University of Oxford

Department of Chemistry



Olefin polymerisation using group 4 permethylindenyl complexes

Thomas James Williams

Balliol College

Hilary 2020

This thesis is submitted in partial fulfilment of the requirement for the degree of Doctor of Philosophy at the University of Oxford

Preface

The work described in this thesis was carried out in the Chemistry Research Laboratory at the University of Oxford between October 2016 and March 2020 under the supervision of Professor Dermot O'Hare. All the work was performed by the author unless otherwise stated and no part has been previously submitted for any other degree.

Part of the work contained in this thesis has been published in the following journal papers:

T. J. Williams, J.-C. Buffet, Z. R. Turner and D. O'Hare, *Catal. Sci. Technol.*, 2018, **8**, 5454-5461.

T. J. Williams, A. D. H. Smith, J.-C. Buffet, Z. R. Turner and D. O'Hare, *Mol. Catal.*, 2020, **486**, 110872.

Abstract

Olefin polymerisation using group 4 permethylindenyl complexes

Thomas J. Williams **D.Phil Thesis**

Balliol College **Hilary Term 2020**

This thesis discusses the development of permethylindenyl constrained geometry complexes (CGCs) as highly efficient slurry-phase polymerisation catalysts capable of incorporating olefins at high and controllable levels and a niobium imido complex as an ethylene oligomerisation catalyst. Finally, a CGC and a niobium imido complex were combined on a single inorganic solid support with the aim of forming short chain branched linear low-density polyethylene (LLDPE) from a single ethylene feedsource.

Ethylene (co)polymerisation, oligomerisation and tandem catalysis are introduced, with discussion of previously reported examples of catalysis of these processes. The synthesis, characterisation and immobilisation on inorganic solid supports of a range of permethylindenyl based CGCs ($^{Me,R^1}$SB($^{t\text{Bu}}$N,$^{3\text{-R}}$I*)MX_2 where ($^{Me,R^1}$SB($^{t\text{Bu}}$N,$^{3\text{-R}}$I*) = {(3-R-η^5-C_9Me_5)(Me,R^1)Si($^{t\text{Bu}}$N)}$^{2-}$), ^{Me_2}SB(^{R}N,I*)$TiCl_2$ and ^{Me_2}SB($^{t\text{Bu}}$N,I*)Ti(Cl)CH_2SiMe_3) is discussed.

Slurry-phase ethylene polymerisation studies were undertaken to investigate the effect of the amido fragment, initiator group, *ansa* bridge, metal centre and permethylindenyl moiety. Factors including temperature, time, scale, catalyst loading, scavenger, pressure and inorganic solid support were all investigated. High-throughput polymerisations were also undertaken for the most active catalysts, and hydrogen response also studied.

Selected complexes were tested as ethylene/1-hexene, ethylene/1-octene and ethylene/styrene copolymerisation catalysts, with ethylene/1-hexene copolymerisations carried out under high-throughput conditions and ^{Me_2}SB($^{t\text{Bu}}$N,I*)TiR_2 (R = Cl and CH_2Ph) tested on a large scale at SCG Chemicals Co., Ltd. (Rayong, Thailand). Solution copolymerisations were also carried out with ^{Me_2}SB($^{t\text{Bu}}$N,I*)$TiCl_2$, ^{Me_2}SB($^{t\text{Bu}}$N,$^{3\text{-Et}}$I*)$TiCl_2$ and ^{Me_2}SB($^{t\text{Bu}}$N,Cp*)$TiCl_2$.

Nb(NDipp)Cl_3.THF.pyr was synthesised and used as a slurry and solution-phase oligomerisation catalyst, with work undertaken to optimise conditions for ethylene trimerisation. Finally, both Nb(NDipp)Cl_3.THF.pyr and ^{Me_2}SB($^{t\text{Bu}}$N,I*)$TiCl_2$ were simultaneously supported on solid polymethylaluminoxane (sMAO) for use in the tandem catalysis of ethylene to form short chain branched LLDPE from a single ethylene feedsource.

Acknowledgements

This work would not have been possible if not for the help of a significant number of people and I am immensely grateful for their help and guidance over the past three and a half years. Firstly, I would like to thank Professor Dermot O'Hare for giving me the opportunity to be part of and study within his research group, and for his advice and help throughout my studies. Secondly, I would like to thank both the EPSRC and SCG Chemicals Co., Ltd. (Thailand) for their financial support through a CASE studentship, allowing me not only to undertake my research, but also enabling me to travel to SCG Chemicals Co., Ltd. in Thailand, HTExplore in Naples and present my work at both national and international conferences.

To both JC and Zoë; thank you for all your help, guidance and patience! I am so grateful for all time you have given to helping me during the past four and half years of being in the group with your advice and tuition being invaluable. I can only apologise for the number of times I had to come and tell you I'd injured myself playing sport! Jess, thanks for being such a great fumehood neighbour for the past three and a half years, always willing to help both in and out of the lab. Chris and Sandy, thank you for your help and being excellent running and golf partners outside of the labs. I must also thank JC, Zoë, Jess and Phil for all your help with proof reading of this thesis. To all other members of the group, thank you for making the last four years enjoyable and entertaining.

Thanks must also go to those who have helped with various techniques; Nick for solid state NMR spectroscopy, Zoë for single crystal X-ray diffraction, Jess, Golf, Phil and Clem for SEM images, Norner AS (Norway) for GPC and solution copolymerisation

testing, HTExplore (University of Naples) for high-throughput studies and SCG Chemicals Co., Ltd. (Thailand) for large-scale catalyst testing.

Away from the lab, thanks to Sam and Tom; two amazing flatmates who have helped turn the flat into a yoga studio and wine bar. Both OUHC and PWs have been a great escape and kept me sane when work has been tough. To Soph, thanks for all your support, and not minding my extended stay in Oxford; I have so enjoyed our travels and time together and I am so lucky to have you there for me, especially when times have been tough. I can't wait to see what the coming years bring for us both. Finally, thanks to Mum, Dad, Grandad and Harry, I am so grateful for your constant help, support, love and encouragement, I would not be where I am today without you all; I am incredibly lucky to have the most caring and supportive family anyone could ask for.

Nomenclature

Below is a summary of some of the commonly used terms throughout the thesis.

Term	Definition
$\{^1H\}$	Proton decoupled
°C	Degree Celsius
µL	Microlitre (10^{-6} L)
µmol	Micromole (10^{-6} mol)
$^{3\text{-Et}}I^*$	3-ethylpentamethylindenyl (3-Et$C_9Me_5^-$)
$^{3\text{-Et}}I^\#$	3-ethylpentamethylindenyl (3-EtC_9Me_5H)
Å	Ångström (10^{-10} m)
α	Ring tilt angle
acac	Acetylacetonate ($CH_3COCHCOCH_3$)
Ad	Adamantyl ($C_{10}H_{16}$)
Allyl	(CH_2CHCH_2)
atm	Atmospheres (1.013 bar)
BHT	3,5-di-*tert*buty-4-hydroxytoluene (3,5-^{t}Bu-4-OH-$C_6H_2CH_3$)
CEF	Crystallisation elution fractionation
cent	Centroid
CGC	Constrained geometry complex
COSY	2D correlation spectroscopy
Cp	Cyclopentadienyl ($C_5H_5^-$)
Cp*	Pentamethylcyclopentadienyl ($C_5Me_5^-$)
CP-MAS	Cross-polarisation magic-angle spinning
Cy	Cyclohexyl (C_6H_{11})

d	Doublet
dd	Doublet of doublets
δ	Chemical shift; angle about the metal centre
DFT	Density Functional Theory
Dipp	Di*iso*propylphenyl (2,6-^{i}Pr-C_6H_3)
dm	Decimetre (10^{-1} m)
dme	Dimethoxyethane ($CH_3OCH_2CH_2OCH_3$)
DP-MAS	Direct polarisation magic angle spinning
DSC	Differential scanning calorimetry
EB	Ethylene bridged (C_2H_4)
EBI	Ethylenebis(1-indenyl) ($C_9H_6(CH_2CH_2)C_9H_6$)
Eq	Equivalents
Et	Ethyl (C_2H_5)
Flu	Fluorenyl ($C_{13}H_9^-$)
g	Gram
GPC	Gel permeation chromatography
h	Hour/hours
HDPE	High-density polyethylene
HMBC	Heteronuclear multiple bond correlation
HSQC	Heteronuclear single quantum coherence
Hz	Hertz
ICP-MS	Inductively coupled plasma mass spectrometry
ICP-OES	Inductively coupled plasma optical emission spectroscopy
I/Ind	Indenyl ($C_9H_6^-$)
I*/Ind*	Permethylindenyl ($C_9Me_6^-$)
I$^{\#}$/Ind$^{\#}$	Hexamethyl indenyl ligand (C_9Me_6H)

^{i}Pr	Isopropyl ($CHMe_2$)
IR	Infrared
K	Kelvin
kcal	Kilocalorie (4184 J)
kDa	Kilodaltons (kg/mol)
kg	Kilogram
kHz	Kilohertz, 10^3 Hz
L	Litre
LAO	Linear α-olefin
LDH	Layered double hydroxide
LDHMAO	Methyaluminoxane-modified layered double hydroxide
LDPE	Low-density polyethylene
LLDPE	Linear low-density polyethylene
M	Metal; mol/dm^3
m	Multiplet
MAO	Methylaluminoxane
Me	Methyl (CH_3)
Mes	Mesityl (2,4,6-Me-C_6H_2)
^{Me_2}SB	Dimethylsilyl bridge ($SiMe_2$)
^{Me,Allyl}SB	Methylallylsilyl bridge ($Si(Me)CH_2CHCH_2$)
^{Me,Pr}SB	Methylpropylsilyl bridge (SiMePr)
mg	Milligram (10^{-3} g)
MHz	Megahertz (10^6 Hz)
min	Minute
mL	Millilitre (10^{-3} L)
mM	Millimole/dm^3

MMAO	Modified methylaluminoxane
mmol	Millimole (10^{-3} mol)
M_n	Number average molecular weight
mol%	Molar percentage (incorporation)
M_w	Weight average molecular weight
M_w/M_n	Molecular weight distribution, PDI, dispersity
^{n}Bu/Bu	^{n}butyl ($CH_2CH_2CH_2CH_3$)
nm	Nanometre (10^{-9} m)
NMR	Nuclear magnetic resonance
PE	Polyethylene
Ph	Phenyl (C_6H_5)
^{Ph}BB	Phenyl boron bridge (PhB)
Pn*	Permethylpentalene ($C_8Me_6^{2-}$)
ppm	Parts per million
Pr	Propyl ($CH_2CH_2CH_3$)
psi	Pounds per square inch
pyr	Pyridine (C_5H_5N)
ROESY	Rotating-frame nuclear Overhauser effect spectroscopy
rpm	Revolutions per minute
RT	Room temperature (~25 °C)
s	Singlet; Seconds
SBI*	Dimethylsilylbis(1-permethylindenyl) ($C_9Me_6(SiMe_2)C_9Me_6$)
SEM	Scanning electron microscopy
SHOP	Shell Higher Olefin Process
sMAO	Solid polymethylaluminoxane
sMAO(1G)	First generation solid polymethylaluminoxane

sMAO(3G)	Third generation solid polymethylaluminoxane
SSMAO	Methylaluminoxane-modified silica
ssNMR	Solid state nuclear magnetic resonance
t	Triplet
T	Temperature
^{t}Bu	*tert*butyl (CMe_3)
$^{t\mathrm{Bu}}$PB	*tert*butyl phosphine bridge (^{t}BuP)
T_c	Crystallisation temperature
TEA	Triethylaluminium ($AlEt_3$)
$T_{El,max.}$	Temperature at maximum elution
THF	Tetrahydrofuran (C_4H_8O)
TiBA	Tri*iso*butylaluminium ($Al^{i}Bu_3$)
T_m	Melting temperature
TMA	Trimethylaluminium ($AlMe_3$)
TMEDA	tetramethylethylenediamine
TOA	Trioctylaluminium ($Al(C_8H_{17})_3$)
TOF	Turnover frequency ($mol_X/mol_Y/h$)
TON	Turnover number (mol_X/mol_Y)
UHMWPE	Ultra-high molecular weight polyethylene
ULMWPE	Ultra-low molecular weight polyethylene, PE wax
W	Watt
wt%	Weight percentage (incorporation)
X	Initiatior group
XRD	X-ray diffraction
ΔH_c	Enthalpy of crystallisation
ΔH_m	Enthalpy of melting

$\Delta_{M\text{-}C}$	Measure of ring slippage
μ-X	Bridging X atom
η	hapticity
κ^n-bound	hapticity

Complex Identification

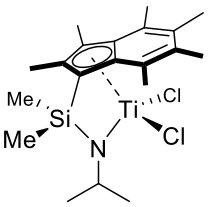

$^{Me2}SB(^{iPr}N,I^*)TiCl_2$

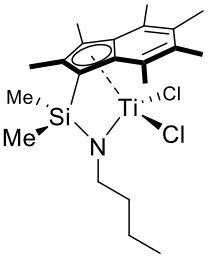

$^{Me2}SB(^{nBu}N,I^*)TiCl_2$

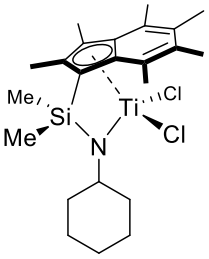

$^{Me2}SB(^{Cy}N,I^*)TiCl_2$

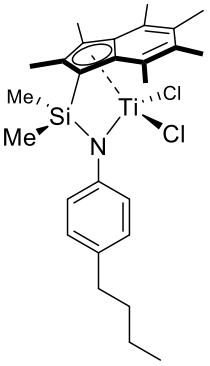

$^{Me2}SB(^{4\text{-}nBuC6H4}N,I^*)TiCl_2$

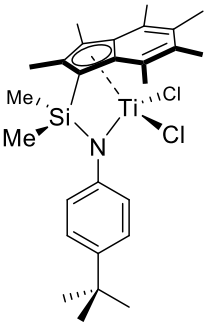

$^{Me2}SB(^{4\text{-}tBuC6H4}N,I^*)TiCl_2$

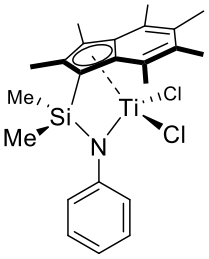

$^{Me2}SB(^{Ph}N,I^*)TiCl_2$

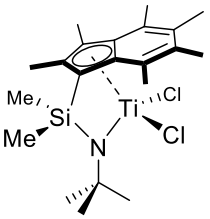

$^{Me2}SB(^{tBu}N,I^*)TiCl_2$

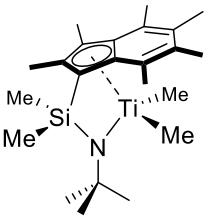

$^{Me2}SB(^{tBu}N,I^*)TiMe_2$

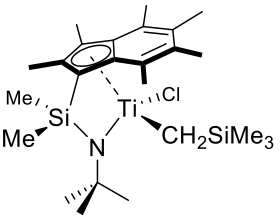

$^{Me2}SB(^{tBu}N,I^*)Ti(Cl)CH_2SiMe_3$

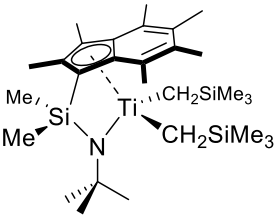

$^{Me2}SB(^{tBu}N,I^*)Ti(CH_2SiMe_3)_2$

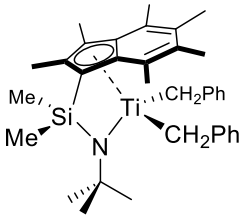

$^{Me2}SB(^{tBu}N,I^*)Ti(CH_2Ph)_2$

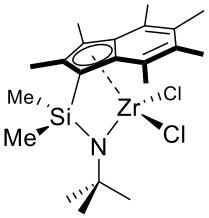

$^{Me2}SB(^{tBu}N,I^*)ZrCl_2$

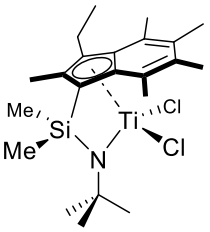

$^{Me2}SB(^{tBu}N,^{3\text{-}Et}I^*)TiCl_2$

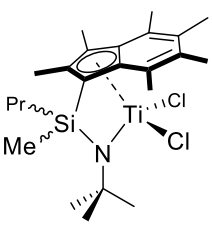

$^{Me,Pr}SB(^{tBu}N,I^*)TiCl_2$

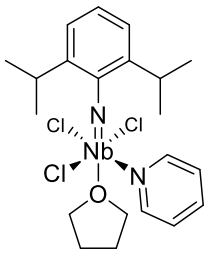

$Nb(NDipp)Cl_3.THF.pyr$

Table of Contents

Preface i

Abstract ii

Acknowledgements iii

Nomenclature v

Complex Identification xi

Table of Contents xii

1 Introduction 1

1.1 Synthesis of constrained geometry complexes 1

1.2 Ethylene homopolymerisation 7

1.2.1 Group four complexes for olefin polymerisation 7

1.2.2 Constrained geometry complexes as ethylene polymerisation catalysts 11

1.2.3 Heterogeneous olefin polymerisation 14

1.2.4 The role of the cocatalyst and scavenger 16

1.2.5 High-throughput ethylene polymerisation 17

1.3 Ethylene/olefin copolymerisation 18

1.3.1 Ethylene/α-olefin copolymerisation 18

1.3.2 Ethylene/styrene copolymerisation 20

1.4 Ethylene oligomerisation 22

1.4.1 Mechanism for ethylene oligomerisation 23

1.4.2 Industrial oligomerisation catalysts 25

1.4.3 Group 5 complexes for ethylene oligomerisation 28

1.5 Tandem catalysis of ethylene 32

1.6 Thesis aims 37

1.7 References 38

2 Complex synthesis 45

2.1 Introduction 45

2.1.1 Synthesis of constrained geometry complexes 45

2.1.2 Chapter synopsis 46

2.2 Synthesis of permethylindenyl constrained geometry complexes 48

2.2.1 Synthesis of $^{Me_2}SB(^{R}N,I^*)TiCl_2$ 48

2.2.2 Synthesis and characterisation of $^{Me_2}SB(^{tBu}N,I^*)Ti(Cl)CH_2SiMe_3$ and $^{Me_2}SB(^{tBu}N,I^*)TiR_2$ 53

2.2.3 Synthesis and characterisation of $^{Me_2}SB(^{tBu}N,^{3\text{-}Et}I^*)TiCl_2$ 58

2.2.4 Synthesis and characterisation of $^{Me,Pr}SB(^{tBu}N,I^*)TiCl_2$ 60

2.2.5 Synthesis and characterisation of $^{Me_2}SB(^{tBu}N,I^*)ZrCl_2$ 61

2.2.6 Attempted synthesis of complexes 61

2.3 Reaction of permethylindenyl CGCs with MAO 65

2.4 Immobilisation of complexes for slurry-phase ethylene polymerisation 67

2.4.1 Immobilisation of complexes on a solid support 67

2.4.2 Immobilisation of complexes on sMAO 67
2.4.3 Immobilisation of complexes on LDHMAO and SSMAO 71

2.5 Conclusions 74

2.6 References 75

3 Constrained geometry complexes for ethylene homopolymerisation 77

3.1 Introduction 77
3.1.1 Overview 77
3.1.2 Ultra-high molecular weight polyethylene (UHMWPE) 78
3.1.3 Hydrogen response 78
3.1.4 Chapter synopsis 79

3.2 Variation of the constrained geometry complex 80
3.2.1 Effect of variation of the amido fragment on slurry-phase ethylene polymerisation 80
3.2.2 Effect of the initiator group on slurry-phase ethylene polymerisation 85
3.2.3 Effect of variation of the permethylindenyl ligand, *ansa* bridge and metal centre on slurry-phase ethylene polymerisation. 91

3.3 Effect of variation of the solid support on polymerisation activity 96
3.3.1 Slurry-phase ethylene polymerisations using sMAO, LDHMAO and SSMAO 96
3.3.2 Variation of complex loading levels on LDHMAO 101
3.3.3 sMAO support variation 103

3.4 Larger scale ethylene polymerisation 107

3.5 Effect of scavenger variation on polymerisation activity 110

3.6 Solution-phase ethylene polymerisation 115

3.7 High-throughput ethylene polymerisation 119
3.7.1 Hydrogen response 121

3.8 Large scale ethylene polymerisation 127

3.9 Conclusions 129

3.10 References 130

4 Constrained geometry complexes for ethylene copolymerisation 133

4.1 Introduction 133
4.1.1 Overview 133
4.1.2 Chapter synopsis 134

4.2 Slurry-phase ethylene copolymerisation 136
4.2.1 Ethylene/1-hexene copolymerisation 136
4.2.2 Ethylene/styrene copolymerisation 145
4.2.3 Ethylene/1-octene copolymerisation 150

4.3 High-throughput ethylene/1-hexene copolymerisation 156
4.3.1 Effect of the amido fragment on ethylene/1-hexene copolymerisation 156
4.3.2 Effect of the initiator group on ethylene/1-hexene copolymerisation 158
4.3.3 Effect of the permethylindenyl moiety on ethylene/1-hexene copolymerisation 161

4.4 Large scale slurry-phase copolymerisation studies 163
4.4.1 Large scale ethylene/1-hexene copolymerisation 163
4.4.2 Large scale ethylene/styrene copolymerisation 165

4.5 Solution-phase copolymerisation 167

4.5.1 Solution-phase ethylene/1-hexene copolymerisation 167
4.5.2 Solution-phase ethylene/1-octene copolymerisation 169

4.6 Conclusions 172

4.7 References 173

5 Niobium imido complex for ethylene oligomerisation and tandem catalysis. 175

5.1 Introduction 175
5.1.1 Ethylene oligomerisation 175
5.1.2 Tandem catalysis of ethylene 176
5.1.3 Chapter synopsis 177

5.2 Synthesis and characterisation of Nb(NDipp)Cl_3.THF.py 178

5.3 Ethylene oligomerisation using Nb(NDipp)Cl_3.THF.py 182
5.3.1 Heterogeneous-phase ethylene oligomerisation 182
5.3.2 Solution-phase ethylene oligomerisation 197

5.4 Tandem catalysis of ethylene 201

5.5 Conclusions 206

5.6 References 207

6 Conclusions and outlook 210

6.1 References 214

7 Experimental details 215

7.1 General preparation and physical methods 215

7.2 Experimental details for Chapter 2 219
7.2.1 Synthesis of constrained geometry complexes 219
7.2.2 Synthesis of ^{Me,Allyl}SB(^{tBu}N,I*)H_2 235
7.2.3 Synthesis of ^{Ph}BB(^{tBu}N,I*)H_2 236
7.2.4 Synthesis of sMAO supported complexes 238
7.2.5 Synthesis of LDHMAO and SSMAO supported complexes 241

7.3 Experimental details for Chapter 3 243
7.3.1 Slurry-phase polymerisation of ethylene 243
7.3.2 Solution-phase polymerisation of ethylene 243
7.3.3 Larger scale slurry-phase ethylene polymerisation 243
7.3.4 High-throughput ethylene, ethylene/hydrogen and ethylene/1-hexene (co)polymerisation 244
7.3.5 Large scale slurry-phase ethylene polymerisation and ethylene/1-hexene copolymerisation 245

7.4 Experimental details for Chapter 4 246
7.4.1 Slurry-phase copolymerisation of ethylene/1-hexene, ethylene/styrene and ethylene/1-octene 246
7.4.2 Solution $^{13}C\{^1H\}$ NMR spectra of copolymer 246
7.4.3 Solution-phase copolymerisation of ethylene/1-hexene and ethylene/1-octene 247

7.5 Experimental details for Chapter 5 248
7.5.1 Synthesis of Nb(NDipp)Cl_3.THF.py 248
7.5.2 Synthesis of sMAO-Nb(NDipp)Cl_3 248
7.5.3 Slurry-phase ethylene oligomerisation 249
7.5.4 Solution-phase ethylene oligomerisation 249
7.5.5 Synthesis of sMAO-Tandem 249
7.5.6 Slurry-phase tandem catalysis 250

7.6 References 251
Appendix A1
Appendix for Chapter 2 ..... A1
Appendix for Chapter 3 ..... A18
Appendix for Chapter 4 ..... A28
Appendix for Chapter 5 ..... A58
References A65

Chapter One

Introduction

1.1 Synthesis of constrained geometry complexes

In 1989, Stevens and co-workers at the Dow Chemical Company filed a patent containing the synthesis of a range of constrained geometry complexes (CGCs) (Figure 1.1) as olefin polymerisation and copolymerisation catalysts.[1] A range of complexes were reported within this patent, with variation of the apical cyclopentadienyl (CpR^3_4) type ligand, amido group (R^1), heteroatom (X), *ansa* bridge (ER^2_2), or metal centre (M).

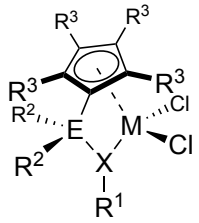

Figure 1.1. General formula for a constrained geometry complex.

Early literature examples of CGCs include $[\{^{Me2}SB(^{tBu}N,Cp^*)\}Sc(PMe_3)]_2(\mu\text{-}H)_2$ ($\{^{Me2}SB(^{tBu}N,Cp^*)\} = \{(\eta^5\text{-}C_5Me_4)Me_2Si(^{tBu}N)\}^{2-}$), synthesised by Bercaw *et al*. in 1990 (Figure 1.2(a)),[2] and Okuda reporting a titanium complex, $^{Me2}SB(^{tBu}N,^{3\text{-}tBu}Cp)TiCl_2$, in the same year (Figure 1.2(b)).[3] CGCs have been of great interest both academically and industrially due to their ability to efficiently polymerise ethylene and incorporate high levels of α-olefins into a polymer chain.[1,4–6]

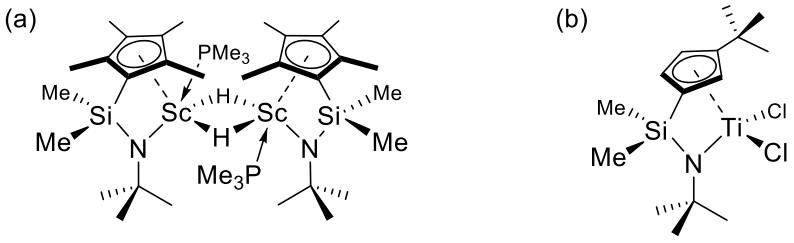

Figure 1.2. Scandium and titanium constrained geometry complexes synthesised by Bercaw *et al*. and Okuda respectively.[2,3]

A range of synthetic methods have been developed, and they can broadly be fitted into two different strategies: either, the synthesis of an *ansa* bridged ligand followed by complexation to a transition metal, or by reaction of coordinated moieties within the ligand sphere of a metal centre to form an *ansa* bridged complex.[5]

The procedure for the synthesis of ^{Me2}SB($^{t\text{Bu}}$N,$^{3\text{-}t\text{Bu}}$Cp)TiCl$_2$ by Okuda in 1990 followed the first method.[3] Firstly, reaction of the protio proligand with ^{n}BuLi to yield the dilithiated ligand ^{Me2}SB($^{t\text{Bu}}$N,$^{3\text{-}t\text{Bu}}$Cp)Li$_2$, then reaction of the ligand with TiCl$_4$.2THF to yield ^{Me2}SB($^{t\text{Bu}}$N,$^{3\text{-}t\text{Bu}}$Cp)TiCl$_2$ in a 35% yield (Equation 1.1).[3] Similar syntheses have been reported for a range of group 4 precursors, including using ZrCl$_4$.2THF,[7] ZrCl$_2$(NEt$_2$)$_2$.2THF,[8] ZrCl$_4$ and HfCl$_4$.[9] Similarly, it is possible to use a range of metal alkyls, such as MeLi, ^{t}BuLi, LiNR$_2$, or Grignard reagents, such as ^{i}PrMgCl, for the double deprotonation of the proligand.[5,10]

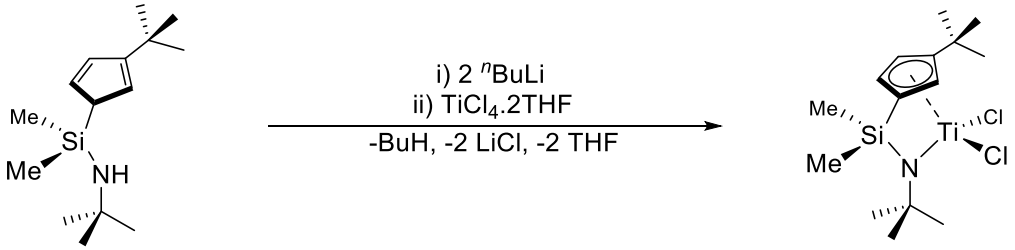

Equation 1.1. Synthesis of ^{Me2}SB($^{t\text{Bu}}$N,$^{3\text{-}t\text{Bu}}$Cp)TiCl$_2$ from ^{Me2}SB($^{t\text{Bu}}$N,$^{3\text{-}t\text{Bu}}$Cp)H$_2$ by dimetallation/salt metathesis.[3]

A disadvantage of this synthetic method is the relatively low yields, partly caused by the facile reduction of titanium (IV) to titanium (III) during complex synthesis. A method to circumvent this was developed, with synthesis of the titanium (III) constrained geometry complex achieved by reaction of the ligand with TiCl$_3$.3THF, followed by oxidation to the final titanium (IV) product. In 1990, Teuben *et al*. reported the use of lead dichloride as an oxidising agent for tervalent titanium complexes to the tetravalent monochloride derivatives.[11] Reaction of half an equivalent of lead dichloride with a range of titanocenes

(Cp_2TiR) (R = Cl, alkoxide, alkyl, hydride) resulted in the clean synthesis of $Cp_2TiR(Cl)$, reaction with lead dibromide resulted in the synthesis of the corresponding monobromide complexes. Okuda *et al*. reported the reaction of $^{Me2}SB(^{tBu}N,^{3\text{-}R}I)Li_2$ ($^{3\text{-}R}I$ is 3-R-indenyl) with $TiCl_3.3THF$ followed by oxidation with lead dichloride to yield $^{Me2}SB(^{tBu}N,^{3\text{-}R}I)TiCl_2$ (R = H, $SiMe_3$) in yields in excess of 90%,[12] far greater than the yield reported for the synthesis of $^{Me2}SB(^{tBu}N,^{3\text{-}tBu}Cp)TiCl_2$.[3]

Another common synthetic method involves elimination of an amine or alkane by reaction of the protio proligand with a metal tetraamide or tetraalkyl. Teuben *et al*. reported the synthesis of propyl bridged constrained geometry complexes by reaction of the proligand, $C_3H_6(^{Me}N,Cp)H_2$, with $M(NMe_2)_4$ (M = Zr and Hf) with yields of over 90% for the zirconium complex.[13] Herrmann *et al*. reported the synthesis of complexes containing *tert*butyl- or phenylamido, cyclopentadienyl or indenyl and titanium or zirconium, all in high yields up to 99%, by reaction of the appropriate proligand with titanium or zirconium tetramethylamine ($Ti(NMe_2)_4$ or $Zr(NMe_2)_4$).[14] Marks *et al.* reported the synthesis of $^{Me2}SB(^{tBu}N,Cp^*)Ti(CH_2Ph)_2$ in a 90% isolated yield by reaction of $^{Me2}SB(^{tBu}N,Cp^*)H_2$ with $Ti(CH_2Ph)_4$ (Equation 1.2).[15] The zirconium analogue was isolated in only 10% yield due to high solubilities of the product.

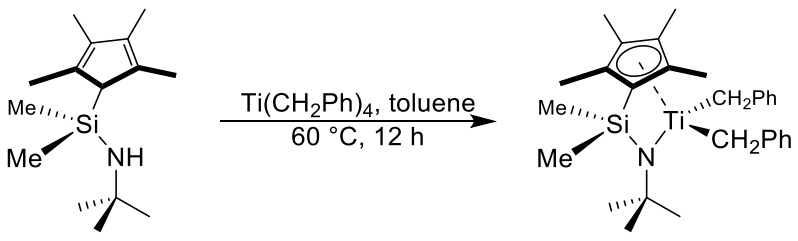

Equation 1.2. Synthesis of $^{Me2}SB(^{tBu}N,Cp^*)Ti(CH_2Ph)_2$ by protonolysis.[15]

Royo *et al*. developed a route to CGCs by templation around a metal centre and formation of an *ansa* bridge within the coordination sphere of the metal centre. Reaction of

Ti(η^5-$C_5H_4SiMe_3$)Cl_3 with LiN(H)R and NEt_3 in a 1:1:1 ratio resulted in the formation of ^{Me_2}SB(^{R}N,Cp)$TiCl_2$ in approximately 70% yields. It is thought that the reaction proceeds *via* the formation of an amido titanium species Ti(η^5-$C_5H_4SiMe_3$)Cl_2(NHR) with loss of LiCl; followed by elimination of HCl in the presence of NEt_3 to yield ^{Me_2}SB(^{R}N,Cp)$TiCl_2$ (where R = ^{t}Bu or CH(Me)Ph).[16] Similarly, Lemenovskii *et al*. reported the synthesis of a phosphorus bridged CGC, $^{t\text{Bu}}$PB($^{t\text{Bu}}$N,$^{3\text{-}t\text{Bu}}$Cp)$TiCl_2$, using this templating method;[17] Jones *et al*. reported the synthesis of constrained geometry complexes with Zr(η^5-$C_5H_4SiMe_3$)Cl_3 pre-supported on aminosilicate, the addition of 2,6-di*tert*butylpyridine led to elimination of HCl and formation of the supported CGC.[18] Okuda *et al*. reported the synthesis of a range of enantiomerically pure chiral constrained geometry complexes using this templation method.[19] Upon activation of these complexes with ^{n}BuLi, they catalysed the hydrogenation of *N*-benzylimine with good conversions, but low selectivities.[20]

It has been shown that it is possible to alter all of the components of a constrained geometry complex in attempts to enhance catalytic activity. A variety of amido groups have been reported in constrained geometry complexes; such as a phenyl amido complex,[21] bulky alkyl groups such as cyclododecyl or adamantyl,[22] or chiral amido complexes.[19] Complexes have been reported with variation of the basal heteroatom; the amido fragment has been replaced by a carbanionic moiety, such as in Figure 1.3 (a),[23] or a phosphido group such as ^{Me_2}SB(^{Cy}P,Cp)Ti(NMe_2)$_2$ (Figure 1.3 (b)).[24]

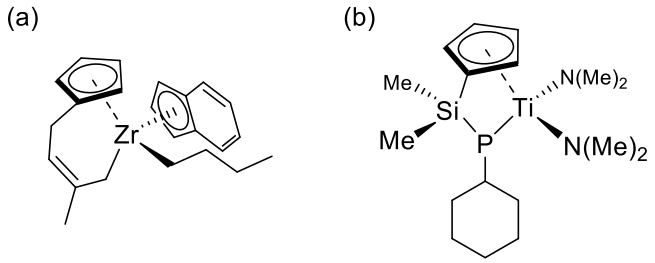

Figure 1.3. Examples of (a) a carbanionic constrained geometry complex,[23] and (b) phosphido constrained geometry complex.[24]

The nature of the *ansa* bridge has been shown to play an important role in the exceptional reactivity and catalytic activity of CGCs, with the high activities and reactivity being attributed to this bridge.[1] The dimethyl silyl bridge was reported in early complexes synthesised by Stevens and co-workers at the Dow Chemical Company,[1] the scandium complex reported by Bercaw *et al*.,[2] and the titanium complex reported by Okuda;[3] this dimethylsilyl bridge is still one of the most commonly employed *ansa* bridges.[5] Aside from silicon, other elements have been reported including boron,[25,26] carbon,[24,27] and phosphorus.[17] Reb *et al*. reported a range of complexes with substitution of one methyl substituent for either a vinyl, phenyl, octenyl or hexenyl group,[28,29] which allowed for the formation of diastereomeric complexes. Substitution of a methyl group for hydrogen or chlorine provides a reactive site whereby it may be possible to bind the complex to an insoluble support *via* the *ansa* bridge,[5,30] or a suitable linker may be attached to allow for the formation of bimetallic complexes, such as the linked CGC–*ansa* bridged zirconocene reported by Alt *et al*..[31]

As demonstrated by Stevens *et al*.,[1] the Cp fragment can be modified, with Okuda *et al*. preparing both indenyl (Ind, I) and fluorenyl (Flu) CGCs.[7,12] Klosin *et al*. reported the modification of indenyl constrained geometry complexes with addition of aryl, alkoxy and amino substituents at the 2- and 3- positions.[32] Rausch *et al.* reported the synthesis of ^{Me_2}SB($^{t\text{Bu}}$N,$^{3\text{-R}}$Cp)TiCl$_2$ (R= H, Me, ^{t}Bu and CH$_2$Ph).[33] Besides scandium and group 4

complexes,[1–3,7,9] constrained geometry complexes have been reported for yttrium and lanthanum,[34–37] group 5,[38–40] 6,[41,42] 7 and 8 metals,[3,43] as well as group 13 and 15 complexes.[44–46]

1.2 Ethylene homopolymerisation

1.2.1 Group four complexes for olefin polymerisation

Since the pioneering work of Ziegler and Natta, ethylene polymerisation has been of great academic and industrial interest.[47,48] While the majority of polyethylene-based polymers are still produced by Ziegler-Natta type catalysts, there has been a small shift towards production of polymers by metallocene-type molecular catalysts, both due to greater control of polymer microstructure,[32] and the ability to incorporate higher levels of α-olefins.[49] A further advantage of these systems is the narrow molecular weight distributions of the polymers produced and the chemical homogeneity through the polymers.[49] In 1957, Natta *et al*. and Breslow *et al*. reported that the bent metallocene Cp_2TiCl_2 with either Et_2AlCl or $AlEt_3$ would polymerise ethylene with low activities.[50,51] A breakthrough in metallocene catalysed polymerisation was the discovery of methylaluminoxane (MAO) by Kaminsky *et al*. in 1980 by addition of a small amount of water to $AlMe_3$, which was found to significantly enhance polymerisation activities for these catalysts.[52,53]

Metallocene complexes are highly tuneable, with variation of the cyclopentadienyl fragment influencing polymerisation activity and polymer properties, as well as the tacticity of the polymer when used in propylene polymerisation.[54–56] The indenyl ligand, a system comprising of fused C_5-C_6 rings (C_9H_6, Ind, I), is a common substitute to cyclopentadienyl. The indenyl ligand can allow for increased substitution at the metal centre due to the ability for the ring to undergo η^5-η^3 ring slip and for the metal to lose valence electrons without the need for oxidation or reduction.[57] Permethylation of the indenyl ring results in the formation of the permethylindenyl ligand (C_9Me_6, Ind*, I*), which has been shown to lead to higher stabilities when compared with the indenyl

ligand, due to inductive donation from the methyl groups, and increased steric bulk about the metal centre.[58–61]

Addition of an *ansa* bridge to a metallocene type complex inhibits ligand rotation in the complex, and as such can enforce rigidity within the complex and introduce chirality.[62,63] The distortion caused by an *ansa* bridge can be measured by the α angle, measuring the degree of ring tilt, the β angle, measuring the angle between the vectors normal to the ring centroids, and the γ angle, which can give an indication of the degree of ring slippage from an ideal η^5 coordination (Figure 1.4).[64] Brintzinger *et al*. demonstrated that *ansa* bridged titanocenes were unreactive under conditions that would cause the corresponding titanocenes to decompose or be transformed to other derivatives;[65] this was attributed to the inability to form the polymeric $[(CH_2)_2Cp_2Ti]_n$ intermediate, in contrast to the unbridged analogue. *Ansa* bridged metallocenes have been shown to be highly efficient ethylene polymerisation catalysts, with *rac*-EBIZrCl_2 (EBI being ethylene-bridged bis-indenyl) having a polymerisation activity of 9377 $kg_{PE}/mol_{Zr}/h/bar$ with an MAO cocatalyst,[66] greater than that reported for Ind_2ZrCl_2 (7600 $kg_{PE}/mol_{Zr}/h/bar$).[67] The higher activities reported for the analogous I* complex *rac*-EBI*ZrCl_2 (61800 $kg_{PE}/mol_{Zr}/h/bar$) and *rac*-SBI*ZrCl_2 (22622 $kg_{PE}mol_{Zr}/h/bar$) highlights the higher activities afforded by permethylation of the indenyl ring.[60,68]

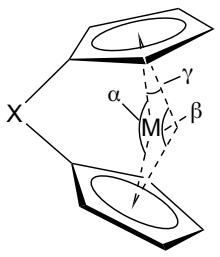

Figure 1.4. Definition of the α, β and γ angles.[64]

Along with the previously synthesised symmetrical I* complexes reported by O'Hare *et al.*,[59,69–71] a range of asymmetric complexes have been produced with substitution of the

basal ligand for cyclopentadienyl (Figure 1.5(b)) and fluorenyl groups (Figure 1.5 (c)), along with further modifications to these.[72–75] This has been facilitated by the optimised synthesis of I*SiMe$_2$Cl (C$_9$Me$_6$(H)SiMe$_2$Cl, Figure 1.5(a)), which can then allow modification of the basal ligand to a wide variety of moieties.

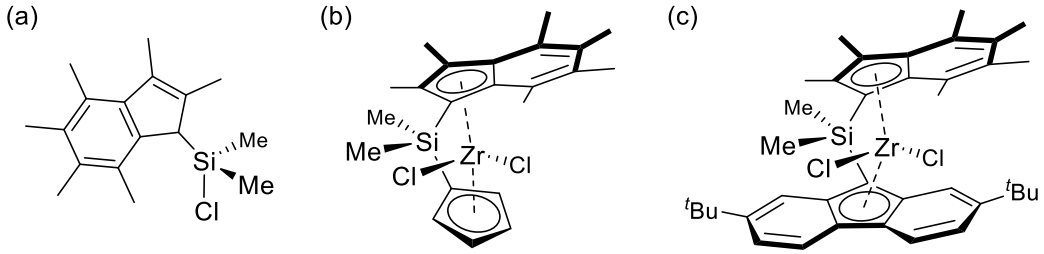

Figure 1.5. Structures of (a) I*SiMe$_2$Cl, and two asymmetric complexes (b) ^{Me_2}SB(I*,Cp)ZrCl$_2$,[72] and (c) ^{Me_2}SB($^{2,7\text{-}t\text{Bu}}$Flu,I*)ZrCl$_2$.[73]

Mechanistically, it is widely accepted that ethylene polymerisation proceeds *via* the Cossee-Arlman ethylene polymerisation mechanism (Scheme 1.1).[76,77] A cationic metallocene with a vacant coordination site is able to bind ethylene in a side-on π-bonding interaction. The monomer inserts into the polymer chain *via* a four-membered ring transition state, with this insertion and rearrangement step being proposed to be the rate determining step. This results in the reformation of the cationic metal centre with a vacant coordination site available for further coordination of ethylene and a pendant polymer chain with an increased chain length of two. The coordination and dissociation of ethylene is thought to be rapid, with many molecules coordinating and dissociating prior to propagation.

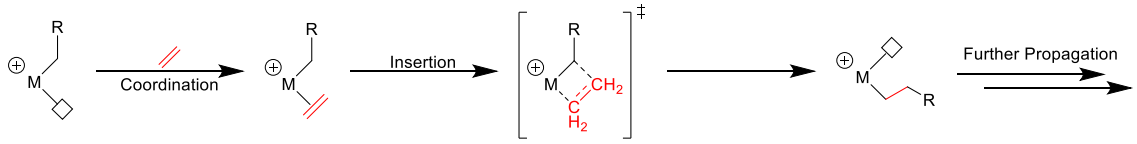

Scheme 1.1. Cossee-Arlman ethylene polymerisation mechanism.[55,76,77] Free coordination site represented by □. Ligands excluded for clarity.

Within this mechanism, there are a number of potential chain termination pathways; these include β-hydride elimination facilitated by a stabilising agostic interaction (Scheme 1.2 (a)), chain transfer to another ethylene monomer and release of the polymer chain (Scheme 1.2 (b)) and chain transfer to an aluminium cocatalyst, such as MAO or $AlMe_3$ (Scheme 1.2 (c)).[78–80]

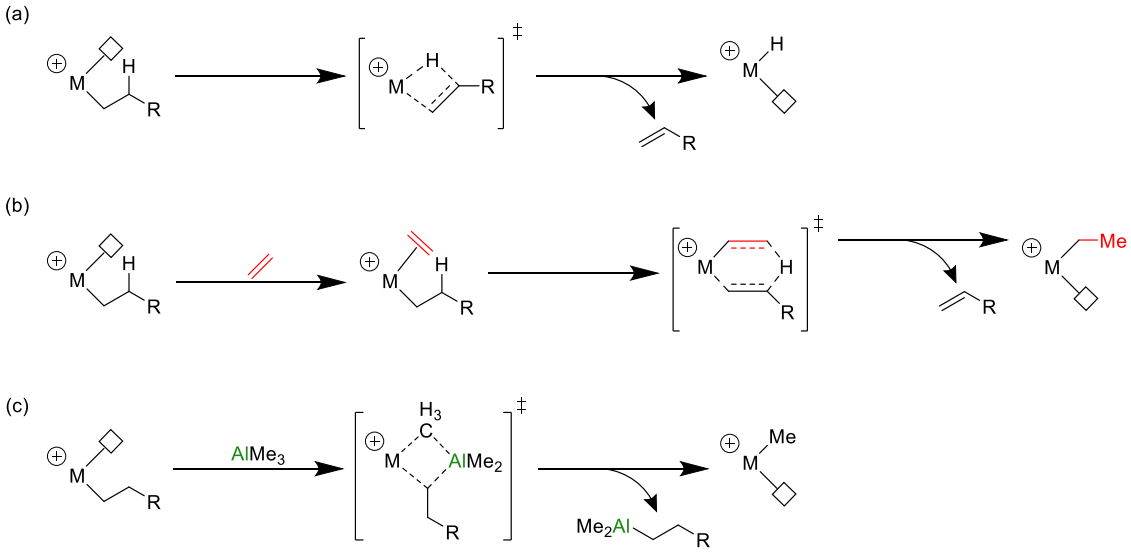

Scheme 1.2. Chain termination pathways for ethylene polymerisation by (a) β-hydride elimination,[78,79] (b) chain transfer to an ethylene comonomer,[78,79] and (c) chain transfer to an alkylaluminium cocatalyst.[80] Free coordination site represented by □. Ligands excluded for clarity.

The difference between the rates of chain propagation, as described in Scheme 1.1, and the various rates of chain termination, Scheme 1.2, results in the polymer molecular weights observed, with these being dependent on the nature of the catalytic system.

Addition of hydrogen to the polymerisation reaction has been shown to result in large decreases in polymer molecular weights, for example Cp_2ZrCl_2 with an MAO cocatalyst at 70 °C and 8 bar pressure produces polyethylenes with molecular weights of 135 kDa and 56 kDa with addition of 0 and 0.04 bar of hydrogen respectively.[81] Seppälä *et al.* showed that molecular weights produced by an $EBIZrCl_2$/MAO system decreased from 136 kDa to 102 kDa with addition of 8300 molar equivalents of hydrogen.[82]

These decreases in molecular weights are attributable to an alternate chain transfer pathway whereby hydrogen can coordinate to the metal centre, and chain transfer can occur resulting in the formation of a metal hydride species (Scheme 1.3).[79]

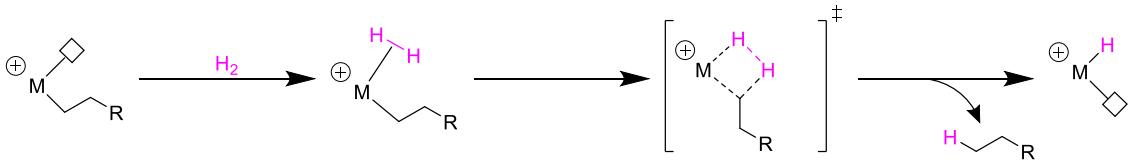

Scheme 1.3. Chain termination mechanism facilitated by hydrogen addition to the polymerisation reaction.[79] Ligands excluded for clarity; free coordination site represented by □.

This reduction in polymer molecular weights is also often commonly paired with large reductions in activity, with the activity decreasing from 45000 to 21400 $kg_{PE}/mol_{Zr}/h/bar$ for the Cp_2ZrCl_2/MAO system.[81] The lower activities of these polymerisations are attributable to the formation of a metal hydride species from chain transfer to hydrogen, that requires reactivation by propagation,[79,81,83] or the formation of a dormant bimetallic species that requires reactivation to form the methyl cationic species.[84,85]

1.2.2 Constrained geometry complexes as ethylene polymerisation catalysts

Stevens *et al*. performed a systematic structural study of a range of constrained geometry complexes, and it was demonstrated that higher polymerisation activities were associated with increasing electron density about the metal centre;[1,4] either with variation of the cyclopentadienyl ligand, where activities follow the trend Cp* > Cp > indenyl,[1,86] or by variation of the amido fragment (with activities following the trend 4-F-C_6H_4 < C_6H_5 < ^{t}Bu).[87] Okuda *et al*. studied ^{Me2}SB(^{R}N,Cp*)Ti($CH_2Ph)_2$ where (R = Me, ^{i}Pr, ^{t}Bu) for ethylene polymerisation which, when activated by $B(C_6F_5)_3$, had activities following the trend Me < ^{i}Pr < ^{t}Bu (activities of 12, 18 and 28 $kg_{PE}/mol_{Ti}/h/bar$ respectively);[88] this

activity trend was inverse to that of the decomposition times of the benzyl cations. Waymouth *et al*. and Nomura *et al.* have both demonstrated that increasing the electron donating nature of the amido group resulted in enhanced activities for ethylene/styrene copolymerisation, with activities increasing in the trend Me < Cy < ^{t}Bu.[87,89]

Rausch *et al.* reported the synthesis of ^{Me2}SB($^{2,6\text{-}Me_2C_6H_3}$N,$^{3\text{-}R}$Cp)TiCl$_2$ (R = H, Me, ^{t}Bu and CH_2Ph) with ethylene polymerisation activities following the trend H > Me > CH_2Ph > ^{t}Bu.[33] Polymerisation with an MAO cocatalyst led to activities of 1500, 1200, 1100 and 62 $kg_{PE}/mol_{Ti}/h/bar$, with the variation in activities being proposed to be due to steric effects of the R group. Klosin *et al*. have reported a range of titanium dimethyl constrained geometry complexes containing an indenyl apical ligand, with variation of the constituents at the 2- and 3- positions (Figure 1.6).[32] These complexes, and ^{Me2}SB($^{t\text{Bu}}$N,Cp*)TiMe$_2$, were tested as ethylene/1-octene copolymerisation catalysts with an MAO cocatalyst. The activity of ^{Me2}SB($^{t\text{Bu}}$N,Cp*)TiMe$_2$ is far greater than that of ^{Me2}SB($^{t\text{Bu}}$N,I)TiMe$_2$, with activities four times greater for the Cp* complex (10150 $kg_{PE}/mol_{Ti}/h/bar$) than the indenyl complex (2490 $kg_{PE}/mol_{Ti}/h/bar$). Variation of the 2- and 3- positions were shown to have a large effect on activities; addition of a methoxy group led to higher activities (8520 and 3910 $kg_{PE}/mol_{Ti}/h/bar$ for the 2- and 3- methoxy complexes respectively) and addition of a pyrrolidine group at the 3- position resulted in a large increase in activity to 69900 $kg_{PE}/mol_{Ti}/h/bar$. Addition of NMe_2 at the 2- position resulted in a decrease in activity to 2170 $kg_{PE}/mol_{Ti}/h/bar$, although with a large variation in the amount of catalyst used. Molecular weights were also found to be affected by variation of the heteroatom; higher polymer molecular weights were observed for complexes with substitution in the 3-position than the 2- position.

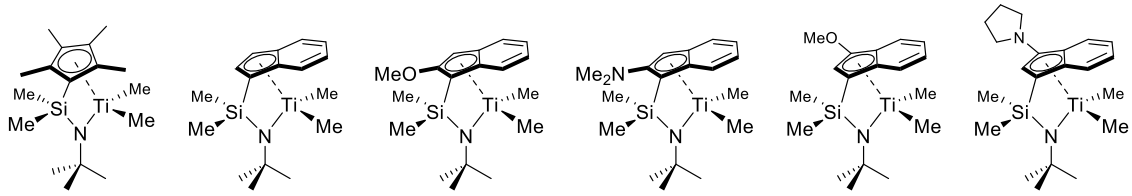

Figure 1.6. Molecular structures of ^{Me2}SB(^{tBu}N,Cp*)TiMe$_2$, ^{Me2}SB(^{tBu}N,I)TiMe$_2$, ^{Me2}SB(^{tBu}N,$^{2\text{-}OMe}$I)TiMe$_2$, ^{Me2}SB(^{tBu}N,$^{2\text{-}NMe2}$I)TiMe$_2$, ^{Me2}SB(^{tBu}N,$^{3\text{-}OMe}$I)TiMe$_2$ and ^{Me2}SB(^{tBu}N,$^{3\text{-}NC4H8}$I)TiMe$_2$.[32]

Numerous constrained geometry complexes have been synthesised with varying leaving groups, including amides,[13,90] and alkylated complexes such as ^{Me2}SB(^{tBu}N,Cp*)TiX$_2$ (X = CH_2Ph and Me) reported by Chen and Marks.[15] Higher activities were observed for the dibenzyl complex (131 $kg_{PE}/mol_{Ti}/h/bar$) compared with the dimethyl complex (114 $kg_{PE}mol_{Ti}/h/bar$) when preactivated with $B(C_6F_5)_3$.

As discussed in 1.2.1, the presence and nature of the *ansa* bridge has been shown to be of great importance in ethylene polymerisation; variation of ^{Me2}SB(^{tBu}N,Cp*)TiCl$_2$ to ^{Me4}DSB(^{tBu}N,Cp*)TiCl$_2$ (^{Me4}DSB corresponds to a disilylmethyl $(SiMe_2)_2$ bridge) has been shown to lead to a lower ethylene polymerisation activity (from 43000 to 6600 $kg_{PE}/mol_{Ti}/h$), whilst higher activities were observed for EB(^{tBu}N,Cp*)TiCl$_2$ (160000 $kg_{PE}/mol_{Ti}/h$) (EB corresponds to a C_2H_4 bridge).[4,91]

Moving down group 4 has been shown to decrease ethylene polymerisation activities, which is in contrast to what has been observed for many metallocene type ethylene polymerisation catalysts,[5] but is commonly observed for CGCs.[25,92] Density functional theory (DFT) studies have shown that this decrease in polymerisation activity is attributable to the ethylene insertion step in the polymerisation mechanism, where the activation barrier for zirconium constrained geometry complexes is much greater than is observed for titanium analogues, resulting in slower polymerisation rates.[93]

Constrained geometry complexes have been shown to produce very high molecular weight polyethylene, with molecular weights in excess of 1000 kDa being produced both by ^{Me2}SB($^{t Bu}$N,Cp*)TiX$_2$ (X = CH_2Ph and Me) (2000 and 1060 kDa respectively) when preactivated with $B(C_6F_5)_3$,[15] and with LDHMAO-supported ^{Me2}SB($^{t Bu}$N,Cp*)$TiCl_2$ at 60 °C (1032 kDa).[94] The polymer molecular weight distributions (M_w/M_n) of the polymers produced by constrained geometry complexes are typically narrower than those produced by heterogeneous Ziegler-Natta complexes,[95] resulting in increased toughness but poorer melt processability. The presence of long chain branching in ethylene polymers produced by constrained geometry complexes at the Dow Chemical Company not only results in advantageous properties such as melt fracture resistance and control of sheer thinning,[96] but also allows for excellent processability for applications such as blown film, injection moulding or thermal forming.[95]

1.2.3 Heterogeneous olefin polymerisation

Heterogeneous-phase catalysts comprising of metallocene type complexes supported on an insoluble solid have been of great industrial interest, due to their ability to control polymer morphology and flowability, and helping to prevent reactor fouling.[97] Heterogeneous catalysts can also be used in slurry-phase or gas-phase polymerisations adding a further advantage over solution-phase analogues.[56] These supports include zirconium oxide,[98] layered double hydroxides (LDHs),[94] clays and zeolites;[99,100] however, the most commonly used support is silica.[68,97,101]

The nature of the support has been shown to influence the polymerisation activities of the catalysts. An example of this is the polymerisation of propylene using $C_2H_4(H_4\text{-Ind})_2ZrCl_2$ supported on a range of insoluble supports with an $AlMe_3$ cocatalyst.[102] Negligible polymerisation activities were observed when the complex was

supported on silica or MgO, with activities of 139, 264, 167 and 13 kg_{PP}/mol_{Zr} when supported on $MgCl_2$, MgF_2, CaF_2 and AlF_3 respectively. Activities were far lower than the unsupported catalyst with an MAO cocatalyst (2070 kg_{PP}/mol_{Zr}), whilst negligible activities were observed using the unsupported catalyst with an $AlMe_3$ cocatalyst.[102]

Pre-treatment of silica with an alkylaluminium species, such as MAO, is often required to activate the support.[97] MAO has been shown to primarily chemisorb onto surface hydroxyl groups, leading to highly Lewis acidic sites.[103] These sites can then interact with metallocene-based pre-catalysts to form an ion pair ($[L_nM\text{-}Me]^+[MAO\text{-}X]^-$) that is active for polymerisation catalysis.[104] The temperature at which silica is pre-treated has been shown to affect ethylene polymerisation rates, with polymerisation productivities for $(Cp^nBu)_2ZrCl_2$ decreasing from 390 to 360 and 190 $g_{PE}/g_{cat}/h/bar$ for silicas pre-treated at 110, 200 and 600 °C respectively.[56]

Kaji *et al*. at Tosoh Finechem Corporation (Japan) developed solid polymethylaluminoxane (sMAO), a modified, polymerised, methylaluminoxane insoluble in many common organic solvents.[105] An optimised laboratory procedure has been developed, with the nature of the solid studied, and sMAO-supported *rac*-$EBIZrCl_2$ has been shown to have a polymerisation activity far greater than that of the MAO-modified LDH (LDHMAO) supported analogue (6533 and 1841 $kg_{PE}/mol_{Zr}/h/bar$ respectively).[106] Modification of sMAO with pentafluorophenyl and pentafluorophenoxy groups has been shown to result in large enhancements in activities compared with the unmodified sMAO support.[107,108] Comparison of ethylene polymerisation activities of complexes supported on sMAO, SSMAO and LDHMAO further highlights the greater activities afforded by the sMAO support; activities for sMAO-supported

^{Me_2}SB(I*,Cp^{R})ZrX$_2$ and ^{Me_2}SB($^{2,7\text{-}t\text{Bu}}$Flu,I*)ZrCl$_2$ far exceed those observed for LDHMAO and SSMAO-supported complexes.[72,73]

1.2.4 The role of the cocatalyst and scavenger

There has been continued research into MAO as a cocatalyst; Ehm *et al*. have investigated the effect of variation of [Al]$_0$:[Ti]$_0$ ratios on supporting Cp*(^{t}Bu$_3$P=N)TiCl$_2$ on 2,6-di*tert*butyl-4-methylphenol (BHT) modified MAO.[109] At high titanium loadings, homodinuclear adducts forming outer sphere ion pairs are dominant, whereas mononuclear inner sphere ion pairs are generally formed at lower loadings; both species were found to be viable precursors to the cationic active species. McIndoe *et al.* have investigated the effect of modifications to MAO, *via* alkyl exchange or oxidation, and the effect in the structure of MAO studied.[110,111]

Like metallocene complexes, constrained geometry complexes also require activation by a cocatalyst to generate a catalytically active species.[104,112] It is generally accepted that the activation of a metallocene type complex occurs by alkylation of the metal centre, followed by abstraction and formation of a cationic metallocene-type active species with a weakly coordinating metal anion (Scheme 1.4).[113,114]

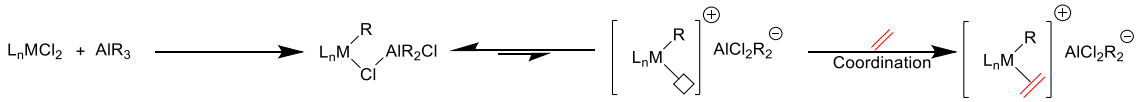

Scheme 1.4. Activation of L_nMCl_2 by AlR_3.[113] Free coordination site represented by □.

Alkyl aluminiums, such as trimethylaluminium (TMA), triethylaluminium (TEA) or tri*iso*butylaluminium (TiBA), are generally present in slurry-phase (co)polymerisation reactors,[115] with the latter two and trioctylaluminium (TOA) generally used due to easier handling compared with TMA. When these are employed as scavengers, they are added in low concentrations so as to minimise the impact on reaction kinetics. When

metallocenes activated by an MAO cocatalyst are used in ethylene polymerisation, the concentration of scavenger is particularly important due the potential to interact with both the metallocene catalyst and the MAO cocatalyst.[116–118] These interactions are often cited as the main reasons for both reduced activity during polymerisations and the cause for reactor fouling when using supported metallocene/MAO catalysts.[115]

1.2.5 High-throughput ethylene polymerisation

The use of a high-throughput reactor allows for the screening of a large number of catalysts under a variety of conditions in shorter amounts of time than conventional systems, leading to faster system optimisation.[119]

Gibson *et al*. have reported the discovery of highly active ethylene polymerisation catalysts based on chromium with tridentate salicylaldimine ligands and tridentate triptycenyl groups through the employment of this method of catalyst screening.[120] Using the same method, Busico *et al*. have reported the optimisation of pyridyl-amide hafnium complexes for ethylene polymerisation.[121] High-throughput screening has also been used to study Ziegler-Natta olefin catalysis;[122] it allows for the ability to study this on a smaller scale, leading to shorter experimental time period, which reduces the risk of decomposition of air sensitive compounds.[122] Despite the high costs of this approach in terms of infrastructure and equipment, and mass transfer limitations from working on a smaller scale,[121] its technical, economic and environmental advantages provides an alternative method for studying not only organometallic catalysis,[121] but also drug screening, materials science and molecular synthesis.[121,123]

1.3 Ethylene/olefin copolymerisation

Addition of an olefin as comonomer to ethylene polymerisation reactions can allow for controlled addition of branches into polymer chains, significantly affecting the polymer properties and end usage. The greater degree of chain branching leads to increased polymer flexibility, allowing for usage as foams, elastic fibres, packaging and adhesives.[124] Constrained geometry complexes have been shown to be highly efficient ethylene/olefin copolymerisation catalysts, with high levels of olefin incorporated into the polymer chain.[1] This improved copolymerisation of ethylene and olefins compared with metallocenes has been attributed to a less crowded coordination sphere, a smaller bite angle (Cp_{cent}-M-N angle), than metallocenes (Cp_{cent}-M-Cp_{cent}) (by approximately 25–30°) and a decreased tendency to undergo chain transfer reactions.[5]

1.3.1 Ethylene/α-olefin copolymerisation

Constrained geometry complexes have been employed industrially on a large scale in high-temperature solution copolymerisation of ethylene with 1-hexene, 1-octene and 1-decene, with comonomer incorporation levels of up to 60 mol%.[125,126] These have been marketed under INSITE, ENGAGE and AFFINITY at the Dow Chemical Company.[91] The importance of the *ansa* bridge on copolymerisation has been demonstrated by Quijada *et al*., comparison of Ind_2ZrCl_2 and $EBIZrCl_2$ with an MAO cocatalyst resulted in a far higher copolymerisation activity for the *ansa* bridged complex, with activities often twice as high, but also much higher levels of comonomer incorporation, with incorporations up to 18 mol% for $EBIZrCl_2$ compared with 6.3 mol% for Ind_2ZrCl_2.[67] Quijada *et al*. have also shown that increased steric bulk and chain length of the linear α-olefin results in lower levels of olefin incorporation, from 26.2 to 9.6 and 11.0 wt% for 1-hexene, 1-octene and 1-decene copolymerisation using $EBIZrCl_2$.[127]

A disadvantage of the addition of a linear α-olefin is the reduction in polymer molecular weights associated with addition of a 1-alkene, which has been proposed to be due to increased chain transfer being facilitated to the comonomer.[128] Klosin *et al*. have been able to negate this large decrease in polymer molecular weights in ethylene/1-octene copolymerisations.[32] Substitution of ^{Me2}SB($^{t Bu}$N,I)TiMe$_2$ in the 2- and 3- positions not only affects copolymerisation activities, but also copolymer molecular weight. It was found that precatalysts with a 3-substituted heteroatom resulted in higher polymer molecular weights than the unsubstituted complex (105 kDa) with molecular weights of 148 kDa for the 3-methoxy complex and 280 kDa for the 3-pyrrolidine complex.

Marks *et al*. reported that the nature of the leaving group in ^{Me2}SB($^{t Bu}$N,Cp*)TiX$_2$ has an effect on both copolymerisation activity and incorporation levels.[15] When ^{Me2}SB($^{t Bu}$N,Cp*)TiX$_2$ (X = Me, CH_2Ph) is pretreated with $B(C_6F_5)_3$, and used in ethylene/1-hexene copolymerisation, the dimethyl complex produced a copolymer with 70% 1-hexene incorporation and an activity of 578 $kg_{PE}/mol_{Ti}/h/bar$, whilst the dibenzyl complex produced a mixture of two homopolymers and an activity of 663 $kg_{PE}/mol_{Ti}/h/bar$. Using an MAO cocatalyst with the dibenzyl complex resulted in a copolymer being produced with 70% incorporation of 1-hexene, highlighting the influence of the cocatalyst on copolymerisation.[15]

Marks *et al*. reported the immobilisation of both mono- and bimetallic constrained geometry complexes on sulfated alumina.[129] Lower incorporation levels of 1-hexene were observed compared with solution copolymerisations, and this was proposed to be due to diffusional resistance of the active sites from both the propagating copolymer chain and the support itself.[130] Workers at the Dow Chemical Company developed a highly effective method of modifying silica with MAO; immobilisation of

^{Me_2}SB($^{t\text{Bu}}$N,Cp*)TiCl$_2$ followed by ethylene/1-octene copolymerisation resulted in high activities and polymers with high bulk densities.[131] Diffusional resistance is observed in ethylene/1-hexene copolymerisation using SSMAO-supported *rac*-^{Me_2}SB($^{2\text{-Me-4-Ph}}$I)$_2$ZrCl$_2$, both homo- and copolymerisation was observed and this was attributed to the formation of a copolymer envelope around the active catalytic site through which only ethylene could diffuse resulting in the formation of polyethylene.[132]

1.3.2 Ethylene/styrene copolymerisation

Introduction of styrene to a polymer chain results in large changes in the elastic and thermo-mechanical properties of the polymer materials,[133] with the crystallisability of the polymer chain being inhibited with increasing levels of styrene incorporation. These polymers have found use as compatibilisers for polyethylene/polystyrene blends, with applications including bitumen modifiers, packaging, adhesives and in automotive and construction uses.[133,134]

Constrained geometry complexes have been shown to be efficient ethylene/styrene copolymerisation catalysts,[1] with incorporations reported up to 48 mol%. The microstructure of these copolymers only showed tail-to-tail styrene-styrene sequences, leading to a maximum theoretical incorporation of 50 mol%. This, therefore, is beneficial in allowing high incorporation levels without the formation of polystyrene blocks,[135] bridging the gap between half-metallocenes, that produce predominantly syndiotactic polystyrene with trace copolymer,[135] and *ansa*-zirconocenes that typically fail to incorporate large amounts of styrene due to a crowded coordination sphere.[136] Mülhaupt *et al.* demonstrated that, as with ethylene homopolymerisation, increased electron density on the Cp ring and amido fragment resulted in higher polymerisation activities.[137] Variation of the Cp ligand followed this trend, with activities following the

order Cp* > Ind > $^{3\text{-SiMe}_3}$Ind (activities of 3074, 435 and 255 $kg_{PE}mol_{Ti}/h$) (Figure 1.7 (a)); the ^{t}Bu amido group also resulted in higher activities than the benzyl amido complex (255 $kg_{PE}mol_{Ti}/h$) for ^{Me_2}SB(^{R}N,Cp*)$TiCl_2$. Bulky substituents result in lower styrene incorporation (1.1 mol% incorporation for the fluorenyl complex (Figure 1.7 (b)) compared with 15.8 mol% for Cp*), due to steric hinderance, but results in an increase in the long-term activity of the catalyst and higher polymer molecular weights.[137] Xu has shown the temperature of polymerisation also has a large effect on the polymer produced using ^{Me_2}SB($^{t\text{Bu}}$N,Flu)TiX_2 with a $B(C_6F_5)_3$ cocatalyst.[138] Copolymerisations at 0 °C resulted in almost exclusively polyethylene produced, but at 50 °C the polymer produced was an ethylene/styrene copolymer.

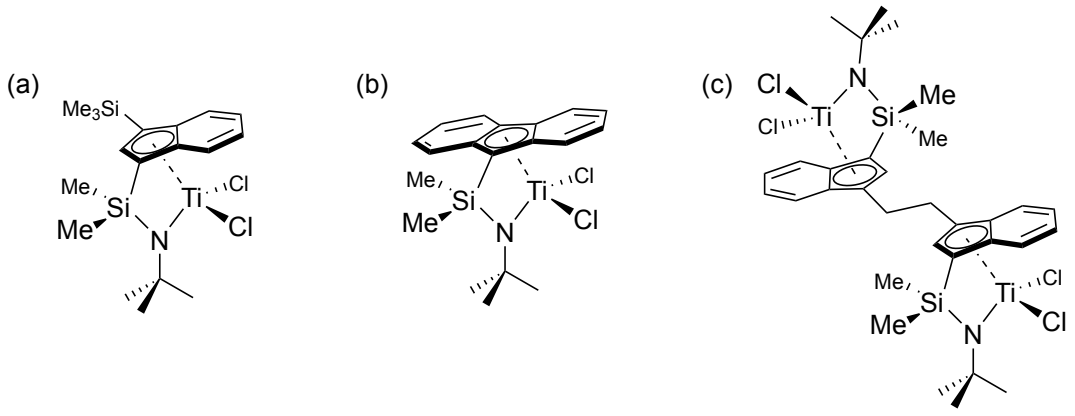

Figure 1.7. Molecular structures of (a) ^{Me_2}SB($^{t\text{Bu}}$N,$^{3\text{-SiMe}_3}$I)$TiCl_2$,[137] (b) ^{Me_2}SB($^{t\text{Bu}}$N,Flu)$TiCl_2$,[137] and (c) $C_2H_4\{^{Me_2}SB(^{t\text{Bu}}N,^{3\text{-SiMe}_3}I)TiCl_2\}_2$.[139]

Bimetallic constrained geometry complexes, such as those developed by Marks *et al*., have been shown to incorporate higher levels of styrene into the polymer chain, over 76 mol% (Figure 1.7 (c)).[139,140] It is proposed that these higher incorporation levels are attributable to bimetallic interactions between the two metal centres.[140]

1.4 Ethylene oligomerisation

The oligomerisation of ethylene to higher value linear α-olefins (LAOs) has been of great industrial interest and widely researched for over 50 years.[141,142] The LAO products have wide ranging uses in today's society, from surfactants and synthetic lubricants to comonomer additives in polymers.[142,143] Whilst demand for LAOs existed in the 1960s, there was no clear commercial process for their production. Ziegler demonstrated that lithium aluminium hydride oligomerised ethylene, with many simple alkylaluminiums (such as TEA) showing the same phenomenon.[144,145] The use of TEA as a catalyst required high temperatures and ethylene pressures (>200 bar) and resulted in a Poisson distribution of even-numbered oligomers,[146] with the Gulf Chemical (now operated by Chevron Phillips Chemical Company LLP) and Ethyl Chemical (now operated by Ineos) companies being the first to receive licenses for this technology.[147]

The Shell Higher Olefin Process (SHOP) uses a nickel-based catalyst under 90 bar ethylene pressure and began operation in 1977; whilst the precise composition of this catalyst has not been disclosed by Shell, most reported systems contain at κ^2-bound phosphorane (P,O) forming a 5-membered chelate.[148–150] This resulted in a distribution of LAO products between C_4 and C_{40}, of which only the C_8 to C_{16} fraction is desired.[151] It is possible to convert the undesired fractions to the desired range by double bond isomerisation over a potassium catalyst followed by olefin metathesis using an alumina supported molybdate catalyst.[152] The poor selectivity is driven by the oligomerisation proceeding *via* a linear coordination mechanism, the Cossee-Arlman mechanism (Scheme 1.5), and increasingly the full range of chain lengths does not match the market demand.[141]

The drive in demand for 1-butene (C_4), 1-hexene (C_6) and 1-octene (C_8) has been fuelled by the growth in use of both high density and linear low-density polyethylenes (HDPE and LLDPE). 1-Hexene and 1-octene are almost exclusively produced by oligomerisation catalysis, whilst 1-butene is produced from both distillation of olefin refinery streams and oligomerisation catalysis.[146] Chevron Phillips commercialised the first trimerisation plant in 2003, producing over half a billion pounds of 1-hexene per year, with Sasol opening a 1-hexene and 1-octene plant in 2014.[153,154]

1.4.1 Mechanism for ethylene oligomerisation

There are two generally accepted mechanisms for ethylene oligomerisation; one accounts for the Schulz-Flory distribution of products, whilst the other can account for the highly selective oligomerisation catalysts that have been more recently developed.

The Cossee-Arlman mechanism involves the successive coordination and insertion of ethylene, similar to the Cossee-Arlman polymerisation mechanism, with competing β-hydride elimination occurring at a similar rate (Scheme 1.5).[76,77] This relationship leads to the Schulz-Flory distribution, as is observed for the Shell Higher Olefin Process.[155,156]

Equation 1.3. Schulz-Flory distribution.[155–157]

$$W_m = \alpha^{m-1}(1 - \alpha)^2 m$$

$$\text{mol(m)\%} = (1 - \alpha)\alpha^{m-1}$$

W_m = weight fraction of m oligomer of oligoethylene

α = rate of propagation/(rate of propagation + rate of chain transfer); $k_1/(k_1 + k_2)$

mol(m)% = mole fraction of the m oligomer of oligoethylene

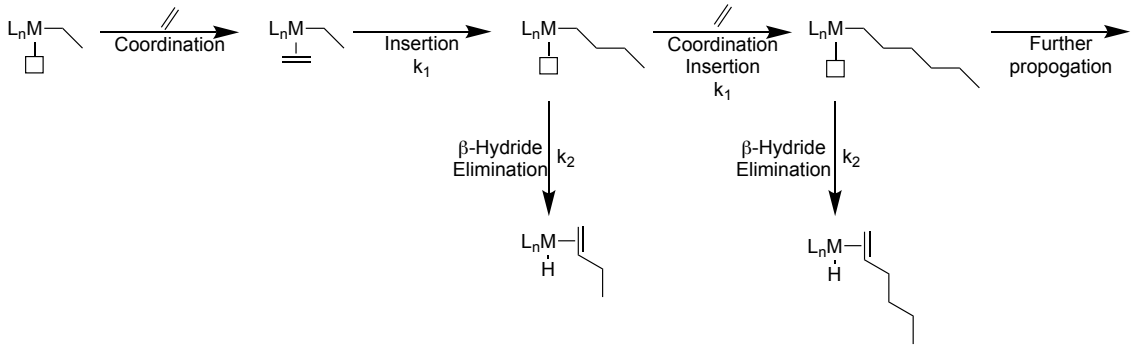

Scheme 1.5. Cossee-Arlman mechanism for ethylene oligomerisation.[76,77] Free coordination site represented by □.

For a given catalytic system, it is possible to modify and manipulate the distribution of products by modification of either temperature or ethylene concentration.[158] Higher reaction temperatures lead to increasing proportions of shorter chain olefins as the rate of chain termination increases faster at higher temperatures than the rate of chain propagation.[159]

This mechanism does not account for the selective dimerisation, trimerisation or tetramerisation processes that are utilised in industry. Manyik and co-workers at Union Carbide were the first to observe highly selective oligomerisation using a chromium (II) 2-ethylhexanoate catalyst, selectively producing 1-hexene and polyethylene.[160] The metallacycle mechanism was proposed in 1997, a metallacyclopentane intermediate is formed by coordination and oxidative coupling of two ethylene monomers (Scheme 1.6). This is followed by further coordination of an ethylene molecule, migratory insertion, and either β-hydride elimination or 3,7-hydride transfer to afford 1-hexene.[161] Bercaw *et al.* have verified the metallacycle mechanism through isotopic labelling studies, with 1-hexene produced from a 50:50 mixture of C_2H_4 and C_2D_4 resulting in the formation of C_6H_{12}, $C_6H_8D_4$, $C_6H_4D_8$, and C_6D_{12} in a 1:3:3:1 ratio, with no H/D scrambling observed.[162,163] This mechanism was further supported by Whitesides *et al*. studying the release of α-olefins through decomposition of platinum metallacycles.[164] The selectivity

of the catalytic system is dependent on the relative stabilities of the metallacyclopentane, metallacycloheptane and metallacyclononane intermediates, and how easily 1-butene, 1-hexene or 1-octene are eliminated.[142]

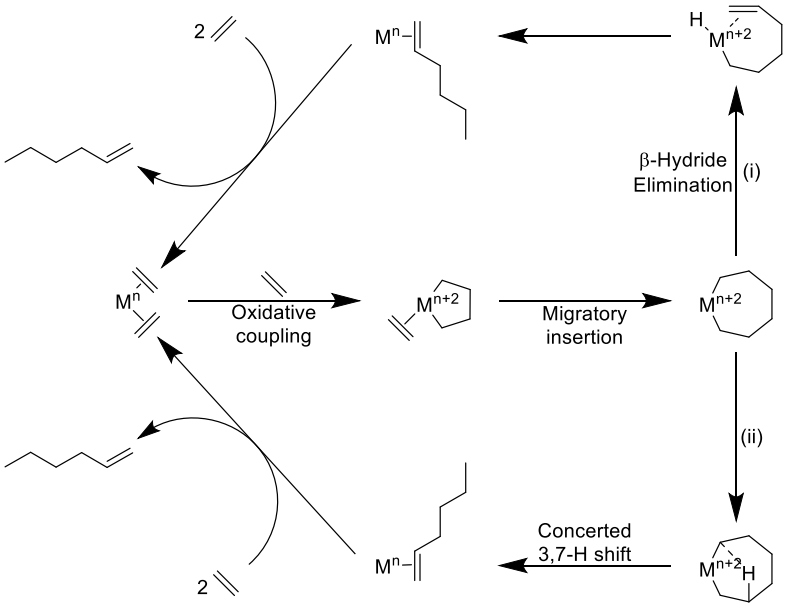

Scheme 1.6. Metallacycle mechanism for ethylene trimerisation.[160] Ligands omitted for clarity.

Whilst it is commonly observed that the metallacycloheptane intermediate is the least stable, with 1-hexene being most readily eliminated, it is possible to tune the catalytic system so as to selectively produce other α-olefins. Schrock *et al*. developed tantalum complexes that selectively dimerised ethylene *via* the metallacycle mechanism;[165,166] Gibson *et al*. have also demonstrated it is possible to form alkenes greater than C_{30} with the use of a MAO activated bis(benzimidazoyl)methylamine chromium catalysts, with the mechanism confirmed by isotopic labelling experiments.[167,168]

1.4.2 Industrial oligomerisation catalysts

The global production of LAOs is dominated by three major companies, Shell, Chevron Phillips Chemicals and Ineos, with other large players including Sasol, Mitsui, Idemitsu and SABIC,[154] with the 2012 capacities shown in Table 1.1. These processes are known as "full-range processes" due to the production of a broad distribution of olefins.

Table 1.1. 2012 production of LAOs by "full-range" process.[154]

Company	Type of catalyst	Typical LAO distribution (wt%)	Production (2012, kt/y)
Chevron Phillips	$AlEt_3$ (1 step)	C_4-C_{10} = 54 (49)[a] C_{12}-C_{14} = 18 (18) C_{16}-C_{20+} = 28 (33)	1053
Ineos	$AlEt_3$ (2 step)	C_4-C_{10} = 70-77 C_{12}-C_{14} = 21-28 C_{16}-C_{20+} = 2	565
Shell	Ni/P-O (biphasic)	C_4-C_{10} = 54 (32)[a,b] C_{12}-C_{14} = 18 (16) C_{16}-C_{20+} = 28 (52)	1251
Idemitsu	Zr/L/$AlR_{3-x}Cl_x$ (solvent)	Non-Disclosed	60
SABIC/Linde	Zr/L/$AlR_{3-x}Cl_x$ (solvent)	C_4-C_{10} = 82 (26)[a] C_{12}-C_{20+} = 88 (74)	250

[a] Typical distribution, in brackets possible flexibility. [b] Possible distribution of LAOs after oligomerisation and before isomerisation and metathesis processing.

Whilst the "full-range process" is still the predominant route to produce LAOs, the increased demand for C_4 to C_{10} LAOs is outgrowing that of other ranges. Progress has been made towards direct product distributions favouring shorter α-olefins or selective production of 1-butene, 1-hexene or 1-octene. Transition metal catalysis allows for this, with a number of newly developed selective industrial catalysts highlighted in Table 1.2. The increased supply of ethane from shale gas production in the US has allowed for vast amounts of ethylene to be produced from cracking, leading to the production of α-olefins becoming cheaper *via* ethylene oligomerisation rather than cracking and distillation of heavier oil sources such naphtha.[169]

Table 1.2. 2012 production of LAOs by selective oligomerisation process.[154]

LAO produced	Process/company	Catalyst type	Production (2012, kt/y)[a]
1-Butene	AlphaButol/Axens	Ti/AlR_3	708
1-Hexene	Chevron Phillips	Cr proprietary/ AlR_3	397
1-Hexene	AlphaHexol/Axens	Cr proprietary/ AlR_3	50[b]
1-Hexene	Mitsui	Ti proprietary/ MAO	30
1-Octene/1-hexene	Sasol	Cr proprietary/ MAO	100

[a] Includes planned capacities. [b] Total capacity for AlphaButol and AlphaHexol units.

Axens AlphaSelect process produces up to 93% selectivity to a narrow range of oligomers (C_4 to C_{10}), with the distribution of oligomers being determined by the metal to cocatalyst ratio.[142] The first AlphaButol unit was opened in 1987 in Thailand, whilst the first AlphaHexol unit was commercialised in 2011.[170]

The industrial Dimersol process, a homogeneous nickel (II)/$EtAlCl_2$ system, was developed by IFPEN and commercialised by Axens.[171] There are three distinct Dimersol processes; Dimersol-E dimerises ethylene to butenes, Dimersol-X dimerises propylene to hexenes and Dimersol-G dimerises butene to octenes.[142] These nickel based systems proceed *via* a Cossee-Arlman mechanism, with the product mainly consisting of dimers due to the high rate of the termination step.[76,77] Thirty five units have been licenced with a capacity of over 4.5 million tons of feed annually.[142]

In 1967, Union Carbide were granted a patent for the selective trimerisation of ethylene to 1-hexene using a chromium (II) hexanoate catalyst with the poly*iso*butylaluminium oxide (PIBAO) cocatalyst with optimal rates found at $[Al]_0$:$[Cr]_0$ ratios of 200:1.[160,161] Chevron Phillips were the first company to be able to fully commercialise an ethylene trimerisation process in 2003;[172] the discovery of the system occurred in the 1990s with the investigation of the catalytic properties of chromium pyrrole compounds. By 1999, the reaction yielded 93% overall selectivity towards 1-hexene and a productivity of 157 $kg_{LAO}/g_{Cr}/h$.[173]

Researchers at Mitsui have reported highly active trimerisation catalysts based on titanium with a tridentate phenoxyimine ligand with pendant oxygen donors. The most active of these having a methoxy pendant donor and a bulky adamantyl substituent, with productivities up to 6590 $kg_{C_6}/g_{cat}/h$ at 5 bar of ethylene pressure with 92% selectivity to 1-hexene.[174] The main by-products are trimers of 1-hexene and ethylene, with this and a

second-order dependence on ethylene concentration suggesting the rate-determining step may be the metallacyclopentane formation.[141]

A highly selective ethylene tetramerisation catalyst has been reported by researchers at Sasol.[153,175] The catalyst, a $Cr(acac)_3$ combined with the PNP pincer ligand $Ph_2PN(^iPr)PPh_2$ and 300 equivalents of MAO produced octenes in 68% selectivity (of which 98.8% was 1-octene), at a productivity of 274 $kg_{LAO}/g_{cat}/h$ at 45 °C and 45 bar of ethylene pressure.[153] Research suggests that this tetramerisation reaction proceeds *via* an extended metallacyclic mechanism; similar to many of the highly selective oligomerisation reactions that have been previously discussed.[175]

1.4.3 Group 5 complexes for ethylene oligomerisation

Whilst no industrial process currently uses group 5 complexes as ethylene oligomerisation catalysts, there are many examples of both tantalum and vanadium complexes as ethylene oligomerisation catalysts in the literature.

Tantalum is well known to promote oligomerisation through metallacycle formation;[166] Sen *et al*. demonstrated highly selective ethylene trimerisation through the combination of $TaCl_5$ with alkylating agents such as $AlMe_3$, SnR_4, $ZnMe_2$ or LiR.[176] Activities up to 460 turnovers per hour were reported, with selectivities up to 99%. Schrock *et al*. reported the highly selective dimerisation of ethylene using $Ta(CH^tBu)(CH_2{}^tBu)(PMe_3)_2$ with 30 bar of ethylene at 0 ºC at a rate of 0.5 turnovers per minute.[177]

Vanadium complexes have also been studied as ethylene oligomerisation catalysts. Teuben *et al.* reported ethylene oligomerisation with a vanadium (III) bis(benzamidinate) alkyl catalyst (Figure 1.8 (a)); the catalysts resulted in a Flory-Schulz distribution of oligomers as well as the presence of 2-alkenes.[178] Fluorination of the ligand resulted in a

fivefold increase of ethylene oligomerisation rates, once again resulting in a Flory-Schulz distribution of α-olefins. Alt *et al.* have also reported vanadium (III) complexes as ethylene oligomerisation catalysts.[179] N,N,N-tridentate vanadium diiminopyridyl complexes (Figure 1.8 (b)) were activated with MAO and tested for oligomerisation activity at 17.2 bar ethylene pressure at 60 ºC. Productivities up to 1140 $kg_{LAO}/g_V/h$ were reported with selectivities up to 96% for 1-hexene.

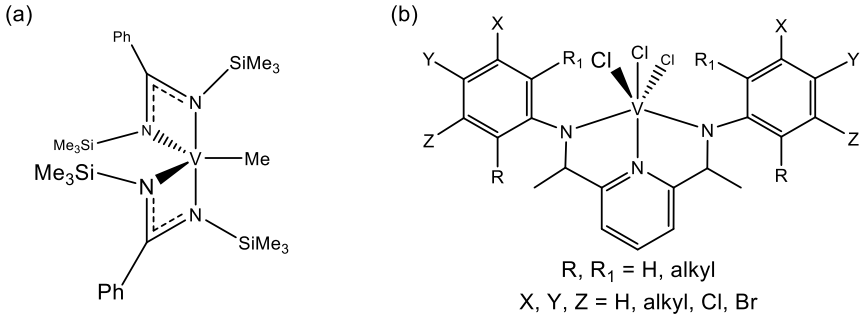

Figure 1.8. (a) Vanadium(III) bis(benzamidinate) alkyl catalyst,[178] and (b) N,N,N-tridentate vanadium diiminopyridyl complex.[179]

Nomura and co-workers have undertaken a large amount of work to study vanadium imido complexes as efficient ethylene dimerisation catalysts. In 2010, Zhang and Nomura reported the dimerisation of ethylene in >90% selectivity, the minor product being 1-hexene, using complexes of the type $V(NR)Cl_2[2\text{-}ArNCH_2(C_5H_4N)]$ (R = Ad, Cy and Ph; Ar = $2,6\text{-}Me_2C_6H_3$ and 2,6-Dipp) with an MAO catalyst.[180] TOF values up to 2670000 $mol_{C_2H_4}/mol_V/h$ were reported under 8.1 bar of ethylene pressure after 60 minutes.

Further studies with these complexes investigated the effect of reaction conditions on the catalytic reactivity; lower catalyst loading levels resulted in higher activities, whilst use of an MAO cocatalyst resulted in higher activities than modified MAO (MMAO).[181] A first order reactivity was observed towards ethylene pressure, suggesting the reaction proceeded *via* a Cossee-Arlman type mechanism rather than a metallacycle mechanism.

It was also observed that the nature of the cocatalyst had a large effect on the catalytic species; whilst MAO and MMAO selectively dimerised ethylene, use of Me_2AlCl or Et_2AlCl as a cocatalyst resulted in solely ultra-high molecular weight polyethylene as a product. Tuning of the ligand set, both the chelating ligand and imido group, has been shown to influence the activity and product distribution.[182] Variation of the imido complex from adamantyl to phenyl and methylphenyl has shown that the steric bulk of the imido ligand can influence the reaction between polymerisation or dimerisation.[183]

Dyer *et al.* have reported tantalum and niobium imido complexes as ethylene dimerisation and polymerisation catalysts.[184] A range of tantalum imido complexes: $Ta(NR)Cl_3(dme)$ (R = ^{t}Bu, Ph, Mes and Dipp), $Ta(NDipp)Cl_2Cp$ and $Ta(NDipp)Cl_3(TMEDA)$ were synthesised and tested for ethylene oligomerisation with an $EtAlCl_2$ cocatalyst (Figure 1.9). These complexes were shown to be highly selective towards 1-butene, with the Cp complex ($Ta(NDipp)Cl_2Cp$) exhibiting the lowest activities towards oligomerisation. Decreased selectivity for 1-butene (from 100 to 74%) with variation of the X group from dme to TMEDA signifies the importance of the Lewis base, whilst analysis of the product mixture shows that the reaction pathway most likely occurs *via* a metallacycle mechanism.

The analogous niobium imido complexes: $Nb(NR)Cl_3(dme)$ (R = ^{t}Bu, Ph, Mes and Dipp), $Nb(NDipp)Cl_2Cp$ and $Nb(NDipp)Cl_3(TMEDA)$ (Figure 1.9) were also synthesised. These complexes typically formed higher percentages of polyethylene than the tantalum analogues. In addition, with increasing steric bulk of the imido group (NPh < NMes < NDipp), the fraction of oligomer ($C_n > 4$) increased as well as the amount of polymer produced. Mechanistically, it is not possible for a single catalytic site to both

selectively dimerise and polymerise, so it is expected that there are multiple active species originating from these complexes.[184]

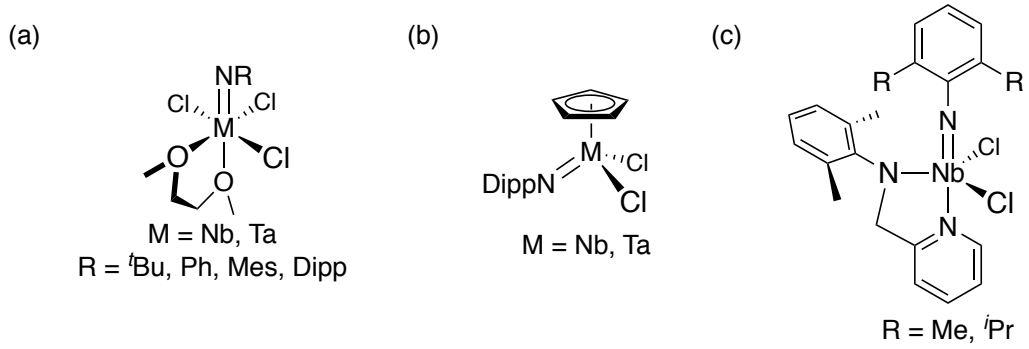

Figure 1.9. (a) and (b) niobium and tantalum imido complexes synthesised by Dyer *et al.*,[184] and (c) niobium arylimido complexes synthesised by Nomura *et al*..[185]

Nomura and Kuboki reported that the complexes $Nb(NAr)Me_2[2\text{-}(2,6\text{-}Me\text{-}C_6H_3)NCH_2(C_5H_4N)]$ (Ar = 2,6-Me-C_6H_3 and 2,6-^{i}Pr-C_6H_3) were active for ethylene dimerisation when activated by $[Ph_3C][B(C_6F_5)_4]$ (Figure 1.9(c)).[185] Optimised conditions led to TON values up to 234000 $mol_{C_2H_4}/mol_{Nb}$ under 8.1 bar ethylene pressure. A reported first order relationship between activity and ethylene pressure suggests that, as with the vanadium complexes discussed earlier, the reaction proceeds *via* a Cossee-Arlman mechanism.[185]

1.5 Tandem catalysis of ethylene

Tandem catalysis (Scheme 1.7), where one catalyst oligomerises ethylene to the desired α-olefin, followed by a second catalyst copolymerising the α-olefin and ethylene to form short chain branched LLDPE,[186] removes the requirement for addition of an often expensive comonomer.[141,187]

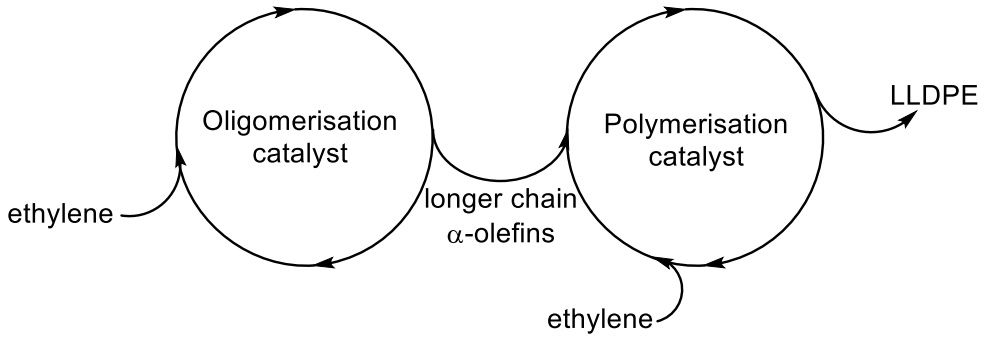

Scheme 1.7. Tandem catalytic cycle with formation of LLDPE from a single ethylene feedsource.

There are a number of factors to be considered when building a tandem catalytic system; the two catalysts must be compatible, with best control achieved when the two species are able to operate independently and the activities being comparable so that one system does not overrun the other.[186] Beach and Kissin reported a tandem catalytic system, based on a Ziegler-Natta type catalyst coupled with either a titanium alkoxide or sulfonated nickel ylide dimerisation catalyst to form short-chain branched LLDPE from a single ethylene feedsource with up to 45 Me/1000C reported for the optimised system.[188] McDaniel and co-workers at Phillips developed a tandem catalytic system in the 1980s based on silica supported chromium.[189] A mixture of chromium oxide and chromium bis-dimethylpentadienyl resulted in the formation of short-chain branched polymer without the addition of a comonomer to the reaction mixture.

Fink *et al*. demonstrated the importance of the reaction conditions in producing a successful tandem catalytic system.[190] With the use of the SHOP oligomerisation catalyst,

a copolymerisation catalyst was required that did not need activation by an alkylaluminium (which in turn would deactivate the oligomerisation catalyst). This was facilitated by the use of Cp_2TiCl_2, with a mixture of magnesium hydride and α-$TiCl_4$ cocatalysts, to produce a tandem catalytic system with the resulting polymer having butyl and ethyl chains from incorporated 1-hexene and 1-butene.[190] Hao *et al*. developed a catalytic cycle with a single zirconium complex, *rac*-EBI$ZrCl_2$, and two cocatalysts: diethyl aluminium chloride and MAO. Incorporations of up to 2.9 mol% were reported.[191]

Zirconocene complexes have also been used to develop tandem catalytic systems using well-defined catalytic species. Duchateau *et al.* reported a tandem catalytic system supported on SSMAO resulting in the formation of ethylene/1-hexene copolymer.[192] Combination of Cp_2ZrCl_2 and the Mitsui phenoxyimine titanium ethylene trimerisation catalyst resulted in the incorporation levels of up to 6.9%. However, immobilisation of both complexes onto a single support was found to inhibit polymerisation activities; this was not observed in a physical mixture of the two supported catalysts.[192]

With constrained geometry complexes having been shown to be highly efficient ethylene/α-olefin copolymerisation catalysts,[1,193] it was proposed that these complexes could form part of a well-defined tandem catalytic system with a suitable oligomerisation catalyst. Bazan and Barnhart demonstrated that the combination $^{Me_2}SB(^{tBu}N,Cp^*)TiCl_2$ and $(C_5H_5BR)_2ZrCl_2$ (R = Ph, OEt) resulted in the formation of branched polyethylene when employed with an MAO cocatalyst.[194] The zirconocene complex oligomerised ethylene to α-olefins in a Schulz-Flory distribution of products; these oligomers were then incorporated by the constrained geometry complex. Due to the array of α-olefins incorporated, it was not possible to precisely determine the incorporation level afforded by this system. Zhu *et al.* reported a tandem catalytic system comprising of

^{Me2}SB($^{t\text{Bu}}$N,Cp*)TiCl$_2$ and [η^5-C$_5$H$_4$CMe$_2$C$_6$H$_5$)]TiCl$_3$ (Figure 1.10 (a)) with an MMAO cocatalyst.[195] [η^5-C$_5$H$_4$CMe$_2$C$_6$H$_5$)]TiCl$_3$ acts as an efficient ethylene trimerisation catalyst, with up to 86 wt% selectivity to 1-hexene (10 wt% C_{10} from concomitant trimerisation of 1-hexene and two ethylene units). 1-Hexene incorporations of up to 12.9 mol% were observed for this system with catalysts employed in a 2:1 ratio of trimerisation catalyst to CGC. Furthermore, Zhu *et al.* reported up to 15 mol% incorporation of 1-hexene branches into the polymer chain using the same CGC with a bis(2-dodecylsulfanyl-ethyl)amine chromium trichloride ethylene trimerisation catalyst with MAO as an activator (Figure 1.10 (b)).[196] When both catalysts were present from the start of the reaction, the polymer produced was observed to be semi-crystalline, with initial long polyethylene sequences later becoming more amorphous with the increased incorporation of 1-hexene into the polymer chain. A pre-trimerisation period of five minutes or more was found to result in entirely amorphous copolymer.

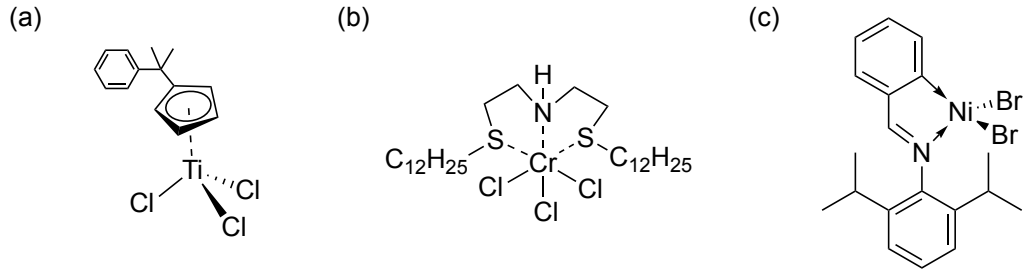

Figure 1.10. Molecular structures of (a) [η^5-C$_5$H$_4$CMe$_2$C$_6$H$_5$)]TiCl$_3$,[195] (b) bis(2-dodecylsulfanyl-ethyl)amine chromium trichloride,[196] and (c) dibromo(pyridylimine)nickel.[197]

Tandem catalysis of a homogeneous oligomerisation catalyst with a heterogeneous CGC polymerisation catalyst has also been reported. Okuda *et al.* developed a system combining MMAO activated dibromo(pyridylimine)nickel [C$_5$H$_4$NCHNAr]NiBr$_2$ (Ar = 2,6-diisopropylphenyl, Figure 1.10 (c)) with ^{Me2}SB(^{R}N,Cp*)TiCl$_2$ (R = Me, ^{t}Bu) supported on pyridylethylsilane-modified silica;[197] incorporations of up 2.9 mol% were reported for ^{Me2}SB(^{Me}N,Cp*)TiCl$_2$ with a [Ni]$_0$:[Ti]$_0$ ratio of 2:1. Marks *et al*. reported a

tandem catalytic system based on two constrained geometry complexes. A zirconium oligomerisation complex, ^{Me2}SB(^{tBu}N,$^{3\text{-}Et}$I)ZrMe$_2$, acting as an oligomerisation catalyst and ^{Me2}SB(^{tBu}N,Cp*)TiMe$_2$ as a polymerisation catalyst with both complexes being activated by a bis-borate cocatalyst.[198] The nature of the borate cocatalyst was demonstrated to affect the polymer produced, and the polymerisation activity.[199]

Bercaw *et al.* developed a heterogeneous tandem catalytic system with two titanium complexes immobilised on SSMAO.[200] This involved the immobilisation of both ^{Me2}SB(^{tBu}N,Cp*)TiCl$_2$ and (FI)TiCl$_3$ (FI = (N-(5-methyl-3-(1-adamantyl)-salicylidene)-2'-(2''-methoxyphenyl)anilinato) (Figure 1.11), with the associated activation of these species by alkylation and anion abstraction. Incorporations of over 50 mol% were observed, with 1-hexene incorporation levels increasing with time. The increased levels of 1-hexene incorporation suggests there is minimal cooperativity of the system with 1-hexene going into solution rather than directly into the catalytic chain.[200]

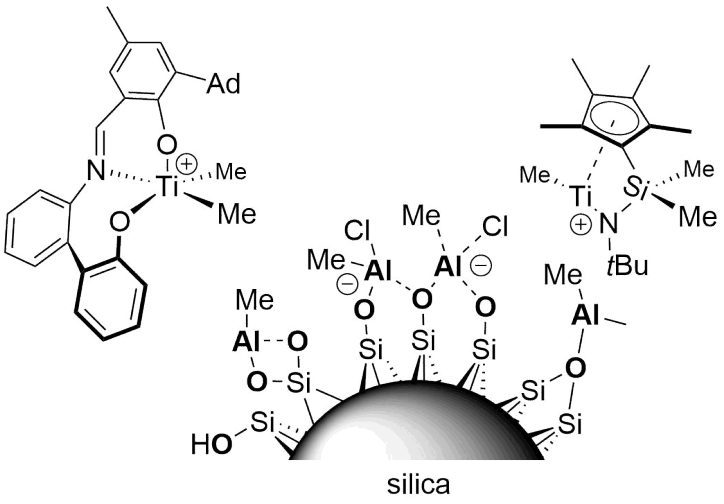

Figure 1.11. SSMAO supported tandem catalytic system developed by Bercaw *et al.*.[200]

Tandem catalytic systems containing three complexes; two separate oligomerisation catalysts coupled with a CGC can result in a polymer with differing chain branches.[201] Bazan *et al.* reported a triple tandem catalytic system for the synthesis of polymers with

varying structures.[202] A mixture of three complexes were used, a CGC acting as a copolymerisation catalyst, with a selective dimerisation catalyst and an unselective oligomerisation catalyst. High-throughput screening experiments showed that the triple tandem catalytic system was feasible, with comonomer incorporations of up to 46% determined by IR spectroscopy and the tailoring of the ratios of catalysts resulting in a variety of incorporation levels.

1.6 Thesis aims

The aims of this thesis are to develop group 4 permethylindenyl constrained geometry complexes as ethylene homopolymerisation and copolymerisation catalysts, and niobium imido complexes as ethylene oligomerisation catalysts. The final aim is to combine both an oligomerisation and copolymerisation catalyst on a single solid support so as to develop a tandem catalyst capable of forming short chain branched LLDPE from a single ethylene feedsource.

1.7 References

1 J. C. Stevens, F. J. Timmers, D. R. Wilson, G. F. Schmidt, P. N. Nickias, R. K. Rosen, G. W. Knight and S. Y. Lai, 1991, EP0416815A2.

2 P. J. Shapiro, E. Bunel, W. P. Schaefer and J. E. Bercaw, *Organometallics*, 1990, **9**, 867–869.

3 J. Okuda, *Chem. Ber.*, 1990, **123**, 1649–1651.

4 J. C. Stevens, *26. Insite™ Catal. Struct. Relationships Olefin Polym. Stud. Surf. Sci. Catal. Vol. 89*, 1994, 277–284.

5 H. Braunschweig and F. M. Breitling, *Coord. Chem. Rev.*, 2006, **250**, 2691–2720.

6 J. Cano and K. Kunz, *J. Organomet. Chem.*, 2007, **692**, 4411–4423.

7 J. Okuda, F. J. Schattenmann, S. Wocadlo and W. Massa, *Organometallics*, 1995, **14**, 789–795.

8 L. Duda, G. Erker, R. Fröhlich and F. Zippel, *Eur. J. Inorg. Chem.*, 1998, **1998**, 1153–1162.

9 H. V. Rasika Dias, Z. Wang and S. G. Bott, *J. Organomet. Chem.*, 1996, **508**, 91–99.

10 A. L. McKnight, M. A. Masood, R. M. Waymouth and D. A. Straus, *Organometallics*, 1997, **16**, 2879–2885.

11 G. A. Luinstra and J. H. Teuben, *J. Chem. Soc., Chem. Commun.*, 1990, 1470–1471.

12 F. Amor and J. Okuda, *J. Organomet. Chem.*, 1996, **520**, 245–248.

13 A. K. Hughes, A. Meetsma and J. H. Teuben, *Organometallics*, 1993, **12**, 1936–1945.

14 W. A. Herrmann and M. J. A. Morawietz, *J. Organomet. Chem.*, 1994, **482**, 169–181.

15 Y.-X. Chen and T. J. Marks, *Organometallics*, 1997, **16**, 3649–3657.

16 S. Ciruelos, T. Cuenca, R. Gómez, P. Gómez-Sal, A. Manzanero and P. Royo, *Organometallics*, 1996, **15**, 5577–5585.

17 V. V. Kotov, E. V. Avtomonov, J. Sundermeyer, K. Harms and D. A. Lemenovskii, *Eur. J. Inorg. Chem.*, 2002, **2002**, 678–691.

18 K. Yu, M. W. McKittrick and C. W. Jones, *Organometallics*, 2004, **23**, 4089–4096.

19 J. Okuda, S. Verch, T. P. Spaniol and R. Stürmer, *Chem. Ber.*, 1996, **129**, 1429–1431.

20 J. Okuda, S. Verch, R. Stürmer and T. P. Spaniol, *J. Organomet. Chem.*, 2000, **605**, 55–67.

21 D. D. Devore, F. J. Timmers, D. L. Hasha, R. K. Rosen, T. J. Marks, P. A. Deck and C. L. Stern, *Organometallics*, 1995, **14**, 3132–3134.

22 J. A. M. Canich, 1996, WO1996000244A1.

23 A. I. Licht and H. G. Alt, *J. Organomet. Chem.*, 2003, **684**, 91–104.

24 K. Kunz, G. Erker, S. Döring, R. Fröhlich and G. Kehr, *J. Am. Chem. Soc.*, 2001, **123**, 6181–6182.

25 H. Braunschweig, F. M. Breitling, C. von Koblinski, A. J. P. White and D. J. Williams, *Dalton Trans.*, 2004, 938–943.

26 H. Braunschweig, F. M. Breitling, K. Radacki and F. Seeler, *J. Organomet. Chem.*, 2005, **690**, 5000–5005.

27 K. Kunz, G. Erker, S. Döring, S. Bredeau, G. Kehr and R. Fröhlich,

Organometallics, 2002, **21**, 1031–1041.
28 A. Reb and H. G. Alt, *J. Mol. Catal. A Chem.*, 2001, **174**, 35–49.
29 H. G. Alt, A. Reb and K. Kundu, *J. Organomet. Chem.*, 2001, **628**, 211–221.
30 A. B. Vázquez and P. Royo, *J. Organomet. Chem.*, 2003, **671**, 172–178.
31 H. G. Alt, R. Ernst and I. K. Böhmer, *J. Organomet. Chem.*, 2002, **658**, 259–265.
32 J. Klosin, P. P. Fontaine and R. Figueroa, *Acc. Chem. Res.*, 2015, **48**, 2004–2016.
33 B. Rhodes, J. C. W. Chien, J. S. Wood, A. Chandrasekaran and M. D. Rausch, *Appl. Organomet. Chem.*, 2002, **16**, 323–330.
34 Y. Mu, W. E. Piers, M.-A. MacDonald and M. J. Zaworotko, *Can. J. Chem.*, 1995, **73**, 2233–2238.
35 K. C. Hultzsch, T. P. Spaniol and J. Okuda, *Angew. Chem. Int. Ed.*, 1999, **38**, 227–230.
36 E. Kirillov, L. Toupet, C. W. Lehmann, A. Razavi and J.-F. Carpentier, *Organometallics*, 2003, **22**, 4467–4479.
37 J. Okuda, *Dalton Trans.*, 2003, 2367–2378.
38 P. T. Witte, A. Meetsma and B. Hessen, *Organometallics*, 1999, **18**, 2944–2946.
39 W. Kaminsky, B. Hinrichs and D. Rehder, *Polymer* , 2002, **43**, 7225–7229.
40 M. I. Alcalde, M. P. Gómez-Sal and P. Royo, *Organometallics*, 1999, **18**, 546–554.
41 Y. Liang, G. P. A. Yap, A. L. Rheingold and K. H. Theopold, *Organometallics*, 1996, **15**, 5284–5286.
42 W. A. Herrmann, W. Baratta and M. J. A. Morawietz, *J. Organomet. Chem.*, 1995, **497**, C4–C6.
43 T.-F. Wang, C.-Y. Lai, C.-C. Hwu and Y.-S. Wen, *Organometallics*, 1997, **16**, 1218–1223.
44 J. M. Pietryga, J. D. Gorden, C. L. B. Macdonald, A. Voigt, R. J. Wiacek and A. H. Cowley, *J. Am. Chem. Soc.*, 2001, **123**, 7713–7714.
45 J. M. Pietryga, J. N. Jones, L. A. Mullins, R. J. Wiacek and A. H. Cowley, *Chem. Commun.*, 2003, 2072–2073.
46 R. J. Wiacek, C. L. B. Macdonald, J. N. Jones, J. M. Pietryga and A. H. Cowley, *Chem. Commun.*, 2003, 430–431.
47 G. Natta, *Angew. Chem.*, 1956, **68**, 393–403.
48 K. Ziegler, E. Holzkamp, H. Breil and H. Martin, *Angew. Chem.*, 1955, **67**, 426.
49 W. Kaminsky, A. Funck and H. Hähnsen, *Dalton Trans.*, 2009, 8803–8810.
50 G. Natta, P. Pino, G. Mazzanti and U. Giannini, *J. Am. Chem. Soc.*, 1957, **79**, 2975–2976.
51 D. S. Breslow and N. R. Newburg, *J. Am. Chem. Soc.*, 1957, **79**, 5072–5073.
52 H. Sinn, W. Kaminsky, H.-J. Vollmer and R. Woldt, *Angew. Chem. Int. Ed.* , 1980, **19**, 390–392.
53 W. Kaminsky, *Macromolecules*, 2012, **45**, 3289–3297.
54 R. A. Collins, A. F. Russell and P. Mountford, *Appl. Petrochemical Res.*, 2015, **5**, 153–171.
55 L. Resconi, L. Cavallo, A. Fait and F. Piemontesi, *Chem. Rev.*, 2000, **100**, 1253–1346.
56 G. G. Hlatky, *Chem. Rev.*, 2000, **100**, 1347–1376.
57 M. J. Calhorda and L. F. Veiros, *Coord. Chem. Rev.*, 1999, **185**–**186**, 37–51.
58 D. O'Hare, J. C. Green, T. Marder, S. Collins, G. Stringer, A. K. Kakkar, N. Kaltsoyannis, A. Kuhn and R. Lewis, *Organometallics*, 1992, **11**, 48–55.
59 P. Ransom, A. Ashley, A. Thompson and D. O'Hare, *J. Organomet. Chem.*, 2009, **694**, 1059–1068.

60 P. Ransom, A. E. Ashley, N. D. Brown, A. L. Thompson and D. O'Hare, *Organometallics*, 2011, **30**, 800–814.
61 T. K. Miyamoto, M. Tsutsui and L.-B. Chen, *Chem. Lett.*, 1981, **10**, 729–730.
62 P. J. Shapiro, *Coord. Chem. Rev.*, 2002, **231**, 67–81.
63 C. E. Zachmanoglou, A. Docrat, B. M. Bridgewater, G. Parkin, C. G. Brandow, J. E. Bercaw, C. N. Jardine, M. Lyall, J. C. Green and J. B. Keister, *J. Am. Chem. Soc.*, 2002, **124**, 9525–9546.
64 J. H. Shin, T. Hascall and G. Parkin, *Organometallics*, 1999, **18**, 6–9.
65 J. A. Smith and H. H. Brintzinger, *J. Organomet. Chem.*, 1981, **218**, 159–167.
66 G. Jany, M. Gustafsson, T. Repo, E. Aitola, J. A. Dobado, M. Klinga and M. Leskelä, *J. Organomet. Chem.*, 1998, **553**, 173–178.
67 R. Quijada, J. Dupont, M. S. L. Miranda, R. B. Scipioni and G. B. Galland, *Macromol. Chem. Phys.*, 1995, **196**, 3991–4000.
68 J.-C. Buffet, T. A. Q. Arnold, Z. R. Turner, P. Angpanitcharoen and D. O'Hare, *RSC Adv.*, 2015, **5**, 87456–87464.
69 P. Ransom, T. A. Q. Arnold, A. L. Thompson, J.-C. Buffet and D. O'Hare, *Dalton Trans.*, 2012, **41**, 11267–11269.
70 P. Angpanitcharoen, G. Hay, J.-C. Buffet, Z. R. Turner, T. A. Q. Arnold and D. O'Hare, *Polyhedron*, 2016, **116**, 216–222.
71 T. A. Q. Arnold, J.-C. Buffet, Z. R. Turner and D. O'Hare, *J. Organomet. Chem.*, 2015, **792**, 55–65.
72 J. V. Lamb, J.-C. Buffet, Z. R. Turner and D. O'Hare, *Polym. Chem.*, 2019, **10**, 1386–1398.
73 J.-C. Buffet, Z. R. Turner and D. O'Hare, *Chem. Commun.*, 2018, **54**, 10970–10973.
74 J. V. Lamb, J.-C. Buffet, J. E. Matley, C. M. R. Wright, Z. R. Turner and D. O'Hare, *Dalton Trans.*, 2019, **48**, 2510–2520.
75 J. V. Lamb, J. C. Abell, J. E. McLaren, J.-C. Buffet, Z. R. Turner and D. O'Hare, *Mol. Catal.*, 2019, 110735.
76 P. Cossee, *J. Catal.*, 1964, **3**, 80–88.
77 E. Arlman, *J. Catal.*, 1964, **3**, 99–104.
78 K. Thorshaug, J. A. Støvneng, E. Rytter and M. Ystenes, *Macromolecules*, 1998, **31**, 7149–7165.
79 A. K. Rappé, W. M. Skiff and C. J. Casewit, *Chem. Rev.*, 2000, **100**, 1435–1456.
80 E. Quintanilla, F. di Lena and P. Chen, *Chem. Commun.*, 2006, 4309.
81 W. Kaminsky and H. Lüker, *Die Makromol. Chemie, Rapid Commun.*, 1984, **5**, 225–228.
82 A. Malmberg, E. Kokko, P. Lehmus, B. Löfgren and J. V. Seppälä, *Macromolecules*, 1998, **31**, 8448–8454.
83 K.-J. Chu, J. B. P. Soares and A. Penlidis, *Macromol. Chem. Phys.*, 2000, **201**, 552–557.
84 F. Song, R. D. Cannon and M. Bochmann, *J. Am. Chem. Soc.*, 2003, **125**, 7641–7653.
85 M. Bochmann, *Organometallics*, 2010, **29**, 4711–4740.
86 A. L. McKnight and R. M. Waymouth, *Chem. Rev.*, 1998, **98**, 2587–2598.
87 M. Kamigaito, T. K. Lal and R. M. Waymouth, *J. Polym. Sci. Part A Polym. Chem.*, 2000, **38**, 4649–4660.
88 J. Okuda, K. Musikabhumma and P.-J. Sinnema, *Isr. J. Chem.*, 2002, **42**, 383–392.
89 K. Nomura, H. Okumura, T. Komatsu, N. Naga and Y. Imanishi, *J. Mol. Catal. A*

Chem., 2002, **190**, 225–234.
90 A. K. Hughes, S. M. B. Marsh, J. A. K. Howard and P. S. Ford, *J. Organomet. Chem.*, 1997, **528**, 195–198.
91 M. C. Baier, M. A. Zuideveld and S. Mecking, *Angew. Chem. Int. Ed.*, 2014, **53**, 9722–9744.
92 H. Juvaste, T. T. Pakkanen and E. I. Iiskola, *Organometallics*, 2000, **19**, 1729–1733.
93 L. Fan, D. Harrison, T. K. Woo and T. Ziegler, *Organometallics*, 1995, **14**, 2018–2026.
94 J.-C. Buffet, Z. R. Turner, R. T. Cooper and D. O'Hare, *Polym. Chem.*, 2015, **6**, 2493–2503.
95 P. S. Chum and K. W. Swogger, *Prog. Polym. Sci.*, 2008, **33**, 797–819.
96 S. Y. Lai, J. R. Wilson, G. W. Knight, J. C. Stevens, S. P. Chum, 1993, US5272236.
97 J. R. Severn, J. C. Chadwick, R. Duchateau and N. Friederichs, *Chem. Rev.*, 2005, **105**, 4073–4147.
98 E. V. Ramos-Fernández, A. Sepúlveda-Escribano and F. Rodríguez-Reinoso, *Catal. Commun.*, 2008, **9**, 1243–1246.
99 P. A. Zapata, C. Belver, R. Quijada, P. Aranda and E. Ruiz-Hitzky, *Appl. Catal. A Gen.*, 2013, **453**, 142–150.
100 H. Rahiala, I. Beurroies, T. Eklund, K. Hakala, R. Gougeon, P. Trens and J. B. Rosenholm, *J. Catal.*, 1999, **188**, 14–23.
101 P. Wongwaiwattanakul and B. Jongsomjit, *Catal. Commun.*, 2008, **10**, 118–122.
102 K. Soga and M. Kaminaka, *Die Makromol. Chemie*, 1993, **194**, 1745–1755.
103 V. N. Panchenko, N. V. Semikolenova, I. G. Danilova, E. A. Paukshtis and V. A. Zakharov, *J. Mol. Catal. A Chem.*, 1999, **142**, 27–37.
104 E. Y.-X. Chen and T. J. Marks, *Chem. Rev.*, 2000, **100**, 1391–1434.
105 E. Kaji and E. Yoshioka, 2010, WO2010055652.
106 A. F. R. Kilpatrick, J.-C. Buffet, P. Nørby, N. H. Rees, N. P. Funnell, S. Sripothongnak and D. O'Hare, *Chem. Mater.*, 2016, **28**, 7444–7450.
107 A. F. R. Kilpatrick, N. H. Rees, S. Sripothongnak, J.-C. Buffet and D. O'Hare, *Organometallics*, 2018, **37**, 156–164.
108 J. V. Lamb, J.-C. Buffet, Z. R. Turner and D. O'Hare, *Macromolecules*, 2020, **53**, 929–935.
109 F. Zaccaria, C. Zuccaccia, R. Cipullo, P. H. M. Budzelaar, A. Macchioni, V. Busico and C. Ehm, *ACS Catal.*, 2019, **9**, 2996–3010.
110 H. S. Zijlstra, A. Joshi, M. Linnolahti, S. Collins and J. S. McIndoe, *Dalton Trans.*, 2018, **47**, 17291–17298.
111 H. S. Zijlstra, S. Collins and J. S. McIndoe, *Chem. Eur. J.*, 2018, **24**, 5506–5512.
112 V. C. Gibson and S. K. Spitzmesser, *Chem. Rev.*, 2003, **103**, 283–316.
113 M. Bochmann, *J. Chem. Soc. Dalt. Trans.*, 1996, 255–270.
114 H. H. Brintzinger, D. Fischer, R. Müllhaupt, B. Rieger and R. M. Waymouth, *Angew. Chem. Int. Ed.* , 1995, **34**, 1143–1170.
115 M. A. Bashir, V. Monteil, C. Boisson and T. F. L. McKenna, *J. Appl. Polym. Sci.*, 2018, **135**, 45670.
116 V. F. Tisse, C. Boisson and T. F. L. McKenna, *Macromol. Chem. Phys.*, 2014, **215**, 1358–1369.
117 H. Hammawa, T. M. Mannan, D. T. Lynch and S. E. Wanke, *J. Appl. Polym. Sci.*, 2004, **92**, 3549–3560.
118 D. E. Babushkin, V. N. Panchenko, M. N. Timofeeva, V. A. Zakharov and H. H.

Brintzinger, *Macromol. Chem. Phys.*, 2008, **209**, 1210–1219.
119 H. Zhang, R. Hoogenboom, M. A. R. Meier and U. S. Schubert, *Meas. Sci. Technol.*, 2005, **16**, 203–211.
120 D. J. Jones, V. C. Gibson, S. M. Green and P. J. Maddox, *Chem. Commun.*, 2002, 1038–1039.
121 V. Busico, R. Pellecchia, F. Cutillo and R. Cipullo, *Macromol. Rapid Commun.*, 2009, **30**, 1697–1708.
122 V. Busico, R. Cipullo, A. Mingione and L. Rongo, *Ind. Eng. Chem. Res.*, 2016, **55**, 2686–2695.
123 M. Goldberg, K. Mahon and D. Anderson, *Adv. Drug Deliv. Rev.*, 2008, **60**, 971–978.
124 W. Kaminsky, *Macromol. Chem. Phys.*, 1996, **197**, 3907–3945.
125 R. E. Lapointe, J. C. Stevens, P. N. Nickias, M. H. Mcadon, 1992, EP0520732B1.
126 J. C. Stevens, in *Studies in Surface Science and Catalysis*, 1996, pp. 11–20.
127 R. Quijada, G. B. Galland and R. S. Mauler, *Macromol. Chem. Phys.*, 1996, **197**, 3091–3098.
128 N. Herfert, P. Montag and G. Fink, *Die Makromol. Chemie*, 1993, **194**, 3167–3182.
129 L. A. Williams and T. J. Marks, *Organometallics*, 2009, **28**, 2053–2061.
130 K. Czaja, L. A. Novokshonova and N. J. Kovaleva, *Macromol. Chem. Phys.*, 1999, **200**, 983–988.
131 G. B. Jacobsen, P. L. Wauteraerts and L. Spencer, 1997, US6043180A.
132 C. Przybyla, B. Tesche and G. Fink, *Macromol. Rapid Commun.*, 1999, **20**, 328–332.
133 P. S. Chum, W. J. Kruper and M. J. Guest, *Adv. Mater.*, 2000, **12**, 1759–1767.
134 Y. W. Cheung and M. J. Guest, in *Modern Styrenic Polymers: Polystyrenes and Styrenic Copolymers*, John Wiley & Sons, Ltd, Chichester, UK, 2003, pp. 605–630.
135 D.-H. Lee, K.-B. Yoon, H.-J. Kim, S.-S. Woo and S. K. Noh, *J. Appl. Polym. Sci.*, 1998, **67**, 2187–2198.
136 J. Ren and G. R. Hatfield, *Macromolecules*, 1995, **28**, 2588–2589.
137 F. G. Sernetz, R. Müllhaupt, F. Amor, T. Eberle and J. Okuda, *J. Polym. Sci. Part A Polym. Chem.*, 1997, **35**, 1571–1578.
138 G. Xu, *Macromolecules*, 1998, **31**, 2395–2402.
139 N. Guo, L. Li and T. J. Marks, *J. Am. Chem. Soc.*, 2004, **126**, 6542–6543.
140 N. Guo, C. L. Stern and T. J. Marks, *J. Am. Chem. Soc.*, 2008, **130**, 2246–2261.
141 D. S. McGuinness, *Chem. Rev.*, 2011, **111**, 2321–2341.
142 A. Forestière, H. Olivier-Bourbigou and L. Saussine, *Oil Gas Sci. Technol. - Rev. l'IFP*, 2009, **64**, 649–667.
143 J. Skupinska, *Chem. Rev.*, 1991, **91**, 613–648.
144 K. Ziegler, *Angew. Chem.*, 1952, **64**, 323–329.
145 K. Ziegler, *Angew. Chem.*, 1964, **76**, 545–553.
146 O. L. Sydora, *Organometallics*, 2019, **38**, 997–1010.
147 G. R. Lappin and J. D. Sauer, *Alpha Olefins Applications Handbook*, CRC Press, 1989.
148 W. Keim, F. H. Kowaldt, R. Goddard and C. Krüger, *Angew. Chem. Int. Ed.* , 1978, **17**, 466–467.
149 M. Peuckert and W. Keim, *Organometallics*, 1983, **2**, 594–597.
150 W. Keim, A. Behr, B. Gruber, B. Hoffmann, F. H. Kowaldt, U. Kuerschner, B.

Limbaecker and F. P. Sistig, *Organometallics*, 1986, **5**, 2356–2359.
151 W. Keim, *Angew. Chem. Int. Ed.*, 2013, **52**, 12492–12496.
152 J. Mol, *J. Mol. Catal. A Chem.*, 2004, **213**, 39–45.
153 A. Bollmann, K. Blann, J. T. Dixon, F. M. Hess, E. Killian, H. Maumela, D. S. McGuinness, D. H. Morgan, A. Neveling, S. Otto, M. Overett, A. M. Z. Slawin, P. Wasserscheid and S. Kuhlmann, *J. Am. Chem. Soc.*, 2004, **126**, 14712–14713.
154 P.-A. R. Breuil, L. Magna and H. Olivier-Bourbigou, *Catal. Letters*, 2015, **145**, 173–192.
155 G. V. Schulz, *Z. Phys. Chem.*, 1935, **30**, 379–398.
156 P. J. Flory, *J. Am. Chem. Soc.*, 1936, **58**, 1877–1885.
157 C. T. Young, R. von Goetze, A. K. Tomov, F. Zaccaria and G. J. P. Britovsek, *Top. Catal.*, 2020.
158 R. H. Crabtree, *Chem. Rev.*, 2015, **115**, 127–150.
159 S. A. Svejda and M. Brookhart, *Organometallics*, 1999, **18**, 65–74.
160 R. M. Manyik, W. E. Walker and T. P. Wilson, 1967, US3300458A.
161 R. Manyik, *J. Catal.*, 1977, **47**, 197–209.
162 T. Agapie, S. J. Schofer, J. A. Labinger and J. E. Bercaw, *J. Am. Chem. Soc.*, 2004, **126**, 1304–1305.
163 T. Agapie, J. A. Labinger and J. E. Bercaw, *J. Am. Chem. Soc.*, 2007, **129**, 14281–14295.
164 J. X. McDermott, J. F. White and G. M. Whitesides, *J. Am. Chem. Soc.*, 1976, **98**, 6521–6528.
165 S. J. McLain and R. R. Schrock, *J. Am. Chem. Soc.*, 1978, **100**, 1315–1317.
166 S. J. McLain, J. Sancho and R. R. Schrock, *J. Am. Chem. Soc.*, 1980, **102**, 5610–5618.
167 A. K. Tomov, J. J. Chirinos, D. J. Jones, R. J. Long and V. C. Gibson, *J. Am. Chem. Soc.*, 2005, **127**, 10166–10167.
168 A. K. Tomov, J. J. Chirinos, R. J. Long, V. C. Gibson and M. R. J. Elsegood, *J. Am. Chem. Soc.*, 2006, **128**, 7704–7705.
169 J. N. Armor, *Catal. Today*, 2014, **236**, 171–181.
170 *Hydrocarb. Process.*, 2012, https://www.axens.net/product/technology-licensing.
171 A. Convers, D. Commereuc and B. Torck, *Rev. l'Institut Français du Pétrole*, 1994, **49**, 437–451.
172 J. T. Dixon, M. J. Green, F. M. Hess and D. H. Morgan, *J. Organomet. Chem.*, 2004, **689**, 3641–3668.
173 J. W. Freeman, J. L. Buster, R. D. Knudsen, 1999, US5856257A.
174 Y. Suzuki, S. Kinoshita, A. Shibahara, S. Ishii, K. Kawamura, Y. Inoue and T. Fujita, *Organometallics*, 2010, **29**, 2394–2396.
175 M. J. Overett, K. Blann, A. Bollmann, J. T. Dixon, D. Haasbroek, E. Killian, H. Maumela, D. S. McGuinness and D. H. Morgan, *J. Am. Chem. Soc.*, 2005, **127**, 10723–10730.
176 C. Andes, S. B. Harkins, S. Murtaza, K. Oyler and A. Sen, *J. Am. Chem. Soc.*, 2001, **123**, 7423–7424.
177 J. D. Fellmann, G. A. Rupprecht and R. R. Schrock, *J. Am. Chem. Soc.*, 1979, **101**, 5099–5101.
178 E. A. C. Brussee, A. Meetsma, B. Hessen and J. H. Teuben, *Organometallics*, 1998, **17**, 4090–4095.
179 R. Schmidt, M. B. Welch, R. D. Knudsen, S. Gottfried and H. G. Alt, *J. Mol. Catal. A Chem.*, 2004, **222**, 17–25.
180 S. Zhang and K. Nomura, *J. Am. Chem. Soc.*, 2010, **132**, 4960–4965.

181 A. Igarashi, S. Zhang and K. Nomura, *Organometallics*, 2012, **31**, 3575–3581.
182 K. Nomura, A. Igarashi, S. Katao, W. Zhang and W.-H. Sun, *Inorg. Chem.*, 2013, **52**, 2607–2614.
183 X.-Y. Tang, A. Igarashi, W.-H. Sun, A. Inagaki, J. Liu, W. Zhang, Y.-S. Li and K. Nomura, *Organometallics*, 2014, **33**, 1053–1060.
184 A. M. Messinis, A. S. Batsanov, J. A. K. Howard, M. J. Hanton and P. W. Dyer, *ChemCatChem*, 2019, **11**, 1756–1764.
185 M. Kuboki and K. Nomura, *Organometallics*, 2019, **38**, 1544–1559.
186 Z. J. A. Komon and G. C. Bazan, *Macromol. Rapid Commun.*, 2001, **22**, 467–478.
187 C. M. Killian, P. B. Mackenzie, G. G. Lavoie, J. A. Ponasik and L. S. Moody, 2000, WO 2000050475.
188 D. L. Beach and Y. V. Kissin, *J. Polym. Sci. Polym. Chem. Ed.*, 1984, **22**, 3027–3042.
189 E. A. Benham, P. D. Smith and M. P. McDaniel, *Polym. Eng. Sci.*, 1988, **28**, 1469–1472.
190 C. Denger, U. Haase and G. Fink, *Macromol. Rapid Commun.*, 1991, **12**, 697–701.
191 M. Yang, Q. Li, X. Li, B. Hu, X. Dong, J. Qu, B. Liu, X. Wang and X. Hao, *Chinese J. Polym. Sci.*, 2016, **34**, 298–306.
192 F. F. Karbach, T. Macko and R. Duchateau, *Macromolecules*, 2016, **49**, 1229–1241.
193 J. Canich and G. Licciardi, 1991, US5057475A.
194 R. W. Barnhart, G. C. Bazan and T. Mourey, *J. Am. Chem. Soc.*, 1998, **120**, 1082–1083.
195 Z. Ye, F. AlObaidi and S. Zhu, *Macromol. Rapid Commun.*, 2004, **25**, 647–652.
196 S. Guo, H. Fan, Z. Bu, B.-G. Li and S. Zhu, *Macromol. Chem. Phys.*, 2014, **215**, 1661–1667.
197 K. Musikabhumma, T. P. Spaniol and J. Okuda, *J. Polym. Sci. Part A Polym. Chem.*, 2003, **41**, 528–544.
198 G. P. Abramo, L. Li and T. J. Marks, *J. Am. Chem. Soc.*, 2002, **124**, 13966–13967.
199 H. Li, L. Li, T. J. Marks, L. Liable-Sands and A. L. Rheingold, *J. Am. Chem. Soc.*, 2003, **125**, 10788–10789.
200 D. C. Aluthge, A. Sattler, M. A. Al-Harthi, J. A. Labinger and J. E. Bercaw, *ACS Catal.*, 2016, **6**, 6581–6584.
201 J.-C. Wasilke, S. J. Obrey, R. T. Baker and G. C. Bazan, *Chem. Rev.*, 2005, **105**, 1001–1020.
202 Z. J. A. Komon, G. M. Diamond, M. K. Leclerc, V. Murphy, M. Okazaki and G. C. Bazan, *J. Am. Chem. Soc.*, 2002, **124**, 15280–15285.

Chapter Two
Complex synthesis

2.1 Introduction

2.1.1 Synthesis of constrained geometry complexes

A range of synthetic methods have been used in the synthesis of group 4 constrained geometry complexes, including salt metathesis, protonolysis and template synthesis.[1] The first synthetic method involves reaction of the proligand with a suitable alkyllithium or other deprotonating agent followed by reaction with a suitable metal dichloride species. Okuda reported the synthesis of $^{Me_2}SB(^{t Bu}N,^{3\text{-}t Bu}Cp)TiCl_2$ (Figure 2.1(a)) *via* this synthetic method using $^{n}BuLi$ proceeded by $TiCl_4.2THF$,[2] with further syntheses reported with the use of $ZrCl_4.2THF$,[3] $ZrCl_2(NEt_2)_2.2THF$,[4] $ZrCl_4$ and $HfCl_4$.[5] Low yields reported for the titanium complexes were due to reduction of the titanium (IV) species to titanium (III) over the course of the reaction. An alternative synthesis was developed to increase reaction yields, by first preparing a titanium (III) species followed by oxidation. This synthetic method has been used by Teuben *et al*. in the oxidation of Cp_2TiR with lead dichloride to yield $Cp_2TiR(Cl)$.[6] This was also employed in the synthesis of $^{Me_2}SB(^{t Bu}N,^{3\text{-}R}I)TiCl_2$ (R = H, $SiMe_3$, Figure 2.1(b)),[7] allowing for increases in product yields to over 90%, far greater than those reported by the traditional synthetic method (35%).[2]

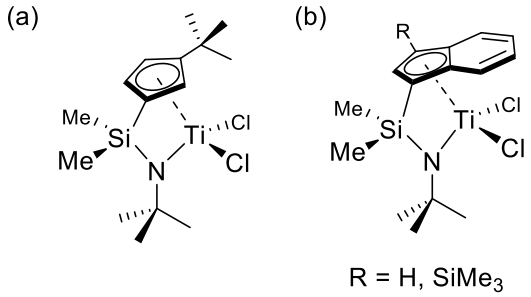

Figure 2.1. Molecular structures of (a) ^{Me2}SB(^{tBu}N,$^{3\text{-}tBu}$Cp)TiCl$_2$ and (b) ^{Me2}SB(^{tBu}N,$^{3\text{-}R}$I)TiCl$_2$.[2,7]

The protonolysis method involves the reaction of the proligand with a metal tetraamide or tetraalkyl to yield the desired complex with moderate conditions.[1] This synthetic method has been used by Teuben *et al*. in the preparation of C$_3$H$_6$(^{Me}N,Cp)Zr(NMe$_2$)$_2$ (Figure 2.2 (a)) from Zr(NMe$_2$)$_4$ and C$_3$H$_6$(^{Me}N,Cp)H$_2$ in 94% yield after 15 minutes reaction time.[8] The template synthesis involves stepwise coordination of the ligands to the metal centre followed by an internal reaction. This method has been employed by Royo *et al*.; C$_5$H$_4$SiMe$_3$SiMe$_2$Cl was reacted with TiCl$_4$ to yield CpSiMe$_2$ClTiCl$_3$, followed by reaction with LiN(H)^{t}Bu to yield ^{Me2}SB(^{tBu}N,Cp)TiCl$_2$ (Figure 2.2 (b)).[9]

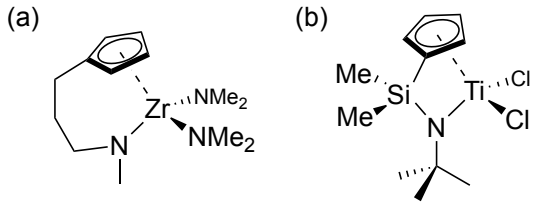

Figure 2.2. Molecular structures of C$_3$H$_6$(^{Me}N,Cp)Zr(NMe$_2$)$_2$ and ^{Me2}SB(^{tBu}N,Cp)TiCl$_2$.

2.1.2 Chapter synopsis

This chapter describes the synthesis and characterisation of a range of constrained geometry complexes with variation of the amido fragment, leaving group, metal centre and *ansa* bridge. The attempted syntheses of two further *ansa* bridge variations are discussed. Two complexes are reacted with methylaluminoxane (MAO) in order to attempt to gain an insight into the nature of the supported complexes.

The synthesis of solid polymethylaluminoxane (sMAO), MAO-modified layered double hydroxide (LDH, LDHMAO) and MAO-modified silica (SSMAO) supported complexes are also described with solid state NMR spectroscopy characterisation of these complexes discussed.

2.2 Synthesis of permethylindenyl constrained geometry complexes

2.2.1 Synthesis of ^{Me2}SB(^{R}N,I*)TiCl$_2$

The proligands, ^{Me2}SB(^{R}N,I*)H$_2$, (I* = C$_9$Me$_6$; R = ^{i}Pr, ^{t}Bu, ^{n}Bu, Cy, Ph, 4-^{t}BuC$_6$H$_4$ and 4-^{n}BuC$_6$H$_4$) were synthesised by addition of LiN(H)R to I*SiMe$_2$Cl in a 1:1 ratio (Equation 2.1). The reactants were combined in cold tetrahydrofuran (THF) and then allowed to warm to room temperature and stirred for 2 hours. Products were obtained as dark orange/yellow oils in quantitative yields.

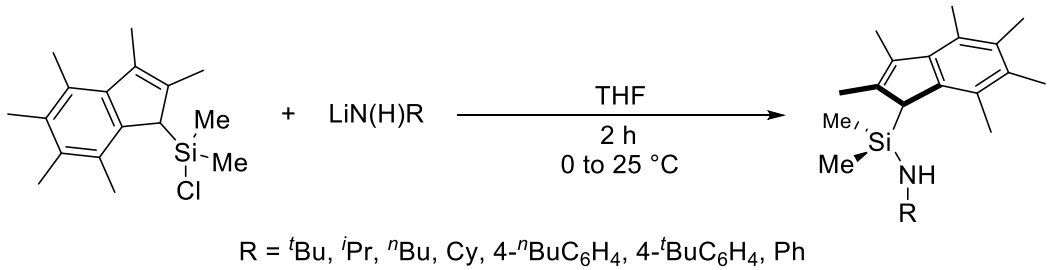

R = ^{t}Bu, ^{i}Pr, ^{n}Bu, Cy, 4-^{n}BuC$_6$H$_4$, 4-^{t}BuC$_6$H$_4$, Ph

Equation 2.1. Preparation of ^{Me2}SB(^{R}N,I*)H$_2$ from I*SiMe$_2$Cl.

The ^{1}H NMR spectra of the proligands show the expected six permethylindenyl (I*-Me) resonances between 1.9–2.6 ppm and two dimethylsilyl (SiMe$_2$) resonances around 0–0.5 ppm. A typical proligand ^{1}H NMR spectrum is shown below in Figure 2.3 for ^{Me2}SB($^{4\text{-}t\text{BuC}6\text{H}4}$N,I*)H$_2$. I*-Me resonances are observed from 1.98 to 2.52 ppm, Si-Me$_2$ resonances at 0.07 and 0.03 ppm and the 4-*tert*butylphenyl resonances observed at 7.17, 6.52 and 1.29 ppm. In addition, resonances are observed at 3.63 and 3.05 ppm that correspond to the N-H and I*-H protons respectively.

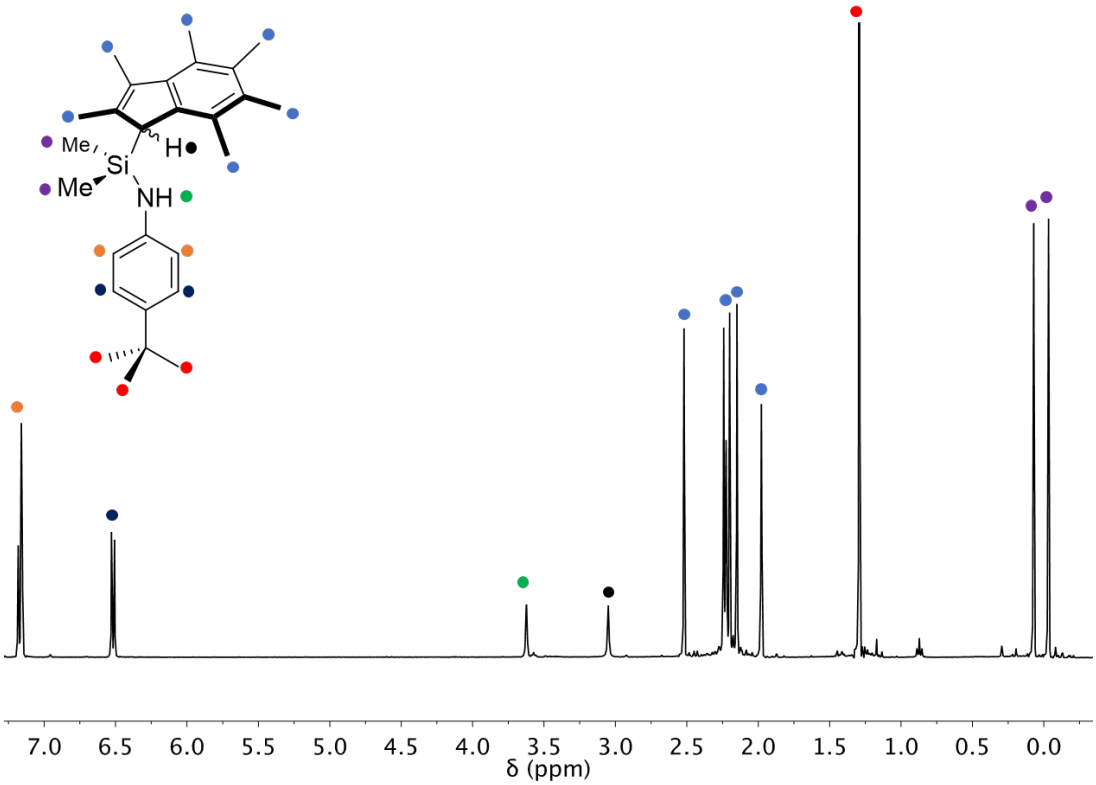

Figure 2.3. ^{1}H NMR spectrum of ^{Me_2}SB($^{4\text{-}t\text{BuC}_6\text{H}_4}$N,I*)H$_2$ (d_6-benzene, 298 K and 400.2 MHz).

The complexes ^{Me_2}SB(^{R}N,I*)TiCl$_2$ were synthesised *via* a salt metathesis procedure (Equation 2.2). ^{Me_2}SB(^{R}N,I*)Li$_2$ was first prepared by dropwise addition of 2.2 equivalents of ^{n}BuLi to a solution of ^{Me_2}SB(^{R}N,I*)H$_2$ in cold THF; work up yielded ^{Me_2}SB(^{R}N,I*)Li$_2$.

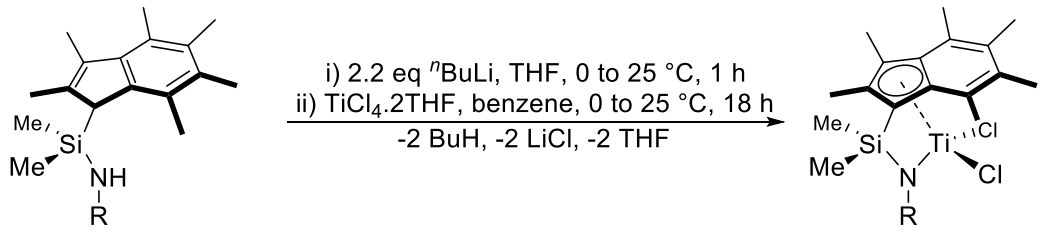

R = ^{t}Bu, ^{i}Pr, ^{n}Bu, Cy, 4-^{n}BuC$_6$H$_4$, 4-^{t}BuC$_6$H$_4$, Ph

Equation 2.2. Preparation of ^{Me_2}SB(^{R}N,I*)TiCl$_2$ from ^{Me_2}SB(^{R}N,I*)H$_2$.

The ^{1}H NMR spectra for these dilithium salts (as exemplified in Figure 2.4 for ^{Me_2}SB($^{i\text{Pr}}$N,I*)Li$_2$) show the loss of the two resonances from the proligand corresponding to both the I*-H and N-H protons. In addition to the expected six resonances for the I*-Me

protons (2.50–3.20 ppm), the resonances attributable to the amido fragments (1.22, 1.24 and 3.52 ppm) and the Si-Me resonance at 0.78 ppm, there are two resonances observed at 1.62 and 3.67 ppm that correspond to residual THF. Integration of these resonances relative to ^{Me_2}SB($^{i\text{Pr}}$N,I*)Li$_2$ corresponds to 0.18 equivalents of THF.

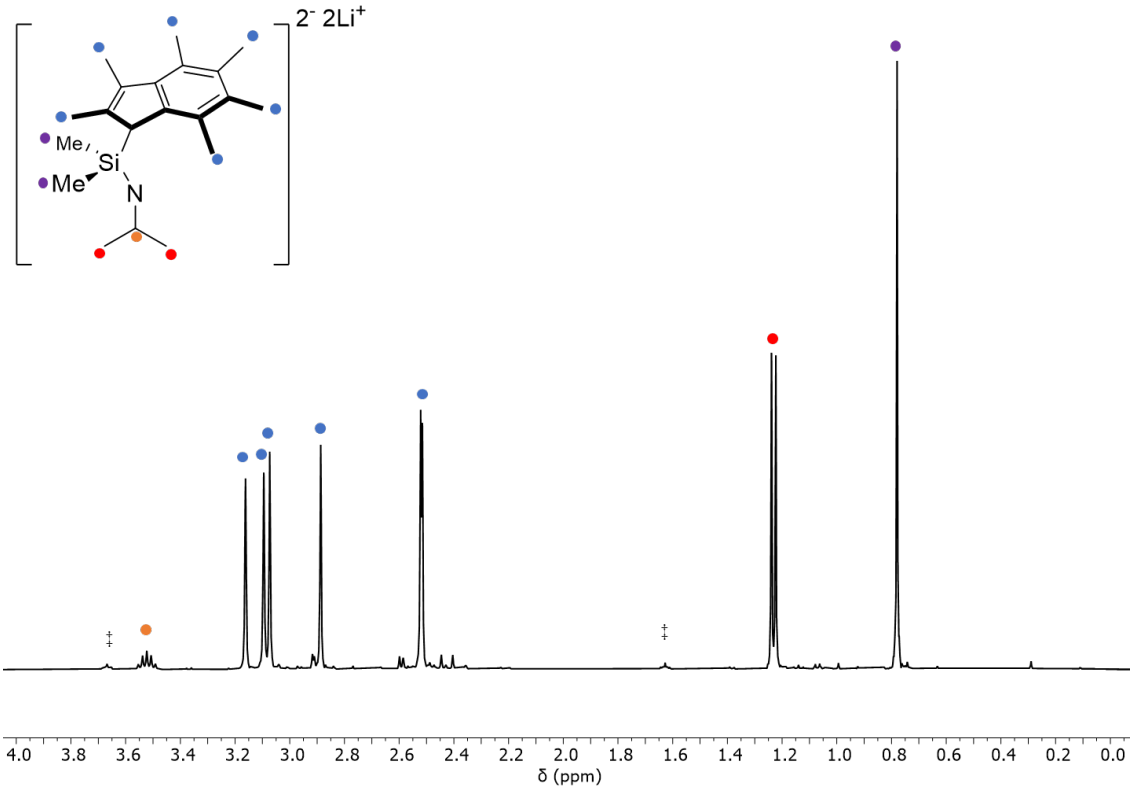

Figure 2.4. ^{1}H NMR spectrum of ^{Me_2}SB($^{i\text{Pr}}$N,I*)Li$_2$ (d_5-pyridine, 298 K and 400.2 MHz). ‡ corresponds to residual THF.

For R = Ph, the dilithium salt of the ligand was reacted in a one pot procedure with TiCl$_4$.2THF to form the complex, whilst for R = 4-^{t}BuC$_6$H$_4$, 4-^{n}BuC$_6$H$_4$, Cy, ^{n}Bu, ^{i}Pr and ^{t}Bu, the ligand was isolated prior to complexation. One equivalent of TiCl$_4$.2THF was added to the ligands in benzene. Following work up, the products, ^{Me_2}SB(^{R}N,I*)TiCl$_2$, were isolated as red/purple solids in yields of 5 to 20%. The ^{1}H NMR spectra are shown in Figures 2.5 and A2.1–A2.6. The ^{1}H NMR spectra show typical I*-Me resonances in the range of 2.00–2.60 ppm in addition to two silyl-methyl resonances between 0.40 and 0.80 ppm. The aromatic amido resonances are observed between 6.80–7.30 ppm. In

Figure 2.5, the ^{i}Pr resonances are seen as a septet at 5.08 ppm and a pair of doublets at 1.01 and 1.11 ppm.

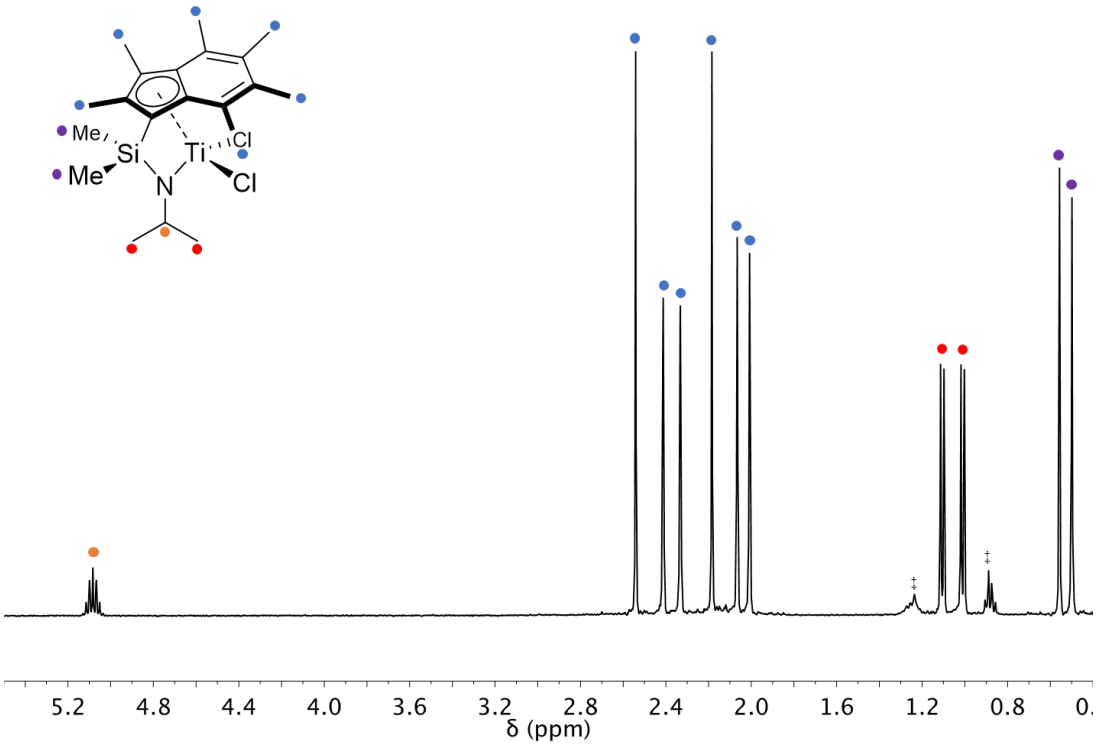

Figure 2.5. ^{1}H NMR spectrum of ^{Me_2}SB(^{iPr}N,I*)TiCl$_2$ (d_6-benzene, 298 K and 499.9 MHz). Resonances at 0.85 and 1.25 ppm correspond to residual pentane (‡).

The most complex ^{1}H NMR spectrum is that of ^{Me_2}SB(^{Cy}N,I*)TiCl$_2$ (Figure A2.6), with all of the individual protons on the cyclohexyl ring being magnetically inequivalent. As well as the characteristic resonances for the I*-Me, and Si-Me groups observed for all ^{Me_2}SB(^{R}N,I*)TiCl$_2$ complexes, the C-H proton of the cyclohexyl amido group can be assigned to the multiplet at 4.75 ppm. By use of ^{1}H-^{1}H COSY, ^{1}H-^{13}C HSQC and ^{1}H-^{13}C HMBC NMR spectroscopy, it is possible to fully assign resonances in the range of 0.87 to 2.13 ppm to the remaining protons of the cyclohexyl group.

There are no large differences in the ^{1}H NMR spectra for the I*-Me resonances of ^{Me_2}SB(^{R}N,I*)TiCl$_2$; resonances between 2.04 and 2.56 ppm for ^{Me_2}SB(^{tBu}N,I*)TiCl$_2$ and 2.07 to 2.55 ppm for ^{Me_2}SB(^{Ph}N,I*)TiCl$_2$, with the resonances of the other complexes

falling in this range. Similarly, there is no large shift for the two complexes ^{Me2}SB(^{R}N,Cp)TiCl$_2$ reported by Royo *et al.*;[9] where the Cp resonances for R = ^{t}Bu are observed between 5.99 and 6.51 ppm and from 6.07–6.60 ppm for R = CH(Me)Ph.

Crystals of ^{Me2}SB($^{i\text{Pr}}$N,I*)TiCl$_2$, ^{Me2}SB($^{t\text{Bu}}$N,I*)TiCl$_2$ and ^{Me2}SB($^{4\text{-}t\text{BuC}_6\text{H}_4}$N,I*)TiCl$_2$ suitable for single crystal X-ray diffraction studies were grown in pentane at −32 °C (Figure 2.6 and Table 2.1).

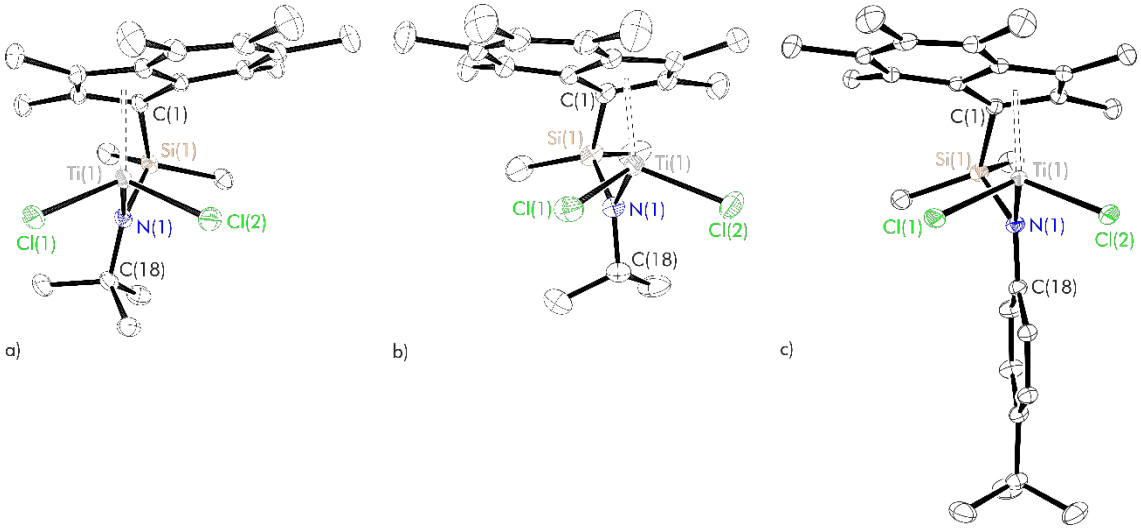

Figure 2.6. Solid-state structures of (a) ^{Me2}SB($^{t\text{Bu}}$N,I*)TiCl$_2$, (b) ^{Me2}SB($^{i\text{Pr}}$N,I*)TiCl$_2$ and (c) ^{Me2}SB($^{4\text{-}t\text{BuC}_6\text{H}_4}$N,I*)TiCl$_2$. Hydrogen atoms have been omitted for clarity; thermal ellipsoids are drawn at 30% probability. Crystals of ^{Me2}SB($^{t\text{Bu}}$N,I*)TiCl$_2$ grown by Dr. J.-C. Buffet.

Table 2.1. Selected bond lengths (Å) and angles (°) for ^{Me2}SB($^{t\text{Bu}}$N,I*)TiCl$_2$, ^{Me2}SB($^{i\text{Pr}}$N,I*)TiCl$_2$ and ^{Me2}SB($^{4\text{-}t\text{BuC}_6\text{H}_4}$N,I*)TiCl$_2$. Estimated standard deviations are given in parentheses.

Complex	^{Me2}SB($^{t\text{Bu}}$N,I*)TiCl$_2$	^{Me2}SB($^{i\text{Pr}}$N,I*)TiCl$_2$	^{Me2}SB($^{4\text{-}t\text{BuC}_6\text{H}_4}$N,I*)TiCl$_2$
Ti(1)-N(1)	1.910(2)	1.8883(13)	1.9378(14)
Ti(1)-Cp$_{cent}$	2.0386(1)	2.0332(1)	2.0301(1)
δ	108.10(1)	107.68(1)	107.49(1)
C(1)-Si(1)-N(1)	91.00(12)	90.37(7)	91.26(7)
C(18)-N(1)	1.497(4)	1.471(2)	1.409(2)
Percent Buried Volume[10]	65.0	62.0	62.6

The solid-state structures show similar bond lengths for Ti-Cp_{cent} to those of comparable CGCs within the literature (2.012–2.115 Å for (*S*-(-)^{Me2}SB(^{PhMeCH}N,Cp)$TiCl_2$ and ^{Me2}SB($^{t Bu}$N,$^{3\text{-}N_4C_4}$I)$TiCl_2$ respectively).[11,12] The observed C(1)-Si(1)-N(1) angle also lies within the range of angles previously reported (88.414° and 92.323° for ^{Me2}SB(^{MeOCH_2CH_2}N,Cp)$TiCl_2$ and ^{Me2}SB($^{t Bu}$N,$^{3\text{-}N(CH_2CH_2SEt)_2}$I)$TiCl_2$ respectively).[13,14] The Ti(1)-N(1) bond length for ^{Me2}SB($^{4\text{-}t BuC_6H_4}$N,I*)$TiCl_2$ is on average longer than those previously reported (1.874(3)–1.930 Å).[13,15] However, longer bond lengths have been reported for constrained geometry complexes which contain multiple ligating N atoms.[16] Kamigaito *et al*. reported the complexes ^{Me2}SB(^{R}N,Cp*)$TiCl_2$ (R = C_6F_5 and SO_2Ph), and when compared with ^{Me2}SB($^{t Bu}$N,Cp*)$TiCl_2$ longer Ti(1)-N(1) bond lengths were observed with more electron-withdrawing amido groups; this was proposed to lead to a more electron-deficient metal centre and lower polymerisation activities.[17] This was not observed in the above complexes, with a shorter bond length for ^{Me2}SB($^{i Pr}$N,I*)$TiCl_2$ (1.8883(3) Å) than ^{Me2}SB($^{t Bu}$N,I*)$TiCl_2$ (1.910(2) Å) implying there is also a steric influence from the nature of the amido group. Comparison of ^{Me2}SB($^{t Bu}$N,Cp)$TiCl_2$, ^{Me2}SB($^{t Bu}$N,Cp*)$TiCl_2$ and ^{Me2}SB($^{t Bu}$N,I*)$TiCl_2$ also shows slight increases in Ti(1)-N(1) bond lengths, from 1.901(3) to 1.907(4) and 1.910(2) Å respectively and increasing Ti(1)-Cp_{cent} bond lengths from 2.019 to 2.030 and 2.0386(1) Å respectively which is likely due to the increasing steric bulk of the apical ligand.[18]

2.2.2 Synthesis and characterisation of ^{Me2}SB($^{t Bu}$N,I*)Ti(Cl)CH_2SiMe_3 and ^{Me2}SB($^{t Bu}$N,I*)TiR_2

The reaction of ^{Me2}SB($^{t Bu}$N,I*)$TiCl_2$ with the appropriate alkali metal salt afforded ^{Me2}SB($^{t Bu}$N,I*)Ti(Cl)CH_2SiMe_3, ^{Me2}SB($^{t Bu}$N,I*)$TiMe_2$, ^{Me2}SB($^{t Bu}$N,I*)Ti$(CH_2Ph)_2$ and

^{Me2}SB($^{t\text{Bu}}$N,I*)Ti(CH_2SiMe_3)$_2$ (Scheme 2.1). ^{Me2}SB($^{t\text{Bu}}$N,I*)TiMe_2, ^{Me2}SB($^{t\text{Bu}}$N,I*)Ti(CH_2Ph)$_2$ and ^{Me2}SB($^{t\text{Bu}}$N,I*)Ti(CH_2SiMe_3)$_2$ were first prepared by Mr. Alexander Smith.[19]

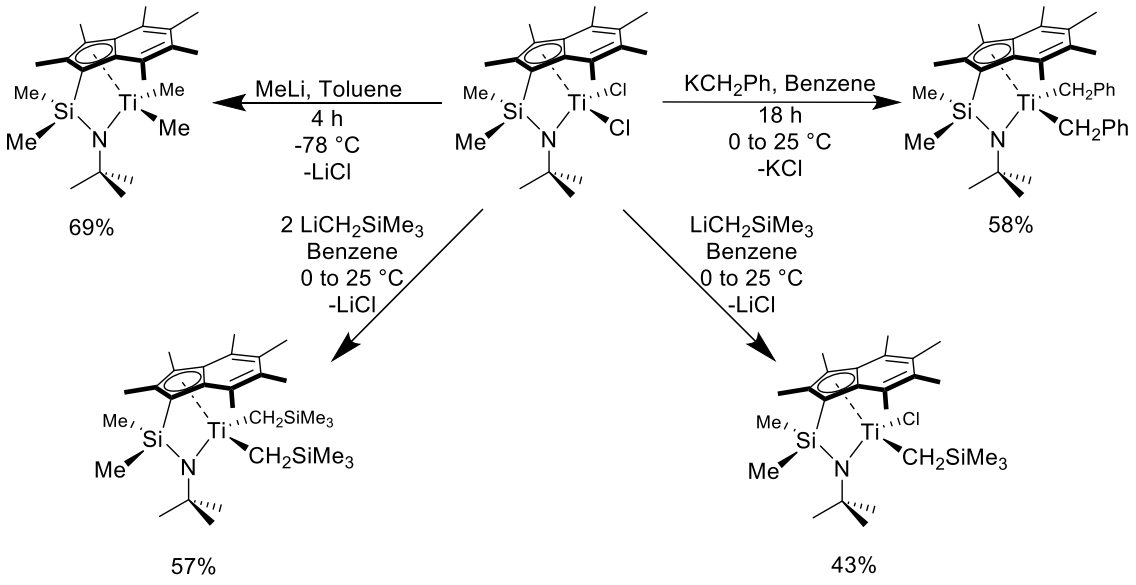

Scheme 2.1. Synthetic procedure for the synthesis of ^{Me2}SB($^{t\text{Bu}}$N,I*)Ti(Cl)CH_2SiMe_3 and ^{Me2}SB($^{t\text{Bu}}$N,I*)TiR_2 (R = Me, CH_2Ph and CH_2SiMe_3) from ^{Me2}SB($^{t\text{Bu}}$N,I*)TiCl_2.

Reaction of ^{Me2}SB($^{t\text{Bu}}$N,I*)TiCl_2 with 2.2 equivalents of either MeLi in toluene or KCH_2Ph in benzene followed by work up yielded ^{Me2}SB($^{t\text{Bu}}$N,I*)TiMe_2 and ^{Me2}SB($^{t\text{Bu}}$N,I*)Ti(CH_2Ph)$_2$ as brown or dark-red solids in 69 and 58% yield respectively (Scheme 2.1). ^{Me2}SB($^{t\text{Bu}}$N,I*)Ti(Cl)CH_2SiMe_3 and ^{Me2}SB($^{t\text{Bu}}$N,I*)Ti(CH_2SiMe_3)$_2$ were synthesised by reaction of ^{Me2}SB($^{t\text{Bu}}$N,I*)TiCl_2 with 1 or 2 equivalents of Li(CH_2SiMe_3)$_2$ in benzene to afford ^{Me2}SB($^{t\text{Bu}}$N,I*)Ti(Cl)CH_2SiMe_3 and ^{Me2}SB($^{t\text{Bu}}$N,I*)Ti(CH_2SiMe_3)$_2$ after work up as orange crystalline solids in 57 and 43% yield respectively (Scheme 2.1).

The ^{1}H NMR spectra of ^{Me2}SB($^{t\text{Bu}}$N,I*)Ti(CH_2Ph)$_2$, ^{Me2}SB($^{t\text{Bu}}$N,I*)TiMe_2, ^{Me2}SB($^{t\text{Bu}}$N,I*)Ti(CH_2SiMe_3)$_2$ and ^{Me2}SB($^{t\text{Bu}}$N,I*)Ti(Cl)CH_2SiMe_3 contain the same diagnostic resonances for the constrained geometry ligand as for ^{Me2}SB($^{t\text{Bu}}$N,I*)TiCl_2. Six singlets can be observed in the 2.00–2.50 ppm region which correspond to the I* methyl

protons, a singlet between 1.42 and 1.51 ppm is assigned to the N-^{t}Bu group, and the silyl-methyl groups are observed as singlets from 0.51 to 0.66 ppm.

In the ^{1}H NMR spectrum of ^{Me2}SB($^{t Bu}$N,I*)Ti(Cl)CH$_2$SiMe$_3$ (Figure 2.7), a singlet at 0.10 ppm corresponds to the SiMe$_3$ group, whilst the methylene protons are observed as a pair of roofed doublets at 1.57 and −0.97 ppm, with a $^2J_{H\text{-}H}$ coupling of 11.9 Hz. In the ^{1}H-^{1}H ROESY NMR spectrum of ^{Me2}SB($^{t Bu}$N,I*)Ti(Cl)CH$_2$SiMe$_3$, coupling between the SiMe$_3$ resonance and the I*-Me resonances confirms that the CH$_2$SiMe$_3$ group is positioned below the I* ring, as seen in the solid state molecular structure.

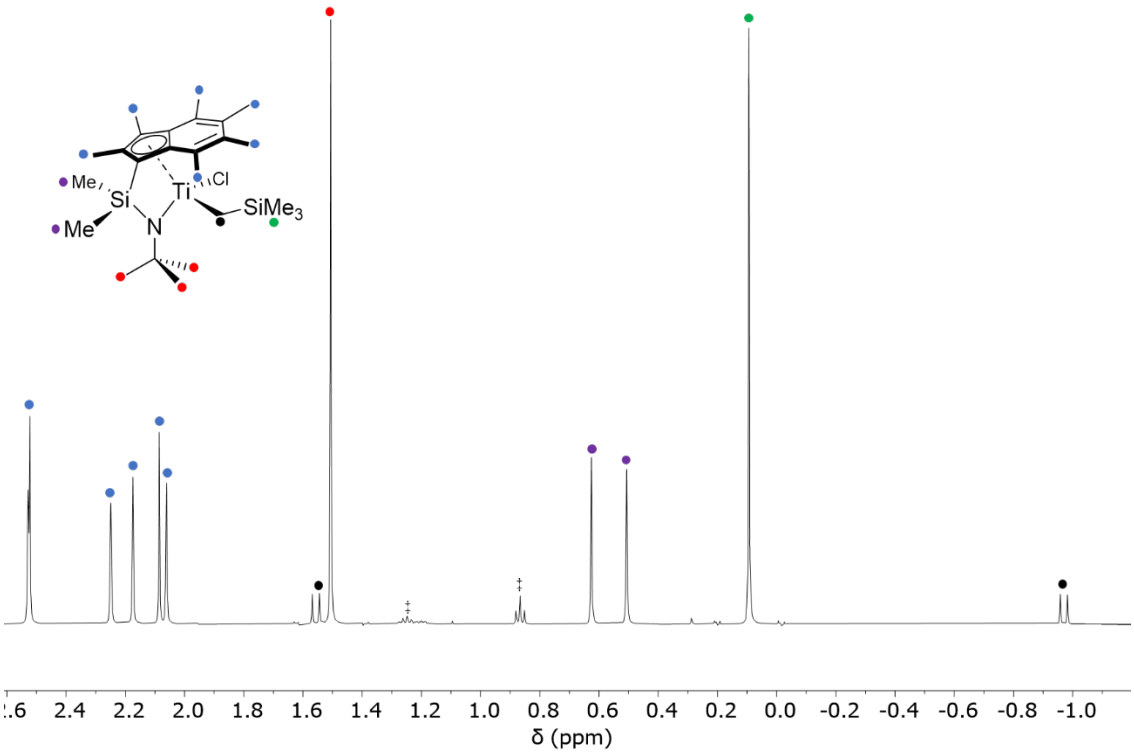

Figure 2.7. ^{1}H NMR spectrum of ^{Me2}SB($^{t Bu}$N,I*)Ti(Cl)CH$_2$SiMe$_3$ (d_6-benzene, 298 K and 400.2 MHz). Resonances at 0.85 and 1.25 ppm correspond to residual pentane (‡).

In the bisneosilyl complex, doublets are also observed at 1.22, 0.98, 0.65 and −0.87 ppm, which correspond to the four protons of the diastereotopic methylene groups bound to the titanium centre. The ^{1}H-^{1}H ROESY NMR spectrum shows that the neosilyl group directly under the I* ring (with correlation to the I*-Me resonances) corresponds to the more

negatively shifted $SiMe_3$ group (0.02 ppm). In the dibenzyl complex, triplets at 7.16, 7.06, 6.92 and 6.83 ppm and doublets at 6.94 and 6.71 ppm have been assigned to the phenyl groups. Doublets observed at 2.70, 2.40, 1.59 and 1.52 ppm correspond to the four protons of the diastereotopic methylene units showing different orientations of the benzyl groups relative to the I* ring as is seen in $^{Me2}SB(^{tBu}N,I^*)Ti(CH_2SiMe_3)_2$. The ^1H NMR spectrum of $^{Me2}SB(^{tBu}N,I^*)TiMe_2$ shows two additional singlets at 0.58 and −0.14 ppm that correspond to two methyl groups bound to the titanium centre.

Crystals suitable for analysis by single crystal X-ray diffraction studies were grown from pentane at −20 ºC for the complexes $^{Me2}SB(^{tBu}N,I^*)TiMe_2$, $^{Me2}SB(^{tBu}N,I^*)Ti(CH_2SiMe_3)_2$ and $^{Me2}SB(^{tBu}N,I^*)Ti(Cl)CH_2SiMe_3$. Selected bond lengths and angles are given in Table 2.2 and the solid-state molecular structures are shown in Figure 2.8.

Table 2.2. Selected bond lengths (Å) and angles (º) for $^{Me2}SB(^{tBu}N,I^*)TiMe_2$, $^{Me2}SB(^{tBu}N,I^*)Ti(CH_2SiMe_3)_2$, and $^{Me2}SB(^{tBu}N,I^*)Ti(Cl)CH_2SiMe_3$. Estimated standard deviations (ESDs) are given in parentheses, (L) = $^{Me2}SB(^{tBu}N,I^*)$.

	(L)$TiMe_2$	(L)$Ti(CH_2SiMe_3)_2$	(L)$Ti(Cl)CH_2SiMe_3$
Ti(1)-Cp_{cent}	2.0555(1)	2.1010(1)	2.0599(1)
Ti(1)-C(22)	2.1093(13)	2.1077(12)	2.1310(16)
Ti(1)-C(23/26)	2.1146(14)	2.1429(12)	-
Ti(1)-N(1)	1.9295(11)	1.9389(10)	1.9242(15)
N(1)-C(^{t}Bu)	1.4871(16)	1.4864(16)	1.491(2)
Δ_{M-C}	0.107	0.132	0.115
δ	109.19	109.12	107.33
C(22)-Ti(1)-C(23/26)	103.05(1)	104.75(5)	-

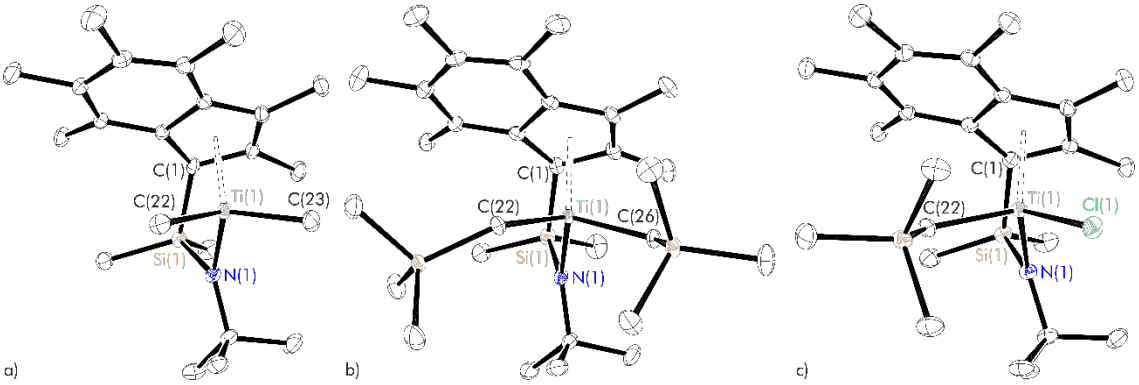

Figure 2.8. Solid-state molecular structures of (a) ^{Me2}SB(^{tBu}N,I*)TiMe$_2$, (b) ^{Me2}SB(^{tBu}N,I*)Ti(CH$_2$SiMe$_3$)$_2$, and (c) ^{Me2}SB(^{tBu}N,I*)Ti(Cl)CH$_2$SiMe$_3$. Hydrogen atoms have been omitted for clarity. Thermal ellipsoids are drawn at 30% probability. Crystals of ^{Me2}SB(^{tBu}N,I*)TiMe$_2$ and ^{Me2}SB(^{tBu}N,I*)Ti(CH$_2$SiMe$_3$)$_2$ were grown by Mr. Alexander Smith.

The shorter Ti(1)-Cp$_{cent}$ distance in ^{Me2}SB(^{tBu}N,I*)TiMe$_2$ compared to ^{Me2}SB(^{tBu}N,I)TiMe$_2$ (2.0555(1) and 2.0913(13) Å respectively) can be attributed to the stronger bonding between the more electron rich I* moiety and titanium.[20] The increased length for ^{Me2}SB(^{tBu}N,I*)Ti(CH$_2$SiMe$_3$)$_2$ (2.1010(1) Å) compared with both ^{Me2}SB(^{tBu}N,I*)TiMe$_2$ (2.0555(1) Å) and ^{Me2}SB(^{tBu}N,I*)Ti(Cl)CH$_2$SiMe$_3$ (2.0599(1) Å) is likely due to the greater steric bulk of the $^{-}$CH$_2$SiMe$_3$ ligands when compared with the methyl group. This trend is also observed in the Ti(1)-N(1) bond length with the longest bond length observed for ^{Me2}SB(^{tBu}N,I*)Ti(CH$_2$SiMe$_3$)$_2$ (1.9389(10) Å). The longer Ti(1)-Cp$_{cent}$ and Ti(1)-N(1) distances relative to ^{Me2}SB(^{tBu}N,I*)TiCl$_2$ (2.0386(1) and 1.910(2) Å) is indicative of the greater electron donating ability of the alkyl initiator groups relative to chloride.

The comparable $\Delta_{M\text{-}C}$ distance (defined in Equation 2.3 and a measure of ring slippage) of ^{Me2}SB(^{tBu}N,I*)TiMe$_2$ (0.107 Å) and ^{Me2}SB(^{tBu}N,I)TiMe$_2$ (0.106 Å) shows a propensity to undergo η^5-η^3 ring slip, characteristic of indenyl metallocenes, when compared to the small $\Delta_{M\text{-}C}$ distance in ^{Me2}SB(^{tBu}N,Cp*)TiMe$_2$ (0.04 Å).[20] The larger $\Delta_{M\text{-}C}$ distance of ^{Me2}SB(^{tBu}N,I*)Ti(CH$_2$SiMe$_3$)$_2$ (0.132 Å) and ^{Me2}SB(^{tBu}N,I*)Ti(Cl)CH$_2$SiMe$_3$ (0.115 Å)

infers a greater propensity to η^5-η^3 ring slip. This could be due to the longer Ti(1)-Cp_{cent} distance of the neosilyl complexes which can allow for the I* moiety to adopt a position with less steric hindrance.

$$\Delta_{M-C} = \left\{\frac{C(8)+C(9)}{2}\right\} - \left\{\frac{C(1)+C(2)+C(3)}{3}\right\}$$

Equation 2.3. Definition of $\Delta_{M\text{-}C}$ where C(n) denotes the bond length for Ti(1)-C(n).

The δ angle (the angle subtended at the metal centre by the I* centroid (Cp_{cent}) and the amido fragment (N(1))) increases as the Cp type ligand is changed from Cp* (108.44°) to I (108.88°) and I* (109.19°).[20,21] Compared with ^{Me_2}SB($^{t\text{Bu}}$N,I*)TiMe$_2$, the δ angles for ^{Me_2}SB($^{t\text{Bu}}$N,I*)Ti(CH$_2$SiMe$_3$)$_2$ (109.12°) and ^{Me_2}SB($^{t\text{Bu}}$N,I*)Ti(Cl)CH$_2$SiMe$_3$ (107.33°) decrease which could once again be due to the greater steric bulk of the neosilyl ligand.

2.2.3 Synthesis and characterisation of ^{Me_2}SB($^{t\text{Bu}}$N,$^{3\text{-Et}}$I*)TiCl$_2$

$^{3\text{-Et}}$I*SiMe$_2$Cl was prepared by reaction of three equivalents of SiMe$_2$Cl$_2$ with $^{3\text{-Et}}$I$^{\#}$Li (3-EtC$_9$Me$_5$LiH)[22] in an 83% yield. $^{3\text{-Et}}$I*SiMe$_2$Cl was then reacted with an equimolar amount of LiN(H)^{t}Bu and, following work up, ^{Me_2}SB($^{t\text{Bu}}$N,$^{3\text{-Et}}$I*)H$_2$ was isolated as a yellow oil in a quantitative yield. Reaction of the proligand with 2.2 equivalents of ^{n}BuLi yielded ^{Me_2}SB($^{t\text{Bu}}$N,$^{3\text{-Et}}$I*)Li$_2$ in a 58% yield. ^{Me_2}SB($^{t\text{Bu}}$N,$^{3\text{-Et}}$I*)Li$_2$ was then reacted with an equimolar amount of TiCl$_4$.2THF to yield ^{Me_2}SB($^{t\text{Bu}}$N,$^{3\text{-Et}}$I*)TiCl$_2$ in an 18% yield as a red solid (Equation 2.4)

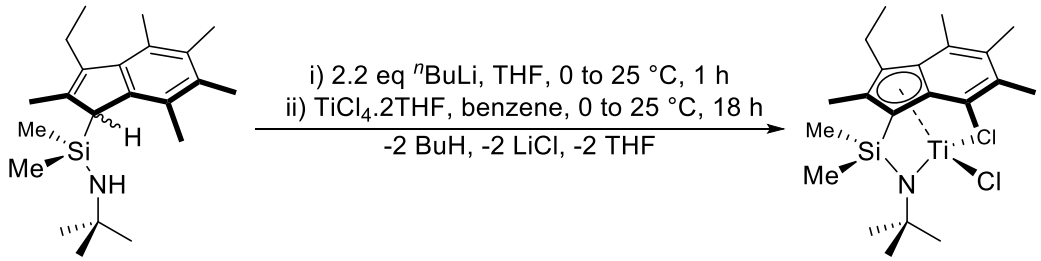

Equation 2.4. Synthetic route to ^{Me_2}SB($^{t\text{Bu}}$N,$^{3\text{-Et}}$I*)TiCl$_2$ from ^{Me_2}SB($^{t\text{Bu}}$N,$^{3\text{-Et}}$I*)H$_2$.

The ^{1}H NMR spectrum of ^{Me_2}SB($^{t\text{Bu}}$N,$^{3\text{-Et}}$I*)TiCl$_2$ (Figure 2.9) confirms the presence of only five I*-Me resonances in the range of 2.03 to 2.45 ppm. Three resonances are observed for the ethyl chain; a pair of multiplets at 3.34 and 3.03 ppm corresponding to the methylene protons, with the presence of both $^{2}J_{\text{H-H}}$ and $^{3}J_{\text{H-H}}$ coupling, and an apparent triplet corresponding to the methyl group as both sets of $^{3}J_{H\text{-H}}$ coupling is 7.6 Hz.

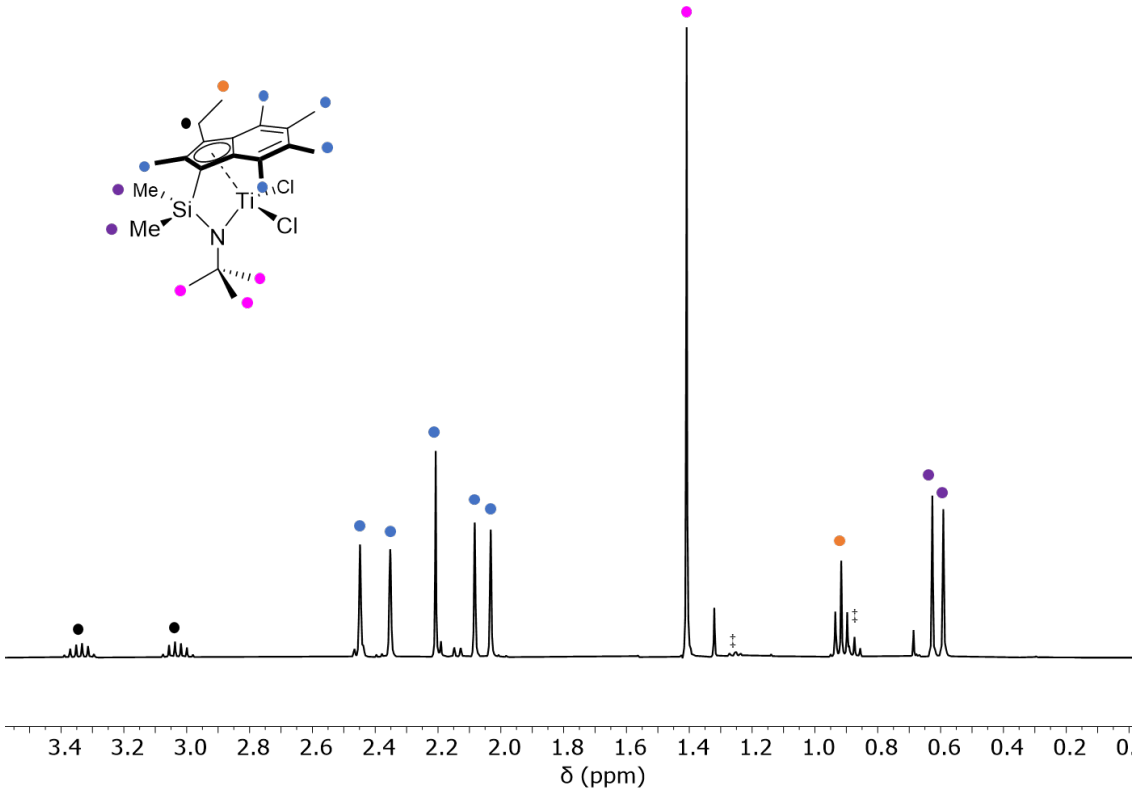

Figure 2.9. ^{1}H NMR spectrum of ^{Me_2}SB($^{t\text{Bu}}$N,$^{3\text{-Et}}$I*)TiCl$_2$ (d_6-benzene, 298 K and 400.2 MHz). Resonances at 0.85 and 1.25 ppm correspond to residual pentane (‡).

The I*-Me resonances are comparable to those of ^{Me_2}SB($^{t\text{Bu}}$N,I*)TiCl$_2$, from 2.04 to 2.56 ppm, with N-^{t}Bu resonance at 1.41 ppm. Rausch *et al*. reported a series of complexes ^{Me_2}SB($^{2,6\text{-Me}_2\text{C}_6\text{H}_3}$N,$^{3\text{-R}}$Cp)TiCl$_2$ where the Cp-H resonances vary from 6.75–7.21 ppm (R = H), to 6.55–6.89 ppm (R = CH$_2$Ph), 6.50–7.12 ppm (R = ^{t}Bu) and 6.49–6.93 ppm (R = Me), whilst the Me groups of the amido fragment are all observed between 2.01 and 2.07 ppm.[23] The polymerisation activities of these complexes followed the trend H > Me

> CH_2Ph > ^{t}Bu with activity variations being proposed to be due to steric rather than electronic effects.

2.2.4 Synthesis and characterisation of ^{Me,Pr}SB(^{tBu}N,I*)TiCl$_2$

I$^{\#}$Li (C_9Me_6HLi) was added dropwise to 1.5 equivalents of Si(Me,Pr)Cl_2 to yield I*Si(Me,Pr)Cl as a pale orange solid in a mixture of two diastereomers. I*Si(Me,Pr)Cl was then reacted with 1.05 equivalents of LiN(H)^{t}Bu and, following work up, ^{Me,Pr}SB(^{tBu}N,I*)H_2 was isolated as a mixture of two isomers. Addition of 2.2 equivalents of ^{n}BuLi to ^{Me,Pr}SB(^{tBu}N,I*)H_2 resulted in the formation of ^{Me,Pr}SB(^{tBu}N,I*)Li_2. ^{Me,Pr}SB(^{tBu}N,I*)Li_2 was reacted with an equimolar amount of $TiCl_4$.2THF (Equation 2.5). Following work up, an isomeric mixture ^{Me,Pr}SB(^{tBu}N,I*)$TiCl_2$ was afforded as red oily solid in 20% yield.

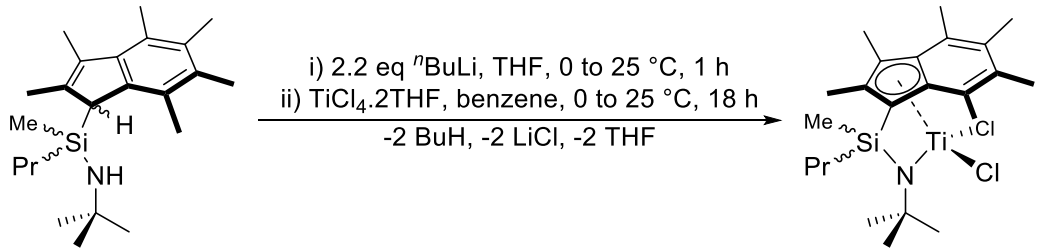

Equation 2.5. Synthetic route to ^{Me,Pr}SB(^{tBu}N,I*)$TiCl_2$.

In ^{Me,Pr}SB(^{tBu}N,I*)$TiCl_2$, the conformationally locked nature of the product leads to a pair of diastereomers in a 57:43 ratio as determined from the ^{1}H NMR spectrum (Figure A2.7). The I*-Me resonances are between 2.02 and 2.56 ppm. Both N-^{t}Bu resonances are observed at 1.42 ppm, the Si-Me resonances at 0.63 and 0.58 ppm, and the Si-Pr resonances between 1.74 and 1.04 ppm. The I*-Me and N-^{t}Bu resonances are similar to both ^{Me_2}SB(^{tBu}N,I*)$TiCl_2$ and ^{Me_2}SB(^{tBu}N,$^{3\text{-}Et}$I*)$TiCl_2$ (2.04–2.56 and 2.03–2.45 ppm, and 1.40 and 1.41 ppm respectively). Similarly for

^{R1R2}SB($^{2,7\text{-}t\text{Bu}}$Flu,I*)ZrCl$_2$ (R^1 = R^2 = Me or Et and R^1 = Me, R^2 = Pr) there are no large changes in the I*-Me resonances.[24]

2.2.5 Synthesis and characterisation of ^{Me2}SB($^{t\text{Bu}}$N,I*)ZrCl$_2$

^{Me2}SB($^{t\text{Bu}}$N,I*)Li$_2$ was reacted with an equimolar amount of ZrCl$_4$ to yield ^{Me2}SB($^{t\text{Bu}}$N,I*)ZrCl$_2$ in a 24% yield as a dark orange/brown solid following work up (Equation 2.6). The ^{1}H NMR spectrum contains the same diagnostic ligand resonances at comparable frequencies as found in the titanium analogue ^{Me2}SB($^{t\text{Bu}}$N,I*)TiCl$_2$ (Figure A2.8).

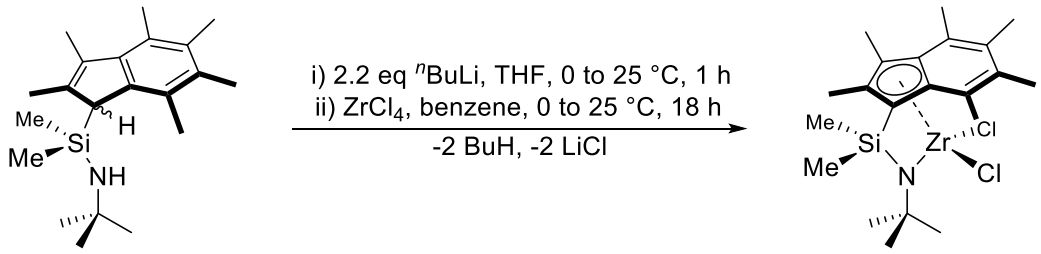

Equation 2.6. Synthetic route to ^{Me2}SB($^{t\text{Bu}}$N,I*)ZrCl$_2$.

2.2.6 Attempted synthesis of complexes

2.2.6.1 Attempted synthesis of ^{Me,Allyl}SB($^{t\text{Bu}}$N,I*)TiCl$_2$

Use of an Si(Me,Allyl) *ansa* bridge has previously been reported for a bispermethylindenyl zirconocene (^{Me,Allyl}SBI*ZrCl$_2$) and for a range of constrained geometry complexes ^{Me,Allyl}SB($^{t\text{Bu}}$N,$^{3\text{-}R}$Cp)TiCl$_2$ and ^{Me,Allyl}SB($^{t\text{Bu}}$N,$^{3\text{-}R}$I)TiCl$_2$.[25,26] The allylic fragment of the *ansa* bridge allows for an alternative route for immobilisation on a solid support, by binding to the *ansa* bridge, that, when combined with activation by alkylation of the metal centre, would allow for a more open metal centre that is proposed to lead to higher ethylene polymerisation activities, whilst being able to maintain the experimental advantages of heterogeneous-phase polymerisations.[27,28]

Both I*Si(Me,Allyl)Cl and ^{Me,Allyl}SB(^{tBu}N,I*)H$_2$ were prepared analogously to I*Si(Me,Pr)Cl and ^{Me,Pr}SB(^{tBu}N,I*)H$_2$; first, by reaction of I$^{\#}$Li with 1.5 equivalents of Si(Me,Allyl)Cl$_2$ and, following work up of I*Si(Me,Allyl)Cl, reaction with 1.1 equivalents of LiN(H)^{t}Bu to yield the proligand ^{Me,Allyl}SB(^{tBu}N,I*)H$_2$. Despite the addition of excess LiN(H)^{t}Bu, and longer reaction times (up to 72 hours), it was not possible to cleanly isolate the proligand without residual I*Si(Me,Allyl)Cl starting material. This can be observed in the ^{1}H NMR spectrum (Figure 2.10), where resonances can be observed at 0.25 and 0.04 ppm that correspond to the silylmethyl resonances of the starting material.

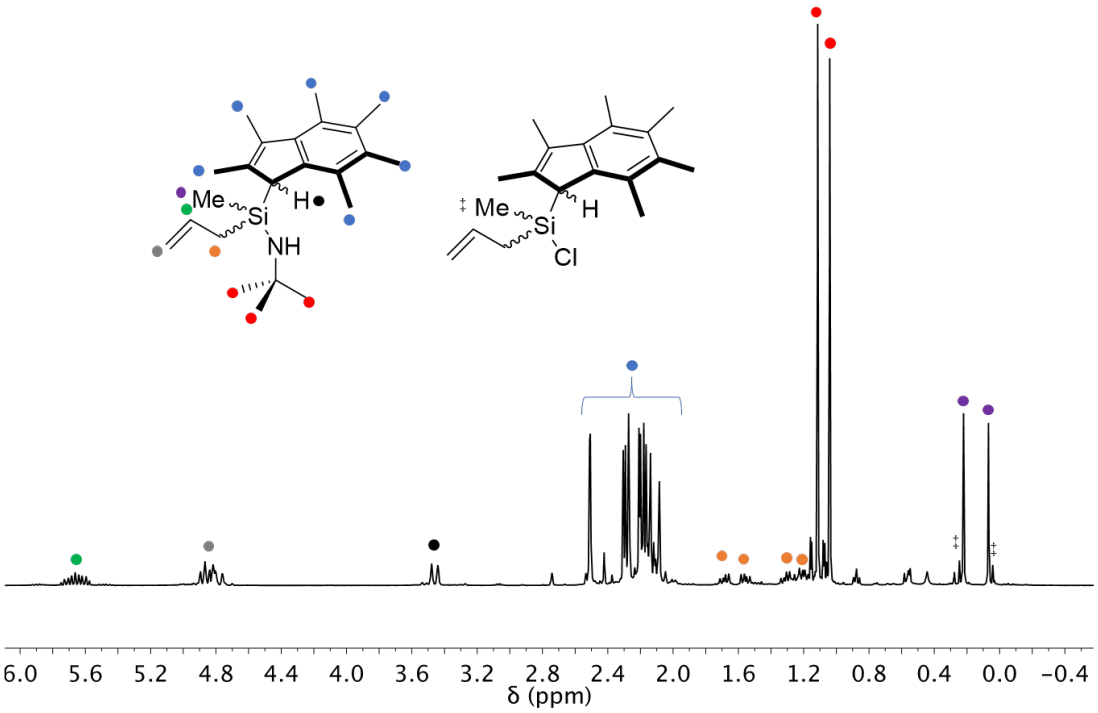

Figure 2.10. ^{1}H NMR spectrum of ^{Me,Allyl}SB(^{tBu}N,I*)H$_2$, residual I*Si(Me,Allyl)Cl can be observed in resonances at 0.25 and 0.04 ppm (d_6-benzene, 298 K, 400.2 MHz).

Further reaction with ^{n}BuLi resulted in the formation of ^{Me,Allyl}SB(^{tBu}N,I*)Li$_2$ and I$^{\#}$Li and reaction of this with TiCl$_4$.2THF resulted in a red oily solid that was an intractable mixture of products from which ^{Me,Allyl}SB(^{tBu}N,I*)TiCl$_2$ could not be isolated.

2.2.6.2 Attempted synthesis of $^{Ph}BB(^{tBu}N,I^*)TiCl_2$

Boron bridged constrained geometry complexes have previously been reported by Braunschweig and co-workers,[29,30] with these complexes shown to be efficient ethylene polymerisation catalysts. O'Hare and co-workers have previously synthesised both *rac*- and *meso*-$^{Ph}BBI^*ZrCl_2$, with high polymerisation activities reported when supported on LDHMAO. Activities of LDHMAO-*rac*-$^{Ph}BBI^*ZrCl_2$ are far in excess of those for LDHMAO-*rac*-$^{Me_2}SBI^*ZrCl_2$.[31] Work was therefore undertaken to synthesise the analogous I* CGC, $^{Ph}BB(^{tBu}N,I^*)TiCl_2$, to investigate whether these enhanced ethylene polymerisation activities could be maintained relative to the dimethylsilyl bridged complex $^{Me_2}SB(^{tBu}N,I^*)TiCl_2$.

I*BPhCl was synthesised by reaction of $I^{\#}Li$ with 1.5 equivalents of $BPhCl_2$, with the product isolated at pale yellow solid in a 15% yield; reaction with 1.05 equivalents of LiN(H)^{t}Bu yields $^{Ph}BB(^{tBu}N,I^*)H_2$ in a 27% yield. In the ^{1}H NMR spectrum, there is a shift to a lower frequency in the phenyl resonances from 8.05, 7.16 and 7.09 ppm in I*BPhCl to 7.20, 7.07 and 7.01 ppm in $^{Ph}BB(^{tBu}N,I^*)H_2$ (Figure 2.11). The I*-Me resonances are comparable, in the range of 1.87–2.50 ppm and 2.00–2.50 ppm for I*BPhCl and $^{Ph}BB(^{tBu}N,I^*)H_2$ respectively. In the proligand, resonances are observed at 1.29 and 0.89 ppm corresponding to the N-H and N-^{t}Bu protons respectively. In both cases, a single resonance is observed in the $^{11}B\{^1H\}$ NMR spectra, at 69 ppm for I*BPhCl and at 44 ppm for $^{Ph}BB(^{tBu}N,I^*)H_2$.

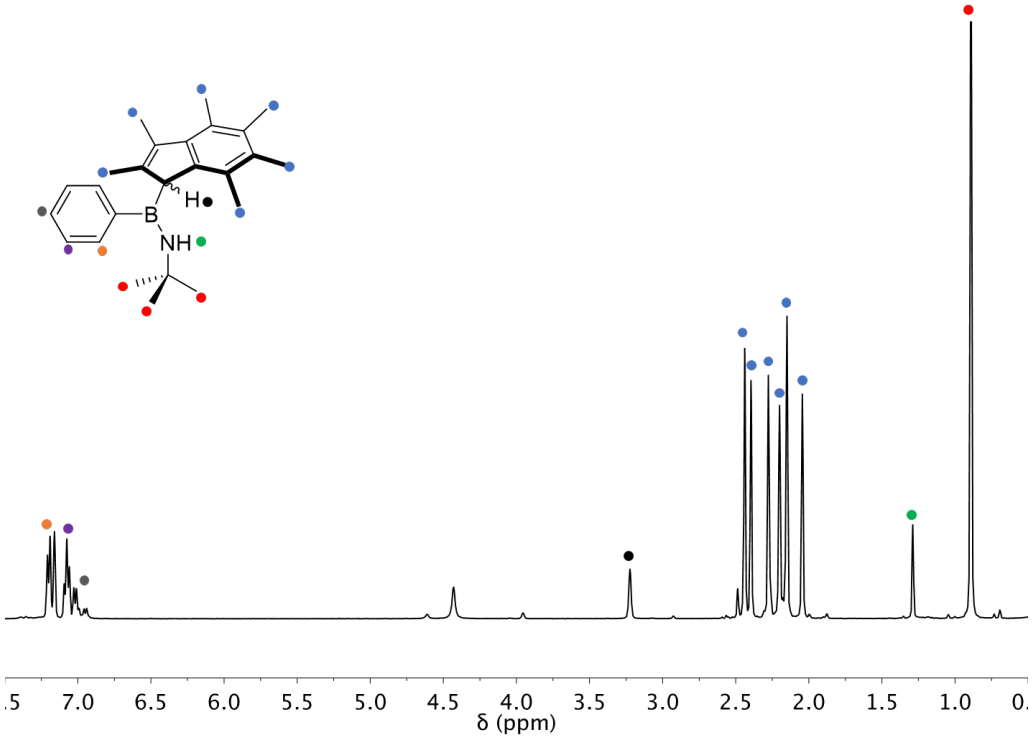

Figure 2.11. ^{1}H NMR spectrum of ^{Ph}BB($^{t\text{Bu}}$N,I*)H$_2$ (d_6-benzene, 298 K, 400.2 MHz).

Reaction with ^{n}BuLi in an attempt to synthesise the ligand ^{Ph}BB($^{t\text{Bu}}$N,I*)Li$_2$ resulted in cleavage of the B-I* bond with only I$^{\#}$Li observed in the ^{1}H NMR spectrum after work up. Further reactions were attempted with less basic potassium salt alternatives, potassium hexamethylsilazide (KHMDS) and potassium hydride (KH), on an NMR spectroscopy scale. KHMDS was insufficiently basic to deprotonate either the amido or I* fragment. Reaction with KH at 80 °C for 8 hours was initially proposed to form the monodeprotonated product ^{Ph}BB($^{t\text{Bu}}$N,I*)KH, where the amido group was deprotonated. However, further work has suggested that what is instead formed is the dianionic product ^{Ph,H}BB($^{t\text{Bu}}$N,I*)K$_2$H.[32]

2.3 Reaction of permethylindenyl CGCs with MAO

In an attempt to gain an insight into the nature of the active species for ethylene polymerisation, ^{Me_2}SB($^{t Bu}$N,I*)TiCl$_2$ and ^{Me_2}SB($^{t Bu}$N,I*)Ti(Cl)CH$_2$SiMe$_3$ were reacted with methylaluminoxane (MAO) on an NMR spectroscopic scale. The ^{1}H NMR spectra for the reaction of ^{Me_2}SB($^{t Bu}$N,I*)TiCl$_2$ with 1, 2, 5 and 10 equivalents of MAO are shown in Figure 2.12.

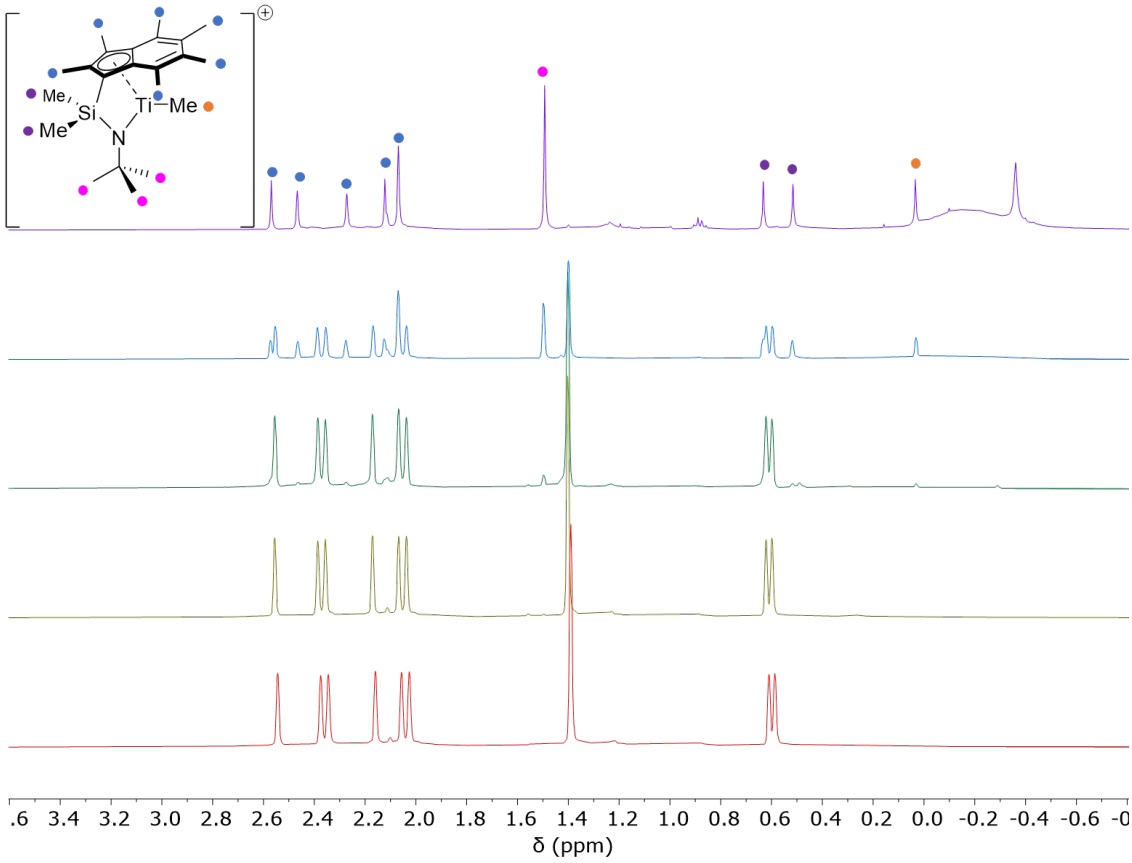

Figure 2.12. ^{1}H NMR spectra of the reaction of ^{Me_2}SB($^{t Bu}$N,I*)TiCl$_2$ with from bottom to top: 0 (red), 1 (gold), 2 (green), 5 (blue) and 10 (purple) equivalents of MAO (d_6-benzene, 298 K, 400.2 MHz).

With addition of increasing amounts of MAO to both ^{Me_2}SB($^{t Bu}$N,I*)TiCl$_2$ (Figure 2.12) and ^{Me_2}SB($^{t Bu}$N,I*)Ti(Cl)CH$_2$SiMe$_3$ (Figure A2.9), growth of a new species is observed in the ^{1}H NMR spectra, with resonances at 2.07, 2.12, 2.27, 2.47 and 2.57 ppm corresponding to the I*-Me resonances, and at 1.49, 0.52 and 0.63 ppm corresponding to

the N-^{t}Bu and two Si-Me resonances respectively. There is growth of a broad resonance from 0.1 to –0.5 ppm and a sharper resonance at –0.36 ppm, both of which are attributable to MAO. Finally, there is a resonance at 0.03 ppm, which is proposed to be a Ti-Me resonance from the formation of a cationic species [^{Me_2}SB($^{t Bu}$N,I*)TiMe]$^+$. In the reaction of MAO with ^{Me_2}SB($^{t Bu}$N,I*)Ti(Cl)CH_2SiMe_3, the pair of doublets of the CH_2Si protons become a single resonance at −0.82 ppm and this is proposed to be due to coordination of the leaving group to MAO and the formation of the counteranionic species [Me_3SiCH_2-MAO]$^-$. Similarly, it is proposed that reaction of MAO with ^{Me_2}SB($^{t Bu}$N,I*)$TiCl_2$ results in the formation of an [^{Me_2}SB($^{t Bu}$N,I*)TiMe][Cl-MAO] ion pair. It is broadly accepted within the literature that addition of an MAO cocatalyst to a metallocene type complex results in the formation a similar, catalytically-active, metal-alkyl cationic species with a weakly coordinating anion.[33,34] Addition of 1 bar ethylene resulted in the formation of polyethylene in the NMR tube, and no decomposition was observed with heating at 70 °C for 30 minutes.

2.4 Immobilisation of complexes for slurry-phase ethylene polymerisation

2.4.1 Immobilisation of complexes on a solid support

The solid support plays a key role in the polymerisation activity of a complex, as well as in polymer properties including molecular weight, molecular weight distribution, and polymer morphology.[35] The use of many common inorganic solid supports have been previously reported,[36–40] with one of the most commonly used being silica.[35,41,42] Many of these solid supports require pre-treatment with an alkylaluminium species, such as MAO, to activate them.[35] MAO has been shown to primarily chemisorb onto surface hydroxyl groups, leading to highly Lewis acidic sites.[43] The site can then interact with metallocene-based precatalysts to form a cation-anion pair, for example ([Cp^R_2M-Me][MAO-X]), active for polymerisation catalysis.[44] Solid polymethylaluminoxane (sMAO) is a modified, polymerised methylaluminoxane, insoluble in many common inorganic solid supports that was developed by Kaji *et al*. at Tosoh Finechem Corporation (Japan).[45] A laboratory procedure for an optimised synthesis of sMAO has since been developed and the nature of the support studied.[46] sMAO-supported complexes have been shown to be highly efficient ethylene polymerisation catalysts with activities far in excess of those on other common inorganic supports such as MAO-modified silica (SSMAO) and MAO-modified LDH (LDHMAO).[24,46]

2.4.2 Immobilisation of complexes on sMAO

The synthesised complexes were supported on sMAO in initial $[Al]_0$:$[Ti]_0$ ratios of 200:1 or 100:1. sMAO and the chosen complex were combined and swirled in toluene at 60 °C

for one hour (Equation 2.7). A brown solid was allowed to settle from a colourless solution (Figure A2.10). The solution was decanted and the brown solid dried under vacuum to yield the sMAO-supported complex in isolated yields of 71–87%.

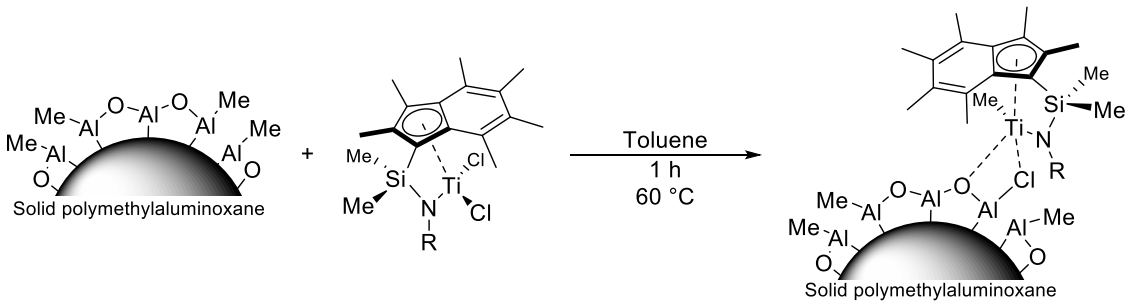

Equation 2.7. Reaction of ^{Me_2}SB(^{R}N,I*)TiCl$_2$ with sMAO. Supported complex is a schematic illustration.

^{13}C CP-MAS NMR spectroscopy was used to characterise a range of sMAO-supported complexes (Figures 2.13 and 2.14, A2.11, A2.12, A2.14, A2.16, A2.18, A2.20, A2.22 and A2.24). Whilst the resonances attributed to the surface supported complex are weak relative to the bulk sMAO (with resonances attributable to sMAO at –8, 128 and 180 ppm), it is possible to tentatively assign resonances to the supported complex by comparison with the solution-phase ^{13}C{^{1}H} NMR spectra. The resonances within the region of 125–140 ppm are due to the aromatic carbons of the I* ring. The resonance in the region of 10–20 ppm corresponds to the methyl carbons of the I* ring. sMAO-^{Me_2}SB($^{t\text{Bu}}$N,I*)TiCl$_2$ shows a resonance at 33 ppm, corresponding to the ^{t}Bu amido group.

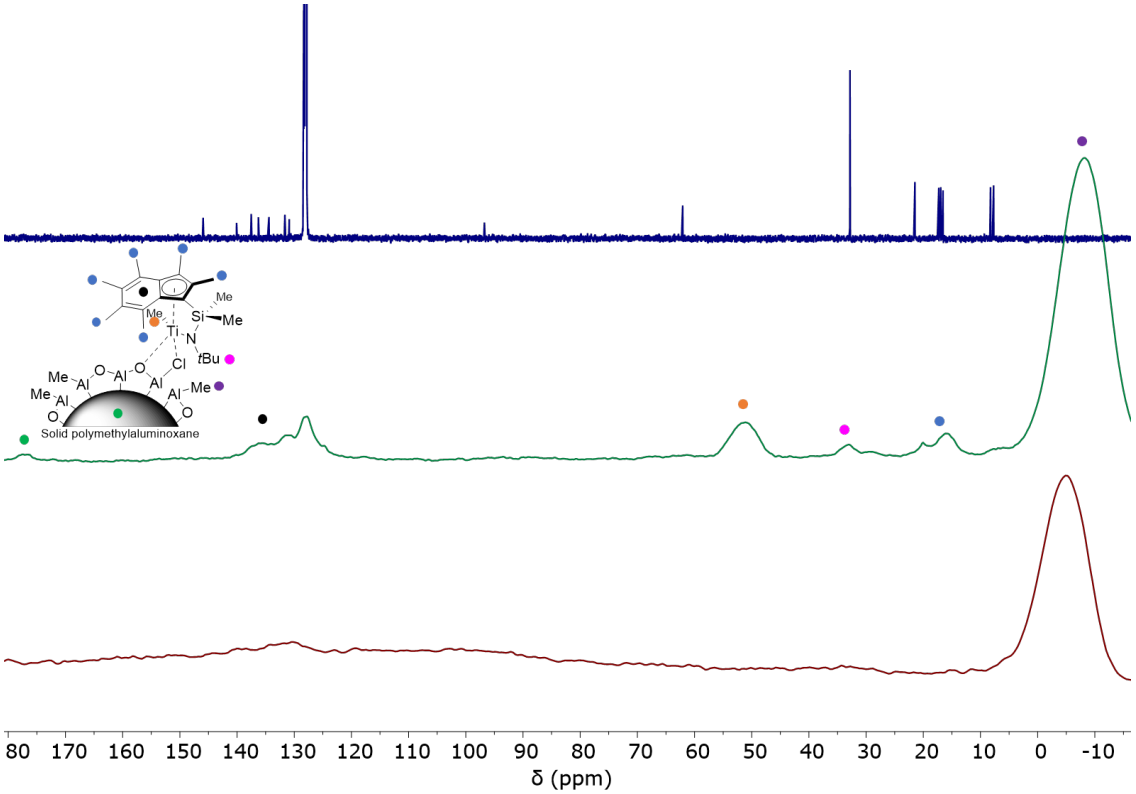

Figure 2.13. Stack plot of (top) $^{13}C\{^{1}H\}$ NMR spectrum of $^{Me_2}SB(^{tBu}N,I^*)TiCl_2$ (d_6-benzene, 125.7 MHz, 298 K), (middle) ^{13}C CP-MAS (100.6 MHz) NMR spectrum of sMAO-$^{Me_2}SB(^{tBu}N,I^*)TiCl_2$ and (bottom) ^{13}C CP-MAS (100.6 MHz) NMR spectrum of sMAO.

Comparison of the ^{13}C CP-MAS NMR spectra of sMAO-$^{Me_2}SB(^{tBu}N,I^*)TiR_2$ (R = CH_2Ph, Me and CH_2SiMe_3) and sMAO-$^{Me_2}SB(^{tBu}N,I^*)Ti(Cl)CH_2SiMe_3$ are shown in Figure 2.14. The resonance at 50 ppm in the spectra may correspond to a Ti-Me resonance (typically observed in the region 45–60 ppm for Cp_2TiMeX complexes) and is in good agreement with the Ti-Me resonances in the solution $^{13}C\{^{1}H\}$ NMR spectrum of $^{Me_2}SB(^{tBu}N,I^*)TiMe_2$.[19,47] This would indicate partial or total methylation of the metal centre, as has been observed by reactions with MAO in Section 2.3. This has been hypothesised to occur both for sMAO-supported complexes, and in solution when metallocene complexes are activated with a MAO cocatalyst.[48] The $[Al]_0$:$[Ti]_0$ ratios were calculated by inductively coupled plasma mass spectrometry (ICP-MS) and inductively coupled plasma optical emission spectrometry (ICP-OES) for sMAO-$^{Me_2}SB(^{tBu}N,I^*)TiCl_2$ and sMAO-$^{Me_2}SB(^{iPr}N,I^*)TiCl_2$; both indicated full

immobilisation of the complexes, and no leaching of the supported catalyst was observed over 3 hours in slurry (Table A2.1).

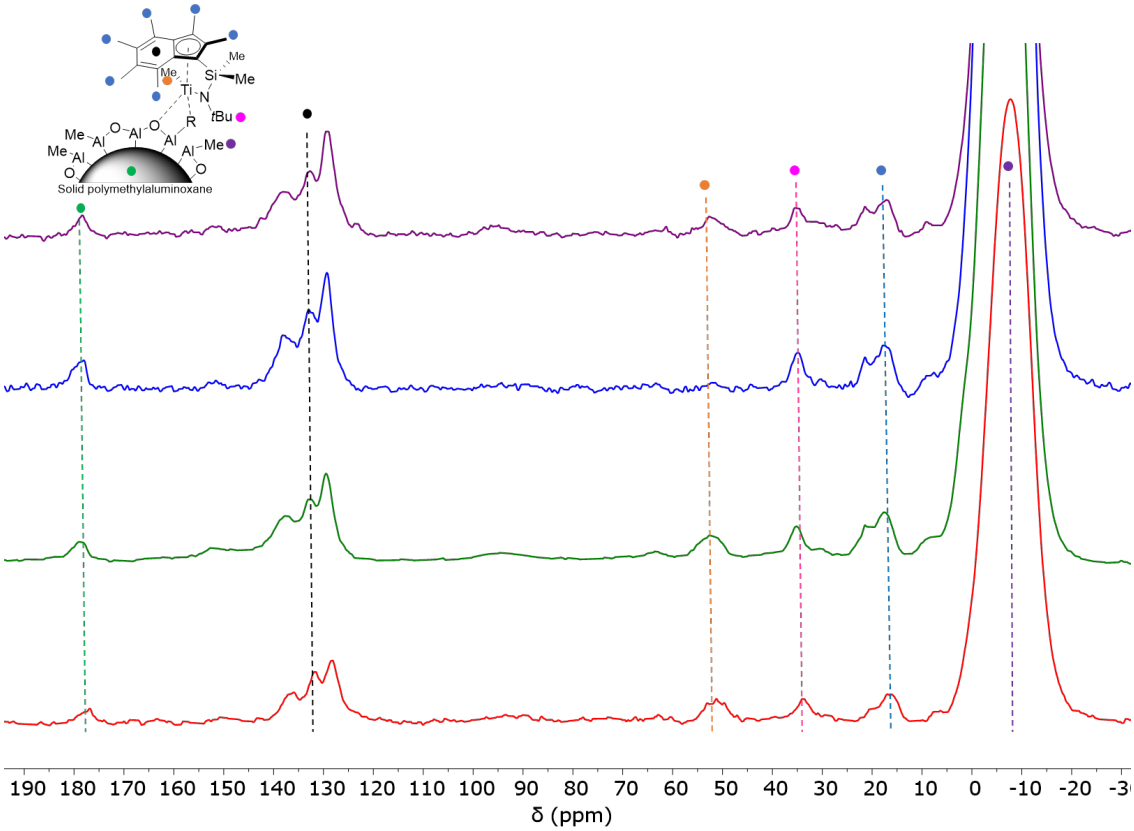

Figure 2.14. ^{13}C CP-MAS (100.6 MHz) NMR spectra of (purple) sMAO-^{Me2}SB(^{tBu}N,I*)Ti($CH_2Ph)_2$, (blue) sMAO-^{Me2}SB(^{tBu}N,I*)$TiMe_2$, (green) sMAO-^{Me2}SB(^{tBu}N,I*)Ti($CH_2SiMe_3)_2$ and (red) sMAO-^{Me2}SB(^{tBu}N,I*)Ti(Cl)CH_2SiMe_3.

All supported complexes show a broad resonance in the ^{27}Al DP-MAS hahnecho NMR spectra (Figure A2.32), indicative of the highly amorphous nature of the sMAO support. In the ^{29}Si CP-MAS NMR spectrum (Figures A2.13, A2.15, A2.17), the complexes all show a resonance at approximately −19 ppm, corresponding to *ansa* bridging silicon in the ligand backbone. In addition, the ^{29}Si CP-MAS NMR spectra of both sMAO-^{Me2}SB(^{tBu}N,I*)Ti($CH_2SiMe_3)_2$ and sMAO-^{Me2}SB(^{tBu}N,I*)Ti(Cl)CH_2SiMe_3 have an extra resonance at 0 ppm respectively (Figures A2.21 and A2.19); attributed to the CH_2SiMe_3 initiator groups that remain bound to the surface of the sMAO particle once the metal centre has been methylated.

2.4.3 Immobilisation of complexes on LDHMAO and SSMAO

The layered double hydroxide (LDH), $Mg_3Al\text{-}CO_3$, was prepared by Drs. Chunping Chen, Hongri (Clara) Suo and Miss Meng Lyu, and silica (PQ E70X) purchased from PQ Corporation. Prior to MAO modification the solids were calcined to remove any residual water that may have chemisorbed/physisorbed to the surface or in between the layers; $Mg_3Al\text{-}CO_3$ was calcined under vacuum at 150 °C for 6 hours, and silica was calcined under vacuum at 600 °C for 6 hours. To the calcined LDH was added MAO (40 wt%), the mixture was swirled in 50 mL toluene at 80 °C for 2 hours and then dried under vacuum. SSMAO was prepared from calcined silica in an analogous manner.

^{Me2}SB($^{t Bu}$N,I*)TiCl$_2$ and LDHMAO were mixed in a variety of ratios ([Al$_{MAO}$]$_0$:[Ti]$_0$ = 50:1, 100:1 and 200:1), whilst ^{Me2}SB($^{t Bu}$N,$^{3\text{-}Et}$I*)TiCl$_2$, ^{Me,Pr}SB($^{t Bu}$N,I*)TiCl$_2$ and ^{Me2}SB($^{t Bu}$N,I*)Ti(Cl)CH$_2$SiMe$_3$ were mixed with LDHMAO in an [Al$_{MAO}$]$_0$:[Ti]$_0$ ratio of 200:1. To this was added 30 mL of toluene and the mixture was swirled at 60 °C for 1 hour (Equation 2.8). The mixture was allowed to settle, yielding a coloured solid and a clear, colourless solution. The solution was decanted away and the solid dried under vacuum. The four complexes and SSMAO were mixed in an [Al$_{MAO}$]$_0$:[Ti]$_0$ ratio of 200:1, with immobilisation carried out using an analogous method.

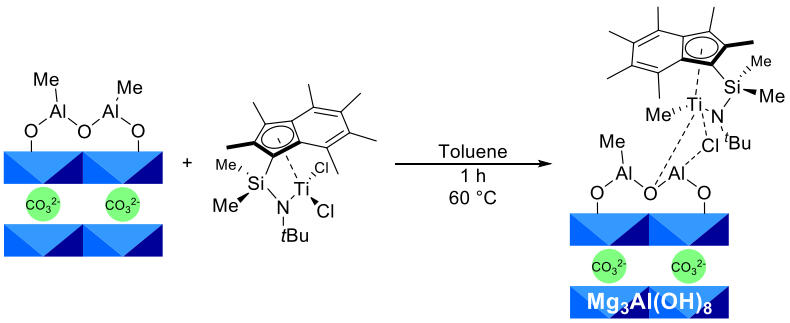

Equation 2.8. Reaction of ^{Me2}SB($^{t Bu}$N,I*)TiCl$_2$ on LDHMAO. Supported complex is a schematic illustration.

In the solid-state ^{13}C CP-MAS NMR spectra of the LDHMAO supported complexes (Figures 2.15, A2.27, A2.29 and A2.31), resonances attributable to LDHMAO are observed at −8 and 165 ppm. As with the ^{13}C CP-MAS NMR spectra of the sMAO-supported complexes it is possible to assign resonances at approximately 20 and 130 ppm to both the I*-Me and I* aromatic carbons respectively whilst the resonances at 32 ppm correspond to the N-^{t}Bu carbons of the supported complex. With the exception of LDHMAO-^{Me_2}SB(^{tBu}N,I*)TiCl$_2$, the other three supported complexes have a resonance at 50 ppm. This, as with the sMAO supported complexes, is proposed to be attributable to a Ti-Me species that is formed on support and activation of the complex.

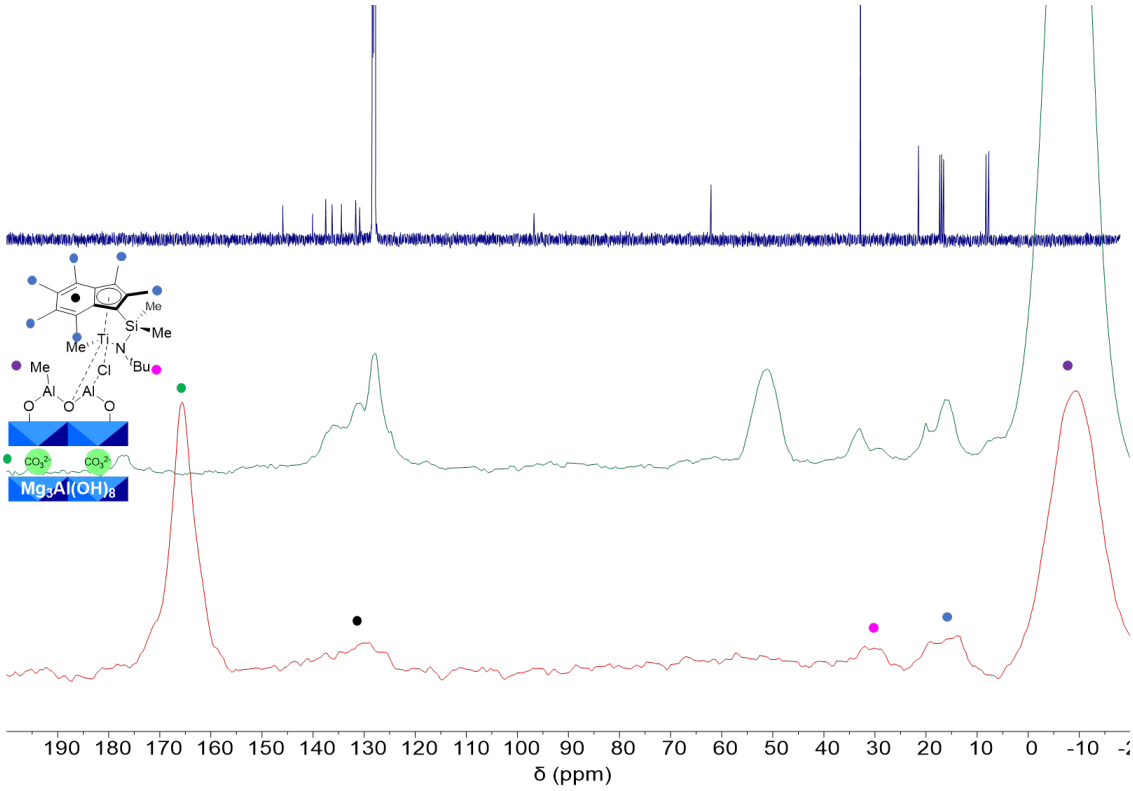

Figure 2.15. Stack plot of (top) $^{13}C\{^{1}H\}$ NMR spectrum of ^{Me_2}SB(^{tBu}N,I*)TiCl$_2$ (d_6-benzene, 125.7 MHz, 298 K), (middle) ^{13}C CP-MAS (100.6 MHz) NMR spectrum of sMAO-^{Me_2}SB(^{tBu}N,I*)TiCl$_2$ and (bottom) ^{13}C CP-MAS (100.6 MHz) NMR spectrum of LDHMAO-^{Me_2}SB(^{tBu}N,I*)TiCl$_2$.

A sharp single resonance is observed at −8 ppm in the ^{27}Al hahnecho spectra (Figure A2.33), which was sharper than the corresponding resonances for the sMAO

supported complexes due to the more ordered nature of LDHMAO. The ^{29}Si DP-MAS spectrum of LDHMAO-^{Me2}SB($^{t\text{Bu}}$N,I*)Ti(Cl)SiMe$_3$ (Figure A2.30) has two resonances at 0 and −79 ppm, one being assigned to the *ansa* bridge of the supported complex, and the other proposed to be due to the CH_2SiMe_3 group that remains coordinated to the solid support on immobilisation of the complex. ICP-MS studies of LDHMAO-^{Me2}SB($^{t\text{Bu}}$N,I*)TiCl$_2$ confirm the loading levels at $[Al]_0$:$[Ti]_0$ ratios of 200:1 to 100:1 providing evidence that there is complete immobilisation of the complex in both cases. Lower support levels were observed for $[Al]_0$:$[Ti]_0$ = 50:1 where a ratio of 67:1 is observed.

2.5 Conclusions

Eleven constrained geometry complexes have been synthesised with variation of the amido fragment, permethylindenyl ring, *ansa* bridge and the metal centre with yields up to 25%. The complexes have been characterised by NMR spectroscopy, elemental analysis and IR spectroscopy; six complexes have been isolated as single crystals and their solid state molecular structures determined by single crystal X-ray diffraction studies. From the solid state structures, alkylation of the metal centre has been shown to increase both the Ti-N and Ti-Cp_{cent} bond lengths.

These complexes have been immobilised on sMAO and the supported complexes characterised by solid-state NMR spectroscopy and metal ratios determined by ICP-MS and ICP-OES analysis showing complete immobilisation and no leaching of the complex in slurry. Four complexes were supported on SSMAO and LDHMAO for slurry-phase ethylene polymerisation studies.

The reaction of ^{Me2}SB($^{t Bu}$N,I*)$TiCl_2$ and ^{Me2}SB($^{t Bu}$N,I*)Ti(Cl)CH_2SiMe_3 with MAO has shown the formation of the cationic species [^{Me2}SB($^{t Bu}$N,I*)TiMe]$^+$ in both cases, probably coupled with a weakly coordinating anion [X-MAO]$^-$; evidence of the formation of [Me_3SiCH_2-MAO]$^-$ was observed in the NMR spectrum for the reaction of ^{Me2}SB($^{t Bu}$N,I*)Ti(Cl)CH_2SiMe_3 with MAO. This, coupled with the solid state NMR spectra of the supported complexes and previous research in this field, would suggest the formation of a methyl cationic species when the complex is immobilised on the solid support. From the results observed from the reaction of ^{Me2}SB($^{t Bu}$N,I*)Ti(Cl)CH_2SiMe_3 with MAO and the ^{29}Si ssNMR for sMAO-supported mono and bisneosilyl complexes, it is expected that the initiator group remains bound the solid support.

2.6 References

1 J. Cano and K. Kunz, *J. Organomet. Chem.*, 2007, **692**, 4411–4423.
2 J. Okuda, *Chem. Ber.*, 1990, **123**, 1649–1651.
3 J. Okuda, F. J. Schattenmann, S. Wocadlo and W. Massa, *Organometallics*, 1995, **14**, 789–795.
4 L. Duda, G. Erker, R. Fröhlich and F. Zippel, *Eur. J. Inorg. Chem.*, 1998, **1998**, 1153–1162.
5 H. V. Rasika Dias, Z. Wang and S. G. Bott, *J. Organomet. Chem.*, 1996, **508**, 91–99.
6 G. A. Luinstra and J. H. Teuben, *J. Chem. Soc., Chem. Commun.*, 1990, 1470–1471.
7 F. Amor and J. Okuda, *J. Organomet. Chem.*, 1996, **520**, 245–248.
8 A. K. Hughes, A. Meetsma and J. H. Teuben, *Organometallics*, 1993, **12**, 1936–1945.
9 S. Ciruelos, T. Cuenca, R. Gómez, P. Gómez-Sal, A. Manzanero and P. Royo, *Organometallics*, 1996, **15**, 5577–5585.
10 L. Falivene, R. Credendino, A. Poater, A. Petta, L. Serra, R. Oliva, V. Scarano and L. Cavallo, *Organometallics*, 2016, **35**, 2286–2293.
11 J. Okuda, S. Verch, T. P. Spaniol and R. Stürmer, *Chem. Ber.*, 1996, **129**, 1429–1431.
12 J. Klosin, W. J. Kruper, P. N. Nickias, G. R. Roof, P. De Waele and K. A. Abboud, *Organometallics*, 2001, **20**, 2663–2665.
13 J. Okuda, K. E. Du Plooy, W. Massa, H. Kang and U. Rose, *Chem. Ber.*, 1996, **129**, 275–277.
14 S. Liu, A. Motta, A. R. Mouat, M. Delferro and T. J. Marks, *J. Am. Chem. Soc.*, 2014, **136**, 10460–10469.
15 T. Liu, *Pol. J. Chem.*, 2001, **75**, 1371–1375.
16 C. Paniagua, M. E. G. Mosquera, H. Jacobsen, G. Jiménez and T. Cuenca, *Organometallics*, 2009, **28**, 6975–6980.
17 M. Kamigaito, T. K. Lal and R. M. Waymouth, *J. Polym. Sci. Part A Polym. Chem.*, 2000, **38**, 4649–4660.
18 D. W. Carpenetti, L. Kloppenburg, J. T. Kupec and J. L. Petersen, *Organometallics*, 1996, **15**, 1572–1581.
19 A. D. H. Smith, Part II Thesis, University of Oxford, 2018.
20 K. Nishii, T. Ikeda, M. Akita and T. Shiono, *J. Mol. Catal. A Chem.*, 2005, **231**, 241–246.
21 J. C. Stevens and D. Neithamer, 1991, EP418044A2.
22 P. Angpanitcharoen, G. Hay, J.-C. Buffet, Z. R. Turner, T. A. Q. Arnold and D. O'Hare, *Polyhedron*, 2016, **116**, 216–222.
23 B. Rhodes, J. C. W. Chien, J. S. Wood, A. Chandrasekaran and M. D. Rausch, *Appl. Organomet. Chem.*, 2002, **16**, 323–330.
24 J.-C. Buffet, Z. R. Turner and D. O'Hare, *Chem. Commun.*, 2018, **54**, 10970–10973.
25 C. J. Miller and D. O'Hare, *Chem. Commun.*, 2004, 1710.
26 A. Reb and H. G. Alt, *J. Mol. Catal. A Chem.*, 2001, **174**, 35–49.
27 A. B. Vázquez and P. Royo, *J. Organomet. Chem.*, 2003, **671**, 172–178.
28 H. Braunschweig and F. M. Breitling, *Coord. Chem. Rev.*, 2006, **250**, 2691–2720.

29 H. Braunschweig, C. von Koblinski and U. Englert, *Chem. Commun.*, 2000, 1049–1050.
30 H. Braunschweig, F. M. Breitling, C. von Koblinski, A. J. P. White and D. J. Williams, *Dalton Trans.*, 2004, 938–943.
31 G. E. Hickman, C. M. R. Wright, A. F. R. Kilpatrick, Z. R. Turner, J.-C. Buffet and D. O'Hare, *Mol. Catal.*, 2019, **468**, 139–147.
32 C. Collins Rice, Part II Thesis, University of Oxford, 2019.
33 H. H. Brintzinger, D. Fischer, R. Müllhaupt, B. Rieger and R. M. Waymouth, *Angew. Chem. Int. Ed.*, 1995, **34**, 1143–1170.
34 M. Bochmann, *J. Chem. Soc. Dalt. Trans.*, 1996, 255–270.
35 J. R. Severn, J. C. Chadwick, R. Duchateau and N. Friederichs, *Chem. Rev.*, 2005, **105**, 4073–4147.
36 E. V. Ramos-Fernández, A. Sepúlveda-Escribano and F. Rodríguez-Reinoso, *Catal. Commun.*, 2008, **9**, 1243–1246.
37 J.-C. Buffet, Z. R. Turner, R. T. Cooper and D. O'Hare, *Polym. Chem.*, 2015, **6**, 2493–2503.
38 J.-C. Buffet, C. F. H. Byles, R. Felton, C. Chen and D. O'Hare, *Chem. Commun.*, 2016, **52**, 4076–4079.
39 P. A. Zapata, C. Belver, R. Quijada, P. Aranda and E. Ruiz-Hitzky, *Appl. Catal. A Gen.*, 2013, **453**, 142–150.
40 H. Rahiala, I. Beurroies, T. Eklund, K. Hakala, R. Gougeon, P. Trens and J. B. Rosenholm, *J. Catal.*, 1999, **188**, 14–23.
41 P. Wongwaiwattanakul and B. Jongsomjit, *Catal. Commun.*, 2008, **10**, 118–122.
42 J.-C. Buffet, T. A. Q. Arnold, Z. R. Turner, P. Angpanitcharoen and D. O'Hare, *RSC Adv.*, 2015, **5**, 87456–87464.
43 V. N. Panchenko, N. V. Semikolenova, I. G. Danilova, E. A. Paukshtis and V. A. Zakharov, *J. Mol. Catal. A Chem.*, 1999, **142**, 27–37.
44 E. Y.-X. Chen and T. J. Marks, *Chem. Rev.*, 2000, **100**, 1391–1434.
45 E. Kaji and E. Yoshioka, 2010, WO2010055652.
46 A. F. R. Kilpatrick, J.-C. Buffet, P. Nørby, N. H. Rees, N. P. Funnell, S. Sripothongnak and D. O'Hare, *Chem. Mater.*, 2016, **28**, 7444–7450.
47 K. P. Bryliakov, E. P. Talsi and M. Bochmann, *Organometallics*, 2004, **23**, 149–152.
48 S. Collins, M. Linnolahti, M. G. Zamora, H. S. Zijlstra, M. T. Rodríguez Hernández and O. Perez-Camacho, *Macromolecules*, 2017, **50**, 8871–8884.

Chapter 3

Constrained geometry complexes for ethylene homopolymerisation

3.1 Introduction

3.1.1 Overview

Since the pioneering work of Ziegler and Natta, ethylene polymerisation has been of great academic and industrial interest,[1,2] with global polyethylene consumption reaching 96 million tons in 2016.[3] While the majority of polyethylene-based polymers are still produced by Ziegler–Natta type catalysts, there has been a small shift towards production of polymers by metallocene-type molecular catalysts. This is due to greater control of polymer microstructure,[4] and the ability to incorporate higher levels of α-olefins.[5] A further advantage of these systems is the narrow molecular weight distributions of the polymer produced and chemical homogeneity through the polymers.[5]

Constrained geometry complexes (CGCs) are highly tuneable and variation of the complex components can dramatically influence polymerisation activities.[6] Waymouth *et al.* and Nomura *et al.* have both demonstrated that increasing the electron donating nature of the amido group results in enhanced polymerisation activities.[7,8] Moving down group 4 has also been shown to decrease ethylene polymerisation activities,[9–11] in contrast to bis(Cp) group 4 complexes.[12] Rausch *et al.* reported the synthesis of $^{Me_2}SB(^{t Bu}N,^{3\text{-}R}Cp)TiCl_2$ (R = H, Me, ^{t}Bu and CH_2Ph) with ethylene polymerisation activities following the trend H > Me > ^{t}Bu > CH_2Ph.[13] Variation of the initiator group also affects polymerisation activity; for the complexes $^{Me_2}SB(^{t Bu}N,Cp^*)TiX_2$ (X = CH_2Ph

and Me) reported by Chen and Marks, higher activities were reported for the dibenzyl complex than the dimethyl complex.[14]

3.1.2 Ultra-high molecular weight polyethylene (UHMWPE)

One advantage of constrained geometry complexes is their ability to produce polyethylenes with very high molecular weights (M_w), often in excess of 1000 kDa.[14,15] Modification of the inorganic support used in slurry-phase ethylene polymerisation not only affects polymerisation activity, but also the properties of the polymer produced, notably morphology and molecular weights.[16] Notably, the use of methylaluminoxane (MAO)-modified silica (SSMAO) or MAO-modified layered double hydroxide (LDHMAO) as a support results in higher polymer molecular weights, but lower polymerisation activities, than using solid polymethylaluminoxane (sMAO) as a support.[17,18] UHMWPE is used to describe polymers with M_w values in excess of 3000 kDa, with the long polymer chain serving to transfer load more effectively resulting in a material with the highest impact strength of any thermoplastic currently produced.[19] The extremely low moisture absorption, very low friction coefficient, high levels of crystallinity (up to 85%) and self-lubricating nature has led to a number of uses including: impact resistant materials in the military, fishing lines and materials in maritime usage.[19] It is also of great medical interest, with UHMWPE being used in one half of total joint replacements, particularly in hips and knees, with joint lifetimes of 15–20 years commonly attained.[20]

3.1.3 Hydrogen response

Addition of hydrogen to a polymerisation reaction typically results in a decrease in polymer molecular weights due to an increase in chain termination facilitated by hydrogen acting as a chain transfer agent.[21] In addition, it often results in lower

polymerisation activities due to the formation of a metal hydride species from chain transfer requiring reactivation by propagation,[21–23] or a dormant bimetallic resting state that requires reactivation to form the active cationic methyl species.[24,25] This allows the possibility to target ultra-low molecular weight polyethylene (ULMWPE), also known as PE wax, with polymer molecular weights below 10 kDa. PE wax finds applications in areas such as asphalt, electric cable, coatings and plastics.[26]

3.1.4 Chapter synopsis

This chapter investigates the use of fourteen constrained complexes as slurry-phase ethylene polymerisation catalysts and the effect of various structural modifications on ethylene polymerisation activities. The effect of the choice and amount of scavenger used on ethylene polymerisation was also investigated. The nature of the inorganic solid support was also varied, from sMAO to SSMAO and LDHMAO, with the aim of forming UHMWPE while maintaining high polymerisation activities and narrow molecular weight dispersities. Six of the most promising catalysts were tested in high-throughput polymerisations, with the response to hydrogen addition also studied. sMAO-^{Me_2}SB($^{t Bu}$N,I*)TiCl$_2$, sMAO-^{Me_2}SB($^{t Bu}$N,I*)Ti(CH$_2$Ph)$_2$ and sMAO-^{Me_2}SB($^{t Bu}$N,I*)TiMe$_2$ were also tested for large scale polymerisation applications at SCG Chemicals Co., Ltd. (Rayong, Thailand).

3.2 Variation of the constrained geometry complex

3.2.1 Effect of variation of the amido fragment on slurry-phase ethylene polymerisation

Seven sMAO-supported complexes were studied for ethylene polymerisation with various amido fragments (Figure 3.1); variation in temperature and time were performed (Figures 3.2 and A3.1, and Tables A3.1 and A3.2). The catalysts were prepared as described in 2.4.2.

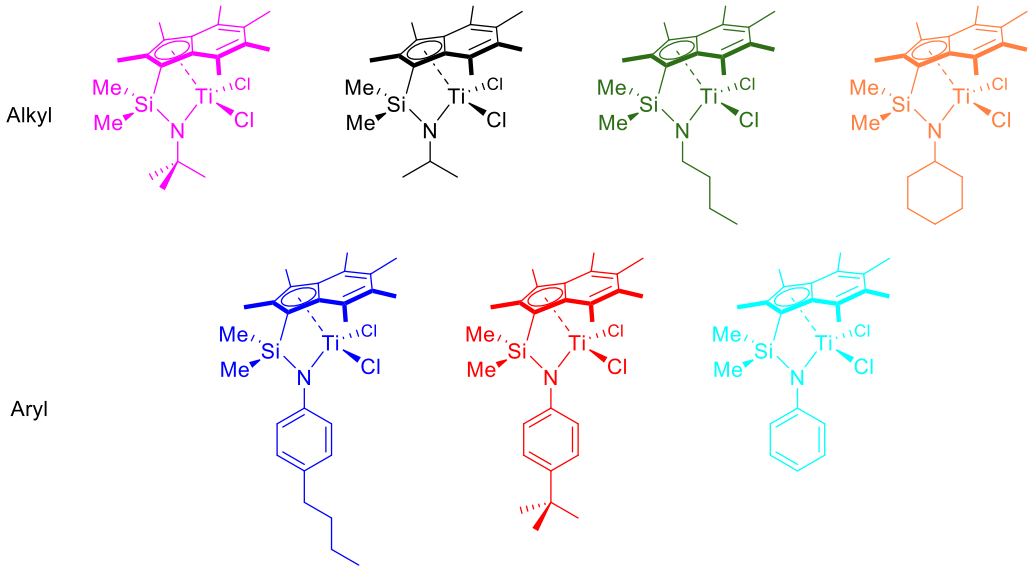

Figure 3.1. Molecular structures of the seven complexes tested in this section. Colours correspond to colours of the lines used on the graphs.

The complex sMAO-^{Me2}SB($^{t Bu}$N,I*)TiCl$_2$ shows the highest activity of the seven catalysts, with a maximum activity of 3602 kg$_{PE}$/mol$_{Ti}$/h/bar after 30 minutes at 60 °C (Figure 3.2). This activity is significantly higher than that observed for the Cp* analogue ^{Me2}SB($^{t Bu}$N,Cp*)TiCl$_2$ supported on sMAO (1301 kg$_{PE}$/mol$_{Ti}$/h/bar), LDHMAO (243 kg$_{PE}$/mol$_{Ti}$/h/bar),[15] borate-modified silica (17 kg$_{PE}$/mol$_{Ti}$/h/bar),[27] and SSMAO (2110 kg$_{PE}$/mol$_{Ti}$/h/bar),[28] demonstrating the enhancement in activity afforded by the I* ligand relative to Cp* and the superiority of sMAO as a catalyst support (Table 3.1).

Increasing the loading of complex on sMAO leads to a significant decrease in polymerisation activities. For sMAO-^{Me2}SB(^{tBu}N,I*)TiCl$_2$, ethylene polymerisation activities decrease from 3524 to 1160 kg$_{PE}$/mol$_{Ti}$/h/bar at 70 °C with [Al]$_0$:[Ti]$_0$ = 200:1 and 100:1 respectively (Table A3.1). It is proposed that increased complex loading leads to an increase in steric congestion on the surface and catalyst deactivation resulting in fewer catalytically active sites. A similar observation has been seen for zirconocene complexes in solution, where lower [Al$_{MAO}$]$_0$:[Zr]$_0$ ratios result in formation of homodinuclear cation pairs which are less active for polymerisation.[29–31]

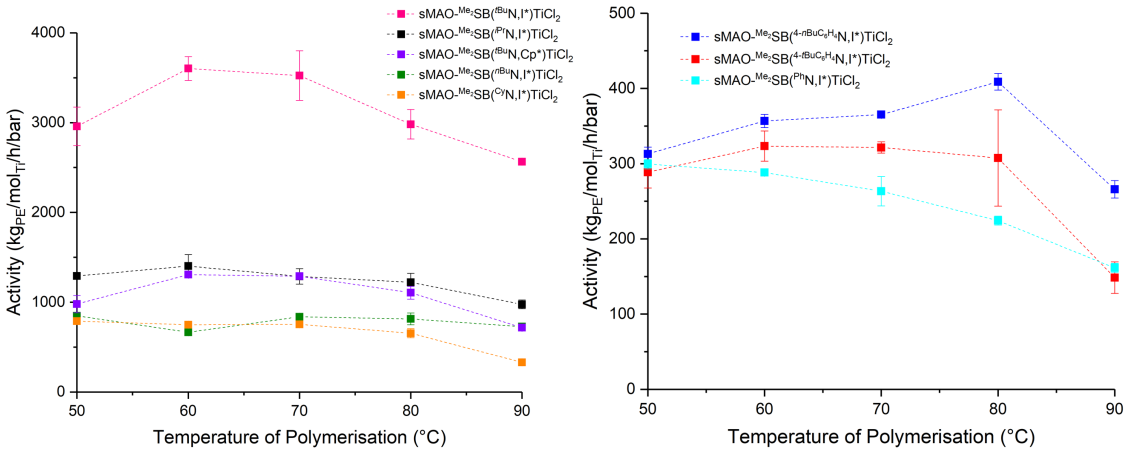

Figure 3.2. Slurry phase ethylene polymerisation activity dependence of sMAO-^{Me2}SB(^{R}N,I*)TiCl$_2$ in function of the temperature; 2 bar ethylene, 50 mL hexanes, 10 mg catalyst ([Al]$_0$:[Ti]$_0$ = 200:1), 150 mg TiBA and 30 minutes. Error bars as 1 standard deviation.

Polymerisation activities of sMAO-^{Me2}SB(^{Cy}N,I*)TiCl$_2$ are more comparable to those of sMAO-^{Me2}SB(^{nBu}N,I*)TiCl$_2$ (848 kg$_{PE}$/mol$_{Ti}$/h/bar after 30 minutes at 50 °C) than sMAO-^{Me2}SB(^{iPr}N,I*)TiCl$_2$ (1402 kg$_{PE}$/mol$_{Ti}$/h/bar after 30 minutes at 60 °C), with a maximum activity of 788 kg$_{PE}$/mol$_{Ti}$/h/bar after 30 minutes at 50 °C. This would suggest that in addition to the electronic effects the amido group has on the polymerisation activity, where there is a much greater positive inductive effect of ^{t}Bu compared with ^{i}Pr, ^{n}Bu and Cy,[32] there is also a steric effect with the increased steric bulk lowering

polymerisation activities, possibly by hindering close approach of the monomer to the metal centre.

Table 3.1. Selected slurry-phase ethylene polymerisation activities of some metallocene based complexes, and varying solid supports.

Complex	Support	Activity[a]	Ref
^{Me2}SB($^{t Bu}$N,I*)TiCl$_2$	sMAO	3602	This work
^{Me2}SB($^{t Bu}$N,Cp*)TiCl$_2$	sMAO	1301	This work
^{Me2}SB($^{t Bu}$N,Cp*)TiCl$_2$	MAO-modified LDH	243	15
^{Me2}SB($^{t Bu}$N,Cp*)Ti(CH$_2$Ph)$_2$	Borate-modified silica	120	27
^{Me2}SB($^{t Bu}$N,Cp*)TiCl$_2$	MAO-modified silica	2110	28
rac-(SBI*)ZrCl$_2$	sMAO	5791	33
rac-(EBI)ZrCl$_2$	sMAO	6533	34

[a] Activity in kg$_{PE}$/mol$_M$/h/bar

The activities of sMAO-^{Me2}SB($^{t Bu}$N,I*)TiCl$_2$ are comparable to previously reported polymerisation activities for metallocene type complexes supported on sMAO; activities are lower than both *rac*-(SBI*)ZrCl$_2$ (5791 kg$_{PE}$/mol$_{Zr}$/h/bar), *rac*-(EBI)ZrCl$_2$ (6533 kg$_{PE}$/mol$_{Zr}$/h/bar),[33,34] and Pn*ZrCpCl (4209 kg$_{PE}$/mol$_{Zr}$/h/bar, Pn* corresponds to permethylpentalene)[35] (Table 3.1). Polymerisation activity follows the order ^{t}Bu > ^{i}Pr > ^{n}Bu > Cy > 4-^{n}BuC$_6$H$_4$ > 4-^{t}BuC$_6$H$_4$ > Ph with electron-donating amido groups leading to higher activities. Maximum activity was observed between 60 and 80 °C for all catalysts, with time variation showing the expected trend of decreasing activity with time as the catalyst deactivates (Figure A3.1, and Table A3.2). It has previously been reported that there is a correlation between decreased Ti-N bond length resulting in increased ethylene polymerisation activities.[7] However, here it is not possible to draw a conclusion on this from the available solid state crystal structures described in Section 2.2.1.

Scanning electron microscopy (SEM) images of the polymers produced (Figure 3.3 and A3.2–A3.7) show that the polymers exhibit a "popcorn-like" morphology; mimicking the sMAO support.[34] The polymers produced by sMAO-^{Me2}SB($^{t Bu}$N,I*)TiCl$_2$ and

sMAO-^{Me_2}SB($^{i Pr}$N,I*)$TiCl_2$ are also approximately twice the diameter of that produced by the other catalysts, this may be due to increased activity of these two catalysts.[36]

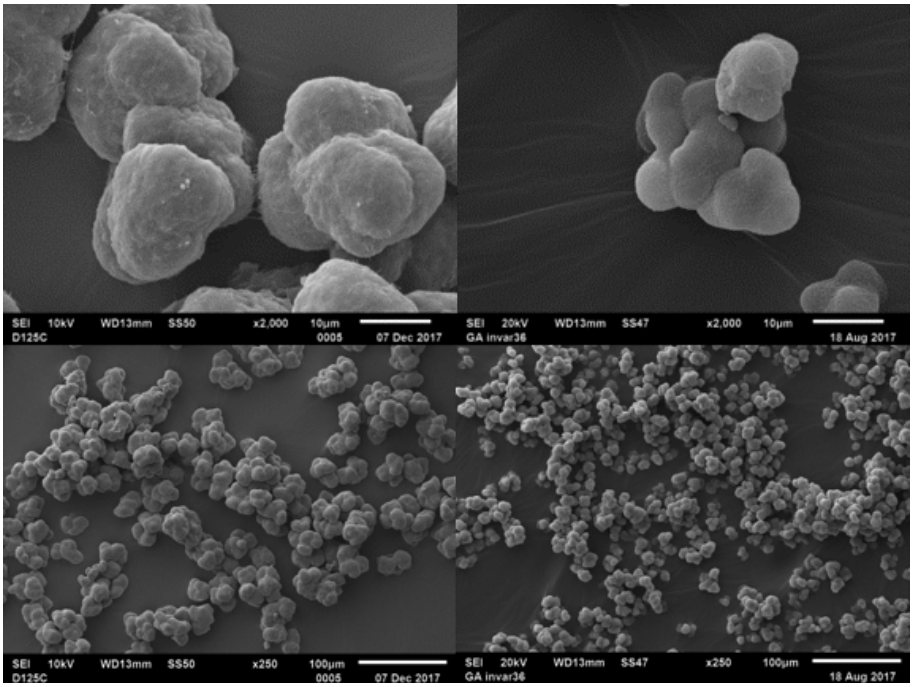

Figure 3.3. Scanning electron microscopy images of (left) sMAO-^{Me_2}SB($^{t Bu}$N,I*)$TiCl_2$ and (right) sMAO-^{Me_2}SB($^{4\text{-}n BuC_6H_4}$N,I*)$TiCl_2$; 2 bar ethylene, 50 mL hexanes, 10 mg catalyst ($[Al]_0$:$[Ti]_0$ = 200:1), 150 mg TiBA, 70 °C and 30 minutes.

The molecular weights of the polymers produced were determined by gel permeation chromatography (GPC) (Figures 3.4 and 3.5). The polyethylenes produced show high molecular weights (up to 1631 kDa at 50 °C for sMAO-^{Me_2}SB($^{n Bu}$N,I*)$TiCl_2$). The molecular weights tend to increase with decreased ethylene polymerisation activity and steric bulk of the amido fragment. The broad molecular weight distributions can be partly attributed to the low ethylene pressures for polymerisation. The melt temperatures (T_m around 134 °C) were attributed to linear high density polyethylenes.

Polymer molecular weights decrease with increased polymerisation temperature (868 kDa at 30 °C to 247 kDa at 90 °C), due to the relative rates of chain propagation and termination changing with temperature,[37] and chain transfer reactions increasing at higher

temperatures.[38] In addition, there are greater values of dispersities (M_w/M_n) for the less active catalysts; at 70 °C, M_w/M_n for sMAO-^{Me2}SB(^{tBu}N,I*)TiCl$_2$ is 3.9 compared with 8.4, 7.6 and 5.7 for sMAO-^{Me2}SB(^{Cy}N,I*)TiCl$_2$, sMAO-^{Me2}SB(^{iPr}N,I*)TiCl$_2$ and sMAO-^{Me2}SB(^{nBu}N,I*)TiCl$_2$ respectively.

The polymer molecular weight distributions of the polymers produced by aromatic amido complexes are in general much greater than those of the aliphatic amido complexes, with values up to 30.8. The ^{29}Si CP-MAS ssNMR of sMAO-^{Me2}SB(^{Ph}N,I*)TiCl$_2$ shows multiple resonances at 6, 2, −4, −16, −98 ppm. In contrast, the ^{29}Si CP-MAS ssNMR of sMAO-^{Me2}SB(^{tBu}N,I*)TiCl$_2$ shows one resonance at −19 ppm which would imply the presence of multiple silicon species in the immobilised aromatic CGC and only one in sMAO-^{Me2}SB(^{tBu}N,I*)TiCl$_2$. These broad molecular weight distributions and the multiple resonances observed in the ssNMR would imply poor control of the polymerisation mechanism with aromatic CGCs, and the possibility of multiple active sites.

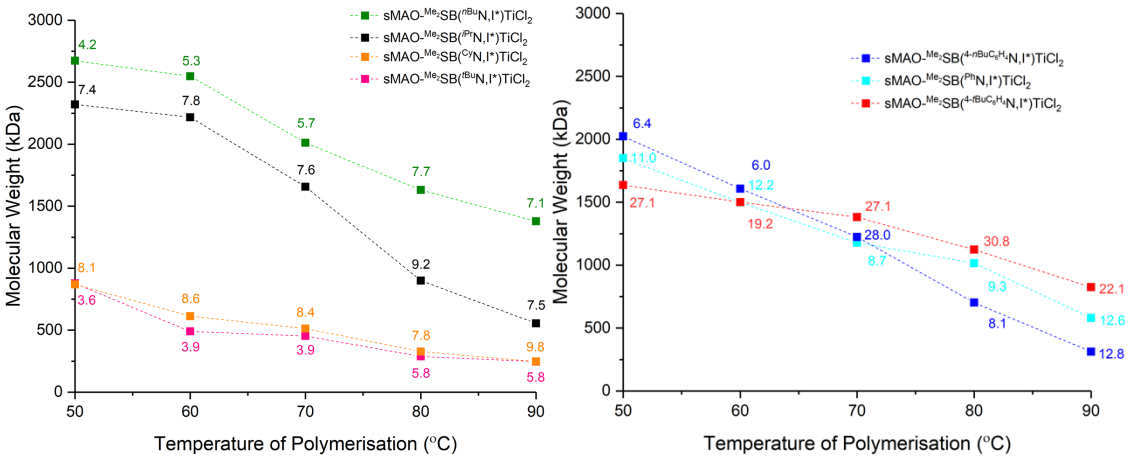

Figure 3.4. Molecular weights and dispersities of the polyethylenes produced for the complexes sMAO-^{Me2}SB(^{R}N,I*)TiCl$_2$ (left: R = ^{t}Bu, ^{i}Pr, ^{n}Bu, Cy; right R = Ph, 4-^{t}BuC$_6$H$_4$ and 4-^{n}BuC$_6$H$_4$); 2 bar ethylene, 50 mL hexanes, 10 mg catalyst ([Al]$_0$:[Ti]$_0$ = 200:1), 150 mg TiBA and 30 minutes. M_w/M_n values given.

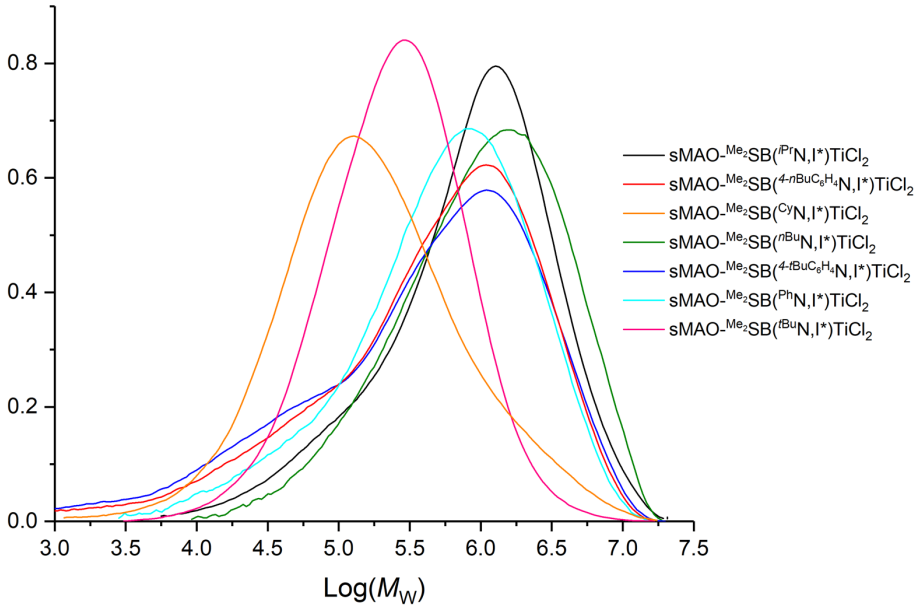

Figure 3.5. GPC traces of the polymers produced by sMAO-^{Me2}SB(^{R}N,I*)TiCl$_2$ (R = ^{t}Bu, ^{n}Bu, ^{i}Pr, Cy, Ph, 4-^{t}BuC$_6$H$_4$ and 4-^{n}BuC$_6$H$_4$); 2 bar ethylene, 50 mL hexanes, 10 mg catalyst ([Al]$_0$:[Ti]$_0$ = 200:1), 150 mg TiBA, 70 °C and 30 minutes.

3.2.2 Effect of the initiator group on slurry-phase ethylene polymerisation

Solid polymethylaluminoxane-immobilised ^{Me2}SB(^{tBu}N,I*)TiR$_2$ (R = Me, CH$_2$SiMe$_3$ or CH$_2$Ph) and ^{Me2}SB(^{tBu}N,I*)Ti(Cl)CH$_2$SiMe$_3$ (Figure 3.6) catalysts were tested for their ethylene homopolymerisation activity in the slurry phase (Figures 3.7 and A3.8). Polymerisations using sMAO-^{Me2}SB(^{tBu}N,I*)TiR$_2$ (R = Me, CH$_2$SiMe$_3$ or CH$_2$Ph) were first carried out by Mr. Alexander Smith.

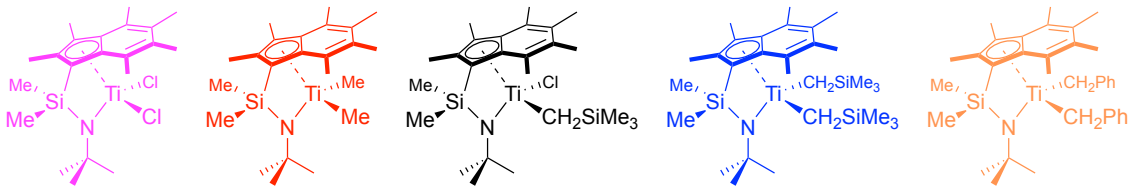

Figure 3.6. Molecular structures of the five complexes tested in this section. Colours correspond to colours of the lines used on the graphs.

At 60 °C, the dialkyl complexes exhibit significantly higher polymerisation activities (6865, 5792 and 5375 $kg_{PE}/mol_{Ti}/h/bar$ for sMAO-^{Me2}SB($^{t Bu}$N,I*)Ti(CH_2SiMe_3)$_2$, sMAO-^{Me2}SB($^{t Bu}$N,I*)Ti(CH_2Ph)$_2$ and sMAO-^{Me2}SB($^{t Bu}$N,I*)$TiMe_2$ respectively) than sMAO-^{Me2}SB($^{t Bu}$N,I*)$TiCl_2$ (3602 $kg_{PE}/mol_{Ti}/h/bar$) and sMAO-^{Me2}SB($^{t Bu}$N,I*)Ti(Cl)CH_2SiMe_3 (2942 $kg_{PE}/mol_{Ti}/h/bar$) (Figures 3.7 and A3.8). The effect of alkylation of metallocene-type permethylindenyl complexes on polymerisation activity has been studied previously,[17] with alkylation of the complexes leading to significantly enhanced polymerisation activities. The increase in polymerisation activities has been proposed to be due to a number of reasons: firstly, the alkyl initiator groups are electron donating, whilst the chloride group is electron withdrawing. Since it has previously been shown that addition of electron donating groups to an indenyl ring enhances polymerisation activity, and conversely electron withdrawing groups lead to decreased activities,[39] it is proposed that a similar effect would be observed with variation of the initiator group. Secondly, it is thought that formation of the active species occurs by alkylation followed by abstraction to form a cationic species that is bound to the solid support. This is seen by reaction of ^{Me2}SB($^{t Bu}$N,I*)$TiCl_2$ and ^{Me2}SB($^{t Bu}$N,I*)Ti(Cl)CH_2SiMe_3 with MAO (Section 2.3) and so activation is proposed to be easier with an alkylated complex compared with a dichloride complex. Finally, the initiatior group likely remains bound to the surface of the solid support, and it is believed that this group exerts a secondary coordination influence on the active site of the catalyst. The initiator group also affects the molecular weights (M_w) of the polymer that is formed (Figures 3.9 and 3.10), which is further evidence of the secondary coordination effect. Waymouth *et al*. have demonstrated how the oxidation state of the titanium metal centre can affect the rate of styrene polymerisation and selectivities in copolymerisations;[40] it is possible that variation of the leaving group could

lead to differing levels of titanium (III) and titanium (IV) species, and as such change the number and nature of the active sites. Large activity enhancements are also observed for borate-modified silica-supported ^{Me_2}SB(^{tBu}N,Cp*)TiX$_2$; where activities for the dibenzyl complex (120 kg$_{PE}$/mol$_{Ti}$/h/bar) are greater than those afforded by the dimethyl and dichloride complex (50 and 17 kg$_{PE}$/mol$_{Ti}$/h/bar respectively).[41]

In all cases, polymerisation activities decrease at higher temperatures, and this can be attributed to both decreased solubility of ethylene in hexanes and thermal decomposition of the catalyst.[42] The alkylated complexes show a greater decrease in polymerisation activities at 90 °C compared with 60 °C when compared with sMAO-^{Me_2}SB(^{tBu}N,I*)TiCl$_2$. Polymerisation activities decrease by 46 and 32% for sMAO-^{Me_2}SB(^{tBu}N,I*)TiMe$_2$ (5375 to 2926 kg$_{PE}$/mol$_{Ti}$/h/bar) and sMAO-^{Me_2}SB(^{tBu}N,I*)Ti(CH$_2$Ph)$_2$ (5793 to 3935 kg$_{PE}$/mol$_{Ti}$/h/bar) respectively, while activities of sMAO-^{Me_2}SB(^{tBu}N,I*)Ti(CH$_2$SiMe$_3$)$_2$ (6866 to 1977 kg$_{PE}$/mol$_{Ti}$/h/bar) and sMAO-^{Me_2}SB(^{tBu}N,I*)Ti(Cl)CH$_2$SiMe$_3$ (2943 to 862 kg$_{PE}$/mol$_{Ti}$/h/bar) decrease by 71%, the activity of sMAO-^{Me_2}SB(^{tBu}N,I*)TiCl$_2$ only decreases by 29% (3602 to 2565 kg$_{PE}$/mol$_{Ti}$/h/bar).

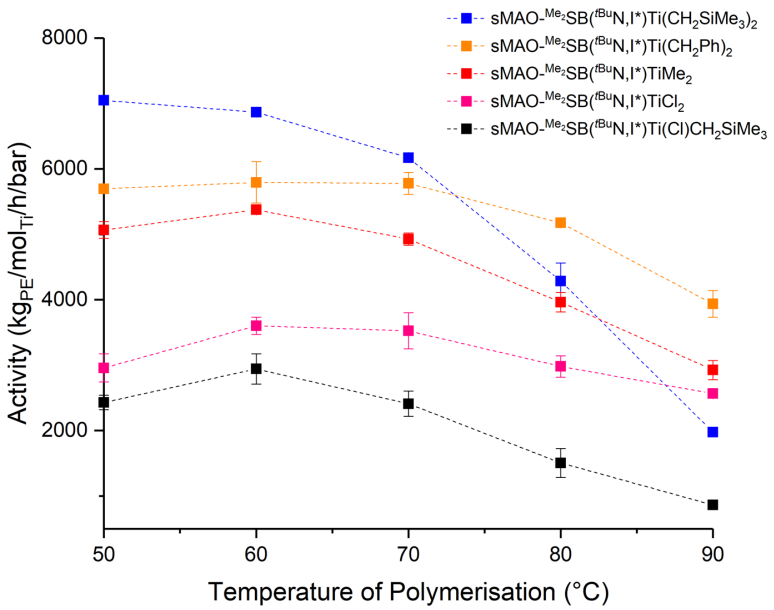

Figure 3.7. Ethylene polymerisation activities for sMAO-^{Me2}SB($^{t Bu}$N,I*)Ti(Cl)CH_2SiMe_3 and sMAO-^{Me2}SB($^{t Bu}$N,I*)TiR_2 (R = Cl, Me, CH_2Ph and CH_2SiMe_3); 2 bar ethylene, 50 mL hexanes, 10 mg catalyst ($[Al]_0$:$[Ti]_0$ = 200:1), 150 mg TiBA and 30 minutes. Error bars at 1 standard deviation.

Polymerisation studies were also conducted to investigate how polymerisation activities decreased with time at 70 °C (Figure A3.8). When comparing the activities after 5 and 60 minutes, the decrease in polymerisation activity of sMAO-^{Me2}SB($^{t Bu}$N,I*)$TiCl_2$ is less than that of sMAO-^{Me2}SB($^{t Bu}$N,I*)$TiMe_2$, sMAO-^{Me2}SB($^{t Bu}$N,I*)$Ti(CH_2Ph)_2$, sMAO-^{Me2}SB($^{t Bu}$N,I*)Ti(Cl)CH_2SiMe_3 and sMAO-^{Me2}SB($^{t Bu}$N,I*)$Ti(CH_2SiMe_3)_2$ (decreases of 47, 56, 59, 66 and 61% respectively). These decreases in activity are caused both by catalyst deactivation and the polymer templation effect which results in blocked active sites leading to decreased activities.[16] The polymer takes on the form of discrete "popcorn-shaped" particles (Figure 3.11), mimicking that of the solid support.[17,18]

GPC studies also demonstrate the effect of the leaving group on the polymer properties (Figures 3.9 and 3.10). sMAO-^{Me2}SB($^{t Bu}$N,I*)Ti(Cl)CH_2SiMe_3 and sMAO-^{Me2}SB($^{t Bu}$N,I*)$Ti(CH_2SiMe_3)_2$ produce polymer with much higher molecular weights (1509 and 1860 kDa at 50 °C respectively) compared with 654, 877 and 979 kDa for sMAO-^{Me2}SB($^{t Bu}$N,I*)$TiMe_2$, sMAO-^{Me2}SB($^{t Bu}$N,I*)$TiCl_2$ and

sMAO-^{Me_2}SB($^{t Bu}$N,I*)Ti(CH_2Ph)$_2$. This highlights that the leaving group still has an effect on the polymerisation mechanism, further suggesting that the initiator group remains bound to the solid support surface and exerts a secondary coordination influence (Figure 3.8).

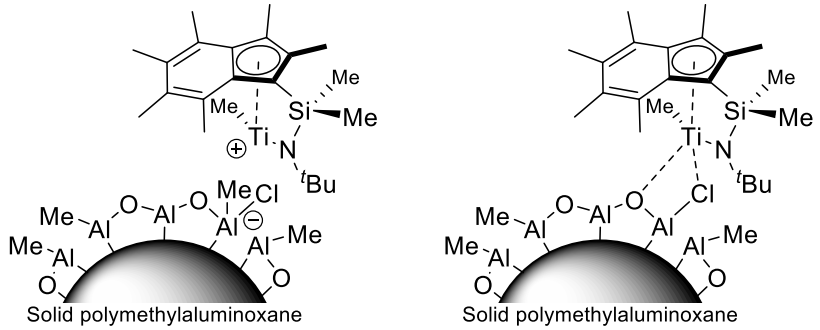

Figure 3.8. ^{Me_2}SB($^{t Bu}$N,I*)$TiCl_2$ immobilised on sMAO, with the chloride leaving group remaining bound to the solid support. Diagram is a schematic representation.

The decrease in polymer molecular weight with increased temperature is expected, and has previously been observed for a variety of solid-supported catalysts.[15,17] At higher polymerisation temperatures, the rate of chain termination increases more rapidly than the rate of propagation, hence resulting in lower polymer molecular weights. M_w/M_n values have also been shown to decrease at higher ethylene pressures, presumably as the higher ethylene pressure leads to improved control of the polymerisation reaction. The monomodal nature of the GPC traces would suggest that the catalysts are single site in nature and the relatively narrow molecular weight distributions would also suggest a relatively high degree of control in the polymerisation reactions; M_w/M_n values are in the range of 3.5 to 6.0. In the ^{29}Si CP-MAS ssNMR spectra, the dimethyl, dibenzyl and dichloride complexes (Figures A2.13, A2.15 and A2.17) all show a single resonance, with two resonances observed for the neosilyl complexes (Figures A2.19 and A2.21), implying there is a single species on the solid support.

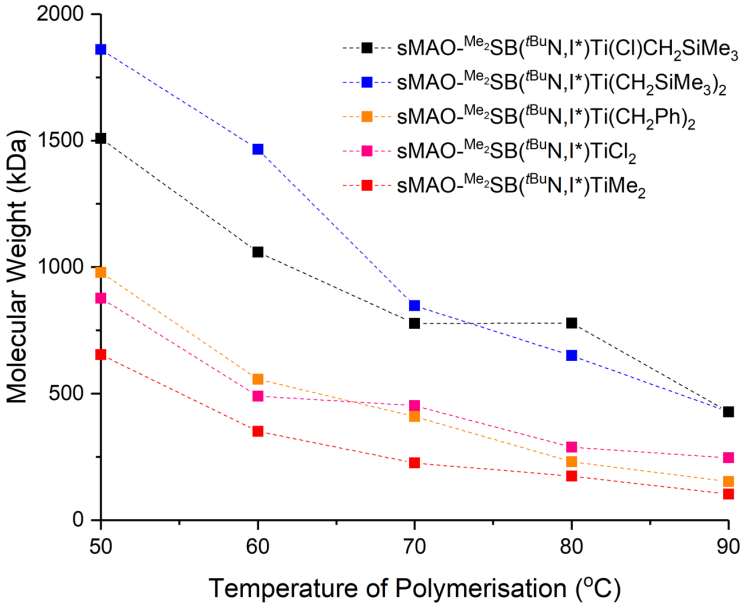

Figure 3.9. Molecular weights of the polyethylenes produced for the complexes sMAO-^{Me_2}SB($^{t Bu}$N,I*)Ti(Cl)CH_2SiMe_3 and sMAO-^{Me_2}SB($^{t Bu}$N,I*)TiR_2 (R = Cl, Me, CH_2Ph and CH_2SiMe_3); 2 bar ethylene, 50 mL hexanes, 10 mg catalyst ($[Al]_0$:$[Ti]_0$ = 200:1), 150 mg TiBA and 30 minutes.

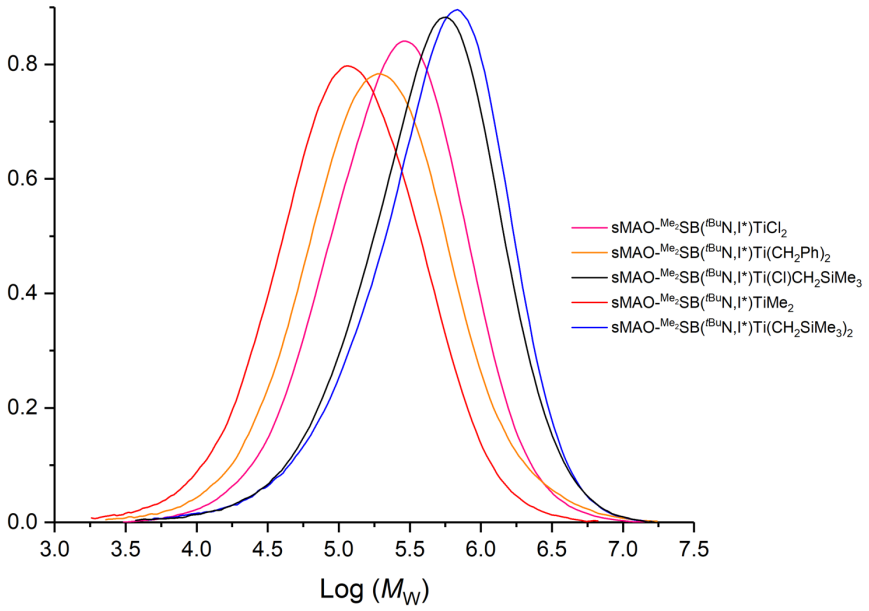

Figure 3.10. GPC traces of the polyethylenes produced for the complexes sMAO-^{Me_2}SB($^{t Bu}$N,I*)Ti(Cl)CH_2SiMe_3 and sMAO-^{Me_2}SB($^{t Bu}$N,I*)TiR_2 (R = Cl, Me, CH_2Ph and CH_2SiMe_3); 2 bar ethylene, 50 mL hexanes, 10 mg catalyst ($[Al]_0$:$[Ti]_0$ = 200:1), 150 mg TiBA, 70 °C and 30 minutes.

SEM images show that the polyethylenes obtained using sMAO-^{Me_2}SB($^{t Bu}$N,I*)TiR$_2$ (R = Me, CH_2Ph and CH_2SiMe_3) possess a "popcorn" morphology (mimicking the support) and similar to that of sMAO-^{Me_2}SB($^{t Bu}$N,I*)TiCl$_2$ (Figure 3.3).

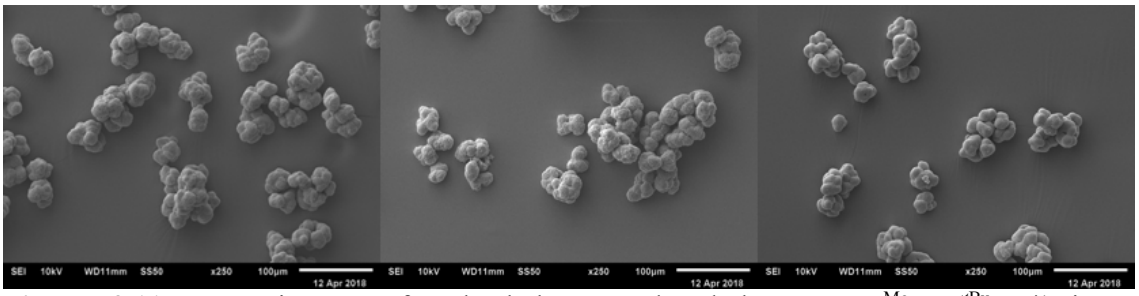

Figure 3.11. SEM images of polyethylene produced by sMAO-^{Me_2}SB($^{t Bu}$N,I*)TiMe$_2$, sMAO-^{Me_2}SB($^{t Bu}$N,I*)Ti(CH_2SiMe_3)$_2$ and sMAO-^{Me_2}SB($^{t Bu}$N,I*)Ti(CH_2Ph)$_2$ (left to right); 2 bar ethylene, 50 mL hexanes, 10 mg catalyst ([Al]$_0$:[Ti]$_0$ = 200:1), 150 mg TiBA, 70 °C and 30 minutes.

3.2.3 Effect of variation of the permethylindenyl ligand, *ansa* bridge and metal centre on slurry-phase ethylene polymerisation.

sMAO-^{Me_2}SB($^{t Bu}$N,$^{3\text{-}R}$I*)TiCl$_2$ (R = Me and Et), sMAO-^{Me,Pr}SB($^{t Bu}$N,I*)TiCl$_2$ (3rd generation sMAO used), and sMAO-^{Me_2}SB($^{t Bu}$N,I*)ZrCl$_2$ (Figure 3.12) were tested for slurry phase ethylene homopolymerisation (Figures 3.13 and A3.9).

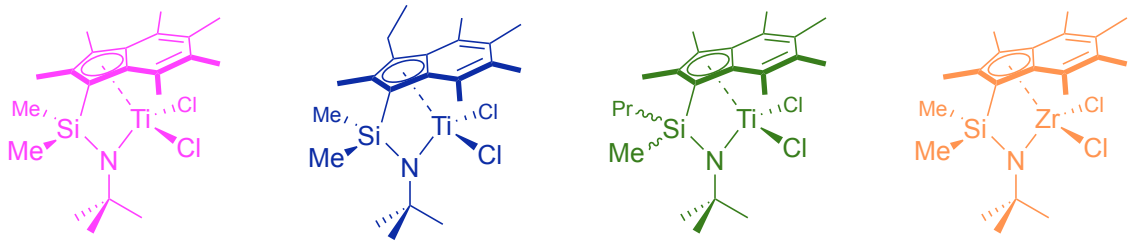

Figure 3.12. Molecular structures of the four complexes tested in this section. Colours correspond to colours of the lines used on the graphs.

At temperatures below 70 ºC, sMAO-^{Me_2}SB($^{t Bu}$N,$^{3\text{-}Et}$I*)TiCl$_2$ exhibits higher activities than sMAO-^{Me_2}SB($^{t Bu}$N,I*)TiCl$_2$, with a maximum activity of 4067 $kg_{PE}/mol_{Ti}/h/bar$ after 30 minutes at 50 °C (Figure 3.13). This increase in activity initially appears unexpected,

since the analogous family of catalysts sMAO-^{Me_2}SB($^{2,7\text{-}t\text{Bu}}$Flu,$^{3\text{-}R}$I*)$ZrCl_2$ shows decreases in activity for the 3-ethyl complex relative to the permethylindenyl complex (4963 and 6755 $kg_{PE}/mol_{Zr}/h/bar$).[18] However, considering that the CGC complexes have two fewer valence electrons than these complexes,[43,44] the additional inductive effect of the ethyl group relative to the methyl is likely to enhance polymerisation activity, similarly to what has been observed for amido group variation. As with sMAO-^{Me_2}SB($^{2,7\text{-}t\text{Bu}}$Flu,$^{3\text{-}R}$I*)$ZrCl_2$ catalysts, there are much greater decreases in polymerisation activities at higher temperatures for sMAO-^{Me_2}SB($^{t\text{Bu}}$N,$^{3\text{-}Et}$I*)$TiCl_2$ (3913 and 2323 $kg_{PE}/mol_{Ti}/h/bar$ for 60 and 90 °C) compared with sMAO-^{Me_2}SB($^{t\text{Bu}}$N,I*)$TiCl_2$ (3602 and 2565 $kg_{PE}/mol_{Ti}/h/bar$ for 60 and 90 °C), indicating a decrease in thermal stability of these 3-ethylpentamethylindenyl supported complexes relative to the permethylindenyl analogues.

sMAO-^{Me,Pr}SB($^{t\text{Bu}}$N,I*)$TiCl_2$ also shows higher activities than sMAO-^{Me_2}SB($^{t\text{Bu}}$N,I*)$TiCl_2$ at all temperatures with a maximum value of 4197 $kg_{PE}/mol_{Ti}/h/bar$ after 30 minutes at 60 °C. This is in contrast to the related complexes sMAO-^{R_1,R_2}SB($^{2,7\text{-}t\text{Bu}}$Flu,I*)$ZrCl_2$ (R_1 = R_2 = Me, Et, and R_1 = Me, R_2 = Pr) where the dimethylsilyl bridged complex shows higher activities (6755 $kg_{PE}/mol_{Zr}/h/bar$) compared to the diethylsilyl bridged complex (5550 $kg_{PE}/mol_{Zr}/h/bar$) and the methylpropylsilyl bridged complex (5059 $kg_{PE}/mol_{Zr}/h/bar$).[18] Alt and co-workers have previously reported the synthesis of constrained geometry complexes of the form ^{Me,R}SB($^{t\text{Bu}}$N,$^{3\text{-}R}$Cp)$TiCl_2$ and ^{Me,R}SB($^{t\text{Bu}}$N,$^{3\text{-}R}$I)$TiCl_2$, and shown that variation of the R group leads to enhancements in polymerisation activity for R = vinyl compared with R = phenyl, likely due to the relative electron donating ability of the groups.[45] Similarly for metallocene type complexes, work has been undertaken to investigate how the *ansa*

bridge effects both polymerisation activity and stereospecificity in propylene polymerisation.[46–48]

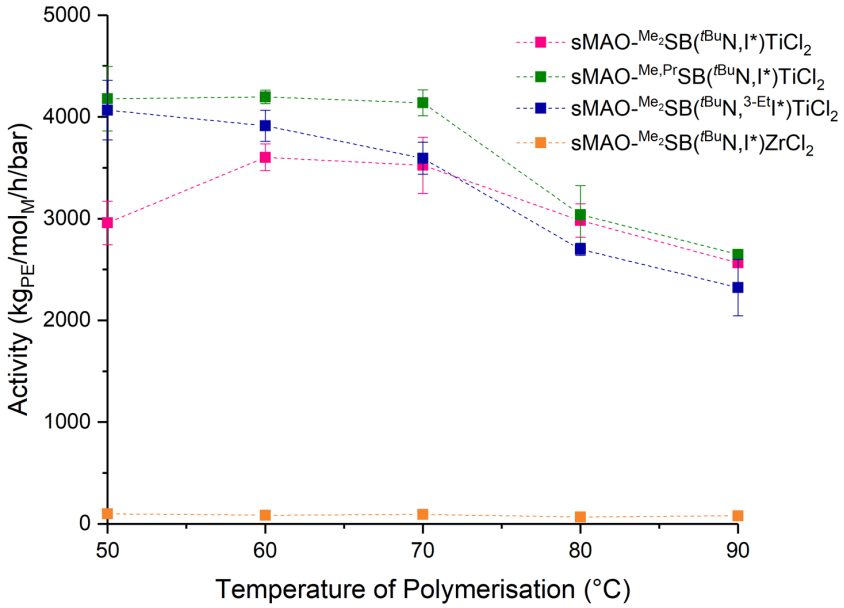

Figure 3.13. Slurry-phase ethylene polymerisation activities for sMAO-^{Me_2}SB($^{t Bu}$N,$^{3\text{-}Et}$I*)TiCl$_2$, sMAO-^{Me,R}SB($^{t Bu}$N,I*)TiCl$_2$ (R = Me and Pr) and sMAO-^{Me_2}SB($^{t Bu}$N,I*)ZrCl$_2$; 2 bar ethylene, 50 mL hexanes, 10 mg catalyst ([Al]$_0$:[Ti]$_0$ = 200:1), 150 mg TiBA and 30 minutes. Error bars as 1 standard deviation.

Pombeiro *et al.* have shown through variation of the 2- position of complexes ^{Me_2}SB($^{t Bu}$N,$^{2\text{-}R}$C$_5$Me$_3$)TiCl$_2$ that addition of alkyl groups, (R = Me, ^{n}Bu) resulted in decreases in polymerisation activity relative to the ^{Me_2}SB($^{t Bu}$N,$^{2\text{-}H}$C$_5$Me$_3$)TiCl$_2$ with an MAO cocatalyst in lower [Al]$_0$:[Ti]$_0$ ratios (1100:1), whereas addition of a phenyl group in the 2- position (^{Me_2}SB($^{t Bu}$N,$^{2\text{-}Ph}$C$_5$Me$_3$)TiCl$_2$) has been shown to increase polymerisation activity.[49] At higher [Al]$_0$:[Ti]$_0$ ratios (3100:1), higher activities are observed in the trend Me > Ph > ^{n}Bu > H. Alt *et al.* proposed that this activity enhancement at lower [Al]$_0$:[Ti]$_0$ ratios could be due to a spacer effect, whereby the phenyl group separates the bulky MAO anion from the catalytic species,[50] this effect has also been seen in *ansa*-bis(fluorenyl)zirconium dichloride systems.[51] Conversely, with (3-R)-pentamethylindenyl complexes ^{Me_2}SB($^{t Bu}$N,I*)TiCl$_2$ and ^{Me_2}SB($^{t Bu}$N,$^{3\text{-}Et}$I*)TiCl$_2$,

this additional steric bulk has been contributed by the I* ring itself, it is proposed that the addition of the 3-ethyl group or a methylpropylsilyl *ansa* bridge can enhance polymerisation activity through a directional and inductive effect of these groups.

Variation of the metal centre down group 4 from titanium to zirconium results in significant decreases in polymerisation activity, which is in contrast to what has been observed for many metallocene type ethylene polymerisation catalysts,[6] but is commonly observed for CGCs.[52,53] DFT studies have shown that this decrease in polymerisation activity is attributable to the ethylene insertion step in the polymerisation mechanism, where the activation barrier for zirconium constrained geometry complexes is much greater than is observed for titanium analogues, resulting in slower polymerisation rates.[54] The maximum activity after 30 minutes for sMAO-^{Me2}SB($^{t Bu}$N,I*)$ZrCl_2$ is 99 $kg_{PE}/mol_{Zr}/h/bar$ (Figure 3.13 and A3.9), and this thirty-fold decrease in activity with respect to the titanium analogue is not uncommon for these complexes, with large decreases in activity observed for the Cp* analogues when supported on silica and activated with MAO.[53] Molecular weights (M_w) and dispersities (M_w/M_n) are given in Table 3.2, with sMAO-^{Me2}SB($^{t Bu}$N,$^{3\text{-}Et}$I*)$TiCl_2$ and sMAO-^{Me,Pr}SB($^{t Bu}$N,I*)$TiCl_2$ generally producing lower molecular weight polyethylenes than sMAO-^{Me2}SB($^{t Bu}$N,I*)$TiCl_2$. The narrow molecular weight distributions indicate relatively controlled polymerisation with a single-site catalytic species in both cases. This can also be observed in the ssNMR ^{29}Si CP-MAS spectrum of sMAO-^{Me2}SB($^{t Bu}$N,$^{3\text{-}Et}$I*)$TiCl_2$ where a single ^{29}Si resonance is observed (Figure A2.25), and is supported by the monomodal GPC traces (Figure 3.14). The complexes produce higher molecular weight polyethylenes than comparable permethylindenyl complexes,

such as sMAO-^{Me_2}SB(Cp,I*)$ZrCl_2$ (130 kDa), and sMAO-*rac*-SBI*$ZrCl_2$ (183 kDa) at 60 ºC.[17]

Table 3.2. Molecular weights (M_w) and dispersities (M_w/M_n) of the polyethylenes produced for sMAO-^{Me,R}SB(^{tBu}N,$^{3\text{-}R}$I*)$TiCl_2$ (R = Me, Et and Pr); 2 bar ethylene, 50 mL hexanes, 10 mg catalyst ($[Al]_0$:$[Ti]_0$ = 200:1), 150 mg TiBA and 30 minutes.

Complex	^{Me_2}SB(^{tBu}N,I*)$TiCl_2$		^{Me_2}SB(^{tBu}N,$^{3\text{-}Et}$I*)$TiCl_2$		^{Me,Pr}SB(^{tBu}N,I*)$TiCl_2$	
T (°C)	M_w (kDa)	M_w/M_n	M_w (kDa)	M_w/M_n	M_w (kDa)	M_w/M_n
50	881	3.6	598	3.7	740	3.2
60	490	3.9	505	3.3	435	3.5
70	474	3.9	276	4.9	480	3.5
80	289	5.8	205	4.7	282	3.4
90	246	5.8	168	4.5	224	3.7

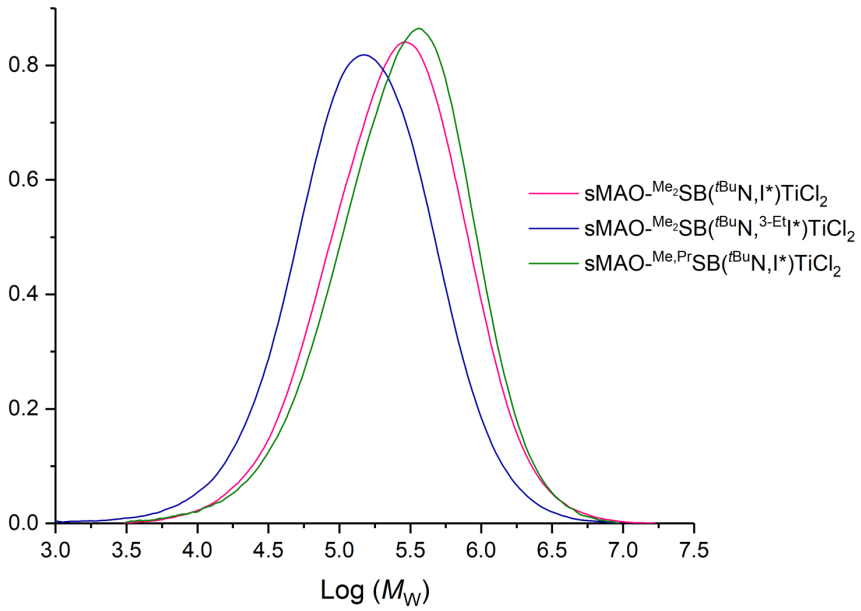

Figure 3.14. GPC traces of the polyethylenes produced for sMAO-^{Me,R}SB(^{tBu}N,$^{3\text{-}R}$I*)$TiCl_2$ (R = Me, Et and Pr); 2 bar ethylene, 50 mL hexanes, 10 mg catalyst ($[Al]_0$:$[Ti]_0$ = 200:1), 150 mg TiBA, 70 °C and 30 minutes.

3.3 Effect of variation of the solid support on polymerisation activity

In this section, three different solid supports were screened for their use in slurry-phase ethylene polymerisation. These were (a) sMAO, (b) LDHMAO and (c) SSMAO and proposed structures are shown in Figure 3.15.

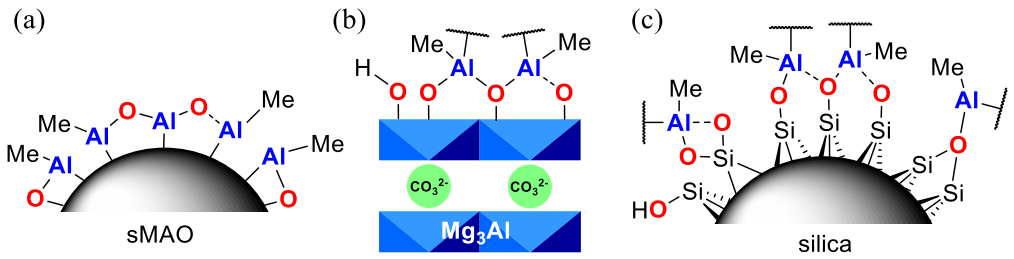

Figure 3.15. Proposed structures of (a) sMAO, (b) LDHMAO and (c) SSMAO.

Four different complexes were tested across these solid supports, ^{Me2}SB(^{tBu}N,I*)TiCl$_2$, ^{Me2}SB(^{tBu}N,$^{3\text{-}Et}$I*)TiCl$_2$, ^{Me,Pr}SB(^{tBu}N,I*)TiCl$_2$ and ^{Me2}SB(^{tBu}N,I*)Ti(Cl)CH$_2$SiMe$_3$ (Figure 3.16).

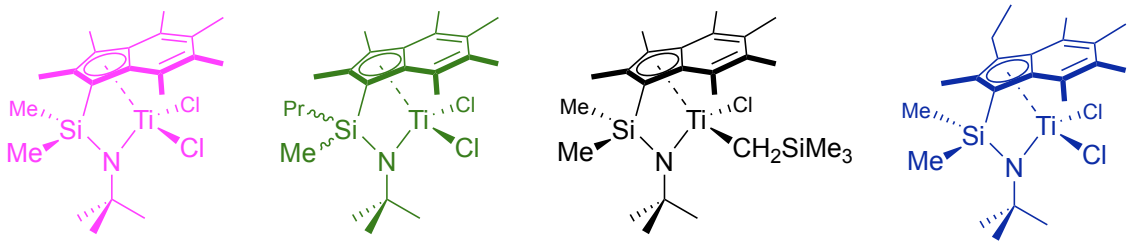

Figure 3.16. Molecular structures of the four complexes tested in this section. Colours correspond to colours of the lines used on the graphs.

3.3.1 Slurry-phase ethylene polymerisations using sMAO, LDHMAO and SSMAO

The process for pre-treatment of LDH and silica to form LDHMAO and SSMAO respectively followed by immobilisation of the four complexes is outlined in 2.4.3.

Polymerisations were performed using standard conditions, with the complexes immobilised on either 3rd generation sMAO (1st generation sMAO for ^{Me2}SB($^{t Bu}$N,$^{3\text{-}Et}$I*)TiCl$_2$), LDHMAO or SSMAO in an $[Al]_0$:$[Ti]_0$ ratio of 200:1; for LDHMAO the molar amount of aluminium does not include the aluminium content of the LDH. Polymerisations were run for 30 minutes with 10 mg of catalyst in 50 mL of hexanes and 150 mg of TiBA scavenger between 50 and 90 °C. The polymerisation activities are shown in Figure 3.17.

Polymerisation activities are significantly greater for the sMAO-supported complexes compared with the complexes immobilised on LDHMAO or SSMAO. The highest polymerisation activity after 30 minutes for ^{Me2}SB($^{t Bu}$N,I*)TiCl$_2$ was 3771 $kg_{PE}/mol_{Ti}/h/bar$ for the sMAO-supported complex compared with 1397 and 1803 $kg_{PE}/mol_{Ti}/h/bar$ for the SSMAO- and LDHMAO-supported complexes respectively. Similarly, for sMAO-supported ^{Me2}SB($^{t Bu}$N,$^{3\text{-}Et}$I*)TiCl$_2$, ^{Me,Pr}SB($^{t Bu}$N,I*)TiCl$_2$ and ^{Me2}SB($^{t Bu}$N,I*)Ti(Cl)CH$_2$SiMe$_3$ activities are 4067, 4197 and 4567 $kg_{PE}/mol_{Ti}/h/bar$, which are much greater than the activities of 1349, 901 and 1468 $kg_{PE}/mol_{Ti}/h/bar$ when supported on SSMAO and 2079, 839 and 1549 $kg_{PE}/mol_{Ti}/h/bar$ supported on LDHMAO.

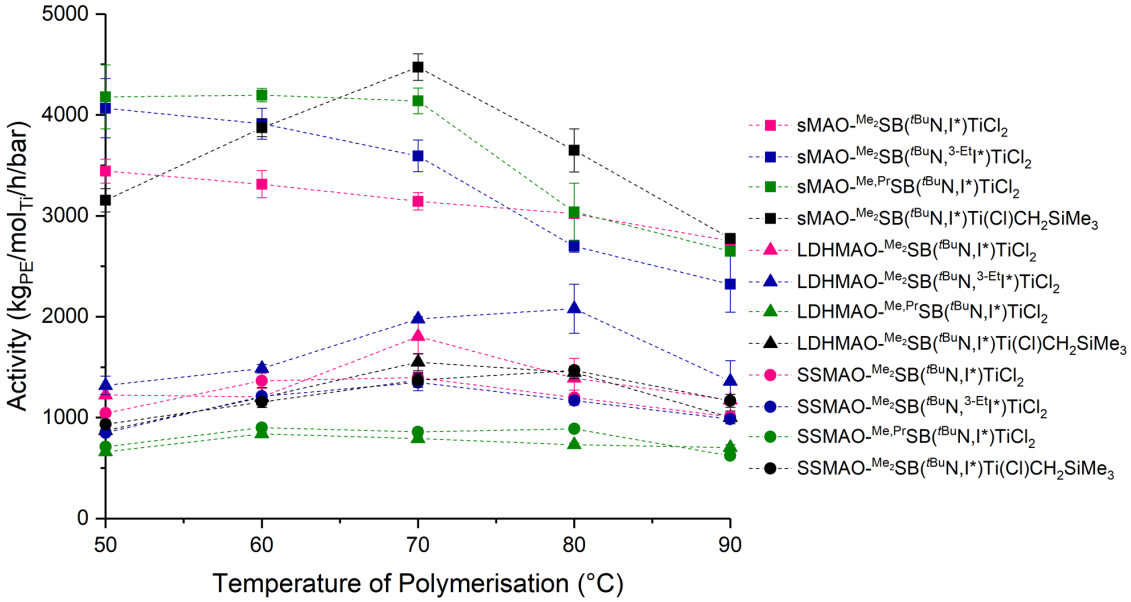

Figure 3.17. Ethylene polymerisation activities for ^{Me_2}SB($^{t Bu}$N,I*)TiCl$_2$, ^{Me_2}SB($^{t Bu}$N,$^{3\text{-Et}}$I*)TiCl$_2$, ^{Me,Pr}SB($^{t Bu}$N,I*)TiCl$_2$ and ^{Me_2}SB($^{t Bu}$N,I*)Ti(Cl)CH$_2$SiMe$_3$ supported on sMAO, LDHMAO and SSMAO; 2 bar ethylene, 50 mL hexanes, 10 mg catalyst ([Al]$_0$:[Ti]$_0$ = 200:1), 150 mg TiBA and 30 minutes. Error bars as 1 standard deviation.

The increase in ethylene polymerisation activities for sMAO compared with SSMAO and LDHMAO is to be expected; Kilpatrick and co-workers reported that the polymerisation activity for sMAO-*rac*-(EBI)ZrCl$_2$ was 6533 kg$_{PE}$/mol$_{Zr}$/h/bar, a five-fold increase on the activity reported for MAO-modified MgAl-CO$_3$ LDH (1276 kg$_{PE}$/mol$_{Zr}$/h/bar).[15,34] Similarly, comparison of the activities with ^{Me_2}SB($^{t Bu}$N,Cp*)TiCl$_2$ shows a much greater activity for the sMAO-supported complex (1301 kg$_{PE}$mol$_{Ti}$/h/bar) compared with LDHMAO (243 kg$_{PE}$/mol$_{Ti}$/h/bar).[15] The SSMAO-supported complex has an activity of 2110 kg$_{PE}$/mol$_{Ti}$/h/bar, as reported by Li and Wu.[28] However, in this case the polymerisations were carried out at 13.8 bar of ethylene pressure and so the results are not directly comparable. For ^{Me_2}SB(I*,Cp)ZrCl$_2$, ^{Me_2}SB(I*,Cp)ZrMe$_2$ and ^{Me_2}SB(I*,Cp)Zr(CH$_2$Ph)$_2$, polymerisation activities of the sMAO-supported complexes were also much higher than the analogous SSMAO and LDHMAO-supported complexes.[17] In contrast to the results above, the SSMAO-supported complexes typically had higher activities (57–84% greater) than the LDHMAO-supported complexes. For

^{Me_2}SB($^{2,7\text{-}t\text{Bu}}$Flu,I*)ZrCl$_2$, the sMAO-supported complex had an activity approximately ten times greater (6755 kg$_{PE}$/mol$_{Zr}$/h/bar) than the SSMAO- and LDHMAO-supported complexes (606 and 687 kg$_{PE}$/mol$_{Zr}$/h/bar respectively).[18]

The inverse trend observed for ^{Me_2}SB($^{t\text{Bu}}$N,I*)TiCl$_2$, ^{Me_2}SB($^{t\text{Bu}}$N,$^{3\text{-Et}}$I*)TiCl$_2$, ^{Me,Pr}SB($^{t\text{Bu}}$N,I*)TiCl$_2$ and ^{Me_2}SB($^{t\text{Bu}}$N,I*)Ti(Cl)CH$_2$SiMe$_3$ with higher activities for LDHMAO than for SSMAO compared with the activities for SSMAO and LDHMAO-supported ^{Me_2}SB(I*,Cp)ZrCl$_2$, ^{Me_2}SB(I*,Cp)ZrMe$_2$ and ^{Me_2}SB(I*,Cp)Zr(CH$_2$Ph)$_2$ could be attributed to the type of MAO used, and also the age of the supported catalyst. The age of the LDHMAO support has been shown to affect the ethylene polymerisation activity, with polymerisation activities decreasing by almost 50% with two week old LDHMAO-^{Me_2}SB($^{t\text{Bu}}$N,I*)TiCl$_2$ compared with freshly prepared LDHMAO-^{Me_2}SB($^{t\text{Bu}}$N,I*)TiCl$_2$ (Table 3.3). In the above polymerisations (Figure 3.17), all the supports were freshly prepared, with the catalysts prepared and used within a week of making the support.

Table 3.3. Slurry-phase ethylene polymerisation activities for ^{Me_2}SB($^{t\text{Bu}}$N,I*)TiCl$_2$, supported on fresh LDHMAO and two week old LDHMAO; 2 bar ethylene, 50 mL hexanes, 10 mg catalyst ([Al]$_0$:[Ti]$_0$ = 200:1), 150 mg TiBA and 30 minutes. Error given as 1 standard deviation.

Temperature	Fresh LDHMAO	Two week old LDHMAO
(°C)	Activity (kg$_{PE}$/mol$_{Ti}$/h/bar)	Activity (kg$_{PE}$/mol$_{Ti}$/h/bar)
30	787±1	293±21
40	838±22	428±20
50	1099±120	544±120
60	1867±60	935±93
70	1295±96	861±35
80	1322±51	706±55
90	1006±59	363±4

The molecular weights of the polymer produced vary with the different supports (Figure 3.18). In all cases, the SSMAO and LDHMAO-supported complexes have higher molecular weights than the sMAO-supported complexes. The lower molecular weights

produced by the sMAO-supported complexes are to be expected. The presence of free trimethylaluminium (TMA) in sMAO leads to an increase in the rate of chain termination, facilitated by chain transfer to the aluminium alkyl species, which does not occur in either SSMAO or LDHMAO where there is absence of free TMA.[34,55,56]

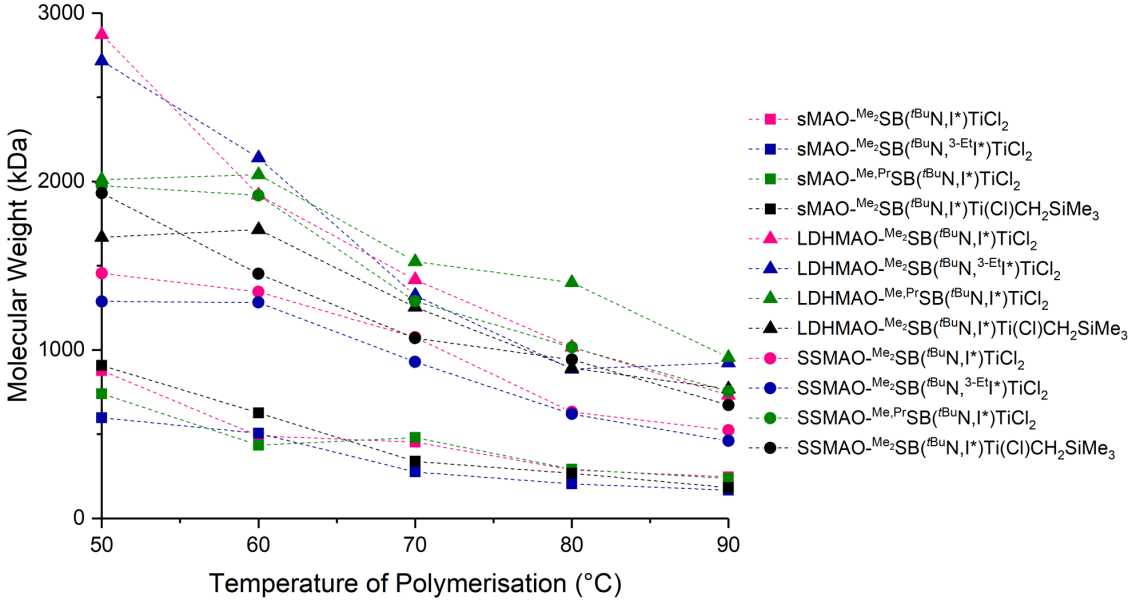

Figure 3.18. Polymer molecular weights for ^{Me_2}SB(^{tBu}N,I*)TiCl$_2$, ^{Me_2}SB(^{tBu}N,$^{3\text{-}Et}$I*)TiCl$_2$, ^{Me,Pr}SB(^{tBu}N,I*)TiCl$_2$ and ^{Me_2}SB(^{tBu}N,I*)Ti(Cl)CH$_2$SiMe$_3$ supported on sMAO, LDHMAO and SSMAO; 2 bar ethylene, 50 mL hexanes, 10 mg catalyst ([Al]$_0$:[Ti]$_0$ = 200:1), 150 mg TiBA and 30 minutes.

Polymer molecular weight distributions tend to increase with increasing temperature of polymerisation (for example, M_w/M_n values increase from 3.2 to 4.3 for LDHMAO-^{Me_2}SB(^{tBu}N,I*)TiCl$_2$) (Table A3.3). The low molecular weight distributions at low temperatures, such as 3.2 for LDHMAO-^{Me_2}SB(^{tBu}N,I*)TiCl$_2$ at 50 and 60 °C, indicate that there is a relatively high degree of control in these polymerisations.[57] Broader molecular weight distributions at higher temperatures would suggest that higher polymerisation temperatures result in poorer control in the polymerisation reaction. Both LDHMAO-^{Me_2}SB(^{tBu}N,I*)TiCl$_2$ and LDHMAO-^{Me_2}SB(^{tBu}N,$^{3\text{-}Et}$I*)TiCl$_2$ produced polyethylene with molecular weights in excess of 2500 kDa, maintaining relatively

narrow molecular weight distributions (3.2 and 3.9 respectively) and with activities still being very high (greater than 1000 $kg_{PE}/mol_{Ti}/h/bar$).[58]

3.3.2 Variation of complex loading levels on LDHMAO

Having previously observed the very high polymer molecular weights produced by LDHMAO-^{Me2}SB($^{t Bu}$N,I*)$TiCl_2$ at 50 °C with relatively narrow dispersities (M_w = 2873 kDa, M_w/M_n = 3.2), investigations were carried out to determine if UHMWPE could be produced at high productivities and activities, while maintaining relatively narrow molecular weight distributions. Polymerisations were undertaken between 30 and 90 °C, with ^{Me2}SB($^{t Bu}$N,I*)$TiCl_2$ supported on LDHMAO in $[Al]_0$:$[Ti]_0$ ratios of 200:1, 100:1 and 50:1.

Polymerisation activities for the LDHMAO-supported complexes in $[Al]_0$:$[Ti]_0$ ratios of 200:1 and 100:1 have activities comparable to each other (maximum activities of 1759 and 1867 $kg_{PE}/mol_{Ti}/h/bar$ respectively, Figure 3.19) and would suggest that bimetallic deactivation does not occur at these loading levels. However, the large decrease in activities observed for the 50:1 loading (maximum activity of 754 $kg_{PE}/mol_{Ti}/h/bar$) would suggest that at the highest loading, the proposed bimetallic decomposition pathways occur through deactivation and blocking of active sites.[17,59]

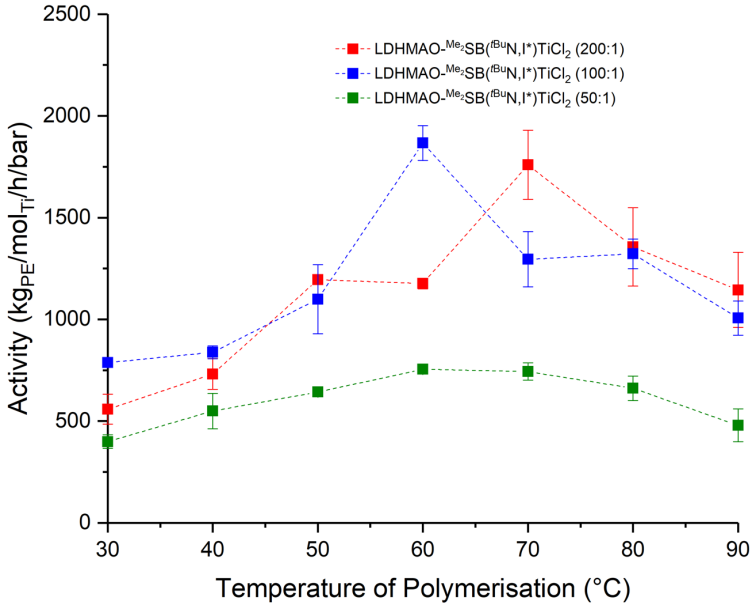

Figure 3.19. Ethylene polymerisation activities for ^{Me2}SB(^{tBu}N,I*)TiCl$_2$ supported on LDHMAO in a variety of [Al]$_0$:[Ti]$_0$ ratios; 2 bar ethylene, 50 mL hexanes, 10 mg catalyst ([Al]$_0$:[Ti]$_0$ = 200:1, 100:1 or 50:1), 150 mg TiBA and 30 minutes. Error bars as 1 standard deviation.

Comparison of productivities (mass$_{polymer}$/mass$_{catalyst}$/bar/h) demonstrates that higher productivities are afforded by the 100:1 loadings, with values (up to 0.177 kg$_{PE}$/g$_{cat}$/h/bar) almost double that of the 200:1 loadings (up to 0.086 kg$_{PE}$/g$_{cat}$/h/bar). Productivities of the 50:1 loading are more comparable to those of the 100:1 loading (up to 0.143 kg$_{PE}$/g$_{cat}$/h/bar). By comparison to these values, the highest productivity obtained for sMAO-^{Me2}SB(^{tBu}N,I*)TiCl$_2$ is 0.574 kg$_{PE}$/g$_{cat}$/h/bar, highlighting the greater productivity and activity afforded by sMAO than LDHMAO.

The molecular weights of the polymers produced by the LDHMAO-supported complexes are far greater than those produced by the sMAO-supported complexes; over three times greater at 50 °C (2888 and 3325 kDa for 1:200 and 1:100 loadings compared with 881 kDa for the sMAO support) (Figure 3.20). At temperatures below 50 °C, the polymers produced have molecular weights in excess of 3000 kDa with narrow molecular weight distributions; the actual molecular weights of these polymers are likely to be in excess of those given due to the molecular weights reaching the limits of the GPC

instrument. The relatively narrow molecular weight dispersities of the polymers indicate a relatively high degree of control in the polymerisation mechanism,[57] with increasing molecular weight distributions at higher temperatures suggesting that there is reduced control over the polymerisation reaction at higher temperatures. The production of UHMWPE with relatively narrow dispersities is extremely desirable for industrial applications as discussed in 3.1.2, with molecular weights of up to 3510 kDa obtained.

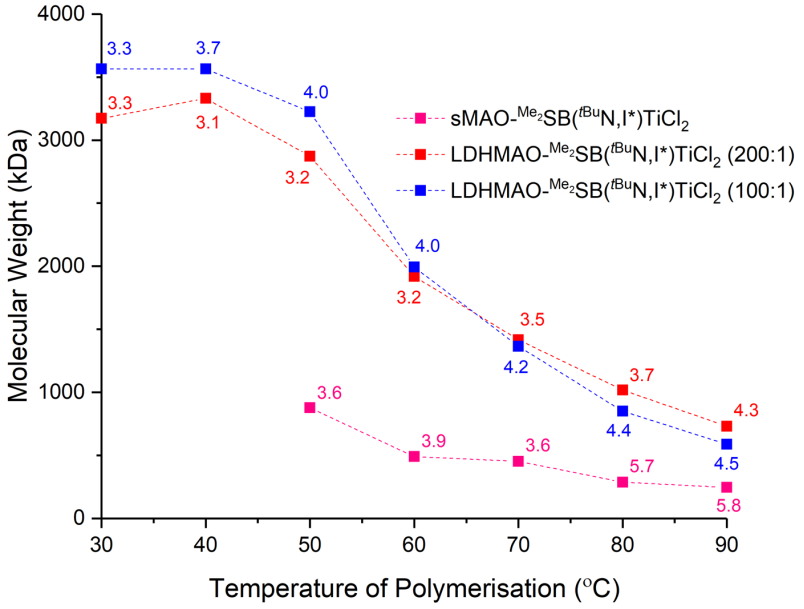

Figure 3.20. Polymer molecular weights for $^{Me2}SB(^{tBu}N,I^*)TiCl_2$ supported on LDHMAO with $[Al]_0$:$[Ti]_0$ ratios of 200:1 and 100:1 compared with sMAO-$^{Me2}SB(^{tBu}N,I^*)TiCl_2$; 2 bar ethylene, 50 mL hexanes, 10 mg catalyst ($[Al]_0$:$[Ti]_0$ = 200:1 or 100:1), 150 mg TiBA and 30 minutes. M_w/M_n values given.

3.3.3 sMAO support variation

sMAO has been shown to be an efficient support in the production of polyethylene, affording enhanced polymerisation activities in comparison with both LDHMAO and SSMAO. To further investigate the effect of sMAO on ethylene polymerisation catalysis, two differing types of sMAO have been investigated. Both types were produced by TOSOH Finechem Corp. (Japan) as slurries in toluene and were dried under vacuum prior

to use. The difference between the two generations of sMAO (1st and 3rd) is a result of alternative synthetic methods that affect both the nucleation and crystallisation rates. Aluminium contents of the two generations (41.1 and 40.2 wt% for 1st and 3rd generation respectively) and particle sizes (~5 μm) are similar.

Five complexes, ^{Me2}SB($^{t Bu}$N,I*)TiCl$_2$, ^{Me2}SB($^{t Bu}$N,I*)Ti(CH$_2$Ph)$_2$, ^{Me2}SB($^{t Bu}$N,I*)Ti(CH$_2$SiMe$_3$)$_2$, ^{Me2}SB($^{t Bu}$N,I*)Ti(Cl)CH$_2$SiMe$_3$ and ^{Me2}SB($^{t Bu}$N,$^{3\text{-}Et}$I*)TiCl$_2$, were tested using both 1st and 3rd generation sMAO. Polymerisations were undertaken at 70 °C for 30 minutes. The polymerisation activities remain approximately constant at 70 °C for both ^{Me2}SB($^{t Bu}$N,I*)TiCl$_2$ and ^{Me2}SB($^{t Bu}$N,$^{3\text{-}Et}$I*)TiCl$_2$, with activities of 3524 and 3443 kg$_{PE}$/mol$_{Ti}$/h/bar, and 3593 and 3880 kg$_{PE}$/mol$_{Ti}$/h/bar respectively for 1st and 3rd generation sMAO (Figure 3.21). Large decreases in polymerisation activity are observed for both ^{Me2}SB($^{t Bu}$N,I*)Ti(CH$_2$Ph)$_2$ and ^{Me2}SB($^{t Bu}$N,I*)Ti(CH$_2$SiMe$_3$)$_2$, with decreases in activities from 5777 and 4377 kg$_{PE}$/mol$_{Ti}$/h/bar and 6171 to 3314 kg$_{PE}$/mol$_{Ti}$/h/bar; there is a large increase in polymerisation activity for ^{Me2}SB($^{t Bu}$N,I*)Ti(Cl)CH$_2$SiMe$_3$ with an increase from 2411 to 4905 kg$_{PE}$/mol$_{Ti}$/h/bar. Previously reported activities for complexes supported on 1st and 3rd generation sMAO, sMAO-^{Me2}SB(I*,Cp)ZrCl$_2$ and sMAO-(Cp$^{n Bu}$)$_2$ZrCl$_2$, both show decreases in activity from 5144 to 4622 kg$_{PE}$/mol$_{Zr}$/h/bar and 3459 to 2912 kg$_{PE}$/mol$_{Zr}$/h/bar respectively.[60]

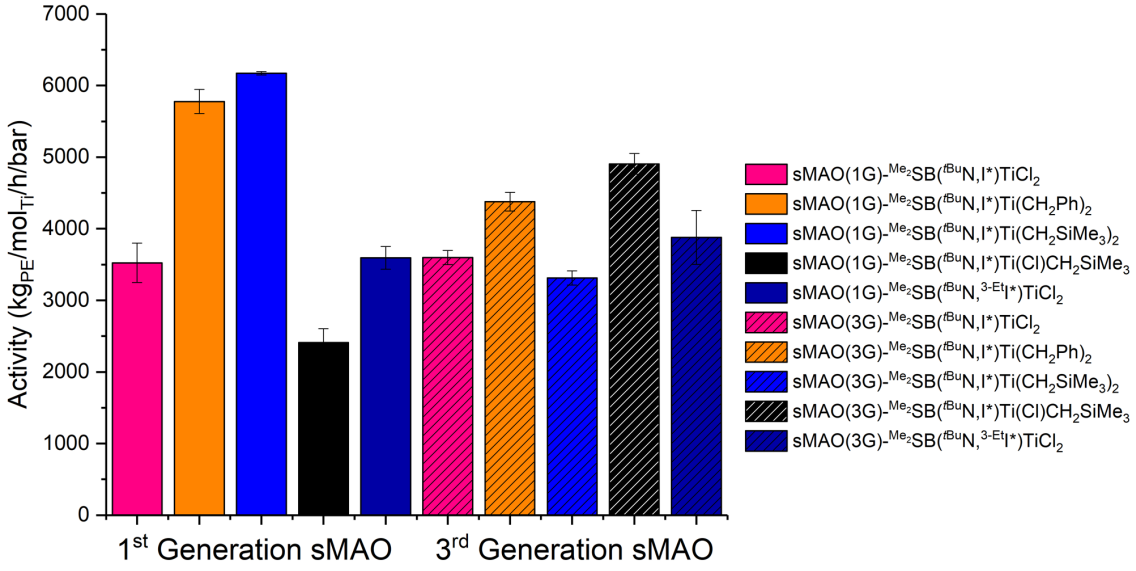

Figure 3.21. Ethylene polymerisation activities for complexes supported on 1st and 3rd generation sMAO; 2 bar ethylene, 50 mL hexanes, 10 mg catalyst ($[Al]_0$:$[Ti]_0$ = 200:1), 150 mg TiBA, 70 °C and 30 minutes. Error bars as 1 standard deviation.

Having observed the large increase in polymerisation activity for ^{Me2}SB($^{t Bu}$N,I*)Ti(Cl)CH_2SiMe_3 on 3rd generation sMAO compared with 1st generation sMAO, ethylene polymerisation studies were carried out over a range of temperatures, 50 to 90 °C, to determine how the temperature dependence varies on the two different supports (Figure 3.22).

The large difference in polymerisation activities is maintained across all temperatures for 1st and 3rd generation sMAO-supported ^{Me2}SB($^{t Bu}$N,I*)Ti(Cl)CH_2SiMe_3, with a maximum activity of 2943 and 4474 $kg_{PE}/mol_{Ti}/h/bar$ at 60 and 70 °C respectively for the two supports. Conversely, polymerisation activities for sMAO-^{Me2}SB($^{t Bu}$N,I*)$TiCl_2$ remain similar across a range of temperatures, with minimal difference in polymerisation activities between the two supports (less than 14%). Polymerisation activities below 50 °C decrease for the 3rd generation sMAO-supported ^{Me2}SB($^{t Bu}$N,I*)$TiCl_2$, with a decrease from 3443 $kg_{PE}/mol_{Ti}/h/bar$ to 2715 $kg_{PE}/mol_{Ti}/h/bar$ at 40 °C and 1276 $kg_{PE}/mol_{Ti}/h/bar$ at 30 °C. The change in polymerisation activities are most likely

attributable to the differing structure of the sMAO particles, caused by the different synthetic methods affecting both the size and properties of the sMAO support.

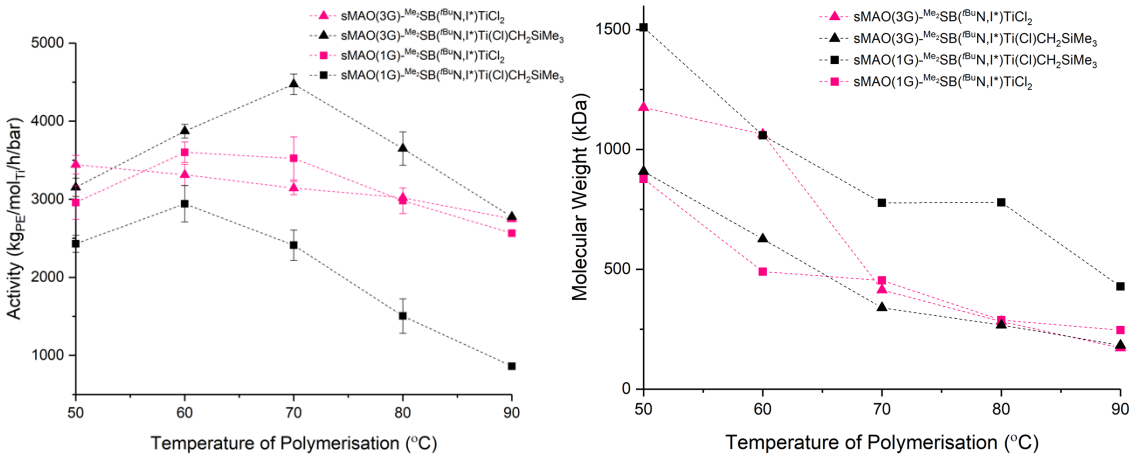

Figure 3.22. Ethylene polymerisation activities (left) and polymer molecular weights (right) for ^{Me2}SB($^{t\text{Bu}}$N,I*)TiCl$_2$ and ^{Me2}SB($^{t\text{Bu}}$N,I*)Ti(Cl)CH$_2$SiMe$_3$ supported on 1st (square) and 3rd (triangle) generation sMAO; 2 bar ethylene, 50 mL hexanes, 10 mg catalyst ([Al]$_0$:[Ti]$_0$ = 200:1), 150 mg TiBA and 30 minutes. Error bars as 1 standard deviation.

The polymer molecular weights and molecular weight distributions have been determined by GPC, with these values given in Figure 3.22 (right) and Table A3.4. Polymer molecular weights decrease with increasing polymerisation temperature in all cases, as would be expected. Similar molecular weights are observed for 1st and 3rd generation sMAO-^{Me2}SB($^{t\text{Bu}}$N,I*)TiCl$_2$ between 70 and 90 °C, but much larger values are observed for 3rd generation sMAO at 50 and 60 °C (1175 and 1063 kDa compared with 881 and 490 kDa). In contrast, much higher molecular weights are observed for 1st generation sMAO-supported ^{Me2}SB($^{t\text{Bu}}$N,I*)Ti(Cl)CH$_2$SiMe$_3$ than the 3rd generation sMAO-supported complex, exemplified by the values at 50 °C of 1509 and 908 kDa respectively. Polymer molecular weight distributions remain relatively narrow for both complexes on both supports and the dispersities observed (3.2–4.1) would indicate that the polymerisations are relatively well controlled, with increasing M_w/M_n values at higher temperatures suggesting that higher temperatures result in poorer control of the polymerisation reaction.

3.4 Larger scale ethylene polymerisation

The effect of increasing the size of the polymerisation vessel was investigated for five supported complexes: sMAO(3G)-^{Me_2}SB($^{t Bu}$N,I*)TiCl$_2$, sMAO(3G)-^{Me_2}SB($^{t Bu}$N,$^{3\text{-}Et}$I*)TiCl$_2$, sMAO(3G)-^{Me,Pr}SB($^{t Bu}$N,I*)TiCl$_2$, sMAO(3G)-^{Me_2}SB($^{t Bu}$N,I*)Ti(CH$_2$SiMe$_3$)$_2$ and sMAO(3G)-^{Me_2}SB($^{t Bu}$N,I*)Ti(Cl)CH$_2$SiMe$_3$ (Figure 3.23), all supported in an [Al]$_0$:[Ti]$_0$ ratio of 200:1.

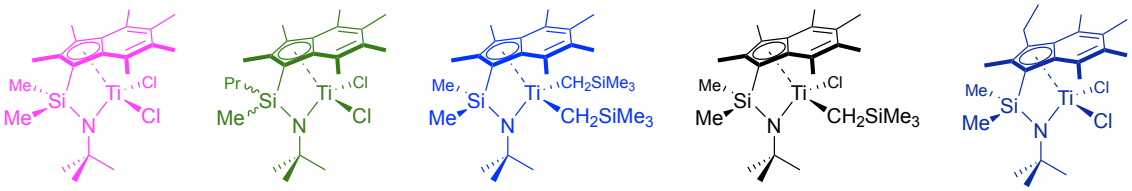

Figure 3.23. Molecular structure of the five complexes tested in this section. Colours correspond to colours of the lines used on the graphs.

The reaction flask size was increased from 150 to 500 mL, with the amount of hexanes used increased from 50 to 250 mL and the amount of TiBA scavenger increased from 150 to 750 mg. The amount of catalyst added (10 mg) was kept constant, and ethylene pressure was maintained at 2 bar. Polymerisations were undertaken at 70 °C for 30 minutes. Comparisons of the activities on both polymerisation scales for these polymerisations are shown in Figure 3.24 and Table 3.4, the molecular weights and molecular weight distributions of the polymers produced are also shown in Table 3.4.

No large increases in activity are observed with the larger scale polymerisations, in contrast to what has previously been observed for sMAO-supported complexes based on ^{Me_2}SB(I*,Cp^R)ZrX$_2$ where activities almost doubled.[17,60] Activities remained approximately equal for sMAO(3G)-^{Me_2}SB($^{t Bu}$N,I*)TiCl$_2$ and sMAO(3G)-^{Me_2}SB($^{t Bu}$N,I*)Ti(Cl)CH$_2$SiMe$_3$ (3343 and 3654 kg$_{PE}$/mol$_{Ti}$/h/bar and 4905

and 4795 $kg_{PE}/mol_{Ti}/h/bar$ respectively), while polymerisation activities decreased on scale-up for the remaining three complexes. Polymerisation activities would be expected to increase due to mass-transfer limiting effects in the smaller scale polymerisation reactions. The ethylene molecules encounter diffusional resistance in multiple places to reach the active site: at the gas-liquid interface, there is a liquid film surrounding the polymer macroparticle, the small pores of the polymer macroparticle and a polymeric shell encapsulating the active catalytic fragment.[61] Increasing the size of the polymerisation apparatus should help to overcome some of these mass-transfer limitations; a larger surface area for the gas-liquid phase barrier should lead to higher ethylene polymerisation rates.[62,63]

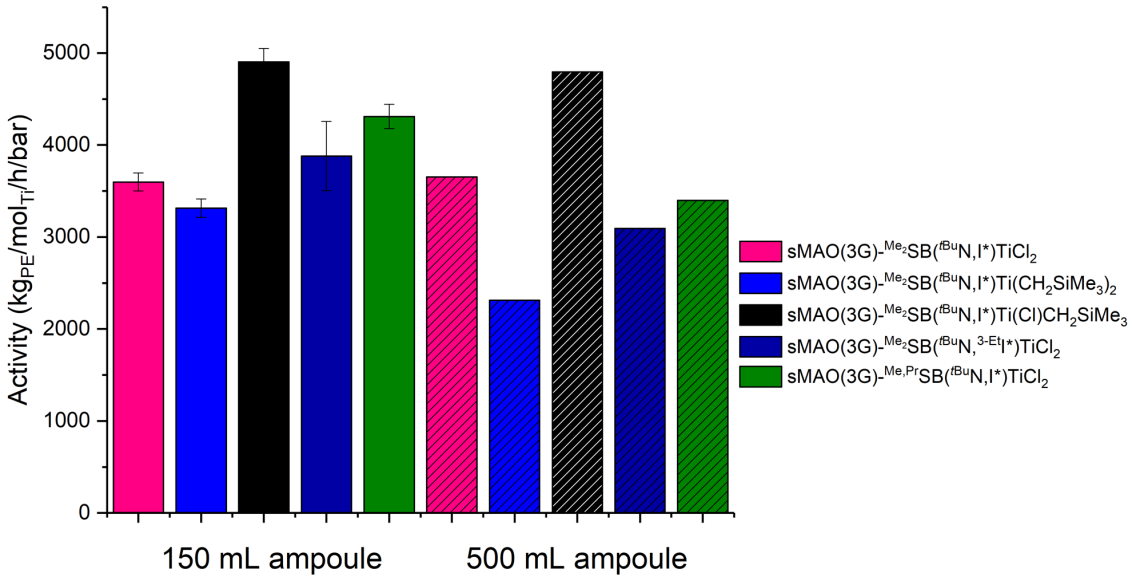

Figure 3.24. Slurry-phase ethylene polymerisation activities for standard (150 mL ampoule) and larger scale (500 mL ampoule) ethylene polymerisations. Standard scale conditions: 10 mg catalyst ($[Al]_0:[Ti]_0$ = 200:1), 2 bar ethylene, 50 mL hexanes, 150 mg TiBA, 30 minutes and 70 °C. Larger scale conditions: 10 mg catalyst ($[Al]_0:[Ti]_0$ = 200:1), 2 bar ethylene, 250 mL hexanes, 750 mg TiBA, 30 minutes and 70 °C. Error bars as 1 standard deviation.

Table 3.4. Slurry-phase ethylene polymerisation activities and polymer molecular weights for sMAO(3G)-supported complexes with standard scale (150 mL ampoule) and larger scale (500 mL ampoule) ethylene polymerisations. Error given as 1 standard deviation.

Catalyst	Standard scale			Larger Scale		
	Activity[a]	M_w (kDa)	M_w/M_n	Activity[a]	M_w (kDa)	M_w/M_n
^{Me2}SB($^{t Bu}$N,I*)TiCl$_2$	3443±94	414	6.6	3654	1355	5.3
^{Me2}SB($^{t Bu}$N,I*)Ti(CH$_2$SiMe$_3$)$_2$	3314±99	667	3.7	2311	1734	3.9
^{Me2}SB($^{t Bu}$N,I*)Ti(Cl)CH$_2$SiMe$_3$	4905±144	369	3.3	4795	1019	3.6
^{Me2}SB($^{t Bu}$N,$^{3\text{-}Et}$I*)TiCl$_2$	3880±376	395	3.2	3094	1152	4.3
^{Me,Pr}SB($^{t Bu}$N,I*)TiCl$_2$	4146±32	554	3.8	3397	1432	3.9

[a] Activity in kg$_{PE}$/mol$_{Ti}$/mol/h/bar

As is seen in Table 3.4, increased size of the polymerisation vessel results in increased polymer molecular weights. Polymer molecular weights more than doubled in all cases, with an increase of 227% observed for sMAO(3G)-^{Me2}SB($^{t Bu}$N,I*)TiCl$_2$ with increasing scale. These increases in the molecular weights for all complexes would suggest that increasing the scale of the reaction leads to a decrease in the rate of chain termination relative to the rate of propagation resulting in longer chain polymers being formed. The molecular weight distributions of the polymers produced remain approximately constant for each complex on the two different scales, suggesting that changing the size of the reactor does not affect the relative control of the polymerisation reactions.

3.5 Effect of scavenger variation on polymerisation activity

The use of a scavenger has been shown to be important in slurry-phase ethylene polymerisation studies. McKenna *et al*. have carried out ethylene polymerisation studies with $(Cp^{nBu})_2ZrCl_2$ and an MAO cocatalyst with a range of scavengers; lower polymerisation rates were reported for triethylaluminium (TEA) when compared with TiBA and trioctylaluminium (TOA), with molecular weights of the polymers produced also affected.[64] In this study, three alkylaluminium species (TMA, TEA and TiBA) and MAO were used as scavenger and polymerisations were carried out for 30 minutes at temperatures from 50 to 90 °C, with the exception of the MAO scavenger, where polymerisations were carried out for 5 minutes. The results of this are shown below in Figure 3.25.

Highest activities for the three alkylaluminium scavengers are observed for TiBA. Between 50 and 70 °C, activities with TEA scavenger are between 56 and 59% of the activity of the TiBA scavenger, larger decreases are observed at 80 and 90 °C with activities at 34 and 24% of those of the TiBA scavenger. Activities with a TMA scavenger increase with temperature, in contrast to both TEA and TiBA, with activities increasing from 597 to 979 $kg_{PE}/mol_{Ti}/h/bar$ from 50 to 90 °C. These activities are between 17 and 36% of the activities observed for the TiBA scavenger, and the activities lower than all other scavengers apart from TEA at 90 °C.

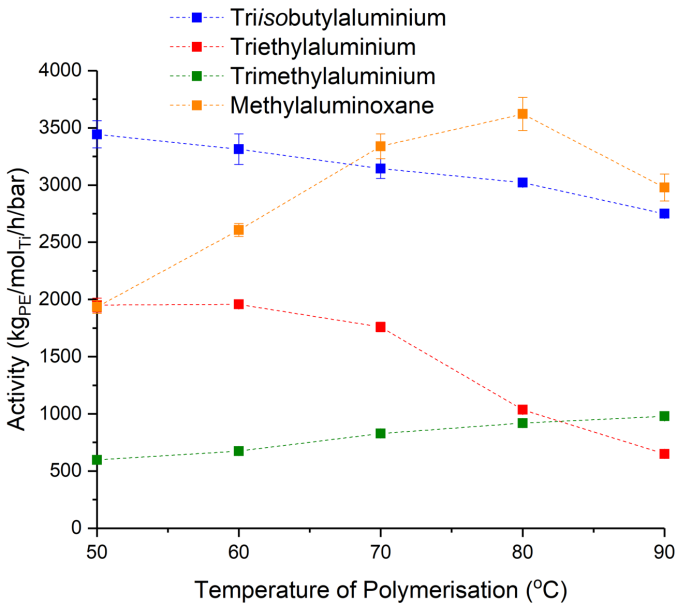

Figure 3.25. Ethylene polymerisation activities of sMAO-^{Me2}SB(^{tBu}N,I*)TiCl$_2$ with various scavengers (TiBA, TEA, TMA and MAO); 2 bar ethylene, 50 mL hexanes, 10 mg catalyst ([Al]$_0$:[Ti]$_0$ = 200:1), 1000 equivalents of scavenger and 30 minutes (5 minutes MAO). Error bars as 1 standard deviation.

Polymerisations with the MAO scavenger were only run for 5 minutes, further polymerisation time resulted in stirring being inhibited and the polymer produced was much more clumpy and aggregated, as can be seen in the SEM images in Figure 3.26. With an MAO scavenger, activities are highest at 80 °C with an activity of 3621 kg$_{PE}$/mol$_{Ti}$/h/bar.

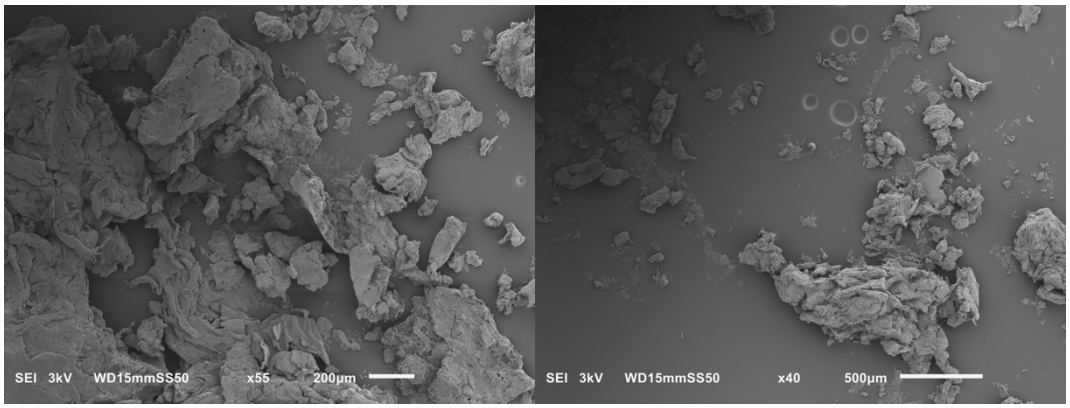

Figure 3.26. SEM images of the polymer produced by sMAO-^{Me2}SB(^{tBu}N,I*)TiCl$_2$ with an MAO scavenger.

Lower activities for TMA and TEA have both been previously observed for sMAO-^{Me2}SB(I*,Cp)$ZrCl_2$ and sMAO-^{Me2}SB(I*,Cp^{Me})$Zr(CH_2Ph)_2$,[60] with the use of an MAO scavenger also resulting in polymer aggregation. Boisson *et al.* have reported that polymerisation of SSMAO-$(Cp^{nBu})_2ZrCl_2$ with TiBA and TEA scavenger resulted in lower activities for the TEA scavenger (166 $kg_{PE}/mol_{Zr}/h/bar$) compared with TiBA (226 $kg_{PE}/mol_{Zr}/h/bar$).[57] It has been proposed that the difference in polymerisation activity is attributed to the relative stabilities of the heterobimetallic species $[Cp_2M(\mu\text{-}CH_2R')(\mu\text{-}R)AlR_2]^+$ formed.[65–67] Fink *et al*. have demonstrated that increasing the steric bulk of the alkyl fragment of AlR_3 results in lower stability of the heterobimetallic species.[68] Heating of the supported complexes at 70 °C for 30 minutes with the four different scavengers shows no sign of catalyst leaching, with neither colouring of the solutions or any changes observed in the ^{1}H NMR spectra. The scavenger used also affects the molecular weights of the polymer produced, with molecular weights and molecular weight distributions shown in Figure 3.27.

The much lower molecular weights observed for the polymers produced with TMA scavenger (up to 270 kDa) are to be expected, due to the alternative chain transfer pathways facilitated by TMA that are less commonly observed for either TiBA, TEA or MAO (with molecular weights up to 1175, 1852 and 1118 kDa respectively).[55] With TiBA, TEA and MAO, the increased bulk of the alkyl aluminium species (acting as a chain transfer agent) reduces the levels of chain transfer that occurs.[69,70]

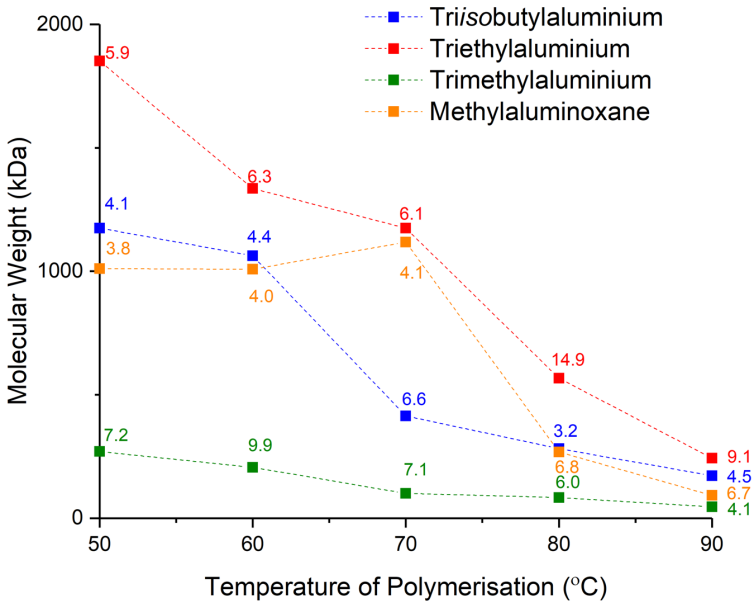

Figure 3.27. Polymer molecular weights of sMAO-^{Me2}SB(^{tBu}N,I*)TiCl$_2$ with various scavengers (TiBA, TEA, TMA and MAO); 2 bar ethylene, 50 mL hexanes, 10 mg catalyst ([Al]$_0$:[Ti]$_0$ = 200:1), 1000 equivalents of scavenger and 30 minutes (5 minutes MAO). M_w/M_n values given.

Variation of the amount of scavenger shows that polymerisation activities are highest on addition on 2500 equivalents of TiBA (4573 kg$_{PE}$/mol$_{Ti}$/h/bar). Similar activities are observed with addition of 250 to 1000 equivalents of TiBA (4011, 3870 and 4031 kg$_{PE}$/mol$_{Ti}$/h/bar, Table 3.5). With addition of 5000 equivalents of TiBA, a lower polymerisation activity is observed (3497 kg$_{PE}$/mol$_{Ti}$/h/bar). This decrease in polymerisation activity could be caused by catalyst poisoning and decomposition facilitated by the excess amount of TiBA added.[24] In addition, it has been proposed that increasing the concentration of the scavenger also increases the probability of formation of the inactive heterobimetallic species, leading to lower activities.[67] Similarly, addition of smaller amounts of TiBA scavenger hinders ethylene polymerisation activity, with activities of 73 and 2341 kg$_{PE}$/mol$_{Ti}$/h/bar for addition of 0 and 100 equivalents of TiBA respectively. The lower activities associated with small amounts of TiBA addition can be attributed to deactivation of the active species due to any residual water or oxygen that remains in the ethylene or hexanes causing catalytic decomposition.

Table 3.5. Ethylene polymerisation activities ($kg_{PE}/mol_{Ti}/h/bar$) and the molecular weights (kDa) and molecular weight distributions of the polymers produced at varying amounts of TiBA scavenger; 2 bar ethylene, 50 mL hexanes, 10 mg catalyst ($[Al]_0:[Ti]_0$ = 200:1), 70 °C and 30 minutes. Errors as 1 standard deviation

TiBA Equivalents	Activity	M_w	M_w/M_n
	($kg_{PE}/mol_{Ti}/h/bar$)	(kDa)	
0	73±48	-	-
100	2341±4	882	3.2
250	4011±184	477	4.0
500	3870±112	591	3.3
1000	4031±4	452	3.5
2500	4573±254	307	4.0
5000	3497±277	162	6.8

Polymer molecular weights decrease with increased addition of TiBA, with molecular weights decreasing from 882 kDa with addition of 100 equivalents of TiBA to 162 kDa with addition of 5000 equivalents of TiBA. Lower molecular weights with increased addition of TiBA are to be expected as a result of increased probability of chain transfer to TiBA.[55]

3.6 Solution-phase ethylene polymerisation

Solution-phase ethylene polymerisation studies were undertaken with four complexes: ^{Me2}SB($^{t Bu}$N,I*)TiCl$_2$, ^{Me2}SB($^{t Bu}$N,$^{3\text{-}Et}$I*)TiCl$_2$, ^{Me,Pr}SB($^{t Bu}$N,I*)TiCl$_2$ and ^{Me2}SB($^{t Bu}$N,I*)Ti(Cl)CH$_2$SiMe$_3$ (Figure 3.16, Section 3.3). Solution-phase polymerisations were undertaken in a 150 mL ampoule containing 0.5 mg of complex with 1000 equivalents of MAO cocatalyst and 50 mL of hexanes under 2 bar of ethylene pressure. Polymerisations were carried out for five minutes, with longer polymerisation times resulting in stirring stopping due to the amount and morphology of the polymer produced. The activities of these polymerisations are shown below and compared with those of the sMAO-supported slurry-phase polymerisations in Table 3.6, with the polymer molecular weights and molecular weight distributions shown in Table 3.7.

In all cases, solution polymerisation activities are lower than those of the equivalent slurry-phase ethylene polymerisation activities, with the significantly lower polymerisation activity of ^{Me2}SB($^{t Bu}$N,I*)Ti(Cl)CH$_2$SiMe$_3$ attributable to the stirring being stopped after approximately two and a half minutes during polymerisation experiments. All activities are rated as very good on the Gibson scale (activities greater than 1000 $kg_{PE}/mol_{Ti}/h/bar$),[58] with the relative activities of ^{Me2}SB($^{t Bu}$N,I*)TiCl$_2$, ^{Me2}SB($^{t Bu}$N,$^{3\text{-}Et}$I*)TiCl$_2$ and ^{Me,Pr}SB($^{t Bu}$N,I*)TiCl$_2$ following the same trend in both solution and slurry-phase: ^{Me,Pr}SB($^{t Bu}$N,I*)TiCl$_2$ > ^{Me2}SB($^{t Bu}$N,$^{3\text{-}Et}$I*)TiCl$_2$ > ^{Me2}SB($^{t Bu}$N,I*)TiCl$_2$. The poor morphology of the polymer produced led to reactor fouling, and also likely inhibited stirring in all polymerisations, limiting the larger scale solution-phase polymerisation potential of these complexes. Polymerisation activities were much greater than those reported for [^{Me2}SB($^{t Bu}$N,Cp*)TiMe][MeB(C$_6$F$_5$)$_3$] and [^{Me2}SB($^{t Bu}$N,Cp*$^{-H}$)Ti][PhCH$_2$B(C$_6$F$_5$)$_3$], formed by reaction of ^{Me2}SB($^{t Bu}$N,Cp*)TiMe$_2$

and ^{Me2}SB($^{t\text{Bu}}$N,Cp*)Ti(CH_2Ph)$_2$ with B(C_6F_5)$_3$ (Figure 3.28), with activities of 114 and 131 $kg_{PE}/mol_{Ti}/h/bar$ respectively,[14] but lower than that of ^{Me2}SB(I*,Cp)$ZrCl_2$ (6284 $kg_{PE}/mol_{Zr}/h/bar$) activated with 200 equivalents of MAO at 80 °C under analogous conditions.[60] Activities were also higher than those reported for the unbridged zirconocenes ($^{2,4\text{-Me}}$I)$_2ZrCl_2$ and ($^{2,4,6\text{-Me}}$I)$_2ZrCl_2$ activated with 3000 equivalents of MAO cocatalyst with activities of 3590 and 3890 $kg_{PE}/mol_{Zr}/h/bar$ respectively.[71]

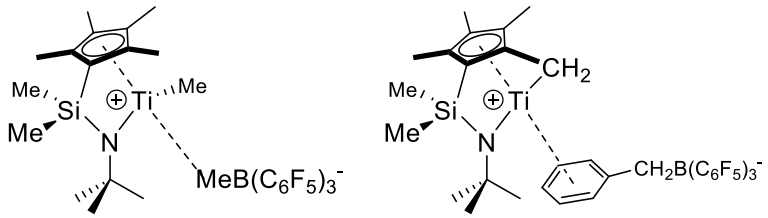

Figure 3.28. [^{Me2}SB($^{t\text{Bu}}$N,Cp*)TiMe][MeB(C_6F_5)$_3$] and [^{Me2}SB($^{t\text{Bu}}$N,Cp*$^{-H}$)Ti][$PhCH_2B(C_6F_5)_3$], formed by reaction of ^{Me2}SB($^{t\text{Bu}}$N,Cp*)$TiMe_2$ and ^{Me2}SB($^{t\text{Bu}}$N,Cp*)Ti(CH_2Ph)$_2$ with B(C_6F_5)$_3$.[14]

The reactor fouling that occurs in solution polymerisations along with the hindered stirring caused by the poor polymer morphology compared with the "popcorn-shaped" particles formed in sMAO-supported slurry-phase polymerisations would likely account for the lower activities observed. In addition, the greater amount of complex present in the solution-phase reaction (~1–1.1x10^{-6} moles compared with ~7–8x10^{-7} moles in slurry-phase) coupled with the inhibited stirring could lead to activities being limited by mass transfer effects and the ability to solubilise ethylene rapidly enough during the reactions.[62,63]

Table 3.6. Ethylene polymerisation activities for solution and slurry (sMAO) phase polymerisations with ^{Me2}SB(^{tBu}N,I*)TiCl$_2$, ^{Me2}SB(^{tBu}N,$^{3\text{-}Et}$I*)TiCl$_2$, ^{Me,Pr}SB(^{tBu}N,I*)TiCl$_2$ and ^{Me2}SB(^{tBu}N,I*)Ti(Cl)CH$_2$SiMe$_3$. Slurry-phase conditions: 10 mg catalyst ([Al]$_0$:[Ti]$_0$ = 200:1), 2 bar ethylene, 50 mL hexanes, 150 mg TiBA, 70 °C and 5 minutes. Solution-phase conditions: 0.5 mg complex, 1000 equivalents of MAO, 2 bar ethylene, 50 mL hexanes, 70 °C and 5 minutes. Polymerisations were carried out, at least, in duplicate. Error given as 1 standard deviation.

Complex	Solution	Slurry
	Activity[a]	Activity[a]
^{Me2}SB(^{tBu}N,I*)TiCl$_2$	4421±153	5562±363
^{Me2}SB(^{tBu}N,$^{3\text{-}Et}$I*)TiCl$_2$	4538±102	6012±5
^{Me,Pr}SB(^{tBu}N,I*)TiCl$_2$	4881±43	7021±101
^{Me2}SB(^{tBu}N,I*)Ti(Cl)CH$_2$SiMe$_3$	2681±87[b]	6532±13

[a] Activity in kg$_{PE}$/mol$_{Ti}$/h/bar; [b] polymerisations stopped stirring after approximately 2.5 minutes.

Molecular weights of the polymers produced in both solution and slurry-phase polymerisations are shown in Table 3.7. The polymer molecular weights for the polymer produced by solution-phase polymerisations are lower than those produced in slurry-phase polymerisations with molecular weight distributions remaining relatively narrow (3.4–3.7), with the exception of ^{Me2}SB(^{tBu}N,I*)Ti(Cl)CH$_2$SiMe$_3$ (M_w/M_n = 6.5). The GPC traces all suggest a monomodal distribution of polymer molecular weights, suggesting that there is one major active species. Reaction of ^{Me2}SB(^{tBu}N,I*)TiCl$_2$ and ^{Me2}SB(^{tBu}N,I*)Ti(Cl)CH$_2$SiMe$_3$ with sequential amounts of MAO in Section 2.3 leads to the formation of [^{Me2}SB(^{tBu}N,I*)TiMe]$^+$ most likely coupled with an anionic [X-MAO]$^-$ species, which was then shown to polymerise ethylene. It is broadly accepted that addition of an MAO cocatalyst results in the formation of the catalytically active metal-alkyl cationic species paired with weakly coordinating anions.[72,73] It seems reasonable to propose that in the above case the catalytically active species are [^{Me2}SB(^{tBu}N,I*)TiMe]$^+$, [^{Me2}SB(^{tBu}N,$^{3\text{-}Et}$I*)TiMe]$^+$ and [^{Me,Pr}SB(^{tBu}N,I*)TiMe]$^+$ for ^{Me2}SB(^{tBu}N,I*)TiCl$_2$, ^{Me2}SB(^{tBu}N,$^{3\text{-}Et}$I*)TiCl$_2$ and ^{Me,Pr}SB(^{tBu}N,I*)TiCl$_2$ respectively with a [Cl-MAO]$^-$ anion in all cases. With the proposed formation of [^{Me2}SB(^{tBu}N,I*)TiMe][SiMe$_3$CH$_2$-MAO] when MAO is added to ^{Me2}SB(^{tBu}N,I*)Ti(Cl)CH$_2$SiMe$_3$, the different polymerisation activities and polymer

properties compared with $^{Me_2}SB(^{tBu}N,I^*)TiCl_2$ would suggest that the nature of the anion influences the polymerisation mechanism and the degree of control in the polymerisation reaction.[74,75]

Table 3.7. Molecular weights (M_w) and dispersities (M_w/M_n) of the polyethylenes produced for solution and slurry-phase polymerisations with $^{Me_2}SB(^{tBu}N,I^*)TiCl_2$, $^{Me_2}SB(^{tBu}N,^{3\text{-}Et}I^*)TiCl_2$, $^{Me,Pr}SB(^{tBu}N,I^*)TiCl_2$ and $^{Me_2}SB(^{tBu}N,I^*)Ti(Cl)CH_2SiMe_3$. Slurry-phase conditions: 10 mg catalyst ($[Al]_0:[Ti]_0 = 200:1$), 2 bar ethylene, 50 mL hexanes, 150 mg TiBA, 70 °C and 5 minutes. Solution-phase conditions: 0.5 mg complex, 1000 equivalents of MAO, 2 bar ethylene, 50 mL hexanes, 70 °C and 5 minutes.

Complex	Solution		Slurry	
	M_w (kDa)	M_w/M_n	M_w (kDa)	M_w/M_n
$^{Me_2}SB(^{tBu}N,I^*)TiCl_2$	159	3.7	453	3.6
$^{Me_2}SB(^{tBu}N,^{3\text{-}Et}I^*)TiCl_2$	205	3.7	276	4.9
$^{Me,Pr}SB(^{tBu}N,I^*)TiCl_2$	240	3.4	480	3.5
$^{Me_2}SB(^{tBu}N,I^*)Ti(Cl)CH_2SiMe_3$	86	6.5	339	3.2

3.7 High-throughput ethylene polymerisation

Catalysts that demonstrated high ethylene polymerisation activities under University of Oxford conditions were studied under high-throughput conditions for ethylene homopolymerisation and hydrogen response. The catalysts tested were sMAO-^{Me2}SB($^{t Bu}$N,I*)TiMe$_2$, sMAO-^{Me2}SB($^{t Bu}$N,I*)Ti(CH$_2$Ph)$_2$, sMAO-^{Me2}SB($^{t Bu}$N,I*)Ti(CH$_2$SiMe$_3$)$_2$, sMAO-^{Me2}SB($^{t Bu}$N,I*)Ti(Cl)CH$_2$SiMe$_3$, sMAO-^{Me2}SB($^{t Bu}$N,I*)TiCl$_2$ and sMAO-^{Me2}SB($^{t Bu}$N,$^{3\text{-}Et}$I*)TiCl$_2$ (Figure 3.29).

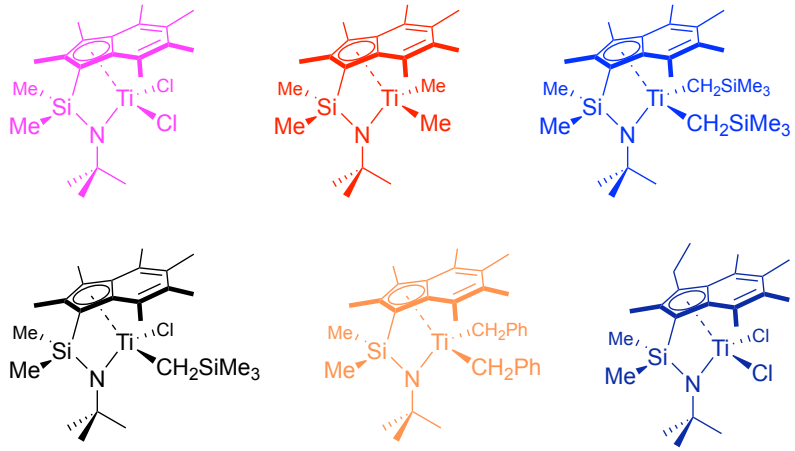

Figure 3.29. Molecular structures of the six complexes tested in this section. Colours correspond to colours of the lines used on the graphs.

High-throughput ethylene polymerisation experiments were carried out at HTExplore (University of Naples) in collaboration with Prof. Vincenzo Busico, with the experiments run by Dr. Alessio Mingione. High-throughput experiments allow for a large number of simultaneous, parallel experiments to be run at the same time, screening a number of different conditions in a shorter time period and are of common use in pharmaceutical, organometallic and organic chemistry.[76,77] Polymerisations were conducted at 8.27 bar ethylene pressure at 80 °C and overhead stirring in 23 mL cells with 5 mL of heptane, 10 µmol TiBA scavenger, 0.075–0.40 mg catalyst ([Al]$_0$:[Ti]$_0$ ratio of 200:1). The reactions were run for 1 hour or until 8.3 bar of ethylene uptake was reached.

Ethylene homopolymerisation activities typically increase under high-throughput conditions (with respect to polymerisations in Sections 3.2.2 and 3.2.3); increasing from 5112 to 8379 $kg_{PE}/mol_{Ti}/h/bar$ for sMAO-^{Me2}SB(^{tBu}N,I*)Ti($CH_2Ph)_2$, 1505 to 4708 $kg_{PE}/mol_{Ti}/h/bar$ for sMAO-^{Me2}SB(^{tBu}N,I*)Ti(Cl)CH_2SiMe_3 and 2981 to 6738 $kg_{PE}/mol_{Ti}/h/bar$ for sMAO-^{Me2}SB(^{tBu}N,I*)$TiCl_2$ (Figure 3.30). Activities however decrease for sMAO-^{Me2}SB(^{tBu}N,I*)$TiMe_2$ (3964 to 1411 $kg_{PE}/mol_{Ti}/h/bar$) and activities remaining approximately constant for sMAO-^{Me2}SB(^{tBu}N,I*)Ti($CH_2SiMe_3)_2$ and sMAO-^{Me2}SB(^{tBu}N,$^{3\text{-}Et}$I*)$TiCl_2$; 4285 to 4388 $kg_{PE}/mol_{Ti}/h/bar$, and 2698 to 2564 $kg_{PE}/mol_{Ti}/h/bar$ respectively.

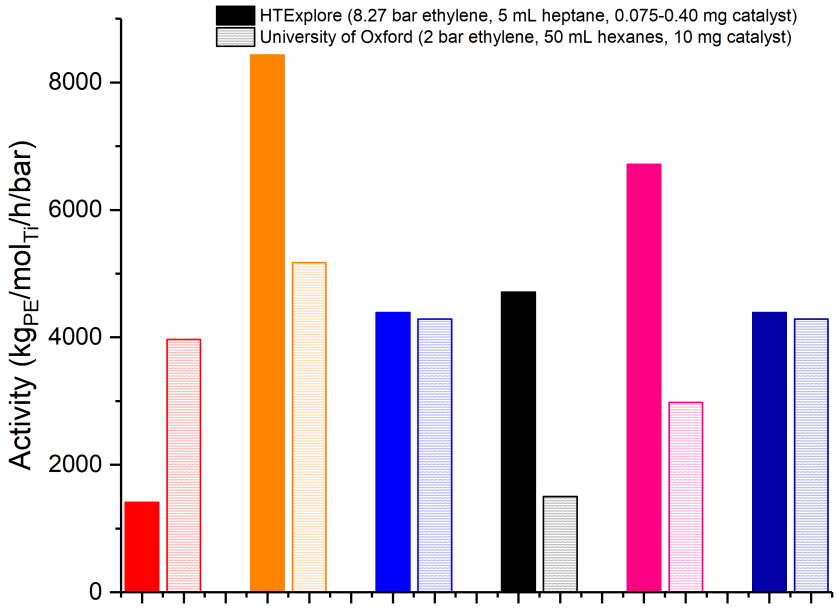

Figure 3.30. Ethylene homopolymerisation activity of sMAO-^{Me2}SB(^{tBu}N,I*)$TiMe_2$ (red), sMAO-^{Me2}SB(^{tBu}N,I*)Ti($CH_2Ph)_2$ (orange), sMAO-^{Me2}SB(^{tBu}N,I*)Ti($CH_2SiMe_3)_2$ (blue), sMAO-^{Me2}SB(^{tBu}N,I*)Ti(Cl)CH_2SiMe_3 (black), sMAO-^{Me2}SB(^{tBu}N,I*)$TiCl_2$ (pink), sMAO-^{Me2}SB(^{tBu}N,$^{3\text{-}Et}$I*)$TiCl_2$ (royal blue) at University of Oxford (unfilled) and HTExplore (filled).

The higher ethylene pressure of the high-throughput experiments leads to large increases in the polymer molecular weights; 2 to 3 times greater for sMAO-^{Me2}SB(^{tBu}N,I*)Ti($CH_2SiMe_3)_2$ and sMAO-^{Me2}SB(^{tBu}N,I*)Ti(Cl)CH_2SiMe_3, and 6.5 to 9.2 times greater for sMAO-^{Me2}SB(^{tBu}N,I*)$TiMe_2$,

sMAO-^{Me_2}SB(^{tBu}N,I*)Ti(CH_2Ph)$_2$, sMAO-^{Me_2}SB(^{tBu}N,$^{3\text{-}Et}$I*)$TiCl_2$ and sMAO-^{Me_2}SB(^{tBu}N,I*)$TiCl_2$ (Table 3.8). Increasing ethylene pressure of polymerisation is likely to lead to increased rates of ethylene propagation relative to chain termination and as such molecular weights increase.[78] The narrower molecular weight distributions of the polymer produced would signify a greater degree of control in the polymerisation mechanism with the higher pressure of reaction and the high-throughput experimental set up, and the relatively narrow distributions (3.2–3.8) would suggest polymerisations are likely single-site in nature.[57]

Table 3.8. Molecular weights (M_w) and dispersities (M_w/M_n) of the polyethylenes produced using sMAO-^{Me_2}SB(^{tBu}N,I*)$TiMe_2$, sMAO-^{Me_2}SB(^{tBu}N,I*)Ti(CH_2Ph)$_2$, sMAO-^{Me_2}SB(^{tBu}N,I*)Ti(CH_2SiMe_3)$_2$, sMAO-^{Me_2}SB(^{tBu}N,I*)Ti(Cl)CH_2SiMe_3, sMAO-^{Me_2}SB(^{tBu}N,$^{3\text{-}Et}$I*)$TiCl_2$ and sMAO-^{Me_2}SB(^{tBu}N,I*)$TiCl_2$ at University of Oxford and HTExplore at 80 °C.

Catalyst	University of Oxford		HTExplore	
	M_w (kDa)	M_w/M_n	M_w (kDa)	M_w/M_n
sMAO-^{Me_2}SB(^{tBu}N,I*)$TiCl_2$	288	5.7	2667	3.2
sMAO-^{Me_2}SB(^{tBu}N,I*)Ti(CH_2Ph)$_2$	231	5.1	1.6×10^3	3.3
sMAO-^{Me_2}SB(^{tBu}N,I*)$TiMe_2$	174	3.8	1.4×10^3	3.4
sMAO-^{Me_2}SB(^{tBu}N,I*)Ti(CH_2SiMe_3)$_2$	650	4.4	1.8×10^3	3.5
sMAO-^{Me_2}SB(^{tBu}N,I*)Ti(Cl)CH_2SiMe_3	769	4.3	1.5×10^3	3.8
sMAO-^{Me_2}SB(^{tBu}N,$^{3\text{-}Et}$I*)$TiCl_2$	205	4.7	1.4×10^3	3.4

3.7.1 Hydrogen response

During these hydrogen response experiments, 0.075–0.30 mg of catalyst was used, and hydrogen supplied at 0.8% (0.07 bar) or 1.6% (0.13 bar) by a mixed hydrogen/nitrogen feed. Activities and uptake rates are shown in Figures 3.31 to 3.34 and Table 3.9.

Polymerisation activities decrease with increased addition of hydrogen, with the decreases in polymerisation activity being greater for the alkylated complexes than the dichloride and the mono-neosilyl complexes. The decreases in activity compared to

homopolymerisation with 1.6% hydrogen addition for sMAO-^{Me2}SB($^{t Bu}$N,I*)Ti(Cl)CH_2SiMe_3, sMAO-^{Me2}SB($^{t Bu}$N,$^{3\text{-}Et}$I*)$TiCl_2$ and sMAO-^{Me2}SB($^{t Bu}$N,I*)$TiCl_2$ are 31, 40 and 28% respectively compared with decreases of 43, 55 and 66% for sMAO-^{Me2}SB($^{t Bu}$N,I*)Ti(CH_2SiMe_3)$_2$, sMAO-^{Me2}SB($^{t Bu}$N,I*)$TiMe_2$ and sMAO-^{Me2}SB($^{t Bu}$N,I*)Ti(CH_2Ph)$_2$. The alkylated complexes also typically have greater decreases in activity than the dichloride complexes at higher temperatures, as shown in Section 3.2.2, and would suggest there is intrinsically a poorer stability associated with these alkylated complexes compared with the parent dichloride complex.

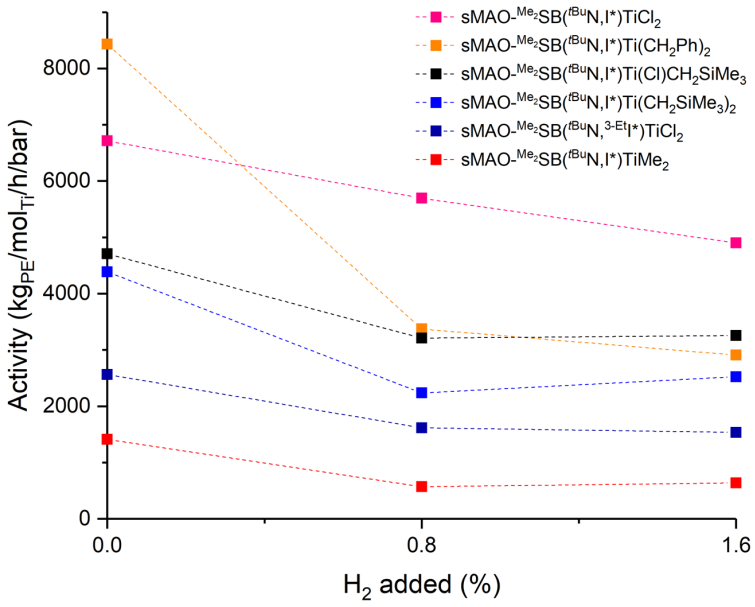

Figure 3.31. Ethylene polymerisation activities of sMAO-supported complexes with 0, 0.8 and 1.6% hydrogen addition; 8.27 bar ethylene, 0.075–0.40 mg catalyst ($[Al]_0$:$[Ti]_0$ = 200:1), 5.0 mL heptane, 10 µmol TiBA and 80 °C. Reactions quenched at 8.27 bar maximum ethylene uptake or after 60 minutes.

Table 3.9. Ethylene polymerisation activities produced using sMAO-supported complexes with 0, 0.8 and 1.6% hydrogen addition; 8.27 bar ethylene, 0.075–0.40 mg catalyst ($[Al]_0$:$[Ti]_0$ = 200:1), 5.0 mL heptane, 10 μmol TiBA and 80 °C. Reactions quenched at 8.27 bar maximum ethylene uptake or after 60 minutes.

Catalyst	Activity ($kg_{PE}/mol_{Ti}/h/bar$)		
Hydrogen (%)	0	0.8	1.6
sMAO-^{Me2}SB($^{t Bu}$N,I*)$TiCl_2$	6738	5734	4874
sMAO-^{Me2}SB($^{t Bu}$N,I*)$Ti(CH_2Ph)_2$	8433	3373	2908
sMAO-^{Me2}SB($^{t Bu}$N,I*)$TiMe_2$	1411	570	639
sMAO-^{Me2}SB($^{t Bu}$N,I*)$Ti(CH_2SiMe_3)_2$	4388	2237	2523
sMAO-^{Me2}SB($^{t Bu}$N,I*)$Ti(Cl)CH_2SiMe_3$	4708	3209	3256
sMAO-^{Me2}SB($^{t Bu}$N,$^{3\text{-}Et}$I*)$TiCl_2$	2564	1618	1536

The uptake rate plots in Figures 3.32–3.34 show the lower uptake rates of the ethylene/hydrogen polymerisations compared with ethylene homopolymerisations. This corresponds to the lower activities of the ethylene/hydrogen polymerisations observed in Figure 3.31. The lower activities of these polymerisations are attributable to the formation of a metal hydride species from chain transfer to hydrogen. The metal hydride species requires reactivation by propagation,[21–23] or forms a dormant bimetallic resting state with a bridging hydride, as has been proposed in the solution-phase, that requires reactivation to form the methyl cationic species.[24,25] The difference in the relative changes in activities and the absolute activities of the alkylated complexes and the dichloride complex of ^{Me2}SB($^{t Bu}$N,I*)TiR_2 would suggest that the initiator group remains coordinated to the surface of the support and influences the nature of the active species through a secondary coordination effect.

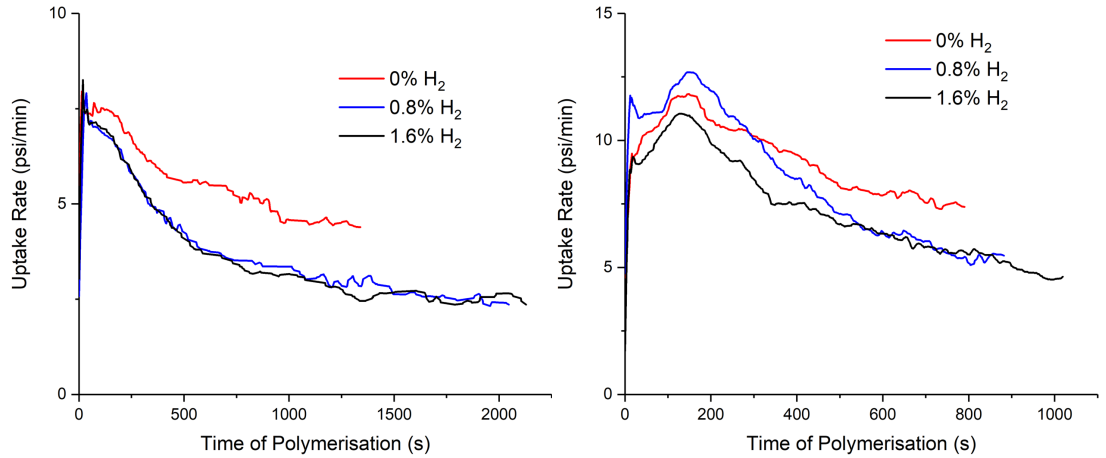

Figure 3.32. Ethylene uptake rate profiles for sMAO-^{Me_2}SB($^{t\text{Bu}}$N,$^{3\text{-Et}}$I*)TiCl$_2$ (left) and sMAO-^{Me_2}SB($^{t\text{Bu}}$N,I*)TiCl$_2$ (right) with varying amounts of hydrogen; 8.27 bar ethylene, 0.20–0.30 mg catalyst ([Al]$_0$:[Ti]$_0$ = 200:1), 5.0 mL heptane, 10 µmol TiBA and 80 °C. Reactions quenched at 8.27 bar maximum ethylene uptake or after 60 minutes.

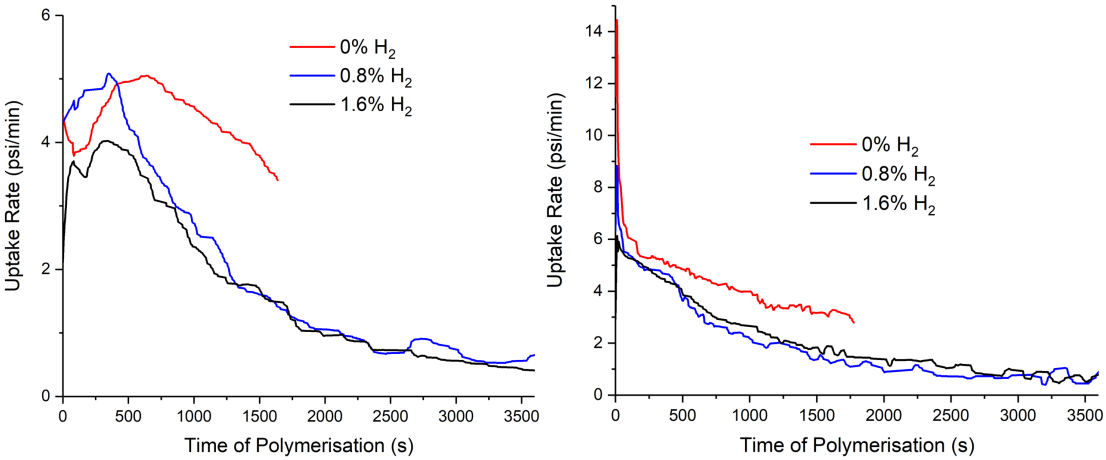

Figure 3.33. Ethylene uptake rate profiles for sMAO-^{Me_2}SB($^{t\text{Bu}}$N,I*)Ti(CH$_2$Ph)$_2$ (left) and sMAO-^{Me_2}SB($^{t\text{Bu}}$N,I*)TiMe$_2$ (right) with varying amounts of hydrogen; 8.27 bar ethylene, 0.075–0.40 mg catalyst ([Al]$_0$:[Ti]$_0$ = 200:1), 5.0 mL heptane, 10 µmol TiBA and 80 °C. Reactions quenched at 8.27 bar maximum ethylene uptake or after 60 minutes.

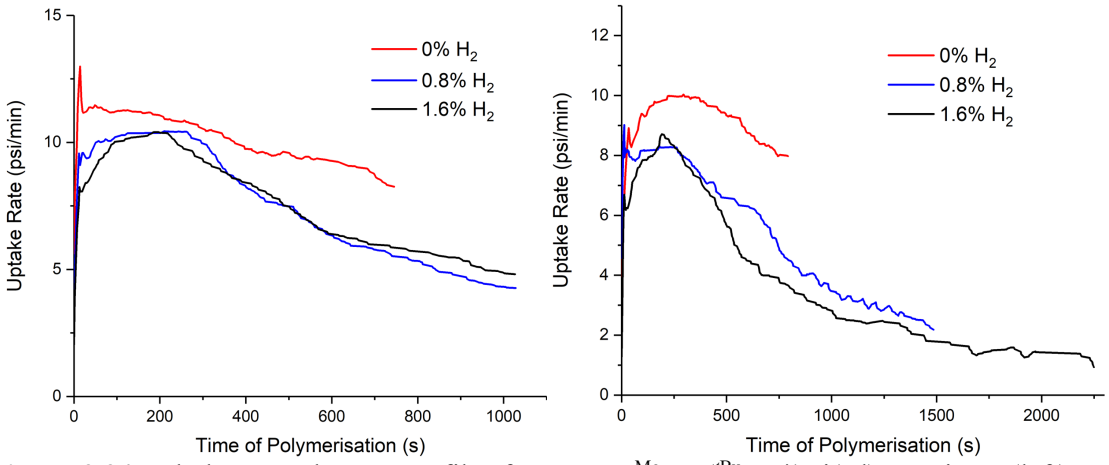

Figure 3.34. Ethylene uptake rate profiles for sMAO-^{Me2}SB(^{tBu}N,I*)Ti(Cl)CH_2SiMe_3 (left) and sMAO-^{Me2}SB(^{tBu}N,I*)Ti(CH_2SiMe_3)$_2$ (right) with varying amounts of hydrogen; 8.27 bar ethylene, 0.20–0.30 mg catalyst ([Al]$_0$:[Ti]$_0$ = 200:1), 5.0 mL heptane, 10 µmol TiBA and 80 °C. Reactions quenched at 8.27 bar maximum ethylene uptake or after 60 minutes.

The polymer molecular weights and molecular weight distributions are shown in Table 3.10. As would be expected, polymer molecular weights decrease with increased addition of hydrogen. Addition of hydrogen to the polymerisation reaction allows for an alternative chain transfer and termination pathway whereby the coordination of hydrogen leads to the formation of a metal hydride species. Computational studies have shown that the energy barrier for hydrogen insertion (4.5 kcal/mol) is far lower than that of ethylene insertion (7.5 kcal/mol) when modelled for Cp_2ZrCl_2.[79] This much lower activation barrier can therefore explain why such large decreases in molecular weights are observed when relatively small amounts of hydrogen are added. The narrowing of the molecular weight distributions with increased addition of hydrogen, such as from 3.8 to 2.7 with sMAO-^{Me2}SB(^{tBu}N,I*)Ti(Cl)CH_2SiMe_3, would suggest that there is increased control in the reaction with hydrogen addition.

Table 3.10. Molecular weights (M_w) (kDa) and dispersities (M_w/M_n) of the polyethylenes produced using sMAO-supported complexes with 0, 0.8 and 1.6% hydrogen addition; 8.27 bar ethylene, 0.075–0.30 mg catalyst ($[Al]_0:[Ti]_0 = 200:1$), 5.0 mL heptane, 10 μmol TiBA and 80 °C. Reactions quenched at 8.27 bar maximum ethylene uptake or after 60 minutes.

Catalyst	0%		0.8%		1.6%	
	M_w	M_w/M_n	M_w	M_w/M_n	M_w	M_w/M_n
sMAO-^{Me_2}SB($^{t Bu}$N,I*)TiCl$_2$	2667	3.2	80	2.4	41	2.9
sMAO-^{Me_2}SB($^{t Bu}$N,I*)Ti(CH$_2$Ph)$_2$	1.6×10^3	3.3	84	2.8	47	2.7
sMAO-^{Me_2}SB($^{t Bu}$N,I*)TiMe$_2$	1.4×10^3	3.4	85	2.7	45	2.7
sMAO-^{Me_2}SB($^{t Bu}$N,I*)Ti(CH$_2$SiMe$_3$)$_2$	1.8×10^3	3.5	82	2.6	43	2.6
sMAO-^{Me_2}SB($^{t Bu}$N,I*)Ti(Cl)CH$_2$SiMe$_3$	1.5×10^3	3.8	73	2.7	42	2.7
sMAO-^{Me_2}SB($^{t Bu}$N,$^{3\text{-}Et}$I*)TiCl$_2$	1.4×10^3	3.4	80	2.8	42	2.7

3.8 Large scale ethylene polymerisation

Large scale ethylene homopolymerisation reactions were carried at SCG Chemicals Co., Ltd. (Rayong, Thailand) by Mr Thawesak Parawan, Mr Somjet Songnoey and Mr Pongsiri Kaeoyok. Polymerisations were undertaken in a 1 L reactor with 600 mL of hexanes, 25–50 mg supported catalyst, 8 bar ethylene pressure and 3 mmol TiBA scavenger with polymerisations conducted for 1 hour at 70 °C (80 °C for sMAO-^{Me2}SB($^{t Bu}$N,I*)TiCl$_2$). sMAO-^{Me2}SB($^{t Bu}$N,I*)TiCl$_2$, sMAO-^{Me2}SB($^{t Bu}$N,I*)Ti(CH$_2$Ph)$_2$ and sMAO-^{Me2}SB($^{t Bu}$N,I*)TiMe$_2$ (molecular structures of the complexes are shown in Figure 3.35) were studied with the polymerisation activities obtained at University of Oxford, HTExplore and in Rayong are shown below in Table 3.11.

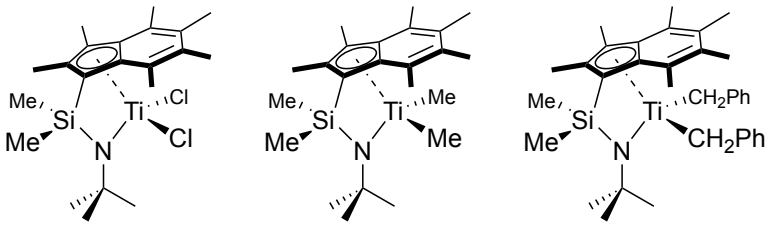

Figure 3.35. Molecular structures of the three complexes tested in this section.

Table 3.11. Ethylene polymerisation activities, M_w and M_w/M_n for sMAO-^{Me2}SB($^{t Bu}$N,I*)TiCl$_2$, sMAO-^{Me2}SB($^{t Bu}$N,I*)TiMe$_2$ and sMAO-^{Me2}SB($^{t Bu}$N,I*)Ti(CH$_2$Ph)$_2$. Rayong conditions: 8 bar ethylene, 25–50 mg catalyst ([Al]$_0$:[Ti]$_0$ = 200:1), 70 °C (80 °C for sMAO-^{Me2}SB($^{t Bu}$N,I*)TiCl$_2$), 1 hour, 600 mL hexanes, and 3 mmol TiBA. High-throughput conditions: 8.27 bar ethylene, 0.075–0.30 mg catalyst ([Al]$_0$:[Ti]$_0$ = 200:1), 5.0 mL heptane, 10 μmol TiBA and 80 °C. Reactions quenched at 8.27 bar maximum ethylene uptake or after 60 minutes. University of Oxford conditions: 2 bar ethylene, 50 mL hexanes, 10 mg catalyst ([Al]$_0$:[Ti]$_0$ = 200:1), 150 mg TiBA, 80 °C and 30 minutes.

	^{Me2}SB($^{t Bu}$N,I*)TiCl$_2$			^{Me2}SB($^{t Bu}$N,I*)Ti(CH$_2$Ph)$_2$			^{Me2}SB($^{t Bu}$N,I*)TiMe$_2$		
	Activity[a]	M_w[b]	M_w/M_n	Activity	M_w	M_w/M_n	Activity	M_w	M_w/M_n
Rayong	4098[c]	1104	15.7	8412	1090	4.0	2056	-	-
HTExplore	6738	2667	3.2	8433	1600	3.3	1411	1400	3.4
Oxford	2981	288	5.7	5112	231	5.1	3964	174	3.8

[a] Activity in kg$_{PE}$/mol$_{Ti}$/h/bar; [b] M_w value in kDa (kg/mol). [c] Homopolymerisation conducted at 80 °C.

Polymerisation activities for both sMAO-^{Me_2}SB($^{t Bu}$N,I*)$TiCl_2$ and sMAO-^{Me_2}SB($^{t Bu}$N,I*)$Ti(CH_2Ph)_2$ increase with increasing ethylene pressure. Activities increase by 65% for sMAO-^{Me_2}SB($^{t Bu}$N,I*)$Ti(CH_2Ph)_2$ at Rayong and HTExplore compared with University of Oxford, and by 37 and 126% for sMAO-^{Me_2}SB($^{t Bu}$N,I*)$TiCl_2$. The activities for sMAO-^{Me_2}SB($^{t Bu}$N,I*)$TiMe_2$ decrease by 48 and 64% with higher pressure at HTExplore and Rayong, suggesting that there is an inherent instability of the supported complex, sMAO-^{Me_2}SB($^{t Bu}$N,I*)$TiMe_2$. The larger decreases with increased polymerisation temperature from 80 to 90 °C shown in 3.2.2 (from 3964 to 2926 $kg_{PE}/mol_{Ti}/h/bar$) when compared with sMAO-^{Me_2}SB($^{t Bu}$N,I*)$TiCl_2$ (from 2981 to 2565 $kg_{PE}/mol_{Ti}/h/bar$) would also suggest a lower thermal stability of the dimethyl complex compared with the parent dichloride complex.

Polymer molecular weights increase with higher ethylene pressures, with this being attributable to the larger increase in the rate of chain propagation compared with chain termination. With the exception of sMAO-^{Me_2}SB($^{t Bu}$N,I*)$TiCl_2$ at Rayong, polymer molecular weight distributions narrow at higher pressures. This is likely due to improved mechanical stirring resulting in a more homogeneous reaction mixture and a greater degree of control in the polymerisation reaction. There is no clear reason why the polymer molecular weight distribution for sMAO-^{Me_2}SB($^{t Bu}$N,I*)$TiCl_2$ at Rayong is much higher than would be expected.

3.9 Conclusions

Fourteen sMAO-supported catalysts have been tested for the slurry-phase polymerisation of ethylene. Variation of the amido group shows that sMAO-^{Me2}SB(^{tBu}N,I*)TiCl$_2$ has the highest ethylene polymerisation activity of 3602 kg$_{PE}$/mol$_{Ti}$/h/bar, three times greater than an sMAO-supported industrial standard ^{Me2}SB(^{tBu}N,Cp*)TiCl$_2$. Modification of the initiator group has shown that alkyl groups lead to higher polymerisation activities, up to 7048 kg$_{PE}$/mol$_{Ti}$/h/bar for sMAO-^{Me2}SB(^{tBu}N,I*)Ti(CH$_2$SiMe$_3$)$_2$. Modification of both the *ansa* bridge and permethylindenyl fragment both increase activities compared with sMAO-^{Me2}SB(^{tBu}N,I*)TiCl$_2$. By variation of the inorganic support, use of LDHMAO-^{Me2}SB(^{tBu}N,I*)TiCl$_2$ has allowed for the production of the industrially desirable UHMWPE, with molecular weights in excess of 3000 kDa, whilst being able to maintain relatively good activities (up to 1867 kg$_{PE}$/mol$_{Ti}$/h/bar).

High-throughput studies of six catalysts led to enhancements in activities, with a maximum activity of 8433 kg$_{PE}$/mol$_{Ti}$/h/bar for sMAO-^{Me2}SB(^{tBu}N,I*)Ti(CH$_2$Ph)$_2$. sMAO-^{Me2}SB(^{tBu}N,I*)TiCl$_2$ performed best for hydrogen response, with modest decreases in activity, from 6738 to 4874 kg$_{PE}$/mol$_{Ti}$/h/bar, large decreases in molecular weights, from 2667 to 41 kDa, and narrow molecular weight distributions maintained.

Scale up homopolymerisations at SCG Chemicals Co., Ltd. (Rayong, Thailand) resulted in activities of 8412 and 4098 kg$_{PE}$/mol$_{Ti}$/h/bar for sMAO-^{Me2}SB(^{tBu}N,I*)Ti(CH$_2$Ph)$_2$ and sMAO-^{Me2}SB(^{tBu}N,I*)TiCl$_2$ respectively, 65 and 37% increases in activity compared with University of Oxford conditions.

3.10 References

1 G. Natta, *Angew. Chem.*, 1956, **68**, 393–403.
2 K. Ziegler, E. Holzkamp, H. Breil and H. Martin, *Angew. Chem.*, 1955, **67**, 426–426.
3 Y. Guo, L. Wang, H. Wang, Y. Chen, S. Zhu, T. Chen and P. Luo, *J. Appl. Polym. Sci.*, 2020, 48971.
4 J. Klosin, P. P. Fontaine and R. Figueroa, *Acc. Chem. Res.*, 2015, **48**, 2004–2016.
5 W. Kaminsky, A. Funck and H. Hähnsen, *Dalton Trans.*, 2009, 8803–8810.
6 H. Braunschweig and F. M. Breitling, *Coord. Chem. Rev.*, 2006, **250**, 2691–2720.
7 M. Kamigaito, T. K. Lal and R. M. Waymouth, *J. Polym. Sci. Part A Polym. Chem.*, 2000, **38**, 4649–4660.
8 K. Nomura, H. Okumura, T. Komatsu, N. Naga and Y. Imanishi, *J. Mol. Catal. A Chem.*, 2002, **190**, 225–234.
9 A. L. McKnight and R. M. Waymouth, *Chem. Rev.*, 1998, **98**, 2587–2598.
10 J. C. Stevens, *26. Insite™ Catal. Struct. Relationships Olefin Polym. Stud. Surf. Sci. Catal. Vol. 89*, 1994, 277–284.
11 J. C. Stevens, F. J. Timmers, D. R. Wilson, G. F. Schmidt, P. N. Nickias, R. K. Rosen, G. W. Knight and S. Y. Lai, 1991, EP0416815A2.
12 A. Togni and R. L. Halterman, Eds., *Metallocenes*, Wiley-VCH Verlag GmbH, Weinheim, Germany, 1998.
13 B. Rhodes, J. C. W. Chien, J. S. Wood, A. Chandrasekaran and M. D. Rausch, *Appl. Organomet. Chem.*, 2002, **16**, 323–330.
14 Y.-X. Chen and T. J. Marks, *Organometallics*, 1997, **16**, 3649–3657.
15 J.-C. Buffet, Z. R. Turner, R. T. Cooper and D. O'Hare, *Polym. Chem.*, 2015, **6**, 2493–2503.
16 J. R. Severn, J. C. Chadwick, R. Duchateau and N. Friederichs, *Chem. Rev.*, 2005, **105**, 4073–4147.
17 J. V. Lamb, J.-C. Buffet, Z. R. Turner and D. O'Hare, *Polym. Chem.*, 2019, **10**, 1386–1398.
18 J.-C. Buffet, Z. R. Turner and D. O'Hare, *Chem. Commun.*, 2018, **54**, 10970–10973.
19 S.-J. Park and M.-K. Seo, in *Interface Science and Technology*, 2011, pp. 431–499.
20 A. Wang, D. C. Sun, C. Stark and J. H. Dumbleton, *Wear*, 1995, **181**, 241–249.
21 A. K. Rappé, W. M. Skiff and C. J. Casewit, *Chem. Rev.*, 2000, **100**, 1435–1456.
22 W. Kaminsky and H. Lüker, *Die Makromol. Chemie, Rapid Commun.*, 1984, **5**, 225–228.
23 K.-J. Chu, J. B. P. Soares and A. Penlidis, *Macromol. Chem. Phys.*, 2000, **201**, 552–557.
24 F. Song, R. D. Cannon and M. Bochmann, *J. Am. Chem. Soc.*, 2003, **125**, 7641–7653.
25 M. Bochmann, *Organometallics*, 2010, **29**, 4711–4740.
26 Y. Jia and L. Zhang, *J. Appl. Polym. Sci.*, 2013, **129**, 1476–1483.
27 K. Musikabhumma, T. P. Spaniol and J. Okuda, *Macromol. Chem. Phys.*, 2002, **203**, 115–121.
28 L.-H. Wu and K.-T. Li, *Molecules*, 2017, **22**, 751–762.
29 T. K. Trefz, M. A. Henderson, M. Linnolahti, S. Collins and J. S. McIndoe,

Chem. Eur., 2015, **21**, 2980–2991.
30 D. Coevoet, H. Cramail and A. Deffieux, *Macromol. Chem. Phys.*, 1998, **199**, 1451–1457.
31 U. Wieser, F. Schaper and H.-H. Brintzinger, *Macromol. Symp.*, 2006, **236**, 63–68.
32 C. Hansch, A. Leo and R. W. Taft, *Chem. Rev.*, 1991, **91**, 165–195.
33 T. A. Q. Arnold, Z. R. Turner, J.-C. Buffet and D. O'Hare, *J. Organomet. Chem.*, 2016, **822**, 85–90.
34 A. F. R. Kilpatrick, J.-C. Buffet, P. Nørby, N. H. Rees, N. P. Funnell, S. Sripothongnak and D. O'Hare, *Chem. Mater.*, 2016, **28**, 7444–7450.
35 D. A. X. Fraser, Z. R. Turner, J.-C. Buffet and D. O'Hare, *Organometallics*, 2016, **35**, 2664–2674.
36 M. Velikova, L. Minkova, D. Damyanov and S. Rangelov, *Eur. Polym. J.*, 1997, **33**, 403–409.
37 M. Eskelinen and J. V. Seppälä, *Eur. Polym. J.*, 1996, **32**, 331–335.
38 M. Rahaman, M. A. Parvez, J. B. P. Soares and I. A. Hussein, *Int. J. Polym. Sci.*, 2014, **2014**, 1–10.
39 I. M. Lee, W. J. Gauthier, J. M. Ball, B. Iyengar and S. Collins, *Organometallics*, 1992, **11**, 2115–2122.
40 M. K. Mahanthappa and R. M. Waymouth, *J. Am. Chem. Soc.*, 2001, **123**, 12093–12094.
41 J. Okuda, K. Musikabhumma and P.-J. Sinnema, *Isr. J. Chem.*, 2002, **42**, 383–392.
42 G. Sivalingam, V. Natarajan, K. R. Sarma and U. Parasuveera, *Ind. Eng. Chem. Res.*, 2008, **47**, 8940–8946.
43 P. J. Shapiro, E. Bunel, W. P. Schaefer and J. E. Bercaw, *Organometallics*, 1990, **9**, 867–869.
44 W. E. Piers, P. J. Shapiro, E. E. Bunel and J. E. Bercaw, *Synlett*, 1990, **1990**, 74–84.
45 A. Reb and H. G. Alt, *J. Mol. Catal. A Chem.*, 2001, **174**, 35–49.
46 H. G. Alt and A. Köppl, *Chem. Rev.*, 2000, **100**, 1205–1222.
47 J. A. Ewen, R. L. Jones, A. Razavi and J. D. Ferrara, *J. Am. Chem. Soc.*, 1988, **110**, 6255–6256.
48 H. G. Alt and R. Zenk, *J. Organomet. Chem.*, 1996, **526**, 295–301.
49 M. F. N. N. Carvalho, K. Mach, A. R. Dias, J. F. Mano, M. M. Marques, A. M. Soares and A. J. L. Pombeiro, *Inorg. Chem. Commun.*, 2003, **6**, 331–334.
50 H. G. Alt, A. Reb and K. Kundu, *J. Organomet. Chem.*, 2001, **628**, 211–221.
51 P. Schertl and H. G. Alt, *J. Organomet. Chem.*, 1999, **582**, 328–337.
52 H. Braunschweig, F. M. Breitling, C. von Koblinski, A. J. P. White and D. J. Williams, *Dalton Trans.*, 2004, 938–943.
53 H. Juvaste, T. T. Pakkanen and E. I. Iiskola, *Organometallics*, 2000, **19**, 1729–1733.
54 L. Fan, D. Harrison, T. K. Woo and T. Ziegler, *Organometallics*, 1995, **14**, 2018–2026.
55 A. Tynys, J. L. Eilertsen and E. Rytter, *Macromol. Chem. Phys.*, 2006, **207**, 295–303.
56 E. Kaji and E. Yoshioka, 2010, WO2010055652.
57 M. A. Bashir, T. Vancompernolle, R. M. Gauvin, L. Delevoye, N. Merle, V. Monteil, M. Taoufik, T. F. L. McKenna and C. Boisson, *Catal. Sci. Technol.*, 2016, **6**, 2962–2974.

58 G. J. P. Britovsek, V. C. Gibson and D. F. Wass, *Angew. Chem. Int. Ed.*, 1999, **38**, 428–447.
59 C. M. R. Wright, T. J. Williams, Z. R. Turner, J.-C. Buffet and D. O'Hare, *Inorg. Chem. Front.*, 2017, **4**, 1048–1060.
60 J. V. Lamb, DPhil Thesis, University of Oxford, 2019.
61 M. S. Bhagwat, S. S. Bhagwat and M. M. Sharma, *Ind. Eng. Chem. Res.*, 1994, **33**, 2322–2330.
62 J. Li, Z. Tekie, T. I. Mizan, B. I. Morsi, E. E. Maier and C. P. P. Singh, *Chem. Eng. Sci.*, 1996, **51**, 549–559.
63 S. Floyd, R. A. Hutchinson and W. H. Ray, *J. Appl. Polym. Sci.*, 1986, **32**, 5451–5479.
64 M. A. Bashir, V. Monteil, C. Boisson and T. F. L. McKenna, *J. Appl. Polym. Sci.*, 2018, **135**, 45670.
65 J. T. Hirvi, M. Bochmann, J. R. Severn and M. Linnolahti, *ChemPhysChem*, 2014, **15**, 2732–2742.
66 F. Song, R. D. Cannon, S. J. Lancaster and M. Bochmann, *J. Mol. Catal. A Chem.*, 2004, **218**, 21–28.
67 M. Bochmann and S. J. Lancaster, *Angew. Chem. Int. Ed.*, 1994, **33**, 1634–1637.
68 R. Kleinschmidt, Y. van der Leek, M. Reffke and G. Fink, *J. Mol. Catal. A Chem.*, 1999, **148**, 29–41.
69 V. F. Tisse, C. Boisson and T. F. L. McKenna, *Macromol. Chem. Phys.*, 2014, **215**, 1358–1369.
70 F. Ghiotto, C. Pateraki, J. R. Severn, N. Friederichs and M. Bochmann, *Dalton Trans.*, 2013, **42**, 9040.
71 W. Wang, Z. Fan and L. Feng, *Eur. Polym. J.*, 2005, **41**, 2380–2387.
72 H. H. Brintzinger, D. Fischer, R. Müllhaupt, B. Rieger and R. M. Waymouth, *Angew. Chem. Int. Ed.*, 1995, **34**, 1143–1170.
73 M. Bochmann, *J. Chem. Soc. Dalt. Trans.*, 1996, 255–270.
74 S. S. Reddy and S. Sivaram, *Prog. Polym. Sci.*, 1995, **20**, 309–367.
75 E. Giannetti, G. M. Nicoletti and R. Mazzocchi, *J. Polym. Sci. Polym. Chem. Ed.*, 1985, **23**, 2117–2134.
76 M. Goldberg, K. Mahon and D. Anderson, *Adv. Drug Deliv. Rev.*, 2008, **60**, 971–978.
77 V. Busico, R. Pellecchia, F. Cutillo and R. Cipullo, *Macromol. Rapid Commun.*, 2009, **30**, 1697–1708.
78 D. P. Gates, S. A. Svejda, E. Oñate, C. M. Killian, L. K. Johnson, P. S. White and M. Brookhart, *Macromolecules*, 2000, **33**, 2320–2334.
79 J. Ramos, V. Cruz, A. Muñoz-Escalona and J. Martínez-Salazar, *Polymer*, 2000, **41**, 6161–6169.

Chapter Four

Constrained geometry complexes for ethylene copolymerisation

4.1 Introduction

4.1.1 Overview

Addition of an α-olefin as a comonomer to ethylene polymerisation reactions can allow for controlled addition of branches into polymer chains, significantly affecting the polymer properties and end usage. The greater degree of chain branching leads to increased polymer flexibility, allowing for usage as foams, elastic fibres, packaging and adhesives.[1] Quijada *et al*. have also reported the use of *ansa* bridged metallocenes, $^{Me_2}SBCp_2ZrCl_2$ and $EBIZrCl_2$, for ethylene/1-hexene copolymerisation with a methylaluminoxane (MAO) activator.[2] It was found that the presence of the *ansa* bridge resulted in greater levels of 1-hexene incorporation compared with the unbridged analogues, and lower polymer molecular weights due to the facilitation of β-hydride transfer reactions.

Since the development of group 4 CGCs in the late 1980s and early 1990s,[3,4] there have been a vast number of patents filed for the use of this family of complexes for ethylene/α-olefin copolymerisation.[5–7] It was proposed that the strain inducing *ansa* bridge opened up the metal centre relative to the unbridged analogues, allowing for more facile coordination of comonomers such as 1-hexene or 1-octene. Klosin and co-workers have investigated the effects of the apical moiety for ethylene/1-octene copolymerisation. With use of a substituted indenyl fragment, the addition of electron-donating substituents

led to both increased copolymerisation activity and polymer molecular weight, whilst still maintaining very high levels of comonomer incorporation.[8] Marks and Chen investigated ^{Me2}SB($^{t Bu}$N,Cp*)TiX$_2$ (X = CH_2Ph and Me) for homogeneous-phase ethylene/1-hexene copolymerisation with MAO and borane cocatalysts; the dimethyl complex showed high levels of 1-hexene incorporation, whilst the dibenzyl complex resulted in the formation of a mixture of two homopolymers.[9] Ethylene/1-hexene copolymerisation has also been studied in heterogeneous systems; Marks and Williams reported the use of CGCs supported by MAO-activated sulfated alumina for slurry-phase ethylene/1-hexene copolymerisation.[10] The supported species resulted in significantly lower levels of 1-hexene incorporation due to mass transfer effects, where both the support and the propagating polymer chain cause diffusional resistance of the comonomer.[11]

CGCs have also been shown to be highly active ethylene/styrene copolymerisation catalysts,[5] they bridge the gap between half-metallocene complexes that produce predominantly syndiotactic polystyrene with a trace of copolymer,[12] and *ansa*-zirconocene dichlorides that only incorporate small amounts of styrene into the polymer chain.[13] Mülhaupt and co-workers demonstrated CGC derived systems incorporated styrene in either a tail-to-tail manner or in an isolated fashion,[14] with this preference in the incorporation of styrene units leading to maximum incorporations of up to 50 mol%.[5] Marks and co-workers were able to achieve up to 92 mol% styrene incorporation utilising a bimetallic CGC [{^{Me2}SB($^{t Bu}$N,I)TiCl$_2$}$_2$(μ-C_2H_4)] with the close proximity of the two active sites facilitating these high incorporation levels.[15]

4.1.2 Chapter synopsis

This chapter investigates how selected complexes synthesised in Chapter 2 perform as ethylene/1-hexene and ethylene/styrene copolymerisation catalysts when supported on

sMAO, as well as how sMAO-supported ^{Me2}SB($^{t\text{Bu}}$N,I*)TiCl$_2$ and ^{Me2}SB($^{t\text{Bu}}$N,$^{3\text{-Et}}$I*)TiCl$_2$ performed as ethylene/1-octene copolymerisation catalysts. Eight supported complexes were tested for ethylene/1-hexene copolymerisations under high-throughput conditions. sMAO-^{Me2}SB($^{t\text{Bu}}$N,I*)TiCl$_2$ and sMAO-^{Me2}SB($^{t\text{Bu}}$N,I*)Ti(CH$_2$Ph)$_2$ were studied as slurry-phase ethylene/1-hexene and ethylene/styrene copolymerisation catalysts on a larger scale at SCG Chemicals Co., Ltd. (Rayong, Thailand). Finally, ^{Me2}SB($^{t\text{Bu}}$N,I*)TiCl$_2$ and ^{Me2}SB($^{t\text{Bu}}$N,$^{3\text{-Et}}$I*)TiCl$_2$ were studied as solution-phase ethylene/1-hexene and ethylene/1-octene copolymerisation catalysts.

4.2 Slurry-phase ethylene copolymerisation

4.2.1 Ethylene/1-hexene copolymerisation

The effect of temperature on ethylene/1-hexene copolymerisation has been studied using sMAO(3G)-^{Me_2}SB($^{t Bu}$N,I*)TiCl$_2$. Copolymerisations were carried out for 30 minutes in a 150 mL ampoule with a sidearm containing 0.156, 0.312 or 0.625 mL of 1-hexene (1710, 3421 and 6852 mol$_{1\text{-hexene}}$/mol$_{Ti}$) in 5 mL of hexanes that was added at the start of the polymerisation, a total volume of 50 mL hexanes, 10 mg of 3rd generation sMAO-supported complex ([Al]$_0$:[Ti]$_0$ ratio of 200:1), 150 mg TiBA scavenger and 2 bar ethylene pressure. The temperature of polymerisation was varied from 30 to 90 °C. A picture of the reaction set-up is shown in Figure 4.1, and the results of these studies are shown in Figure 4.2 and Table A4.1.

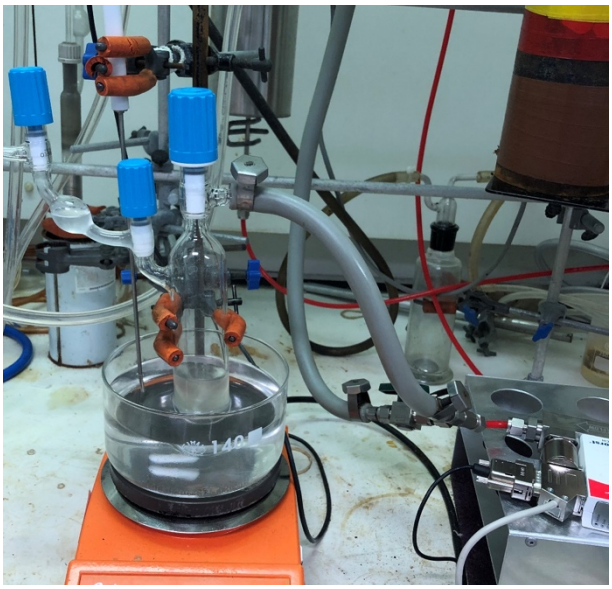

Figure 4.1. Experimental reaction set-up for ethylene/olefin copolymerisations at University of Oxford.

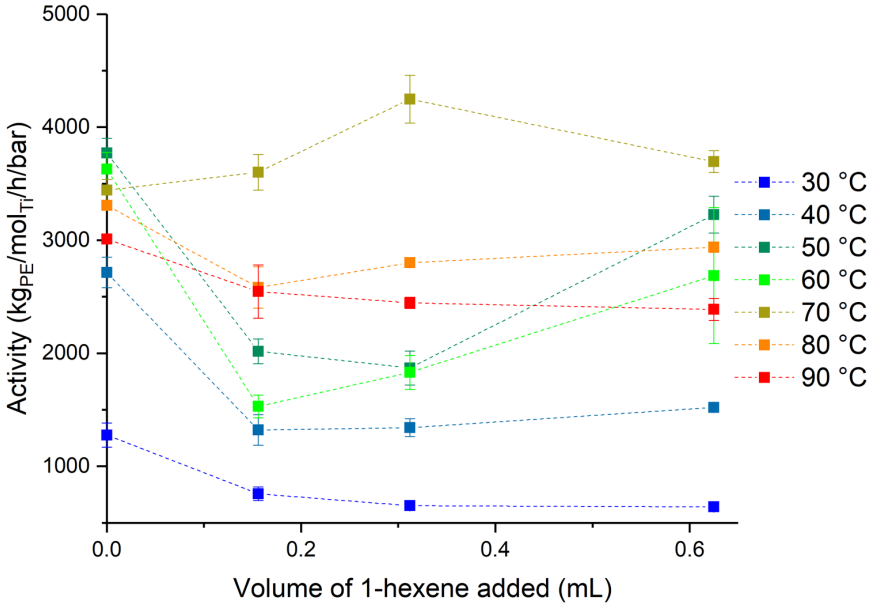

Figure 4.2. Slurry-phase ethylene copolymerisation activities for sMAO-^{Me_2}SB($^{t Bu}$N,I*)TiCl$_2$; 10 mg catalyst ([Al]$_0$:[Ti]$_0$ = 200:1), 2 bar ethylene, 0, 0.156, 0.312 or 0.625 mL 1-hexene, 50 mL hexanes, 150 mg TiBA and 30 minutes. Error bars as 1 standard deviation.

At temperatures below 70 °C, activities decrease with addition of 1-hexene compared with homopolymerisation. This is likely due to a higher activation energy for chain propagation of an α-olefin compared with ethylene,[16] causing activities to be lower for copolymerisation than homopolymerisation. At 80 and 90 °C, activities also decrease with addition of 1-hexene (from 3308 and 3010 kg$_{PE}$/mol$_{Ti}$/h/bar for homopolymerisation to 2939 and 2388 kg$_{PE}$/mol$_{Ti}$/h/bar with addition of 0.625 mL of 1-hexene respectively), due to a proposed exothermic spike (similar to what is observed in high-throughput studies where it was possible to constantly monitor the temperature of the reaction mixture) leading to catalyst deactivation. At 70 °C, activities increase with addition of 1-hexene from 3443 to 4248 kg$_{PE}$/mol$_{Ti}$/h/bar with 0 and 0.312 mL 1-hexene, possibly due to the enthalpic barrier of 1-hexene insertion at low temperatures being overcome,[16] along with 1-hexene increasing ethylene solubility,[17] and increased ability for monomer close approach to the catalyst site that occurs at all temperatures.[18] The uptake rate graphs show the relative ethylene uptake rates for (co)polymerisations at 70, 80 and 90 °C

(Figure A4.1–A4.3). These appear to indicate that there is not significantly greater catalyst deactivation in the copolymerisation reactions compared with the homopolymerisations, with uptake rates remaining constant through the polymerisations. At 70 °C, with addition of 0.625 mL 1-hexene, an increase in uptake rate is observed after 750 seconds.

The levels of 1-hexene incorporation have been determined using high temperature $^{13}C\{^{1}H\}$ NMR spectroscopy, an assigned spectrum is shown in Figure A4.47, with the side chain and carbon resonances in close proximity being assigned by comparison to literature values.[22,23] It has previously been shown that for ethylene/1-octene copolymerisations, incorporation levels decrease with increased temperature of reaction.[16] However, as is seen in Table 4.1, the levels of 1-hexene incorporation increase with increasing temperature from 1.9 mol% at 30 °C to 2.6 mol% at 90 °C.

Table 4.1. 1-hexene incorporation levels and melt temperatures (T_m) of the copolymers produced; 10 mg catalyst ($[Al]_0$:$[Ti]_0$ = 200:1), 2 bar ethylene, 0, 0.156, 0.312 or 0.625 mL 1-hexene, 50 mL hexanes, 150 mg TiBA and 30 minutes.

Volume of 1-hexene (mL)	0	0.156		0.312		0.625	
Temperature of polymerisation (ºC)	T_m (°C)	T_m (°C)	Incorporation (mol%)	T_m (°C)	Incorporation (mol%)	T_m (°C)	Incorporation (mol%)
30	135	126	-	123	-	114	1.9
40	135	125	-	119	-	113	2.0
50	136	125	-	120	-	114	2.2
60	136	123	-	116	-	115	2.1
70	138	125	0.6	122	1.0	122	2.1
80	136	123	-	119	-	122	2.3
90	134	126	-	122	-	119	2.6

Large decreases in polymer molecular weights were observed with addition of 1-hexene. At 70 °C, molecular weights decrease from homopolymerisation to addition of 0.625 mL of 1-hexene (414 and 95 kDa respectively) (Table 4.2). This effect has been observed in the literature, with the molecular weight decrease resulting from frequent chain

termination following addition of 1-hexene and chain transfer to 1-hexene monomers.[24] Klosin and co-workers have undertaken work to negate this molecular weight decrease by addition of heteroatom substituents to the indenyl ligand.[8,25,26] The tendency for molecular weight distributions to become narrower with addition of increasing amounts of comonomer has also been observed by Quijada *et al.* with 1-hexene, 1-octene and 1-decene comonomers with *rac*-EBIZrCl$_2$.[27]

Table 4.2. Polymer molecular weights (M_w) and molecular weight distributions (M_w/M_n); 10 mg catalyst ($[Al]_0$:$[Ti]_0$ = 200:1), 2 bar ethylene, 0, 0.156, 0.312 or 0.625 mL 1-hexene, 50 mL hexanes, 150 mg TiBA and 30 minutes.

Volume of 1-hexene (mL)	0		0.156		0.312		0.625	
Temperature of polymerisation (°C)	M_w (kDa)	M_w/M_n	M_w (kDa)	M_w/M_n	M_w (kDa)	M_w/M_n	M_w (kDa)	M_w/M_n
30	2313	4.2	1291	2.8	1133	3.1	894	3.0
40	2197	3.9	856	2.8	781	2.8	695	2.7
50	1175	4.1	740	2.8	700	2.8	393	2.8
60	1063	4.4	637	3.0	499	3.1	203	2.7
70	414	6.6	313	3.0	213	3.2	95	3.0
80	282	6.8	294	3.6	243	3.1	95	4.1
90	172	6.7	87	3.7	49	3.5	51	3.4

The polymers produced have also been studied by differential scanning calorimetry (DSC) to determine polymer melt and crystallisation temperatures and enthalpies (Tables A4.2 and A4.3, Figure 4.3 and Figures A4.17–A4.22). DSC is a common method of studying polymers of this type, as it gives an indication of the incorporation of comonomer into a polymer chain.[19] With addition of 1-hexene, there are large decreases in all values measured across the temperature range (melt temperatures decrease from 138 to 125, 122 and 122 °C and crystallisation temperatures decrease from 116 to 111, 111 and 108 °C with 0, 0.156, 0.312 and 0.625 mL 1-hexene at 70 °C). The decrease in polymer melt temperatures with increasing 1-hexene incorporation is thought to be due to both the reduced spacing between butyl chains and a reduction in polymer molecular weight. The butyl chains are generally excluded from the lamella;[20] with increasing

comonomer incorporation these lamella become thinner and this reduction in thickness is a major factor in polymer melt temperatures decreasing. The broadening of the melting peaks can be attributed to the variation of lamella size, which has been seen previously through comparison of random and precisely branched polymers, with the precisely branched polymers resulting in sharp melting peaks.[21]

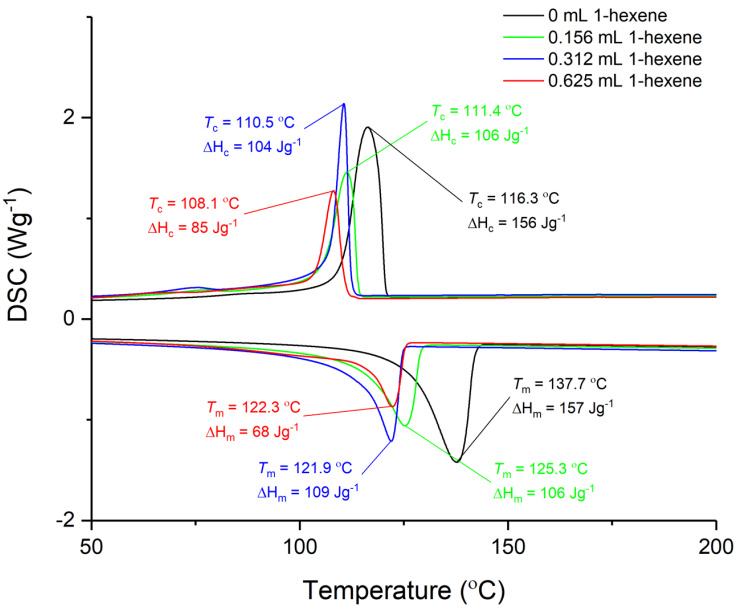

Figure 4.3. DSC plot for polymers produced by sMAO-^{Me_2}SB($^{t\text{Bu}}$N,I*)TiCl$_2$ at 70 °C for 0 (black), 0.156 mL (green), 0.312 mL (blue) and 0.625 mL 1-hexene (red).

Scanning electron microscopy (SEM) images of the copolymer produced (Figures A4.40–A4.43) show that on addition of 0.156 and 0.312 mL of 1-hexene the copolymer particles are still discrete with a "popcorn-shaped" morphology. However, with addition of 0.625 mL of 1-hexene the polymer forms large aggregated clumps, with the individual particles stuck together.

Six other catalysts, sMAO(3G)-^{Me,Pr}SB($^{t\text{Bu}}$N,I*)TiCl$_2$, sMAO(3G)-^{Me_2}SB($^{t\text{Bu}}$N,$^{3\text{-Et}}$I*)TiCl$_2$, sMAO(3G)-^{Me_2}SB($^{t\text{Bu}}$N,I*)Ti(CH$_2$Ph)$_2$, sMAO(3G)-^{Me_2}SB($^{t\text{Bu}}$N,I*)Ti(Cl)CH$_2$SiMe$_3$, sMAO(3G)-^{Me_2}SB($^{t\text{Bu}}$N,I*)Ti(CH$_2$SiMe$_3$)$_2$, and an industrial standard sMAO(3G)-^{Me_2}SB($^{t\text{Bu}}$N,Cp*)TiCl$_2$ (Figure 4.4) were also

tested for ethylene/1-hexene copolymerisation at 70 °C under the previously described conditions.

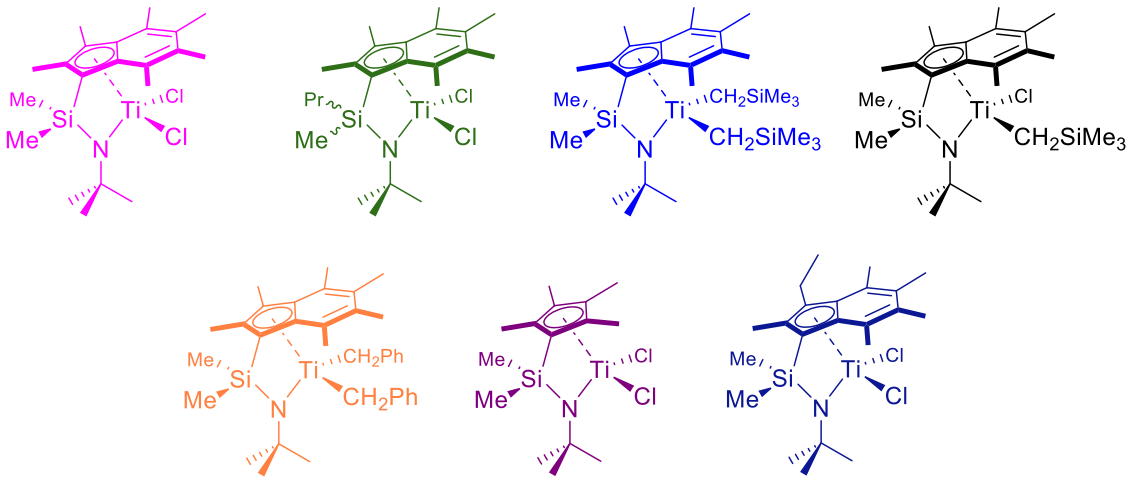

Figure 4.4. Molecular structures of the seven complexes tested in this section. Colours correspond to colours of the lines used on the graphs.

As can be seen in Figures 4.5 and 4.6 and uptake rate plots in Figures A4.1 and A4.4–A4.9, with the exception of sMAO(3G)-^{Me_2}SB($^{t Bu}$N,I*)TiCl$_2$, copolymerisation activities decrease relative to homopolymerisation, and typically the maximum activities for copolymerisations are seen for addition of the largest amount of 1-hexene (0.625 mL). Copolymerisation activities decrease for sMAO(3G)-^{Me,Pr}SB($^{t Bu}$N,I*)TiCl$_2$ and sMAO(3G)-^{Me_2}SB($^{t Bu}$N,$^{3\text{-}Et}$I*)TiCl$_2$ relative to homopolymerisation. Temperature variation of ethylene homopolymerisation has shown that both sMAO(3G)-^{Me,Pr}SB($^{t Bu}$N,I*)TiCl$_2$ and sMAO(1G)-^{Me_2}SB($^{t Bu}$N,$^{3\text{-}Et}$I*)TiCl$_2$ exhibit much greater decreases in polymerisation activity compared with sMAO(1G)-^{Me_2}SB($^{t Bu}$N,I*)TiCl$_2$ when temperature is increased from 70 to 80 °C (4138 to 3038 kg$_{PE}$/mol$_{Ti}$/h/bar (27%) and 3593 to 2698 kg$_{PE}$/mol$_{Ti}$/h/bar (25%) respectively compared with 3524 to 2981 kg$_{PE}$/mol$_{Ti}$/h/bar (15%)).

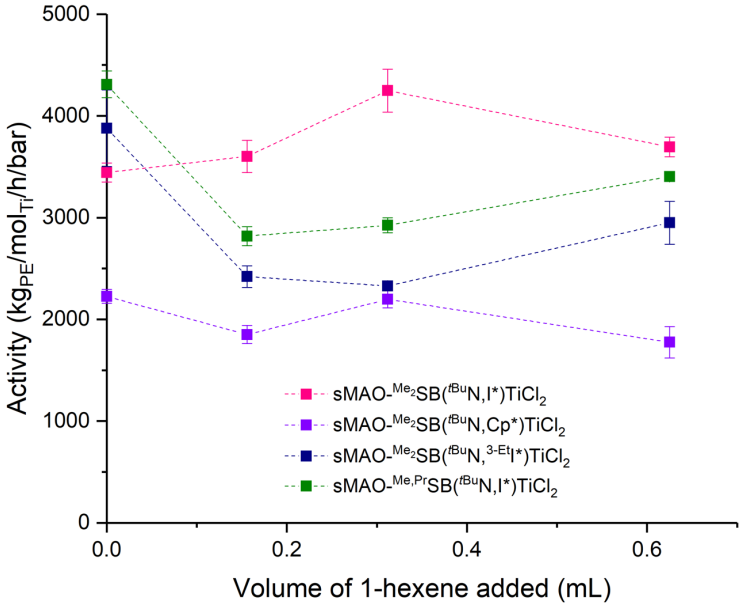

Figure 4.5. Ethylene/1-hexene copolymerisation activities; 10 mg catalyst ($[Al]_0$:$[Ti]_0$ = 200:1), 2 bar ethylene, 0, 0.156, 0.312 or 0.625 mL 1-hexene, 50 mL hexanes, 150 mg TiBA, 70 °C and 30 minutes. Error bars as 1 standard deviation.

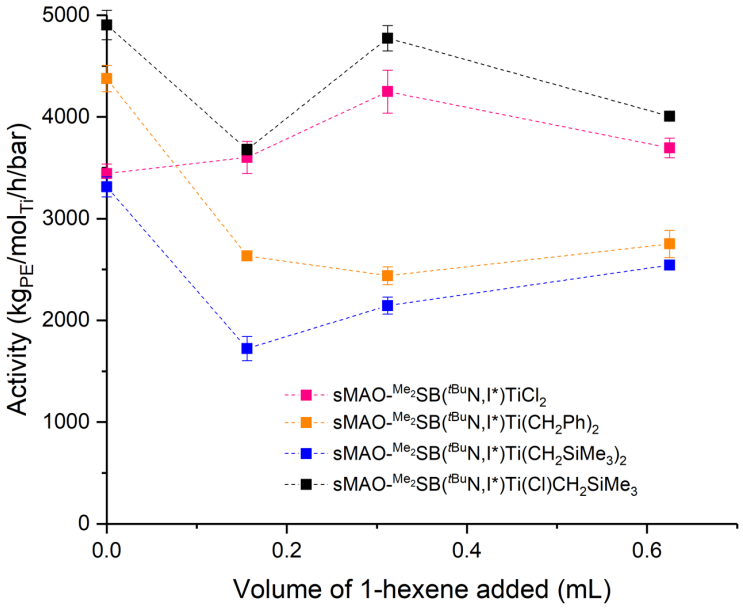

Figure 4.6. Ethylene/1-hexene copolymerisation activities; 10 mg catalyst ($[Al]_0$:$[Ti]_0$ = 200:1), 2 bar ethylene, 0, 0.156, 0.312 or 0.625 mL 1-hexene, 50 mL hexanes, 150 mg TiBA, 70 °C and 30 minutes. Error bars as 1 standard deviation.

As shown in Chapter 3, sMAO(1G)-^{Me_2}SB(^{tBu}N,I*)Ti(CH$_2$Ph)$_2$ and sMAO(1G)-^{Me_2}SB(^{tBu}N,I*)Ti(CH$_2$SiMe$_3$)$_2$ are less thermally stable than sMAO(1G)-^{Me_2}SB(^{tBu}N,I*)TiCl$_2$. A 40% decrease is seen in the copolymerisation activity for sMAO(3G)-^{Me_2}SB(^{tBu}N,I*)Ti(CH$_2$Ph)$_2$ (4377 to 2421 $kg_{PE}/mol_{Ti}/h/bar$) and 48%

decrease for sMAO(3G)-^{Me_2}SB($^{t Bu}$N,I*)Ti(CH_2SiMe_3)$_2$ (3243 to 1639 $kg_{PE}/mol_{Ti}/h/bar$) compared with the 5% increase in activity for sMAO(3G)-^{Me_2}SB($^{t Bu}$N,I*)$TiCl_2$ (3443 to 3602 $kg_{PE}/mol_{Ti}/h/bar$) on addition of 0.156 mL 1-hexene (Figure 4.6). For sMAO(3G)-^{Me_2}SB($^{t Bu}$N,I*)Ti(Cl)CH_2SiMe_3, which appears to be more thermally stable than the two bis-alkylated complexes, where a maximum activity of 4474 $kg_{PE}/mol_{Ti}/h/bar$ is observed at 70 °C which decreases to 3648 $kg_{PE}/mol_{Ti}/h/bar$ at 80 °C (Sections 3.2.2 and 3.2.3), the activity decreases by 25% to 3678 $kg_{PE}/mol_{Ti}/h/bar$ with addition of 0.156 mL of 1-hexene. These decreases in activities would suggest that there is some thermal decomposition of the catalyst caused by addition of a comonomer that can partly contribute to the negative comonomer effect observed in some cases.

This effect can also be seen in Figures A4.1 and A4.7–A4.9, where the uptake rate plots remain approximately constant for the duration of the (co)polymerisations for the dichloride complex. In contrast, uptake rate profiles decrease rapidly for the copolymerisations for the dibenzyl and bis-neosilyl complexes, whilst the uptake rates for the homopolymerisation are more constant. 1-hexene incorporation levels have been calculated for all of the catalysts for copolymerisation with 0.625 mL of 1-hexene by high temperature $^{13}C\{^1H\}$ NMR spectroscopy, and the melting points of all (co)polymers determined by DSC (Table 4.3 and Figures A4.23−A4.28).

Table 4.3. Polymer melt temperatures (T_m), and 1-hexene incorporation levels for the sMAO(3G)-supported complexes; 10 mg catalyst ($[Al]_0$:$[Ti]_0$ = 200:1), 2 bar ethylene, 0, 0.156, 0.312 or 0.625 mL 1-hexene, 50 mL hexanes, 150 mg TiBA, 70 °C and 30 minutes.

Volume of 1-hexene (mL)	0	0.156	0.312		0.625	
Supported Complex	T_m (°C)	T_m (°C)	T_m (°C)	Incorporation (%)	T_m (°C)	Incorporation (%)
^{Me2}SB(^{tBu}N,I*)TiCl$_2$	138	125	122	1.0	122	2.1
^{Me2}SB(^{tBu}N,$^{3\text{-}Et}$I*)TiCl$_2$	133	122	117	-	114	2.4
^{Me,Pr}SB(^{tBu}N,I*)TiCl$_2$	133	123	117	-	114	1.9
^{Me2}SB(^{tBu}N,I*)Ti(CH$_2$Ph)$_2$	133	122	117	-	114	2.2
^{Me2}SB(^{tBu}N,Cp*)TiCl$_2$	134	120	117	-	107	3.5
^{Me2}SB(^{tBu}N,I*)Ti(CH$_2$SiMe$_3$)$_2$	134	121	116	-	112	2.4
^{Me2}SB(^{tBu}N,I*)Ti(Cl)CH$_2$SiMe$_3$	133	135	123	-	121	2.3

Incorporation levels for the permethylindenyl complexes (1.9–2.4 mol%) are lower than that of ^{Me2}SB(^{tBu}N,Cp*)TiCl$_2$ (3.5 mol%). The incorporation levels are lower than typically observed for solution-phase copolymerisations.[8] Marks and Williams previously synthesised a range of constrained geometry complexes supported on MAO-activated sulfated alumina which showed lower levels of 1-hexene incorporation compared with solution-phase reactions.[10] The lower incorporation levels were attributed to mass transfer effects, where both the support and the propagating polymer chain cause diffusional resistance of the comonomer.[11]

Table 4.4. Polymer molecular weights (M_w) and molecular weight distributions (M_w/M_n); 10 mg catalyst ($[Al]_0$:$[Ti]_0$ = 200:1), 2 bar ethylene, 0, 0.156, 0.312 or 0.625 mL 1-hexene, 50 mL hexanes, 150 mg TiBA, 70 °C and 30 minutes.

Volume of 1-hexene (mL)	0		0.156		0.312		0.625	
Supported Complex	M_w (kDa)	M_w/M_n	M_w (kDa)	M_w/M_n	M_w (kDa)	M_w/M_n	M_w (kDa)	M_w/M_n
^{Me2}SB(^{tBu}N,I*)TiCl$_2$	414	6.6	313	3.0	213	3.2	95	3.0
^{Me2}SB(^{tBu}N,$^{3\text{-}Et}$I*)TiCl$_2$	395	3.2	269	4.4	255	3.7	175	2.5
^{Me,Pr}SB(^{tBu}N,I*)TiCl$_2$	554	3.8	340	2.8	351	2.7	249	2.7
^{Me2}SB(^{tBu}N,I*)Ti(CH$_2$Ph)$_2$	449	4.0	344	3.5	364	3.8	201	3.0
^{Me2}SB(^{tBu}N,Cp*)TiCl$_2$	365	3.2	307	3.1	251	3.0	127	3.4
^{Me2}SB(^{tBu}N,I*)Ti(CH$_2$SiMe$_3$)$_2$	667	3.7	480	3.3	381	3.5	233	3.0
^{Me2}SB(^{tBu}N,I*)Ti(Cl)CH$_2$SiMe$_3$	369	3.3	347	3.2	214	5.1	105	4.1

The general decrease in molecular weight and narrowing of M_w/M_n values reported in Table 4.4 has also previously been reported by Fink *et al.* and Quijada *et al.*.[24,27] Fink *et al.* proposed that the change in the polymer molecular weight was due to a balance of higher rates of chain propagation facilitated by the addition of a comonomer which increases M_w, an increased rate β-hydride transfer facilitated by the metal–1-hexene species and also an increased rate of chain transfer to 1-hexene which decrease M_w. By comparison of two systems cocatalysed with MAO, $Me_2C(Flu,Cp)ZrCl_2$ and $SBIZrCl_2$, it was found that that these factors were catalyst dependent. Polymer molecular weights increased for $Me_2C(Flu,Cp)ZrCl_2$ at low 1-hexene levels due to the polymerisation rate enhancing effect having a stronger influence than that of the chain transfer and termination effects facilitated by 1-hexene. Conversely, in the $SBIZrCl_2$/MAO system polymer molecular weights decreased to a much larger extent.[24] The tendency for reducing polymer molecular weight distributions was also reported by Quijada *et al.* who observed the same phenomenon across three catalytic systems ($SBIZrCl_2$, $EBIZrCl_2$ and Cp_2ZrCl_2) with an MAO cocatalyst.[27] For all catalysts, polymer melt temperatures decrease with increasing addition of 1-hexene comonomer and decreasing polymer molecular weights.

4.2.2 Ethylene/styrene copolymerisation

The same seven solid supported catalysts have been tested for the slurry-phase ethylene/styrene copolymerisation under the same conditions as 4.2.1 in a styrene to catalyst ratio of 1867, 3733 and 7479 $mol_{styrene}/mol_{Ti}$ with addition of 0.156, 0.312 and 0.625 mL of styrene respectively. Ethylene/styrene copolymerisation activities (Figures 4.7 and 4.8) decrease to a greater extent than was seen for ethylene/1-hexene copolymerisations, which can also be seen in the lower uptake rates in

Figures A4.10–A4.16. Mülhaupt *et al.* have previously reported similar results in solution-phase using ^{Me2}SB(^{tBu}N,Cp*)TiCl$_2$.[28]

For the dichloride complexes, the decrease in copolymerisation activities are greater for I* derived ligands than the Cp* analogue, where the activity increases from 2227 to 2346 kg$_{PE}$/mol$_{Ti}$/h/bar on addition of 0.156 mL of styrene followed by a decline in activities on addition of higher amounts of styrene (Figure 4.7). Klosin *et al*. reported that substitution of the 3- and 4- positions of the Cp ring with phenyl groups resulted in higher copolymerisation activities than the Cp* complex, 4423 kg$_{PE}$/mol$_{cat}$/h/bar for ^{Me2}SB(^{tBu}N,$^{3,4\text{-}Ph}$Cp)TiMe$_2$ compared with 1721 kg$_{PE}$/mol$_{cat}$/h/bar for ^{Me2}SB(^{tBu}N,Cp*)TiMe$_2$, indicating the electronics of the ring substituents can greatly effect copolymerisation activities.[25]

For sMAO(3G)-^{Me2}SB(^{tBu}N,I*)TiCl$_2$, activities decrease from 3442 to 1193 and 1236 kg$_{PE}$/mol$_{Ti}$/h/bar for additions of 0.156 and 0.312 mL of styrene, and increases to 2036 kg$_{PE}$/mol$_{Ti}$/h/bar with addition of 0.625 mL. This is in contrast to the other I* complexes where no increase in activities are seen for higher levels of styrene addition. The activity of sMAO(3G)-^{Me2}SB(^{tBu}N,$^{3\text{-}Et}$I*)TiCl$_2$ of decreases from 3759 to 1431, 1324 and 1272 kg$_{PE}$/mol$_{Ti}$/h/bar and sMAO(3G)-^{Me,Pr}SB(^{tBu}N,I*)TiCl$_2$ from 4145 to 954, 853 and 713 kg$_{PE}$/mol$_{Ti}$/h/bar.

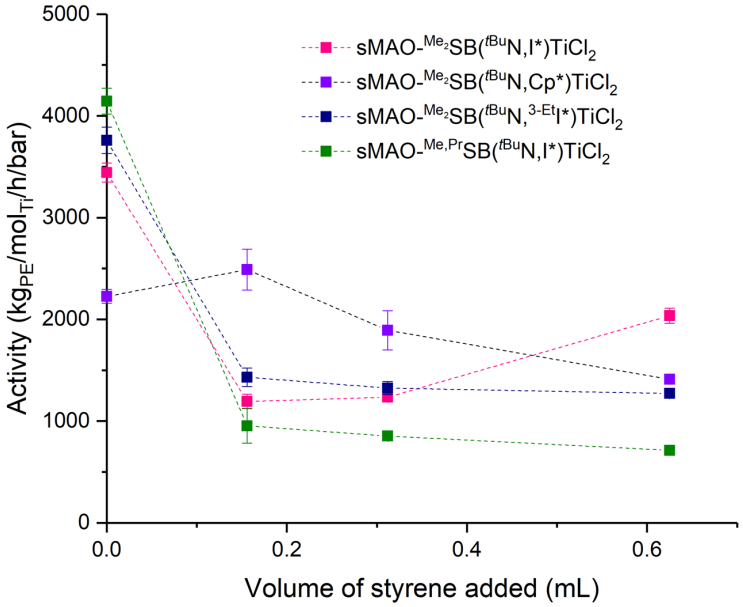

Figure 4.7. Ethylene/styrene copolymerisation activities; 10 mg catalyst ($[Al]_0$:$[Ti]_0$ = 200:1), 2 bar ethylene, 0, 0.156, 0.312 or 0.625 mL styrene, 50 mL hexanes, 150 mg TiBA, 70 °C and 30 minutes. Error bars as 1 standard deviation.

Greatest decreases are observed for the alkylated complexes with increasing amounts of styrene (Figure 4.8): from 4380 to 728 $kg_{PE}/mol_{Ti}/h/bar$, an 83% decrease, for sMAO(3G)-^{Me2}SB($^{t Bu}$N,I*)Ti($CH_2Ph)_2$, and from 3314 to 735 $kg_{PE}/mol_{Ti}/h/bar$, a 78% decrease for sMAO(3G)-^{Me2}SB($^{t Bu}$N,I*)Ti($CH_2SiMe_3)_2$. This is compared to a 41% decrease in activity for sMAO(3G)-^{Me2}SB($^{t Bu}$N,I*)$TiCl_2$. The reduction in activity for sMAO(3G)-^{Me2}SB($^{t Bu}$N,I*)Ti(Cl)CH_2SiMe_3 is more modest than the two bis-alkylated complexes, with activities decreasing from 4905 to 2291 $kg_{PE}/mol_{Ti}/h/bar$ with increasing styrene addition, a 56% decrease in activity. This decrease in activity is more comparable to the change observed for sMAO(3G)-^{Me2}SB($^{t Bu}$N,I*)$TiCl_2$ than the two bis-alkylated complexes and further suggests the nature of the leaving group plays a key role in catalytic copolymerisation activities.

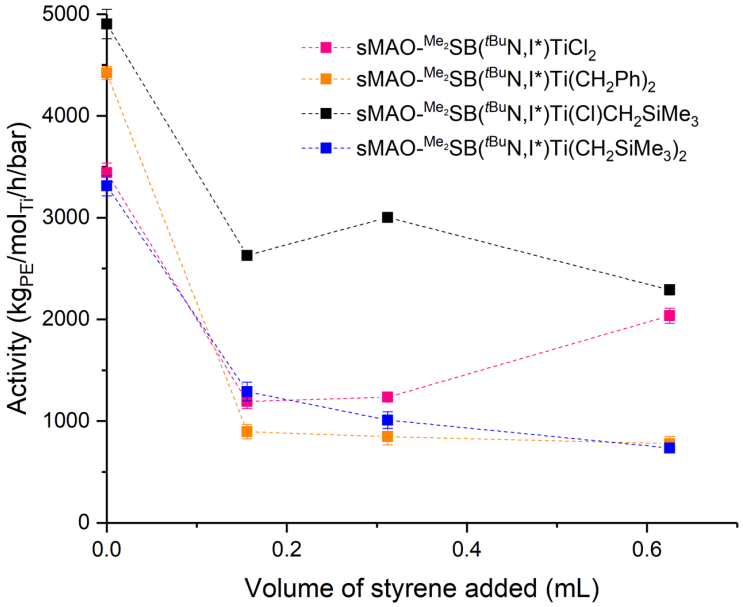

Figure 4.8. Ethylene/styrene copolymerisation activities; 10 mg catalyst ($[Al]_0$:$[Ti]_0$ = 200:1), 2 bar ethylene, 0, 0.156, 0.312 or 0.625 mL styrene, 50 mL hexanes, 150 mg TiBA, 70 °C and 30 minutes. Error bars as 1 standard deviation.

The polymer melt temperatures have been measured for the copolymers produced (Figures A4.29−A4.35), and styrene incorporation levels determined by $^{13}C\{^1H\}$ NMR spectroscopy for addition of 0.625 mL of styrene (Table 4.5). The Cp* complex shows higher levels of styrene incorporation relative to the I* complexes (3.8 mol% compared with 1.6–2.5 mol%) as is to be expected due to the reduced sterics of the apical ligand. Similar effects have been observed in the literature; Okuda and co-workers reported that ^{Me2}SB($^{t\text{Bu}}$N,Cp*)TiCl$_2$ incorporated 15.8 mol% of styrene into the copolymer with a MAO cocatalyst. The fluorenyl analogue, ^{Me2}SB($^{t\text{Bu}}$N,Flu)TiCl$_2$, resulted in only 1.1 mol% styrene incorporation and ^{Me2}SB($^{t\text{Bu}}$N,$^{3\text{-SiMe3}}$I)TiCl$_2$ resulted in 5.7 mol% incorporation under the same conditions.[14] Klosin *et al*. showed that modification of the Cp ring could lead to far higher styrene incorporation and polymer molecular weights, with incorporations of up to 30 mol% for ^{Me2}SB($^{t\text{Bu}}$N,$^{2,3\text{-phenanthrene}}$Cp)TiMe$_2$.[25]

sMAO(3G)-^{Me2}SB($^{t\text{Bu}}$N,$^{3\text{-Et}}$I*)TiCl$_2$ (2.5 mol%) and sMAO(3G)-^{Me2}SB($^{t\text{Bu}}$N,I*)TiCl$_2$ (2.3 mol%) show comparable levels of styrene incorporation with addition of 0.625 mL

of styrene. Lower levels of incorporation were observed for sMAO(3G)-^{Me,Pr}SB($^{t Bu}$N,I*)TiCl$_2$ compared with the other dichloride complexes, which is also coupled with lower copolymerisation activities. A similar decrease in incorporation levels with decreasing copolymerisation activities is also seen when comparing the two bis-alkylated complexes with sMAO(3G)-^{Me_2}SB($^{t Bu}$N,I*)TiCl$_2$. Smaller decreases in activity for copolymerisations with respect to homopolymerisations with sMAO(3G)-^{Me_2}SB($^{t Bu}$N,I*)TiCl$_2$ and sMAO(3G)-^{Me_2}SB($^{t Bu}$N,I*)Ti(Cl)CH$_2$SiMe$_3$ are coupled with higher incorporation levels (both 2.3 mol%) compared with sMAO(3G)-^{Me_2}SB($^{t Bu}$N,I*)Ti(CH$_2$Ph)$_2$ (1.8 mol% and an 83% decrease in activity) and sMAO(3G)-^{Me_2}SB($^{t Bu}$N,I*)Ti(CH$_2$SiMe$_3$)$_2$ (2.1 mol% and a 78% decrease in activity).

Table 4.5. Polymer melt temperatures (T_m), and styrene incorporation levels for the sMAO-supported complexes; 10 mg catalyst ([Al]$_0$:[Ti]$_0$ = 200:1), 2 bar ethylene, 0, 0.156, 0.312 or 0.625 mL styrene, 50 mL hexanes, 150 mg TiBA, 70 °C and 30 minutes.

Volume of styrene (mL)	0	0.156	0.312	0.625	
Supported Complex	T_m (°C)	T_m (°C)	T_m (°C)	T_m (°C)	Incorporation (%)
^{Me_2}SB($^{t Bu}$N,I*)TiCl$_2$	138	119	105	98	2.3
^{Me_2}SB($^{t Bu}$N,$^{3\text{-}Et}$I*)TiCl$_2$	133	120	114	107	2.5
^{Me,Pr}SB($^{t Bu}$N,I*)TiCl$_2$	133	122	119	113	1.6
^{Me_2}SB($^{t Bu}$N,I*)Ti(CH$_2$Ph)$_2$	133	120	116	110	1.8
^{Me_2}SB($^{t Bu}$N,Cp*)TiCl$_2$	134	115	109	98	3.8
^{Me_2}SB($^{t Bu}$N,I*)Ti(CH$_2$SiMe$_3$)$_2$	134	120	116	110	2.1
^{Me_2}SB($^{t Bu}$N,I*)Ti(Cl)CH$_2$SiMe$_3$	133	121	117	110	2.3

As with ethylene/1-hexene copolymerisations in 4.2.1, increased addition of styrene results in decreases in polymer molecular weights (Table 4.6). Waymouth and Son have previously observed this in ethylene/styrene copolymerisations; in a system of {C$_5$H$_4$CH$_2$CH$_2$N(CH$_3$)$_2$}TiCl$_3$ with a MAO cocatalyst, polymer molecular weights decrease from 118 kDa with addition of 10 g styrene to 94 kDa with 20 g of styrene, both under 0.34 bar ethylene.[29]

Table 4.6. Polymer molecular weights (M_w) and molecular weight distributions (M_w/M_n); 10 mg catalyst ($[Al]_0:[Ti]_0 = 200:1$), 2 bar ethylene, 0, 0.156, 0.312 or 0.625 mL styrene, 50 mL hexanes, 150 mg TiBA, 70 °C and 30 minutes.

Volume of styrene (mL)	0		0.156		0.312		0.625	
Supported Complex	M_w (kDa)	M_w/M_n	M_w (kDa)	M_w/M_n	M_w (kDa)	M_w/M_n	M_w (kDa)	M_w/M_n
^{Me2}SB(^{tBu}N,I*)TiCl$_2$	414	6.6	333	3.1	287	3.1	178	2.8
^{Me2}SB(^{tBu}N,$^{3\text{-}Et}$I*)TiCl$_2$	395	3.2	331	3.2	284	3.1	204	2.9
^{Me,Pr}SB(^{tBu}N,I*)TiCl$_2$	554	3.8	507	3.3	459	3.2	321	3.1
^{Me2}SB(^{tBu}N,I*)Ti(CH$_2$Ph)$_2$	449	4.0	405	6.5	341	5.2	280	4.7
^{Me2}SB(^{tBu}N,Cp*)TiCl$_2$	365	3.2	338	3.1	255	3.1	180	2.7
^{Me2}SB(^{tBu}N,I*)Ti(CH$_2$SiMe$_3$)$_2$	667	3.7	410	3.5	358	5.8	306	4.4
^{Me2}SB(^{tBu}N,I*)Ti(Cl)CH$_2$SiMe$_3$	369	3.3	327	3.7	261	5.2	252	4.4

For the supported dichloride complexes, molecular weight dispersities decrease with increasing addition of styrene; for example for sMAO(3G)-^{Me2}SB(^{tBu}N,I*)TiCl$_2$ where M_w/M_n values decrease from 6.6 in homopolymerisation to 3.1, 3.1 and 2.8 for addition of 0.156, 0.312 and 0.635 mL of styrene respectively. There is no clear reason as to why this decrease occurs, but the narrower molecular weight distributions would suggest that there is a greater degree of control in the polymerisation reaction during copolymerisations than homopolymerisations. In contrast, the alkylated complexes demonstrate broader molecular weight distributions with addition of styrene compared to the polymer produced by homopolymerisation. This is also in contrast to what was observed in ethylene/1-hexene copolymerisations in 4.2.1. SEM images of the ethylene/styrene copolymer (Figures A4.44–A4.46) show that the discrete "popcorn-shaped" morphology is maintained on addition of 0.156, 0.312 and 0.625 mL of styrene.

4.2.3 Ethylene/1-octene copolymerisation

Ethylene/1-octene copolymerisation studies were carried out for 30 minutes in a 150 mL ampoule with a sidearm with 0.156, 0.312 or 0.625 mL of 1-octene (1363, 2725 and 5459 $mol_{1\text{-octene}}/mol_{Ti}$) in 5 mL of hexanes that was added at the start of the

polymerisation, a total volume of 50 mL hexanes, 10 mg of catalyst, 150 mg TiBA scavenger, 2 bar ethylene and an $[Al]_0$:$[Ti]_0$ ratio of 200:1. Two supported complexes were tested for ethylene/1-octene copolymerisation, sMAO(3G)-^{Me_2}SB($^{t Bu}$N,I*)$TiCl_2$ and sMAO(3G)-^{Me_2}SB($^{t Bu}$N,$^{3\text{-}Et}$I*)$TiCl_2$ (Figure 4.9), with copolymerisations carried out at 70 °C. The activities obtained are compared with those of ethylene/1-hexene and ethylene/styrene copolymerisations in Figures 4.10 and 4.11.

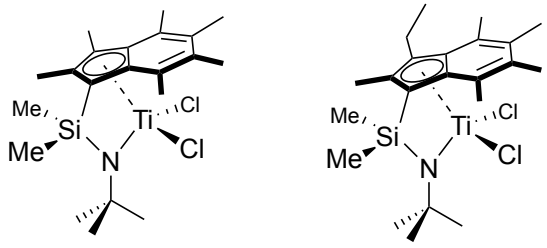

Figure 4.9. Molecular structures of the two complexes tested for ethylene/1-octene copolymerisation.

Ethylene/1-octene copolymerisation activities do not significantly change with addition of 1-octene when compared with homopolymerisation and the activity changes observed in ethylene/1-hexene and ethylene/styrene copolymerisations. For sMAO(3G)-^{Me_2}SB($^{t Bu}$N,I*)$TiCl_2$, copolymerisation activities vary from a 5% decrease to a 10% increase for addition of 0.625 and 0.312 mL of 1-octene respectively (a 4% decrease with 0.156 mL of 1-octene) with respect to homopolymerisation. This is compared to a range of a 5–23% increase in activity in ethylene/1-hexene copolymerisation and a 41–65% decrease in activities in ethylene/styrene copolymerisations. Moderate changes are also seen for sMAO(3G)-^{Me_2}SB($^{t Bu}$N,$^{3\text{-}Et}$I*)$TiCl_2$ ethylene/1-octene copolymerisation activities with these varying from a 3–11% decrease, compared with a 24–40% decrease in activity for ethylene/1-hexene copolymerisation and a 62–66% decrease in activity for ethylene/styrene copolymerisations. This smaller change in activities is unexpected,

especially in comparison to ethylene/1-hexene copolymerisations. Since there is not a large decrease in the level of incorporation of 1-octene compared with 1-hexene (2.0 and 1.8 mol% compared with 2.1 and 2.4 mol% with addition of 0.625 mL of comonomer) this smaller change in activity cannot be fully attributed to incorporation of lower levels of comonomer. Transition to 1-octene from 1-hexene could lead to reductions in both positive and negative comonomer effects, be it exothermic spikes leading to catalytic deactivation and reduction in activities, or increasing ethylene solubility and increased ability for monomer close approach to the catalyst site which can contribute to higher activities.[17,18]

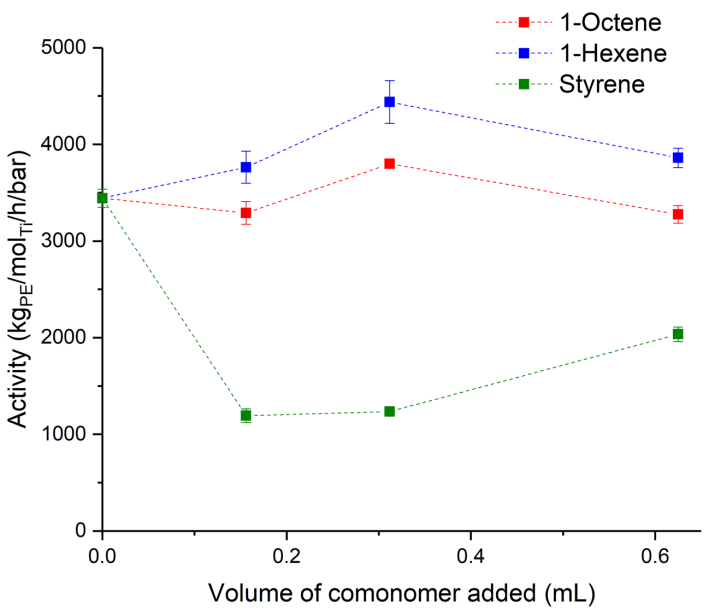

Figure 4.10. Ethylene copolymerisation activities with sMAO(3G)-^{Me_2}SB($^{t Bu}$N,I*)TiCl$_2$; 10 mg catalyst ([Al]$_0$:[Ti]$_0$ = 200:1), 2 bar ethylene, 0, 0.156, 0.312 or 0.625 mL of 1-octene (red), 1-hexene (blue) and styrene (green), 50 mL hexanes, 150 mg TiBA, 70 °C and 30 minutes.

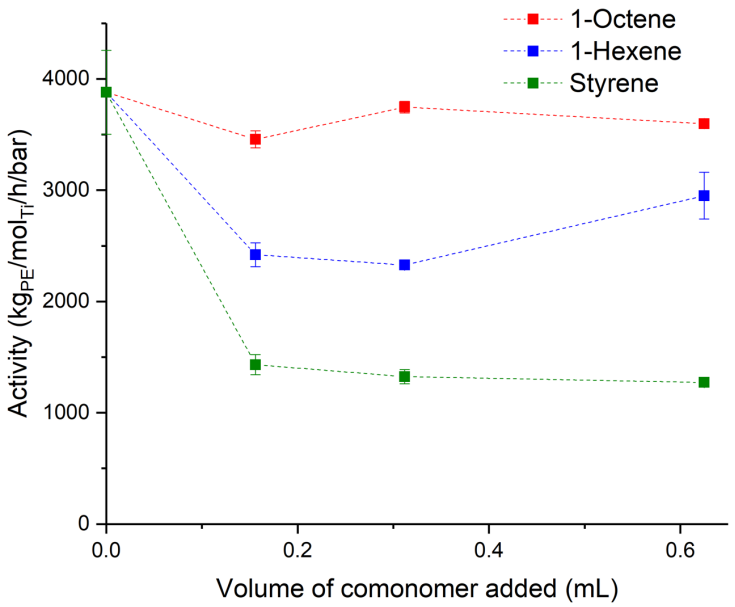

Figure 4.11. Ethylene copolymerisation activities with sMAO(3G)-^{Me2}SB(^{tBu}N,$^{3\text{-}Et}$I*)TiCl$_2$; 10 mg catalyst ([Al]$_0$:[Ti]$_0$ = 200:1), 2 bar ethylene, 0, 0.156, 0.312 or 0.625 mL of 1-octene (red), 1-hexene (blue) and styrene (green), 50 mL hexanes, 150 mg TiBA, 70 °C and 30 minutes.

The polymer produced was studied using DSC (Figures 4.12 and 4.13 and Table 4.7), and the polymers produced with addition of 0.625 mL of 1-octene studied by high temperature ^{13}C{^{1}H} NMR spectroscopy (Table 4.7).

Table 4.7. Polymer melt temperatures (T_m), and 1-octene incorporation levels for the catalysts: sMAO-^{Me2}SB(^{tBu}N,I*)TiCl$_2$ and sMAO-^{Me2}SB(^{tBu}N,$^{3\text{-}Et}$I*)TiCl$_2$; 10 mg catalyst ([Al]$_0$:[Ti]$_0$ = 200:1), 2 bar ethylene, 0, 0.156, 0.312 or 0.625 mL of 1-octene, 50 mL hexanes, 150 mg TiBA, 70 °C and 30 minutes.

Volume of 1-octene (mL) Supported complex	0 T_m (°C)	0.156 T_m (°C)	0.312 T_m (°C)	0.625 T_m (°C)	0.625 Incorporation (mol%)
sMAO-^{Me2}SB(^{tBu}N,I*)TiCl$_2$	138	124	122	119	2.0
sMAO-^{Me2}SB(^{tBu}N,$^{3\text{-}Et}$I*)TiCl$_2$	133	125	123	122	1.8

The lower incorporation level observed for sMAO(3G)-^{Me2}SB(^{tBu}N,$^{3\text{-}Et}$I*)TiCl$_2$ compared with sMAO(3G)-^{Me2}SB(^{tBu}N,I*)TiCl$_2$ could be due to a steric effect of the 3-ethyl group, which when coupled with the sterically bulky sMAO support could hinder the close approach of 1-octene. Quijada *et al.* have previously demonstrated that increased steric bulk of a linear α-olefin results in lower levels of incorporation, with both EBIZrCl$_2$ and

^{Me_2}SBCp$_2$ZrCl$_2$ incorporating higher levels of 1-hexene than 1-octene and 1-decene with equivalent amounts of comonomer in solution,[27] as is observed here.

Polymer molecular weights decrease with increased addition of 1-octene, as observed for both ethylene/1-hexene and ethylene/styrene copolymerisations (Table 4.8). As previously discussed in 4.2.1, the changes in molecular weights have been proposed to be due to a balance of higher rates of chain propagation facilitated by the addition of a comonomer competing with an increased rate of β-hydride transfer facilitated by the metal–α-olefin species and also an increased rated of chain transfer to the α-olefin.[24,27]

Table 4.8. Molecular weights (M_w) and molecular weight distributions (M_w/M_n) of the polymers produced; 10 mg catalyst ([Al]$_0$:[Ti]$_0$ = 200:1), 2 bar ethylene, 0, 0.156, 0.312 or 0.625 mL of 1-octene, 50 mL hexanes, 150 mg TiBA, 70 °C and 30 minutes.

Volume of 1-octene (mL)	0		0.156		0.312		0.625	
Supported Complex	M_w (kDa)	M_w/M_n	M_w (kDa)	M_w/M_n	M_w (kDa)	M_w/M_n	M_w (kDa)	M_w/M_n
^{Me_2}SB($^{t\text{Bu}}$N,I*)TiCl$_2$	414	6.6	356	3.1	282	3.0	103	4.2
^{Me_2}SB($^{t\text{Bu}}$N,$^{3\text{-Et}}$I*)TiCl$_2$	395	3.2	243	2.8	226	2.8	93	3.0

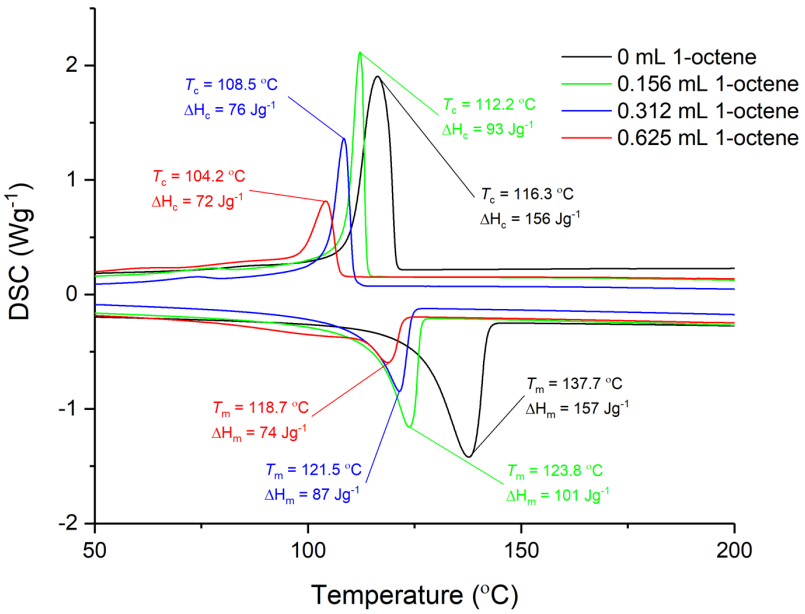

Figure 4.12. DSC plot for polymers produced by sMAO-^{Me_2}SB($^{t\text{Bu}}$N,I*)TiCl$_2$ at 70 °C for 0 mL (black), 0.156 mL (green), 0.312 mL (blue), and 0.625 mL 1-octene (red).

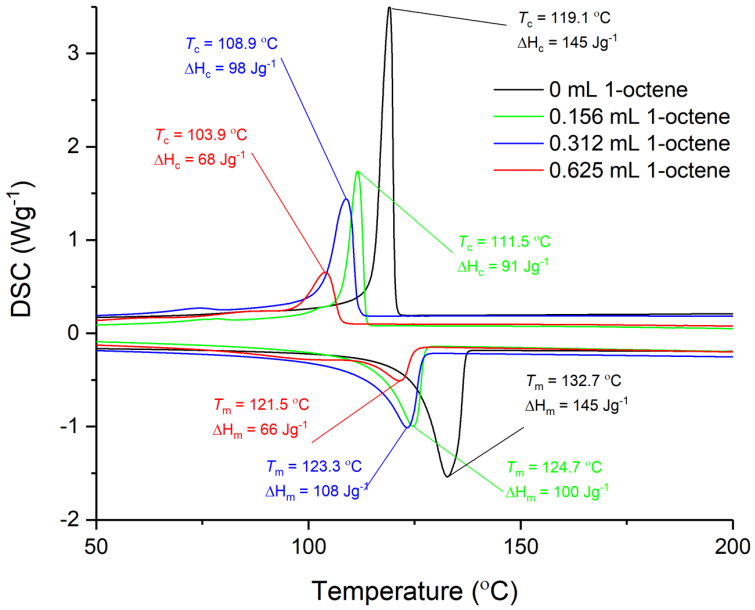

Figure 4.13. DSC plot for polymers produced by sMAO-^{Me2}SB($^{t\text{Bu}}$N,$^{3\text{-Et}}$I*)TiCl$_2$ at 70 °C for 0 mL (black), 0.156 mL (green), 0.312 mL (blue), and 0.625 mL 1-octene (red).

As has been observed for both ethylene/1-hexene and ethylene/styrene copolymerisations, polymer melt enthalpies and temperatures and crystallisation enthalpies and temperatures decrease with increased addition of 1-octene. The similar changes in polymer melt temperatures compared with ethylene/1-hexene copolymerisation align with the comparable levels of comonomer incorporation with addition of both 1-octene and 1-hexene (2.0 and 1.8 mol% compared with 2.1 and 2.3 mol%) for ^{Me2}SB($^{t\text{Bu}}$N,I*)TiCl$_2$ and ^{Me2}SB($^{t\text{Bu}}$N,$^{3\text{-Et}}$I*)TiCl$_2$ respectively.

As discussed in 4.2.1, increased addition of 1-octene results in a decrease in the average chain length between hexyl chain defects and a decreased polymer molecular weight. The hexyl chains are generally excluded from the lamella, with the narrowing of these being a major factor in the reduction in melt temperatures.[20,21] The comparable changes in polymer melt temperatures with all three comonomers further suggests that these defects are excluded from the lamella.

4.3 High-throughput ethylene/1-hexene copolymerisation

High-throughput ethylene/1-hexene copolymerisation experiments were carried out at HTExplore (University of Naples) in collaboration with Prof. Vincenzo Busico, with the experiments run by Dr. Alessio Mingione. High-throughput experiments allow for a large number of simultaneous, parallel, experiments screening a number of different conditions in a shorter time period, and are of common use in pharmaceutical, organometallic and organic chemistry.[30,31] Copolymerisations were conducted at 8.27 bar of ethylene in 23 mL cells with 5 mL of heptane, 10 μmol TiBA scavenger, 0.075–0.40 mg catalyst ($[Al]_0$:$[Ti]_0$ ratio of 200:1 on 1st generation sMAO) and the desired volume of 1-hexene (0, 125 or 250 μL).

4.3.1 Effect of the amido fragment on ethylene/1-hexene copolymerisation

Three catalysts with differing amido fragments, sMAO-^{Me2}SB($^{t Bu}$N,I*)$TiCl_2$, sMAO-^{Me2}SB($^{i Pr}$N,I*)$TiCl_2$ and sMAO-^{Me2}SB($^{n Bu}$N,I*)$TiCl_2$ (Figure 4.14), were tested as ethylene/1-hexene copolymerisation catalysts with the results shown in Table 4.9.

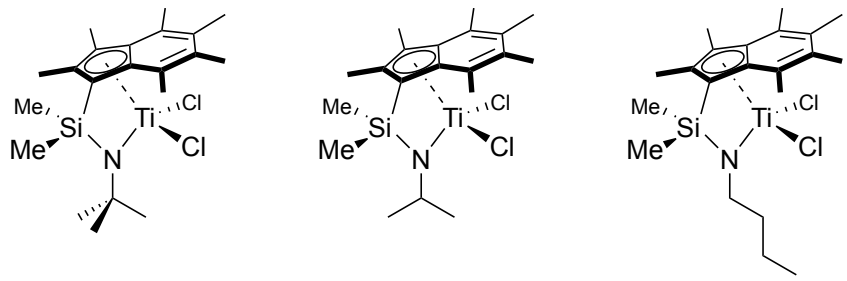

Figure 4.14. Molecular structures of the three complexes tested for ethylene/1-hexene copolymerisation under high-throughput conditions.

As has been previously reported for these complexes and demonstrated in Chapter 3, there is a trend of increased polymerisation activity with increased electron donating ability of the amido fragment (^{t}Bu > ^{i}Pr > ^{n}Bu).[32] The activity of the ^{n}Bu complex under

high-throughput conditions was found to be lower than had been previously found for the complex under 2 bar ethylene pressure in Section 3.2.1, and it is proposed that this low activity could be due to rapid catalyst decomposition from thermal instability, which could be overcome by prepolymerisation.[33]

Table 4.9. Ethylene/1-hexene copolymerisation activities and 1-hexene incorporation levels using sMAO-^{Me2}SB($^{t Bu}$N,I*)TiCl$_2$, sMAO-^{Me2}SB($^{i Pr}$N,I*)TiCl$_2$ and sMAO-^{Me2}SB($^{n Bu}$N,I*)TiCl$_2$; 8.27 bar ethylene, 0.075–0.40 mg catalyst ([Al]$_0$:[Ti]$_0$ = 200:1), 5.0 mL heptane, 10 μmol TiBA and 80 °C. Reactions quenched at 8.27 bar maximum ethylene uptake or after 60 minutes.

Volume of 1-Hexene (μL)	^{Me2}SB($^{t Bu}$N,I*)TiCl$_2$		^{Me2}SB($^{i Pr}$N,I*)TiCl$_2$		^{Me2}SB($^{n Bu}$N,I*)TiCl$_2$	
	Activity[a]	Incorporation (mol%)	Activity[a]	Incorporation (mol%)	Activity[a]	Incorporation (mol%)
0	6714	-	1224	-	485	-
125	5246	5.6	377	6.3	216	1.6
250	3598	6.6	394	14.2	193	4.7

[a] Activity in kg$_{PE}$/mol$_{Ti}$/h/bar.

Across the three complexes, there are high levels of 1-hexene incorporation, a trait commonly observed for CGC complexes that is attributable to the more open metal centre due to the strain inducing *ansa* bridge.[4–6] sMAO-^{Me2}SB($^{i Pr}$N,I*)TiCl$_2$ shows much higher levels of 1-hexene incorporation with respect to sMAO-^{Me2}SB($^{t Bu}$N,I*)TiCl$_2$ (6.3 and 14.2 mol% compared with 5.6 and 6.6 mol%), likely to be due to the reduced steric bulk of the ^{i}Pr ligand, which leads to easier coordination of 1-hexene to the metal centre compared with the ^{t}Bu ligand. These incorporation levels are lower than have been reported for other CGCs, over 60% for ^{Me2}SB($^{t Bu}$N,Cp*)TiMe$_2$ with an MAO cocatalyst.[9] However, it should be noted that these were conducted with higher concentrations of 1-hexene and in solution-phase, where higher incorporation levels are often observed.[10]

There are also large reductions in activity on addition of 1-hexene in comparison with homopolymerisation activities, 6714 to 3598 kg$_{PE}$/mol$_{Ti}$/h/bar and 1224 to 394 kg$_{PE}$/mol$_{Ti}$/h/bar for the two complexes with decreases in activity indicating the negative comonomer effects outweigh the positive effects. Many theories have been

proposed for the positive comonomer effect, including the fracturing of catalyst particles exposing new sites, formation of new active species by coordination of α-olefins, or activation of dormant active sites, but many of these have been refuted for molecular catalyst systems.[34] Studies have shown that addition of 1-hexene to an alkane reaction mixture leads to a 7–10% increase in ethylene solubility between 70–90 °C,[17] as well as improved diffusion of ethylene close to the catalytic site.[18] With metallocene-type complexes, the comonomer effect is often not observed or is even negative. This has been proposed to be due to competitive binding between ethylene and α-olefins and, if the rate of migratory insertion of the α-olefin is slower than that of ethylene, the rate of chain propagation will decrease and as such polymerisation activities can decrease.[34] These negative comonomer effects can lead to the reduced activities observed for copolymerisations compared with homopolymerisations.

4.3.2 Effect of the initiator group on ethylene/1-hexene copolymerisation

Four complexes of the type sMAO-^{Me2}SB($^{t Bu}$N,I*)TiR$_2$ (R = Cl, Me, CH_2Ph and CH_2SiMe_3) and sMAO-^{Me2}SB($^{t Bu}$N,I*)Ti(Cl)CH_2SiMe_3 (Figure 4.15) were tested for ethylene/1-hexene copolymerisation.

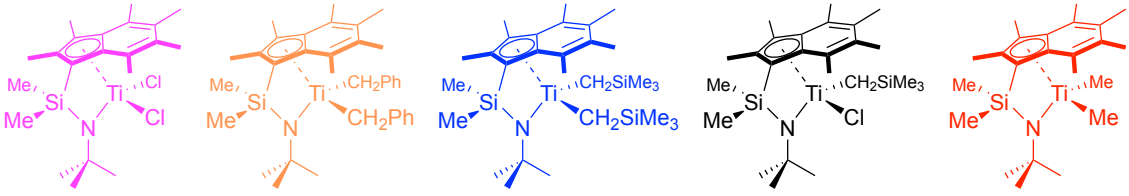

Figure 4.15. Molecular structures of the five complexes tested for ethylene/1-hexene copolymerisation under high-throughput conditions. Colours correspond to colours of the lines used on the graphs.

Figure 4.16 shows the ethylene/1-hexene copolymerisation activities with varying amounts of 1-hexene comonomer. There is a large decrease in ethylene polymerisation

activity with addition of 1-hexene to the reaction mixture. For example, a decrease from 4708 to 1518 $kg_{PE}/mol_{Ti}/h/bar$ is observed for sMAO-^{Me2}SB(^{tBu}N,I*)Ti(Cl)CH_2SiMe_3 with 0 and 250 µL 1-hexene respectively. The decreases in activity can be attributed to the reasons discussed in 4.3.1. In addition to this, there is also an exothermic spike up to approximately 85 °C at the start of these copolymerisation experiments. The alkylated complexes are much more sensitive to polymerisation temperature than the dichloride complex, and so a thermal spike from 80 °C is likely to have a larger effect on activities. Secondly, the copolymer produced is much stickier compared to polyethylene, wrapping around the stirrer mechanism, resulting in a lollipop-like appearance. This inhibits the stirring efficiency and can result in a bi-layered mixture forming, leading to a further barrier for ethylene diffusion in solution and hindering polymerisation.

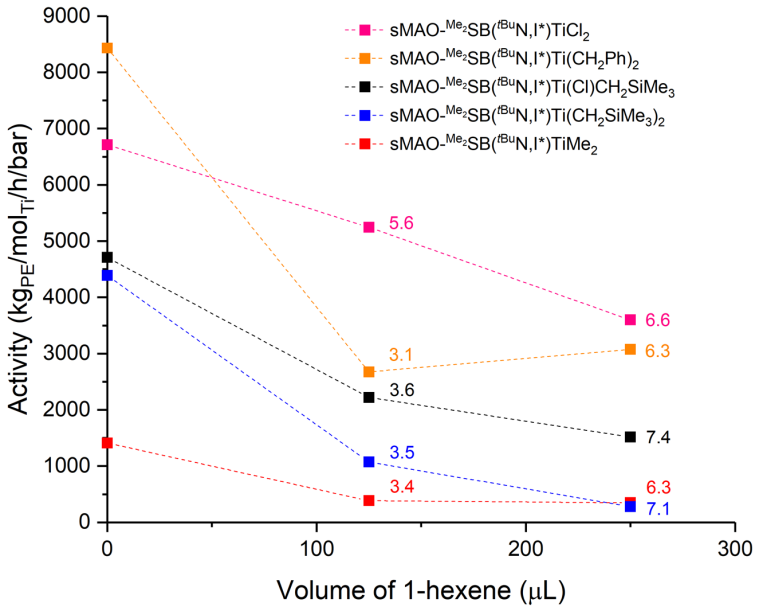

Figure 4.16. Ethylene/1-hexene copolymerisation activities of sMAO-^{Me2}SB(^{tBu}N,I*)TiR_2 (R = Cl, Me, CH_2Ph and CH_2SiMe_3) and sMAO-^{Me2}SB(^{tBu}N,I*)Ti(Cl)CH_2SiMe_3; 1-hexene incorporation percentages shown on the graph. 8.27 bar ethylene, 0.075–0.40 mg catalyst ($[Al]_0$:$[Ti]_0$ = 200:1), 5.0 mL heptane, 10 µmol TiBA and 80 °C. Reactions quenched at 8.27 bar maximum ethylene uptake or after 60 minutes.

This effect can be seen in the uptake rate graphs shown in Figure 4.17 and Figures A4.36−A4.39. Sharp decreases in uptake rates with 125 and 250 µL addition of 1-hexene can be attributed to this phenomenon.

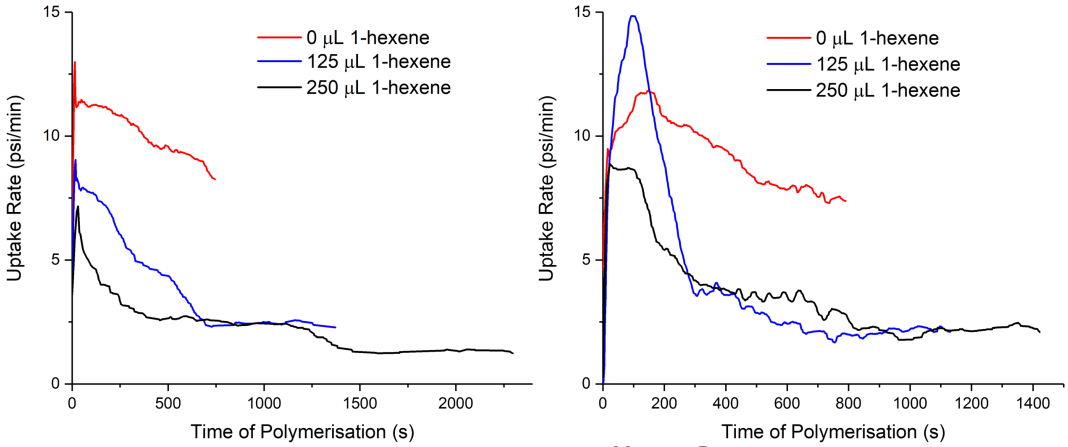

Figure 4.17. Ethylene uptake rate profiles for sMAO-^{Me2}SB($^{t\text{Bu}}$N,I*)Ti(Cl)CH_2SiMe_3 (left) and sMAO-^{Me2}SB($^{t\text{Bu}}$N,I*)$TiCl_2$ (right) with varying amounts of 1-hexene. Polymerisation conditions: 8.27 bar ethylene, 0.075–0.40 mg catalyst ($[Al]_0$:$[Ti]_0$ = 200:1), 5.0 mL heptane, 10 µmol TiBA and 80 °C. Reactions quenched at 8.27 bar maximum ethylene uptake or after 60 minutes.

These complexes all show very high levels of α-olefin incorporation (Figure 4.16), typical of CGCs.[4–6] sMAO-^{Me2}SB($^{t\text{Bu}}$N,I*)$TiCl_2$ shows higher levels of 1-hexene incorporation on addition of 125 µL of 1-hexene when compared to the alkylated complexes, 5.6 mol% compared with 3.1–3.6 mol%. It is possible this may be due to the steric and electronic effects of the initiator group remaining coordinated to the catalyst surface interacting with the active species by a secondary coordination effect. The effects of $^{-}CH_2Ph$ and $^{-}CH_2SiMe_3$ appear to be much greater than that of Cl^{-}, reducing the rate of diffusion of the comonomer close to the active site, similar to how supported catalysts typically exhibit lower incorporation than homogeneous catalysts.[10] This effect is no longer observed on addition of 250 µL 1-hexene with incorporation levels of 6.6 mol% for sMAO-^{Me2}SB($^{t\text{Bu}}$N,I*)$TiCl_2$ and 6.3–7.1 mol% for the alkylated complexes. However, what is observed for the alkyl complexes is a more proportionate increase in 1-hexene incorporation, and this can be of great use to controllably tune the amount of 1-hexene

being incorporated into the polymer chain. Higher incorporation levels compared with 4.2.1 are likely due to higher 1-hexene concentrations, and higher molar ratios of 1-hexene relative to the amount of catalyst used.

Crystallisation Elution Fraction (CEF) was also used to analyse the polymer produced. It showed that maximum elution temperatures ($T_{El,max}$) decrease with increased addition of 1-hexene, and higher incorporation levels (Table A4.11). For example, maximum elution temperatures decrease from 113.3 to 88.0 and 70.9 °C with increased addition of 1-hexene for sMAO-^{Me2}SB($^{t Bu}$N,I*)Ti(Cl)CH_2SiMe_3 and from 112.1 to 85.1 and 73.5 °C for sMAO-^{Me2}SB($^{t Bu}$N,I*)$TiCl_2$. The decreases in $T_{El,max}$ are attributable to the weakening of intramolecular forces between the polymer chains with increasing incorporation of 1-hexene.[35]

4.3.3 Effect of the permethylindenyl moiety on ethylene/1-hexene copolymerisation

The catalysts sMAO-^{Me2}SB($^{t Bu}$N,$^{3\text{-}R}$I*)$TiCl_2$ (R = Me and Et) (Figure 4.9) were tested for ethylene/1-hexene copolymerisation under the conditions described in 4.3. Klosin *et al.* have previously reported the effect of variation of the indenyl moiety on ethylene/1-octene copolymerisation, finding that increased electron-donating ability led to higher activities and polymer molecular weights.[8,25] The polymerisation activities, polymer molecular weights and 1-hexene incorporation levels are shown in Table 4.10.

Both complexes show decreases in activity for ethylene/1-hexene copolymerisation compared with ethylene homopolymerisation. sMAO-^{Me2}SB($^{t Bu}$N,$^{3\text{-}Et}$I*)$TiCl_2$ shows greater decreases in activities (34 and 56% for 125 and 250 μL 1-hexene respectively) compared with sMAO-^{Me2}SB($^{t Bu}$N,I*)$TiCl_2$ (22 and 46% respectively) attributed to the decreased thermal stability of the 3-ethylpentamethylindenyl complex compared with the

permethylindenyl complex. This is also observed in ethylene homopolymerisation for analogous sMAO-^{Me_2}SB($^{2,7\text{-}t\text{Bu}}$Flu,$^{3\text{-R}}$I*)$ZrCl_2$ catalysts and homopolymerisation in 3.2.3 where there are greater decreases in polymerisation activities with increased temperatures for the 3-ethylpentamethylindenyl complex compared with the permethylindenyl complex.[36] High levels of 1-hexene incorporation are observed for both catalysts; 5.6 mol% for 125 µL 1-hexene and 6.6 mol% and 8.4 mol% for 250 µL 1-hexene (Table 4.10). The increased incorporation at 250 µL for sMAO-^{Me_2}SB($^{t\text{Bu}}$N,$^{3\text{-Et}}$I*)$TiCl_2$ compared with sMAO-^{Me_2}SB($^{t\text{Bu}}$N,I*)$TiCl_2$ is also seen in the analogous sMAO-^{Me_2}SB($^{2,7\text{-}t\text{Bu}}$Flu,$^{3\text{-R}}$I*)$ZrCl_2$ complexes.[37]

Table 4.10. Ethylene/1-hexene copolymerisation activities, 1-hexene incorporation levels and polymer molecular weights for sMAO-^{Me_2}SB($^{t\text{Bu}}$N,I*)$TiCl_2$ and sMAO-^{Me_2}SB($^{t\text{Bu}}$N,$^{3\text{-Et}}$I*)$TiCl_2$; 8.27 bar ethylene, 0.20–0.30 mg catalyst ($[Al]_0$:$[Ti]_0$ = 200:1), 5.0 mL heptane, 10 µmol TiBA and 80 °C. Reactions quenched at 8.27 bar maximum ethylene uptake or after 60 minutes.

Volume of 1-Hexene (µL)	^{Me_2}SB($^{t\text{Bu}}$N,I*)$TiCl_2$				^{Me_2}SB($^{t\text{Bu}}$N,$^{3\text{-Et}}$I*)$TiCl_2$			
	Activity[a]	Incorporation (mol%)	M_w[b]	M_w/M_n	Activity[a]	Incorporation (mol%)	M_w[b]	M_w/M_n
0	6714	-	2667	3.2	2564	-	1.4×10^3	4.0
125	5246	5.6	269	3.0	1681	5.6	247	2.9
250	3598	6.6	332	2.7	1139	8.4	224	2.6

[a] Activity in $kg_{PE}/mol_{Ti}/h/bar$; [b] M_w value in kDa.

Both complexes show over a five-fold decrease in polymer molecular weights with addition of 1-hexene, with relatively narrow molecular weight distributions (M_w/M_n) maintained (2.7–3.0 for copolymers, compared with 3.2 and 4.0 for the I* and $^{3\text{-Et}}$I* homopolymers respectively). This decrease results from frequent chain termination following 1-hexene insertion and chain transfer to 1-hexene monomers, coupled with a decrease in the rate of chain propagation.[24,27] This effect has been observed and studied for ^{Me_2}SB($^{t\text{Bu}}$N,Cp*)$TiMe_2$, ^{Me_2}SB($^{t\text{Bu}}$N,$^{2\text{-R}}$I)$TiMe_2$ and ^{Me_2}SB($^{t\text{Bu}}$N,$^{3\text{-R}}$I)$TiMe_2$, with work having been undertaken in an attempt to negate this molecular weight decrease with addition of heteroatom substituents in the 2- and 3- positions on the indenyl moiety.[8,25]

4.4 Large scale slurry-phase copolymerisation studies

4.4.1 Large scale ethylene/1-hexene copolymerisation

Large scale copolymerisation studies were conducted at SCG Chemicals Co. Ltd., (Rayong, Thailand) by Mr Thawesak Parawan, Mr Somjet Songnoey and Mr Pongsiri Kaeoyok. Polymerisations were undertaken in a 1 L reactor with 600 mL of hexanes, 25–50 mg of catalyst ($[Al]_0$:$[Ti]_0$ = 200:1), 6 or 8 bar ethylene, 3 mmol TiBA scavenger, 5, 10 or 20 mL of 1-hexene with polymerisations conducted for 1 hour at 70 °C. sMAO-^{Me2}SB($^{t Bu}$N,I*)$TiCl_2$ and sMAO-^{Me2}SB($^{t Bu}$N,I*)$Ti(CH_2Ph)_2$ were studied (Figure 4.18). Ethylene homo- and copolymerisation activities are shown in Tables 4.11 and 4.12, along with incorporation levels and polymer molecular weights.

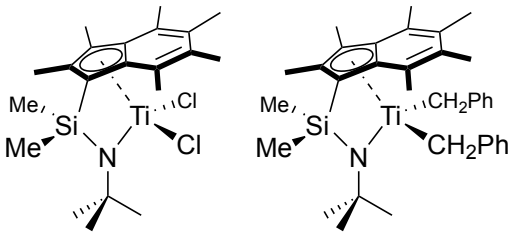

Figure 4.18. Molecular structures of the two complexes tested for ethylene/1-hexene copolymerisation at SCG Chemicals Co. Ltd., (Rayong, Thailand).

Table 4.11. Ethylene/1-hexene copolymerisation activities, 1-hexene incorporation levels and polymer molecular weights for sMAO-^{Me2}SB($^{t Bu}$N,I*)$TiCl_2$ and sMAO-^{Me2}SB($^{t Bu}$N,I*)$Ti(CH_2Ph)_2$; 8 bar ethylene, 25–50 mg catalyst ($[Al]_0$:$[Ti]_0$ = 200:1), 70 °C, 1 hour, 600 mL hexanes, and 3 mmol TiBA.

Volume of 1-Hexene (mL)	^{Me2}SB($^{t Bu}$N,I*)$TiCl_2$				^{Me2}SB($^{t Bu}$N,I*)$Ti(CH_2Ph)_2$			
	Activity[a]	Incorporation (mol%)	M_w[b]	M_w/M_n	Activity[a]	Incorporation (mol%)	M_w[b]	M_w/M_n
0	4098[c]	-	1104	15.7	8412	-	1090	3.9
5	-	-	-		2211	0.94	697	5.0
10	1591[d]	0.99	-		3423	3.36	395	3.9
20	1135[e]	3.99	158	4.7	2924	2.62	473	3.3

[a] Activity in $kg_{PE}/mol_{Ti}/h/bar$; [b] M_w value in kDa. [c] Homopolymerisation conducted at 80 °C. [d] 2 hour reaction time. [e] 100 mg solid catalyst.

With increased addition of 1-hexene comonomer, in both cases a decrease in polymerisation activity is observed; for sMAO-^{Me2}SB($^{t Bu}$N,I*)TiCl$_2$, polymerisation activities decrease by 61 and 72% respectively for addition of 10 and 20 mL of 1-hexene, and for sMAO-^{Me2}SB($^{t Bu}$N,I*)Ti(CH$_2$Ph)$_2$, activities decrease by 74, 59 and 65% with addition of 5, 10 and 20 mL of 1-hexene respectively. This larger than expected decrease for sMAO-^{Me2}SB($^{t Bu}$N,I*)TiCl$_2$ when compared with the two previous studies is attributable to two factors. Firstly, on addition of 10 mL of 1-hexene, the copolymerisation experiment was undertaken for two hours compared to 1 hour for other (co)polymerisations; it has been broadly demonstrated in Chapter 3 that polymerisation activities decrease with increased reaction time due to blocking of active sites and deactivation of the active species. Secondly, on addition of 20 mL of 1-hexene, four times more supported catalyst is used compared with the homopolymerisation reaction which is likely to lead to lower activities due to lower relative concentrations of ethylene in the reaction mixture compared with the amount of supported catalyst present. With both catalysts, incorporation levels typically increase with increased addition of 1-hexene as has been observed in both HTExplore and University of Oxford conditions; similarly to the high-throughput experiments, sMAO-^{Me2}SB($^{t Bu}$N,I*)Ti(CH$_2$Ph)$_2$ shows a more proportionate increase in incorporation levels than is observed for sMAO-^{Me2}SB($^{t Bu}$N,I*)TiCl$_2$. Higher levels of incorporation are observed when compared with Section 4.2.1 with maximum incorporations of 3.36 and 3.99 mol% for sMAO-^{Me2}SB($^{t Bu}$N,I*)Ti(CH$_2$Ph)$_2$ and sMAO-^{Me2}SB($^{t Bu}$N,I*)TiCl$_2$ respectively compared with 2.1 and 2.2 mol%). This is likely due to higher concentrations of 1-hexene in solution during the larger scale copolymerisations (up to 0.27 mol/dm^3 compared with up to 0.10 mol/dm^3). Polymer molecular weights also reduce significantly with addition of 1-hexene, from 1104 to 158 kDa and 1090 to 473 kDa for sMAO-^{Me2}SB($^{t Bu}$N,I*)TiCl$_2$

and sMAO-^{Me_2}SB(^{tBu}N,I*)Ti(CH_2Ph)$_2$ respectively. An effect observed for all other copolymerisation experiments and attributable to an increase in chain termination and chain transfer pathways afforded by addition of a 1-hexene comonomer, and a decrease in the rate of chain propagation.[24]

Table 4.12. Ethylene/1-hexene copolymerisation activities, 1-hexene incorporation levels and polymer molecular weights for sMAO-^{Me_2}SB(^{tBu}N,I*)Ti(CH_2Ph)$_2$; 25–50 mg catalyst ([Al]$_0$:[Ti]$_0$ = 200:1), 70 °C, 1 hour, 600 mL hexanes, and 3 mmol TiBA.

Volume of 1-Hexene (mL)	6 bar				8 bar			
	Activity[a]	Incorporation (mol%)	M_w[b]	M_w/M_n	Activity[a]	Incorporation (mol%)	M_w[b]	M_w/M_n
0	-	-	-		8412	-	1090	3.9
5	671	0.79	1408	3.9	2211	0.94	697	5.0
10	2010	1.62	584	4.6	3423	3.36	395	3.9
20	1342	3.05	511	3.6	2924	2.62	473	3.3

[a] Activity in $kg_{PE}/mol_{Ti}/h/bar$; [b] M_w value in kDa.

Table 4.12 demonstrates how pressure can affect copolymerisation activities and the molecular weight of the polymer produced. As expected, activities decrease with decreasing ethylene pressure (41–70% decrease), due to the decreasing amount of ethylene in solution and reduced availability of the monomer in the reaction mixture.[38] The change in pressure does not appear to result in a definitive change in incorporation levels between 6 and 8 bar of ethylene. Reduced polymer molecular weights with increased ethylene pressure is in contrast to what has been observed previously in homopolymerisations. In both cases molecular weights decrease with increased 1-hexene incorporation as discussed above.

4.4.2 Large scale ethylene/styrene copolymerisation

Large scale ethylene/styrene copolymerisation experiments were carried out using the same method described in Section 4.4.1, with sMAO-^{Me_2}SB(^{tBu}N,I*)$TiCl_2$ and sMAO-^{Me_2}SB(^{tBu}N,I*)Ti(CH_2Ph)$_2$ studied. The (co)polymerisation activities, comonomer incorporations and polymer molecular weights are given in Table 4.13.

Table 4.13. Ethylene/styrene copolymerisation activities, styrene incorporation levels and polymer molecular weights for sMAO-^{Me2}SB($^{t Bu}$N,I*)TiCl$_2$ and sMAO-^{Me2}SB($^{t Bu}$N,I*)Ti(CH$_2$Ph)$_2$; 8 bar ethylene, 25–50 mg catalyst ([Al]$_0$:[Ti]$_0$ = 200:1), 70 °C, 1 hour, 600 mL hexanes, and 3 mmol TiBA.

Volume of styrene (mL)	^{Me2}SB($^{t Bu}$N,I*)TiCl$_2$			^{Me2}SB($^{t Bu}$N,I*)Ti(CH$_2$Ph)$_2$		
	Activity[a]	Incorporation (mol%)	M_w[b]	Activity[a]	Incorporation (mol%)	M_w[b]
0	4098[c]	-	1104	8412	-	1090
5	-	-	-	446	0.38	629
10	1895[c]	0.52	669	440	0.72	739
20	-	-	-	292	1.46	614

[a] Activity in kg$_{PE}$/mol$_{Ti}$/h/bar; [b] M_w value in kDa. [c] Experiments carried out at 80 °C.

Copolymerisation activities significantly decrease on addition of comonomer as is also observed in polymerisations carried out in Section 4.2.2. Activities decrease by 54% for sMAO-^{Me2}SB($^{t Bu}$N,I*)TiCl$_2$ and by 95–97% for sMAO-^{Me2}SB($^{t Bu}$N,I*)Ti(CH$_2$Ph)$_2$. The larger decreases in copolymerisation activities for ethylene/styrene copolymerisation relative to ethylene/1-hexene copolymerisation are also observed in 4.2. This reduction in activity could be due to the coordination of the aromatic ring of styrene to the metal centre during the polymerisation cycle.[39] Decreasing polymer molecular weights with addition of styrene compared with homopolymerisation would once again suggest that alternative chain transfer and termination pathways are facilitated by addition of a comonomer in addition to the decreased rate of chain propagation, similar to as was previously observed with addition of 1-hexene. Styrene incorporation levels are lower than those observed for ethylene/1-hexene copolymerisations under the same conditions, with 0.52 mol% incorporation for sMAO-^{Me2}SB($^{t Bu}$N,I*)TiCl$_2$ with addition of 10 mL of styrene (compared with 0.99 mol% for 1-hexene) and 0.38, 0.72 and 1.46 mol% for sMAO-^{Me2}SB($^{t Bu}$N,I*)Ti(CH$_2$Ph)$_2$ with 5, 10 and 20 mL styrene (compared with 0.94, 3.36 and 2.62 mol% for 1-hexene).

4.5 Solution-phase copolymerisation

4.5.1 Solution-phase ethylene/1-hexene copolymerisation

Solution-phase ethylene/1-hexene copolymerisations were performed at Norner AS by Tina Kristiansen Voss, Svein Nenseth, Knut Fosse and Jarmo Lindroos. Copolymerisations were carried out in a 1 L reactor in an Isopar-E reaction solvent. 1–2 mg of complex was used with 1000 equivalents of MAO cocatalyst, 35 bar ethylene, 10–20 minutes reaction time between 140 and 150 °C, 10–30 mL of 1-hexene and 4300–8800 ppm of dihydrogen. Three complexes were tested for ethylene/1-hexene copolymerisation: ^{Me2}SB($^{t Bu}$N,I*)TiCl$_2$, ^{Me2}SB($^{t Bu}$N,$^{3\text{-}Et}$I*)TiCl$_2$ and ^{Me2}SB($^{t Bu}$N,Cp*)TiCl$_2$ (Figure 4.19).

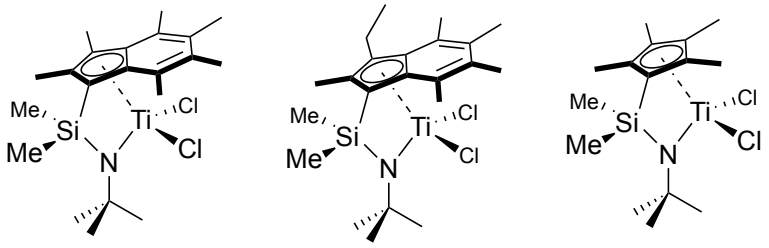

Figure 4.19. Molecular structures of the three complexes tested for solution-phase copolymerisations of ethylene/1-hexene and ethylene/1-octene.

Copolymerisation activities, polymer density and comonomer incorporations are shown in Table 4.14 for additions of 10, 20 and 30 mL of 1-hexene to the reaction mixture. Due to a contaminated batch of Isopar-E it is not possible to compare results with those of ethylene homopolymerisation with uncharacteristically low activities being observed.

Table 4.14. Solution-phase ethylene/1-hexene copolymerisation activities, densities and comonomer incorporations with addition of 10, 20 and 30 mL 1-hexene for ^{Me_2}SB($^{t Bu}$N,I*)TiCl$_2$, ^{Me_2}SB($^{t Bu}$N,$^{3\text{-Et}}$I*)TiCl$_2$ and ^{Me_2}SB($^{t Bu}$N,Cp*)TiCl$_2$; 1–2 mg complex, 1000 equivalents MAO, 35 bar ethylene, 140–150 °C, 10–20 minutes, Isopar-E.

Complex	Activity ($kg_{PE}/mol_{Ti}/h/bar$)	Volume 1-hexene (mL)	Polymer density (g/dm^3)	Comonomer incorporation (wt%)
^{Me_2}SB($^{t Bu}$N,I*)TiCl$_2$	4888	10	929	3.7
	4910	20	916	7.5
	5153	30	912	8.3
^{Me_2}SB($^{t Bu}$N,$^{3\text{-Et}}$I*)TiCl$_2$	3500	10	935	4.1
	6032	20	916	8.3
	3197	30	920	8.1
^{Me_2}SB($^{t Bu}$N,Cp*)TiCl$_2$	1463	10	936	3.3
	1861	20	926	6.9
	1533	30	907	11.3

Comonomer incorporations calculated by FTIR.

On addition of 10, 20 and 30 mL of 1-hexene the I* and $^{3\text{-Et}}$I* complexes have activities 2 to 3.5 times greater than that of the Cp* complex, demonstrating the increased ethylene polymerisation activities afforded by the permethylindenyl ring relative to permethylcyclopentadienyl ligands. Copolymerisation activities increase with increasing addition of 1-hexene for ^{Me_2}SB($^{t Bu}$N,I*)TiCl$_2$, from 4888 to 4910 and 5153 $kg_{PE}/mol_{Ti}/h/bar$ with addition of 10, 20 and 30 mL of 1-hexene respectively demonstrating a positive comonomer effect. In the case of ^{Me_2}SB($^{t Bu}$N,$^{3\text{-Et}}$I*)TiCl$_2$ and ^{Me_2}SB($^{t Bu}$N,Cp*)TiCl$_2$, activities are greatest on addition of 20 mL of 1-hexene; 3500, 6032 and 3193 $kg_{PE}/mol_{Ti}/h/bar$ for ^{Me_2}SB($^{t Bu}$N,$^{3\text{-Et}}$I*)TiCl$_2$ and 1463, 1861 and 1533 $kg_{PE}/mol_{Ti}/h/bar$ for ^{Me_2}SB($^{t Bu}$N,Cp*)TiCl$_2$ with addition of 10, 20 and 30 mL of 1-hexene respectively.

Increasing 1-hexene incorporation is also observed with increased amount of 1-hexene being added to the reaction mixture. At lower levels of comonomer addition (10 and 20 mL), incorporation levels are higher for ^{Me_2}SB($^{t Bu}$N,I*)TiCl$_2$ (3.7 and 7.5%) and ^{Me_2}SB($^{t Bu}$N,$^{3\text{-Et}}$I*)TiCl$_2$ (4.1 and 8.3%) than ^{Me_2}SB($^{t Bu}$N,Cp*)TiCl$_2$ (3.3 and 6.9%).

However, on addition of 30 mL of 1-hexene, ^{Me2}SB(^{tBu}N,Cp*)TiCl$_2$ incorporates more 1-hexene (11.3%) compared with ^{Me2}SB(^{tBu}N,I*)TiCl$_2$ (8.3%) and ^{Me2}SB(^{tBu}N,$^{3\text{-}Et}$I*)TiCl$_2$ (8.1%). Polymer densities typically decrease with increasing comonomer incorporation, with densities between 907 and 936 g/dm^3, in the region of those previously reported for LLDPE (920 g/dm^3).[40]

4.5.2 Solution-phase ethylene/1-octene copolymerisation

Solution-phase ethylene/1-octene copolymerisations were performed as described in 4.5.1. The activities of the same three complexes (Figure 4.19) on addition of 10, 20 and 30 mL of 1-octene, the densities and incorporations of the polymer produced are shown in Table 4.15.

Table 4.15. Solution-phase ethylene/1-octene copolymerisation activities, densities and comonomer incorporations with addition of 10, 20 and 30 mL 1-octene for ^{Me2}SB(^{tBu}N,I*)TiCl$_2$, ^{Me2}SB(^{tBu}N,$^{3\text{-}Et}$I*)TiCl$_2$ and ^{Me2}SB(^{tBu}N,Cp*)TiCl$_2$; 1–2 mg complex, 1000 equivalents MAO, 35 bar ethylene, 140–150 °C, 10–20 minutes, Isopar-E.

Complex	Activity ($kg_{PE}/mol_{Ti}/h/bar$)	Volume 1-octene (mL)	Density (g/dm^3)	Comonomer incorporation (wt%)
^{Me2}SB(^{tBu}N,I*)TiCl$_2$	4337	20	920	6.7
	4464	30	908	11.2
^{Me2}SB(^{tBu}N,$^{3\text{-}Et}$I*)TiCl$_2$	5336	10	931	4.7
	4699	20	919	8.0
^{Me2}SB(^{tBu}N,Cp*)TiCl$_2$	1810	10	933	5.0
	1883	20	924	8.1
	1883	30	905	12.3

Comonomer incorporations calculated by FTIR.

As with the ethylene/1-hexene copolymerisations, activities for ^{Me2}SB(^{tBu}N,$^{3\text{-}R}$I*)TiCl$_2$ are between 2 and 3 times greater than the ^{Me2}SB(^{tBu}N,Cp*)TiCl$_2$, again highlighting the increased activity afforded by the permethylindenyl ligand. Copolymerisation activities vary between 1810 to 1883 $kg_{PE}/mol_{Ti}/h/bar$ for ^{Me2}SB(^{tBu}N,Cp*)TiCl$_2$, compared with 4699 to 5336 $kg_{PE}/mol_{Ti}/h/bar$ for ^{Me2}SB(^{tBu}N,$^{3\text{-}Et}$I*)TiCl$_2$ and 4337 and 4464 $kg_{PE}/mol_{Ti}/h/bar$ for ^{Me2}SB(^{tBu}N,I*)TiCl$_2$.

Klosin *et al.* have studied a number of constrained geometry complexes under similar conditions.[25] Under these conditions, ^{Me2}SB(^{tBu}N,Cp*)TiMe$_2$ on addition of 165 mL 1-octene had an activity of 10144 kg$_{PE}$/mol$_{Ti}$/h/bar after 15 minutes of polymerisation. The activity of this complex is over 4 times greater than that observed for the indenyl complex, ^{Me2}SB(^{tBu}N,I)TiMe$_2$ (2493 kg$_{PE}$/mol$_{Ti}$/h/bar) under the same conditions. Addition of electron donating groups such as alkoxy or amido groups led to enhanced polymerisation activities with substituents in the 3- position leading to greater enhancements than the 2- position, with the complex ^{Me2}SB(^{tBu}N,$^{3\text{-}NC4H8}$I)TiMe$_2$ having an activity almost thirty times greater than that of ^{Me2}SB(^{tBu}N,I)TiMe$_2$ (69855 kg$_{PE}$/mol$_{Ti}$/h/bar) as well as producing polymers with much greater molecular weight (280 kDa and 105 kDa). It should be noted that a significantly smaller amount of catalyst was used for ^{Me2}SB(^{tBu}N,$^{3\text{-}NC4H8}$I)TiMe$_2$ (0.05 μmol) than ^{Me2}SB(^{tBu}N,I)TiMe$_2$ (1.2 μmol).

As with the slurry-phase ethylene/1-hexene and ethylene/1-octene copolymerisations, higher activities are observed for ethylene/1-hexene copolymerisation compared with ethylene/1-octene using ^{Me2}SB(^{tBu}N,I*)TiCl$_2$, with higher activities observed for ethylene/1-octene copolymerisations using ^{Me2}SB(^{tBu}N,$^{3\text{-}Et}$I*)TiCl$_2$. There does not appear to be a clear reason for this change in relative activities, although it is possible that the comonomer effect associated with 1-octene is smaller than that from 1-hexene. This would lead to a result similar to slurry-phase copolymerisations where ethylene/1-octene copolymerisation activities were closer to homopolymerisation activities than ethylene/1-hexene copolymerisations.

Incorporation levels increase with increased addition of 1-octene. Comparable incorporation levels are observed for the three complexes across all three levels of

1-octene addition. Incorporation levels of 4.7 and 5.0 wt% for ^{Me_2}SB($^{t\text{Bu}}$N,$^{3\text{-Et}}$I*)TiCl$_2$ and ^{Me_2}SB($^{t\text{Bu}}$N,Cp*)TiCl$_2$ respectively on addition of 10 mL of 1-octene. Addition of 20 mL of 1-octene leads to incorporation levels of 6.7, 8.0 and 8.1 wt% for ^{Me_2}SB($^{t\text{Bu}}$N,I*)TiCl$_2$, ^{Me_2}SB($^{t\text{Bu}}$N,$^{3\text{-Et}}$I*)TiCl$_2$ and ^{Me_2}SB($^{t\text{Bu}}$N,Cp*)TiCl$_2$; 11.2 and 12.3 wt% incorporation was seen for ^{Me_2}SB($^{t\text{Bu}}$N,I*)TiCl$_2$ and ^{Me_2}SB($^{t\text{Bu}}$N,Cp*)TiCl$_2$ on addition of 30 mL of 1-octene. At all levels of 1-octene addition, polymer densities are within a narrow range, 931 to 905 g/dm^3, and as with the ethylene/1-hexene copolymerisations the densities decrease with increased comonomer incorporation.

4.6 Conclusions

A temperature study using sMAO-^{Me2}SB(^{tBu}N,I*)TiCl$_2$ for ethylene/1-hexene copolymerisation showed a positive comonomer effect at 70 °C with increases in activity of up to 23%, 1-hexene incorporations of 2.1 mol% and a proportionate increase in incorporation with increased addition of 1-hexene comonomer.

Slurry-phase ethylene/1-hexene and ethylene/styrene copolymerisations were carried out with six sMAO supported I* CGCs and an industrially used complex ^{Me2}SB(^{tBu}N,Cp*)TiCl$_2$. The supported I* CGCs all showed activities greater than that of sMAO-^{Me2}SB(^{tBu}N,Cp*)TiCl$_2$ with incorporations up to 2.4 mol% compared with 3.5 mol%. Ethylene/styrene copolymerisations resulted in large activity decreases in all cases for the I* catalysts with incorporation levels up to 2.5 mol%. Ethylene/1-octene copolymerisations resulted in lower incorporations (up to 2.0 mol%) and a smaller comonomer effect was observed, with smaller changes in activity compared with ethylene/1-hexene and ethylene/styrene copolymerisations.

High-throughput ethylene/1-hexene copolymerisations were undertaken with eight I* CGCs, with incorporations of up to 8.4 mol% reported for sMAO-^{Me2}SB(^{tBu}N,$^{3\text{-}Et}$I*)TiCl$_2$. The dichloride complexes were found to be more stable to increased addition of comonomer, with smaller decreases in activity observed.

Solution-phase ethylene/1-hexene and ethylene/1-octene copolymerisations showed ^{Me2}SB(^{tBu}N,$^{3\text{-}Et}$I*)TiCl$_2$ and ^{Me2}SB(^{tBu}N,I*)TiCl$_2$ produced copolymer with comparable incorporation levels to ^{Me2}SB(^{tBu}N,Cp*)TiCl$_2$; up to 8.3 and 11.2 wt% for the two comonomers with almost three times greater activities.

4.7 References

1 W. Kaminsky, *Macromol. Chem. Phys.*, 1996, **197**, 3907–3945.
2 R. Quijada, J. Dupont, M. S. L. Miranda, R. B. Scipioni and G. B. Galland, *Macromol. Chem. Phys.*, 1995, **196**, 3991–4000.
3 J. Okuda, *Chem. Ber.*, 1990, **123**, 1649–1651.
4 J. C. Stevens, F. J. Timmers, D. R. Wilson, G. F. Schmidt, P. N. Nickias, R. K. Rosen, G. W. Knight and S. Y. Lai, 1991, EP0416815A2.
5 H. Braunschweig and F. M. Breitling, *Coord. Chem. Rev.*, 2006, **250**, 2691–2720.
6 J. Canich and G. Licciardi, 1991, US5057475A.
7 J. Canich, 1991, US5055438A.
8 J. Klosin, W. J. Kruper, P. N. Nickias, G. R. Roof, P. De Waele and K. A. Abboud, *Organometallics*, 2001, **20**, 2663–2665.
9 Y.-X. Chen and T. J. Marks, *Organometallics*, 1997, **16**, 3649–3657.
10 L. A. Williams and T. J. Marks, *Organometallics*, 2009, **28**, 2053–2061.
11 K. Czaja, L. A. Novokshonova and N. J. Kovaleva, *Macromol. Chem. Phys.*, 1999, **200**, 983–988.
12 D.-H. Lee, K.-B. Yoon, H.-J. Kim, S.-S. Woo and S. K. Noh, *J. Appl. Polym. Sci.*, 1998, **67**, 2187–2198.
13 J. Ren and G. R. Hatfield, *Macromolecules*, 1995, **28**, 2588–2589.
14 F. G. Sernetz, R. Müllhaupt, F. Amor, T. Eberle and J. Okuda, *J. Polym. Sci. Part A Polym. Chem.*, 1997, **35**, 1571–1578.
15 N. Guo, L. Li and T. J. Marks, *J. Am. Chem. Soc.*, 2004, **126**, 6542–6543.
16 J. Suhm, M. J. Schneider and R. Mülhaupt, *J. Polym. Sci. Part A Polym. Chem.*, 1997, **35**, 735–740.
17 B. J. Banaszak, D. Lo, T. Widya, W. H. Ray, J. J. de Pablo, A. Novak and J. Kosek, *Macromolecules*, 2004, **37**, 9139–9150.
18 A. Novak, M. Bobak, J. Kosek, B. J. Banaszak, D. Lo, T. Widya, W. Harmon Ray and J. J. de Pablo, *J. Appl. Polym. Sci.*, 2006, **100**, 1124–1136.
19 P. Starck, P. Lehmus and J. V. Seppälä, *Polym. Eng. Sci.*, 1999, **39**, 1444–1455.
20 G. Rojas, B. Inci, Y. Wei and K. B. Wagener, *J. Am. Chem. Soc.*, 2009, **131**, 17376–17386.
21 S. Hosoda, Y. Nozue, Y. Kawashima, K. Suita, S. Seno, T. Nagamatsu, K. B. Wagener, B. Inci, F. Zuluaga, G. Rojas and J. K. Leonard, *Macromolecules*, 2011, **44**, 313–319.
22 T. Wiedemann, G. Voit, A. Tchernook, P. Roesle, I. Göttker-Schnetmann and S. Mecking, *J. Am. Chem. Soc.*, 2014, **136**, 2078–2085.
23 K. Czaja and M. Bialek, *Polimery*, 2000, **45**, 353–357.
24 N. Herfert, P. Montag and G. Fink, *Die Makromol. Chemie*, 1993, **194**, 3167–3182.
25 J. Klosin, P. P. Fontaine and R. Figueroa, *Acc. Chem. Res.*, 2015, **48**, 2004–2016.
26 Y. He, X. Qiu, J. Klosin, R. Cong, G. R. Roof and D. Redwine, *Macromolecules*, 2014, **47**, 3782–3790.
27 R. Quijada, G. B. Galland and R. S. Mauler, *Macromol. Chem. Phys.*, 1996, **197**, 3091–3098.
28 F. G. Sernetz, R. Mülhaupt and R. M. Waymouth, *Macromol. Chem. Phys.*, 1996, **197**, 1071–1083.
29 K.-S. Son and R. M. Waymouth, *J. Polym. Sci. Part A Polym. Chem.*, 2010, **48**,

1579–1585.
30 M. Goldberg, K. Mahon and D. Anderson, *Adv. Drug Deliv. Rev.*, 2008, **60**, 971–978.
31 V. Busico, R. Pellecchia, F. Cutillo and R. Cipullo, *Macromol. Rapid Commun.*, 2009, **30**, 1697–1708.
32 K. Nomura, H. Okumura, T. Komatsu and N. Naga, *Macromolecules*, 2002, **35**, 5388–5395.
33 K.-J. Chu, J. B. P. Soares, A. Penlidis and S.-K. Ihm, *Eur. Polym. J.*, 2000, **36**, 3–11.
34 J. C. W. Chien and T. Nozaki, *J. Polym. Sci. Part A Polym. Chem.*, 1993, **31**, 227–237.
35 M. D. E. F. V Marques, R. B. Tiosso and P. E. Mano, *J. Mater. Sci. Eng.* , 2011, **4**, 149–173.
36 J.-C. Buffet, Z. R. Turner and D. O'Hare, *Chem. Commun.*, 2018, **54**, 10970–10973.
37 J.-C. Buffet, Unpublished Data.
38 G. Sivalingam, V. Natarajan, K. R. Sarma and U. Parasuveera, *Ind. Eng. Chem. Res.*, 2008, **47**, 8940–8946.
39 N. Guo, C. L. Stern and T. J. Marks, *J. Am. Chem. Soc.*, 2008, **130**, 2246–2261.
40 R. K. Krishnaswamy and M. J. Lamborn, *Polym. Eng. Sci.*, 2000, **40**, 2385–2396.

Chapter Five

Niobium imido complex for ethylene oligomerisation and tandem catalysis

5.1 Introduction

5.1.1 Ethylene oligomerisation

Ethylene oligomerisation has been of great industrial interest over the past 50 years,[1] with linear α-olefins having wide ranging usage in today's society such as surfactants, synthetic lubricants and comonomer additives to polymers.[2,3] Ziegler first reported the oligomerisation of ethylene with lithium aluminium hydride and many simple alkylaluminium species.[4,5] Whilst this method was licensed and commercialised, it was non-selective, resulting in a Poisson distribution of even-numbered α-olefins and required ethylene pressures in excess of 200 bar.[6] The Shell Higher Olefin Process (SHOP), using a nickel based catalyst, began operation in 1977; the process operates at lower pressures (90 bar), however, it still produces a mixture of α-olefins between C_4 and C_{40}, of which only the fraction up to C_{16} is desired.[7] The demand for 1-hexene and 1-octene has been driven by their use as comonomers in linear low-density polyethylene (LLDPE) synthesis; to cater for this demand Chevron-Phillips commercialised the first trimerisation plant in 2003 and Sasol opened 1-hexene and 1-octene production plants in 2014.[8,9]

Metal imido complexes have been shown to be efficient ethylene oligomerisation catalysts, with the dimerisation of ethylene by *in situ* tungsten imido complexes first reported by Wideman *et al.* in 1975.[10] Dyer *et al.* have reported the use of various group 6

mono and bis-imido complexes selectively dimerising ethylene,[11,12] with tungsten mono-imido complexes producing activities comparable to, and better than, that of the industrial AlphaButol Process.[13] Group 5 complexes have been shown to act as olefin oligomerisation catalysts in the presence of a cocatalyst.[14–17] Nomura and Zhang have reported the selective dimerisation of ethylene using vanadium imido complexes (>90% selectivity) with a TOF of up to 2670000 $mol_{C_2H_4}/mol_V/h$.[18] Dyer *et al.* have reported ethylene oligomerisation using niobium and tantalum imido complexes with an $EtAlCl_2$ cocatalyst;[19] higher selectivities were observed for the tantalum complexes than with niobium analogues. The high amounts of polymer produced by the niobium complexes along with selective dimerisation lead to the assertation that there were multiple active species formed. Nomura and Kuboki reported that niobium imido complexes activated by $[Ph_3C][B(C_6F_5)_4]$ were active for selective dimerisation of ethylene with TON values up to 234000 $mol_{C_2H_4}/mol_{Nb}$ under 8 atm of ethylene pressure.[17]

5.1.2 Tandem catalysis of ethylene

Tandem catalysis, where cooperative ethylene oligomerisation and copolymerisation leads to the formation of short-chain branched LLDPE from a single ethylene feedsource, has attracted attention due to the ability to remove the required addition of a comonomer.[1,20] The first tandem catalytic system was reported by Beach and Kissin, based on a Ziegler-Natta type catalyst with a titanium or nickel dimerisation catalyst;[21] McDaniel and co-workers at Phillips developed a tandem catalytic system in the 1980s based on silica supported chromium.[22] There have been various reports of CGCs used as the copolymerisation catalyst in a tandem catalytic system with both components of the system being homogeneous catalysts.[23–25] Okuda *et al.* developed a system combining modified methylaluminoxane (MMAO) activated dibromo(pyridylimine)nickel catalyst with $^{Me_2}SB(^{R}N,Cp^*)TiCl_2$ (R = Me and ^{t}Bu) supported on pyridylethylsilane-modified

silica,[26] whilst Bercaw *et al.* reported a tandem catalytic system where two titanium complexes were simultaneously supported on a single modified silica support.[27]

5.1.3 Chapter synopsis

This chapter describes the synthesis and characterisation of Nb(Dipp)Cl_3.THF.py, the testing of various reaction parameters on ethylene oligomerisation activity and selectivity, and the development of a tandem catalytic system with the aim of forming short-chain branched LLDPE from a single ethylene feedsource.

5.2 Synthesis and characterisation of Nb(NDipp)Cl$_3$.THF.py

Nb(NDipp)Cl$_3$.THF.py was synthesised *via* a modified literature procedure as reported by Nomura *et al*. (Equation 5.1).[28] A mixture of $NbCl_5$, $ZnCl_2$ and THF in DCM was cooled to −40 °C and to this mixture was added a solution of 2,6-di*iso*propylphenylamine ($DippNH_2$) and pyridine in DCM. Work up and extraction resulted in pink crystals isolated at −23 °C in a 24% yield, which were suitable for single crystal X-ray diffraction studies.

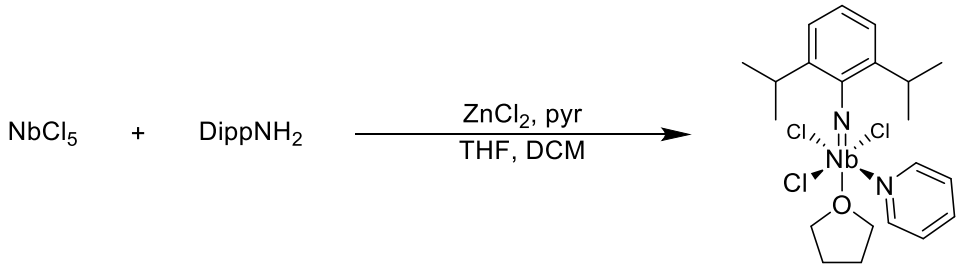

Equation 5.1. Synthesis of Nb(NDipp)Cl$_3$.THF.py.

The ^{1}H NMR spectrum (Figure 5.1) shows three broad resonances at 8.93, 7.91 and 7.47 ppm corresponding to a coordinated pyridine ligand, and two broad resonances at 4.29 and 2.01 ppm corresponding to the bound THF. The resonances attributable to aromatic ring are observed as a doublet at 7.10 ppm and a triplet at 6.98 ppm for the meta and para aromatic protons respectively with a $^3J_{H\text{-}H}$ coupling of 7.6 Hz. A broad multiplet observed at 1.31 ppm and a doublet at 1.19 ppm correspond to the two ^{i}Pr groups of the imido fragment. Integration of the resonances confirms the coordination of one equivalent of both THF and pyridine.

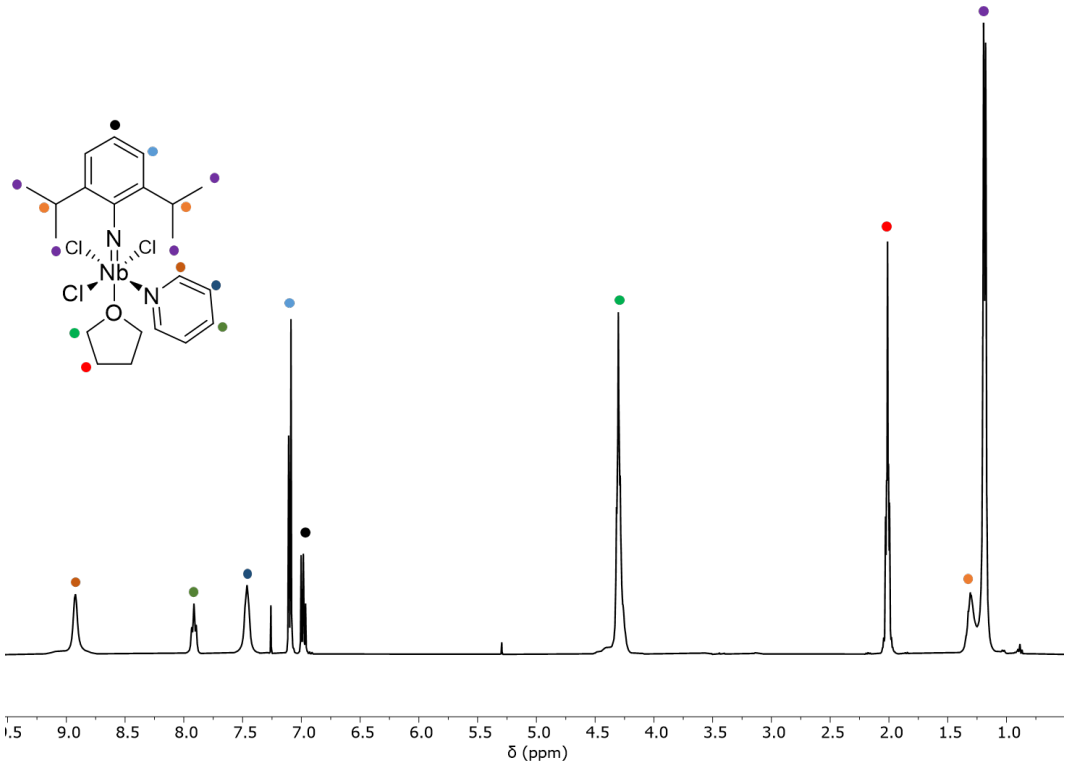

Figure 5.1. ^{1}H NMR spectrum of Nb(NDipp)Cl_3.THF.py ($CDCl_3$, 298 K, 400 MHz).

In the solid-state, the complex adopts a distorted octahedral structure, caused by the steric bulk of the di*iso*propylphenyl imido group (Figure 5.2 and Table 5.1). This is exemplified by the average N(1)-Nb-Cl bond angles being 97.7° and the average of the O-Nb-Cl bond angles being 82.8°. A similar distortion is observed for Nb(N^{t}Bu)Cl_3(dme) reported by Kovalev *et al*..[29] The near linear bond angle of N(1)-Nb-O (177.91(5)°) is comparable to many previously reported examples (177.8(2)° for N(1)-Nb-N(2) in [Nb(N^{t}Bu)Cl_4.py]$^-$).[30] This bond angle has been observed to decrease with the use of a bidentate ligand, such as dme, with the strain induced resulting in bending away from linear such as for Nb(N^{t}Bu)Cl_3(dme) (168.1(3)°),[31] Nb(NDipp)Cl_3(dme) (169.7(2)°)[32] and Nb(N$NC_{12}H_8$)Cl_3(dme) (166.5°).[33]

The Nb-N(1) bond length (1.7632(13) Å) is within the range previously reported for similar niobium imido complexes, 1.721–1.781 Å.[31,34] The steric bulk of the imido fragment does not appear to influence this bond length, as shown by Nb(NR)Cl_3.py_2

(R = ^{t}Bu and ^{i}Pr) (1.734(4) and 1.733(3) Å respectively).[35] The variation of the X group from pyr_2 to dme, Nb(N^{t}Bu)Cl_3(dme) (1.722(7) Å),[31] suggests the coordinating solvent has a larger effect on this bond length. Dyer *et al.* reported that aromatic imido complexes generally resulted in longer Nb-N(1) bond lengths than comparable aliphatic imido complexes due to conjugation between the aromatic ring and the metal-nitrogen bond.[19] Comparison with a reported Nb-N triple bond, Nb(NDipp)Cl_3(dme) (1.746(4) Å) indicates there is not significant lengthening of the bond for a double bond compared with a triple bond.[32]

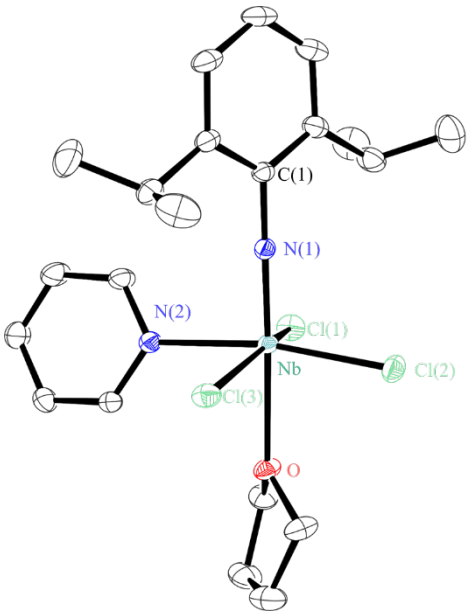

Figure 5.2. Solid state molecular structure of Nb(NDipp)Cl_3.THF.py. Hydrogen atoms are omitted for clarity, thermal ellipsoids drawn at 30% probability.

Table 5.1. Selected bond lengths (Å) and angles (º) for Nb(NDipp)Cl_3.THF.py. Estimated standard deviations (ESDs) are given in parentheses.

C(1)-N(1)	1.3880(19)	N(1)-Nb-N(2)	92.28(5)
N(1)-Nb	1.7632(13)	N(1)-Nb-O	177.91(5)
N(2)-Nb	2.2925(13)	N(2)-Nb-O	85.63(4)
Cl(1)-Nb	2.3886(4)	Cl(2)-Nb-Cl(1)	96.923(16)
Cl(2)-Nb	2.3716(4)	Cl(3)-Nb-Cl(2)	96.937(16)
Cl(3)-Nb	2.3979(4)	Cl(1)-Nb-Cl(3)	157.803(17)
C(1)-N(1)-Nb	177.51(11)	O-Nb-Cl(1)	82.56(3)
N(1)-Nb-Cl(1)	97.01(4)	O-Nb-Cl(2)	84.23(3)
N(1)-Nb-Cl(2)	97.86(4)	O-Nb-Cl(3)	81.68(3)
N(1)-Nb-Cl(3)	98.17(4)		

5.3 Ethylene oligomerisation using Nb(NDipp)Cl_3.THF.py

5.3.1 Heterogeneous-phase ethylene oligomerisation

Nb(NDipp)Cl_3.THF.py was immobilised on sMAO and the oligomerisations were undertaken on an NMR scale, using a similar procedure used previously by O'Hare *et al.* to study related sMAO-supported tungsten imido complexes.[36,37] To a Young's tap NMR tube was added 5 mg of supported complex, with 500 μL of deuterated solvent and 2.8 μL of mesitylene as a standard. The NMR tube was then freeze-pump-thaw degassed three times and backfilled with 1 bar ethylene. The reaction was then heated in an oil bath with the reaction stopped and studied by NMR spectroscopy after specified time periods. Whilst this screening method has limitations, it allows for an indication of relative activities between different reaction conditions. These limitations include the relative small amounts of monomer present (making full analysis of the range of products difficult), and the low boiling point of butenes (likely to be present in the atmosphere of the NMR tube rather than in solution). Thus, the full amount of butenes present and actual alkene selectivities cannot be fully determined. In addition, the lack of stirring in the reaction and small scale of the catalytic studies can also result in mass transfer effects inhibiting activities.

Previously reported oligomerisation studies are typically performed on a larger scale; with reactions carried out in reactors with mechanical stirring under a constant flow of ethylene. To analyse the products, the reaction is first quenched and cooled below the boiling point of butenes, and then the mixture analysed by GC-FID (gas chromatography – flame ionisation detection) to quantitatively determine to product mixture and relative selectivities.[19,38]

5.3.1.1 Immobilisation of Nb(NDipp)Cl_3.THF.py

Immobilisation of Nb(NDipp)Cl_3.THF.py was carried out using a standard procedure; sMAO and Nb(NDipp)Cl_3.THF.py were mixed in a Schlenk tube in the desired $[Al]_0$:$[Nb]_0$ ratios (250:1, 200:1, 150:1, and 100:1). The mixture was then swirled in toluene at 60 °C for 1 hour, during which the pink solution decolourised to leave a pale pink solid and a colourless supernatant. The supernatant was decanted and the solid product dried *in vacuo* to yield to the supported catalyst sMAO-Nb(Dipp)Cl_3 (Equation 5.2).

The nature of the supported complex has been studied by solid state NMR spectroscopy. The ^{13}C CP-MAS solid state NMR spectrum is shown in Figure 5.3, and by comparison with the solution-phase $^{13}C\{^1H\}$ NMR spectrum, it is possible to assign resonances both to sMAO and the supported complex.

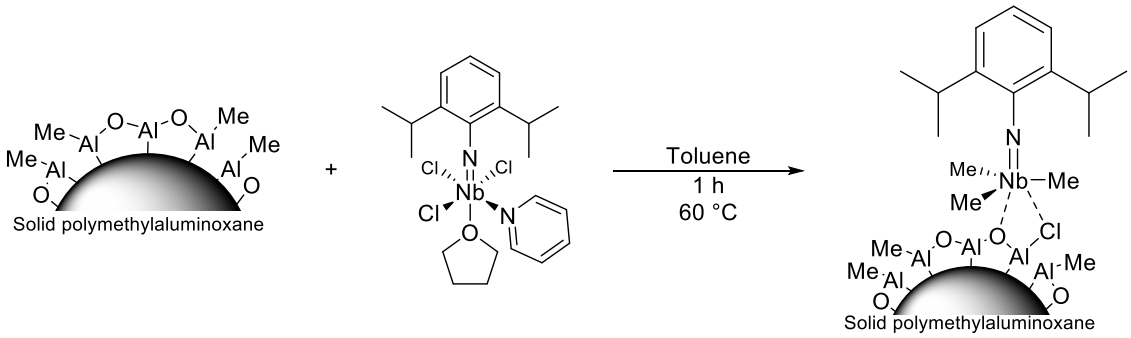

Equation 5.2. Immobilisation of Nb(NDipp)Cl_3.THF.py on sMAO. Immobilised complex is a representative image.

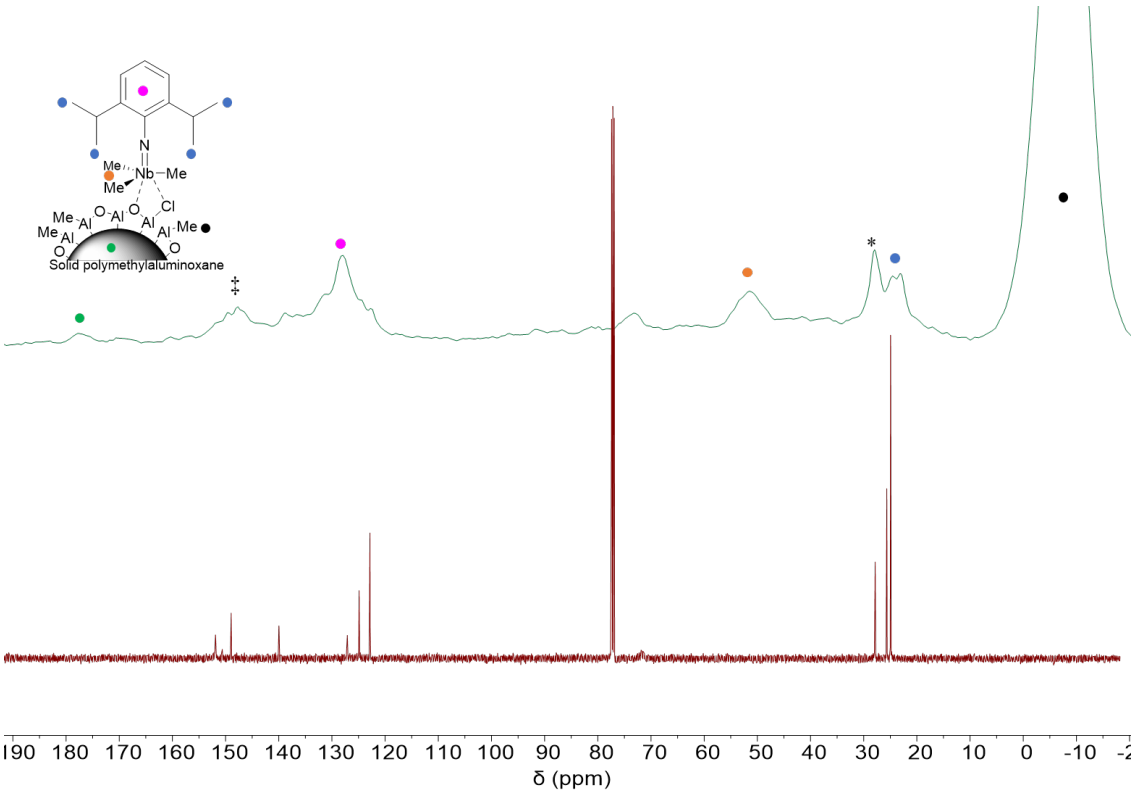

Figure 5.3. (top) Solid state ^{13}C CP-MAS spectrum of sMAO-Nb(NDipp)Cl_3 (100.6 MHz, 298 K), and (bottom) $^{13}C\{^1H\}$ NMR spectrum of Nb(NDipp)Cl_3.THF.py ($CDCl_3$, 125.7 MHz, 298 K, resonance at 77.23 ppm corresponds to d_1-chloroform). ‡ corresponds to bound pyridine, * corresponds to THF.

In addition to the resonances attributable to sMAO at –8, 128 and 181 ppm, it is possible to assign resonances to the immobilised complex by comparison with the solution-phase $^{13}C\{^1H\}$ NMR spectrum. The resonances between 20 and 30 ppm are attributable to the *iso*propyl groups of the imido ligand and THF that may remain bound to either the metal centre or on the support. The aromatic resonances of the imido fragment at 123 and 127 ppm in the spectrum of the complex are likely to be buried within the broad resonance at 128 ppm corresponding to sMAO and may contribute to the shoulder observed at 132 ppm. The resonance at 147 ppm could be assigned to the coordinated pyridine, and as such would suggest that pyridine remains bound to either the metal centre or to the sMAO support. A resonance is also observed at 51 ppm, that cannot be attributed to either sMAO or Nb(NDipp)Cl_3.THF.py. Similar to the supported CGC complexes discussed in Chapter 2, it is possible that this resonance may be attributable to a methyl group bound

to the niobium metal centre, since the process of immobilisation is proposed to involve alkylation followed by alkyl abstraction. Unfortunately, it was not possible to cleanly isolate an alkylated niobium imido complex to confirm this assignment. Nikonov and co-workers have previously synthesised and characterised the niobium methyl complex $[CpNb(\mu\text{-}Ar)Me]_2$ and a resonance at 21 ppm was assigned to the methyl group in the $^{13}C\{^1H\}$ NMR spectrum.[39] Whilst this gives an indication of where a resonance may be observed, the proposed cationic nature of the catalytic species would likely result in a shift to higher frequency of this methyl resonance.

5.3.1.2 Effect of temperature on oligomerisation activity

Oligomerisation studies were carried out at 50, 70, 75 and 100 °C to investigate the effect of temperature on activities and selectivities. The rate of oligomerisation was highest at 50 °C (up to 50 $mol_{C_2H_4}/mol_{Nb}$), with activities decreasing with increasing temperature (Figure 5.4). In all cases, polymerisation activities exceed oligomerisation activities, with polymer selectivities of 88 to 96% after 10 hours of reaction (Table A5.1).

Ethylene oligomerisation activities remain approximately constant or decrease after 30–45 minutes, with visible polymer formation from 45 minutes to 1 hour of heating. Whilst this polymer formation is proposed to incorporate some of the oligomeric product leading to reduced TON values; unfortunately, not enough polymer was produced in these conditions for characterisation by high temperature $^{13}C\{^1H\}$ NMR spectroscopy. A similar effect has previously been observed at 100 °C for supported tungsten imido complexes; where no further ethylene oligomerisation was observed after 4 hours of reaction.[37] No colouring of the solution or observation of the complex in the NMR spectra was seen during the course of the reaction at any temperature, indicating that there was no complex leaching during the reactions. However, decreased activities with increasing

temperatures would suggest that at higher temperatures some active sites become deactivated.

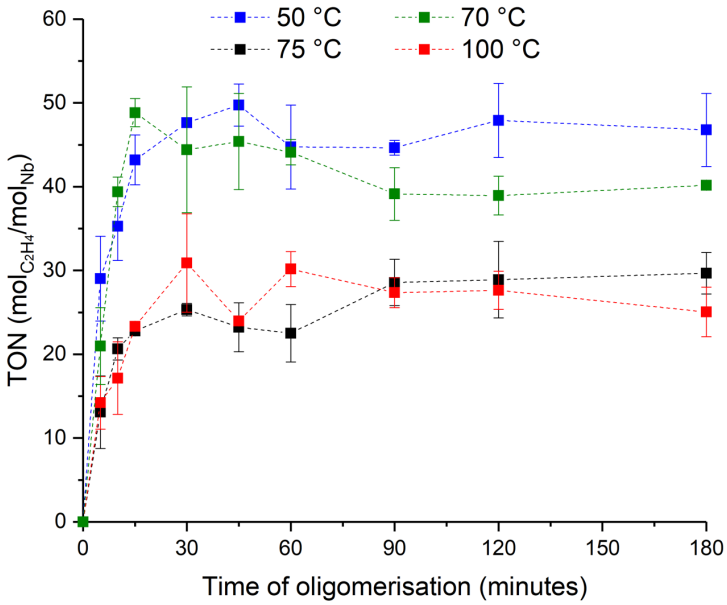

Figure 5.4. Temperature study using sMAO-Nb(NDipp)Cl_3 at 50, 70, 75 and 100 °C; 1 bar ethylene, 5 mg catalyst ($[Al]_0$:$[Nb]_0$ = 200:1), 500 µL d_6-benzene and mesitylene standard.

The observed selectivities towards 1-hexene are relatively high for all temperatures (Table 5.2) with up to 92% 1-hexene selectivity at 50 °C after 15 minutes with the remainder of the alkene fraction being 1-butene, this would suggest that oligomerisation may proceed *via* a metallacyclic mechanism.[40] However, as discussed in 5.3.1, a limitation of this experimental method is that the full amount of butenes produced may not be observed due to the low boiling points. To conclusively determine the mechanism, isotopic labelling studies would have to be performed as described by Bercaw *et al.*.[41,42] Messinis and co-workers reported that solution-phase ethylene oligomerisation using an analogous Nb(NDipp)Cl_3(dme) activated with $EtAlCl_2$ resulted in selective dimerisation to 1-butene, with a small fraction to 1-hexene also being observed.[19] Higher activities (up to 104200 $mol_{C_2H_4}/mol_{Nb}/h$ after 7.9 minutes) were observed in the solution-phase. However, this can be partly attributed to the larger reaction scale and higher ethylene pressure. A similar effect of ethylene pressure has been observed for (α-diimine)nickel

complexes, Brookhart *et al*. have shown that increasing oligomerisation pressure from 1 to 15 bar resulted in turnover numbers increasing from 22000 to 116000 $mol_{C_2H_4}/mol_{Ni}$.[43]

Table 5.2. Ethylene oligomerisation activities and observed 1-hexene selectivities for selected time periods at 50, 70, 75 and 100 °C.

Time (minutes)	50 °C		70 °C		75 °C		100 °C	
	TON[a]	Observed 1-hexene selectivity (%)[b]	TON[a]	Observed 1-hexene selectivity (%)[b]	TON[a]	Observed 1-hexene selectivity (%)[b]	TON[a]	Observed 1-hexene selectivity (%)[b]
15	43	92	49	84	23	91	23	86
30	48	91	44	84	25	90	31	89
45	50	91	45	81	23	88	24	86
60	45	91	44	79	23	88	30	86
180	47	87	40	75	30	88	25	88
600	732[c]	5[d]	312[c]	3[d]	227[c]	10[d]	461[c]	4[d]

[a] TON values in $mol_{C_2H_4}/mol_{Nb}$. [b] Due to its volatility, the actual amount of butenes produced may be higher than that observed. [c] TON for both oligomerisation and polymerisation. [d] 1-hexene selectivity from all observed products. Reaction conditions: 1 bar ethylene, 5 mg catalyst ($[Al]_0$:$[Nb]_0$ = 200:1), 500 µL d_6-benzene and mesitylene standard. Selectivities determined by integration of triplets corresponding to 1-butene and 1-hexene between 0.95 and 0.80 ppm. Turnover numbers calculated by integration of the resonance at 5.00 ppm corresponding to the terminal CH_2 resonances of both 1-butene and 1-hexene.

As highlighted in Tables 5.2 and A5.1, the rate of ethylene polymerisation exceeds that of ethylene oligomerisation, with turnover numbers of 42 and 690 $mol_{C_2H_4}/mol_{Nb}$ for oligomerisation and polymerisation respectively at 50 °C. This would suggest the presence of two active catalytic species in both cases, one promoting selective oligomerisation, and one promoting ethylene polymerisation due to the inability for a single catalytic site to both selectively oligomerise and polymerise ethylene.[19] It is also proposed that the active species for polymerisation incorporates some of the linear α-olefins produced into the polymer chain; this results in the production of short chain branched polyethylene and is known as concurrent tandem catalysis.[44]

5.3.1.3 Effect of solvent on ethylene oligomerisation

Oligomerisation studies were undertaken with a range of aromatic and aliphatic solvents to determine the effect the reaction solvent has on both activity and selectivity. The

activities over 60 minutes are shown in Figure 5.5, with observed activities and selectivities for selected time periods in Tables 5.3 and 5.4.

Activities are highest when using aromatic solvents, and activities decrease with increasing polarity of the solvent (Figure 5.5). A table of the dielectric constants of these solvents can be found in Table A5.2. Aliphatic solvents resulted in selective dimerisation of ethylene, with the highest activity observed for d_{18}-octane (up to 12 $mol_{C_2H_4}/mol_{Nb}$ after 60 minutes); activities with aliphatic solvents were also far lower than those observed for aromatic solvents. The use of d_8-THF resulted in complete inactivity, possibly due to its highly coordinating nature. Similarly, use of d_1-chloroform also resulted in very low activities; the reaction mixture turning pink would suggest that complex leached from the sMAO support or that the d_1-chloroform reacts with the active species forming an inactive, unsupported, chloride complex. Bercaw *et al.* demonstrated with a chromium PNP diphosphine complex that use of chlorobenzene resulted in increased rates of oligomerisation and higher selectivity with respect to reactions carried out in toluene.[45] Similarly, Hanton and co-workers investigated the effect of variation of reaction solvent on *in situ* tungsten imido complexes for ethylene oligomerisation;[46] strong donor solvents were shown to inhibit catalytic activity, presumably due to coordination to and deactivation of the active species. O'Hare *et al.* have previously demonstrated the effect solvent has on supported tungsten imido complexes for ethylene dimerisation;[37] as with the supported niobium imido complex, aromatic solvents were shown to lead to higher oligomerisation activities than aliphatic solvents, increased polarity of the aromatic solvent was also shown to increase activity. It was proposed that this trend was a balance between a polar solvent stabilising the proposed cationic transition state of the catalytic cycle and the solvent coordinating to the catalytic centre and inhibiting catalytic activity.

It is proposed that the change in selectivity from 1-hexene to 1-butene for aliphatic solvents could be due to the low activities observed for the aliphatic solvents resulting in solely the production of 1-butene. The trend in activity between solvents is maintained through to 10 hours of heating (Figure A5.1). With the exception of bromobenzene (6 hours) all activities are maximised within 1 to 2 hours, with polymer formation being observed throughout the reaction.

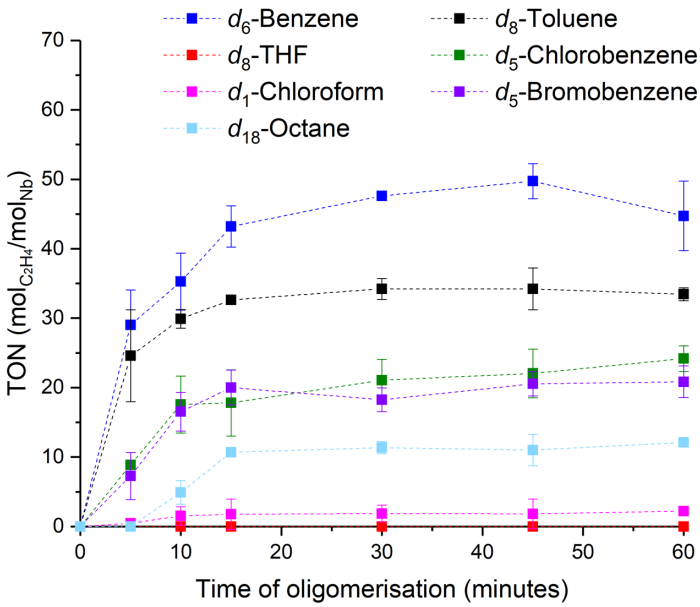

Figure 5.5. Solvent study using sMAO-Nb(NDipp)Cl_3; 1 bar ethylene, 5 mg catalyst ($[Al]_0$:$[Nb]_0$ = 200:1), 500 µL solvent, 50 °C and mesitylene standard.

Table 5.3. Ethylene oligomerisation activities and observed 1-hexene selectivities for selected time periods with different solvents.

Time (minutes)	d_6-benzene		d_8-toluene		d_5-chlorobenzene		d_5-bromobenzene	
	TON[a]	Observed 1-hexene selectivity (%)[b]	TON[a]	Observed 1-hexene selectivity (%)[b]	TON[a]	Observed 1-hexene selectivity (%)[b]	TON[a]	Observed 1-hexene selectivity (%)[b]
15	43	92	33	83	18	86	20	86
30	48	91	34	81	21	85	19	74
45	50	91	34	83	22	85	21	71
60	45	91	33	84	24	84	21	82
600	732[c]	5[d]	571[c]	4[d]	613[c]	3[d]	271[c]	8[d]

[a] TON values in $mol_{C_2H_4}/mol_{Nb}$. [b] Due to its volatility, the actual amount of butene produced may be higher than that observed. [c] TON for both oligomerisation and polymerisation. [d] 1-hexene selectivity from all observed products. Reaction conditions: 1 bar ethylene, 5 mg catalyst ($[Al]_0$:$[Nb]_0$ = 200:1), 500 µL d_6-benzene and mesitylene standard. Selectivities determined by integration of triplets corresponding to 1-butene and 1-hexene between 0.95 and 0.80 ppm. Turnover numbers calculated by integration of the resonance at 5.00 ppm corresponding to the terminal CH_2 resonances of both 1-butene and 1-hexene.

Table 5.4. Ethylene oligomerisation activities and observed 1-butene selectivities for selected time periods with different solvents.

Time (minutes)	d_{18}-octane		d_8-THF	d_1-chloroform	
	TON[a]	Observed 1-butene selectivity (%)[b]	TON[a]	TON[a]	Observed 1-butene selectivity (%)[b]
15	11	100	0	2	100
30	11	100	0	2	100
45	11	100	0	2	100
60	12	100	0	2	100
600	749[c]	1[d]	0[c]	100[c]	2[d]

[a] TON values in $mol_{C_2H_4}/mol_{Nb}$. [b] Due to its volatility, the actual amount of butene produced may be higher than that observed. [c] TON for both oligomerisation and polymerisation. [d] 1-hexene selectivity from all observed products. Reaction conditions: 1 bar ethylene, 5 mg catalyst ($[Al]_0$:$[Nb]_0$ = 200:1), 500 µL d_6-benzene and mesitylene standard. Selectivities determined by integration of triplets corresponding to 1-butene and 1-hexene between 0.95 and 0.80 ppm. Turnover numbers calculated by integration of the resonance at 5.00 ppm corresponding to the terminal CH_2 resonances of both 1-butene and 1-hexene.

Whilst activities for both oligomerisation and polymerisation are low (Tables 5.3, 5.4 and A5.3), it would appear that d_{18}-octane results in higher selectivities towards polymerisation than oligomerisation, although in all cases, selectivity towards polymerisation is high (>90%) compared with oligomerisation.

5.3.1.4 Effect of catalyst loading on ethylene oligomerisation

Oligomerisation studies were undertaken with complex loadings in the $[Al]_0$:$[Nb]_0$ ratios of 250:1, 200:1, 150:1 and 100:1 to investigate the effect of catalyst loading on activity and selectivity with observed activities in Figure 5.6 and observed activities and selectivities in Table 5.5. Highest turnover numbers were observed for a loading level of 200:1 (50 $mol_{C_2H_4}/mol_{Nb}$ after 45 minutes), with lower activities observed for 250:1 (36 $mol_{C_2H_4}/mol_{Nb}$ after 90 minutes), 150:1 (27 $mol_{C_2H_4}/mol_{Nb}$ after 2 hours) and 100:1 (25 $mol_{C_2H_4}/mol_{Nb}$ after 90 minutes). Highest combined turnover numbers were also observed for the 200:1 loading (732 $mol_{C_2H_4}/mol_{Nb}$ after 10 hours), with high selectivities towards polymerisation observed at all loading levels.

Observed selectivities towards 1-hexene remain approximately the same for all loadings (Table 5.5), indicating that loading levels does not appear to affect the nature of the active species. However, as discussed previously, the high volatility of 1-butene means that the apparent amount of 1-butene produced is likely lower than the actual amount produced, influencing both observed activities and selectivities. It is proposed that higher loadings of complex on the support causes lower activities due to a combination of blocking of active sites and bimetallic deactivation pathways facilitated by the close proximity of adjacent metal centres. It is also important to note that given the reaction is a closed system, the relative amounts of ethylene present per niobium metal centre will decrease with higher catalyst loadings, which may also contribute to decreased oligomerisation activities.

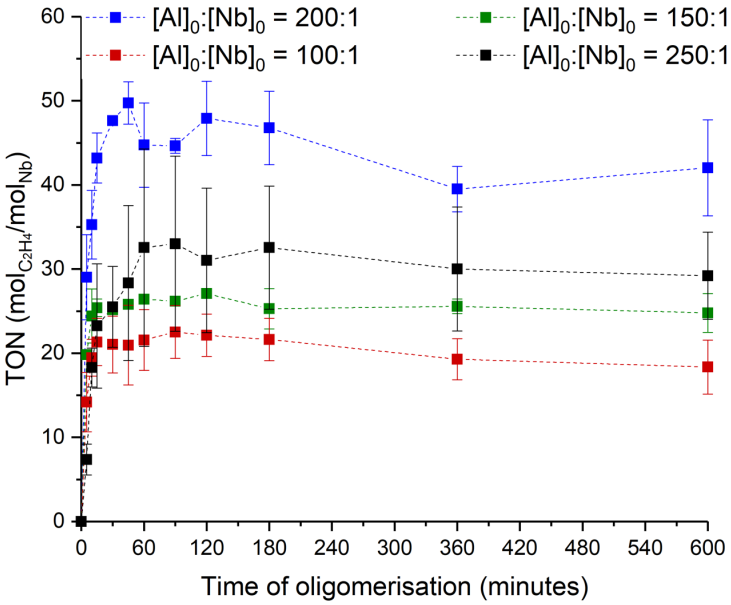

Figure 5.6. Catalyst loading study using sMAO-Nb(NDipp)Cl_3; 1 bar ethylene, 5 mg catalyst, 500 µL d_6-benzene, 50 °C and mesitylene standard.

Table 5.5. Ethylene oligomerisation activities and observed 1-hexene selectivities for selected time periods with different catalyst loadings.

Time (minutes)	250:1 TON[a]	250:1 Observed 1-hexene selectivity (%)[b]	200:1 TON[a]	200:1 Observed 1-hexene selectivity (%)[b]	150:1 TON[a]	150:1 Observed 1-hexene selectivity (%)[b]	100:1 TON[a]	100:1 Observed 1-hexene selectivity (%)[b]
15	26	91	43	92	25	91	21	91
30	26	91	48	91	25	91	21	91
45	35	91	50	91	26	92	21	92
60	34	90	45	91	26	91	22	90
180	40	88	47	87	25	91	22	89
600	525[c]	5[d]	732[c]	5[d]	225[c]	14[d]	121[c]	9[d]

[a] TON values in $mol_{C_2H_4}/mol_{Nb}$. [b] Due to its volatility, the actual amount of butene produced may be higher than that observed. [c] TON for both oligomerisation and polymerisation. [d] 1-hexene selectivity from all observed products. Reaction conditions: 1 bar ethylene, 5 mg catalyst ($[Al]_0:[Nb]_0$ = 200:1), 500 µL d_6-benzene and mesitylene standard. Selectivities determined by integration of triplets corresponding to 1-butene and 1-hexene between 0.95 and 0.80 ppm. Turnover numbers calculated by integration of the resonance at 5.00 ppm corresponding to the terminal CH_2 resonances of both 1-butene and 1-hexene.

The amount of polymer produced decreases with higher loadings (Tables 5.5 and A5.4), with alkene selectivities increasing from approximately 5% for 200:1 and 250:1 loadings up to 15% (150:1) and 10% (100:1). This may partly account for the lower oligomerisation activities of the 250:1 loading, with blocking of active sites facilitated by the templating of the polymer formed around the catalyst particles. It is possible that the

bimetallic interactions facilitated by the closer proximity of the niobium centres at higher loadings could hinder ethylene polymerisation to a greater extent than ethylene oligomerisation.

5.3.1.5 Effect of ethylene pressure on oligomerisation

Ethylene pressure has been shown to have a marked effect in the rate of oligomerisation observed with the effect of pressure being dependent on the specific catalyst system. Dixon *et al.* demonstrated a $(p_{C_2H_4})^{1.6}$ rate dependence for a chromium based tetramerisation catalyst.[49] Fujita and co-workers have reported a second order ethylene dependence for a phenoxyimine (FI) titanium catalyst employed for the selective trimerisation of ethylene.[1,50] Nomura *et al*. have shown that oligomerisation activities had a first order relationship with ethylene pressure for a niobium arylimido/MAO catalytic system.[17] This dependence of the rate of ethylene oligomerisation on ethylene pressure is one of the reasons that can be attributed to the far higher activities reported by Dyer *et al*. (up to 104200 $mol_{C_2H_4}/mol_{Nb}/h$ at 45 bar of ethylene pressure).[19]

Increased ethylene pressure results in higher oligomerisation activities (Figure 5.7 and Table 5.6), with a maximum of 59 $mol_{C_2H_4}/mol_{Nb}$ after 30 minutes for 2 bar of ethylene pressure, compared with a maximum of 50 $mol_{C_2H_4}/mol_{Nb}$ after 45 minutes at 1 bar. Initial activities are also greater for 2 bar of ethylene pressure than 1 bar, with activities of 56 and 43 $mol_{C_2H_4}/mol_{Nb}$ after 15 minutes respectively. In both cases the dominant catalytic pathway is polymerisation, with polymer being over 90% of the observed product (Tables 5.6 and A5.5). The observed 1-hexene selectivities are approximately the same for both 1 and 2 bar of ethylene pressure (92 and 85% after 15 minutes respectively, however, the full amount of 1-butene produced may not be observed due to the high volatility), a greater decrease in observed selectivity over time is seen at higher ethylene

pressure. Selectivities between polymer and alkene fractions also remain approximately constant for the two pressures with 6 to 8% of the product after 10 hours being alkenes (1-hexene or 1-butene, Table A5.5).

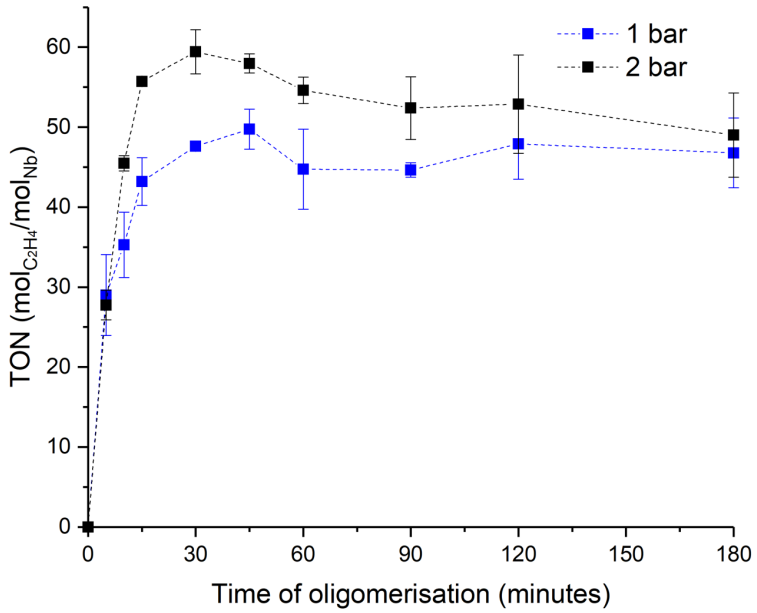

Figure 5.7. Pressure study using sMAO-Nb(NDipp)Cl_3; 5 mg catalyst ($[Al]_0$:$[Nb]_0$ = 200:1), 500 µL d_6-benzene, 50 °C and mesitylene standard.

Table 5.6. Ethylene oligomerisation activities and observed 1-hexene selectivities for selected time periods with ethylene pressures.

Time (minutes)	1 bar		2 bar	
	TON[a]	Observed 1-hexene selectivity (%)[b]	TON[a]	Observed 1-hexene selectivity (%)[b]
15	43	92	56	85
30	48	91	59	82
45	50	91	58	81
60	45	91	55	79
600	732[c]	5[d]	533[c]	6[d]

[a] TON values in mol$_{C_2H_4}$/mol$_{Nb}$. [b] Due to its volatility, the actual amount of butene produced may be higher than that observed. [c] TON for both oligomerisation and polymerisation. [d] 1-hexene selectivity from all observed products. Reaction conditions: 1 bar ethylene, 5 mg catalyst ($[Al]_0$:$[Nb]_0$ = 200:1), 500 µL d_6-benzene and mesitylene standard. Selectivities determined by integration of triplets corresponding to 1-butene and 1-hexene between 0.95 and 0.80 ppm. Turnover numbers calculated by integration of the resonance at 5.00 ppm corresponding to the terminal CH_2 resonances of both 1-butene and 1-hexene.

5.3.1.6 Effect of a scavenger on ethylene oligomerisation

With the ultimate aim of this project being to combine an oligomerisation and polymerisation catalyst to produce a tandem catalytic system producing short chain

branched LLDPE from a single ethylene feedsource, it is important to use reaction conditions such that both catalysts are able to function effectively.[51] It has been demonstrated in Chapter 3, and with other catalytic systems,[52] that addition of a scavenger, and the nature of that scavenger, is important in allowing the species to be catalytically active and efficient in ethylene polymerisation.

The first study carried out, investigated the use of trimethylaluminium (TMA), triethylaluminium (TEA), tri*iso*butylaluminium (TiBA) and methylaluminoxane (MAO) as scavengers for the ethylene oligomerisation system, with addition of 1000 equivalents of the scavenger to replicate conditions used in ethylene polymerisations. This leads to almost complete deactivation of the catalyst (Figure 5.8). This deactivation could be due to a deactivating reaction of the scavengers with the immobilised complex.[53] To investigate further, sMAO-Nb(NDipp)Cl_3 was heated to 50 °C for 3 hours both alone and with addition of 100 equivalents of MAO, with the reaction monitored by ^{1}H NMR spectroscopy (Figures A5.7–A5.8). In both cases, there is no clear evidence of leaching of the niobium complex on heating in either case; both solutions remain colourless through the duration of the reaction. In all four ^{1}H NMR spectra there are four resonances observed, between 0.16 and 2.11 ppm which cannot be attributed to the supported complex or sMAO which are insoluble in benzene, or Nb(NDipp)Cl_3.THF.py.

Following this result, the amount of scavenger was varied to investigate whether lowering the amount of scavenger used would result in increased oligomerisation activity (Figure 5.9). MAO was chosen as a scavenger because it had resulted in slightly higher productivities after 10 hours (3 $mol_{C_2H_4}/mol_{Nb}$) compared with TMA (2 $mol_{C_2H_4}/mol_{Nb}$), TEA (2 $mol_{C_2H_4}/mol_{Nb}$) and TiBA (0 $mol_{C_2H_4}/mol_{Nb}$).

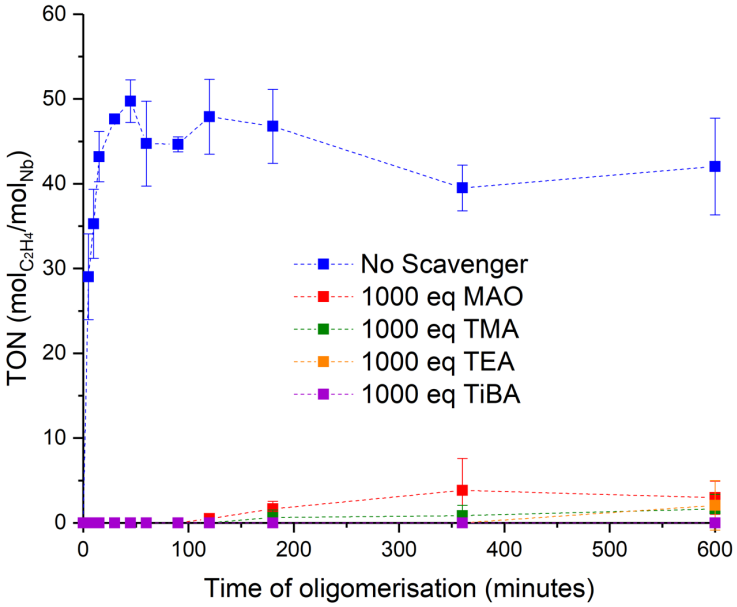

Figure 5.8. Scavenger study using sMAO-Nb(NDipp)Cl_3; 1 bar ethylene, 5 mg catalyst ($[Al]_0$:$[Nb]_0$ = 200:1), 500 µL d_6-benzene, 50 °C and mesitylene standard.

Oligomerisation studies were run with 0, 10, 50, 100 and 1000 equivalents of MAO and the results are shown in Figure 5.9, and Tables 5.7 and A5.6. With decreasing amounts of scavenger, the observed oligomerisation activities increase highlighting the inhibiting scavenger effect on catalytic activity. The scavenger may deactivate or modify the catalytically active sites resulting in lower activities.[54] The relative amounts of alkene and polymer produced does not vary significantly with increasing addition of scavenger (Table A5.6).

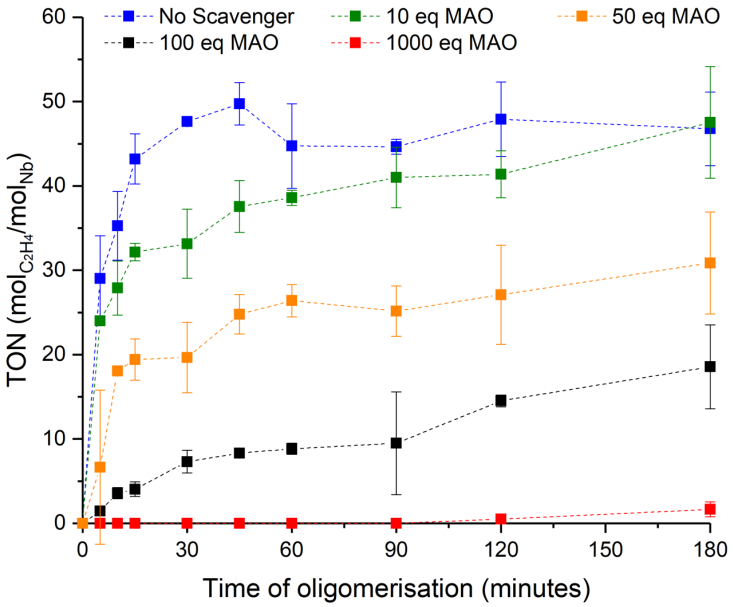

Figure 5.9. Scavenger study using sMAO-Nb(NDipp)Cl_3; 1 bar ethylene, 5 mg catalyst ($[Al]_0$:$[Nb]_0$ = 200:1), 500 µL d_6-benzene, 50 °C and mesitylene standard.

Table 5.7. Ethylene oligomerisation activities and observed 1-hexene selectivities for selected time periods; 1 bar ethylene, 5 mg catalyst ($[Al]_0$:$[Nb]_0$ = 200:1).

Time (minutes)	0 equivalents		10 equivalents		50 equivalents		100 equivalents	
	TON[a]	Observed 1-hexene selectivity (%)[b]	TON[a]	Observed 1-hexene selectivity (%)[b]	TON[a]	Observed 1-hexene selectivity (%)[b]	TON[a]	Observed 1-hexene selectivity (%)[b]
15	43	92	32	86	19	88	4	90
30	48	91	33	87	20	88	7	89
45	50	91	38	86	25	88	8	88
60	45	91	39	86	26	88	9	89
180	47	87	47	81	31	85	21	84
600	732[c]	5[d]	531[c]	6[d]	322[c]	7[d]	416[c]	4[d]

[a] TON values in $mol_{C_2H_4}/mol_{Nb}$. [b] Due to its volatility, the actual amount of butene produced may be higher than that observed. [c] TON for both oligomerisation and polymerisation. [d] 1-hexene selectivity from all observed products. Reaction conditions: 1 bar ethylene, 5 mg catalyst ($[Al]_0$:$[Nb]_0$ = 200:1), 500 µL d_6-benzene and mesitylene standard. Selectivities determined by integration of triplets corresponding to 1-butene and 1-hexene between 0.95 and 0.80 ppm. Turnover numbers calculated by integration of the resonance at 5.00 ppm corresponding to the terminal CH_2 resonances of both 1-butene and 1-hexene.

5.3.2 Solution-phase ethylene oligomerisation

The nature of the cocatalyst has been shown to be highly important in the nature of the active species and as such in the selectivity of the final oligomerisation product; Duchateau *et al.* observed that switching from an MAO cocatalyst to $AlMeCl_2$ transformed the oligomerisation products from a statistical mixture to selective

trimerisation when using [{$Ph_2C(C_4H_3N)(C_5H_6N$}Cr(THF)(μ-Cl)]$_2$.[48] Oligomerisations were carried out on an NMR scale with 2 mg of Nb(NDipp)Cl_3.THF.py with an MAO cocatalyst, 500 μL d_6-benzene, at 50 °C and a mesitylene standard. The results of these studies are shown in Figure 5.10 and selectivities at selected time periods in Table 5.8.

With the addition of no MAO, the niobium complex was completely inactive to oligomerisation or polymerisation, confirming that the process of alkylation followed by alkyl abstraction afforded by addition of an MAO cocatalyst is vitally important in facilitating oligomerisation. Increased catalytic activities are observed with increasing addition of MAO cocatalyst, with a maximum activity of 8.4 $mol_{C_2H_4}/mol_{Nb}$ after 6 hours with addition of 100 equivalents of MAO. A similar effect of increased oligomerisation activities with higher $[Al]_0$:$[M]_0$ ratios has been previously reported. Redshaw *et al*. demonstrated that increasing the amount of $MeAlCl_2$ cocatalyst added to a niobium imidazole complex resulted in increased ethylene polymerisation activities; activities increased from 1600 to 3032 and 4200 kg_{PE}/mol/h/bar with 2000, 4000 and 6000 equivalents of MAO respectively.[55] Nomura *et al.* have also reported that ethylene oligomerisation activities increased with increasing amounts of MAO cocatalyst with a range of vanadium imido complexes; the $[Al]_0$:$[V]_0$ ratio was shown to greatly effect oligomerisation activities, activities generally increased up to 1000 equivalents of cocatalyst. However, further addition up to 1500 equivalents can lead to reduced activities.[56]

Duchateau *et al.* reported that the oligomerisation selectivity can be tuned by variation of the cocatalyst,[48] which can explain the change in selectivity towards 1-hexene presented here compared with the high 1-butene selectivity reported by Messinis and co-workers with niobium imido catalysts with an $EtAlCl_2$ cocatalyst.[19] The lower selectivities

towards 1-hexene in the solution Nb(NDipp)Cl_3.THF.py/MAO system (up to 78% after 60 minutes) compared with sMAO-Nb(NDipp)Cl_3 (91% after 60 minutes) may be due to less well defined nature of MAO or incomplete alkylation resulting in multiple active species; these could promote dimerisation, trimerisation and polymerisation resulting in reduced 1-hexene selectivity.

Whilst the TON values for solution-phase oligomerisation are much lower than those observed for heterogeneous-phase oligomerisations reported in 5.3.1.2, it is important to note that equivalent amounts of oligomer are produced in both cases: 6.5×10^{-6} moles of oligomer after 45 minutes (a TON of 4.7 $mol_{C_2H_4}/mol_{Nb}$) with 100 equivalents of MAO compared with 6.4×10^{-6} moles after the same time in the heterogeneous-phase oligomerisation at 50 °C in d_6-benzene (a TON of 45 $mol_{C_2H_4}/mol_{Nb}$), the most comparable experiment. Increased 1-hexene selectivity for heterogeneous oligomerisations compared with solution-phase has been observed by Jiang *et al*. using a chromium (III) diphosphinoamine catalyst;[57] it was proposed this was due a confinement effect of the solid support increasing the stability of the chromacycloheptane intermediate.

As with heterogeneous-phase oligomerisations, and with the results reported by Dyer *et al.*,[19] the major product of the reaction is polyethylene (Tables 5.8 and A5.7). The selectivity in oligomeric products coupled with the high levels of polymer produced would also support the proposal that multiple active catalysts are produced in the reaction of Nb(NDipp)Cl_3.THF.py with MAO, with the ratios of these active sites produced determining the relative selectivities between the oligomeric and polymeric fractions.

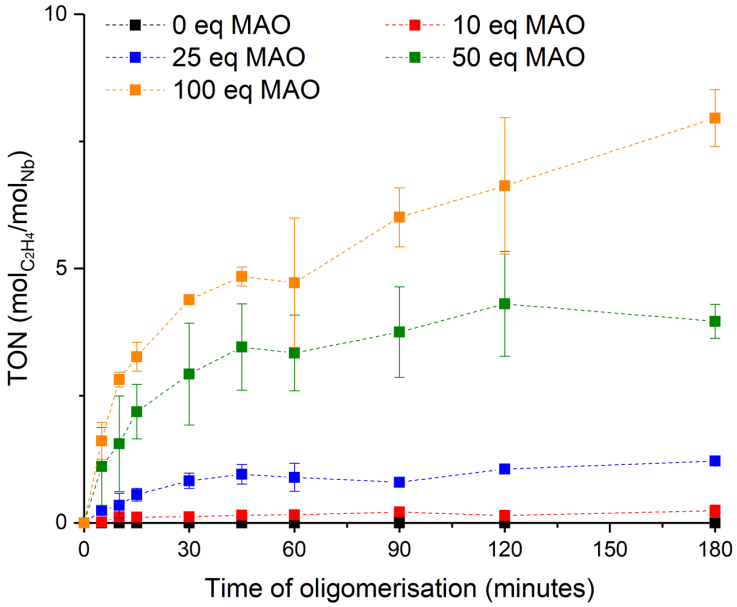

Figure 5.10. Solution-phase ethylene oligomerisation using Nb(NDipp)Cl_3.THF.py with different amounts of MAO cocatalyst; 2 mg of Nb(NDipp)Cl_3.THF.py, MAO cocatalyst, 1 bar ethylene, 500 µL d_6-benzene, mesitylene standard.

Table 5.8. Ethylene oligomerisation activities and observed 1-hexene selectivities for selected time periods for solution-phase oligomerisation with an MAO cocatalyst.

Time (minutes)	10 equivalents		25 equivalents		50 equivalents		100 equivalents	
	TON[a]	Observed 1-hexene selectivity (%)[b]	TON[a]	Observed 1-hexene selectivity (%)[b]	TON[a]	Observed 1-hexene selectivity (%)[b]	TON[a]	Observed 1-hexene selectivity (%)[b]
15	0.1	61	0.6	69	2.2	63	3.3	74
30	0.1	63	0.8	71	2.9	66	4.4	75
45	0.2	64	1.0	72	3.5	67	4.8	75
60	0.2	64	0.9	72	3.3	67	4.7	78
180	0.2	62	1.2	73	4.0	71	8.0	78
600	9.8[c]	3[d]	25.1[c]	5[d]	38.0[c]	10[d]	111.1[c]	6[d]

[a] TON values in mol$_{C_2H_4}$/mol$_{Nb}$. [b] Due to its volatility, the actual amount of butene produced may be higher than that observed. [c] TON for both oligomerisation and polymerisation. [d] 1-hexene selectivity from all observed products. Reaction conditions: 2 mg of Nb(NDipp)Cl_3.THF.py, MAO cocatalyst, 1 bar ethylene, 500 µL d_6-benzene, mesitylene standard. Selectivities determined by integration of triplets corresponding to 1-butene and 1-hexene between 0.95 and 0.80 ppm. Turnover numbers calculated by integration of the resonance at 5.00 ppm corresponding to the terminal CH_2 resonances of both 1-butene and 1-hexene.

5.4 Tandem catalysis of ethylene

A challenge of building a tandem catalytic system is that the conditions needed to be able to facilitate activity of both catalysts, and the activities of both catalysts need to be comparable in order to allow the production of enough α-olefin for it to be successfully incorporated into the polymer chain in levels detectable by various characterising methods.[51]

Given the large disparity between the activities of Nb(NDipp)Cl_3.THF.py for ethylene trimerisation and ^{Me2}SB($^{t Bu}$N,I*)$TiCl_2$ for ethylene polymerisation when supported on sMAO, conditions were chosen to maximise oligomerisation activities, whilst still allowing for ethylene polymerisation. A tandem catalytic experiment was carried out in benzene, with both complexes supported on sMAO in an $[Al]_0$:$[Nb]_0$:$[Ti]_0$ ratio of 2000:10:1 with 10 equivalents (relative to Nb(NDipp)Cl_3.THF.py) of MAO as a scavenger. These were carried out for 3 hours under a constant flow of 2 bar ethylene pressure. In addition to this, analogous experiments were carried out under the same conditions using solely the oligomerisation catalyst (sMAO-Nb(NDipp)Cl_3) in an $[Al]_0$:$[Nb]_0$ ratio of 200:1, solely the polymerisation catalyst (sMAO-^{Me2}SB($^{t Bu}$N,I*)$TiCl_2$) in an $[Al]_0$:$[Ti]_0$ ratio of 2000:1 and a physical mixture of 1 mg of sMAO-^{Me2}SB($^{t Bu}$N,I*)$TiCl_2$ in an $[Al]_0$:$[Ti]_0$ ratio of 200:1 and 9 mg of sMAO-Nb(NDipp)Cl_3 in an $[Al]_0$:$[Nb]_0$ ratio of 180:1.

The ^{13}C CP-MAS solid state NMR spectra of sMAO-Tandem, sMAO-Nb(NDipp)Cl_3 and sMAO-^{Me2}SB($^{t Bu}$N,I*)$TiCl_2$ are shown below in Figure 5.11. Within the solid state NMR spectrum of sMAO-Tandem, it is possible to tentatively assign resonances to sMAO, Nb(NDipp)Cl_3.THF.py and ^{Me2}SB($^{t Bu}$N,I*)$TiCl_2$. Resonances at –8 and 128 ppm correspond to sMAO, those at 147, 130, 74, 50, 30 and 20 ppm are assigned to

Nb(NDipp)Cl_3.THF.py, and resonances at 125–140, 50, 31 and 15–20 ppm to ^{Me_2}SB(^{tBu}N,I*)$TiCl_2$.

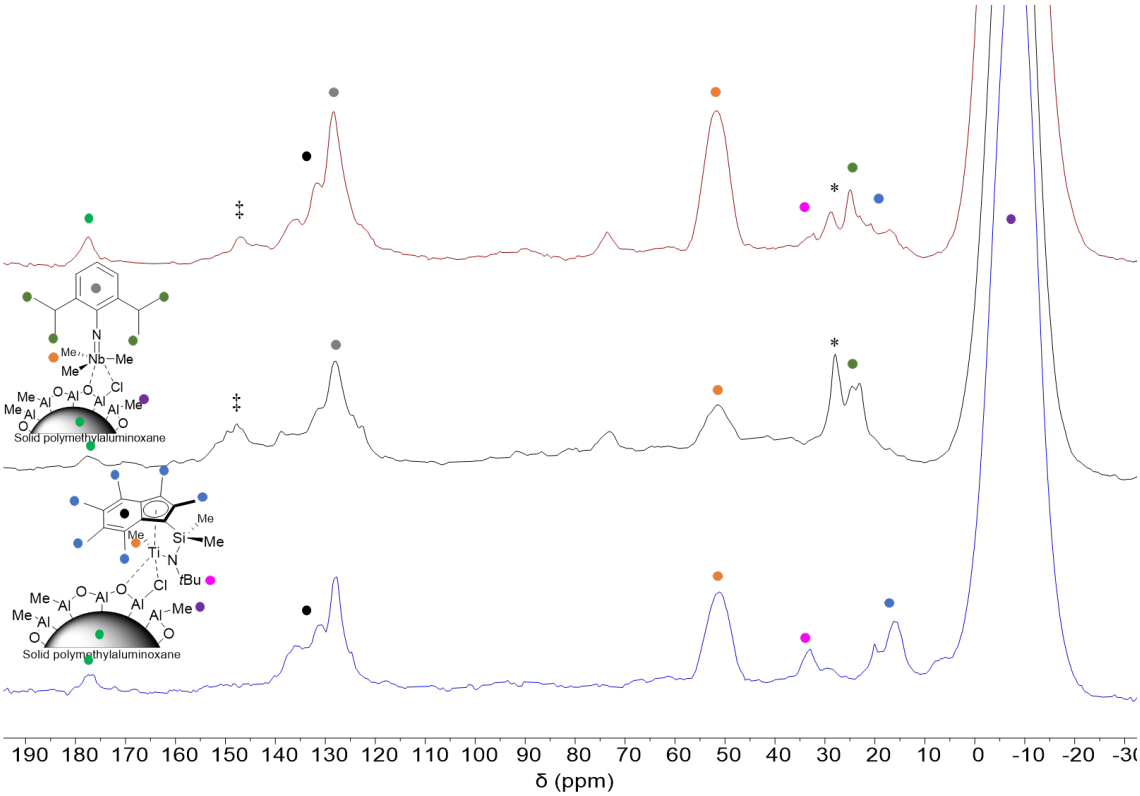

Figure 5.11. ^{13}C CP-MAS solid state NMR spectra of (red) sMAO-Tandem, (black) sMAO-Nb(NDipp)Cl_3 and (blue) sMAO-^{Me_2}SB(^{tBu}N,I*)$TiCl_2$. 100.6 MHz, 298 K.

The activities of the three supported catalysts, along with the physical mixture, are given in Table 5.9 as well at the polymer melt and crystallisation temperatures and enthalpies. Given the unfavourable conditions for ethylene polymerisation, low activities are to be expected, with the amount of polymer produced being between 50 and 90 mg. The ten-fold greater activity reported for the polymerisation with sMAO-^{Me_2}SB(^{tBu}N,I*)$TiCl_2$ can be attributed to the significantly lower amount of complex supported on the catalyst surface. If activities are instead given relative the moles of titanium in the reaction mixture, then this activity is lower than for sMAO-Tandem (214 $kg_{PE}/mol_{Ti}/h/bar$) and the physical mixture (168 $kg_{PE}/mol_{Ti}/h/bar$).

Table 5.9. Polymerisation activities, melt (T_m) and crystallisation temperatures (T_c), and melt (ΔH_m) and crystallisation (ΔH_c) enthalpies for the four tested catalyst compositions; 10 mg catalyst, 50 mL benzene, 2 bar ethylene, 0.4 mg MAO, 50 °C and 3 hours.

	Activity[a]	T_m[b]	T_c[b]	ΔH_m[c]	ΔH_c[c]
sMAO-Tandem	19.0±0.6	133.1	118.0	116	118
sMAO-Nb(NDipp)Cl_3	12.9±1.2	132.6	118.6	116	119
sMAO-^{Me2}SB(^{tBu}N,I*)$TiCl_2$	142.5±1.2	133.7	118.4	134	137
Physical mixture	14.9±1.2	132.1	115.5	85	77

[a] Activity in $kg_{PE}/mol_M/h/bar$; mol_M is the sum of mol_{Nb} and mol_{Ti}. [b] T_m and T_c in °C. [c] ΔH_m and ΔH_c in Jg^{-1}, ΔH values calculated by integration of the melt and crystallisation peaks in DSC traces.

To determine whether there has been any incorporation, the polymer produced was studied using differential scanning calorimetry (DSC) (Figure 5.12) and high temperature $^{13}C\{^1H\}$ NMR spectroscopy (Figure 5.13). DSC is a method that allows determination of both melt and crystallisation temperatures and enthalpies, and is able to indicate whether there has been incorporation of short chain branches into the polymer chain.[58]

In both sMAO-Tandem and sMAO-Nb(NDipp)Cl_3, there are low temperature shoulders in both heating and cooling traces that would suggest that there is a mixture of polymers, with the lower melting temperature possibly corresponding to a branched low molecular weight polyethylene, most likely from incorporation of oligomeric products into a polymer chain. Whilst there is also a decrease in polymer melt temperatures and melt enthalpies for both sMAO-Tandem, sMAO-Nb(NDipp)Cl_3 and the physical mixture relative to sMAO-^{Me2}SB(^{tBu}N,I*)$TiCl_2$, the relatively small decrease does not allow for confirmation conclusively from this that there has been the incorporation of α-olefins into the polymer chain using this technique.

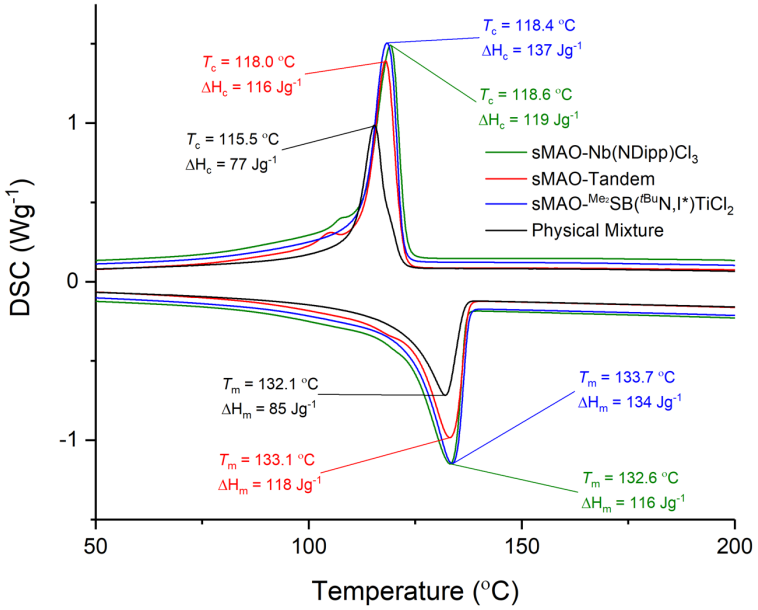

Figure 5.12. DSC plot for polymers produced at 50 °C for sMAO-Nb(NDipp)Cl$_3$ (green), sMAO-Tandem (red), sMAO-^{Me2}SB(^{t}BuN,I*)TiCl$_2$ (blue) and physical mixture (black).

In the polymer NMR spectra (Figure 5.13), no resonances are observed in any of the spectra that could be associated with chain branching formed by incorporation of comonomer. Analysis of the reaction solvent by GCMS shows the presence of 1-butene in the reaction involving sMAO-Nb(NDipp)Cl$_3$, with no 1-hexene observed and no oligomer observed in either of the other reaction mixtures. The reason for the observation of solely 1-butene is unclear, especially since no 1-hexene incorporation is observed in the high temperature ^{13}C{^{1}H} NMR spectra; one possibility is that there is a switch in catalytic activity facilitated both by the change in scale and pressure (5.3.1.5), and scavenger addition (5.3.1.6). It has been shown both previously and in the literature that the nature and amount of scavenger, the reaction pressure and other factors can have a large effect on the selectivity of a catalyst.[59] It is proposed that a combination of these factors results in the transition in the observed selectivity of this catalyst.

From these there are two possible conclusions to draw from the tandem catalytic study: either the oligomerisation part of system is deactivated, potentially through a bimetallic deactivation caused by the presence of the supported ^{Me2}SB(^{t}BuN,I*)TiCl$_2$ resulting in the

formation of polymer with no short chain branches, or there is production of short chain branched polyethylene, but the number of short chain branches are so low that they are not observed in the NMR spectrum.

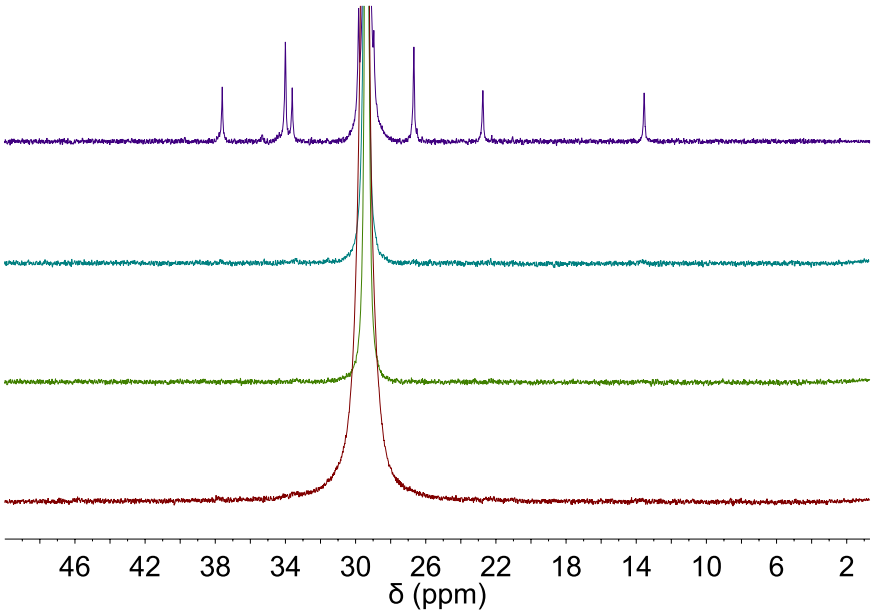

Figure 5.13. $^{13}C\{^{1}H\}$ NMR spectra of polymer produced from (purple) ethylene/1-hexene copolymerisation with sMAO-^{Me_2}SB($^{t\text{Bu}}$N,I*)TiCl$_2$ (0.625 mL 1-hexene, 2.1 mol% incorporation), (blue) sMAO-Nb(NDipp)Cl$_3$, (green) sMAO-Tandem, and (red) physical mixture of sMAO-Nb(NDipp)Cl$_3$ and sMAO-^{Me_2}SB($^{t\text{Bu}}$N,I*)TiCl$_2$; d_2-1,1,2,2-tetrachloroethane at 393 K, 500 MHz.

5.5 Conclusions

Nb(NDipp)Cl_3.THF.py was synthesised in a 24% yield and supported on sMAO in a range of $[Al]_0$:$[Nb]_0$ ratios. Ethylene oligomerisation studies were carried out to study the effect of catalyst loading, reaction solvent, temperature, scavenger and pressure on oligomerisation rates and selectivities.

Despite the discussed limitations of the experimental method, oligomerisation studies found that the major product was 1-hexene (in aromatic solvents), with highest turnovers were found when the complex was supported in a 200:1 $[Al]_0$:$[Nb]_0$ ratio, 50 °C, and in d_6-benzene at 2 bar of ethylene pressure with an observed turnover of 59 $mol_{C_2H_4}/mol_{Nb}$ after 30 minutes. In all cases, oligomerisation was paired with high levels of ethylene polymerisation, with polymer often being greater than 90% of the observed final product from catalysis. The reaction solvent was found to play a key role on the oligomerisation activities, with aromatic solvents resulting in higher activities and selective trimerisation, whilst use of d_{18}-octane resulted solely in dimerisation and lower activities. Both sMAO-Nb(NDipp) and sMAO-Tandem produced polymer where low temperature shoulders were observed in the DSC traces suggesting there is the presence of branched polyethylene.

5.6 References

1 D. S. McGuinness, *Chem. Rev.*, 2011, **111**, 2321–2341.
2 A. Forestière, H. Olivier-Bourbigou and L. Saussine, *Oil Gas Sci. Technol. - Rev. l'IFP*, 2009, **64**, 649–667.
3 J. Skupinska, *Chem. Rev.*, 1991, **91**, 613–648.
4 K. Ziegler, *Angew. Chem.*, 1952, **64**, 323–329.
5 K. Ziegler, *Angew. Chem.*, 1964, **76**, 545–553.
6 O. L. Sydora, *Organometallics*, 2019, **38**, 997–1010.
7 W. Keim, *Angew. Chem. Int. Ed.*, 2013, **52**, 12492–12496.
8 A. Bollmann, K. Blann, J. T. Dixon, F. M. Hess, E. Killian, H. Maumela, D. S. McGuinness, D. H. Morgan, A. Neveling, S. Otto, M. Overett, A. M. Z. Slawin, P. Wasserscheid and S. Kuhlmann, *J. Am. Chem. Soc.*, 2004, **126**, 14712–14713.
9 P.-A. R. Breuil, L. Magna and H. Olivier-Bourbigou, *Catal. Letters*, 2015, **145**, 173–192.
10 H. R. Menapace, N. A. Maly, J. L. Wang and L. G. Wideman, *J. Org. Chem.*, 1975, **40**, 2983–2985.
11 W. R. H. Wright, A. S. Batsanov, J. A. K. Howard, R. P. Tooze, M. J. Hanton and P. W. Dyer, *Dalton Trans.*, 2010, **39**, 7038–7045.
12 W. R. H. Wright, A. S. Batsanov, A. M. Messinis, J. A. K. Howard, R. P. Tooze, M. J. Hanton and P. W. Dyer, *Dalton Trans.*, 2012, **41**, 5502–5511.
13 A. M. Messinis, W. R. H. Wright, A. S. Batsanov, J. A. K. Howard, M. J. Hanton and P. W. Dyer, *ACS Catal.*, 2018, **8**, 11235–11248.
14 C. Andes, S. B. Harkins, S. Murtaza, K. Oyler and A. Sen, *J. Am. Chem. Soc.*, 2001, **123**, 7423–7424.
15 J. D. Fellmann, G. A. Rupprecht and R. R. Schrock, *J. Am. Chem. Soc.*, 1979, **101**, 5099–5101.
16 E. A. C. Brussee, A. Meetsma, B. Hessen and J. H. Teuben, *Organometallics*, 1998, **17**, 4090–4095.
17 M. Kuboki and K. Nomura, *Organometallics*, 2019, **38**, 1544–1559.
18 S. Zhang and K. Nomura, *J. Am. Chem. Soc.*, 2010, **132**, 4960–4965.
19 A. M. Messinis, A. S. Batsanov, J. A. K. Howard, M. J. Hanton and P. W. Dyer, *ChemCatChem*, 2019, **11**, 1756–1764.
20 C. M. Killian, P. B. Mackenzie, G. G. Lavoie, J. A. Ponasik and L. S. Moody, 2000, WO 2000050475.
21 D. L. Beach and Y. V. Kissin, *J. Polym. Sci. Polym. Chem. Ed.*, 1984, **22**, 3027–3042.
22 E. A. Benham, P. D. Smith and M. P. McDaniel, *Polym. Eng. Sci.*, 1988, **28**, 1469–1472.
23 Z. Ye, F. AlObaidi and S. Zhu, *Macromol. Rapid Commun.*, 2004, **25**, 647–652.
24 R. W. Barnhart, G. C. Bazan and T. Mourey, *J. Am. Chem. Soc.*, 1998, **120**, 1082–1083.
25 S. Guo, H. Fan, Z. Bu, B.-G. Li and S. Zhu, *Macromol. Chem. Phys.*, 2014, **215**, 1661–1667.
26 K. Musikabhumma, T. P. Spaniol and J. Okuda, *Macromol. Chem. Phys.*, 2002, **203**, 115–121.
27 D. C. Aluthge, A. Sattler, M. A. Al-Harthi, J. A. Labinger and J. E. Bercaw, *ACS Catal.*, 2016, **6**, 6581–6584.
28 K. Wised and K. Nomura, *Organometallics*, 2016, **35**, 2773–2777.

29 K. Czaja, L. A. Novokshonova and N. J. Kovaleva, *Macromol. Chem. Phys.*, 1999, **200**, 983–988.

30 W. Clegg, R. John Errington, D. C. R. Hockless and C. Redshaw, *Polyhedron*, 1991, **10**, 1959–1961.

31 A. V. Korolev, A. L. Rheingold and D. S. Williams, *Inorg. Chem.*, 1997, **36**, 2647–2655.

32 K. S. Heinselman, V. M. Miskowski, S. J. Geib, L. C. Wang and M. D. Hopkins, *Inorg. Chem.*, 1997, **36**, 5530–5538.

33 I. A. Tonks, A. C. Durrell, H. B. Gray and J. E. Bercaw, *J. Am. Chem. Soc.*, 2012, **134**, 7301–7304.

34 P. Olms, H. W. Roesky, K. Keller and M. Noltemeyer, *Zeitschrift für Naturforsch. B*, 1992, **47**, 1609–1613.

35 H.-T. Chiu, J.-C. Lin, S.-H. Chuang, G.-H. Lee and S.-M. Peng, *J. Chinese Chem. Soc.*, 1998, **45**, 355–360.

36 C. M. R. Wright, Z. R. Turner, J.-C. Buffet and D. O'Hare, *Chem. Commun.*, 2016, **52**, 2850–2853.

37 C. M. R. Wright, T. J. Williams, Z. R. Turner, J.-C. Buffet and D. O'Hare, *Inorg. Chem. Front.*, 2017, **4**, 1048–1060.

38 G. J. P. Britovsek, D. S. McGuinness, T. S. Wierenga and C. T. Young, *ACS Catal.*, 2015, **5**, 4152–4166.

39 G. I. Nikonov, P. Mountford, L. G. Kuzmina, J. A. K. Howard, D. A. Lemenovskii and D. M. Roitershtein, *J. Organomet. Chem.*, 2001, **628**, 25–29.

40 R. M. Manyik, W. E. Walker and T. P. Wilson, 1967, US3300458A.

41 T. Agapie, S. J. Schofer, J. A. Labinger and J. E. Bercaw, *J. Am. Chem. Soc.*, 2004, **126**, 1304–1305.

42 T. Agapie, J. A. Labinger and J. E. Bercaw, *J. Am. Chem. Soc.*, 2007, **129**, 14281–14295.

43 S. A. Svejda and M. Brookhart, *Organometallics*, 1999, **18**, 65–74.

44 Z. J. A. Komon, X. Bu and G. C. Bazan, *J. Am. Chem. Soc.*, 2000, **122**, 1830–1831.

45 P. R. Elowe, C. McCann, P. G. Pringle, S. K. Spitzmesser and J. E. Bercaw, *Organometallics*, 2006, **25**, 5255–5260.

46 M. J. Hanton, L. Daubney, T. Lebl, S. Polas, D. M. Smith and A. Willemse, *Dalton Trans.*, 2010, **39**, 7025.

47 M. Peuckert and W. Keim, *J. Mol. Catal.*, 1984, **22**, 289–295.

48 S. Vadake Kulangara, D. Haveman, B. Vidjayacoumar, I. Korobkov, S. Gambarotta and R. Duchateau, *Organometallics*, 2015, **34**, 1203–1210.

49 R. Walsh, D. H. Morgan, A. Bollmann and J. T. Dixon, *Appl. Catal. A Gen.*, 2006, **306**, 184–191.

50 M. Mitani, J. Saito, S. Ishii, Y. Nakayama, H. Makio, N. Matsukawa, S. Matsui, J. Mohri, R. Furuyama, H. Terao, H. Bando, H. Tanaka and T. Fujita, *Chem. Rec.*, 2004, **4**, 137–158.

51 Z. J. A. Komon and G. C. Bazan, *Macromol. Rapid Commun.*, 2001, **22**, 467–478.

52 J. V. Lamb, J.-C. Buffet, Z. R. Turner and D. O'Hare, *Polym. Chem.*, 2019, **10**, 1386–1398.

53 G. J. P. Britovsek, S. Mastroianni, G. A. Solan, S. P. D. Baugh, C. Redshaw, V. C. Gibson, A. J. P. White, D. J. Williams and M. R. J. Elsegood, *Chem. Eur. J.*, 2000, **6**, 2221–2231.

54 D. E. Babushkin, V. N. Panchenko, M. N. Timofeeva, V. A. Zakharov and H. H. Brintzinger, *Macromol. Chem. Phys.*, 2008, **209**, 1210–1219.
55 C. Redshaw, M. Walton, L. Clowes, D. L. Hughes, A.-M. Fuller, Y. Chao, A. Walton, V. Sumerin, P. Elo, I. Soshnikov, W. Zhao and W.-H. Sun, *Chem. Eur. J.*, 2013, **19**, 8884–8899.
56 K. Nomura, A. Igarashi, S. Katao, W. Zhang and W.-H. Sun, *Inorg. Chem.*, 2013, **52**, 2607–2614.
57 H. Shao, J. Wang, R. Wang, L. Song, X. Guo and T. Jiang, *Appl. Catal. A Gen.*, 2017, **544**, 154–160.
58 P. Starck, P. Lehmus and J. V. Seppälä, *Polym. Eng. Sci.*, 1999, **39**, 1444–1455.
59 T. Jiang, Y. Ning, B. Zhang, J. Li, G. Wang, J. Yi and Q. Huang, *J. Mol. Catal. A Chem.*, 2006, **259**, 161–165.

Chapter 6

Conclusions and outlook

The results discussed in this thesis can be separated into four topics. Permethylindenyl constrained geometry complexes have been synthesised and shown to be both highly efficient catalysts for ethylene homopolymerisation (with good response to hydrogen addition), and for ethylene/α-olefin and ethylene/styrene copolymerisation. A niobium imido complex has also been synthesised, and the reaction system for ethylene oligomerisation optimised with the aim of producing a tandem catalytic system for the production of short-chain branched LLDPE from a single ethylene feedsource.

i) Novel permethylindenyl constrained geometry complexes.

Eleven permethylindenyl constrained geometry complexes have been synthesised and characterised; six solid-state structures have been reported. The complexes have been immobilised on a range of inorganic solid supports (sMAO, SSMAO and LDHMAO) for use as slurry-phase ethylene polymerisation catalysts. ^{Me2}SB($^{t Bu}$N,I*)TiCl$_2$ and ^{Me2}SB($^{t Bu}$N,I*)Ti(Cl)CH$_2$SiMe$_3$ were reacted with MAO to afford [^{Me2}SB($^{t Bu}$N,I*)TiMe]$^+$ (with formation of the counteranionic [X-MAO]$^-$).

ii) Highly efficient ethylene polymerisation catalysts with good response to hydrogen addition.

The sMAO-supported permethylindenyl complexes were shown to be highly efficient polymerisation catalysts; variation of the amido group showed a clear trend for increasing polymerisation activities with increasing electron donating ability. A three-fold increase in activity was observed for sMAO-^{Me2}SB($^{t Bu}$N,I*)TiCl$_2$ (3602 kg$_{PE}$/mol$_{Ti}$/h/bar), when

compared with an industrial standard sMAO-^{Me2}SB(^{tBu}N,Cp*)TiCl$_2$. Variation of the initiator groups to an alkyl species resulted in enhanced activities, up to 7048 $kg_{PE}/mol_{Ti}/h/bar$ for sMAO-^{Me2}SB(^{tBu}N,I*)Ti(CH$_2$SiMe$_3$)$_2$. Use of LDHMAO-^{Me2}SB(^{tBu}N,I*)TiCl$_2$ allowed for the production of extremely industrially desirable UHMWPE, with molecular weights in excess of 3000 kDa, whilst maintaining good activities.

High-throughput studies resulted in a maximum activity of 8433 $kg_{PE}/mol_{Ti}/h/bar$ for sMAO-^{Me2}SB(^{tBu}N,I*)Ti(CH$_2$Ph)$_2$, with sMAO-^{Me2}SB(^{tBu}N,I*)TiCl$_2$ showing the best response to hydrogen addition; molecular weights decreased from 2667 to 41 kDa with modest activity decreases (from 6738 to 4874 $kg_{PE}/mol_{Ti}/h/bar$). Large scale polymerisations at SCG Chemicals Co., Ltd. showed large increases in activities for both sMAO-^{Me2}SB(^{tBu}N,I*)Ti(CH$_2$Ph)$_2$ and sMAO-^{Me2}SB(^{tBu}N,I*)TiCl$_2$.

iii) Highly efficient ethylene/α-olefin and ethylene/styrene copolymerisation catalysts.

High levels of comonomer incorporations were observed for these complexes, up to 2.4 mol% for 1-hexene, 2.5 mol% for styrene and 2.0 mol% for 1-octene. Temperature studies for ethylene/1-hexene copolymerisations with sMAO-^{Me2}SB(^{tBu}N,I*)TiCl$_2$ showed a positive comonomer effect at 70 °C (activity enhancements of up to 23%). Activities of all the supported I* complexes were typically greater than those of sMAO-^{Me2}SB(^{tBu}N,Cp*)TiCl$_2$.

High-throughput studies for ethylene/1-hexene copolymerisation resulted in a maximum incorporation level of 8.4 mol% for sMAO-^{Me2}SB(^{tBu}N,$^{3\text{-}Et}$I*)TiCl$_2$ with a proportional increase in 1-hexene incorporation observed with changes in 1-hexene concentration.

Solution-phase ethylene/1-hexene and ethylene/1-octene copolymerisations showed ^{Me2}SB(^{tBu}N,$^{3\text{-}Et}$I*)TiCl$_2$ and ^{Me2}SB(^{tBu}N,I*)TiCl$_2$ produced copolymer with comparable incorporation levels to ^{Me2}SB(^{tBu}N,Cp*)TiCl$_2$; up to 8.3 and 11.2 wt% for 1-hexene and 1-octene respectively with almost three times greater activities.

These results have shown the potential for use of these complexes on a large scale as ethylene/α-olefin polymerisation catalysts, with comparable and controllable incorporation levels and far superior polymerisation activities. In addition, it would be of interest to further investigate variations of the basal fragment with the permethylindenyl ligand. The use of silyl-bridged phenoxy complexes (so called PHENICS complexes) could allow for high comonomer incorporation levels without the large decreases in polymer molecular weights observed.[1,2]

iv) Selective ethylene oligomerisation with a niobium imido catalyst.

Nb(NDipp)Cl$_3$.THF.pyr was synthesised and its solid-state molecular structure determined. The complex was immobilised on sMAO, and NMR scale oligomerisation studies showed the highest activities were reported with the use of d_6-benzene at 50 °C and 2 bar ethylene, 59 $mol_{C_2H_4}/mol_{Nb}$ after 30 minutes with observed 1-hexene selectivities of up to 92%. Tandem catalytic studies with Nb(NDipp)Cl$_3$.THF.pyr and ^{Me2}SB(^{tBu}N,I*)TiCl$_2$ supported on sMAO were inconclusive, with no chain branching observed using high temperature ^{13}C{^{1}H} NMR spectroscopy. However, the presence of a low melting point shoulder in the DSC plot would suggest that branched polyethylene has been produced. The oligomerisation results observed for sMAO-Nb(NDipp)Cl$_3$ offer scope for further study and optimisation of the system. Firstly, it would be of interest to gain more of an insight into the mechanism by which this catalysis occurs, and also whether the observed selective trimerisation is maintained on scale up of the reaction;

this could be accomplished first by isotopic labelling experiments as performed by Bercaw *et al*.,[3,4] and with catalytic experiments using methods employed by, for example, Britovsek *et al*. and Dyer *et al*..[5,6] Secondly, it would be of interest to study whether variation of the imido fragment, perhaps by addition of electron withdrawing or donating groups to the phenyl ring, could influence oligomerisation activities and selectivities. With the inconclusive results presented for the tandem catalytic studies, it would of interest whether use of a previously reported oligomerisation catalyst could be used in this system, for example use of titanium phenoxyimine complexes similar to the Mitsui trimerisation catalyst as has previously been used by Duchateau *et al*. and Bercaw *et al*. to allow controllable incorporation of butyl branches into the polymer chain from a single ethylene feedsource.[7,8]

6.1 References

1 H. Katayama, M. Nabika, A. Imai, A. Miyashita, T. Watanabe, H. Johohji, Y. Oda, H. Hanaoka, 1996, EP0842939B1.

2 M. Nabika, H. Katayama, T. Watanabe, H. Kawamura-Kuribayashi, K. Yanagi and A. Imai, *Organometallics*, 2009, **28**, 3785–3792.

3 T. Agapie, S. J. Schofer, J. A. Labinger and J. E. Bercaw, *J. Am. Chem. Soc.*, 2004, **126**, 1304–1305.

4 T. Agapie, J. A. Labinger and J. E. Bercaw, *J. Am. Chem. Soc.*, 2007, **129**, 14281–14295.

5 G. J. P. Britovsek, D. S. McGuinness, T. S. Wierenga and C. T. Young, *ACS Catal.*, 2015, **5**, 4152–4166.

6 A. M. Messinis, A. S. Batsanov, J. A. K. Howard, M. J. Hanton and P. W. Dyer, *ChemCatChem*, 2019, **11**, 1756–1764.

7 F. F. Karbach, T. Macko and R. Duchateau, *Macromolecules*, 2016, **49**, 1229–1241.

8 D. C. Aluthge, A. Sattler, M. A. Al-Harthi, J. A. Labinger and J. E. Bercaw, *ACS Catal.*, 2016, **6**, 6581–6584.

Chapter 7

Experimental details

7.1 General preparation and physical methods

General procedures. Air- and moisture-sensitive techniques were undertaken in an inert atmosphere of nitrogen, using standard Schlenk techniques, on a dual manifold nitrogen/vacuum line or in an MBraun Unilab glovebox.

Commercially supplied reagents. Titanium tetrachloride (Sigma Aldrich), *n*butyllithium (2.5 M in hexanes, Sigma Aldrich), methyl lithium (1.6 M in diethyl ether, Sigma Aldrich), triethylaluminium (Sigma Aldrich), trimethylaluminium (Sigma Aldrich), tri*iso*butylaluminium (Sigma Aldrich), ^{Me2}SB($^{t\text{Bu}}$N,Cp*)TiCl$_2$ (MCat GmbH) and hexamethylindene (I$^{\#}$H, $C_9Me_6H_2$, SCG Chemicals Co., Ltd. (Thailand)) were used as supplied. Prior to use, dimethyldichlorosilane (Sigma Aldrich) was degassed and stored over pre-activated 4 Å molecular sieves; zirconium tetrachloride (Sigma Aldrich) was dried under vacuum; 1-hexene (Sigma Aldrich), styrene (Sigma Aldrich) and 1-octene (Sigma Aldrich) were dried over calcium hydride, freeze-thaw degassed and stored over pre-activated 4 Å molecular sieves; PQ E70X silica was purchased from PQ Corporation and calcined at 600 °C under vacuum for 6 hours; Mg_3AlCO_3-LDH (prepared by Dr. Chunping Chen, Dr. Hongri (Clara) Suo and Miss Meng Lyu) was calcined at 150 °C under vacuum for 6 hours; solid polymethylaluminoxane (sMAO, Tosoh Finechem Corporation) and methylaluminoxane (MAO, Chemtura) were supplied as slurries in toluene which were dried under vacuum. Ethylene, CONCOA regulators and flashback arrestors were supplied by CK Gas Products Limited. Pentane, hexane, toluene, dichloromethane (DCM) and benzene were dried using an MBraun SPS 800

solvent purification system. Tetrahydrofuran (THF) and diethyl ether were distilled from purple Na/benzophenone. Amines (*tert*butylamine, *iso*propylamine, cyclohexylamine, 4-*tert*butylaniline, 4-*n*butylaniline, aniline, *n*butylamine and 2,6-di*iso*propylaniline) were dried over CaH_2 and then freeze-pump-thaw degassed three times. The amines, DCM and THF were stored over pre-activated 4 Å molecular sieves; hexane, pentane, benzene and toluene were stored on a potassium mirror. Deuterated solvents were dried over potassium (d_6-benzene, d_8-THF, d_8-toluene and d_{18}-octane) or CaH_2 (d_5-pyridine, d_1-chloroform, d_5-chlorobenzene and d_5-bromobenzene), freeze-pump-thaw degassed, vacuum transferred and stored over pre-activated 4 Å molecular sieves. I*$SiMe_2Cl$ was synthesised using a literature procedure from hexamethylindene (I$^{\#}$H).[1] Lithium amides were prepared *via* lithiation of an amine with 1.1 equivalents of ^{n}BuLi. $TiCl_4$.2THF was synthesised *via* a literature procedure from $TiCl_4$.[2]

Solution phase NMR spectroscopy. NMR spectra were recorded on either a 400 MHz Bruker Avance III HD nanobay spectrometer or a 500 MHz Bruker Avance III HD nanobay spectrometer. ^{1}H and ^{13}C{^{1}H} NMR spectra were recorded at 298 K unless otherwise stated, referenced internally to the residual protio-solvent resonance in the deuterated solvent. Air-sensitive samples were prepared in a glovebox under an inert atmosphere, using dried, deuterated solvents in Young's tap NMR spectroscopy tubes.

For polyethylene samples, NMR spectra were recorded in d_2-1,1,2,2-tetrachloroethane at 393 K with chromium (III) acetylacetonate as a relaxation agent (0.5 wt%).

Solid-state NMR spectroscopy. All experiments were carried out by Dr. Nicholas Rees (University of Oxford). Compounds were prepared in a glovebox under a nitrogen atmosphere and sealed in 5 mm zirconia rotors. Spectra were recorded on a Bruker Avance III HD NanoBay 400.2 MHz solid-state NMR spectrometer, samples were spun

at the magic angle (54.71°) at spin rates of 10 kHz for ^{13}C CP-MAS, ^{27}Al DP-MAS, and ^{29}Si CP-MAS. ^{13}C NMR spectra were referenced to adamantane, ^{27}Al to $Al(NO_3)_3$ and ^{29}Si to kaolinite.

Single crystal X-ray crystallography. X-ray crystallography was carried out by Dr. Zoë Turner (University of Oxford). Crystals were mounted on MiTeGen MicroMounts using perfluoropolyether oil and rapidly transferred to a goniometer head on a diffractometer fitted with an Oxford Cryosystems Cryostream open-flow nitrogen cooling device.[3] Data collections were carried out at 150 K using an Oxford Diffraction Supernova diffractometer using mirror-monochromated Cu *Kα* radiation (λ = 1.54178 Å) and data were processed using CrysAlisPro.[4] The structures were solved using direct methods (SIR-92)[5] or a charge flipping algorithm (SUPERFLIP)[6] and refined by full-matrix least-squares procedures using the Win-GX software suite.[7]

Elemental analysis. Samples were prepared in a glovebox and analysed by Mr Stephen Boyer (London Metropolitan University).

Differential scanning calorimetry (DSC). Samples were run on a DSC3+ (Mettler Toledo, Ltd) using 5 mg of polymer in a sealed aluminium 100 µL crucible. An empty crucible was used as a reference, and the DSC was calibrated using indium. Samples were heated from 25 to 250 °C and cooled back again at a rate of 5 °C per minute, a total of three cycles were run. Polymer melt temperature and enthalpy values were taken from the third heating cycle.

Scanning electron microscopy (SEM). Analyses was performed by Dr. Jessica Lamb, Dr. Phakpoom Angpanitcharoen, Dr. Philip Kenyon and Mr Clement Collins Rice on a JOEL JSM 6610LV scanning electron microscope with an accelerating voltage of 3.0 kV. Polymer samples were spread on carbon tape adhered to an SEM stage. Air- and

moisture-sensitive samples were prepared in glove box whereby a suspension of the sample in pentane was prepared and placed onto a silicon wafer adhered to carbon tape on an SEM stage. Before imaging, the samples were coated with a thin platinum layer (20 nm) to prevent charging and improve image quality.

Gel Permeation Chromatography (GPC). GPC samples were collected by Ms Liv Thobru at Norner AS (Norway) on a high temperature gel permeation chromatograph with an IR5 infrared detector (GPC-IR5). Samples were dissolved in 1,2,4-trichlorobenzene (TCB) containing 300 ppm of 3,5-di*ert*butyl-4-hydroxytoluene (BHT) at 160 °C for 90 minutes and then filtered with a 10 μm SS filter before being passed through the GPC column. The samples were run under a flow rate of 0.5 mL/min using TCB containing 300 ppm of BHT as mobile phase with 1 mg/mL BHT added as a flow rate marker. The GPC column and detector temperature were set at 145 and 160 °C respectively.

7.2 Experimental details for Chapter 2

7.2.1 Synthesis of constrained geometry complexes

7.2.1.1 Synthesis of $^{3\text{-Et}}$I*SiMe$_2$Cl

$^{3\text{-Et}}$I$^{\#}$Li (2.00 g, 9.07 mmol) was dissolved in THF (40 mL). This was then added dropwise to a THF solution (25 mL) of three equivalents of $SiMe_2Cl_2$ (3.28 mL, 27.2 mmol) and the reaction mixture was stirred for 3 hours at 23 °C. The volatiles were removed under vacuum and the product was extracted in pentane (4 × 20 mL). The solution was concentrated and a yellow solid precipitated at −20 °C. The solid melted to form a yellow oil at room temperature and was isolated in 83% yield (2.30 g, 7.49 mmol).

^{1}H NMR (C_6D_6, 298 K, 400.2 MHz): δ (ppm) 3.50 (1H, s, I*-**H**), 2.66 (2H, m, I*-**CH$_2$**-CH$_3$), 2.44 (3H, s, I*-**Me**), 2.14 (3H, s, I*-**Me**), 2.13 (3H, s, I*-**Me**), 2.12 (3H, s, I*-**Me**), 2.12 (3H, s, I*-**Me**), 1.13 (3H, dd, I*-CH$_2$-**CH$_3$**, $^3J_{H\text{-}H}$ = 7.5 Hz, $^3J_{H\text{-}H}$ = 7.5 Hz), 0.20 (3H, s, Si-**Me**) and −0.08 (3H, s, Si-**Me**).

7.2.1.2 Synthesis of I*Si(Me,Pr)Cl

I$^{\#}$Li (5.00 g, 24.3 mmol) was dissolved in THF (25 mL) and added dropwise over 30 minutes to a solution of 1.5 equivalents of $SiMePrCl_2$ (5.46 mL, 36.5 mmol) in THF (20 mL) at 23 °C. The reaction mixture was stirred for 3 hours and the volatiles were removed under vacuum. The product was extracted in pentane (4 × 25 mL) as a pale orange solution, the solution was concentrated and I*Si(Me,Pr)Cl precipitated as a pale orange solid at −20 °C in a 73% yield (7.28 g, 17.4 mmol) as two isomers.

^{1}H NMR (C_6D_6, 298 K, 499.9 MHz): δ (ppm) 3.55 (1H, s, I*-**H**), 3.52 (1H, s, I*-**H**), 2.44 (6H, s, I*-**Me**), 2.22 (3H, s, I*-**Me**), 2.19 (3H, s, I*-**Me**), 2.18 (6H, s, I*-**Me**), 2.13 (6H, s, I*-**Me**), 2.12 (6H, s, I*-**Me**), 2.11 (3H, s, I*-**Me**), 2.09 (3H, s, I*-**Me**), 1.29 (2H,

s, Si-CH_2-**CH_2**-CH_3), 1.09 (2H, m, Si-CH_2-**CH_2**-CH_3), 0.80 (3H, m, Si-CH_2-CH_2-**CH_3**), 0.75 (3H, m, Si-CH_2-CH_2-**CH_3**), 0.53 (2H, m, Si-**CH_2**-CH_2-CH_3), 0.32 (2H, m, Si-**CH_2**-CH_2-CH_3), 0.21 (3H, s, Si-**Me**) and −0.01 (3H, s, Si-**Me**). Resonances cannot be specifically assigned to either isomer.

7.2.1.3 Synthesis of ^{Me2}SB(^{R}N,I*)H_2 (R = ^{t}Bu, ^{i}Pr, ^{n}Bu, Cy, 4-^{t}BuC$_6$H$_4$, 4-^{n}BuC$_6$H$_4$ and Ph)

Equimolar amounts of I*$SiMe_2$Cl (1.00 g, 3.41 mmol) and LiN(H)R were added into a Schlenk tube. The reaction mixture was cooled to 5 °C, and THF (30 mL) was added. The solution was allowed to warm up to 25 °C (room temperature) and the reaction mixture was stirred for 2 hours. The THF was removed under vacuum and the resulting oil dissolved in pentane (30 mL). The solution was filtered and dried under vacuum to yield an oil in quantitative yield.

^{Me2}SB($^{t Bu}$N,I*)H_2. Yellow oil.

^{1}H NMR (C_6D_6, 400.2 MHz, 298 K): δ (ppm) 3.32 (1H, s, I*-**H**), 2.52 (3H, s, I*-**Me**), 2.30 (3H, s, I*-**Me**), 2.30 (3H, s, I*-**Me**), 2.22 (3H, s, I*-**Me**), 2.19 (3H, s, I*-**Me**), 2.11 (3H, s, I*-**Me**), 1.09 (9H, s, N-^{t}**Bu**), 0.46 (1H, s, N-**H**), 0.15 (3H, s, Si-**Me**) and −0.15 (3H, s, Si-**Me**).

^{Me2}SB($^{i Pr}$N,I*)H_2. Dark yellow oil.

^{1}H NMR (C_6D_6, 400.2 MHz, 298 K): δ (ppm) 3.33 (1H, s, I*-**H**), 2.85 (1H, sep, **CH**Me_2, $^{3}J_{H-H}$ = 6.2 Hz), 2.53 (3H, s, I*-**Me**), 2.29 (6H, s, I*-**Me**), 2.22 (3H, s, I*-**Me**), 2.19 (3H, s, I*-**Me**), 2.06 (3H, s, I*-**Me**), 0.92 (6H, m, CH**Me_2**, $^{3}J_{H-H}$ = 6.2 Hz), 0.10 (1H, b, N-**H**), 0.06 (3H, s, Si-**Me**) and −0.12 (3H, s, Si-**Me**).

^{Me2}SB(^{Cy}N,I*)H$_2$. Yellow oil.

^{1}H NMR (C$_6$D$_6$, 298 K, 400.2 MHz): δ (ppm) 3.35 (1H, s, I*-**H**), 2.53 (3H, s, I*-**Me**), 2.45 (1H, m, N-**CyH$_{ipso}$**), 2.30 (3H, s, I*-**Me**), 2.30 (3H, s, I*-**Me**), 2.22 (3H, s, I*-**Me**), 2.20 (3H, s, I*-**Me**), 2.08 (3H, s, I*-**Me**), 1.71 (2H, m, N-**CyH$_{ortho}$**), 1.58 (2H, m, N-**CyH$_{meta}$**), 1.46 (1H, m, N-**CyH$_{para}$**), 1.14 (2H, m, N-**CyH$_{meta}$**), 1.03 (1H, m, N-**CyH$_{para}$**), 0.89 (2H, m, N-**CyH$_{ortho}$**), 0.26 (1H, m, N-**H**), 0.08 (3H, s, Si-**Me**) and −0.08 (3H, s, Si-**Me**).

^{13}C{^{1}H} NMR (C$_6$D$_6$, 298 K, 125.7 MHz): δ (ppm) 142.6 (**I***), 142.0 (**I***), 139.7 (**I***), 132.2 (**I***), 131.8 (**I***), 129.5 (**I***), 126.8 (**I***), 126.1 (**I***), 51.0 (N-**Cy$_{ipso}$**), 50.2 (**I***-Si), 39.0 (N-**Cy$_{ortho}$**), 38.9 (N-**Cy$_{ortho}$**), 26.2 (N-**Cy$_{para}$**), 25.9 (2 × N-**Cy$_{meta}$**), 19.3 (I*-**Me**), 16.5 (I*-**Me**), 16.4 (I*-**Me**), 16.4 (I*-**Me**), 15.7 (I*-**Me**), 13.4 (I*-**Me**), −0.8 (Si-**Me**) and −1.2 (Si-**Me**).

^{Me2}SB($^{n Bu}$N,I*)H$_2$. Yellow oil.

^{1}H NMR (C$_6$D$_6$, 499.9 MHz, 298 K): δ (ppm) 3.37 (1H, s, I*-**H**), 2.54 (3H, s, I*-**Me**), 2.52 (2H, t, N-**C$_α$H$_2$**, $^3J_{H-H}$ = 6.7 Hz), 2.30 (3H, s, I*-**Me**), 2.29 (3H, s, I*-**Me**), 2.23 (3H, s, I*-**Me**), 2.21 (3H, s, I*-**Me**), 2.05 (3H, s, I*-**Me**), 1.19 (2H, m, N-**C$_β$H$_2$**), 1.19 (2H, m, N-**C$_γ$H$_2$**), 0.84 (3H, t, N-**C$_δ$H$_3$**, $^3J_{H-H}$ = 7.1 Hz), 0.12 (1H, s, N-**H**), −0.02 (3H, s, Si-**Me**) and −0.05 (3H, s, Si-**Me**).

^{13}C{^{1}H} NMR (C$_6$D$_6$, 125.7 MHz, 298 K): δ (ppm) 142.6 (**I***), 142.0 (**I***), 139.5 (**I***), 132.2 (**I***), 131.8 (**I***), 129.5 (**I***), 126.9 (**I***), 126.1 (**I***), 50.3 (Si-**I***), 42.0 (N-**C$_α$**), 37.2 (N-**C$_β$**), 20.3 (N-**Cγ**), 19.1 (I*-**Me**), 16.5 (I*-**Me**), 16.4 (I*-**Me**), 16.4 (I*-**Me**), 15.5 (I*-**Me**), 15.4 (I*-**Me**), 14.2 (N-**C$_δ$**), –1.1 (Si-**Me**) and –1.7 (Si-**Me**).

^{Me2}SB($^{4\text{-}n\text{Bu}}$C$_6$H$_4$N,I*)H$_2$. Dark yellow oil.

^{1}H NMR (C$_6$D$_6$, 400.2 MHz, 298 K): δ (ppm) 6.98 (2H, d, Ph-**H$_{meta}$**, $^3J_{H\text{-}H}$ = 7.9 Hz), 6.53 (2H, d, Ph-**H$_{ortho}$**, $^3J_{H\text{-}H}$ = 7.9 Hz), 3.61 (1H, s, N-**H**), 3.05 (1H, s, I*-**H**), 2.52 (3H, s, I*-**Me**), 2.52 (2H, t, **C$_\alpha$H$_2$**, $^3J_{H\text{-}H}$ = 8.0 Hz), 2.24 (3H, s, I*-**Me**), 2.23 (3H, s, I*-**Me**), 2.20 (3H, s, I*-**Me**), 2.16 (3H, s, I*-**Me**), 1.98 (3H, s, I*-**Me**), 1.56 (2H, m, **C$_\beta$H$_2$**), 1.32 (2H, m, **C$_\gamma$H$_2$**), 0.89 (3H, t, **C$_\delta$H$_3$**, $^3J_{H\text{-}H}$ = 7.4 Hz), 0.06 (3H, s, Si-**Me**) and −0.03 (3H, s, Si-**Me**).

^{Me2}SB($^{4\text{-}t\text{Bu}}$C$_6$H$_4$N,I*)H$_2$. Orange oil.

^{1}H NMR (C$_6$D$_6$, 400.2 MHz, 298 K): δ (ppm) 7.17 (2H, d, Ph-**H$_{ortho}$**, $^3J_{H\text{-}H}$ = 8.6 Hz), 6.52 (2H, d, Ph-**H$_{meta}$**, $^3J_{H\text{-}H}$ = 8.6 Hz), 3.62 (1H, s, N-**H**), 3.05 (1H, s, I*-**H**), 2.52 (3H, s, I*-**Me**), 2.24 (3H, s, I*-**Me**), 2.22 (3H, s, I*-**Me**), 2.20 (3H, s, I*-**Me**), 2.15 (3H, s, I*-**Me**), 1.98 (3H, s, I*-**Me**), 1.29 (9H, s, Ph-**^{t}Bu**), 0.07 (3H, s, Si-**Me**), 0.03 (3H, s, Si-**Me**).

7.2.1.4 Synthesis of ^{Me2}SB($^{t\text{Bu}}$N,$^{3\text{-Et}}$I*)H$_2$

$^{3\text{-Et}}$I*SiMe$_2$Cl (1.16 g, 3.78 mmol) was added to 1.05 equivalents of LiN(H)^{t}Bu (0.310 g, 3.97 mmol), and the mixture was cooled to 5 °C. THF (30 mL) was added, and the reaction mixture was allowed to warm to 23 °C and stirred for 2 hours. The volatiles were removed under vacuum and the product then extracted in pentane. The solution was dried *in vacuo* to yield ^{Me2}SB($^{t\text{Bu}}$N,$^{3\text{-Et}}$I*)H$_2$ as a pale yellow oil in a quantitative yield.

^{1}H NMR (C$_6$D$_6$, 298 K, 400.2 MHz): δ (ppm) 3.32 (1H, s, I*-**H**), 2.77 (2H, m, I*-**CH$_2$**-CH$_3$), 2.52 (3H, s, I*-**Me**), 2.30 (3H, s, I*-**Me**), 2.22 (3H, s, I*-**Me**), 2.19 (3H, s, I*-**Me**), 2.13 (3H, s, I*-**Me**), 1.24 (3H, dd, I*-CH$_2$-**CH$_3$**, $^3J_{H\text{-}H}$ = 7.5 Hz, $^3J_{H\text{-}H}$ = 7.5 Hz), 1.08 (9H, s, N-**^{t}Bu**), 0.47 (1H, s, N-**H**), 0.16 (3H, s, Si-**Me**) and −0.13 (3H, s, Si-**Me**).

$^{13}C\{^{1}H\}$ NMR (C_6D_6, 298 K, 125.7 MHz): δ (ppm) 143.0 (**I***), 140.9 (**I***), 140.2 (**I***), 138.6 (**I***), 132.0 (**I***), 129.5 (**I***), 127.0 (**I***), 125.6 (**I***), 50.2 (**I***-Si), 49.5 (N-**C**Me_3), 33.9 (N-C**Me$_3$**), 21.3 (I*-**CH$_2$**-CH_3), 19.5 (I*-**Me**), 16.5 (I*-**Me**), 16.4 (I*-**Me**), 16.1 (I*-**Me**), 15.4 (I*-**Me**), 15.2 (I*-CH_2-**CH$_3$**), 3.7 (Si-**Me**) and 0.2 (Si-**Me**).

7.2.1.5 Synthesis of ^{Me,Pr}SB($^{t Bu}$N,I*)H_2

I*Si(Me,Pr)Cl (2.00 g, 6.23 mmol) was added to 1.05 equivalents of LiN(H)^{t}Bu (0.520 g, 6.59 mmol) and the mixture was cooled to 5 °C. THF (30 mL) was added and the reaction mixture was allowed to warm to 23 °C and stirred for 2 hours. The volatiles were removed under vacuum and the product extracted in pentane as a pale yellow solution. The mixture was dried *in vacuo* to yield ^{Me,Pr}SB($^{t Bu}$N,I*)H_2 as a dark yellow oil in a quantitative yield.

^{1}H NMR (C_6D_6, 298 K, 499.9 MHz): δ (ppm) 2.53 (6H, s, I*-**Me**), 2.33 (6H, s, I*-**Me**), 2.30 (6H, s, I*-**Me**), 2.22 (6H, s, I*-**Me**), 2.18 (6H, s, I*-**Me**), 2.14 (3H, s, I*-**Me**), 2.11 (3H, s, I*-**Me**). **Major Isomer (55%):** δ (ppm) 3.45 (1H, s, I*-**H**), 1.14 (2H, m, Si-CH_2-**CH$_2$**-CH_3), 1.11 (9H, s, N-**^{t}Bu**), 0.87 (3H, t, Si-CH_2-CH_2-**CH$_3$**, $^3J_{H\text{-}H}$ = 7.1 Hz), 0.68 (2H, m, Si-**CH$_2$**-CH_2-CH_3), 0.41 (1H, s, N-**H**), 0.18 (3H, s, Si-**Me**). **Minor isomer (45%):** δ (ppm) 3.41 (1H, s, I*-**H**), 1.22 (2H, m, Si-CH_2-**CH$_2$**-CH_3), 1.06 (9H, s, N-**^{t}Bu**), 0.93 (3H, t, Si-CH_2-CH_2-**CH$_3$**, $^3J_{H\text{-}H}$ = 7.4 Hz), 0.57 (2H, m, Si-**CH$_2$**-CH_2-CH_3), 0.36 (1H, s, N-**H**) and −0.02 (3H, s, Si-**Me**).

7.2.1.6 Synthesis of ^{Me_2}SB(^{R}N,I*)Li_2 (R = ^{t}Bu, ^{i}Pr, ^{n}Bu, Cy, 4-^{t}BuC_6H_4 and 4-^{n}BuC_6H_4).

^{Me_2}SB(^{R}N,I*)H_2 (3.41 mmol) was dissolved in THF (25 mL) and cooled to 5 °C. 2.2 equivalents of ^{n}BuLi (2.5 M in hexanes, 2.97 mL, 7.41 mmol) was added dropwise over 5 minutes. The resulting solution was allowed to warm up to 25 °C and stirred for

30 minutes. The THF was removed under vacuum and the solid product was washed with pentane (2 × 20 mL) and then dried *in vacuo*.

^{Me2}SB(^{tBu}N,I*)Li$_2$. Yellow solid, reacted *in situ*.

^{1}H NMR (C_5D_5N, 400.2 MHz, 298 K): δ (ppm) 3.22 (3H, s, I*-**Me**), 3.10 (3H, s, I*-**Me**), 3.10 (3H, s, I*-**Me**), 2.91 (3H, s, I*-**Me**), 2.52 (3H, s, I*-**Me**), 2.52 (3H, s, I*-**Me**), 1.52 1.40 (9H, s, N-^{t}**Bu**) and 0.84 (6H, s, Si-**Me$_2$**).

^{Me2}SB(^{iPr}N,I*)Li$_2$. Yellow solid in 32% yield (0.35 g, 1.07 mmol).

^{1}H NMR (C_5D_5N, 400.2 MHz, 298 K): δ (ppm) 3.52 (1H, sept, **CH**Me$_2$, $^3J_{H\text{-}H}$ = 6.3 Hz), 3.16 (3H, s, I*-**Me**), 3.10 (3H, s, I*-**Me**), 3.07 (3H, s, I*-**Me**), 2.89 (3H, s, I*-**Me**), 2.52 (3H, s, I*-**Me**), 2.52 (3H, s, I*-**Me**), 1.23 (6H, d, CH**Me$_2$**, $^3J_{H\text{-}H}$ = 6.3 Hz), 0.78 (6H, s, Si-**Me$_2$**).

^{Me2}SB(^{Cy}N,I*)Li$_2$. Pale yellow solid in 48% yield (1.20 g, 3.27 mmol).

^{1}H NMR (C_6D_5N, 298 K, 400.2 MHz): δ (ppm) 3.17 (3H, s, I*-**Me**), 3.13 (1H, m, N-**Cy**), 3.07 (3H, s, I*-**Me**), 3.05 (3H, s, I*-**Me**), 2.87 (3H, s, I*-**Me**), 2.51 (3H, s, I*-**Me**), 2.51 (3H, s, I*-**Me**), 2.13 (2H, m, N-**Cy**), 1.67 (2H, m, N-**Cy**), 1.47 (1H, m, N-**Cy**), 1.26 (4H, m, N-**Cy**), 1.11 (1H, m, N-**Cy**) and 0.79 (6H, s, Si-**Me**).

^{7}Li NMR (C_6D_5N, 298 K, 155.5 MHz): δ (ppm) 2.21.

^{Me2}SB(^{nBu}N,I*)Li$_2$. Yellow solid in 49% yield (0.56 g, 1.65 mmol).

^{1}H NMR (C_5D_5N, 400.2 MHz, 298 K): δ (ppm) 3.15 (3H, s, I*-**Me**), 3.13 (2H, t, N-**C$_\alpha$H$_2$**, $^3J_{H\text{-}H}$ = 6.8 Hz), 3.09 (3H, s, I*-**Me**), 3.07 (3H, s, I*-**Me**), 2.89 (3H, s, I*-**Me**),

2.51 (3H, s, I*-**Me**), 2.51 (3H, s, I*-**Me**), 1.55 (2H, m, N-**C$_\beta$H$_2$**), 1.40 (2H, m, N-**C$_\gamma$H$_2$**), 0.87 (3H, t, N-**C$_\delta$H$_3$**, $^3J_{H\text{-}H}$ = 7.3 Hz) and 0.79 (6H, s, Si-**Me**).

^{Me_2}SB($^{4\text{-}n\text{BuC}_6H_4}$N,I*)Li$_2$. Dark yellow solid in 77% yield (1.08 g, 2.59 mmol).

^{1}H NMR (C$_5$D$_5$N, 400.2 MHz, 298 K): δ (ppm) 7.28 (2H, d, Ph-**H$_{meta}$**, $^3J_{H\text{-}H}$ = 8.3 Hz), 7.16 (2H, d, Ph-**H$_{ortho}$**, $^3J_{H\text{-}H}$ = 8.3 Hz), 3.17 (3H, s, I*-**Me**), 3.06 (3H, s, I*-**Me**), 2.98 (3H, s, I*-**Me**), 2.67 (2H, t, N-**C$_\alpha$H$_2$**, $^3J_{H\text{-}H}$ = 7.4 Hz), 2.51 (3H, s, I*-**Me**), 2.50 (3H, s, I*-**Me**), 2.17 (3H, s, I*-**Me**), 1.72 (2H, m, N-**C$_\beta$H$_2$**), 1.43 (2H, m, N-**C$_\gamma$H$_2$**), 1.15 (6H, s, Si-**Me**) and 0.90 (3H, t, N-**C$_\delta$H$_3$**, $^3J_{H\text{-}H}$ = 7.3 Hz).

^{Me_2}SB($^{4\text{-}t\text{BuC}_6H_4}$N,I*)Li$_2$. Orange solid in 71% yield (1.00 g, 2.40 mmol).

^{1}H NMR (C$_5$D$_5$N, 400.2 MHz, 298 K): δ (ppm) 7.31 (2H, d, Ph-**H$_{ortho}$**, $^3J_{H\text{-}H}$ = 8.7 Hz), 7.25 (2H, d, Ph-**H$_{meta}$**, $^3J_{H\text{-}H}$ = 8.7 Hz), 3.19 (3H, s, I*-**Me**), 3.07 (3H, s, I*-**Me**), 2.99 (3H, s, I*-**Me**), 2.53 (3H, s, I*-**Me**), 2.51 (3H, s, I*-**Me**), 2.19 (3H, s, I*-**Me**), 1.46 (9H, s, Ph-^{t}**Bu**), 1.17 (6H, s, Si-**Me**).

7.2.1.7 Synthesis of ^{Me_2}SB(^{Ph}N,I*)Li$_2$

Equimolar amounts of I*SiMe$_2$Cl (1.00 g, 3.41 mmol) and lithium anilide (0.34 g, 3.41 mmol) were added into a Schlenk tube. The reaction mixture was cooled to 5 °C, and THF (30 mL) was added. The solution was allowed to warm up to 25 °C and the reaction mixture was stirred for 18 hours. The THF was removed *in vacuo* and the resulting oil dissolved in the pentane. The solution was filtered and dried under vacuum to yield a dark yellow oil. The oil was dissolved in THF (25 mL) and cooled to 5 °C. 2.2 equivalents of ^{n}BuLi (2.5 M in hexanes, 2.97 mL, 7.41 mmol) was added dropwise over 5 minutes. The resulting solution was allowed to warm to 25 °C and stirred for 30 minutes. The THF was removed under vacuum and the yellow/orange solid product

was washed with pentane (2 × 20 mL) and then dried *in vacuo*. The product was then reacted *in situ*.

^{1}H NMR (C_5D_5N, 400.2 MHz, 298 K): δ (ppm) 7.33 (4H, s, Ph-**H$_{meta}$** and Ph-**H$_{ortho}$**), 3.19 (3H, s, I*-**Me**), 3.08 (3H, s, I*-**Me**), 2.99 (3H, s, I*-**Me**), 2.52 (6H, s, I*-**Me**), 2.19 (3H, s, I*-**Me**) and 1.17 (6H, s, Si-**Me**). Ph-**H$_{para}$** not observed as obscured by the solvent resonances.

7.2.1.8 Synthesis of ^{Me_2}SB($^{t Bu}$N,$^{3\text{-}Et}$I*)Li$_2$.1.5THF

^{Me_2}SB($^{t Bu}$N,$^{3\text{-}Et}$I*)H$_2$ (1.30 g, 3.78 mmol) was dissolved in THF (30 mL) and cooled to 5 °C. 2.2 equivalents of ^{n}BuLi (1.6 M in hexanes, 5.2 mL, 8.32 mmol) was added dropwise to the solution, the reaction mixture allowed to warm to 23 °C and stirred for 30 minutes. The mixture was dried under vacuum and the residue was washed with pentane at 5 °C (4 × 25 mL). The resulting pale yellow solid was then dried *in vacuo* to yield ^{Me_2}SB($^{t Bu}$N,$^{3\text{-}Et}$I*)Li$_2$.1.5THF in a 43% yield (0.76 g, 1.64 mmol).

^{1}H NMR (C_6D_5N, 298 K, 400.2 MHz): δ (ppm) 3.68 (4H, m, O-**CH$_2$**-CH$_2$), 3.43 (2H, quartet, I*-**CH$_2$**-CH$_3$, $^{3}J_{H\text{-}H}$ = 7.2 Hz), 3.19 (3H, s, I*-**Me**), 3.02 (3H, s, I*-**Me**), 2.93 (3H, s, I*-**Me**), 2.53 (3H, s, I*-**Me**), 2.52 (3H, s, I*-**Me**), 1.64 (4H, m, O-CH$_2$-**CH$_2$**), 1.47 (3H, t, I*-CH$_2$-**CH$_3$**, $^{3}J_{H\text{-}H}$ = 7.2 Hz), 1.38 (9H, s, N-^{t}**Bu**) and 0.82 (6H, s, Si-**Me$_2$**).

^{7}Li NMR (C_6D_5N, 298 K, 155.5 MHz): δ (ppm) 1.84.

7.2.1.9 Synthesis of ^{Me,Pr}SB($^{t Bu}$N,I*)Li$_2$

^{Me,Pr}SB($^{t Bu}$N,I*)H$_2$ (2.23 g, 6.23 mmol) was dissolved in THF (30 mL) and cooled to 5 °C. 2.2 equivalents of ^{n}BuLi (1.6 M in hexanes, 8.60 mL, 13.7 mmol) was added dropwise, and the reaction mixture allowed to warm to 23 °C and stirred for 30 minutes. The reaction mixture was dried under vacuum and the dark yellow solid was washed with

cold pentane (4 × 25 mL) to yield ^{Me,Pr}SB(^{tBu}N,I*)Li$_2$.1.2THF as a pale yellow solid in 31% yield (0.71 g, 1.93 mmol).

^{1}H NMR (C_6D_5N, 298 K, 499.9 MHz): δ (ppm) 3.69 (4H, m, O-C**H$_2$**-CH$_2$), 3.20 (3H, s, I*-**Me**), 2.05 (3H, s, I*-**Me**), 3.05 (3H, s, I*-**Me**), 2.90 (3H, s, I*-**Me**), 2.52 (3H, s, I*-**Me**), 2.50 (3H, s, I*-**Me**), 1.70 (2H, m, Si-**CH$_2$**-CH$_2$-CH$_3$), 1.65 (4H, m, O-CH$_2$-**CH$_2$**), 1.40 (9H, s, N-^{t}**Bu**), 1.25 (2H, m, Si-CH$_2$-**CH$_2$**-CH$_3$), 1.06 (3H, m, Si-CH$_2$-CH$_2$-**CH$_3$**) and 0.84 (3H, s, Si-**Me**).

7.2.1.10 Synthesis of ^{Me2}SB(^{R}N,I*)TiCl$_2$ (R = ^{t}Bu, ^{i}Pr, ^{n}Bu, Cy, 4-^{t}BuC$_6$H$_4$, 4-^{n}BuC$_6$H$_4$ and Ph).

^{Me2}SB(^{R}N,I*)Li$_2$ (0.35–1.23 g) and 1 equivalent of TiCl$_4$.2THF were added to a Schlenk tube and cooled to 5 °C in an ice bath. Benzene (30 mL) was added; the reaction mixture was allowed to warm to 25 °C and stirred for 2–18 hours. The reaction mixture was dried to yield a red solid and the product extracted with pentane (3 × 50 mL).

^{Me2}SB(^{tBu}N,I*)TiCl$_2$. Red solid precipitated at −32 °C in 14% yield (0.20 g, 0.46 mmol).

^{1}H NMR (C_6D_6, 400.2 MHz, 298 K): δ (ppm) 2.56 (3H, s, I*-**Me**), 2.39 (3H, s, I*-**Me**), 2.36 (3H, s, I*-**Me**), 2.17 (3H, s, I*-**Me**), 2.07 (3H, s, I*-**Me**), 2.04 (3H, s, I*-**Me**), 1.40 (9H, s, N-^{t}**Bu**), 0.62 (3H, s, Si-**Me**) and 0.60 (3H, s, Si-**Me**).

^{13}C{^{1}H} NMR (C_6D_6, 125.7 MHz, 298 K): δ (ppm) 145.9 (**I***), 140.1 (**I***), 137.5 (**I***), 136.3 (**I***), 134.4 (**I***), 131.7 (**I***), 131.6 (**I***), 130.9 (**I***), 96.8 (Si-**I***), 62.1 (N-**C**Me$_3$), 32.8 (N-C**Me$_3$**), 21.5 (I*-**Me**), 17.3 (I*-**Me**), 17.1 (I*-**Me**), 17.0 (I*-**Me**), 17.0 (I*-**Me**), 16.6 (I*-**Me**), 8.3 (Si-**Me**) and 7.7 (Si-**Me**).

CHN Analysis (%): Expected: C 56.51, H 7.45, N 3.14. Found: C 56.63, H 7.50, N 3.25.

IR (KBr) (cm^{-1}): 3423 (b), 2973 (b), 2592, 2496, 2031, 1624, 1394, 1386, 900 and 832.

^{Me2}SB(^{iPr}N,I*)TiCl$_2$. Red crystals evolved at −32 °C in 17% yield (0.08 g, 0.18 mmol).

^{1}H NMR (C_6D_6, 400.2 MHz, 298 K): δ (ppm) 5.08 (1H, m, **CH**Me_2), 2.54 (3H, s, I*-**Me**), 2.41 (3H, s, I*-**Me**), 2.33 (3H, s, I*-**Me**), 2.18 (3H, s, I*-**Me**), 2.07 (3H, s, I*-**Me**), 2.01 (3H, s, I*-**Me**), 1.11 (3H, d, CH**Me**, $^3J_{H\text{-}H}$ = 6.5 Hz), 1.01 (3H, d, CH**Me**, $^3J_{H\text{-}H}$ = 6.5 Hz), 0.56 (3H, s, Si-**Me**) and 0.50 (3H, s, Si-**Me**).

^{13}C{^{1}H} NMR (C_6D_6, 125.7 MHz, 298 K): δ (ppm) 146.4 (**I***), 140.3 (**I***), 137.2 (**I***), 135.8 (**I***), 131.7 (**I***), 131.6 (**I***), 131.1 (**I***), 130.0 (**I***), 93.5 (Si-**I***), 56.2 (**C**Me_2), 24.2 (C**Me**), 23.9 (C**Me**), 21.3 (I*-**Me**), 17.2 (I*-**Me**), 17.1 (I*-**Me**), 16.9 (I*-**Me**), 16.9 (I*-**Me**), 16.5 (I*-**Me**), 7.3 (Si-**Me**) and 6.9 (Si-**Me**).

IR (KBr) (cm^{-1}): 3446 (b), 2941 (b), 1625, 1455, 1409, 1254, 909 and 809.

^{Me2}SB(^{Cy}N,I*)TiCl$_2$. Dark red solid precipitated at −20 °C in 14% yield (0.22 g, 0.46 mmol).

^{1}H NMR (C_6D_6, 298 K, 499.9 MHz): δ (ppm) 4.25 (1H, m, N-Cy**H$_{ipso}$**), 2.55 (3H, s, I*-**Me**), 2.42 (3H, s, I*-**Me**), 2.36 (3H, s, I*-**Me**), 2.22 (3H, s, I*-**Me**), 2.13 (1H, m, N-Cy**H$_{ortho}$**), 2.07 (3H, s, I*-**Me**), 2.02 (3H, s, I*-**Me**), 1.99 (1H, m, N-Cy**H$_{ortho}$**), 1.64 (1H, m, N-Cy**H$_{meta}$**), 1.56 (1H, m, N-Cy**H$_{meta}$**), 1.43 (1H, m, N-Cy**H$_{para}$**), 1.26 (1H, m, N-Cy**H$_{meta}$**), 1.15 (1H, m, N-Cy**H$_{meta}$**), 1.02 (1H, m, N-Cy**H$_{ortho}$**), 0.94 (1H, m, N-Cy**H$_{ortho}$**), 0.87 (1H, m, N-Cy**H$_{para}$**), 0.60 (3H, s, Si-**Me**) and 0.54 (3H, s, Si-**Me**).

^{13}C{^{1}H} NMR (C_6D_6, 298 K, 125.7 MHz): δ (ppm) 146.4 (**I***), 140.3 (**I***), 137.2 (**I***), 135.8 (**I***), 131.7 (**I***), 131.6 (**I***), 131.1 (**I***), 131.0 (**I***), 93.8 (**I***-Si), 64.9 (N-**Cy$_{ipso}$**), 35.4 (N-**Cy$_{ortho}$**), 35.0 (N-**Cy$_{ortho}$**), 26.6 (N-**Cy$_{meta}$**), 26.4 (N-**Cy$_{meta}$**), 26.1 (N-**Cy$_{para}$**)

21.3 (I*-**Me**), 17.3 (I*-**Me**), 17.1 (I*-**Me**), 17.0 (I*-**Me**), 16.9 (I*-**Me**), 16.5 (I*-**Me**), 7.4 (Si-**Me**) and 7.1 (Si-**Me**).

CHN Analysis (%): Expected: C 58.48, H 7.47, N 2.97. Found: C 58.46, H 8.12, N 2.69.

IR (KBr) (cm^{-1}): 3441 (b), 2940 (b), 1598, 1428, 1377, 1251, 1104 and 901.

^{Me2}SB($^{n Bu}$N,I*)TiCl$_2$. Red solid precipitated at −32 °C in 13% yield (0.10 g, 0.22 mmol).

^{1}H NMR (C_6D_6, 400.2 MHz, 298 K): δ (ppm) 4.68 (1H, m, N-**C$_\alpha$H**), 3.61 (1H, m, N-**C$_\alpha$H**), 2.54 (3H, s, I*-**Me**), 2.40 (3H, s, I*-**Me**), 2.32 (3H, s, I*-**Me**), 2.24 (3H, s, I*-**Me**), 2.06 (3H, s, I*-**Me**), 2.02 (3H, s, I*-**Me**), 1.49 (1H, m, N-**C$_\beta$H**), 1.39 (1H, m, N-**C$_\beta$H**), 1.24 (2H, m, N-**C$_\gamma$H$_2$**), 0.85 (3H, t, N-**C$_\delta$H$_3$**, $^3J_{H\text{-}H}$ = 7.4 Hz), 0.57 (3H, s, Si-**Me**) and 0.40 (3H, s, Si-**Me**).

^{13}C{^{1}H} NMR (C_6D_6, 125.7 MHz, 298 K): δ (ppm) 146.5 (**I***), 140.2 (**I***), 137.3 (**I***), 135.9 (**I***), 131.5 (**I***), 131.1 (**I***), 130.8 (**I***), 129.8 (**I***), 94.4 (Si-**I***), 55.7 (N-**C$_\alpha$**), 34.7 (N-**C$_\beta$**), 21.1 (I*-**Me**), 20.9 (N-**C$_\gamma$**), 17.2 (I*-**Me**), 17.0 (I*-**Me**), 16.9 (I*-**Me**), 16.8 (I*-**Me**), 16.5 (I*-**Me**), 14.1 (N-**C$_\delta$**), 5.9 (Si-**Me**) and 3.4 (Si-**Me**).

CHN Analysis (%): Expected: C 56.51, H 7.45, N 3.14. Found: C 56.28, H 7.47, N 3.11.

IR (KBr) (cm^{-1}): 3441 (b), 2944 (b), 1626, 1451, 1390, 1247, 1102, 1026 and 920.

^{Me2}SB($^{4\text{-}n Bu C_6H_4}$N,I*)TiCl$_2$. Red solid precipitated at −32 °C in 24% yield (0.28 g, 0.51 mmol).

^{1}H NMR (C_6D_6, 499.9 MHz, 298 K): δ (ppm) 7.25 (2H, d, Ph-**H$_{meta}$**, $^3J_{H\text{-}H}$ = 8.4 Hz), 7.03 (2H, d, Ph-**H$_{ortho}$**, $^3J_{H\text{-}H}$ = 8.4 Hz), 2.56 (3H, s, I*-**Me**), 2.40 (2H, t, N-**C$_\alpha$H$_2$**, $^3J_{H\text{-}H}$ = 7.7 Hz), 2.39 (3H, s, I*-**Me**), 2.31 (3H, s, I*-**Me**), 2.30 (3H, s, I*-**Me**), 2.07 (3H, s,

I*-**Me**), 2.04 (3H, s, I*-**Me**), 1.42 (2H, m, N-$\mathbf{C_\beta H_2}$), 1.19 (2H, m, N-$\mathbf{C_\gamma H_2}$), 0.80 (3H, t, N-$\mathbf{C_\delta H_3}$, $^3J_{H\text{-}H}$ = 7.3 Hz), 0.74 (3H, s, Si-**Me**) and 0.48 (3H, s, Si-**Me**).

^{13}C{^{1}H} NMR (C_6D_6, 125.7 MHz, 298 K): δ (ppm) 151.1 (Ph$\mathbf{C_{ipso}}$), 147.3 (**I***), 140.6 (**I***), 139.2 (Ph$\mathbf{C_{para}}$), 138.0 (**I***), 136.6 (**I***), 133.1 (**I***), 132.1 (**I***), 131.6 (**I***), 130.4 (**I***), 129.2 (Ph$\mathbf{C_{ortho}}$), 119.9 (Ph$\mathbf{C_{meta}}$), 98.2 (Si-**I***), 35.4 (N-$\mathbf{C_\alpha}$), 34.0 (N-$\mathbf{C_\beta}$), 22.7 (N-$\mathbf{C_\gamma}$), 21.2 (I*-**Me**), 17.1 (I*-**Me**), 17.0 (I*-**Me**), 17.0 (I*-**Me**), 16.6 (I*-**Me**), 14.3 (I*-**Me**), 14.2 (N-$\mathbf{C_\delta}$), 6.0 (Si-**Me**) and 3.9 (Si-**Me**).

CHN Analysis (%): Expected: C 62.07, H 7.14, N 2.68. Found: C 61.92, H 7.19, N 2.85.

IR (KBr) (cm^{-1}): 3417 (b), 2942 (b), 1618, 1506, 1442, 1372, 1244, 891, 836, 724 and 596.

$^{Me}_2$SB($^{4\text{-}t\text{Bu}C_6H_4}$N,I*)TiCl$_2$. Red crystals evolved at −32 °C in 28% yield (0.36 g, 0.68 mmol).

^{1}H NMR (C_6D_6, 499.9 MHz, 298 K): δ (ppm) 7.27 (2H, d, Ph-$\mathbf{H_{ortho}}$, $^3J_{H\text{-}H}$ = 9.2 Hz), 7.21 (2H, d, Ph-$\mathbf{H_{meta}}$, $^3J_{H\text{-}H}$ = 9.2 Hz), 2.56 (3H, s, I*-**Me**), 2.39 (3H, s, I*-**Me**), 2.31 (3H, s, I*-**Me**), 2.30 (3H, s, I*-**Me**), 2.08 (3H, s, I*-**Me**), 2.03 (3H, s, I*-**Me**), 1.17 (9H, s, Ph-^{t}**Bu**), 0.77 (3H, s, Si-**Me**) and 0.48 (3H, s, Si-**Me**).

^{13}C{^{1}H} NMR (C_6D_6, 125.7 MHz, 298 K): δ (ppm) 150.8 (Ph$\mathbf{C_{ipso}}$), 147.3 (Ph$\mathbf{C_{para}}$), 147.2 (**I***), 140.6 (**I***), 138.0 (**I***), 136.6 (**I***), 133.2 (**I***), 132.1 (**I***), 131.7 (**I***), 130.4 (**I***), 126.0 (Ph$\mathbf{C_{ortho}}$), 119.5 (Ph$\mathbf{C_{meta}}$), 98.3 (Si-**I***), 34.4 (**C**Me$_3$), 31.5 (C**Me$_3$**), 21.2 (I*-**Me**), 17.3 (I*-**Me**), 17.1 (I*-**Me**), 17.0 (I*-**Me**), 17.0 (I*-**Me**), 16.6 (I*-**Me**), 6.1 (Si-**Me**) and 3.9 (Si-**Me**).

CHN Analysis (%): Expected: C 62.07, H 7.14, N 2.68. Found: C 61.83, H 7.23, N 2.79.

IR (KBr) (cm^{-1}): 3414 (b), 2945 (b), 1690, 1617, 1462, 1392, 1258, 1102, 1023, 904 and 810.

^{Me2}SB(^{Ph}N,I*)TiCl$_2$. Red solid precipitated at −32 °C in 13% yield (0.17 g, 0.46 mmol).

^{1}H NMR (C_6D_6, 499.9 MHz, 298 K): δ (ppm) 7.26 (2H, d, Ph-**H$_{ortho}$**, $^3J_{H-H}$ = 7.7 Hz), 7.13 (2H, m, Ph-**H$_{meta}$**), 6.83 (1H, t, Ph-**H$_{para}$**, $^3J_{H-H}$ = 7.4 Hz), 2.55 (3H, s, I*-**Me**), 2.38 (3H, s, I*-**Me**), 2.29 (3H, s, I*-**Me**), 2.28 (3H, s, I*-**Me**), 2.07 (3H, s, I*-**Me**), 2.03 (3H, s, I*-**Me**), 0.70 (3H, s, Si-**Me**) and 0.44 (3H, s, Si-**Me**).

^{13}C{^{1}H} NMR (C_6D_6, 125.7 MHz, 298 K): δ (ppm) 153.0 (**I***), 147.5 (**I***), 140.7 (**I***), 138.1 (**I***), 136.7 (**I***), 133.2 (**I***), 132.1 (**I***), 131.6 (**I***), 130.4 (**I***), 129.2 (Ph-**C$_{meta}$**), 124.6 (Ph-**C$_{para}$**), 120.1 (Ph-**C$_{ortho}$**), 98.4 (Si-**I***), 21.1 (I*-**Me**), 17.3 (I*-**Me**), 17.1 (I*-**Me**), 17.0 (I*-**Me**), 17.0 (I*-**Me**), 16.6 (I*-**Me**), 5.9 (Si-**Me**) and 3.9 (Si-**Me**). Ph-**C$_{ipso}$** not observed.

CHN Analysis (%): Expected: C 59.24, H 6.27, N 3.00. Found: C 59.31, H 6.32, N 2.94.

IR (KBr) (cm^{-1}): 3394 (b), 2935 (b), 1946, 1696, 1576, 1492, 1458, 1247, 1119, 1022, 895 and 778.

7.2.1.11 Synthesis of ^{Me2}SB(^{tBu}N,$^{3\text{-}Et}$I*)TiCl$_2$

^{Me2}SB(^{tBu}N,$^{3\text{-}Et}$I*)Li$_2$.1.5THF (0.76 g, 1.64 mmol) was mixed with an equimolar amount of TiCl$_4$.2THF (0.63 g, 1.64 mmol) and cooled to 5 °C. The mixture was dissolved in benzene, allowed to warm to 23 °C and stirred for 18 hours resulting in a dark red solution. The volatiles were removed under vacuum, and the product extracted in pentane as a dark red solution. The solution was concentrated and ^{Me2}SB(^{tBu}N,$^{3\text{-}Et}$I*)TiCl$_2$ precipitated at −20 °C as a dark red solid in a yield of 25% (0.19 g, 0.41 mmol).

^{1}H NMR (C_6D_6, 298 K, 400.2 MHz): δ (ppm) 3.34 (1H, m, I*-**CH_2**-CH_3, $^{3}J_{H\text{-}H}$ = 7.6 Hz), 3.03 (1H, m, I*-**CH_2**-CH_3, $^{3}J_{H\text{-}H}$ = 7.6 Hz), 2.45 (3H, s, I*-**Me**), 2.35 (3H, s, I*-**Me**), 2.21 (3H, s, I*-**Me**), 2.08 (3H, s, I*-**Me**), 2.03 (3H, s, I*-**Me**), 1.41 (9H, s, N-***t***Bu**), 0.92 (3H, dd, I*-CH_2-**CH_3**, $^{3}J_{H\text{-}H}$ = 7.6 Hz), 0.63 (3H, s, Si-**Me**) and 0.59 (3H, s, Si-**Me**).

^{13}C{^{1}H} NMR (C_6D_6, 298 K, 125.7 MHz): δ (ppm) 145.7 (**I***), 139.7 (**I***), 137.7 (**I***), 136.4 (**I***), 131.6 (**I***), 131.4 (**I***), 130.4 (**I***), 129.3 (**I***), 96.6 (**I***-Si), 62.0 (N-**C**Me_3), 32.8 (N-C**Me_3**), 23.7 (I*-**CH_2**-CH_3), 21.7 (I*-**Me**), 17.3 (I*-**Me**), 16.7 (I*-**Me**), 16.4 (I*-**Me**), 16.2 (I*-**Me**), 15.0 (I*-CH_2-**CH_3**), 8.2 (Si-**Me**) and 7.7 (Si-**Me**).

CHN Analysis (%): Expected: C 57.40, H 7.66, N 3.04. Found: C 57.56, H 7.73, N 3.16.

IR (KBr) (cm^{-1}): 3440 (b), 2965 (b), 1618, 1463, 1379, 1212, 1029, 842 and 749.

^{7}Li NMR (C_6D_5N, 298 K, 155.5 MHz): δ (ppm) 2.21.

7.2.1.12 Synthesis of ^{Me,Pr}SB(^{tBu}N,I*)$TiCl_2$

^{Me,Pr}SB($^{t\text{Bu}}$N,I*)Li_2.1.2THF (0.88 g, 1.93 mmol) was mixed with an equimolar amount of $TiCl_4$.2THF (0.64 g, 1.93 mmol). The mixture was cooled to 5 °C and dissolved in benzene (30 mL) resulting in a dark red solution. The reaction mixture was allowed to warm to 23 °C and stirred for 18 hours. The volatiles were removed under vacuum, followed by extraction into pentane to yield a dark red solution. The volatiles were removed under vacuum and the residue was dissolved in trimethylsilylether (15 mL), concentrated and stored at −20 °C to afford ^{Me,Pr}SB($^{t\text{Bu}}$N,I*)$TiCl_2$ as a dark red solid which was isolated in a 20% yield (0.18 g, 0.38 mmol).

^{1}H NMR (C_6D_6, 298 K, 499.9 MHz): δ (ppm) 2.56 (3H, s, I*-**Me**), 2.55 (3H, s, I*-**Me**), 2.44 (3H, s, I*-**Me**), 2.40 (3H, s, I*-**Me**), 2.39 (3H, s, I*-**Me**), 2.36 (3H, s, I*-**Me**), 2.19 (3H, s, I*-**Me**), 2.17 (3H, s, I*-**Me**), 2.08 (3H, s, I*-**Me**), 2.07 (3H, s, I*-**Me**), 2.06 (3H,

s, I*-**Me**) and 2.02 (3H, s, I*-**Me**). **Major Isomer (57%):** δ (ppm) 1.74 (2H, m, Si-CH_2-**CH_2**-CH_3), 1.42 (9H, s, N-***t*Bu**), 1.24 (2H, t, Si-**CH_2**-CH_2-CH_3, $^3J_{H-H}$ = 5.6 Hz), 1.04 (3H, t, Si-CH_2-CH_2-**CH_3**, $^3J_{H-H}$ = 7.2 Hz) and 0.63 (3H, s, Si-**Me**). **Minor isomer (43%):** δ (ppm) 1.52 (2H, m, Si-CH_2-**CH_2**-CH_3), 1.42 (9H, s, N-***t*Bu**), 1.10 (3H, t, Si-CH_2-CH_2-**CH_3**, $^3J_{H-H}$ = 7.2 Hz), 0.89 (2H, t, Si-**CH_2**-CH_2-CH_3, $^3J_{H-H}$ = 6.6 Hz) and 0.58 (3H, s, Si-**Me**).

$^{13}C\{^1H\}$ NMR (C_6D_6, 298 K, 125.7 MHz): δ (ppm) 146.4 (**I***), 146.0 (**I***), 140.7 (**I***), 138.0 (**I***), 137.0 (**I***), 136.3 (**I***), 136.2 (**I***), 134.7 (**I***), 134.7 (**I***), 134.0 (**I***), 131.9 (**I***), 131.6 (**I***), 131.5 (**I***), 131.5 (**I***), 131.4 (**I***), 130.5 (**I***), 97.6 (**I***-Si), 96.3 (**I***-Si), 32.9 (N-***t*Bu**), 32.8 (N-***t*Bu**), 21.5 (I*-**Me**), 19.9 (I*-**Me**), 17.4 (I*-**Me**), 17.3 (I*-**Me**), 17.1 (I*-**Me**), 17.0 (I*-**Me**), 17.0 (I*-**Me**), 16.9 (I*-**Me**), 16.7 (I*-**Me**), 16.6 (I*-**Me**), 16.5 (I*-**Me**) and 16.5 (I*-**Me**) **Major isomer (57%):** δ (ppm) 24.9 (Si-CH_2-**CH_2**-CH_3), 18.4 (Si-CH_2-CH_2-**CH_3**), 18.0 (Si-**CH_2**-CH_2-CH_3) and 6.5 (Si-**Me**). **Minor isomer (43%):** δ (ppm) 24.5 (Si-CH_2-**CH_2**-CH_3), 18.4 (Si-CH_2-CH_2-**CH_3**), 18.0 (Si-**CH_2**-CH_2-CH_3) and 5.8 (Si-**Me**).

CHN Analysis (%): Expected: C 58.23, H 7.86, N 2.95. Found: C 58.40, H 8.12, N 2.86.

IR (KBr) (cm^{-1}): 3412 (b), 2941 (b), 2596, 2499, 2043, 1618, 1452, 909, 783.

7.2.1.13 Synthesis of ^{Me2}SB(^{tBu}N,I*)$ZrCl_2$

^{Me2}SB($^{t\text{Bu}}$N,I*)Li_2.1.25THF (1.20 g, 2.78 mmol) was mixed with an equimolar amount of $ZrCl_4$ (0.65 g, 2.78 mmol). The mixture was cooled to 5 °C and dissolved in benzene (30 mL) resulting in an orange/brown solution. The reaction mixture was allowed to warm to 23 °C and stirred for 18 hours. The volatiles were removed under vacuum and the product extracted in pentane (4 × 25 mL) as a dark orange solution. The solution was

concentrated and stored at −20 °C to afford ^{Me2}SB(^{tBu}N,I*)ZrCl$_2$ as an orange solid which was isolated in 24% yield (0.33 g, 0.67 mmol).

^{1}H NMR (C$_6$D$_6$, 499.9 MHz): δ (ppm) 2.55 (3H, s, I*-**Me**), 2.42 (6H, s, I*-**Me**), 2.20 (3H, s, I*-**Me**), 2.08 (3H, s, I*-**Me**), 2.04 (3H, s, I*-**Me**), 1.31 (9H, s, N-^{t}**Bu**) and 0.69 (3H, s, Si-**Me**), 0.60 (3H, s, Si-**Me**).

^{13}C{^{1}H} NMR (C$_6$D$_6$, 125.7 MHz): δ (ppm) 143.2 (**I***), 137.0 (**I***), 135.7 (**I***), 135.0 (**I***), 130.1 (**I***), 129.1 (**I***), 128.4 (**I***), 124.1 (**I***), 88.7 (**I***-Si), 56.7 (N-**C**Me$_3$), 33.3 (N-C**Me$_3$**), 21.4 (I*-**Me**), 17.3 (I*-**Me**), 17.2 (I*-**Me**), 16.5 (I*-**Me**), 16.3 (I*-**Me**), 15.9 (I*-**Me**), 10.0 (Si-**Me**) and 9.0 (Si-**Me**).

CHN Analysis (%): Expected: C 51.29, H 7.17, N 2.85. Found: C 51.70, H 6.82, N 2.89.

IR (KBr) (cm^{-1}): 3435 (b), 2962 (b), 1611, 1449, 1376, 1179, 1089, 1010 and 774.

7.2.1.14 Synthesis of ^{Me2}SB(^{tBu}N,I*)Ti(Cl)CH$_2$SiMe$_3$

^{Me2}SB(^{tBu}N,I*)TiCl$_2$ (0.20 g, 0.45 mmol) was dissolved in benzene (5 mL) and cooled to 5 ºC. A solution of 1 equivalent of LiCH$_2$SiMe$_3$ (42.2 mg, 0.45 mmol) in benzene (~5 mL) was added dropwise over 45 minutes. The orange reaction mixture was allowed to warm to room temperature and stirred for 20 hours. The resultant mixture was filtered, dried *in vacuo,* and the product extracted in pentane (3 × 5 mL). The solution was left at −30 ºC (18 hours) affording ^{Me2}SB(^{tBu}N,I*)Ti(Cl)CH$_2$SiMe$_3$ as a bright orange precipitate in a 43% yield (96 mg, 0.19 mmol).

^{1}H NMR (C$_6$D$_6$, 298 K, 400.2 MHz): δ (ppm) 2.54 (3H, s, I*-**Me**), 2.53 (2H, s, I*-**Me**), 2.26 (3H, s, I*-**Me**), 2.18 (3H, s, I*-**Me**), 2.09 (3H, s, I*-**Me**), 2.07 (3H, s, I*-**Me**), 1.57 (1H, d, Ti-**CH$_2$**-Si, $^2J_{HH}$ = 11.9 Hz), 1.51 (9H, s, N-^{t}**Bu**), 0.63 (3H, s, Si-**Me**), 0.51 (3H, s, Si-**Me**), 0.10 (9H, s, CH$_2$Si-**Me$_3$**) and −0.97 (1H, d, Ti-**CH$_2$**-Si, $^2J_{HH}$ = 11.9 Hz).

$^{13}C\{^{1}H\}$ NMR (C_6D_6, 298 K, 125.7 MHz): δ (ppm) 142.5 (**I***), 137.0 (**I***), 136.0 (**I***), 134.3 (**I***), 132.0 (**I***), 130.9 (**I***), 130.6 (**I***), 95.8 (Si-**I***), 73.1 (Ti-**CH_2**), 60.3 (N-**C**Me_3), 34.0 (N-C**Me_3**), 21.5 (I*-**Me**), 17.8 (I*-**Me**), 17.1 (I*-**Me**), 16.6 (I*-**Me**), 16.6 (I*-**Me**), 16.6 (I*-**Me**), 8.5 (Si-**Me**), 7.9 (Si-**Me**) and 2.5 (Si-**Me_3**). One I* resonance is not observed and is likely to be obscured by the solvent signals.

^{29}Si NMR (HMBC ^{1}H-observed, C_6D_6, 499.9 MHz, 298 K): δ (ppm) −22.0 (CH_2**Si**Me_3) and 2.2 (**Si**Me_2).

CHN Analysis (%): Expected: C 60.28, H 9.01, N 2.81. Found: C 60.14, H 9.01, N 2.83.

IR (KBr) (cm^{-1}): 3450 (b), 2953 (b), 1630, 1456, 1387, 1254, 1206, 1164, 1000 and 837.

7.2.2 Synthesis of $^{Me,Allyl}SB(^{tBu}N,I^*)H_2$

7.2.2.1 Synthesis of I*Si(Me,Allyl)Cl

$I^{\#}Li$ (5.00 g, 24.25 mmol) was dissolved in THF (25 mL) and added dropwise over 30 minutes to a solution of THF (30 mL) and 1.5 equivalents of $SiMeAllylCl_2$ (5.30 mL, 36.38 mmol) at 23 °C. The reaction mixture was stirred for 3 hours and the THF then was removed under vacuum. The product was extracted in pentane (4 × 25 mL) as a pale orange solution, the solution was concentrated and I*Si(Me,Allyl)Cl precipitated as a pale orange solid at −20 °C in a 69% yield (5.30 g, 16.73 mmol) as two isomers.

^{1}H NMR (C_6D_6, 298 K, 400.2 MHz): δ (ppm) **Major Isomer (59%)** 5.48 (1H, m, Si-CH_2-**C**H=CH_2), 4.79 (2H, m, Si-CH_2-CH=**CH_2**), 1.49 (1H, m, Si-**CH_2**-CH=CH_2), 1.28 (1H, m, Si-**CH_2**-CH=CH_2) and 0.25 (3H, s, Si-**Me**). **Minor Isomer (41%)** 5.61 (1H, m, Si-CH_2-**C**H=CH_2), 4.79 (2H, m, Si-CH_2-CH=**CH_2**), 1.71 (1H, m, Si-**CH_2**-CH=CH_2), 1.53 (1H, m, Si-**CH_2**-CH=CH_2) and 0.04 (3H, s, Si-**Me**).

I*-**Me** resonances at 2.42, 2.42, 2.18, 2.15, 2.15, 2.15, 2.14, 2.12, 2.11, 2.11, 2.09 and 2.05 ppm cannot be assigned specifically to either isomer.

7.2.2.2 Synthesis of ^{Me,Allyl}SB(^{tBu}N,I*)H$_2$

I*Si(Me,Allyl)Cl (1.04 g, 3.26 mmol) was added to 1.1 equivalents of LiN(H)^{t}Bu (3.59 mmol, 0.28 g) and the mixture was cooled to 5 °C. THF (30 mL) was added and the reaction mixture was allowed to warm to 23 °C and was stirred for 2 hours. The THF was removed under vacuum and the product extracted in pentane (4 × 25 mL) as a pale yellow solution. The mixture was dried *in vacuo* to yield ^{Me,Allyl}SB(^{tBu}N,I*)H$_2$ as a dark yellow oil in a quantitative yield.

^{1}H NMR (C$_6$D$_6$, 298 K, 400.2 MHz): δ (ppm) 5.66 (1H, m, Si-CH$_2$-**CH**=CH$_2$), 5.66 (1H, m, Si-CH$_2$-**CH**=CH$_2$), 4.87 (2H, m, Si-CH$_2$-CH=**CH$_2$**), 4.87 (2H, m, Si-CH$_2$-CH=**CH$_2$**), 3.48 (1H, s I*-**H**), 3.44 (1H, s I*-**H**), 2.51 (3H, s, I*-**Me**), 2.51 (3H, s, I*-**Me**), 2.31 (3H, s, I*-**Me**), 2.29 (3H, s, I*-**Me**), 2.27 (3H, s, I*-**Me**), 2.21 (3H, s, I*-**Me**), 2.20 (3H, s, I*-**Me**), 2.18 (3H, s, I*-**Me**), 2.17 (3H, s, I*-**Me**), 2.14 (3H, s, I*-**Me**), 2.08 (3H, s, I*-**Me**), 1.68 (1H, m, Si-**CH$_2$**-CH=CH$_2$), 1.56 (1H, m, Si-**CH$_2$**-CH=CH$_2$), 1.29 (1H, m, Si-**CH$_2$**-CH=CH$_2$), 1.21(1H, m, Si-**CH$_2$**-CH=CH$_2$), 1.11 (9H, s, N-**^{t}Bu**), 1.04 (9H, s, N-**^{t}Bu**), 0.22 (3H, s, Si-**Me**) and 0.07 (3H, s, Si-**Me**).

7.2.3 Synthesis of ^{Ph}BB(^{tBu}N,I*)H$_2$

7.2.3.1 Synthesis of I*BPhCl

I$^{\#}$Li (10.31 g, 50.0 mmol) was slurried in Et$_2$O (50 mL) for 18 hours before being added dropwise *via* a teflon canula to 1.5 equivalents of BPhCl$_2$ (9.8 mL, 75.0 mmol) in Et$_2$O (15 mL). The reaction mixture was stirred for 4 hours and then dried under vacuum. The product was extracted in pentane (4 × 25 mL) as a pale yellow solution, the solution was reduced and the product precipitated at −20 °C in a 17% yield (2.71 g, 8.40 mmol).

^{1}H NMR (C_6D_6, 298 K, 499.9 MHz): δ (ppm) 8.05 (2H, d, B-Ph**H$_{ortho}$** $^{3}J_{H-H}$ = 5.8 Hz), 7.16 (1H, m, B-Ph**H$_{para}$**), 7.09 (2H, m, B-Ph**H$_{meta}$**), 4.36 (1H, s, I*-**H**), 2.50 (3H, s, I*-**Me**), 2.23 (3H, s, I*-**Me**), 2.17 (3H, s, I*-**Me**), 2.09 (3H, s, I*-**Me**), 2.08 (3H, s, I*-**Me**) and 1.87 (3H, s, I*-**Me**).

^{11}B{^{1}H} NMR (C_6D_6, 298 K, 128.4 MHz): δ (ppm) 69.0.

^{13}C{^{1}H} NMR (C_6D_6, 298 K, 125.7 MHz): δ (ppm) 144.4 (**I***), 143.1 (**I***), 137.2 (**I***), 137.0 (**I***), 136.4 (B-**Ph$_{ortho}$**), 134.5 (B-**Ph$_{para}$**), 133.7 (**I***), 131.0 (**I***), 128.5 (B-**Ph$_{meta}$**), 127.6 (**I***), 126.8 (**I***), 54.1 (**I***-B), 18.5 (I*-**Me**), 16.5 (I*-**Me**), 16.5 (I*-**Me**), 16.3 (I*-**Me**), 15.7 (I*-**Me**) and 14.6 (I*-**Me**).

7.2.3.2 Synthesis of ^{Ph}BB(^{tBu}N,I*)H$_2$

I*BPhCl (1.55 g, 4.42 mmol) was mixed with 1.05 equivalents of LiN(H)^{t}Bu (0.37 g, 4.64 mmol) in a Schlenk tube and cooled to 5 °C. The mixture was dissolved in Et_2O (30 mL) and allowed to warm to room temperature. The mixture was stirred for 55 hours and then dried under vacuum to give a yellow solid. The product was extracted in pentane (2 × 30 mL) as a pale yellow solution, which was concentrated and the product precipitated as an off white solid at −20 °C in a 30% yield (0.47 g, 1.31 mmol).

^{1}H NMR (C_6D_6, 298 K, 499.9 MHz): δ (ppm) 7.20 (2H, m, B-Ph**H**$_{ortho}$), 7.07 (2H, m, B-Ph**H**$_{meta}$), 7.01 (1H, m, B-Ph**H$_{para}$**), 3.22 (1H, s, I*-**H**), 2.44 (3H, s, I*-**Me**), 2.40 (3H, s, I*-**Me**), 2.28 (3H, s, I*-**Me**), 2.20 (3H, s, I*-**Me**), 2.15 (3H, s, I*-**Me**), 2.04 (3H, s, I*-**Me**), 1.29 (1H, s, N-**H**) and 0.89 (9H, s, N-^{t}**Bu**).

^{11}B{^{1}H} NMR (C_6D_6, 298 K, 128.4 MHz): δ (ppm) 43.5.

^{13}C{^{1}H} NMR (C_6D_6, 298 K, 125.7 MHz): δ (ppm) 143.9 (**I***), 142.8 (**I***), 139.5 (**I***), 133.2 (B-**Ph$_{ipso}$**), 132.4 (**I***), 131.0 (B-**Ph$_{ortho}$**), 129.7 (**I***), 127.5 (**I***), 127.4 (**I***), 127.1

(B-**Ph$_{para}$**), 126.9 (B-**Ph$_{meta}$**), 126.1 (**I***), 55.3 (**I***-B), 33.4 (N-**C**Me$_3$), 33.0 (N-C**Me$_3$**), 17.9 (I*-**Me**), 16.5 (I*-**Me**), 16.5 (I*-**Me**), 16.2 (I*-**Me**), 15.5 (I*-**Me**) and 14.8 (I*-**Me**).

7.2.4 Synthesis of sMAO supported complexes

0.019 mmol of complex and 200 equivalents of sMAO (250 mg, 3.78 mmol) were mixed in toluene (30 mL) at 25 °C, warmed to 60 °C and regularly swirled for 1 hour. The product was allowed to settle and the supernatant was decanted. The brown solid product was then dried under vacuum at room temperature.

sMAO-^{Me_2}SB(^{tBu}N,I*)TiCl$_2$. Isolated in 78% yield (201 mg).

^{13}C CP-MAS NMR (100.6 MHz): δ (ppm) −8 (**Me-sMAO**), 16 (I*-**Me**), 20 (I*-**Me**), 33 (N-*t*-**Bu**), 128 (**sMAO**), 132 (**I***), 136 (**I***) and 177 (**C=O-sMAO**).

^{29}Si CP-MAS NMR (79.4 MHz): δ (ppm) −19.

^{27}Al DP-MAS hahnecho NMR (104.2 MHz): δ (ppm) 329, 185, −95 and −247.

IR (KBr) (cm^{-1}): 3590 (b), 2957, 1560, 1384, 1261, 1219, 1022, 803 and 714.

sMAO-^{Me_2}SB(^{tBu}N,I*)TiCl$_2$ ([Al]$_0$:[Ti]$_0$ =100:1). Isolated in 85% yield (453 mg).

^{13}C CP-MAS NMR (100.6 MHz): δ (ppm) −8 (**Me-sMAO**), 16 (I*-**Me**), 20 (I*-**Me**), 51 (Ti-**Me**) 33 (N-*t*-**Bu**), 128 (**sMAO**), 131 (**I***), 136 (**I***) and 177 (**C=O-sMAO**).

sMAO-^{Me_2}SB(^{iPr}N,I*)TiCl$_2$. Isolated in 72% yield (187 mg).

sMAO-^{Me_2}SB($^{4\text{-}tBuC_6H_4}$N,I*)TiCl$_2$. Isolated in 87% yield (225 mg).

sMAO-^{Me_2}SB($^{4\text{-}nBuC_6H_4}$N,I*)TiCl$_2$. Isolated in 82% yield (212 mg).

sMAO-^{Me_2}SB($^{n Bu}$N,I*)TiCl$_2$. Isolated in 80% yield (207 mg).

sMAO-^{Me_2}SB(^{Ph}N,I*)TiCl$_2$. Isolated in 85% yield (221 mg).

^{13}C CP-MAS NMR (100.6 MHz): δ (ppm) −8 (**Me-sMAO**), 17 (I*-**Me**), 51 (Ti-**Me**), 128 (**sMAO**), 132 (**I*/Ph**), 136 (**I*/Ph**) and 177 (**C=O-sMAO**).

^{29}Si CP-MAS NMR (79.4 MHz): δ (ppm) 6, 2, −4, −16 and −98.

^{27}Al DP-MAS hahnecho NMR (104.2 MHz): δ (ppm) −43.

sMAO-^{Me_2}SB($^{t Bu}$N,I*)Ti(CH$_2$Ph)$_2$. Isolated in 77% yield.

^{13}C CP-MAS NMR (100.6 MHz): δ (ppm) −7 (**Me-sMAO**), 17 (I*-**Me**), 21 (I*-**Me**), 35 (N-^{t}**Bu**), 53 (Ti-**Me**), 129 (**sMAO**), 132 (**I*/Ph**), 138 (**I*/Ph**) and 178 (**C=O-sMAO**).

^{29}Si CP-MAS NMR (79.4 MHz): δ (ppm) −18.

^{27}Al DP-MAS hahnecho NMR (104.2 MHz): δ (ppm) 349, 211, 79, −85 and −243.

sMAO-^{Me_2}SB($^{t Bu}$N,I*)TiMe$_2$. Isolated in 75% yield.

^{13}C CP-MAS NMR (100.6 MHz): δ (ppm) −7 (**Me-sMAO**), 17 (I*-**Me**), 21 (I*-**Me**), 35 (I*-**Me**), 129 (**sMAO**), 133 (**I***), 138 (**I***) and 178 (**C=O-sMAO**).

^{29}Si CP-MAS NMR (79.4 MHz): δ (ppm) −43.

^{27}Al DP-MAS hahnecho NMR (104.2 MHz): δ (ppm) 346, 208, 81, −84 and −241.

sMAO-^{Me_2}SB($^{t Bu}$N,I*)Ti(CH$_2$SiMe$_3$)$_2$. Isolated in 71% yield.

^{13}C CP-MAS NMR (100.6 MHz): δ (ppm) −7 (**Me-sMAO**), 17 (I*-**Me**), 21 (I*-**Me**), 35 (N-^{t}**Bu**), 53 (Ti-**Me**), 129 (**sMAO**), 133 (**I***), 137 (**I***) and 178 (**C=O-sMAO**).

^{29}Si CP-MAS NMR (79.4 MHz): δ (ppm) 0 and −18.

^{27}Al DP-MAS hahnecho NMR (104.2 MHz): δ (ppm) 344, 205, 80, −85 and −242.

sMAO-^{Me_2}SB(^{tBu}N,I*)Ti(Cl)CH_2SiMe_3. Isolated in 73% yield.

^{13}C CP-MAS NMR (100.6 MHz): δ (ppm) −8 (**Me-sMAO**), 17 (I*-**Me**), 34 (N-^{t}**Bu**), 51 (Ti-**Me**), 128 (**sMAO**), 132 (**I***), 136 (**I***) and 177 (**C=O-sMAO**).

^{29}Si CP-MAS NMR (79.4 MHz): δ (ppm) 0 and −19.

^{27}Al DP-MAS hahnecho NMR (104.2 MHz): δ (ppm) 327, 182, −92 and −249.

sMAO-^{Me_2}SB(^{tBu}N,Cp*)$TiCl_2$. Isolated in 68% yield.

^{13}C CP-MAS NMR (100.6 MHz): δ (ppm) −8 (**Me-sMAO**), 18 (Cp*-**Me**), 32 (N-^{t}**Bu**), 51 (Ti-**Me**), 128 (**sMAO**), 132 (**Cp***), 135 (**Cp***) and 179 (**C=O-sMAO**).

^{29}Si CP-MAS NMR (79.4 MHz): δ (ppm) −19.

^{27}Al DP-MAS hahnecho NMR (104.2 MHz): δ (ppm) 326, 184, −93 and −249.

sMAO-^{Me_2}SB(^{tBu}N,$^{3\text{-}Et}$I*)$TiCl_2$. Isolated in 77% yield.

^{13}C CP-MAS NMR (100.6 MHz): δ (ppm) −8 (**Me-sMAO**), 17 (I*-**Me/Et**), 22 (I*-**Me/Et**), 32 (N-^{t}**Bu**), 51 (**Ti-Me**), 128 (**sMAO**), 131 (**I***), 136 (**I***) and 177 (**C=O-sMAO**).

^{29}Si CP-MAS NMR (79.4 MHz): δ (ppm) −20.

^{27}Al DP-MAS hahnecho NMR (104.2 MHz): δ (ppm) 327, 183, −92 and −249.

IR (KBr) (cm^{-1}): 3616 (b), 2950, 1557, 1401, 1218 and 677.

sMAO-^{Me,Pr}SB(^{tBu}N,I*)TiCl$_2$. Isolated in 85% yield.

sMAO-^{Me_2}SB(^{tBu}N,I*)ZrCl$_2$. Isolated in 81% yield as a pale yellow solid.

7.2.5 Synthesis of LDHMAO and SSMAO supported complexes

0.019 mmol of complex and 200 Al_{MAO} equivalents of LDHMAO or SSMAO (500 mg, 3.78 mmol) were mixed in toluene (30 mL) at 25 °C, warmed to 60 °C and regularly swirled for 1 hour. The product was allowed to settle and the supernatant was decanted. The pale red/brown solid product was then dried under vacuum at room temperature.

LDHMAO-^{Me_2}SB(^{tBu}N,I*)TiCl$_2$. Isolated in 90% yield.

^{13}C CP-MAS NMR (100.6 MHz): δ (ppm) −9 (**Me from MAO in LDHMAO**), 14 (I*-**Me**), 19 (I*-**Me**), 30 (I*-**Me**), 32 (N-^{t}**Bu**), 129 (**I***) and 166 (**CO_3 in LDHMAO**).

^{27}Al DP-MAS NMR (104.2 MHz): δ (ppm) 158, 70, −10 and −132.

SSMAO-^{Me_2}SB(^{tBu}N,I*)TiCl$_2$. Isolated in 76% yield.

^{13}C CP-MAS NMR (100.6 MHz): δ (ppm) −8 (**Me from MAO in SSMAO**) and 51.

^{29}Si CP-MAS NMR (79.4 MHz): δ (ppm) −102.

^{27}Al DP-MAS hahnecho NMR (104.2 MHz): δ (ppm) 332, 191, −93 and −252.

LDHMAO-^{Me_2}SB(^{tBu}N,$^{3\text{-}Et}$I*)TiCl$_2$. Isolated in 92% yield.

^{13}C CP-MAS NMR (100.6 MHz): δ (ppm) −9 (**Me from MAO in LDHMAO**), 20 (I*-**Me/Et**), 22 (I*-**Me/Et**), 32 (N-^{t}**Bu**), 128 (**I***) and 165 (**CO_3 in LDHMAO**).

^{29}Si CP-MAS NMR (79.4 MHz): δ (ppm) −23.

^{27}Al DP-MAS hahnecho NMR (104.2 MHz): δ (ppm) 319, 172, −116 and −308.

SSMAO-^{Me_2}SB($^{t Bu}$N,$^{3\text{-}Et}$I*)TiCl$_2$. Isolated in 82% yield.

LDHMAO-^{Me,Pr}SB($^{t Bu}$N,I*)TiCl$_2$. Isolated in 87% yield.

^{13}C CP-MAS NMR (100.6 MHz): δ (ppm) −8 (**Me from MAO in LDHMAO**), 17 (I*-**Me**), 19 (I*-**Me**), 21 (I*-**Me**), 32 (N-^{t}**Bu**), 51 (Ti-**Me**), 129 (**I***) and 165 (**CO_3 in LDHMAO**).

^{27}Al DP-MAS NMR (104.2 MHz): δ (ppm) −8.

SSMAO-^{Me,Pr}SB($^{t Bu}$N,I*)TiCl$_2$. Isolated in 76% yield.

LDHMAO-^{Me_2}SB($^{t Bu}$N,I*)Ti(Cl)CH$_2$SiMe$_3$. Isolated in 94% yield.

^{13}C CP-MAS NMR (100.6 MHz): δ (ppm) −8 (**Me from MAO in LDHMAO**), 19 (I*-**Me**), 21 (I*-**Me**), 32 (N-^{t}**Bu**), 52 (Ti-**Me**), 130 (**I***) and 165 (**CO_3 in LDHMAO**).

^{27}Al DP-MAS NMR (104.2 MHz): δ (ppm) −8.

^{29}Si CP-MAS NMR (79.4 MHz): δ (ppm) 0 and −79.

SSMAO-^{Me_2}SB($^{t Bu}$N,I*)Ti(Cl)CH$_2$SiMe$_3$. Isolated in 73% yield.

7.3 Experimental details for Chapter 3

7.3.1 Slurry-phase polymerisation of ethylene

150 mg of tri*iso*butylaluminium (TiBA) was mixed with 10 mL of hexanes in a 150 mL ampoule. 10 mg of supported catalyst was added, followed by 40 mL of hexanes. The ampoule was allowed to warm to the desired temperature in an oil bath and the headspace degassed, after which it was opened up to 2 bar ethylene while stirring (1000 rpm) and then left under a continuous flow for a specified time. The ampoule was then degassed and the mixture filtered. The polyethylene was then washed with pentane, dried and weighed. All polymerisations were carried out, at least, in duplicate.

7.3.2 Solution-phase polymerisation of ethylene

1000 equivalents of MAO were added to a 150 mL ampoule with 10 mL of hexanes. A stock solution of 5 mg of complex in 10 mL of toluene was prepared and 1 mL of stock solution was added to the ampoule followed by 39 mL of hexanes. The ampoule was allowed to warm to the desired temperature in an oil bath and the headspace degassed, after which it was opened up to 2 bar ethylene while stirring (1000 rpm) and then left under a continuous flow for a specified time. The ampoule was then degassed and the mixture filtered. The polyethylene was then washed with pentane, dried and weighed. All polymerisations were carried out in duplicate.

7.3.3 Larger scale slurry-phase ethylene polymerisation

750 mg of TiBA in 10 mL of hexanes was added to a 500 mL ampoule. 10 mg of supported catalyst was added followed by 240 mL of hexanes. The ampoule was allowed to warm up to the desired temperature in an oil bath and the headspace degassed, after which it was opened up to 2 bar ethylene while stirring (1000 rpm) and then left under a

continuous flow for a specified time. The ampoule was then degassed and the mixture filtered. The polyethylene was then washed with pentane, dried and weighed.

7.3.4 High-throughput ethylene, ethylene/hydrogen and ethylene/1-hexene (co)polymerisation

Polymerisation experiments were undertaken by Dr Alessio Mingione (HTExplore, University of Naples) in a Freeslate Parallel Pressure Reactor platform consisting of 48 reaction cells within a triple MBraun LabMaster Glovebox. The cells (volume ~23 mL, working volume 5 mL) were individually controlled with monitoring of temperature and pressure. Slurry-phase polymerisations were run in a semi continuous mode. Two vortex stir plates fitted with 6 × 8 racks held the catalysts system components (pre-catalyst and scavenger). The injection system consisted of a dual arm robot with specialised needles and injectors. Liquid solvents, diluents and monomers were fed through syringe pumps, with gaseous monomers and diluents fed through direct lines and solenoid valves to individual cells.[8]

Heptane solvent (5 mL) and TiBA scavenger (10 μmol) were added to the reactors *via* robotic syringes which were then heated to 80 °C and pressurised to 8.3 bar with ethylene. When necessary, hydrogen was added to the reaction vessel *via* a 0.8 or 1.6% mixed hydrogen/nitrogen feed. Pre-catalyst (0.075–0.40 mg in a heptane slurry) and 1-hexene (when required) were injected with robotic syringes and chased by heptane solvent. The reactions were run for 1 hour or until a prescribed ethylene uptake was reached (8.3 bar for ethylene homopolymerisation and 5.5 bar for ethylene/1-hexene copolymerisation), following which the reaction was quenched by excess dry air. The polymer samples were transferred to a Genevac EZ-Plus centrifugal evaporator to remove volatiles and then dried under vacuum overnight.

The polymers produced were characterised by $^{13}C\{^{1}H\}$ NMR spectroscopy, high-temperature gel permeation chromatography (GPC) and analytical crystallisation elution fraction (CEF). $^{13}C\{^{1}H\}$ NMR spectra were collected at 393 K in d_2-1,1,2,2-tetrachloroethane on a 400 MHz Bruker Avance III spectrometer equipped with a 5 mm high-temperature cryoprobe and a robotic sample changer. GPC curves were recorded with a FreeSlate Rapid GPC setup, equipped with a set of two mixed-bed Agilent PLgel 10 μm columns and a Polymer Char IR4 detector. CEF curves were collected with a Polymer Char CEF setup, equipped with a 42-well auto sampler, an IR5 detector and a dual-capillary viscometer detector.

7.3.5 Large scale slurry-phase ethylene polymerisation and ethylene/1-hexene copolymerisation

Polymerisations were performed by Mr Thawesak Parawan, Mr Somjet Songnoey or Mr Pongsiri Kaeoyok at SCG Chemicals Co., Ltd. (Rayong, Thailand). A 1 L steel reactor was charged with hexanes (450 mL) and 3 mmol of TiBA scavenger and saturated with 2 bar ethylene gas. 1-hexene was added at an overpressure when required. The reactor was heated to temperature and a mixture of 0.025–0.05 g catalyst in 20 mL hexanes was added and washed in with a further 130 mL hexanes. The ethylene pressure was set at either 6 or 8 bar and the polymerisations run for 1 hour. On completion, the polymer was decanted and dried in an oven overnight.

7.4 Experimental details for Chapter 4

7.4.1 Slurry-phase copolymerisation of ethylene/1-hexene, ethylene/styrene and ethylene/1-octene

150 mg of TiBA was mixed with 10 mL of hexanes in a 150 mL ampoule. 10 mg of supported catalyst was added, followed by 35 mL of hexanes. In a sidearm, the desired amount of comonomer was added in 5 mL of hexanes. The ampoule was allowed to warm to the desired temperature in an oil bath and the headspace degassed, after which it was opened up to 2 bar of ethylene while stirring (1000 rpm) and then left under a continuous flow for a specified time. The ampoule was then degassed and the mixture filtered. The polymer was then washed with pentane, dried and weighed. All polymerisations were carried out, at least, in duplicate.

7.4.2 Solution $^{13}C\{^{1}H\}$ NMR spectra of copolymer

The NMR resonances observed in high temperature NMR spectra of the copolymer produced are shown below as exemplified for sMAO-^{Me_2}SB($^{t Bu}$N,I*)$TiCl_2$.

Ethylene/1-hexene copolymer.

$^{13}C\{^{1}H\}$ NMR (1,1,2,2-$C_2D_2Cl_4$, 125.7 MHz, 393 K): δ (ppm) CγCβCαC$_{BR}$(C4C3C2C1)CαCβCγ), 37.67 (**C$_{BR}$**), 34.01 (**Cα**), 33.61 (**C2**) 29.83 (**Cγ**), 29.33 (**PE chain**), 28.96 (**C4**), 26.68 (**Cβ**), 22.74 (**C2**) and 13.55 (**C1**).

Ethylene/styrene copolymer.

$^{13}C\{^{1}H\}$ NMR (1,1,2,2-$C_2D_2Cl_4$, 125.7 MHz, 393 K): δ (ppm) 146.43 ($CH_2CHPh\mathbf{C_{ipso}}CH_2$), 127.81 ($CH_2CH\mathbf{Ph}CH_2$), 127.43 ($CH_2CH\mathbf{Ph}CH_2$), 125.31

($CH_2CHPh\mathbf{C_{para}}CH_2$), 45.86 ($CH_2\mathbf{C}\mathbf{H}PhCH_2$), 36.57 ($CH_2\mathbf{CH_2}CHPh\mathbf{CH_2}CH_2$), 29.34 (**PE chain**) and 27.28 ($\mathbf{CH_2}CH_2CHPhCH_2\mathbf{CH_2}$).

Ethylene/1-octene copolymer.

$^{13}C\{^1H\}$ NMR (1,1,2,2-$C_2D_2Cl_4$, 125.7 MHz, 393 K): δ (ppm) CγCβCαC$_{BR}$(C6C5C4C3C2C1)CαCβCγ), 37.58 (**C$_{BR}$**), 33.95 (**C6**, **Cα**), 31.62 (**C3**), 29.86 (**C4**, **Cγ**), 29.37 (**PE chain**), 26.66 (**C5**, **Cβ**), 22.30 (**C2**) and 13.60 (**C1**).

7.4.3 Solution-phase copolymerisation of ethylene/1-hexene and ethylene/1-octene

Solution-phase ethylene/1-hexene copolymerisations and ethylene/1-octene copolymerisations were carried out in a 1 L reactor by Ms Tina Kristiansen Voss at Norner AS. The reactor was purged with nitrogen at 145 °C, 1–2 mg of complex was loaded into a metal vessel with 1000 equivalents of MAO (30 wt% in toluene), and Isopar-E and 1-hexene or 1-octene comonomer, if required, was added to another metal vessel. The two vessels were connected to the reactor and flushed in using an ethylene/hydrogen mixture with stirring started immediately after loading. The polymerisation was run for 10–20 minutes with a continuous 35 bar ethylene/hydrogen feed throughout the reaction with the temperature controlled by electrical heating/steam pressure on the jacket. After 10–20 minutes of reaction the stirring was reduced, and the hydrogen and ethylene evaporated. The hot polymer/Isopar-E mixture was removed from the reactor by overpressure of nitrogen, the Isopar-E evaporated and the polymer dried at 70 °C under vacuum.

7.5 Experimental details for Chapter 5

7.5.1 Synthesis of Nb(NDipp)Cl_3.THF.py

Nb(NDipp)Cl_3.THF.py was synthesised *via* a modified literature procedure.[9] $NbCl_5$ (3.00 g, 11.10 mmol) was mixed with $ZnCl_2$ (3.03 g, 22.21 mmol) and THF (1.55 mL) in DCM (1.30 mL) and cooled to −40 °C. To this mixture was added a solution of 2,6-di*iso*propylphenylamine (DippNH_2, 2.09 mL) and pyridine (1.79 mL) in DCM (70 mL) dropwise over 45 minutes. The reaction was allowed to warm to 23 °C and then stirred for 18 hours. The reaction mixture was filtered, and the product extracted in a pentane/DCM mixture (4 × 50 mL). Pink crystals suitable for X-ray diffraction studies were isolated at −23 °C in a 24% yield (1.41 g, 2.66 mmol).

^{1}H NMR ($CDCl_3$, 298 K, 400.2 MHz): δ (ppm) 8.93 (2H, m, py-**H$_{ortho}$**), 7.91 (1H, m, py-**H$_{para}$**), 7.47 (2H, m, py-**H$_{meta}$**), 7.10 (2H, d, N-Dipp**H$_{meta}$**, $^3J_{H\text{-}H}$ = 7.7 Hz), 6.98 (1H, t, N-Dipp**H$_{para}$**, $^3J_{H\text{-}H}$ = 7.7 Hz), 4.29 (2H, m, O-**CH_2**-CH_2), 2.01 (2H, m, O-CH_2-**CH_2**), 1.31 (2H, m, **C**HMe_2) and 1.19 (12H, d, CH**Me$_2$**, $^3J_{H\text{-}H}$ = 6.8 Hz).

^{13}C{^{1}H} NMR ($CDCl_3$, 298 K, 125.7 MHz): δ (ppm) 152.0 (py-**C$_{ortho}$**), 150.7 (N-Dipp**C$_{ipso}$**), 149.0 (N-Dipp**C$_{ortho}$**), 140.0 (py-**C$_{para}$**), 127.2 (N-Dipp**C$_{para}$**), 124.9 (py-**C$_{meta}$**), 122.9 (N-Dipp**C$_{meta}$**), 77.4 (O-**CH_2**-CH_2), 27.9 (O-CH_2-**CH_2**), 25.7 (**C**HMe_2) and 24.9 (CH**Me$_2$**).

7.5.2 Synthesis of sMAO-Nb(NDipp)Cl_3

Nb(NDipp)Cl_3.THF.py and sMAO were mixed in toluene (30 mL) at 25 °C, warmed to 60 °C and regularly swirled for 1 hour. The product was allowed to settle and the supernatant was decanted. The pale pink solid product was then dried under vacuum at room temperature in 85% yield.

^{13}C CP-MAS NMR (100.6 MHz): δ (ppm) −8 (**Me-sMAO**), 23 (**^{i}Pr**), 25 (**^{i}Pr**), 28 (**THF**), 51 (Nb-**Me**), 73 (**THF**), 128 (**sMAO**, Nb(N**Dipp**), **py**), 131(Nb(N**Dipp**), **py**), 139 (**py**), 148(Nb(N**Dipp**), **py**) and 181 (**C=O-sMAO**).

^{27}Al DP-MAS hahnecho NMR (104.2 MHz): δ (ppm) 334, 188, −90 and −245.

7.5.3 Slurry-phase ethylene oligomerisation

5 mg of supported catalyst was added to a J. Young's tap NMR spectroscopy tube along with 2.8 μL of mesitylene (20.1 μmol). These were washed in with 500 μL of deuterated solvent added *via* microlitre syringe. The NMR spectroscopy tube was degassed and backfilled with 1 bar ethylene and heated in an oil bath. The runs were periodically analysed by ^{1}H NMR spectroscopy and stopped after 10 hours and analysed by GC-MS. All oligomerisations were carried out, at least, in duplicate.

7.5.4 Solution-phase ethylene oligomerisation

2 mg of complex was added to the J. Young's tap NMR spectroscopy tube with MAO and 2.8 μL of mesitylene (20.1 μmol). These were washed in with 500 μL of deuterated solvent added *via* microlitre syringe. The NMR spectroscopy tube was degassed and backfilled with 1 bar ethylene and heated in an oil bath. The runs were periodically analysed by ^{1}H NMR spectroscopy and stopped after 10 hours and analysed by GC-MS. All oligomerisations were carried out, at least, in duplicate.

7.5.5 Synthesis of sMAO-Tandem

Nb(NDipp)Cl_3.THF.py, ^{Me2}SB(^{tBu}N,I*)$TiCl_2$ and sMAO were mixed in toluene (30 mL) at 25 °C, warmed to 60 °C and regularly swirled for 1 hour. The product was allowed to settle and the supernatant was decanted. The pale pink solid product was then dried under vacuum at room temperature and isolated in 87% yield.

^{13}C CP-MAS NMR (100.6 MHz): δ (ppm) −8 (**Me-sMAO**), 17 (I*-**Me**), 25 (**^{i}Pr**), 29 (**THF**), 32 (I*-**Me**), 52 (Nb-**Me**, Ti-**Me**), 74 (**THF**), 128 (**sMAO**, Nb(N**Dipp**), **py**), 131(Nb(N**Dipp**), **py**, **I***), 136 (**py**, **I***), 145 (Nb(N**Dipp**), **py**) and 181 (**C=O-sMAO**).

^{27}Al DP-MAS hahnecho NMR (104.2 MHz): δ (ppm) 329, 187, −93 and −248.

7.5.6 Slurry-phase tandem catalysis

10 equivalents of MAO (relative to the amount of Nb) was mixed with 10 mL of benzene in a 150 mL ampoule. 10 mg of supported catalyst was added, followed by 40 mL of benzene. The ampoule was allowed to warm to the desired temperature in an oil bath and the headspace degassed, after which it was opened up to 2 bar ethylene while stirring (1000 rpm) and then left under a continuous flow for 3 hours. The ampoule was then degassed and the mixture filtered. The polyethylene was then washed with pentane, dried and weighed. All polymerisations were carried out, at least, in duplicate.

7.6 References

1 J.-C. Buffet, T. A. Q. Arnold, Z. R. Turner, P. Angpanitcharoen and D. O'Hare, *RSC Adv.*, 2015, **5**, 87456–87464.

2 J. P. Fackler, *Inorganic Syntheses*, John Wiley & Sons, Inc., Hoboken, NJ, USA, 1982, vol. 21.

3 J. Cosier and A. M. Glazer, *J. Appl. Crystallogr.*, 1986, **19**, 105–107.

4 CrysAlisPRO, Oxford Diffraction/Agilent Technologies UK Ltd, Yarnton, England.

5 A. Altomare, G. Cascarano, C. Giacovazzo and A. Guagliardi, *J. Appl. Crystallogr.*, 1993, **26**, 343–350.

6 L. Palatinus and G. Chapuis, *J. Appl. Crystallogr.*, 2007, **40**, 786–790.

7 L. J. Farrugia, *J. Appl. Crystallogr.*, 2012, **45**, 849–854.

8 V. Busico, R. Cipullo, A. Mingione and L. Rongo, *Ind. Eng. Chem. Res.*, 2016, **55**, 2686–2695.

9 K. Wised and K. Nomura, *Organometallics*, 2016, **35**, 2773–2777.

Appendix

Supplementary Data for Chapters 2-5

A2. Appendix for Chapter 2

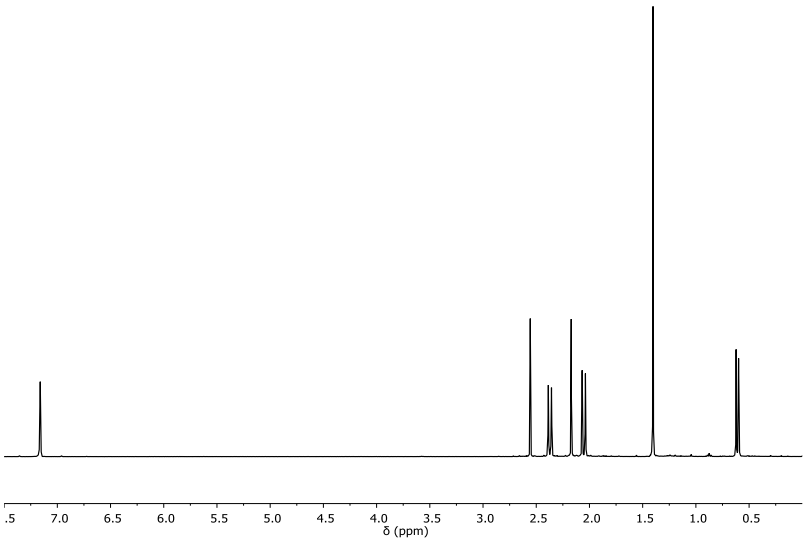

Figure A2.1 ^{1}H NMR spectrum of ^{Me_2}SB($^{t\text{Bu}}$N,I*)TiCl$_2$ (d_6-benzene, 298 K and 400.2 MHz).

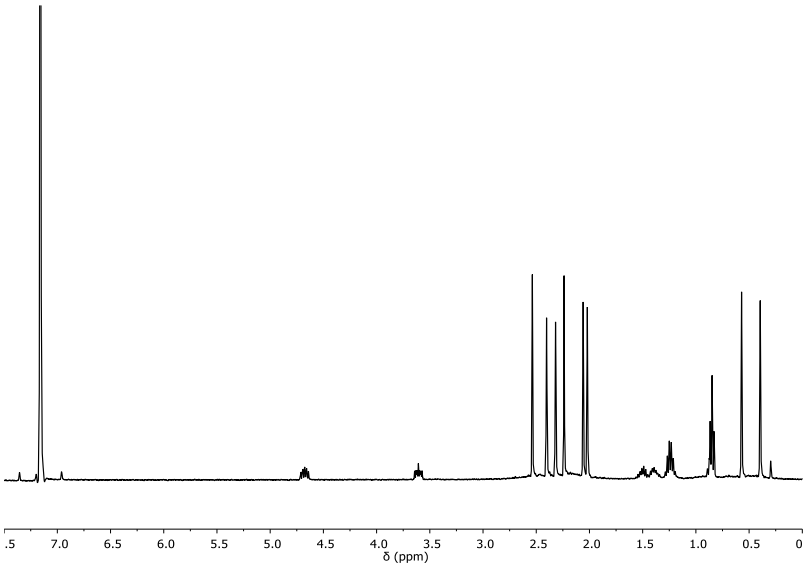

Figure A2.2. ^{1}H NMR spectrum of ^{Me_2}SB($^{n\text{Bu}}$N,I*)TiCl$_2$ (d_6-benzene, 298 K and 400.2 MHz).

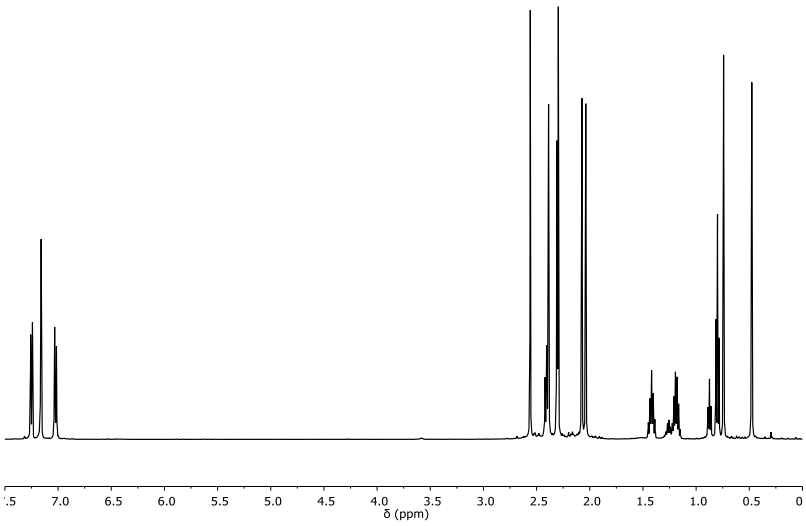

Figure A2.3. ^{1}H NMR spectrum of ^{Me_2}SB($^{4\text{-}n\text{BuC}_6\text{H}_4}$N,I*)TiCl$_2$, resonances at 0.87 and 1.23 ppm correspond to residual pentane (d_6-benzene, 298 K and 499.9 MHz).

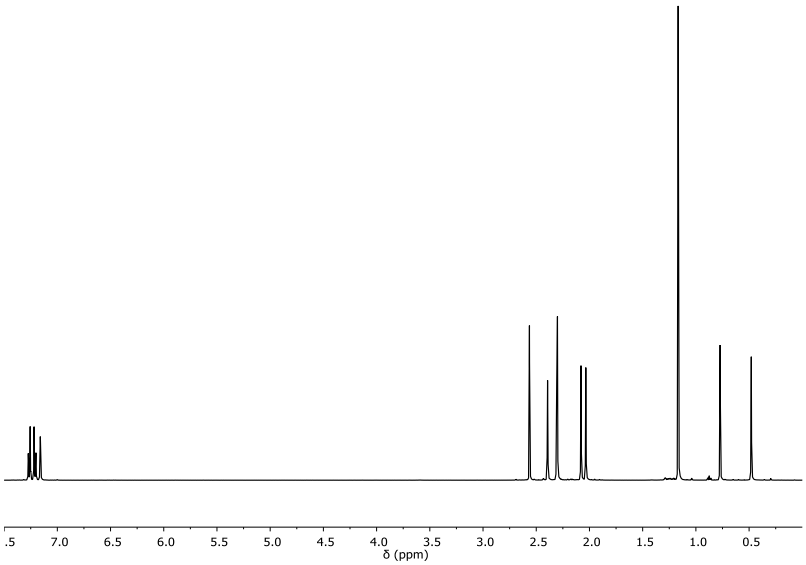

Figure A2.4. ^{1}H NMR spectrum of ^{Me2}SB($^{4\text{-}t\text{Bu}C_6H_4}$N,I*)TiCl$_2$ (d_6-benzene, 298 K and 499.9 MHz).

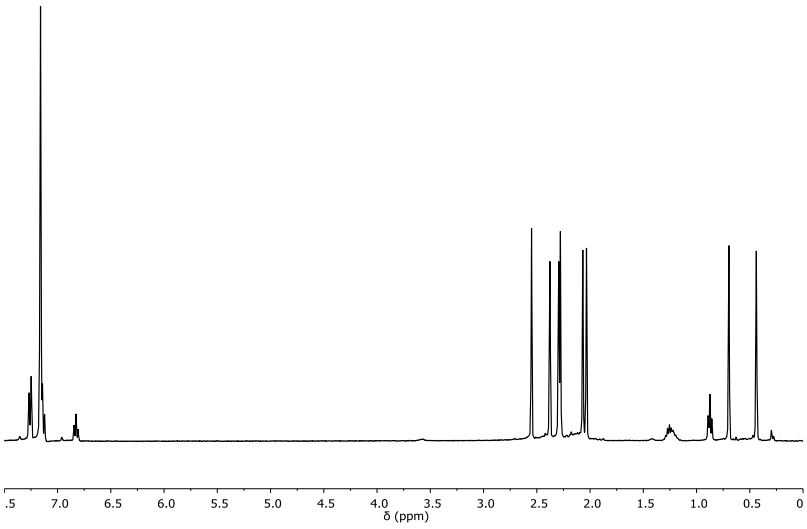

Figure A2.5. ^{1}H NMR spectrum of ^{Me2}SB(^{Ph}N,I*)TiCl$_2$, resonances at 0.87 and 1.23 ppm correspond to residual pentane (d_6-benzene, 298 K and 499.9 MHz).

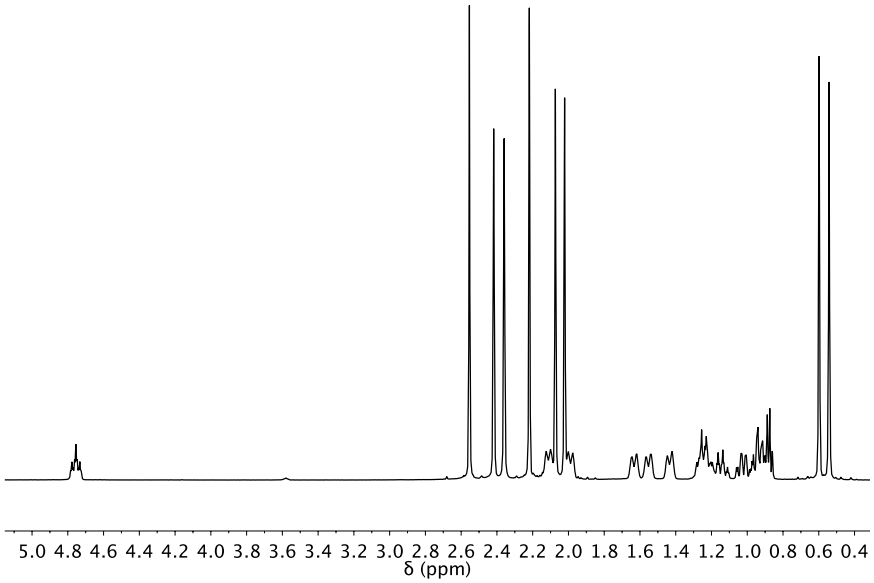

Figure A2.6. ^{1}H NMR spectrum of ^{Me_2}SB(^{Cy}N,I*)TiCl$_2$, solvent resonance omitted for clarity (d_6-benzene, 298 K and 499.9 MHz).

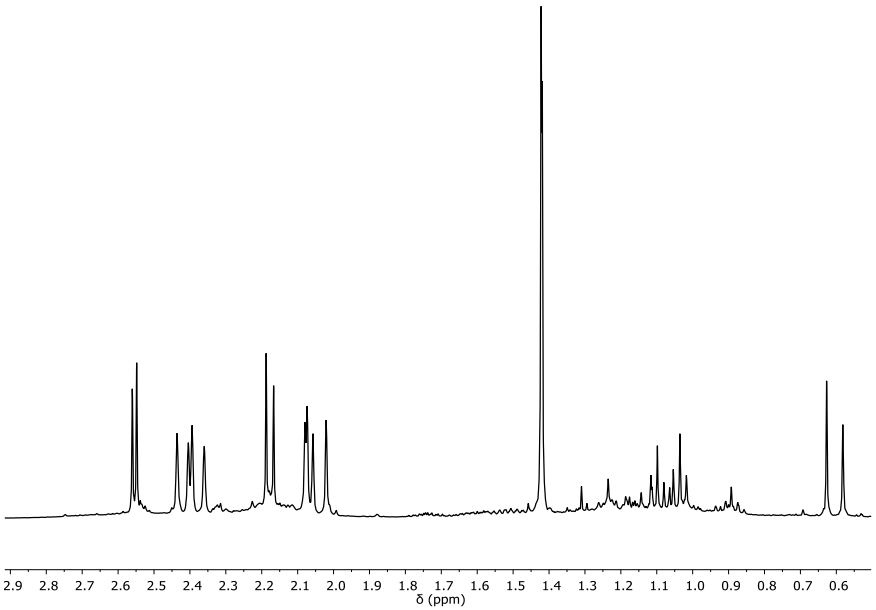

Figure A2.7. ^{1}H NMR spectrum of ^{Me,Pr}SB(^{tBu}N,I*)TiCl$_2$, solvent resonance omitted for clarity. (d_6-benzene, 298 K and 499.9 MHz).

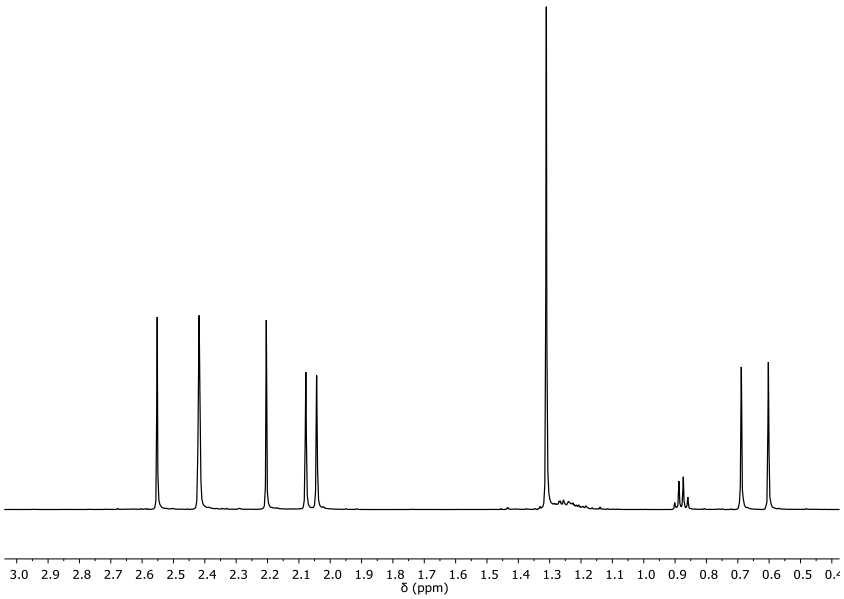

Figure A2.8. ^{1}H NMR spectrum of ^{Me2}SB($^{t\text{Bu}}$N,I*)ZrCl$_2$. Solvent resonance omitted for clarity, resonances at 1.22 and 0.88 ppm correspond to residual pentane (d_6-benzene, 298 K and 400.2 MHz).

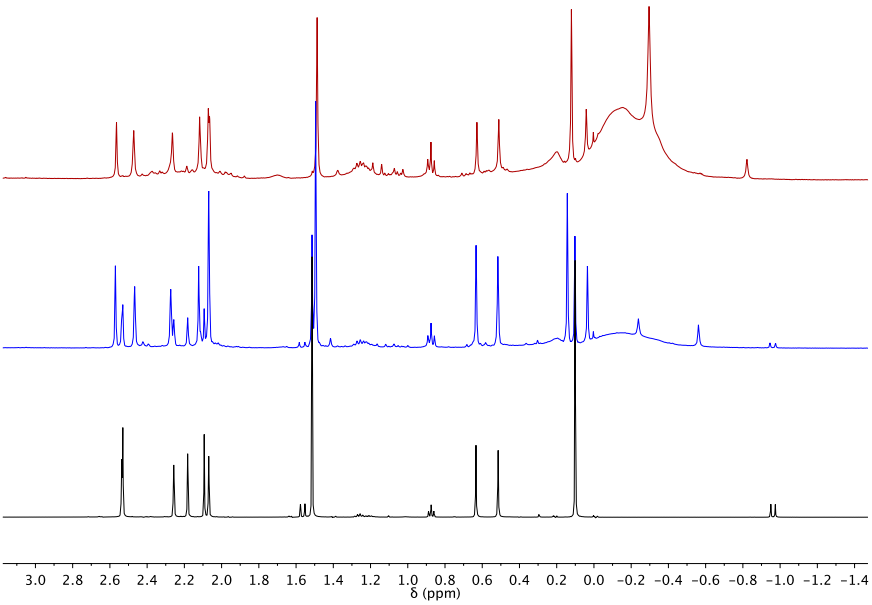

Figure A2.9. ^{1}H NMR spectra of ^{Me2}SB($^{t\text{Bu}}$N,I*)Ti(Cl)SiMe$_3$ with (bottom) 0, (middle) 5 and (top) 10 equivalents of MAO. Solvent resonance omitted for clarity (d_6-benzene, 298 K and 400.2 MHz).

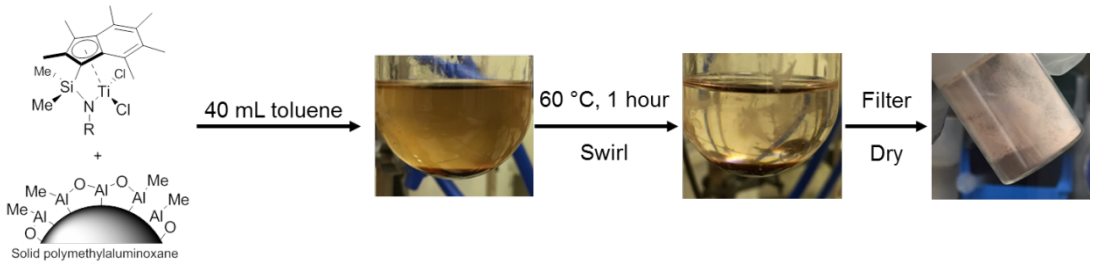

Figure A2.10. Pictorial representation of complex immobilisation on sMAO.

Table A2.1. ICP-OES data of sMAO-^{Me_2}SB($^{t Bu}$N,I*)$TiCl_2$ and sMAO-^{Me_2}SB($^{i Pr}$N,I*)$TiCl_2$.

Complex	Time in slurry (h)	Moles Al	Moles Ti	$[Al]_0$:$[Ti]_0$ ratio
^{Me_2}SB($^{t Bu}$N,I*)$TiCl_2$	0	0.971	0.005	194:1
^{Me_2}SB($^{i Pr}$N,I*)$TiCl_2$	1	1.047	0.005	199:1
^{Me_2}SB($^{i Pr}$N,I*)$TiCl_2$	2	1.061	0.005	208:1
^{Me_2}SB($^{i Pr}$N,I*)$TiCl_2$	3	1.047	0.005	202:1

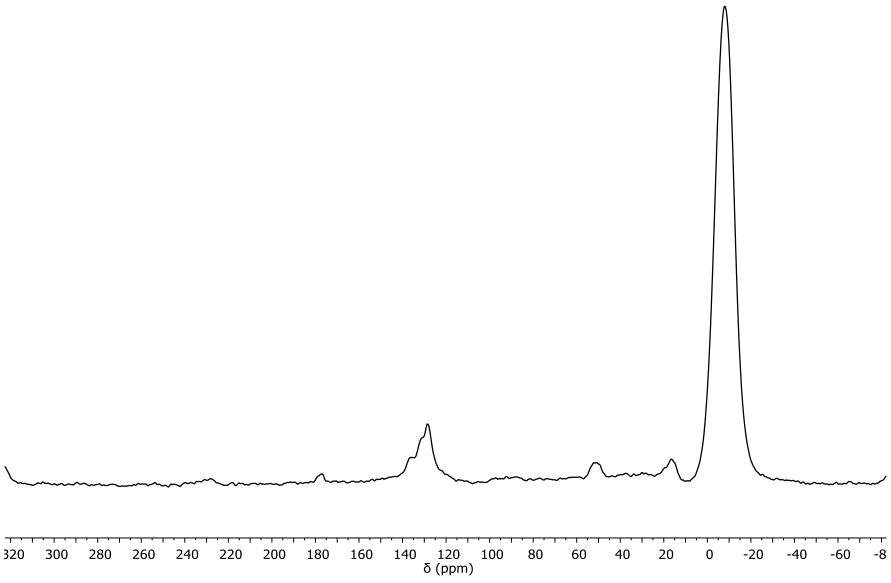

Figure A2.11. ^{13}C CP-MAS (100.6 MHz) NMR spectrum of sMAO-^{Me_2}SB(^{Ph}N,I*)$TiCl_2$.

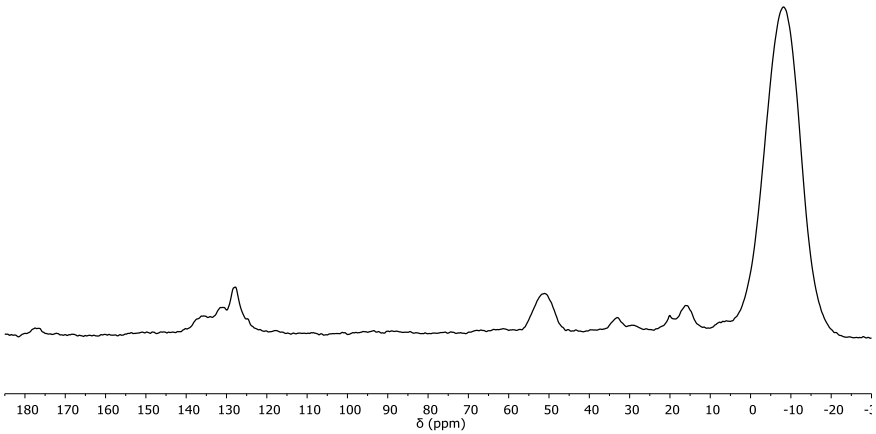

Figure A2.12. ^{13}C CP-MAS (100.6 kHz) NMR spectrum of sMAO-^{Me2}SB($^{t Bu}$N,I*)$TiCl_2$.

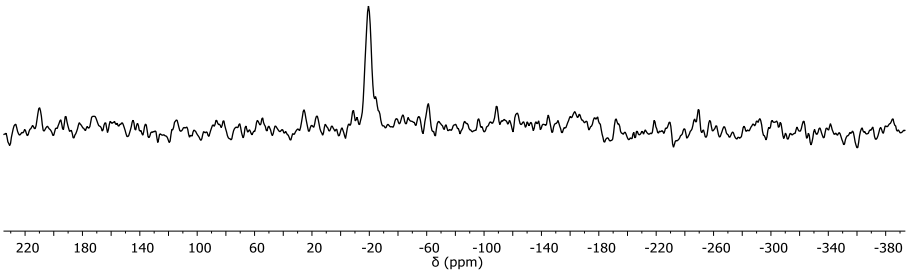

Figure A2.13. ^{29}Si CP-MAS (79.4 MHz) NMR spectrum of sMAO-^{Me2}SB($^{t Bu}$N,I*)$TiCl_2$.

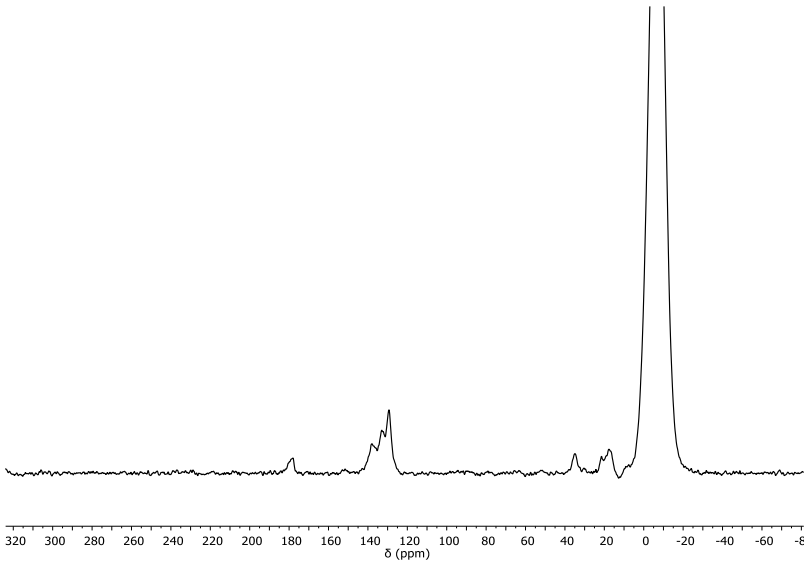

Figure A2.14. ^{13}C CP-MAS (100.6 MHz) NMR spectrum of sMAO-^{Me_2}SB($^{t Bu}$N,I*)TiMe$_2$.

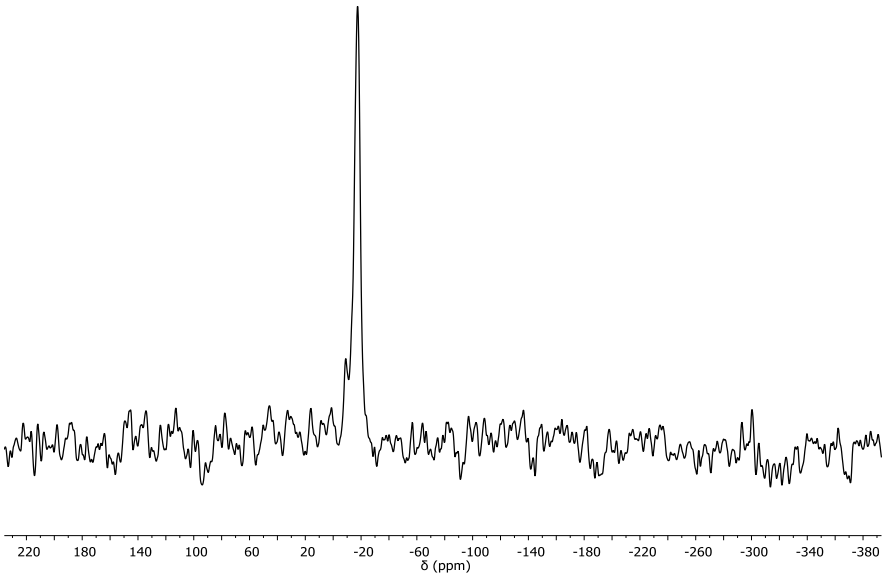

Figure A2.15. ^{29}Si CP-MAS (79.4 MHz) NMR spectrum of sMAO-^{Me_2}SB($^{t Bu}$N,I*)TiMe$_2$.

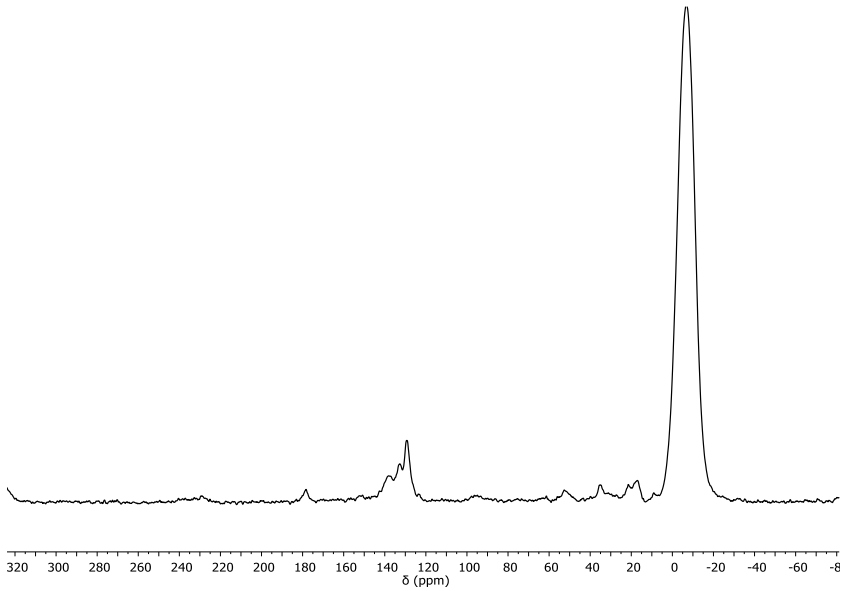

Figure A2.16. ^{13}C CP-MAS (100.6 MHz) NMR spectrum of sMAO-^{Me_2}SB($^{t\text{Bu}}$N,I*)Ti($CH_2Ph)_2$.

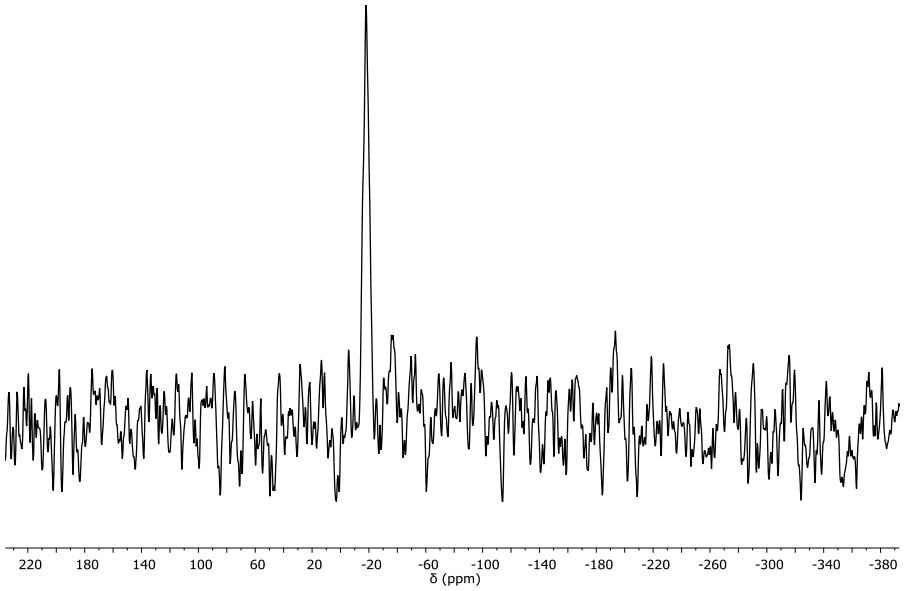

Figure A2.17. ^{29}Si CP-MAS (79.4 MHz) NMR spectrum of sMAO-^{Me_2}SB($^{t\text{Bu}}$N,I*)Ti($CH_2Ph)_2$.

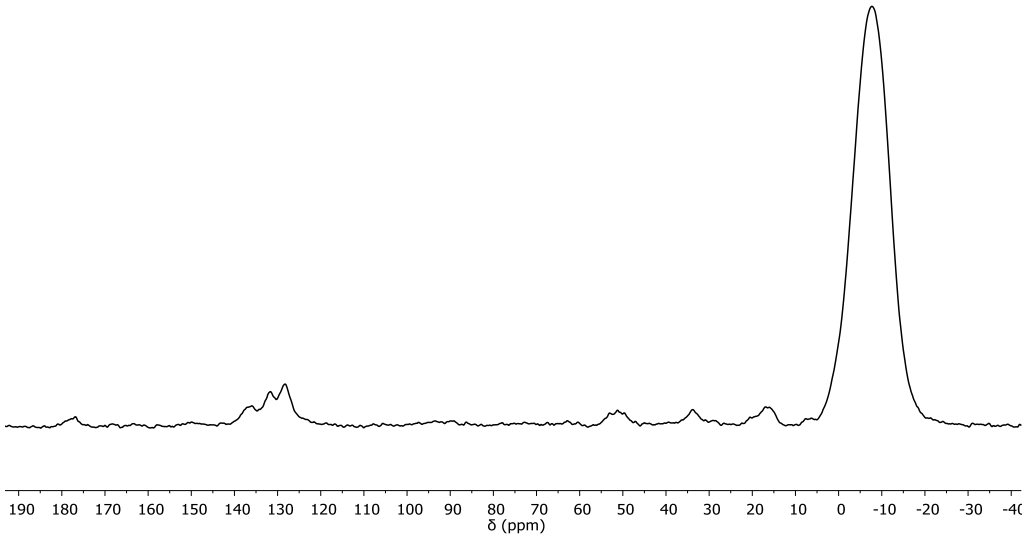

Figure A2.18. ^{13}C CP-MAS (100.6 MHz) NMR spectrum of sMAO-^{Me_2}SB($^{t Bu}$N,I*)Ti(Cl)CH_2SiMe_3.

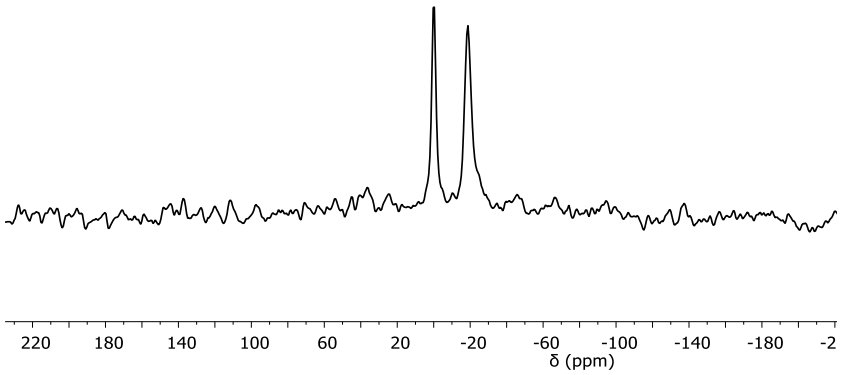

Figure A2.19. ^{29}Si CP-MAS (79.4 MHz) NMR spectrum of sMAO-^{Me_2}SB($^{t Bu}$N,I*)Ti(Cl)CH_2SiMe_3.

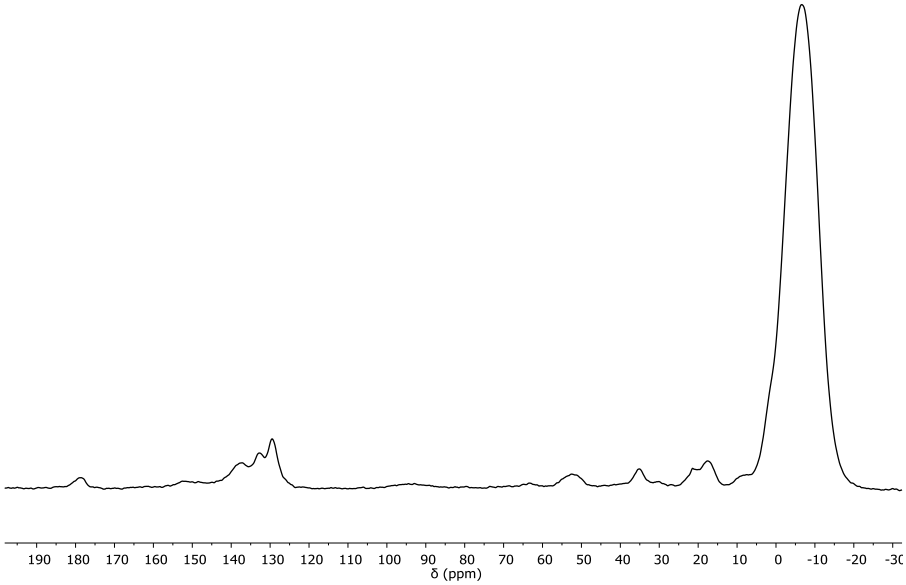

Figure A2.20. ^{13}C CP-MAS (100.6 MHz) NMR spectrum of sMAO-^{Me_2}SB(^{tBu}N,I*)Ti(CH_2SiMe_3)$_2$.

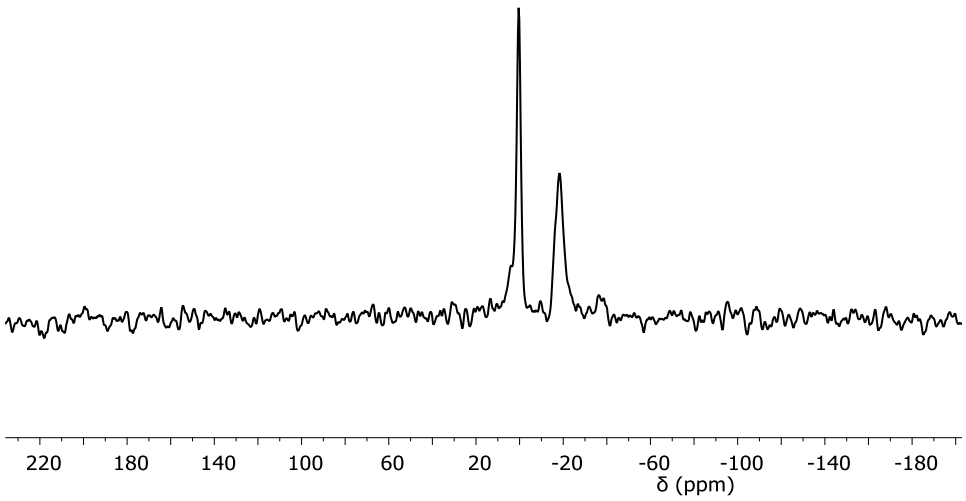

Figure A2.21. ^{29}Si CP-MAS (79.4 MHz) NMR spectrum of sMAO-^{Me_2}SB(^{tBu}N,I*)Ti(CH_2SiMe_3)$_2$.

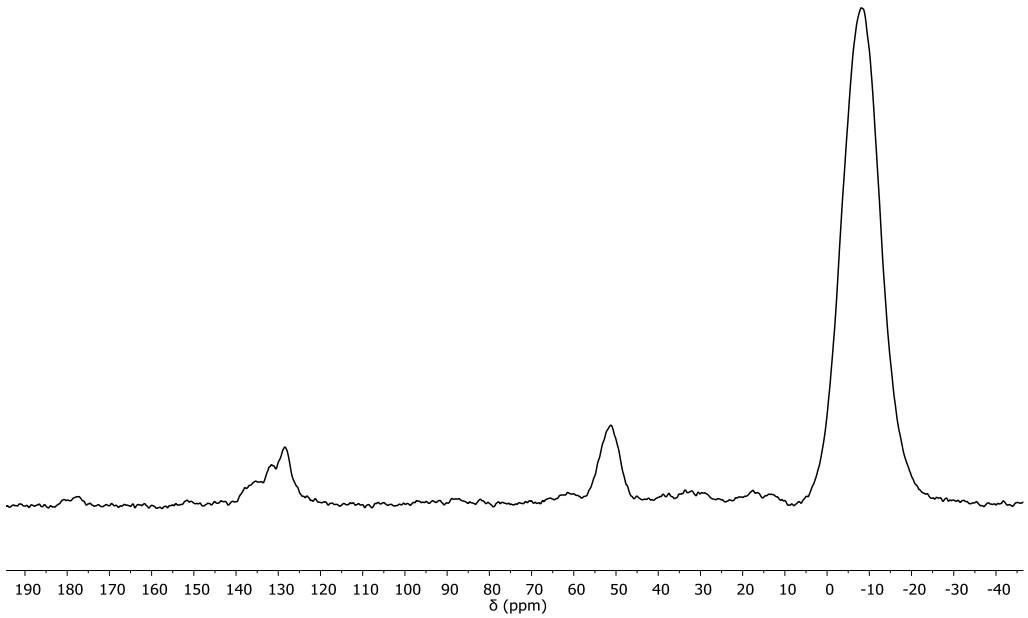

Figure A2.22. ^{13}C CP-MAS (100.6 kHz) NMR spectrum of sMAO-^{Me_2}SB($^{t Bu}$N,Cp*)$TiCl_2$.

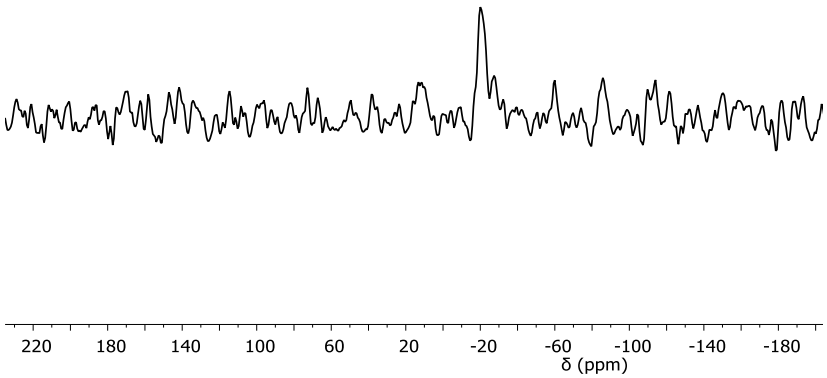

Figure A2.23. ^{29}Si CP-MAS (79.4 MHz) NMR spectrum of sMAO-^{Me_2}SB($^{t Bu}$N,Cp*)$TiCl_2$.

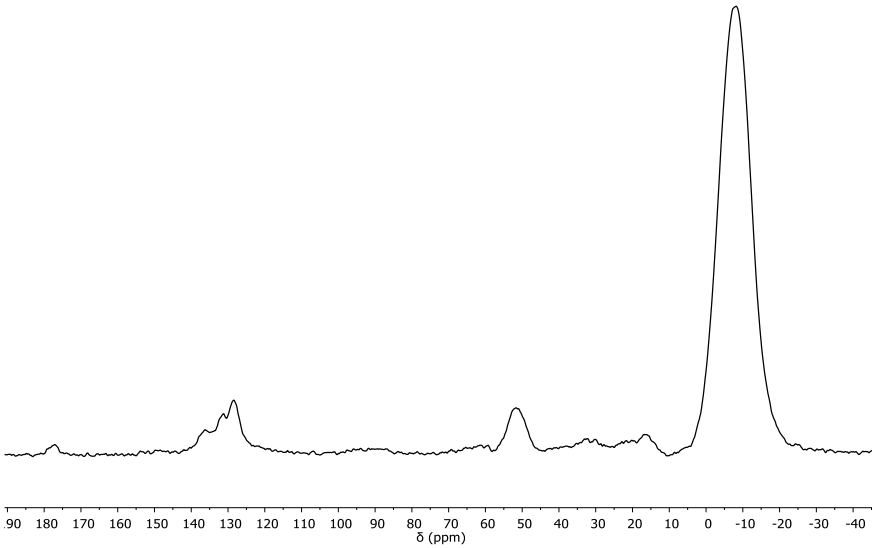

Figure A2.24. ^{13}C CP-MAS (100.6 kHz) NMR spectrum of sMAO-^{Me_2}SB($^{t Bu}$N,$^{3\text{-}Et}$I*)$TiCl_2$.

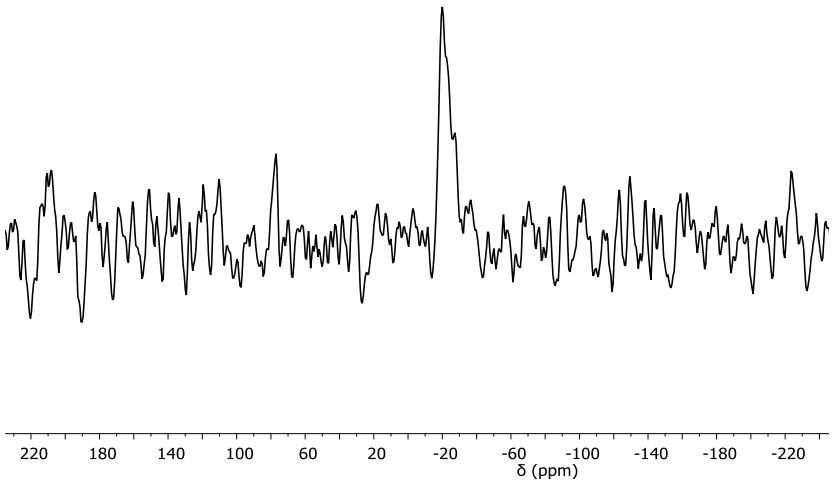

Figure A2.25. ^{29}Si CP-MAS (79.4 MHz) NMR spectrum of sMAO-^{Me_2}SB($^{t Bu}$N,$^{3\text{-}Et}$I*)$TiCl_2$.

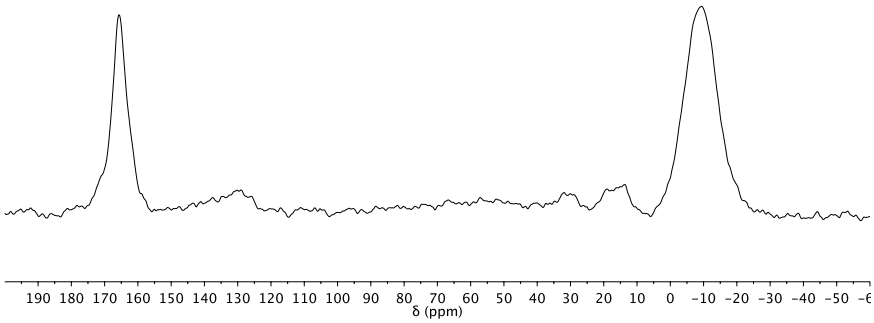

Figure A2.26. ^{13}C CP-MAS (100.6 MHz) NMR spectrum of LDHMAO-^{Me_2}SB($^{t Bu}$N,I*)TiCl$_2$.

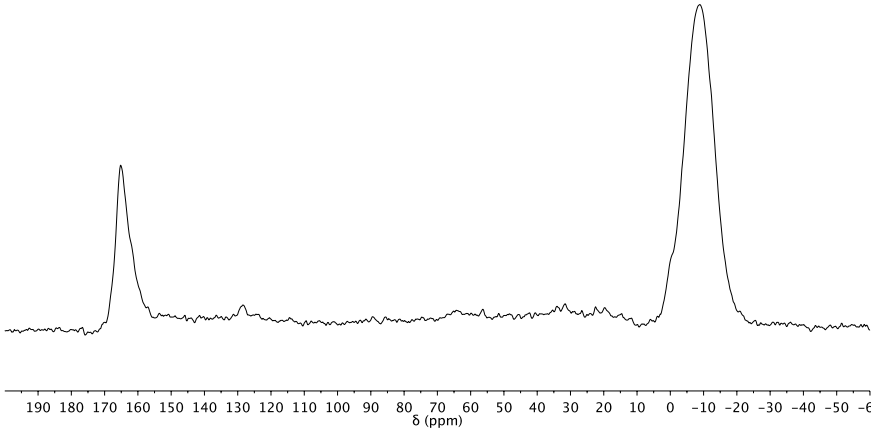

Figure A2.27. ^{13}C CP-MAS (100.6 MHz) NMR spectrum of LDHMAO-^{Me_2}SB($^{t Bu}$N,$^{3\text{-}Et}$I*)TiCl$_2$.

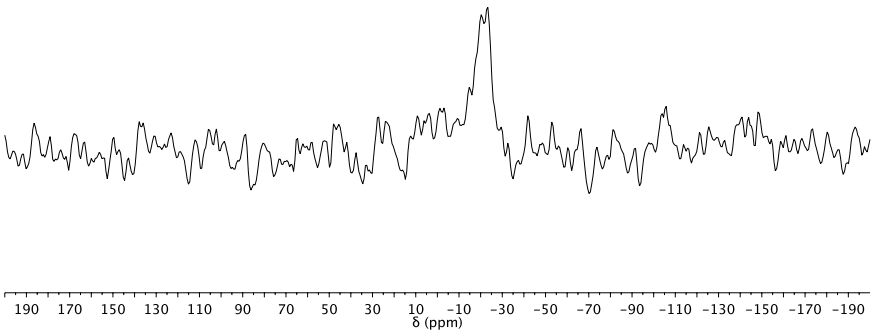

Figure A2.28. ^{29}Si CP-MAS (79.4 MHz) NMR spectrum of LDHMAO-^{Me_2}SB($^{t\text{Bu}}$N,$^{3\text{-Et}}$I*)TiCl$_2$.

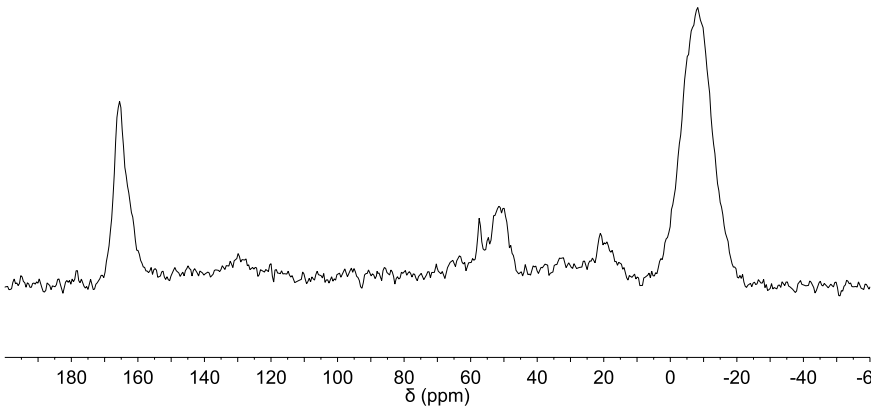

Figure A2.29. ^{13}C CP-MAS (100.6 MHz) NMR spectrum of LDHMAO-^{Me_2}SB($^{t\text{Bu}}$N,I*)Ti(Cl)CH$_2$SiMe$_3$.

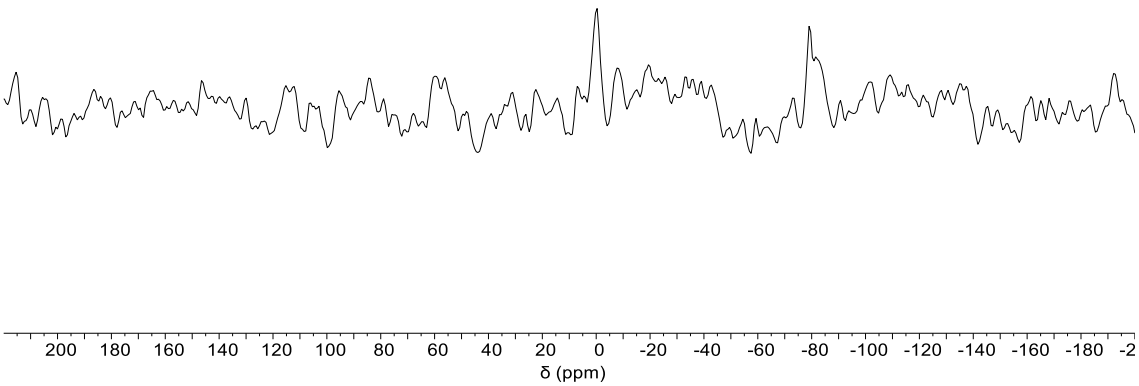

Figure A2.30. ^{29}Si CP-MAS (79.4 MHz) NMR spectrum of LDHMAO-^{Me_2}SB($^{t Bu}$N,I*)Ti(Cl)CH_2SiMe_3.

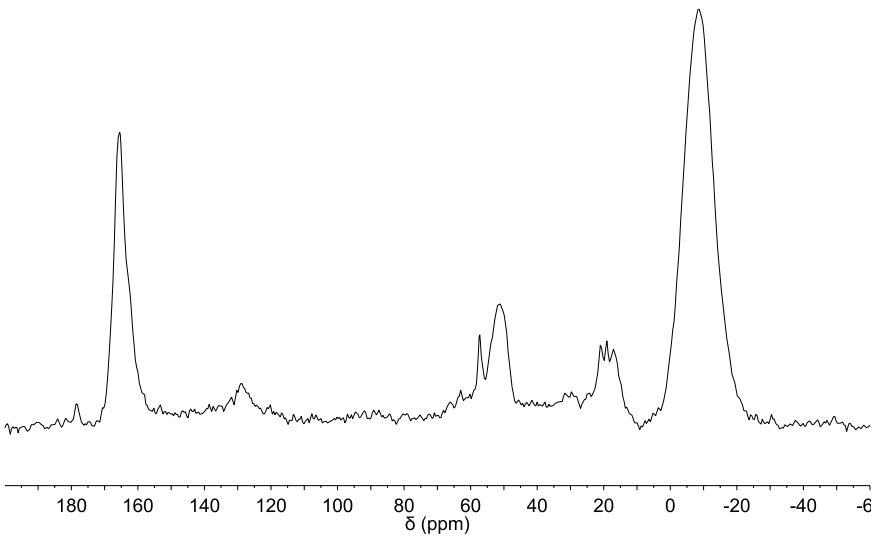

Figure A2.31. ^{13}C CP-MAS (100.6 MHz) NMR spectrum of LDHMAO-^{Me,Pr}SB($^{t Bu}$N,I*)$TiCl_2$.

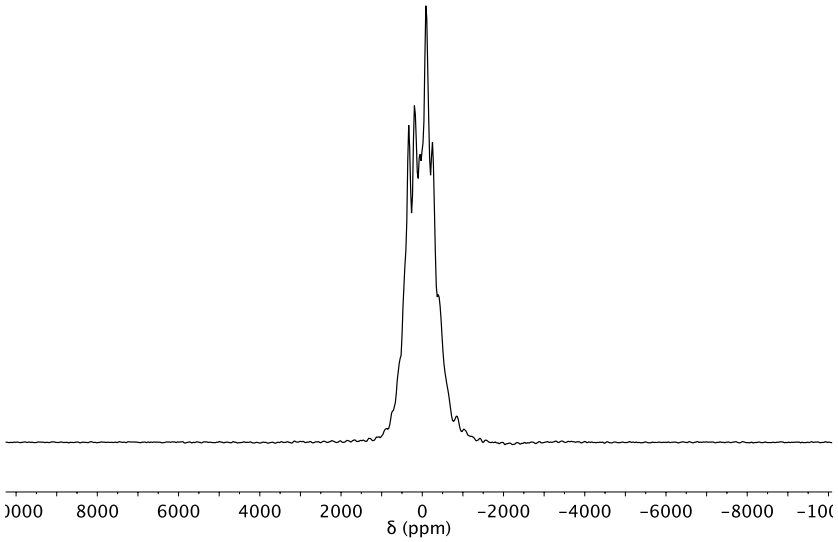

Figure A2.32. ^{27}Al hahnecho (15 kHz) NMR spectrum of sMAO-^{Me_2}SB($^{t\text{Bu}}$N,I*)TiCl$_2$.

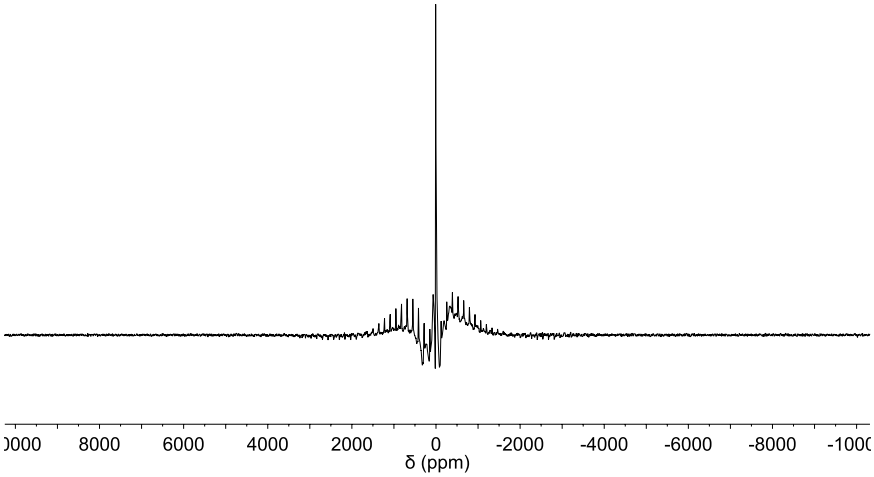

Figure A2.33. ^{27}Al hahnecho (15 kHz) NMR spectrum of LDHMAO-^{Me_2}SB($^{t\text{Bu}}$N,I*)Ti(Cl)CH$_2$SiMe$_3$.

A3. Appendix for Chapter 3

Table A3.1. Polymerisation activities, mass of catalyst used, and mass of polymer produced. Polymerisation conditions; 2 bar ethylene, 50 mL hexanes, 10 mg catalyst ($[Al]_0$:$[Ti]_0$ = 200:1 unless specified), 150 mg TiBA and 30 minutes.

Temperature (°C)	Mass Catalyst (mg)		Mass Polymer (g)		Activity ($kg_{PE}/mol_{Ti}/h/bar$)		Average Activity ($kg_{PE}/mol_{Ti}/h/bar$)
	A	B	A	B	A	B	
sMAO-^{Me_2}SB(^{tBu}N,I*)TiCl$_2$							
50	9.9	10.2	2.216	2.530	2806	3110	2958
60	9.8	10.1	2.743	2.977	3509	3696	3602
70	9.8	9.8	2.602	2.907	3328	3719	3524
80	10.3	10.1	2.354	2.495	2865	3097	2981
90	9.8	10.1	1.984	2.088	2538	2592	2565
sMAO-^{Me_2}SB(^{iPr}N,I*)TiCl$_2$							
50	10.4	9.9	1.080	1.015	1261	1245	1253
60	10.0	10.1	1.047	1.203	1271	1446	1359
70	10.0	10.2	0.979	1.097	1189	1306	1247
80	9.8	9.8	1.011	0.901	1253	1117	1185
90	10.6	10.1	0.796	0.814	912	978	945
sMAO-^{Me_2}SB(^{Cy}N,I*)TiCl$_2$							
50	10.4	10.1	0.557	0.514	808	768	788
60	9.8	10.0	0.477	0.506	735	764	749
70	9.6	9.6	0.464	0.494	730	777	753
80	9.8	10.0	0.402	0.457	619	690	655
90	10.2	10.1	0.228	0.216	337	323	330
sMAO-^{Me_2}SB(^{nBu}N,I*)TiCl$_2$							
50	10.4	9.9	0.660	0.668	796	846	821
60	10.0	9.4	0.522	0.475	654	634	644
70	10.6	10.5	0.690	0.673	816	803	810
80	10.3	10.0	0.610	0.664	743	833	788
90	9.6	10.3	0.527	0.592	688	721	704
sMAO-^{Me_2}SB($^{4\text{-}t\text{Bu}C_6H_4}$N,I*)TiCl$_2$							
50	10.2	10.1	0.185	0.203	274	303	289
60	10.2	10.4	0.228	0.213	337	309	323
70	9.7	9.6	0.210	0.201	327	316	321
80	9.8	10.3	0.229	0.179	353	262	308
90	10.5	9.8	0.093	0.106	134	163	149
sMAO-^{Me_2}SB($^{4\text{-}n\text{Bu}C_6H_4}$N,I*)TiCl$_2$							
50	10.4	10.1	0.220	0.205	319	306	313
60	9.4	9.3	0.226	0.216	363	351	357
70	9.9	9.7	0.238	0.236	363	367	365
80	9.6	10.8	0.255	0.298	401	417	409
90	9.2	9.2	0.167	0.157	274	258	266
sMAO-^{Me_2}SB(^{Ph}N,I*)TiCl$_2$							
50	9.9	10.6	0.223	0.246	295	304	300
60	9.3	10.3	0.206	0.225	290	286	288
70	10.3	10.5	0.218	0.200	277	250	263
80	10.3	9.8	0.173	0.171	220	229	224
90	10.0	9.8	0.120	0.124	157	166	161
sMAO-^{Me_2}SB(^{tBu}N,I*)TiCl$_2$ ($[Al]_0$:$[Ti]_0$ = 1:100)							

50	9.5	9.9	1.317	1.455	869	921	895
60	10.0	10.5	1.579	1.802	990	1076	1033
70	10.1	10.3	1.830	1.947	1136	1185	1160
80	10.3	10.1	1.55	1.643	946	1020	983
90	10.6	9.5	1.320	1.076	781	711	745
sMAO-^{Me_2}SB(^{tBu}N,I*)Ti(CH_2Ph)$_2$							
50	10.0	10.3	3.70	3.87	5651	5739	5695
60	9.9	9.5	3.55	3.80	5477	6109	5793
70	10.2	10.1	3.97	3.71	5945	5610	5777
80	9.5	9.8	3.18	3.36	5112	5236	5174
90	9.7	10.0	2.37	2.71	3732	4139	3935
sMAO-^{Me_2}SB(^{tBu}N,I*)TiMe_2							
50	10.2	9.7	4.42	4.42	4937	5191	5064
60	10.2	10.0	4.77	4.76	5328	5423	5375
70	10.3	9.6	4.37	4.23	4834	5020	4927
80	10.0	10.3	3.61	3.45	4113	3816	3964
90	10.0	10.2	2.44	2.75	2780	3072	2926
sMAO-^{Me_2}SB(^{tBu}N,I*)Ti(CH_2SiMe_3)$_2$							
50	10.1	10.0	4.54	4.63	6944	7152	7048
60	10.5	10.0	4.64	4.47	6826	6905	6866
70	10.0	10.0	3.98	4.01	6148	6195	6171
80	10.4	9.9	3.07	2.57	4560	4010	4285
90	10.0	10.0	1.26	1.30	1946	2008	1977
sMAO-^{Me_2}SB(^{tBu}N,I*)Ti(Cl)CH_2SiMe_3							
50	10.4	10.4	1.863	1.748	2506	2351	2429
60	10.5	10.7	2.085	2.376	2778	3107	2943
70	10.1	9.5	1.730	1.641	2397	2416	2407
80	9.3	9.5	1.104	0.916	1661	1349	1505
90	10.0	10.0	0.618	0.616	865	862	863
sMAO-^{Me,Pr}SB(^{tBu}N,I*)TiCl_2							
50	10.1	10.3	2.899	3.292	3954	4403	4178
60	9.7	10.0	2.988	3.013	4243	4151	4197
70	10.0	10.1	2.939	3.100	4049	4228	4138
80	9.9	10.2	2.329	2.100	3241	2836	3038
90	10.2	10.1	1.965	1.938	2680	2617	2649
sMAO-^{Me_2}SB(^{tBu}N,$^{3\text{-}Et}$I*)TiCl_2							
50	10.5	10.5	3.134	3.470	3860	4272	4067
60	9.6	9.8	2.825	3.047	38.05	4021	3913
70	9.6	9.4	2.750	2.531	3704	3482	3593
80	9.6	9.6	2.034	1.972	2740	2656	2698
90	10.0	10.4	1.948	1.710	2519	2126	2323
sMAO-^{Me_2}SB(^{tBu}N,I*)ZrCl_2							
50	10.6	10.1	0.078	0.085	105	120	112
60	9.7	9.7	0.068	0.064	100	94	97
70	9.5	9.5	0.068	0.071	102	106	104
80	9.6	10.5	0.048	0.062	71	84	78
90	9.5	9.5	0.062	0.057	83	85	89
LDHMAO-^{Me_2}SB(^{tBu}N,I*)TiCl_2 ($[Al]_0$:$[Ti]_0$ = 1:200)							
30	10.5	10.3	0.156	0.127	610	507	558
40	10.2	10.0	0.195	0.165	785	678	732
50	9.9	9.8	0.286	0.287	1187	1203	1195
60	9.8	10.4	0.285	0.293	1195	1157	1176
70	10.3	10.1	0.411	0.462	1639	1879	1759
80	10.1	9.8	0.300	0.356	1220	1492	1356
90	9.8	10.6	0.242	0.329	1015	1275	1145
LDHMAO-^{Me_2}SB(^{tBu}N,I*)TiCl_2 ($[Al]_0$:$[Ti]_0$ = 1:100)							

30	10.6	9.8	0.396	0.365	789	786	787
40	10.4	10.4	0.402	0.424	816	861	838
50	9.8	10.5	0.566	0.487	1219	979	1099
60	10.2	9.7	0.931	0.830	1927	1806	1867
70	10.1	10.0	0.574	0.659	1200	1391	1295
80	10.2	10.3	0.614	0.670	1271	1373	1322
90	10.3	10.3	0.462	0.520	947	1066	1006
LDHMAO-^{Me_2}SB(^{tBu}N,I*)TiCl$_2$ ([Al]$_0$:[Ti]$_0$ = 1:50)							
30	10.7	10.4	0.428	0.370	422	376	399
40	9.9	10.2	0.458	0.590	488	611	549
50	10.2	10.5	0.612	0.650	933	653	643
60	10.1	9.8	0.733	0.690	766	743	755
70	10.1	10.1	0.740	0.683	773	714	744
80	10.2	10.2	0.598	0.680	619	704	661
90	10.8	10.2	0.432	0.518	422	536	479
LDHMAO-^{Me_2}SB(^{tBu}N,$^{3\text{-}Et}$I*)TiCl$_2$							
50	9.8	9.5	0.322	0.283	1384	1254	1319
60	10.0	9.6	0.360	0.332	1516	1456	1486
70	10.8	10.6	0.511	0.494	1992	1963	1978
80	9.5	9.5	0.508	0.430	2252	1906	2079
90	9.8	10.2	0.350	0.294	1504	1214	1359
LDHMAO-^{Me_2}SB(^{tBu}N,I*)Ti(Cl)CH$_2$SiMe$_3$							
50	9.8	9.8	0.210	0.195	904	839	872
60	9.6	9.5	0.257	0.286	1129	1270	1200
70	9.6	9.7	0.339	0.370	1490	1609	1549
80	9.8	10.4	0.326	0.368	1403	1493	1448
90	10.1	10.2	0.229	0.253	956	1046	1001
LDHMAO-^{Me,Pr}SB(^{tBu}N,I*)TiCl$_2$							
50	10.4	9.8	0.167	0.150	677	645	661
60	10.1	9.8	0.203	0.193	847	830	839
70	9.8	10.3	0.183	0.195	787	798	793
80	10.2	10.2	0.174	0.180	719	744	731
90	10.5	10.5	0.170	0.180	682	723	703
SSMAO-^{Me_2}SB(^{tBu}N,I*)TiCl$_2$							
50	10.3	9.8	0.250	0.248	1022	1066	1044
60	9.6	9.5	0.323	0.296	1417	1312	1365
70	9.8	9.3	0.334	0.300	1435	1359	1397
80	10.0	9.6	0.272	0.285	1146	1250	1198
90	10.2	10.7	0.237	0.264	979	1039	1009
SSMAO-^{Me_2}SB(^{tBu}N,$^{3\text{-}Et}$I*)TiCl$_2$							
50	10.3	9.7	0.212	0.192	866	834	850
60	9.7	9.5	0.280	0.272	1216	1206	1211
70	9.4	9.4	0.288	0.314	1290	1407	1349
80	7.6	8.0	0.213	0.220	1180	1158	1169
90	9.3	7.4	0.218	0.173	987	985	986
SSMAO-^{Me_2}SB(^{tBu}N,I*)Ti(Cl)CH$_2$SiMe$_3$							
50	10.0	10.6	0.165	0.183	695	728	712
60	9.8	9.2	0.207	0.199	890	912	901
70	9.6	9.5	0.202	0.187	887	830	858
80	9.8	9.7	0.207	0.204	890	886	888
90	10.5	9.8	0.156	0.144	626	619	623
SSMAO-^{Me,Pr}SB(^{tBu}N,I*)TiCl$_2$							
50	10.0	9.5	0.229	0.203	966	901	933
60	10.5	10.5	0.292	0.283	1173	1137	1155
70	10.0	9.8	0.337	0.307	1422	1321	1372
80	9.5	8.2	0.331	0.285	1470	1466	1468

90	9.3	8.2	0.267	0.218	1211	1121	1166
sMAO(3G)-^{Me_2}SB(^{tBu}N,I*)TiCl$_2$							
50	9.5	9.5	2.673	2.545	3528	3359	3443
60	9.7	9.7	2.490	2.637	3218	3409	3314
70	9.8	10.2	2.410	2.607	3083	3205	3144
80	9.7	10.2	2.337	2.457	3021	3020	3020
90	9.5	9.9	2.064	2.190	2724	2774	2749
sMAO(3G)-^{Me_2}SB(^{tBu}N,I*)Ti(Cl)CH$_2$SiMe$_3$							
50	9.6	9.7	2.478	2.376	3236	3071	3154
60	10.3	9.9	3.232	3.009	2934	3811	3872
70	9.8	9.6	3.424	3.497	4381	4567	4474
80	9.4	9.5	2.622	2.879	3497	3800	3648
90	10.2	9.8	2.257	2.171	2774	2778	2776
sMAO(3G)-^{Me_2}SB(^{tBu}N,I*)TiCl$_2$ (TEA)							
50	10.2	10.3	1.552	1.638	1908	1994	1951
60	9.8	9.9	1.522	1.553	1947	1967	1957
70	10.5	10.3	1.498	1.421	1789	1730	1759
80	9.9	9.8	0.838	0.790	1061	1011	1036
90	9.8	9.7	0.491	0.520	628	672	650
sMAO(3G)-^{Me_2}SB(^{tBu}N,I*)TiCl$_2$ (TMA)							
50	10.3	10.3	0.476	0.505	579	615	597
60	9.8	9.9	0.510	0.550	652	697	675
70	10.3	10.0	0.687	0.654	836	820	828
80	10.1	10.5	0.729	0.782	905	934	919
90	10.5	9.5	0.822	0.740	982	977	979
sMAO(3G)-^{Me_2}SB(^{tBu}N,I*)TiCl$_2$ (MAO)							
50	10.5	10.4	0.551	0.524	1974	1895	1934
60	10.2	10.2	0.718	0.696	2648	2567	2607
70	9.8	9.8	0.890	0.850	3416	3262	3339
80	9.9	10.4	0.980	0.973	3723	3519	3621
90	10.5	10.6	0.808	0.863	2894	3062	2978
^{Me_2}SB(^{tBu}N,I*)TiCl$_2$ solution							
70	0.5	0.5	0.797	0.854	4268	4573	4421
^{Me_2}SB(^{tBu}N,$^{3\text{-}Et}$I*)TiCl$_2$ solution							
70	0.5	0.5	0.840	0.803	4640	4436	4538
^{Me,Pr}SB(^{tBu}N,I*)TiCl$_2$ solution							
70	0.5	0.5	0.856	0.841	4924	4838	4881
^{Me_2}SB(^{tBu}N,I*)Ti(Cl)CH$_2$SiMe$_3$ solution							
70	0.5	0.5	0.434	0.463	2594	2767	2681
sMAO-^{Me_2}SB(^{tBu}N,I*)TiCl$_2$ large scale							
70	9.7		2.827				3654
sMAO-^{Me_2}SB(^{tBu}N,$^{3\text{-}Et}$I*)TiCl$_2$ large scale							
70	9.8		2.402				3093
sMAO-^{Me,Pr}SB(^{tBu}N,I*)TiCl$_2$ large scale							
70	9.6		2.584				3397
sMAO-^{Me_2}SB(^{tBu}N,I*)Ti(Cl)CH$_2$SiMe$_3$ large scale							
70	9.7		3.710				4795
sMAO-^{Me_2}SB(^{tBu}N,I*)Ti(CH$_2$SiMe$_3$)$_2$ large scale							
70	9.9		1.825				2311
sMAO(3G)-^{Me_2}SB(^{tBu}N,I*)Ti(CH$_2$Ph)$_2$							
70	9.7	10.0	3.004	3.230	4285	4469	4377
sMAO(3G)-^{Me_2}SB(^{tBu}N,$^{3\text{-}Et}$I*)TiCl$_2$							
70	9.6	9.5	2.534	2.877	3614	4146	3880
sMAO(3G-^{Me_2}SB(^{tBu}N,I*)Ti(CH$_2$SiMe$_3$)$_2$							

70	9.7	9.4	2.362	2.194	3384	3243	3314

Table A3.2. Polymerisation activities, mass of catalyst used, and mass of polymer produced; 2 bar ethylene, 50 mL hexanes, 10 mg catalyst ($[Al]_0$:$[Ti]_0$ = 200:1), 150 mg TiBA and 70 °C.

Time (minutes)	Mass Catalyst (mg)		Mass Polymer (g)		Activity ($kg_{PE}/mol_{Ti}/h/bar$)		Average Activity ($kg_{PE}/mol_{Ti}/h/bar$)
	A	B	A	B	A	B	
			sMAO-^{Me_2}SB($^{t Bu}$N,I*)$TiCl_2$				
5	9.6	9.8	0.677	0.758	5305	5819	5562
15	10.0	9.9	1.871	1.764	4692	4468	4580
30	9.8	9.8	2.602	2.907	3328	3719	3524
60	9.8	9.8	4.495	4.801	2875	3071	2973
			sMAO-^{Me_2}SB($^{i Pr}$N,I*)$TiCl_2$				
5	9.5	8.5	0.208	0.247	1595	2117	1856
15	4.6	10.0	0.278	0.648	1468	1574	1520
30	10.0	10.2	0.979	1.097	1189	1306	1247
60	9.8	10.2	1.337	1.368	828	814	821
			sMAO-^{Me_2}SB(^{Cy}N,I*)$TiCl_2$				
5	10.1	10.2	0.290	0.305	2601	2709	2655
15	9.6	9.8	0.448	0.427	1409	1316	1362
30	9.6	9.6	0.464	0.494	730	777	753
60	9.6	9.4	0.580	0.501	456	402	429
			sMAO-^{Me_2}SB($^{n Bu}$N,I*)$TiCl_2$				
5	10.1	9.8	0.273	0.325	2033	2495	2264
15	10.4	10.1	0.481	0.502	1160	1246	1203
30	10.6	10.5	0.690	0.673	816	803	810
60	9.9	9.6	0.585	0.500	370	327	348
			sMAO-^{Me_2}SB($^{4\text{-}t Bu C_6H_4}$N,I*)$TiCl_2$				
5	10.1	10.1	0.068	0.073	610	655	632
15	9.5	10.5	0.150	0.155	477	446	461
30	9.7	9.6	0.210	0.201	327	316	321
60	10.5	10.5	0.358	0.351	257	252	255
			sMAO-^{Me_2}SB($^{4\text{-}n Bu C_6H_4}$N,I*)$TiCl_2$				
5	10.4	9.9	0.071	0.078	618	714	666
15	9.8	10.2	0.172	0.175	530	518	524
30	9.9	9.7	0.238	0.236	363	367	365
60	9.8	9.6	0.322	0.344	248	271	259
			sMAO-^{Me_2}SB(^{Ph}N,I*)$TiCl_2$				
5	10.4	9,6	0.056	0.056	423	458	441
15	10.7	9.5	0.144	0.126	353	347	350
30	10.3	10.5	0.218	0.200	277	250	263
60	9.4	10.2	0.348	0.353	242	227	235
			sMAO-^{Me_2}SB($^{t Bu}$N,I*)$Ti(CH_2Ph)_2$				
5	10.1	9.8	1.20	1.24	10888	11595	11241
15	10.3	10.5	2.65	2.72	7859	7913	7886
30	10.2	10.1	3.97	3.71	5945	5610	5777
60	10.0	10.5	6.13	6.1	4681	4436	4559
			sMAO-^{Me_2}SB($^{t Bu}$N,I*)$TiMe_2$				
5	10.4	9.7	1.37	1.25	9004	8809	8907
15	10.2	9.7	2.79	2.54	6232	5966	6099
30	10.3	9.6	4.37	4.23	4834	5020	4927

60	10.0	9.7	6.98	6.54	3976	3840	3908
sMAO-^{Me2}SB($^{t Bu}$N,I*)Ti(CH_2SiMe_3)$_2$							
5	10.1	9.8	1.19	1.20	10920	11349	11135
15	9.7	9.9	2.42	2.43	7708	7583	7646
30	10.0	10.0	3.98	4.01	6148	6195	6171
60	10.2	9.8	5.73	5.47	4339	4311	4325
sMAO-^{Me2}SB($^{t Bu}$N,I*)Ti(Cl)CH_2SiMe_3							
5	9.1	9.1	0.703	0.711	6485	6559	6522
15	10.1	10.1	1.351	1.373	3743	3804	3774
30	10.1	9.5	1.730	1.641	2397	2416	2407
60	9.7	9.5	3.034	3.056	2188	2250	2219
sMAO-^{Me,Pr}SB($^{t Bu}$N,I*)$TiCl_2$							
5	10.5	10.3	0.901	0.866	7092	6949	7021
15	10.4	10.3	1.694	1.866	4488	4991	4739
30	10.0	10.1	2.939	3.100	4049	4228	4138
60	9.3	9.6	4.028	4.154	2983	2980	2982
sMAO-^{Me2}SB($^{t Bu}$N,$^{3\text{-}Et}$I*)$TiCl_2$							
5	10.5	10.5	0.813	0.814	6008	6015	6012
15	10.5	10.3	1.752	1.528	4316	3764	4040
30	9.6	9.4	2.750	2.531	3704	3482	3593
60	9.5	9.6	3.640	3.669	2478	2497	2487
sMAO-^{Me2}SB($^{t Bu}$N,I*)$ZrCl_2$							
5	11.0	10.8	0.024	0.03	186	237	212
15	9.7	10.0	0.043	0.041	126	117	121
30	9.5	9.5	0.068	0.071	102	106	104
60	9.7	10.5	0.187	0.159	137	108	122

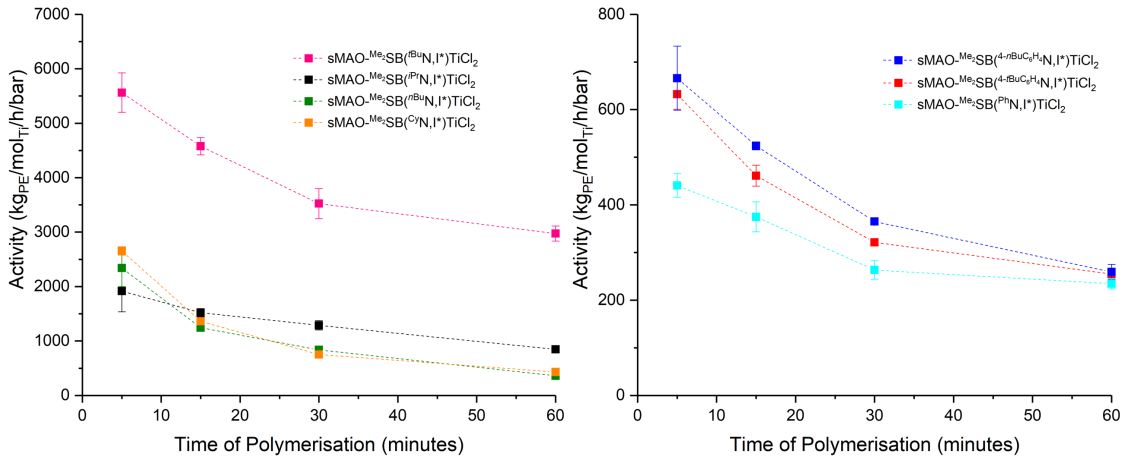

Figure A3.1. Time dependence of slurry phase ethylene polymerisation activity for sMAO-^{Me2}SB(^{R}N,I*)$TiCl_2$ in function of time; 2 bar ethylene, 50 mL hexanes, 10 mg catalyst ($[Al]_0$:$[Ti]_0$ = 200:1), 150 mg TiBA and 70 °C.

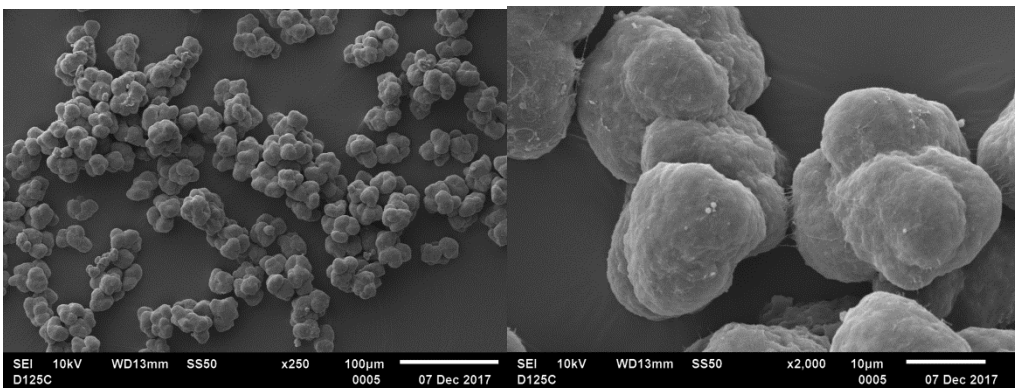

Figure A3.2. SEM images of polyethylene synthesised using sMAO-^{Me_2}SB($^{t\text{Bu}}$N,I*)TiCl$_2$; 2 bar ethylene, 50 mL hexanes, 10 mg catalyst ([Al]$_0$:[Ti]$_0$ = 200:1), 150 mg TiBA, 70 °C and 30 minutes.

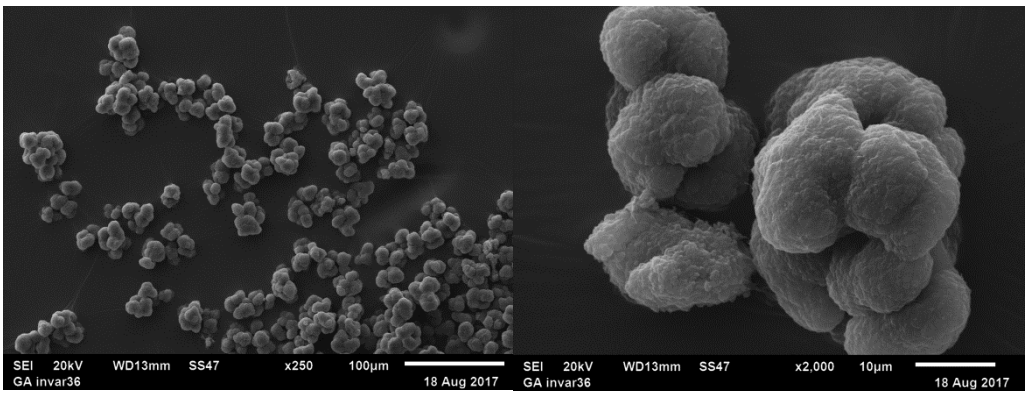

Figure A3.3. SEM images of polyethylene synthesised using sMAO-^{Me_2}SB($^{i\text{Pr}}$N,I*)TiCl$_2$; 2 bar ethylene, 50 mL hexanes, 10 mg catalyst ([Al]$_0$:[Ti]$_0$ = 200:1), 150 mg TiBA, 70 °C and 30 minutes.

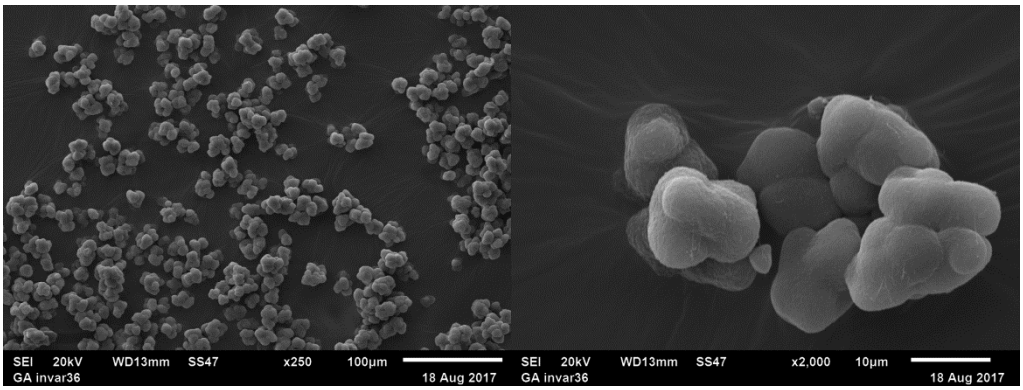

Figure A3.4. SEM images of polyethylene synthesised using sMAO-^{Me_2}SB($^{n\text{Bu}}$N,I*)TiCl$_2$; 2 bar ethylene, 50 mL hexanes, 10 mg catalyst ([Al]$_0$:[Ti]$_0$ = 200:1), 150 mg TiBA, 70 °C and 30 minutes.

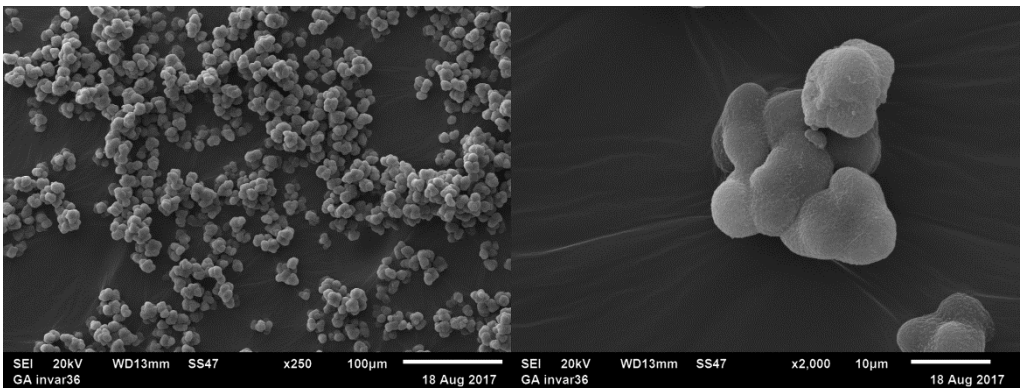

Figure A3.5. SEM images of polyethylene synthesised using sMAO-^{Me_2}SB($^{4\text{-}n\text{BuC}_6\text{H}_4}$N,I*)$TiCl_2$; 2 bar ethylene, 50 mL hexanes, 10 mg catalyst ($[Al]_0$:$[Ti]_0$ = 200:1), 150 mg TiBA, 70 °C and 30 minutes.

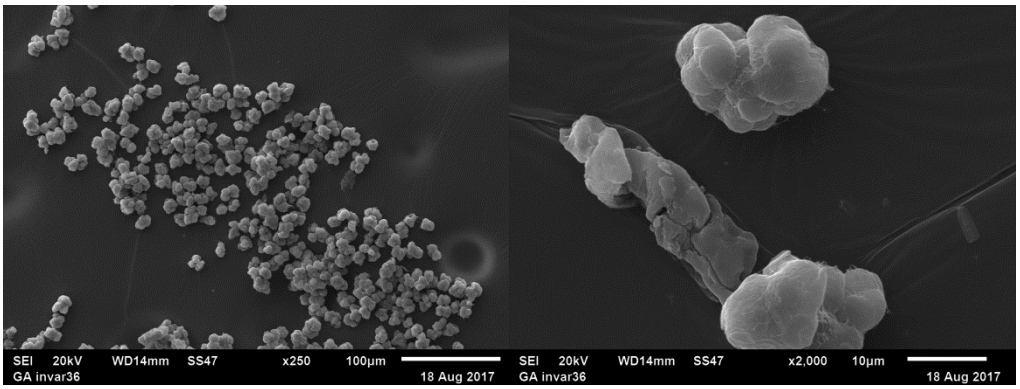

Figure A3.6. SEM images of polyethylene synthesised using sMAO-^{Me_2}SB($^{4\text{-}t\text{BuC}_6\text{H}_4}$N,I*)$TiCl_2$; 2 bar ethylene, 50 mL hexanes, 10 mg catalyst ($[Al]_0$:$[Ti]_0$ = 200:1), 150 mg TiBA, 70 °C and 30 minutes.

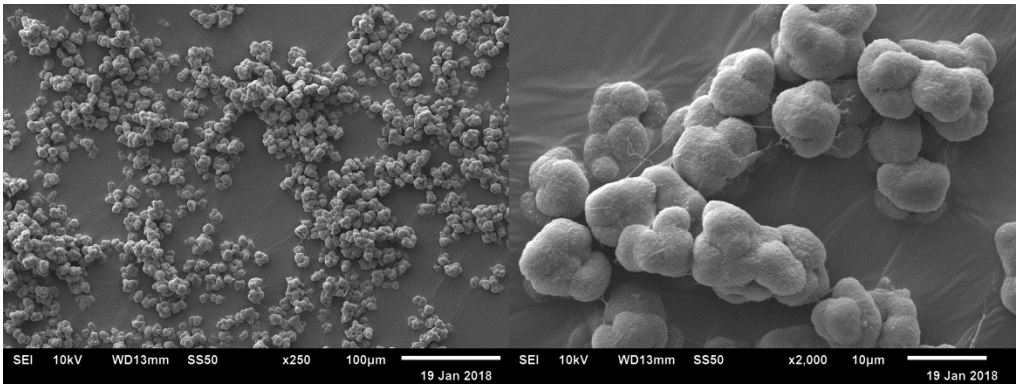

Figure A3.7. SEM images of polyethylene synthesised using sMAO-^{Me_2}SB(^{Ph}N,I*)$TiCl_2$; 2 bar ethylene, 50 mL hexanes, 10 mg catalyst ($[Al]_0$:$[Ti]_0$ = 200:1), 150 mg TiBA, 70 °C and 30 minutes.

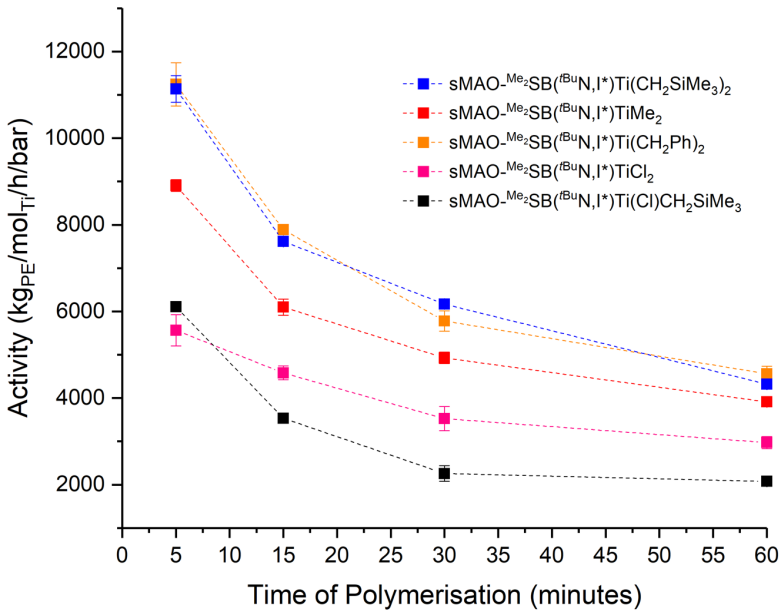

Figure A3.8. Ethylene polymerisation activities for sMAO-^{Me_2}SB($^{t Bu}$N,I*)Ti(Cl)CH_2SiMe_3 and sMAO-^{Me_2}SB($^{t Bu}$N,I*)TiR_2 (R = Cl, Me, CH_2Ph and CH_2SiMe_3); 2 bar ethylene, 50 mL hexanes, 10 mg catalyst ($[Al]_0$:$[Ti]_0$ = 200:1), 150 mg TiBA and 70 °C.

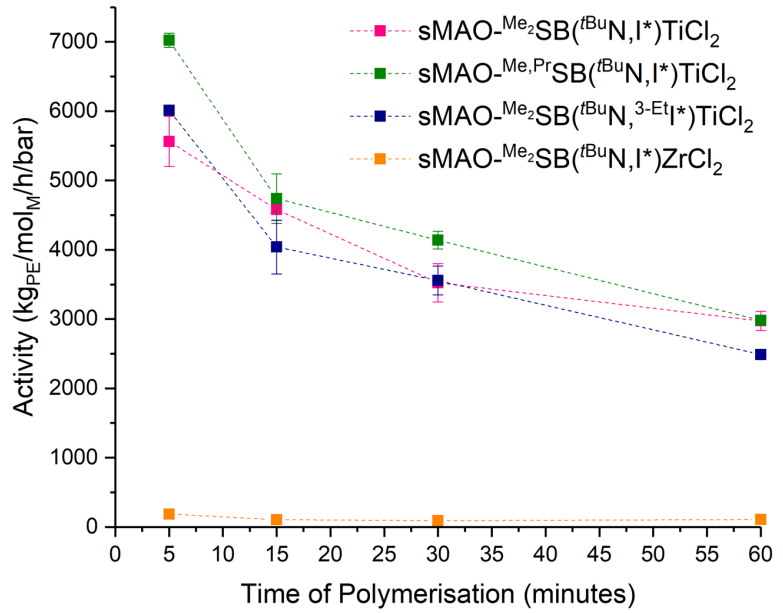

Figure A3.9. Slurry-phase ethylene polymerisation activities for sMAO-^{Me_2}SB($^{t Bu}$N,$^{3\text{-}Et}$I*)$TiCl_2$, sMAO-^{Me,R}SB($^{t Bu}$N,I*)$TiCl_2$ (R = Me and Pr) and sMAO-^{Me_2}SB($^{t Bu}$N,I*)$ZrCl_2$; 2 bar ethylene, 50 mL hexanes, 10 mg catalyst ($[Al]_0$:$[Ti]_0$ = 200:1), 150 mg TiBA and 70 °C.

Table A3.3. Polymer molecular weight distribution values (M_w/M_n) for $^{Me_2}SB(^{tBu}N,I^*)TiCl_2$, $^{Me_2}SB(^{tBu}N,^{3\text{-}Et}I^*)TiCl_2$, $^{Me,Pr}SB(^{tBu}N,I^*)TiCl_2$ and $^{Me_2}SB(^{tBu}N,I^*)Ti(Cl)CH_2SiMe_3$ supported on sMAO, LDHMAO and SSMAO; 2 bar ethylene, 50 mL hexanes, 10 mg catalyst ($[Al]_0:[Ti]_0$ = 200:1), 150 mg TiBA and 30 minutes.

Complex	Support	Temperature (°C)				
		50	60	70	80	90
$^{Me_2}SB(^{tBu}N,I^*)TiCl_2$	sMAO	4.1	4.4	6.6	6.8	6.7
	LDHMAO	3.2	3.2	3.5	3.7	4.3
	SSMAO	4.2	4.1	5.3	6.2	5.4
$^{Me_2}SB(^{tBu}N,^{3\text{-}Et}I^*)TiCl_2$	sMAO	3.7	3.3	4.9	4.7	4.5
	LDHMAO	3.9	3.8	4.2	4.3	4.4
	SSMAO	3.7	5.1	5.0	5.4	6.1
$^{Me,Pr}SB(^{tBu}N,I^*)TiCl_2$	sMAO	3.2	3.5	3.5	3.4	3.9
	LDHMAO	3.7	3.6	4.0	4.0	4.8
	SSMAO	3.5	3.6	4.0	5.2	5.3
$^{Me_2}SB(^{tBu}N,I^*)Ti(Cl)CH_2SiMe_3$	sMAO	3.2	3.8	3.2	3.9	4.1
	LDHMAO	4.2	4.1	3.7	4.4	5.4
	SSMAO	4.3	3.9	4.3	4.1	4.6

Table A3.4. Polymer molecular weight distribution values (M_w/M_n) for $^{Me_2}SB(^{tBu}N,I^*)TiCl_2$, and $^{Me_2}SB(^{tBu}N,I^*)Ti(Cl)CH_2SiMe_3$ supported on 1st and 3rd generation sMAO; 2 bar ethylene, 50 mL hexanes, 10 mg catalyst ($[Al]_0:[Ti]_0$ = 200:1), 150 mg TiBA and 30 minutes.

Complex	Support	Temperature (°C)				
		50	60	70	80	90
$^{Me_2}SB(^{tBu}N,I^*)TiCl_2$	sMAO (1G)	3.6	3.9	3.6	5.7	5.8
	sMAO (3G)	4.1	4.4	6.6	6.8	6.7
$^{Me_2}SB(^{tBu}N,I^*)Ti(Cl)CH_2SiMe_3$	sMAO (1G)	3.6	3.9	3.9	4.4	4.0
	sMAO (3G)	3.2	3.8	3.2	3.9	4.1

A4. Appendix for Chapter 4

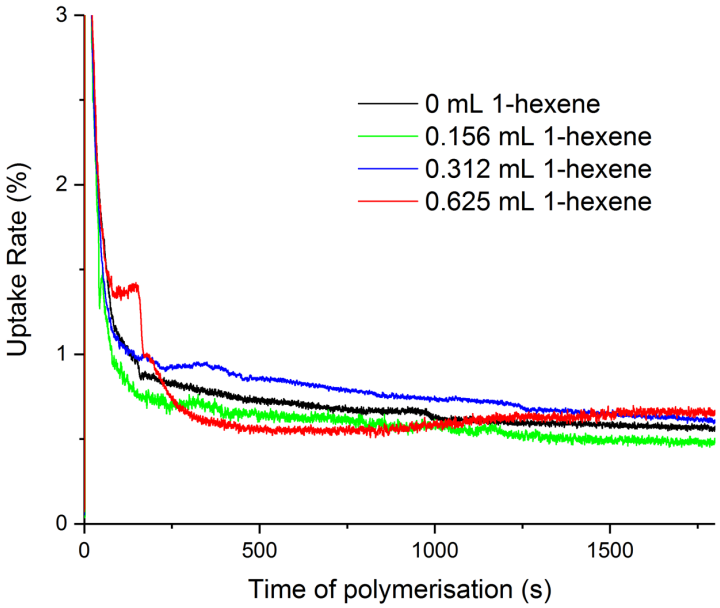

Figure A4.1. Ethylene uptake rate plots for sMAO-^{Me_2}SB(^{tBu}N,I*)TiCl$_2$ at 70 °C; 10 mg catalyst ([Al]$_0$:[Ti]$_0$ = 200:1), 2 bar ethylene, 50 mL hexanes, 150 mg TiBA and 30 minutes. Y-axis is a guide with percentage value providing a quantitative measure of uptake.

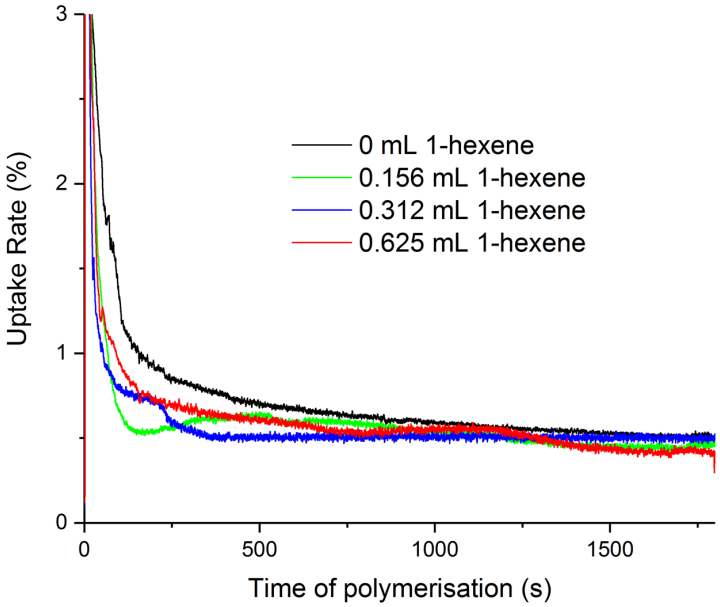

Figure A4.2. Ethylene uptake rate plots for sMAO-^{Me_2}SB(^{tBu}N,I*)TiCl$_2$ at 80 °C; 10 mg catalyst ([Al]$_0$:[Ti]$_0$ = 200:1), 2 bar ethylene, 50 mL hexanes, 150 mg TiBA and 30 minutes. Y-axis is a guide with percentage value providing a quantitative measure of uptake.

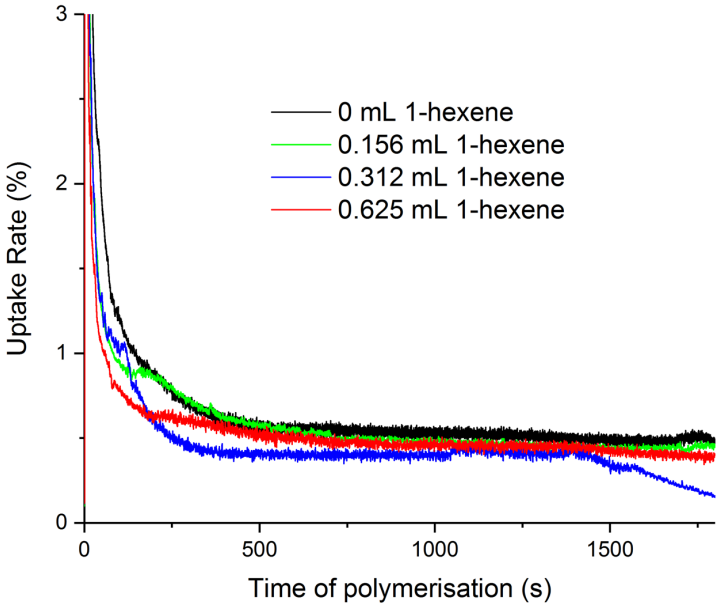

Figure A4.3. Ethylene uptake rate plots for sMAO-^{Me_2}SB(^{tBu}N,I*)TiCl$_2$ at 90 °C; 10 mg catalyst ([Al]$_0$:[Ti]$_0$ = 200:1), 2 bar ethylene, 50 mL hexanes, 150 mg TiBA and 30 minutes. Y-axis is a guide with percentage value providing a quantitative measure of uptake.

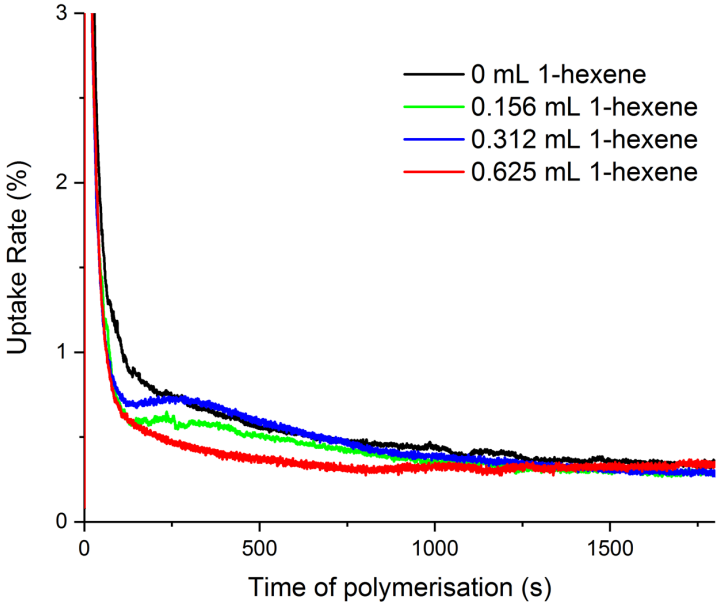

Figure A4.4. Ethylene uptake rate plots for sMAO-^{Me_2}SB(^{tBu}N,Cp*)TiCl$_2$; 10 mg catalyst ([Al]$_0$:[Ti]$_0$ = 200:1), 2 bar ethylene, 50 mL hexanes, 150 mg TiBA, 70 °C and 30 minutes. Y-axis is a guide with percentage value providing a quantitative measure of uptake.

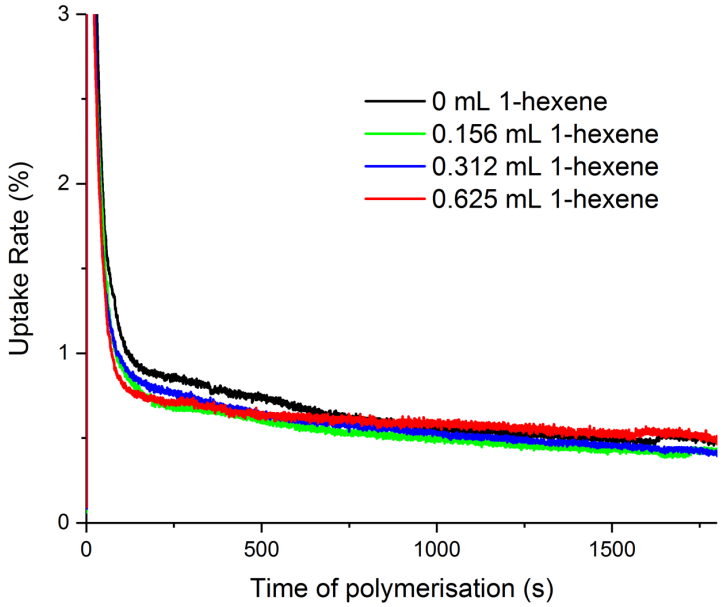

Figure A4.5. Ethylene uptake rate plots for sMAO-^{Me,Pr}SB($^{t Bu}$N,I*)TiCl$_2$; 10 mg catalyst ([Al]$_0$:[Ti]$_0$ = 200:1), 2 bar ethylene, 50 mL hexanes, 150 mg TiBA, 70 °C and 30 minutes. Y-axis is a guide with percentage value providing a quantitative measure of uptake.

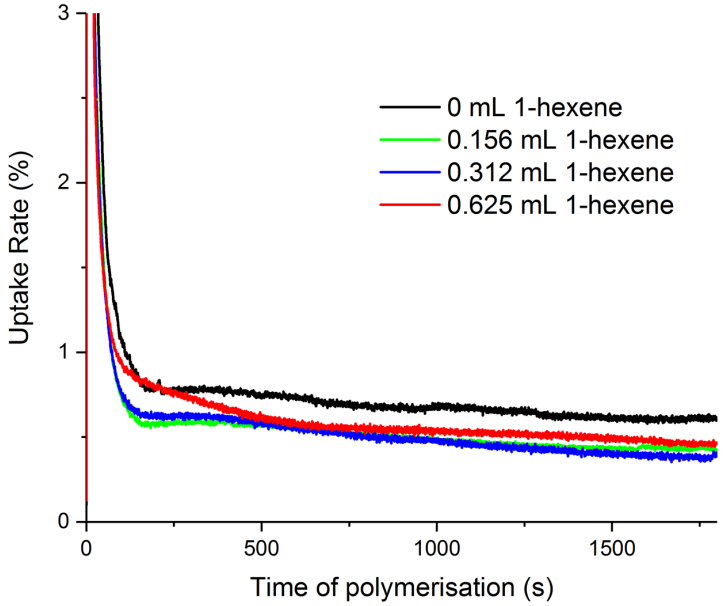

Figure A4.6. Ethylene uptake rate plots for sMAO-^{Me_2}SB($^{t Bu}$N,$^{3\text{-}Et}$I*)TiCl$_2$; 10 mg catalyst ([Al]$_0$:[Ti]$_0$ = 200:1), 2 bar ethylene, 50 mL hexanes, 150 mg TiBA, 70 °C and 30 minutes. Y-axis is a guide with percentage value providing a quantitative measure of uptake.

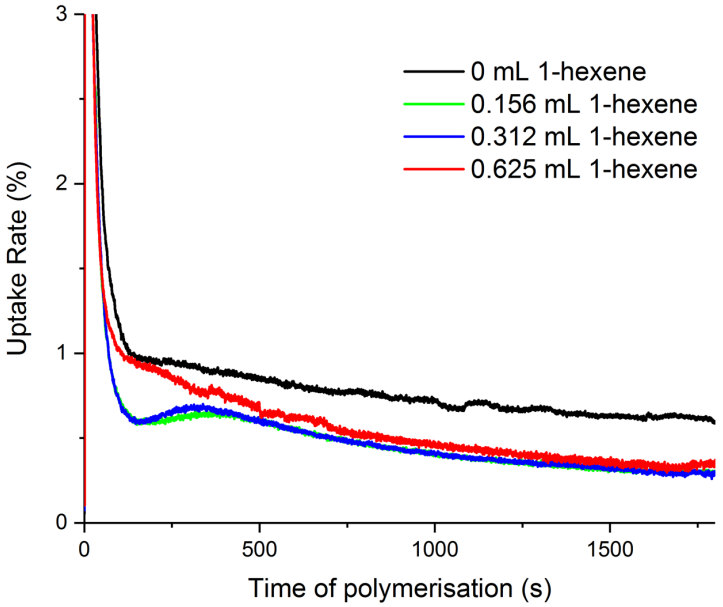

Figure A4.7. Ethylene uptake rate plots for sMAO-^{Me_2}SB($^{t Bu}$N,I*)Ti($CH_2Ph)_2$; 10 mg catalyst ($[Al]_0$:$[Ti]_0$ = 200:1), 2 bar ethylene, 50 mL hexanes, 150 mg TiBA, 70 °C and 30 minutes. Y-axis is a guide with percentage value providing a quantitative measure of uptake.

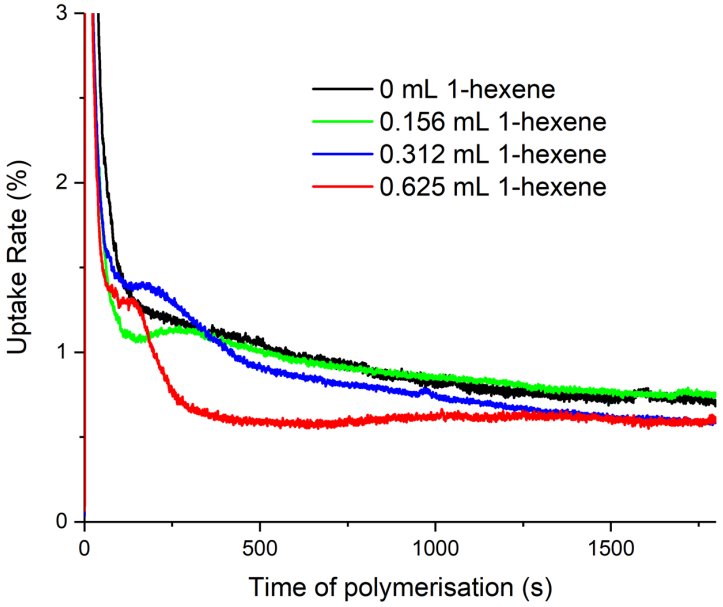

Figure A4.8. Ethylene uptake rate plots for sMAO-^{Me_2}SB($^{t Bu}$N,I*)Ti(Cl)CH_2SiMe_3; 10 mg catalyst ($[Al]_0$:$[Ti]_0$ = 200:1), 2 bar ethylene, 50 mL hexanes, 150 mg TiBA, 70 °C and 30 minutes. Y-axis is a guide with percentage value providing a quantitative measure of uptake.

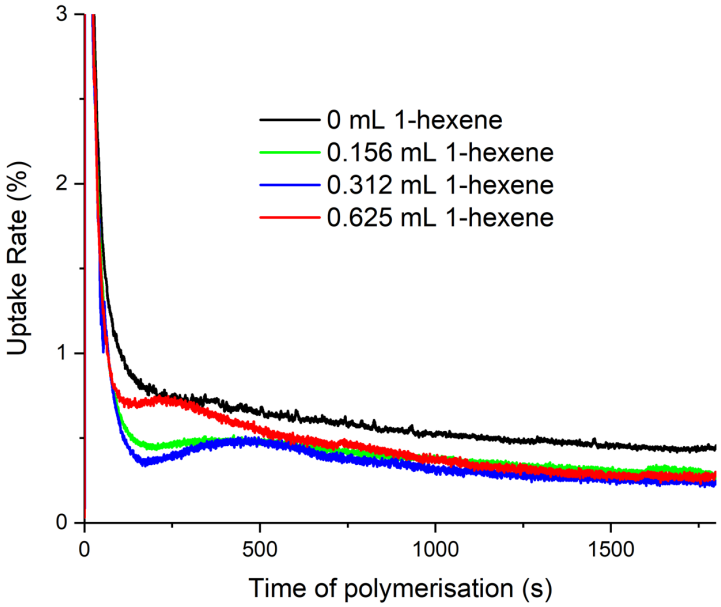

Figure A4.9. Ethylene uptake rate plots for sMAO-^{Me_2}SB($^{t\text{Bu}}$N,I*)Ti(CH_2SiMe_3)$_2$; 10 mg catalyst ([Al]$_0$:[Ti]$_0$ = 200:1), 2 bar ethylene, 50 mL hexanes, 150 mg TiBA, 70 °C and 30 minutes. Y-axis is a guide with percentage value providing a quantitative measure of uptake.

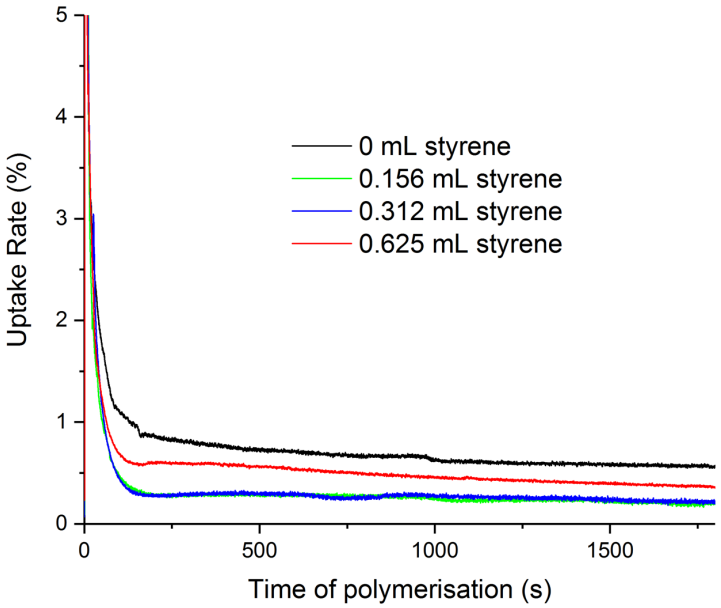

Figure A4.10. Ethylene uptake rate plots for sMAO-^{Me_2}SB($^{t\text{Bu}}$N,I*)$TiCl_2$; 10 mg catalyst ([Al]$_0$:[Ti]$_0$ = 200:1), 2 bar ethylene, 50 mL hexanes, 150 mg TiBA, 70 °C and 30 minutes. Y-axis is a guide with percentage value providing a quantitative measure of uptake.

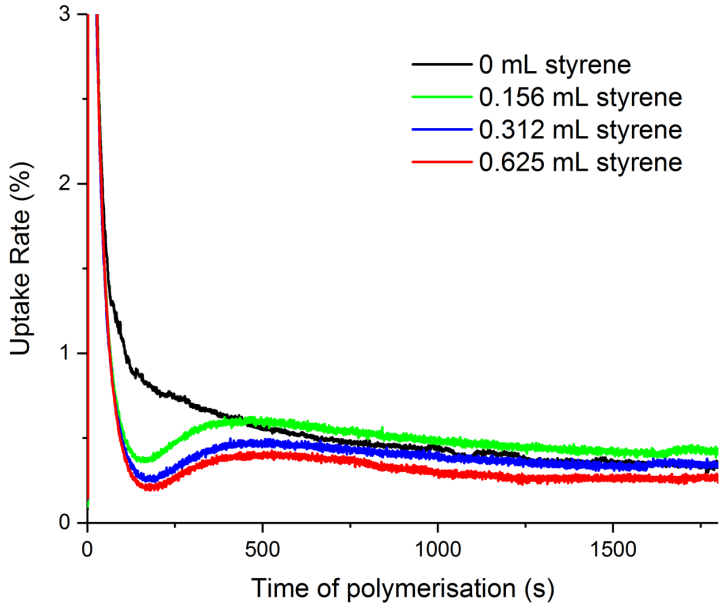

Figure A4.11. Ethylene uptake rate plots for sMAO-^{Me_2}SB(^{tBu}N,Cp*)TiCl$_2$; 10 mg catalyst ([Al]$_0$:[Ti]$_0$ = 200:1), 2 bar ethylene, 50 mL hexanes, 150 mg TiBA, 70 °C and 30 minutes. Y-axis is a guide with percentage value providing a quantitative measure of uptake.

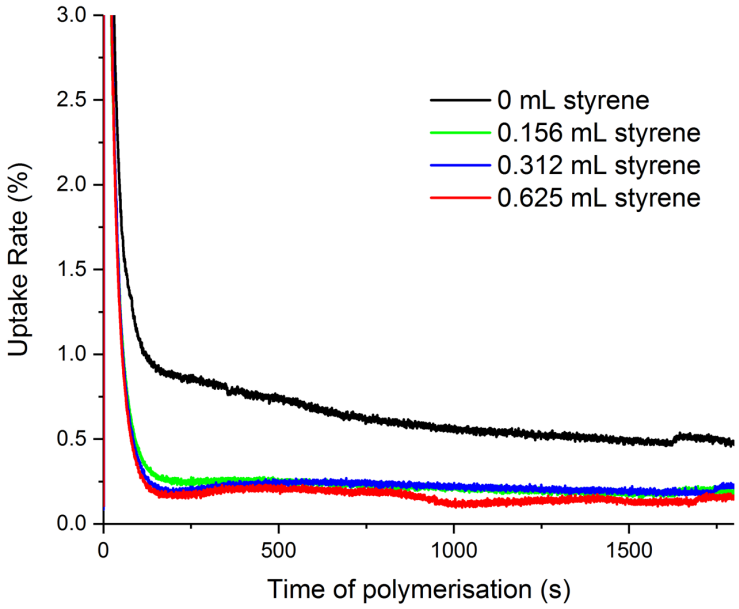

Figure A4.12. Ethylene uptake rate plots for sMAO-^{Me,Pr}SB(^{tBu}N,I*)TiCl$_2$; 10 mg catalyst ([Al]$_0$:[Ti]$_0$ = 200:1), 2 bar ethylene, 50 mL hexanes, 150 mg TiBA, 70 °C and 30 minutes. Y-axis is a guide with percentage value providing a quantitative measure of uptake.

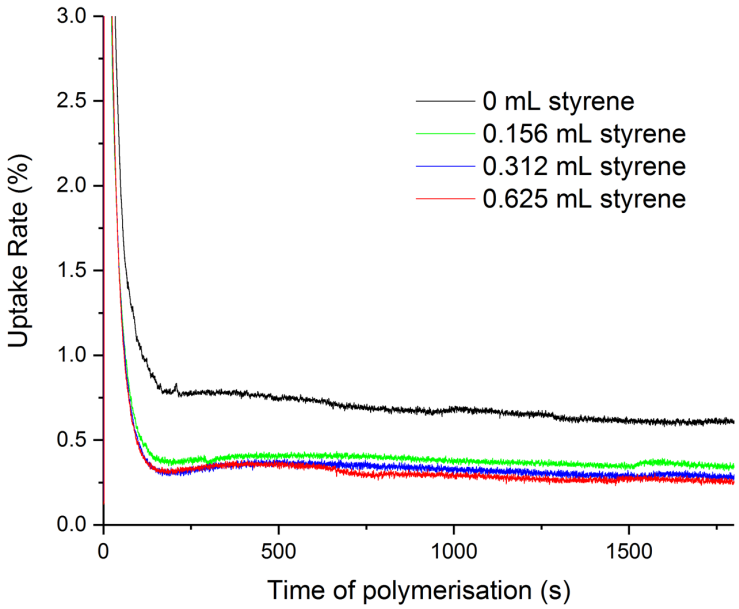

Figure A4.13. Ethylene uptake rate plots for sMAO-^{Me_2}SB($^{t Bu}$N,$^{3\text{-}Et}$I*)TiCl$_2$; 10 mg catalyst ([Al]$_0$:[Ti]$_0$ = 200:1), 2 bar ethylene, 50 mL hexanes, 150 mg TiBA, 70 °C and 30 minutes. Y-axis is a guide with percentage value providing a quantitative measure of uptake.

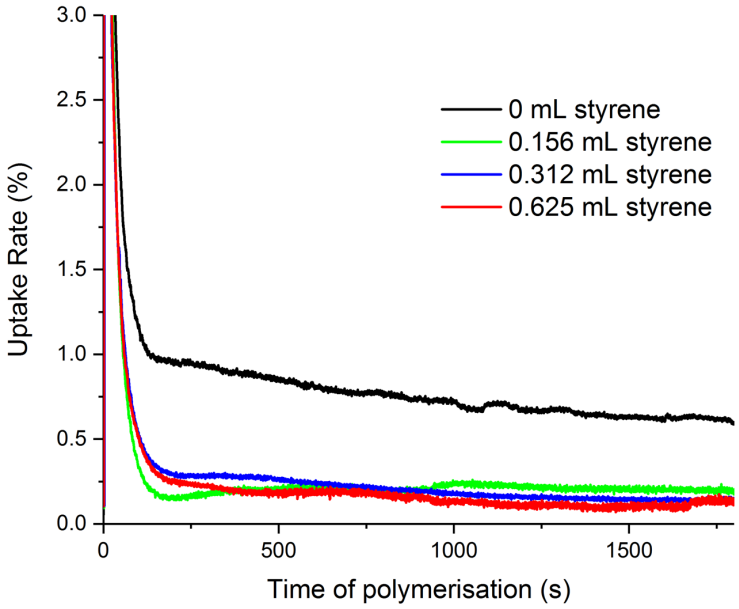

Figure A4.14. Ethylene uptake rate plots for sMAO-^{Me_2}SB($^{t Bu}$N,I*)Ti(CH$_2$Ph)$_2$; 10 mg catalyst ([Al]$_0$:[Ti]$_0$ = 200:1), 2 bar ethylene, 50 mL hexanes, 150 mg TiBA, 70 °C and 30 minutes. Y-axis is a guide with percentage value providing a quantitative measure of uptake.

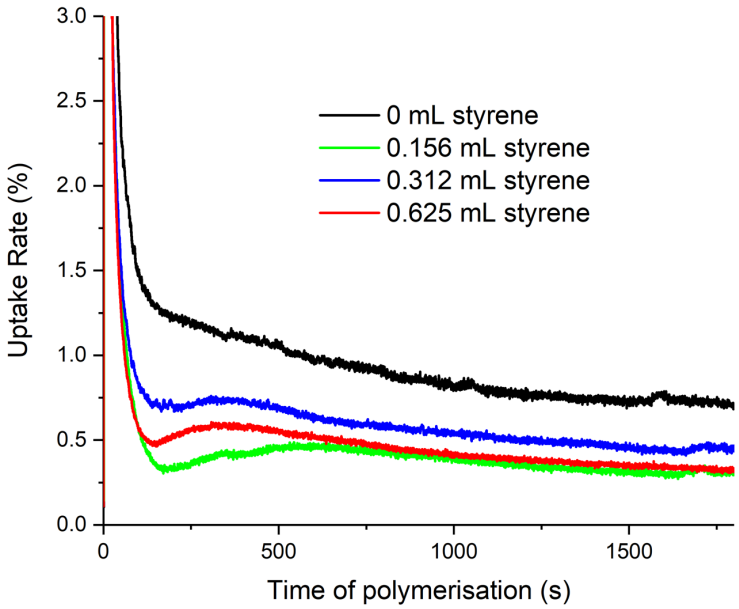

Figure A4.15. Ethylene uptake rate plots for sMAO-^{Me_2}SB($^{t Bu}$N,I*)Ti(Cl)CH_2SiMe_3; 10 mg catalyst ($[Al]_0$:$[Ti]_0$ = 200:1), 2 bar ethylene, 50 mL hexanes, 150 mg TiBA, 70 °C and 30 minutes. Y-axis is a guide with percentage value providing a quantitative measure of uptake.

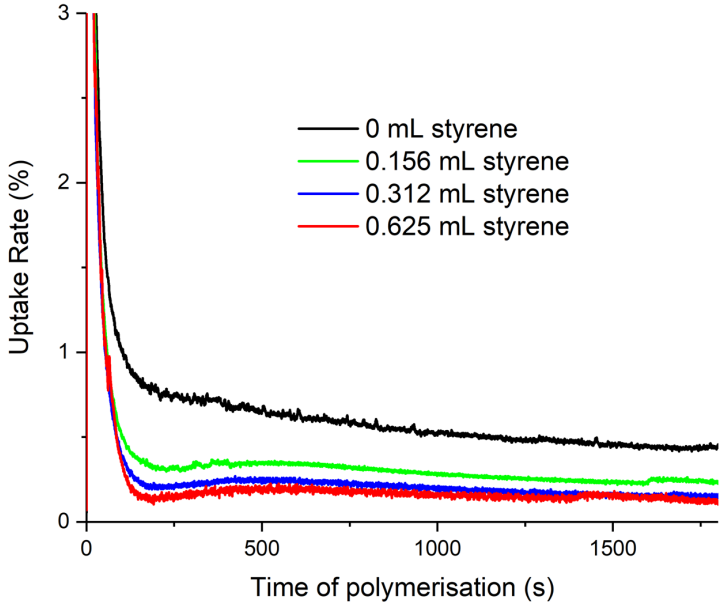

Figure A4.16. Ethylene uptake rate plots for sMAO-^{Me_2}SB($^{t Bu}$N,I*)Ti(CH_2SiMe_3)$_2$; 10 mg catalyst ($[Al]_0$:$[Ti]_0$ = 200:1), 2 bar ethylene, 50 mL hexanes, 150 mg TiBA, 70 °C and 30 minutes. Y-axis is a guide with percentage value providing a quantitative measure of uptake.

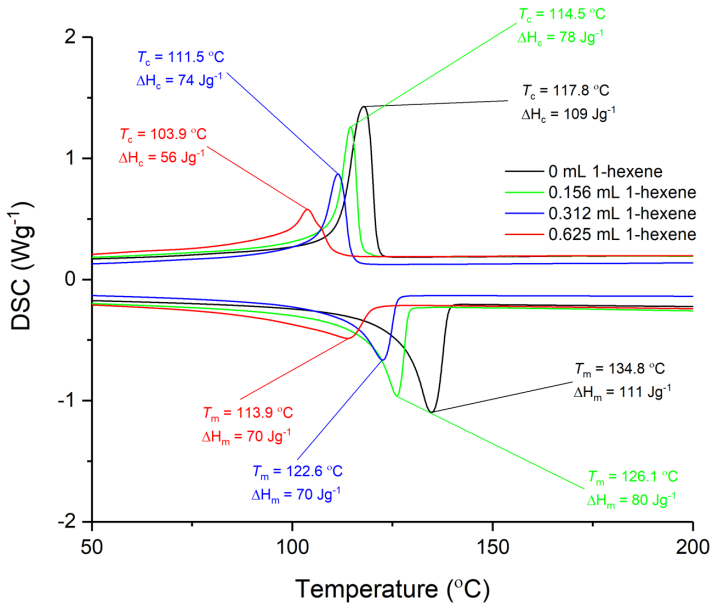

Figure A4.17. DSC plot for polymers produced by sMAO-^{Me2}SB(^{tBu}N,I*)TiCl$_2$ at 30 °C for 0 mL (black), 0.156 mL (green), 0.312 mL (blue), and 0.625 mL 1-hexene (red).

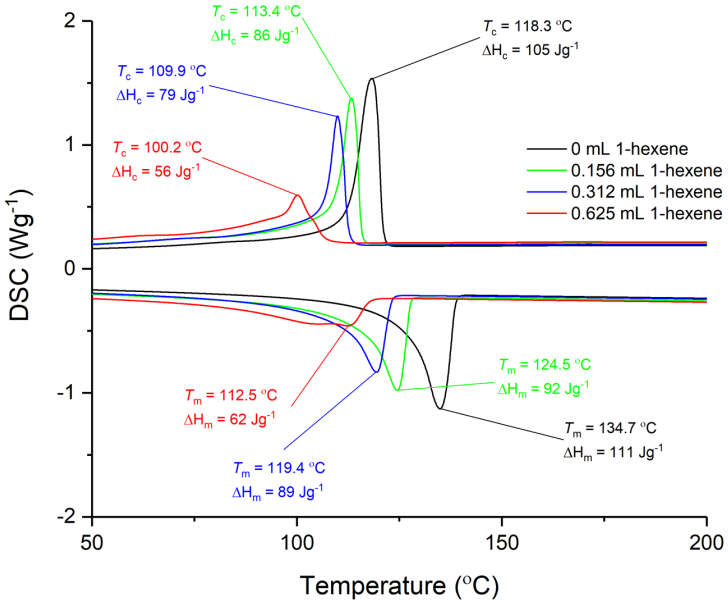

Figure A4.18. DSC plot for polymers produced by sMAO-^{Me2}SB(^{tBu}N,I*)TiCl$_2$ at 40 °C for 0 mL (black), 0.156 mL (green), 0.312 mL (blue), and 0.625 mL 1-hexene (red).

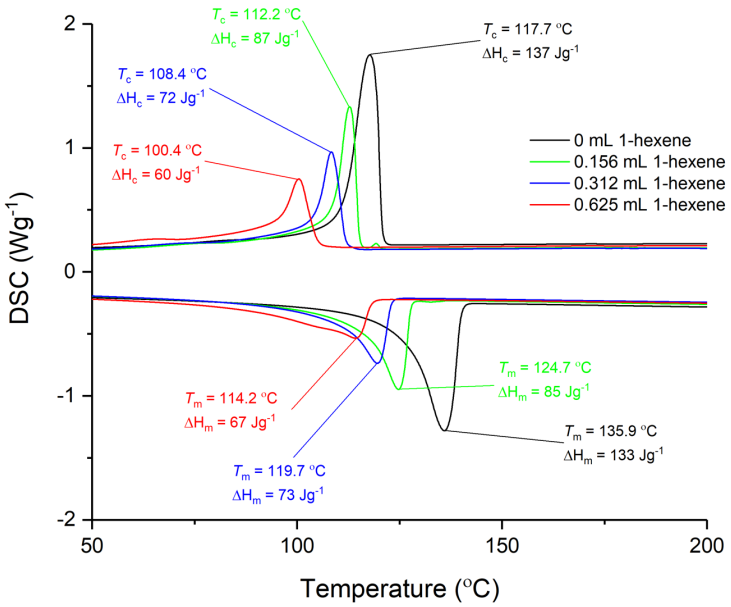

Figure A4.19. DSC plot for polymers produced by sMAO-^{Me2}SB(^{tBu}N,I*)TiCl$_2$ at 50 °C for 0 mL (black), 0.156 mL (green), 0.312 mL (blue), and 0.625 mL 1-hexene (red).

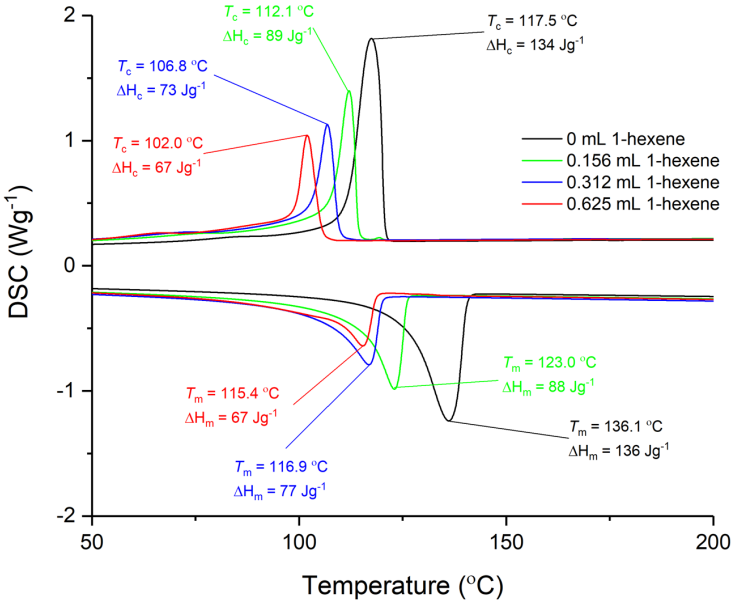

Figure A4.20. DSC plot for polymers produced by sMAO-^{Me2}SB(^{tBu}N,I*)TiCl$_2$ at 60 °C for 0 mL (black), 0.156 mL (green), 0.312 mL (blue), and 0.625 mL 1-hexene (red).

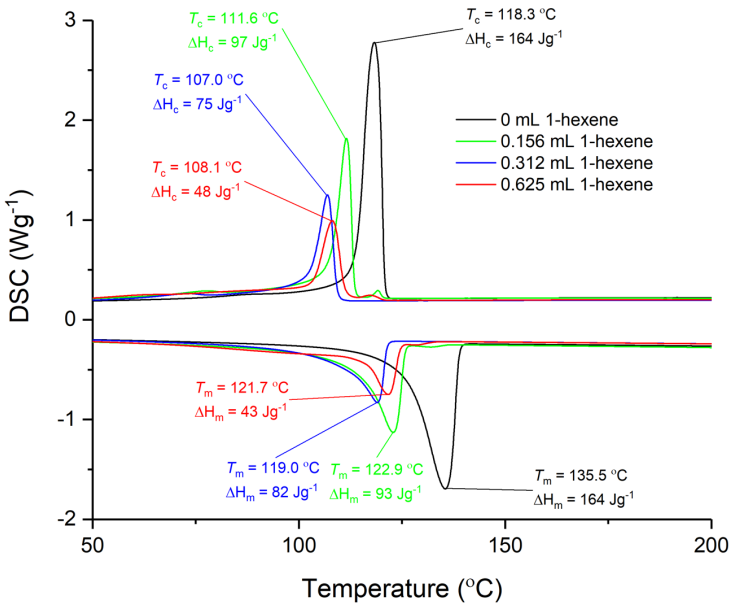

Figure A4.21. DSC plot for polymers produced by sMAO-^{Me2}SB(^{tBu}N,I*)TiCl$_2$ at 80 °C for 0 mL (black), 0.156 mL (green), 0.312 mL (blue), and 0.625 mL 1-hexene (red).

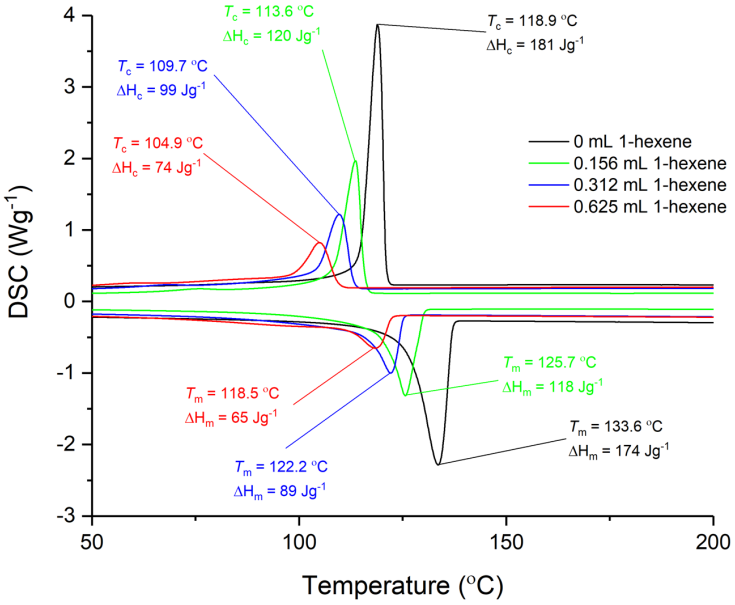

Figure A4.22. DSC plot for polymers produced by sMAO-^{Me2}SB(^{tBu}N,I*)TiCl$_2$ at 90 °C for 0 mL (black), 0.156 mL (green), 0.312 mL (blue), and 0.625 mL 1-hexene (red).

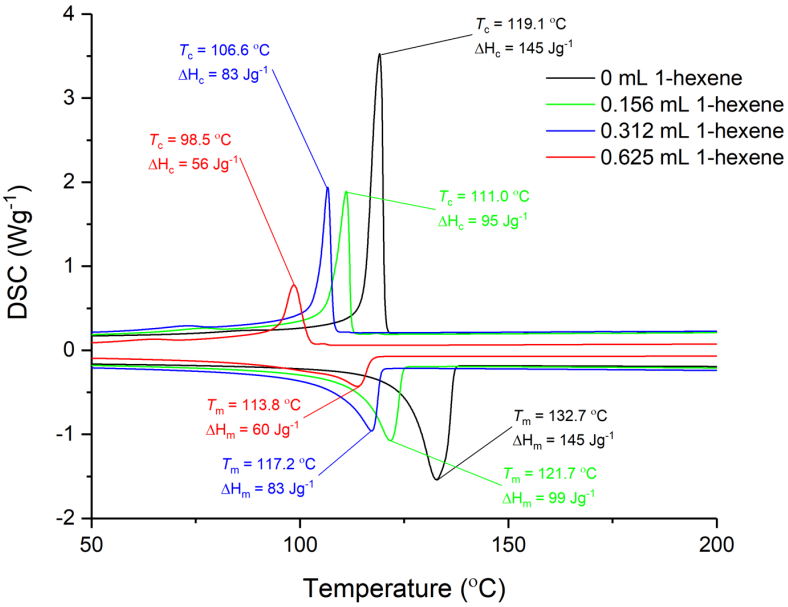

Figure A4.23. DSC plot for polymers produced by sMAO-^{Me2}SB(^{tBu}N,$^{3\text{-}Et}$I*)TiCl$_2$ at 70 °C for 0 mL (black), 0.156 mL (green), 0.312 mL (blue), and 0.625 mL 1-hexene (red).

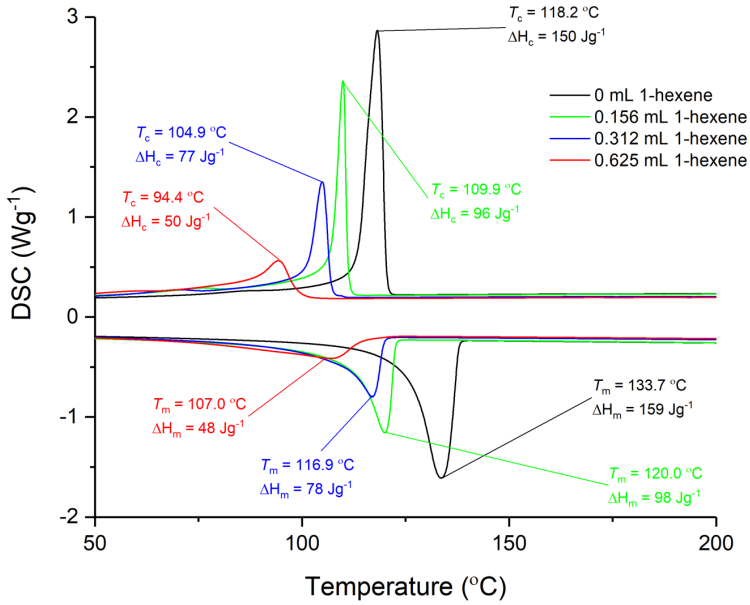

Figure A4.24. DSC plot for polymers produced by sMAO-^{Me2}SB(^{tBu}N,Cp*)TiCl$_2$ at 70 °C for 0 mL (black), 0.156 mL (green), 0.312 mL (blue), and 0.625 mL 1-hexene (red).

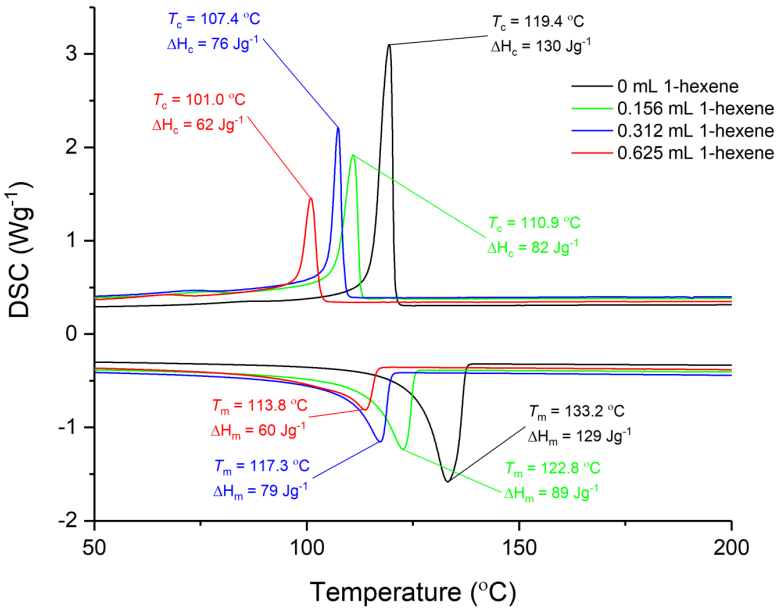

Figure A4.25. DSC plot for polymers produced by sMAO-^{Me,Pr}SB($^{t\text{Bu}}$N,I*)TiCl$_2$ at 70 °C for 0 mL (black), 0.156 mL (green), 0.312 mL (blue), and 0.625 mL 1-hexene (red).

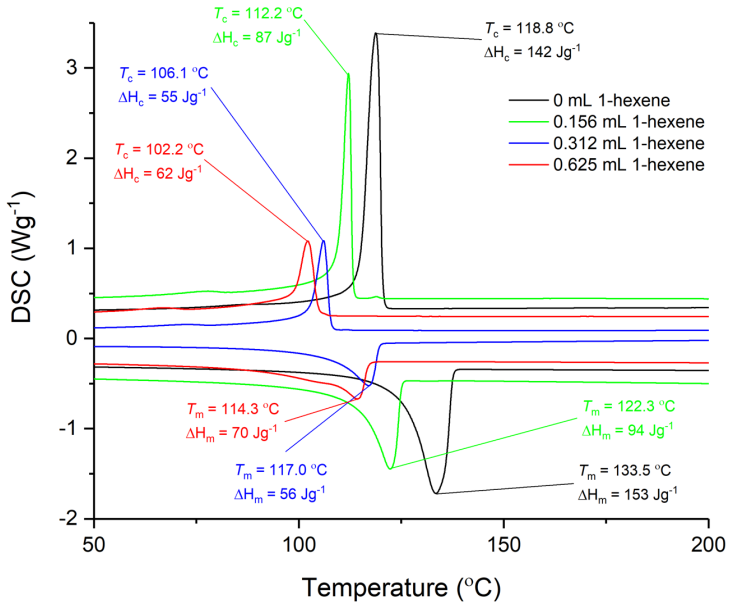

Figure A4.26. DSC plot for polymers produced by sMAO-^{Me_2}SB($^{t\text{Bu}}$N,I*)Ti(CH$_2$Ph)$_2$ at 70 °C for 0 mL (black), 0.156 mL (green), 0.312 mL (blue), and 0.625 mL 1-hexene (red).

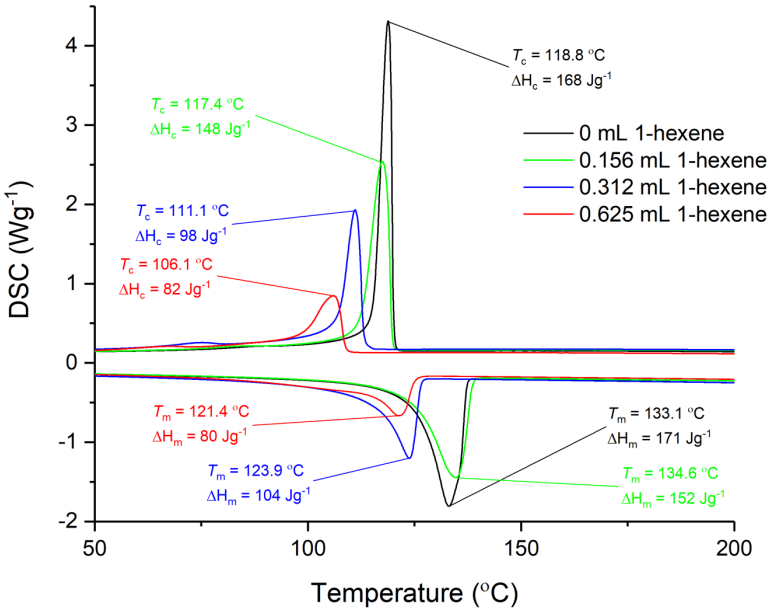

Figure A4.27. DSC plot for polymers produced by sMAO-^{Me2}SB($^{t\text{Bu}}$N,I*)Ti(Cl)CH_2SiMe_3 at 70 °C for 0 mL (black), 0.156 mL (green), 0.312 mL (blue), and 0.625 mL 1-hexene (red).

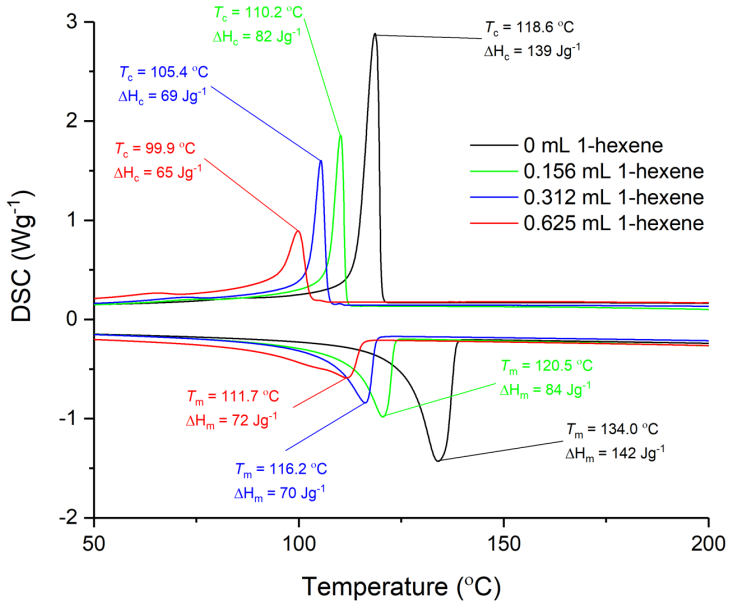

Figure A4.28. DSC plot for polymers produced by sMAO-^{Me2}SB($^{t\text{Bu}}$N,I*)Ti(CH_2SiMe_3)$_2$ at 70 °C for 0 mL (black), 0.156 mL (green), 0.312 mL (blue), and 0.625 mL 1-hexene (red).

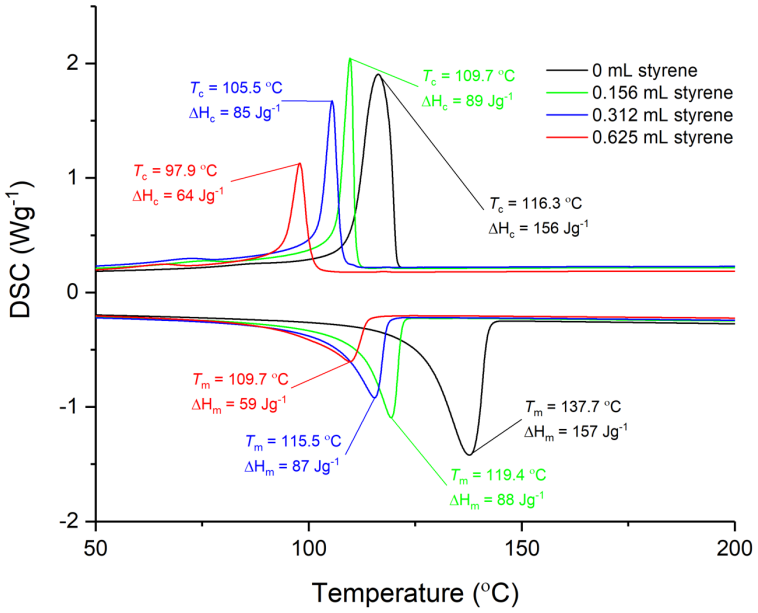

Figure A4.29. DSC plot for polymers produced by sMAO-^{Me2}SB(^{tBu}N,I*)TiCl$_2$ at 70 °C for 0 mL (black), 0.156 mL (green), 0.312 mL (blue), and 0.625 mL styrene (red).

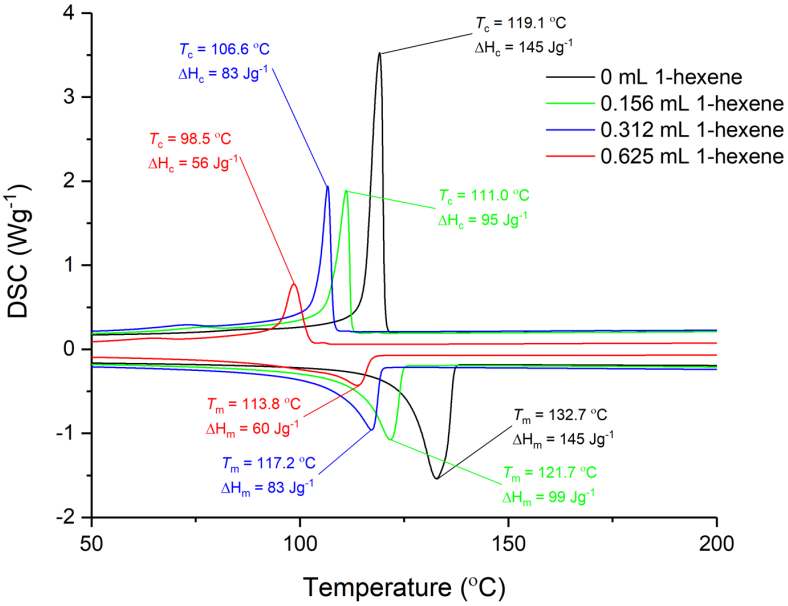

Figure A4.30. DSC plot for polymers produced by sMAO-^{Me2}SB(^{tBu}N,$^{3\text{-}Et}$I*)TiCl$_2$ at 70 °C for 0 mL (black), 0.156 mL (green), 0.312 mL (blue), and 0.625 mL styrene (red).

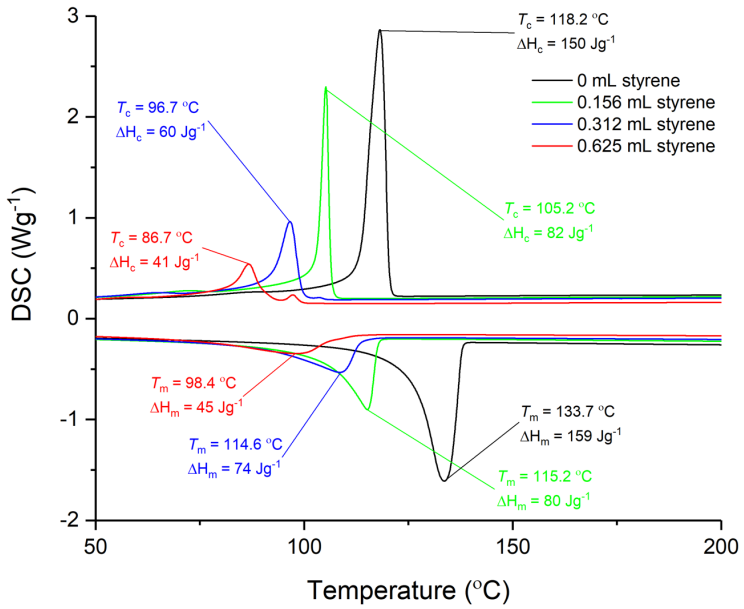

Figure A4.31. DSC plot for polymers produced by sMAO-^{Me_2}SB($^{t\text{Bu}}$N,Cp*)TiCl$_2$ at 70 °C for 0 mL (black), 0.156 mL (green), 0.312 mL (blue), and 0.625 mL styrene (red).

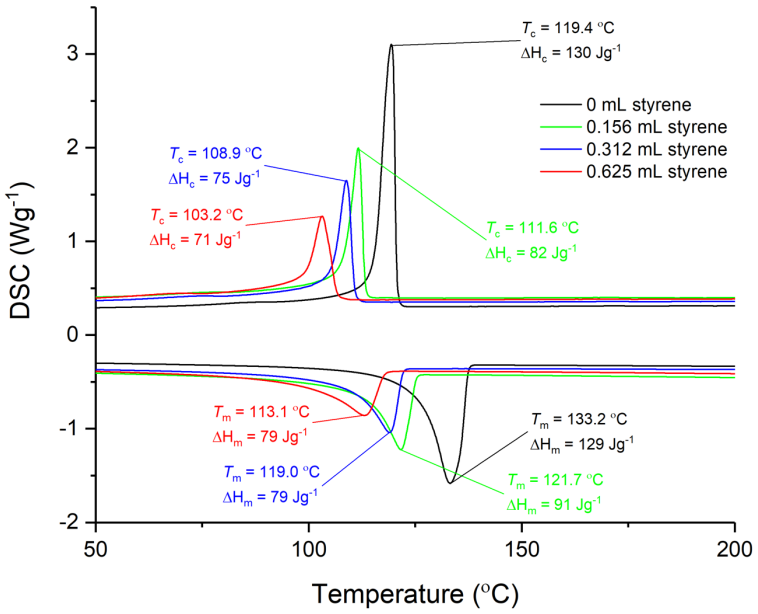

Figure A4.32. DSC plot for polymers produced by sMAO-^{Me,Pr}SB($^{t\text{Bu}}$N,I*)TiCl$_2$ at 70 °C for 0 mL (black), 0.156 mL (green), 0.312 mL (blue), and 0.625 mL styrene (red).

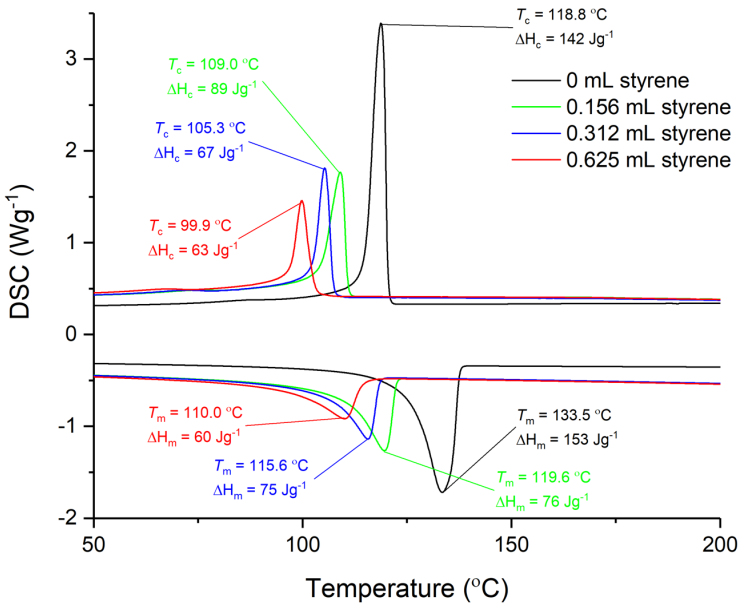

Figure A4.33. DSC plot for polymers produced by sMAO-^{Me2}SB(^{tBu}N,I*)Ti(CH$_2$Ph)$_2$ at 70 °C for 0 mL (black), 0.156 mL (green), 0.312 mL (blue), and 0.625 mL styrene (red).

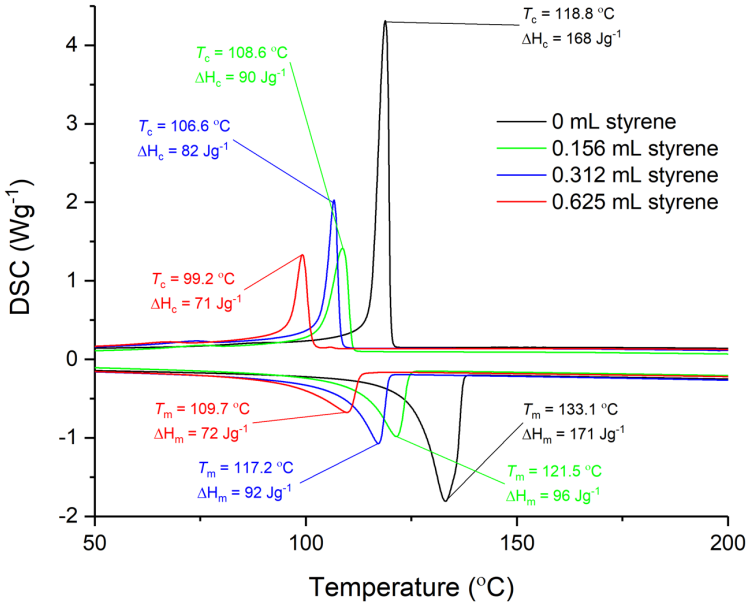

Figure A4.34. DSC plot for polymers produced by sMAO-^{Me2}SB(^{tBu}N,I*)Ti(Cl)CH$_2$SiMe$_3$ at 70 °C for 0 mL (black), 0.156 mL (green), 0.312 mL (blue), and 0.625 mL styrene (red).

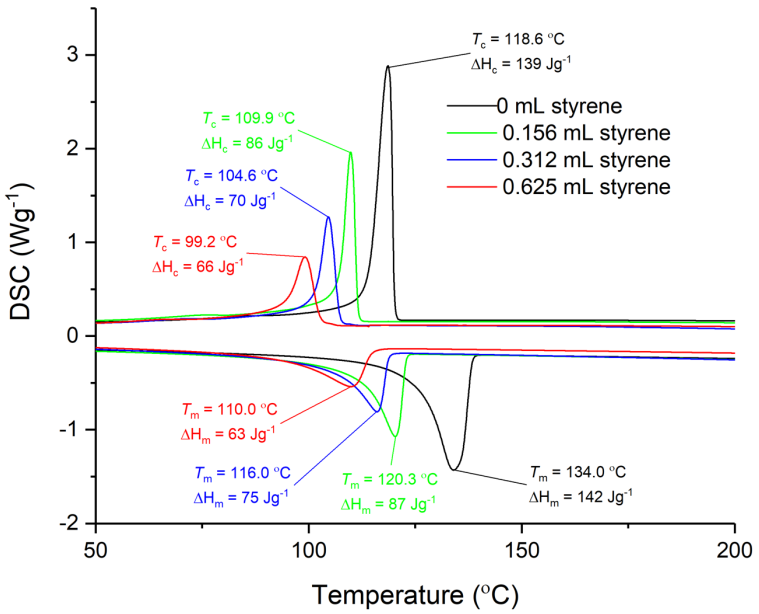

Figure A4.35. DSC plot for polymers produced by sMAO-^{Me_2}SB($^{t\text{Bu}}$N,I*)Ti(CH_2SiMe_3)$_2$ at 70 °C for 0 mL (black), 0.156 mL (green), 0.312 mL (blue), and 0.625 mL styrene (red).

Table A4.1. Polymerisation activities, mass of catalyst used, and mass of polymer produced; 10 mg catalyst $[Al]_0$:$[Ti]_0$ = 200:1), 2 bar ethylene, 0, 0.156, 0.312 or 0.625 mL 1-hexene, 50 mL hexanes, 150 mg TiBA and 30 minutes.

Volume of 1-hexene (mL)	Mass Catalyst (mg)		Mass Polymer (g)		Activity ($kg_{PE}/mol_{Ti}/h/bar$)		Average Activity ($kg_{PE}/mol_{Ti}/h/bar$)
	A	B	A	B	A	B	
			30 °C				
0	10.0	10.5	0.985	0.918	1352	1200	1276
0.156	9.0	10.0	0.469	0.582	716	799	757
0.312	10.5	10.2	0.508	0.475	664	639	652
0.625	10.2	10.0	0.476	0.468	641	643	642
			40 °C				
0	9.5	9.8	1.945	1.869	2811	2619	2715
0.156	9.8	10.2	1.011	0.911	1416	1226	1321
0.312	10.2	9.8	10.38	0.918	1397	1286	1342
0.625	10.5	10.2	1.166	1.127	1525	1517	1520
			50 °C				
0	9.5	9.5	2.673	2.545	3863	3678	3771
0.156	10.0	9.6	1.526	1.357	2095	1941	2018
0.312	9.5	9.8	1.367	1.259	1976	1763	1870
0.625	10.2	9.6	2.311	2.337	3111	3343	3226
			60 °C				
0	9.7	9.7	2.490	2.637	3525	3733	3629
0.156	9.8	10.2	1.143	1.084	1601	1459	1530
0.312	10.0	10.0	1.256	1.411	1725	1937	1831
0.625	9.5	9.4	2.154	2.049	3113	2993	3053
			70 °C				
0	9.8	10.2	2.410	2.607	3377	3509	3443
0.156	9.5	10.2	2.415	2.759	3490	3714	3602
0.312	9.8	9.7	2.925	3.107	4098	4398	4248
0.625	9.5	9.9	2.604	2.615	3764	3627	3695
			80 °C				

0	9.7	10.2	2.337	2.457	3308	3307	3308
0.156	9.9	10.1	1.955	1.804	2711	2452	2582
0.312	9.5	9.7	1.932	1.985	2792	2810	2801
0.625	9.7	10.3	2.053	2.229	2906	2971	2939
			90 °C				
0	9.5	9.9	2.064	2.190	2983	2037	3010
0.156	9.5	10.0	1.877	1.733	2713	2380	2546
0.312	10.1	9.5	1.825	1.668	2481	2410	2446
0.625	9.7	10.0	1.736	1.689	2457	2319	2388

Table A4.2. Polymer melt and crystallisation enthalpies for the polyethylenes/ poly(ethylene-co-1-hexene) produced between 30 and 90 °C using sMAO-^{Me_2}SB($^{t\text{Bu}}$N,I*)TiCl$_2$; 10 mg catalyst [Al]$_0$:[Ti]$_0$ = 200:1), 2 bar ethylene, 0, 0.156, 0.312 or 0.625 mL 1-hexene, 50 mL hexanes, 150 mg TiBA and 30 minutes.

Temperature (°C)	Volume of 1-hexene (mL)							
	0		0.156		0.312		0.625	
	ΔH_m	ΔH_c	ΔH_m	ΔH_c	ΔH_m	ΔH_c	ΔH_m	ΔH_c
30	111	109	80	79	70	74	70	56
40	111	105	92	86	89	79	62	56
50	133	137	84	87	73	72	67	60
60	136	134	88	89	77	73	67	67
70	157	156	106	106	109	103	68	85
80	164	164	93	97	82	75	43	48
90	174	181	118	120	89	99	65	94

ΔH_m and ΔH_c correspond to melt enthalpy and crystallisation enthalpy respectively. Values given as J g^{-1}.

Table A4.3. Polymer melt and crystallisation temperatures for the polyethylenes/poly(ethylene-co-1-hexene) produced between 30 and 90 °C using sMAO-^{Me_2}SB($^{t\text{Bu}}$N,I*)TiCl$_2$; 10 mg catalyst [Al]$_0$:[Ti]$_0$ = 200:1), 2 bar ethylene, 0, 0.156, 0.312 or 0.625 mL 1-hexene, 50 mL hexanes, 150 mg TiBA and 30 minutes.

Temperature (°C)	Volume of 1-hexene (mL)							
	0		0.156		0.312		0.625	
	T_m	T_c	T_m	T_c	T_m	T_c	T_m	T_c
30	134.8	117.8	126.1	114.5	122.6	111.5	113.9	103.9
40	134.7	118.3	124.5	113.4	119.4	109.9	112.5	100.2
50	135.9	117.7	124.7	112.8	119.7	108.4	114.2	100.4
60	136.1	117.5	123.0	112.1	116.1	106.8	115.4	102.0
70	137.7	116.3	125.3	111.4	121.9	110.6	122.3	108.1
80	135.5	118.3	122.9	111.6	119.0	107.0	121.7	108.1
90	133.6	118.9	125.7	113.6	122.2	109.7	118.5	104.9

T_m and T_c in °C; DSC run for 3 cycles between 25 and 250 °C; T_m taken on third heating cycle and T_c from first cooling cycle.

Table A4.4. Polymerisation activities, mass of catalyst used, and mass of polymer produced; 10 mg catalyst $[Al]_0:[Ti]_0 = 200:1$), 2 bar ethylene, 0, 0.156, 0.312 or 0.625 mL 1-hexene, 50 mL hexanes, 150 mg TiBA and 30 minutes.

Volume of 1-hexene (mL)	Mass Catalyst (mg)		Mass Polymer (g)		Activity ($kg_{PE}/mol_{Ti}/h/bar$)		Average Activity ($kg_{PE}/mol_{Ti}/h/bar$)
	A	B	A	B	A	B	
sMAO-^{Me_2}SB(^{tBu}N,I*)$TiCl_2$							
0	9.8	10.2	2.410	2.607	3377	3509	3443
0.156	9.5	10.2	2.415	2.759	3490	3714	3602
0.312	9.8	9.7	2.925	3.107	4098	4398	4248
0.625	9.5	9.9	2.604	2.615	3764	3627	3695
sMAO-^{Me_2}SB(^{tBu}N,$^{3\text{-}Et}$I*)$TiCl_2$							
0	9.6	9.5	2.534	2.877	3614	4146	3880
0.156	9.9	9.7	1.805	1.661	2496	2344	2420
0.312	9.5	9.8	1.627	1.655	2345	2312	2328
0.625	9.5	10.2	1.944	2.309	2801	3099	2950
sMAO-^{Me,Pr}SB(^{tBu}N,I*)$TiCl_2$							
0	10.0	10.1	2.939	3.100	4056	4236	4146
0.156	10.1	10.2	2.030	1.957	2774	2648	2711
0.312	10.3	10.3	2.137	2.063	2863	2764	2814
0.625	9.7	10.1	2.300	2.397	3272	3275	3274
sMAO-^{Me_2}SB(^{tBu}N,I*)$Ti(CH_2Ph)_2$							
0	9.7	10.0	3.004	3.230	4285	4469	4377
0.156	9.7	10.4	1.856	1.970	2647	2621	2634
0.312	9.8	9.8	1.684	1.772	2378	2502	2440
0.625	9.9	9.5	2.037	1.824	2847	2657	2751
sMAO-^{Me_2}SB(^{tBu}N,Cp*)$TiCl_2$							
0	10.0	9.6	1.658	1.525	2273	2178	2226
0.156	9.9	9.9	1.382	1.291	1914	1788	1851
0.312	10.0	9.9	1.559	1.630	2137	2257	2197
0.625	9.7	10.2	1.179	1.402	1666	1884	1775
sMAO-^{Me_2}SB(^{tBu}N,I*)$Ti(CH_2SiMe_3)_2$							
0	9.7	9.4	2.362	2.194	3384	3243	3314
0.156	10.3	9.4	1.340	1.109	1808	1639	1724
0.312	9.8	10.5	1.472	1.665	2087	2204	2145
0.625	10.2	9.8	1.873	1.789	2552	2537	2544
sMAO-^{Me_2}SB(^{tBu}N,I*)$Ti(Cl)CH_2SiMe_3$							
0	9.8	9.6	3.424	3.497	4802	5007	4905
0.156	10.1	10.3	2.676	2.784	3641	3715	3679
0.312	9.7	9.6	2.307	3.396	4686	4863	4774
0.625	9.0	10.1	2.636	2.929	4026	3986	4006

Table A4.5. Polymer melt and crystallisation temperatures for the polyethylenes/poly(ethylene-co-1-hexene) produced for the catalysts (A) sMAO-^{Me_2}SB(^{tBu}N,I*)TiCl$_2$, (B) sMAO-^{Me_2}SB(^{tBu}N,$^{3\text{-}Et}$I*)TiCl$_2$, (C) sMAO-^{Me,Pr}SB(^{tBu}N,I*)TiCl$_2$, (D) sMAO-^{Me_2}SB(^{tBu}N,I*)Ti(CH$_2$Ph)$_2$, (E) sMAO-^{Me_2}SB(^{tBu}N,Cp*)TiCl$_2$, (F) sMAO-^{Me_2}SB(^{tBu}N,I*)Ti(Cl)CH$_2$SiMe$_3$ and (G) sMAO-^{Me_2}SB(^{tBu}N,I*)Ti(CH$_2$SiMe$_3$)$_2$; 10 mg catalyst [Al]$_0$:[Ti]$_0$ = 200:1), 2 bar ethylene, 0, 0.156, 0.312 or 0.625 mL 1-hexene, 50 mL hexanes, 150 mg TiBA and 30 minutes.

Complex	Volume of 1-hexene (mL)							
	0		0.156		0.312		0.625	
	T_m	T_c	T_m	T_c	T_m	T_c	T_m	T_c
A	137.7	116.3	125.3	111.4	121.9	110.6	122.3	108.1
B	132.7	119.1	121.7	111.07	117.2	106.6	113.8	98.5
C	133.2	119.4	122.8	110.9	117.3	107.4	113.8	101.0
D	133.5	118.8	122.3	112.2	117.0	106.1	114.3	102.2
E	133.7	118.2	120.0	109.9	116.9	104.9	107.0	94.4
F	133.1	118.8	134.6	117.4	123.9	111.1	121.4	106.1
G	134.0	118.6	120.5	110.2	116.2	105.4	111.7	99.9

T_m and T_c in °C; DSC run for 3 cycles between 25 and 250 °C; T_m taken on third heating cycle and T_c from first cooling cycle.

Table A4.6. Polymer melt and crystallisation enthalpies for the polyethylenes/ poly(ethylene-co-1-hexene) produced for the catalysts (A) sMAO-^{Me_2}SB(^{tBu}N,I*)TiCl$_2$, (B) sMAO-^{Me_2}SB(^{tBu}N,$^{3\text{-}Et}$I*)TiCl$_2$, (C) sMAO-^{Me,Pr}SB(^{tBu}N,I*)TiCl$_2$, (D) sMAO-^{Me_2}SB(^{tBu}N,I*)Ti(CH$_2$Ph)$_2$, (E) sMAO-^{Me_2}SB(^{tBu}N,Cp*)TiCl$_2$, (F) sMAO-^{Me_2}SB(^{tBu}N,I*)Ti(Cl)CH$_2$SiMe$_3$ and (G) sMAO-^{Me_2}SB(^{tBu}N,I*)Ti(CH$_2$SiMe$_3$)$_2$; 10 mg catalyst [Al]$_0$:[Ti]$_0$ = 200:1), 2 bar ethylene, 0, 0.156, 0.312 or 0.625 mL 1-hexene, 50 mL hexanes, 150 mg TiBA and 30 minutes.

Complex	Volume of 1-hexene (mL)							
	0		0.156		0.312		0.625	
	ΔH_m	ΔH_c	ΔH_m	ΔH_c	ΔH_m	ΔH_c	ΔH_m	ΔH_c
A	157	156	106	106	109	103	68	85
B	145	145	99	95	83	83	60	56
C	129	130	89	82	79	76	60	62
D	153	142	94	87	56	55	70	62
E	159	150	98	96	78	77	48	50
F	171	168	152	148	104	98	80	82
G	142	139	84	82	70	69	72	65

ΔH_m and ΔH_c correspond to melt enthalpy and crystallisation enthalpy respectively. Values given as J g^{-1}.

Table A4.7. Polymerisation activities, mass of catalyst used, and mass of polymer produced; 10 mg catalyst $[Al]_0:[Ti]_0 = 200:1$), 2 bar ethylene, 0, 0.156, 0.312 or 0.625 mL styrene, 50 mL hexanes, 150 mg TiBA and 30 minutes.

Volume of styrene (mL)	Mass Catalyst (mg)		Mass Polymer (g)		Activity ($kg_{PE}/mol_{Ti}/h/bar$)		Average Activity ($kg_{PE}/mol_{Ti}/h/bar$)
	A	B	A	B	A	B	
sMAO-^{Me_2}SB(^{tBu}N,I*)TiCl$_2$							
0	9.8	10.2	2.410	2.607	3377	3509	3443
0.156	9.9	9.7	0.824	0.878	1143	1243	1193
0.312	10.4	9.4	0.918	0.862	1212	1259	1236
0.625	9.7	10.1	1.401	1.537	1983	2089	2036
sMAO-^{Me_2}SB(^{tBu}N,$^{3\text{-}Et}$I*)TiCl$_2$							
0	9.6	9.5	2.534	2.877	3614	4146	3880
0.156	10.1	10.2	1.103	1.019	1495	1368	1431
0.312	9.8	10.0	0.980	0.934	1369	1279	1324
0.625	9.8	10.3	0.912	0.956	1274	1271	1272
sMAO-^{Me,Pr}SB(^{tBu}N,I*)TiCl$_2$							
0	10.0	10.1	2.939	3.100	4056	4236	4146
0.156	9.5	9.8	0.574	0.763	834	1074	954
0.312	10.4	9.9	0.652	0.603	865	841	853
0.625	9.5	10.1	0.472	0.542	686	741	713
sMAO-^{Me_2}SB(^{tBu}N,I*)Ti(CH$_2$Ph)$_2$							
0	9.7	10.0	3.004	3.230	4285	4469	4377
0.156	9.8	10.1	0.527	0.691	744	947	845
0.312	10.5	9.5	0.777	0.542	1024	789	907
0.625	9.3	10.2	0.423	0.610	629	827	728
sMAO-^{Me_2}SB(^{tBu}N,Cp*)TiCl$_2$							
0	10.0	9.6	1.658	1.525	2273	2178	2226
0.156	9.7	9.8	1.660	1.881	2346	2632	2488
0.312	9.8	9.8	1.255	1.449	1756	2027	1891
0.625	10.2	10.2	1.065	1.035	1432	1391	1411
sMAO-^{Me_2}SB(^{tBu}N,I*)Ti(CH$_2$SiMe$_3$)$_2$							
0	9.7	9.4	2.362	2.194	3384	3243	3314
0.156	10.2	10.1	0.995	0.891	1356	1226	1290
0.312	9.4	9.4	0.722	0.644	1067	952	1009
0.625	9.5	9.8	0.483	0.539	707	764	735
sMAO-^{Me_2}SB(^{tBu}N,I*)Ti(Cl)CH$_2$SiMe$_3$							
0	9.8	9.6	3.424	3.497	4802	5007	4905
0.156	10.5	10.0	2.008	1.911	2629	2627	2628
0.312	10.2	9.9	2.228	2.099	3002	2914	2958
0.625	9.5	9.8	1.608	1.608	2326	2255	2291

Table A4.8. Polymer melt and crystallisation temperatures for the polyethylenes/poly(ethylene-co-styrene) produced for the catalysts (A) sMAO-^{Me_2}SB($^{t Bu}$N,I*)TiCl$_2$, (B) sMAO-^{Me_2}SB($^{t Bu}$N,$^{3\text{-}Et}$I*)TiCl$_2$, (C) sMAO-^{Me,Pr}SB($^{t Bu}$N,I*)TiCl$_2$, (D) sMAO-^{Me_2}SB($^{t Bu}$N,I*)Ti(CH$_2$Ph)$_2$, (E) sMAO-^{Me_2}SB($^{t Bu}$N,Cp*)TiCl$_2$, (F) sMAO-^{Me_2}SB($^{t Bu}$N,I*)Ti(Cl)CH$_2$SiMe$_3$ and (G) sMAO-^{Me_2}SB($^{t Bu}$N,I*)Ti(CH$_2$SiMe$_3$)$_2$; 10 mg catalyst [Al]$_0$:[Ti]$_0$ = 200:1), 2 bar ethylene, 0, 0.156, 0.312 or 0.625 mL styrene, 50 mL hexanes, 150 mg TiBA and 30 minutes.

Complex	Volume of styrene (mL)							
	0		0.156		0.312		0.625	
	T_m	T_c	T_m	T_c	T_m	T_c	T_m	T_c
A	137.7	116.3	119.4	109.7	115.5	105.5	109.7	97.9
B	132.7	119.1	120.1	108.9	114.6	104.2	107.8	96.4
C	133.2	119.4	121.7	111.6	119.0	108.9	113.1	103.2
D	133.5	118.8	119.6	109.0	115.6	105.3	110.1	99.9
E	133.7	118.2	115.2	105.2	108.7	96.7	98.4	86.7
F	134.0	118.6	120.3	109.9	116.0	104.6	110.0	99.2
G	133.1	118.8	121.5	108.6	117.2	106.6	109.7	99.2

T_m and T_c in °C; DSC run for 3 cycles between 25 and 250 °C; T_m taken on third heating cycle and T_c from first cooling cycle.

Table A4.9. Polymer melt and crystallisation for the polyethylenes/poly(ethylene-co-styrene) produced for the catalysts (A) sMAO-^{Me_2}SB($^{t Bu}$N,I*)TiCl$_2$, (B) sMAO-^{Me_2}SB($^{t Bu}$N,$^{3\text{-}Et}$I*)TiCl$_2$, (C) sMAO-^{Me,Pr}SB($^{t Bu}$N,I*)TiCl$_2$, (D) sMAO-^{Me_2}SB($^{t Bu}$N,I*)Ti(CH$_2$Ph)$_2$, (E) sMAO-^{Me_2}SB($^{t Bu}$N,Cp*)TiCl$_2$, (F) sMAO-^{Me_2}SB($^{t Bu}$N,I*)Ti(Cl)CH$_2$SiMe$_3$ and (G) sMAO-^{Me_2}SB($^{t Bu}$N,I*)Ti(CH$_2$SiMe$_3$)$_2$; 10 mg catalyst [Al]$_0$:[Ti]$_0$ = 200:1), 2 bar ethylene, 0, 0.156, 0.312 or 0.625 mL styrene, 50 mL hexanes, 150 mg TiBA and 30 minutes.

Complex	Volume of styrene (mL)							
	0		0.156		0.312		0.625	
	ΔH_m	ΔH_c	ΔH_m	ΔH_c	ΔH_m	ΔH_c	ΔH_m	ΔH_c
A	157	156	88	89	85	87	64	59
B	145	145	87	87	74	74	61	60
C	129	130	91	82	79	75	79	71
D	153	142	76	89	75	67	57	63
E	159	150	80	82	61	60	45	41
F	142	139	87	86	75	70	63	66
G	171	168	96	90	92	82	72	71

ΔH_m and ΔH_c correspond to melt enthalpy and crystallisation enthalpy respectively. Values given as J g^{-1}.

Table A4.10. Polymerisation activities, mass of catalyst used, and mass of polymer produced; 10 mg catalyst $[Al]_0:[Ti]_0 = 200:1$), 2 bar ethylene, 0, 0.156, 0.312 or 0.625 mL 1-octene, 50 mL hexanes, 150 mg TiBA and 30 minutes.

Volume of 1-octene (mL)	Mass Catalyst (mg)		Mass Polymer (g)		Activity ($kg_{PE}/mol_{Ti}/h/bar$)		Average Activity ($kg_{PE}/mol_{Ti}/h/bar$)
	A	B	A	B	A	B	
sMAO-^{Me_2}SB(^{tBu}N,I*)$TiCl_2$							
0	9.8	10.2	2.410	2.607	3377	3509	3443
0.156	10.0	9.7	2.457	2.266	3374	3208	3291
0.312	10.3	9.7	2.843	2.690	3790	3808	3799
0.625	10.3	10.4	2.410	2.530	3213	3340	3276
sMAO-^{Me_2}SB(^{tBu}N,$^{3\text{-}Et}$I*)$TiCl_2$							
0	9.6	9.5	2.534	2.877	3614	4146	3880
0.156	10.1	10.2	2.510	2.615	3402	3510	3455
0.312	9.6	9.9	2.653	2.682	3783	2709	3746
0.625	9.5	9.6	2.509	2.510	3616	3579	3597

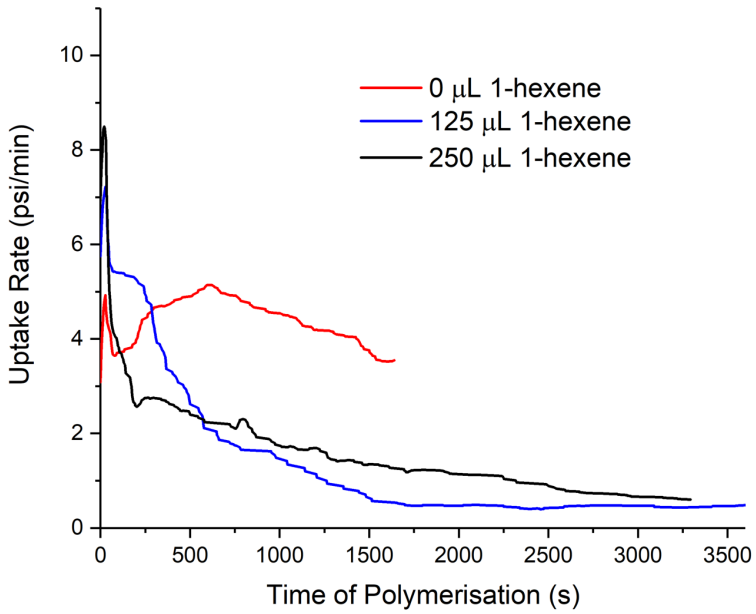

Figure A4.36. Ethylene uptake rate profiles for sMAO-^{Me2}SB($^{t Bu}$N,I*)Ti($CH_2Ph)_2$ with varying amounts of 1-hexene; 8.27 bar ethylene, 0.075 mg catalyst ($[Al]_0$:$[Ti]_0$ = 200:1), 5.0 mL heptane, 10 µmol TiBA and T = 80 °C. Reactions quenched at 8.27 bar maximum ethylene uptake or after 60 minutes.

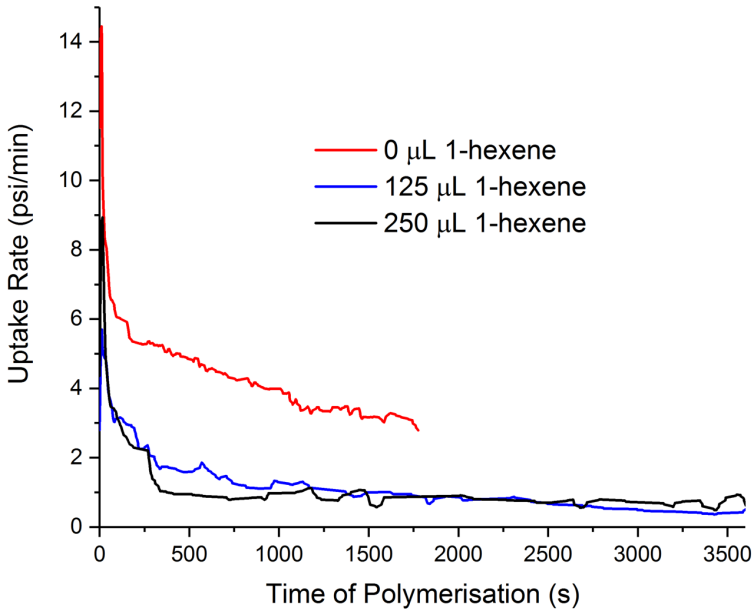

Figure A4.37. Ethylene uptake rate profiles for sMAO-^{Me2}SB($^{t Bu}$N,I*)$TiMe_2$ with varying amounts of 1-hexene; 8.27 bar ethylene, 0.30 mg catalyst ($[Al]_0$:$[Ti]_0$ = 200:1), 5.0 mL heptane, 10 µmol TiBA and T = 80 °C. Reactions quenched at 8.27 bar maximum ethylene uptake or after 60 minutes.

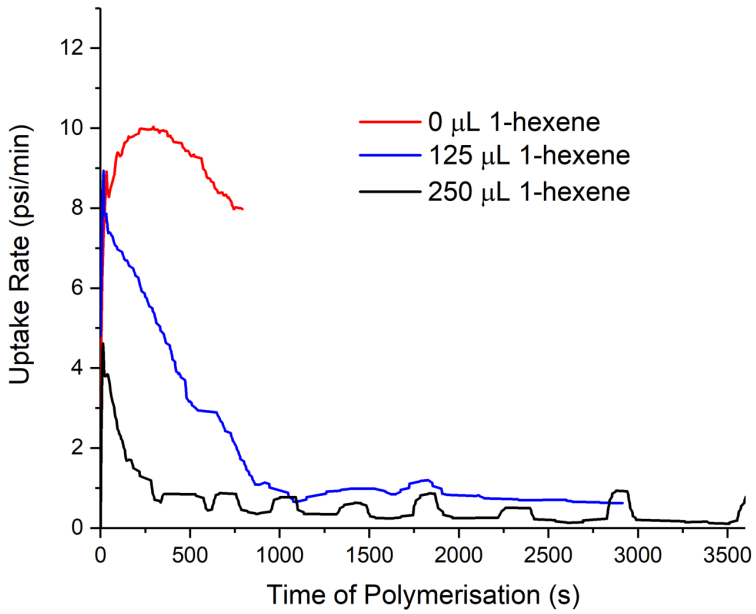

Figure A4.38. Ethylene uptake rate profiles for sMAO-^{Me_2}SB($^{t\text{Bu}}$N,I*)Ti(CH_2SiMe_3)$_2$ with varying amounts of 1-hexene; 8.27 bar ethylene, 0.30 mg catalyst ([Al]$_0$:[Ti]$_0$ = 200:1), 5.0 mL heptane, 10 µmol TiBA and T = 80 °C. Reactions quenched at 8.27 bar maximum ethylene uptake or after 60 minutes.

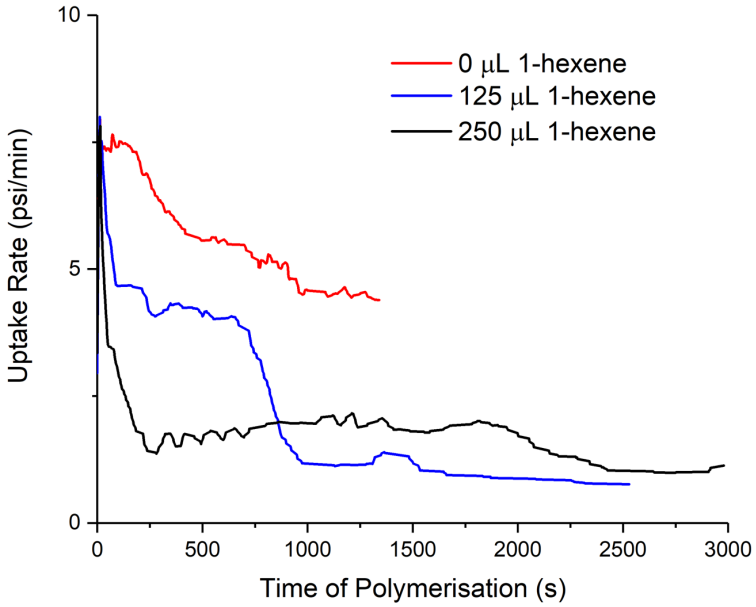

Figure A4.39. Ethylene uptake rate profiles for sMAO-^{Me_2}SB($^{t\text{Bu}}$N,$^{3\text{-Et}}$I*)$TiCl_2$ with varying amounts of 1-hexene; 8.27 bar ethylene, 0.30 mg catalyst ([Al]$_0$:[Ti]$_0$ = 200:1), 5.0 mL heptane, 10 µmol TiBA and T = 80 °C. Reactions quenched at 8.27 bar maximum ethylene uptake or after 60 minutes.

Table A4.11. CEF maximum elution temperatures for the polymers produced by 0, 125 and 250 µL of 1-hexene addition; 8.27 bar ethylene, 0.075−0.30 mg catalyst ($[Al]_0$:$[Ti]_0$ = 200:1), 5.0 mL heptane, 10 µmol TiBA and T = 80 °C. Reactions quenched at 8.27 bar maximum ethylene uptake or after 60 minutes.

Complex	Volume of 1-hexene (µL)		
	0	125	250
	$T_{El,max}$ (°C)	$T_{El,max}$ (°C)	$T_{El,max}$ (°C)
sMAO-^{Me_2}SB($^{t Bu}$N,I*)$TiCl_2$	112.1	85.1	73.5
sMAO-^{Me_2}SB($^{i Pr}$N,I*)$TiCl_2$	113.9	98.8	80.5
sMAO-^{Me_2}SB($^{t Bu}$N,I*)$Ti(CH_2Ph)_2$	111.4	89.8	71.6/105.0
sMAO-^{Me_2}SB($^{t Bu}$N,I*)$TiMe_2$	113.3	84.8	69.5
sMAO-^{Me_2}SB($^{t Bu}$N,I*)$Ti(CH_2SiMe_3)_2$	113.3	89.0	70.5
sMAO-^{Me_2}SB($^{t Bu}$N,I*)$Ti(Cl)CH_2SiMe_3$	113.3	88.0	70.9
sMAO-^{Me_2}SB($^{t Bu}$N,$^{3\text{-}Et}$I*)$TiCl_2$	113.4	81.9	66.0

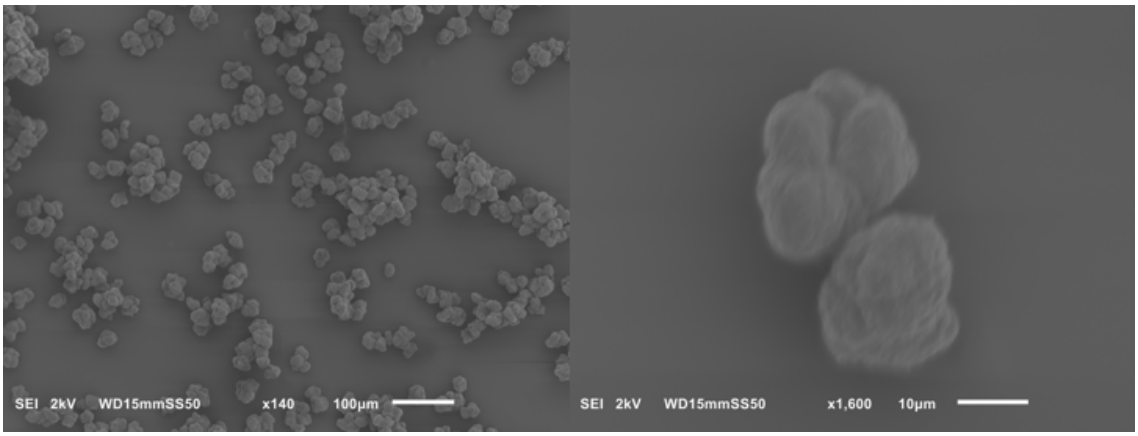

Figure A4.40. SEM image of the polymer produced by sMAO-^{Me_2}SB($^{t Bu}$N,I*)$TiCl_2$ with 0 mL of comonomer; 10 mg catalyst ($[Al]_0$:$[Ti]_0$ = 200:1), 2 bar ethylene, 50 mL hexanes, 150 mg TiBA and 30 minutes.

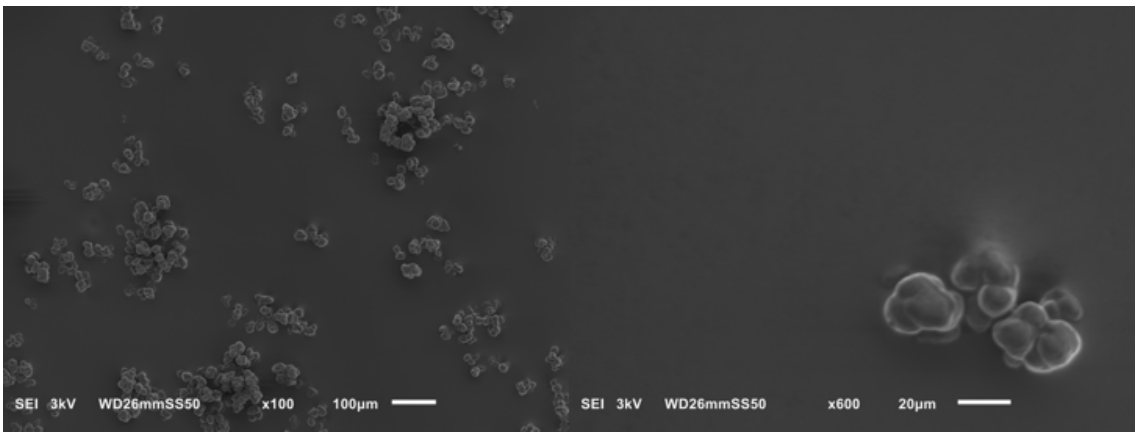

Figure A4.41. SEM image of the polymer produced by sMAO-^{Me2}SB($^{t Bu}$N,I*)TiCl$_2$ with 0.156 mL of 1-hexene; 10 mg catalyst ([Al]$_0$:[Ti]$_0$ = 200:1), 2 bar ethylene, 50 mL hexanes, 150 mg TiBA and 30 minutes.

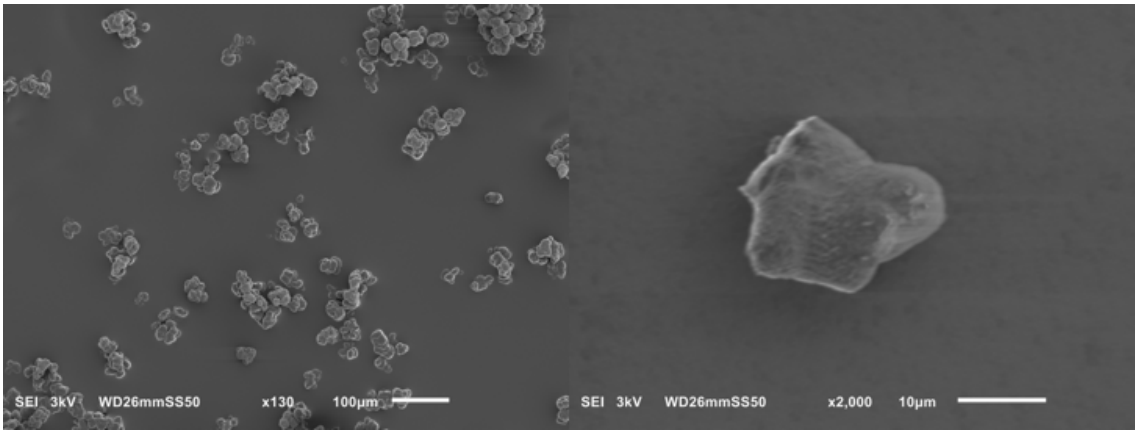

Figure A4.42. SEM image of the polymer produced by sMAO-^{Me2}SB($^{t Bu}$N,I*)TiCl$_2$ with 0.312 mL of 1-hexene; 10 mg catalyst ([Al]$_0$:[Ti]$_0$ = 200:1), 2 bar ethylene, 50 mL hexanes, 150 mg TiBA and 30 minutes.

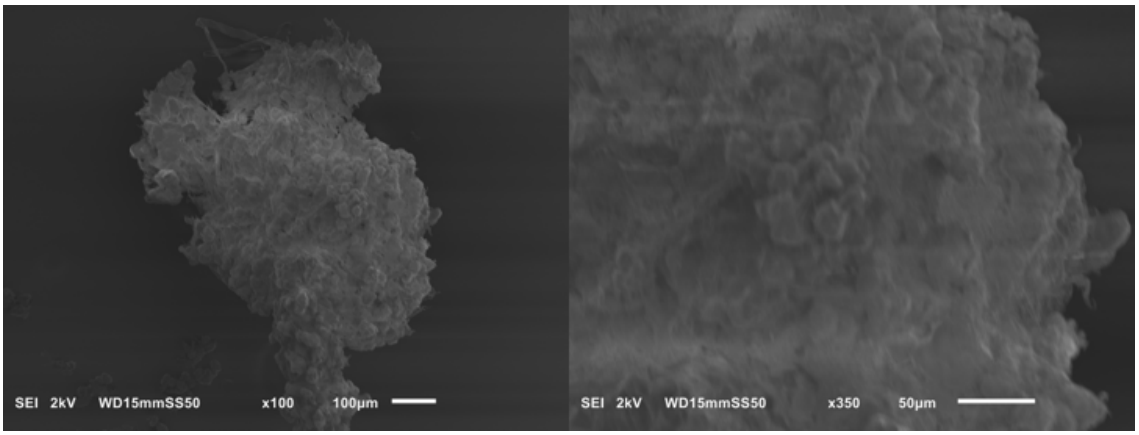

Figure A4.43. SEM image of the polymer produced by sMAO-^{Me2}SB($^{t Bu}$N,I*)TiCl$_2$ with 0.625 mL of 1-hexene; 10 mg catalyst ([Al]$_0$:[Ti]$_0$ = 200:1), 2 bar ethylene, 50 mL hexanes, 150 mg TiBA and 30 minutes.

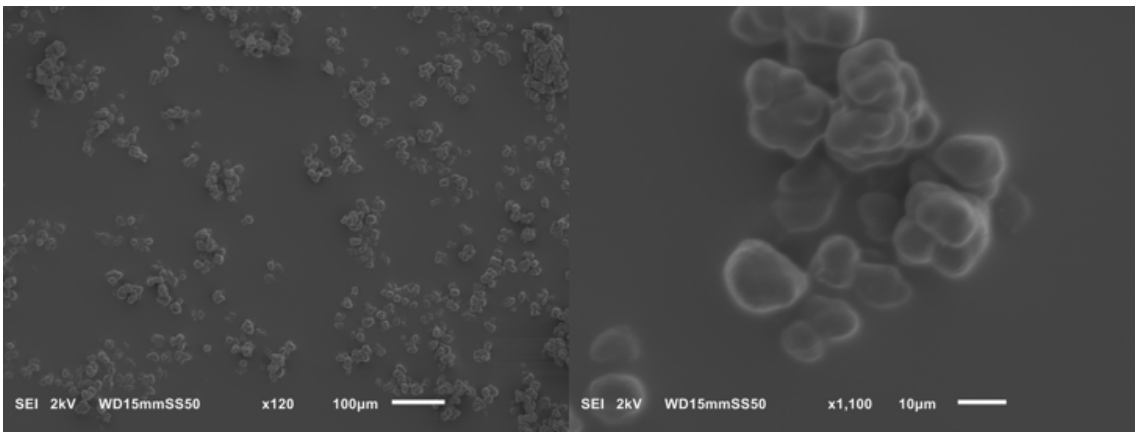

Figure A4.44. SEM image of the polymer produced by sMAO-^{Me2}SB(^{tBu}N,I*)TiCl$_2$ with 0.156 mL of styrene; 10 mg catalyst ([Al]$_0$:[Ti]$_0$ = 200:1), 2 bar ethylene, 50 mL hexanes, 150 mg TiBA and 30 minutes.

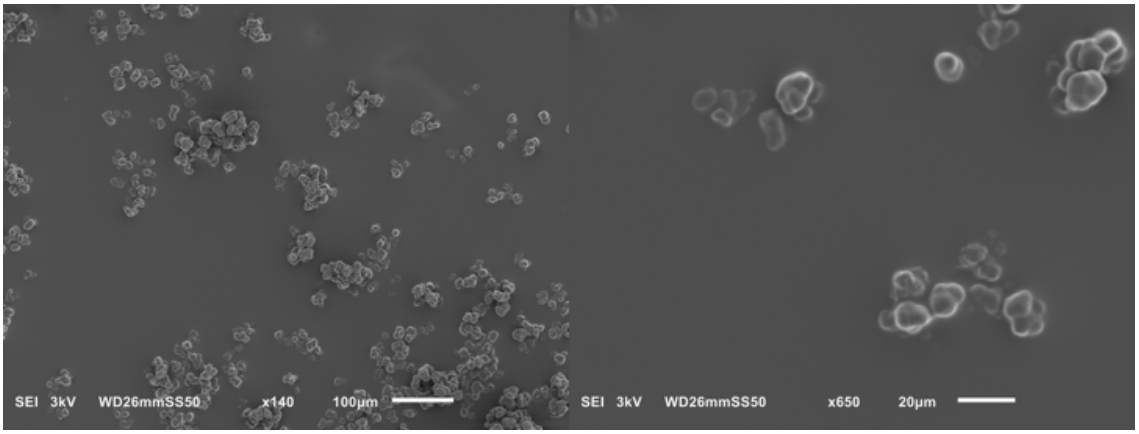

Figure A4.45. SEM image of the polymer produced by sMAO-^{Me2}SB(^{tBu}N,I*)TiCl$_2$ with 0.312 mL of styrene; 10 mg catalyst ([Al]$_0$:[Ti]$_0$ = 200:1), 2 bar ethylene, 50 mL hexanes, 150 mg TiBA and 30 minutes.

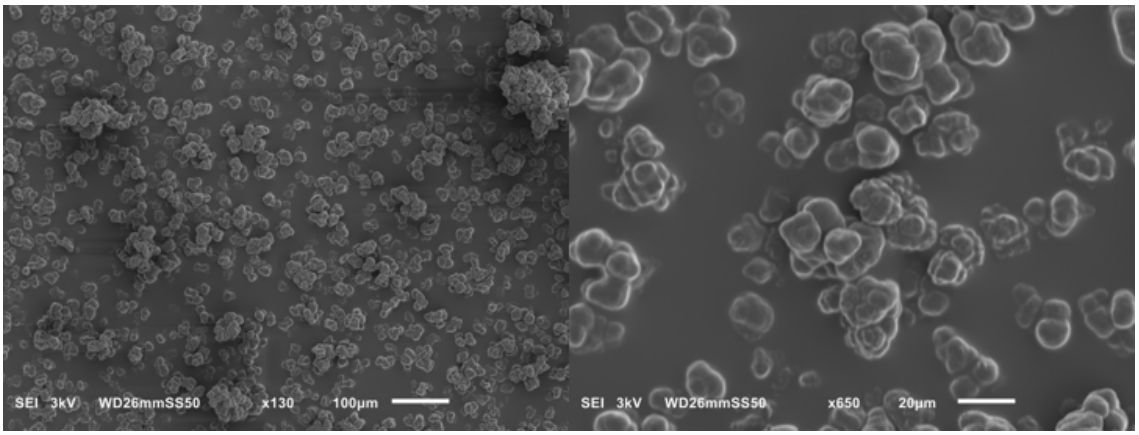

Figure A4.46. SEM image of the polymer produced by sMAO-^{Me2}SB(^{tBu}N,I*)TiCl$_2$ with 0.625 mL of styrene; 10 mg catalyst ([Al]$_0$:[Ti]$_0$ = 200:1), 2 bar ethylene, 50 mL hexanes, 150 mg TiBA and 30 minutes.

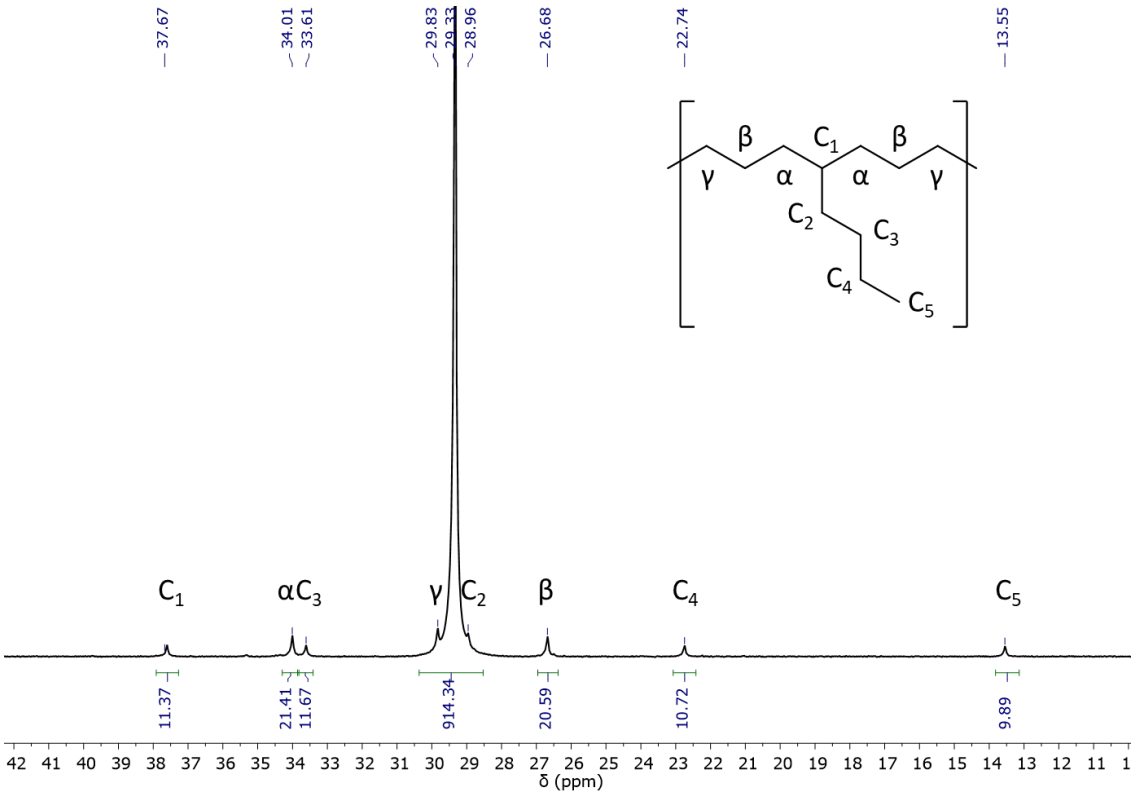

Figure A4.47. $^{13}C\{^{1}H\}$ NMR spectrum of the polymer produced by sMAO-^{Me_2}SB(^{tBu}N,I*)$TiCl_2$ with 0.625 mL of 1-hexene. 30 minutes, 10 mg catalyst, 50 mL hexanes, 150 mg TiBA, 2 bar ethylene and 70 °C (d_2-1,1,2,2-tetrachloroethane, 125.7 MHz, 393 K).

A5. Appendix for Chapter 5

Table A5.1. Ethylene oligomerisation and polymerisation activities and selectivities after 10 hours.

Temperature	50 °C	70 °C	75 °C	100 °C
[b] Alkene TON	42	17	27	18
Mass polymer (mg)	7	3	2	5
Polyethylene TON	690	295	200	443
Alkene selectivity (%)	6	5	12	4
[b] 1-hexene selectivity (%)	87	69	87	88
[b] 1-butene selectivity (%)	13	31	13	12

[a] TON values in $mol_{C_2H_4}/mol_{Nb}$. [b] The observed amount of butene may be lower than the actual amount due to its high volatility. Reaction conditions: 1 bar ethylene, 5 mg catalyst ($[Al]_0$:$[Nb]_0$ = 200:1), 500 µL d_6-benzene and mesitylene standard. Selectivities determined by integration of triplets corresponding to 1-butene and 1-hexene between 0.95 and 0.80 ppm. Turnover numbers calculated by integration of the resonance at 5.00 ppm corresponding to the terminal CH_2 resonances of both 1-butene and 1-hexene.

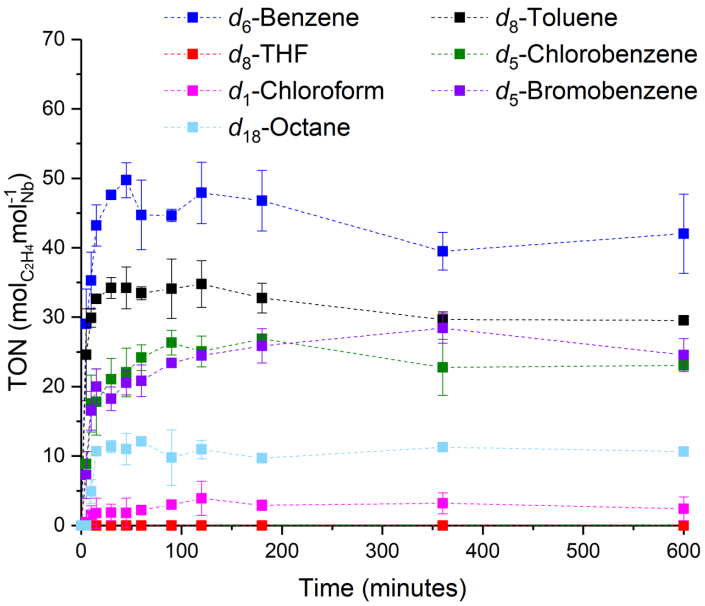

Figure A5.1. Solvent study using sMAO-Nb(NDipp)Cl_3; 1 bar ethylene, 500 µL solvent, 5 mg catalyst ($[Al]_0$:$[Nb]_0$ = of 200:1), 10 hours of reaction time and mesitylene standard.

Table A5.2. Dielectric constants and donor numbers of the solvents used.[1,2]

Solvent	Dielectric constant (ε)	Donor Number
Benzene	2.3	0.1
Toluene	2.4	0.1
Bromobenzene	5.6	3.3
Chlorobenzene	5.4	3
Octane	Heptane = 1.9	Heptane = 0
THF	7.6	20
Chloroform	4.0	4.1

Table A5.3. Ethylene oligomerisation and polymerisation activities and selectivities after 10 hours.

Solvent	C_6D_6	C_7D_8	C_6D_5Cl	C_6D_5Br	C_8D_{18}	C_4H_8O	$CDCl_3$
[b] Alkene TON	42	30	23	25	11	0	2
Mass polymer (mg)	7	5	6	3	8	0	1
Polyethylene TON	690	541	590	246	738	0	98
Alkene selectivity (%)	6	5	4	9	1	0	2
[b] 1-hexene selectivity (%)	87	82	85	84	0	0	0
[b] 1-butene selectivity (%)	13	18	15	16	100	0	100

[a] TON values in $mol_{C_2H_4}/mol_{Nb}$. [b] The observed amount of butene may be lower than the actual amount due to its high volatility. Reaction conditions: 1 bar ethylene, 5 mg catalyst ($[Al]_0$:$[Nb]_0$ = 200:1), 500 µL d_6-benzene and mesitylene standard. Selectivities determined by integration of triplets corresponding to 1-butene and 1-hexene between 0.95 and 0.80 ppm. Turnover numbers calculated by integration of the resonance at 5.00 ppm corresponding to the terminal CH_2 resonances of both 1-butene and 1-hexene.

Table A5.4. Ethylene oligomerisation and polymerisation activities and selectivities after 10 hours.

$[Al]_0$:$[Ti]_0$	250:1	200:1	150:1	100:1
[b] Alkene TON	29	42	25	18
Mass polymer (mg)	4	7	3	2
Polyethylene TON	496	690	200	103
Alkene selectivity (%)	6	6	15	10
[b] 1-hexene selectivity (%)	88	87	90	88
[b] 1-butene selectivity (%)	12	13	10	12

[a] TON values in $mol_{C_2H_4}/mol_{Nb}$. [b] The observed amount of butene may be lower than the actual amount due to its high volatility. Reaction conditions: 1 bar ethylene, 5 mg catalyst ($[Al]_0$:$[Nb]_0$ = 200:1), 500 µL d_6-benzene and mesitylene standard. Selectivities determined by integration of triplets corresponding to 1-butene and 1-hexene between 0.95 and 0.80 ppm. Turnover numbers calculated by integration of the resonance at 5.00 ppm corresponding to the terminal CH_2 resonances of both 1-butene and 1-hexene.

Table A5.5. Ethylene oligomerisation and polymerisation activities and selectivities after 10 hours.

Pressure	1 bar	2 bar
[b] Alkene TON	42	41
Mass polymer (mg)	7	5
Polyethylene TON	690	492
Alkene selectivity (%)	6	8
[b] 1-hexene selectivity (%)	87	74
[b] 1-butene selectivity (%)	13	26

[a] TON values in $mol_{C_2H_4}/mol_{Nb}$. [b] The observed amount of butene may be lower than the actual amount due to its high volatility. Reaction conditions: 1 bar ethylene, 5 mg catalyst ($[Al]_0$:$[Nb]_0$ = 200:1), 500 µL d_6-benzene and mesitylene standard. Selectivities determined by integration of triplets corresponding to 1-butene and 1-hexene between 0.95 and 0.80 ppm. Turnover numbers calculated by integration of the resonance at 5.00 ppm corresponding to the terminal CH_2 resonances of both 1-butene and 1-hexene.

Table A5.6. Ethylene oligomerisation and polymerisation activities and selectivities after 10 hours.

MAO equivalents	0 equivalents	10 equivalents	50 equivalents	100 equivalents
[b] Alkene TON	42	39	27	22
Mass polymer (mg)	7	5	3	4
Polyethylene TON	690	492	295	394
Alkene selectivity (%)	6	7	8	5
[b] 1-hexene selectivity (%)	87	84	84	85
[b] 1-butene selectivity (%)	13	16	16	15

[a] TON values in $mol_{C_2H_4}/mol_{Nb}$. [b] The observed amount of butene may be lower than the actual amount due to its high volatility. Reaction conditions: 1 bar ethylene, 5 mg catalyst ($[Al]_0$:$[Nb]_0$ = 200:1), 500 µL d_6-benzene and mesitylene standard. Selectivities determined by integration of triplets corresponding to 1-butene and 1-hexene between 0.95 and 0.80 ppm. Turnover numbers calculated by integration of the resonance at 5.00 ppm corresponding to the terminal CH_2 resonances of both 1-butene and 1-hexene.

Table A5.7. Ethylene oligomerisation and polymerisation activities and selectivities after 10 hours.

MAO equivalents	10 equivalents	25 equivalents	50 equivalents	100 equivalents
[b] Alkene TON	0.4	1.7	5.2	8.0
Mass polymer (mg)	1	3	4	11
Polyethylene TON	9.4	23.4	32.8	103.1
Alkene selectivity (%)	4	7	14	7
[b] 1-hexene selectivity (%)	62	75	73	77
[b] 1-butene selectivity (%)	38	25	27	23

[a] TON values in $mol_{C_2H_4}/mol_{Nb}$. [b] The observed amount of butene may be lower than the actual amount due to its high volatility. Reaction conditions: 2 mg of Nb(NDipp)Cl_3.THF.pyr, MAO cocatalyst, 1 bar ethylene, 500 µL d_6-benzene, mesitylene standard. Selectivities determined by integration of triplets corresponding to 1-butene and 1-hexene between 0.95 and 0.80 ppm. Turnover numbers calculated by integration of the resonance at 5.00 ppm corresponding to the terminal CH_2 resonances of both 1-butene and 1-hexene.

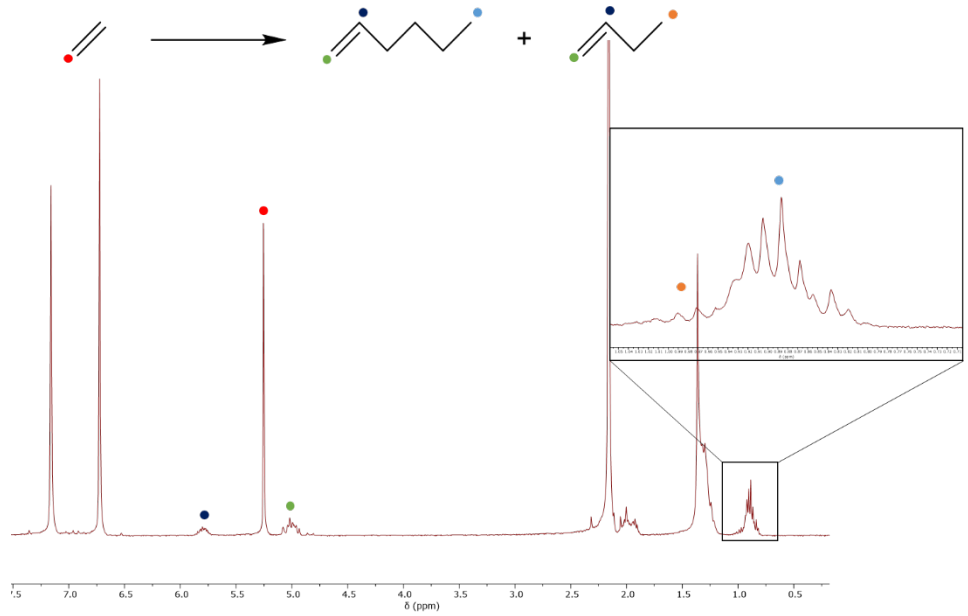

Figure A5.2. ^{1}H NMR spectrum of heterogeneous ethylene oligomerisation; 50 °C, 1 h, $[Al]_0$:$[Nb]_0$ = 200:1 and d_6-benzene.

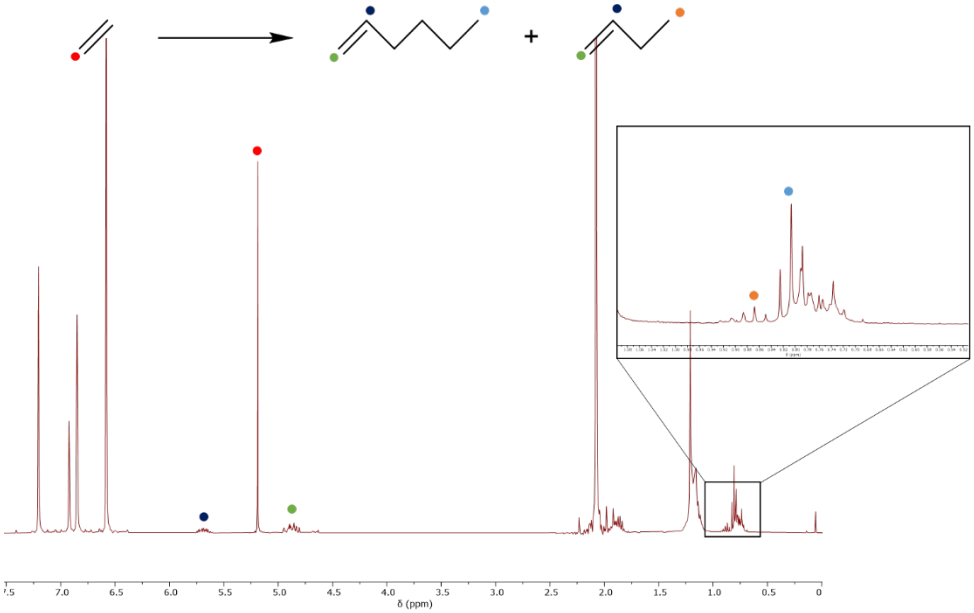

Figure A5.3. ^{1}H NMR spectrum of heterogeneous ethylene oligomerisation; 50 °C, d_5-bromobenzene, 1 h and $[Al]_0$:$[Nb]_0$ = 200:1.

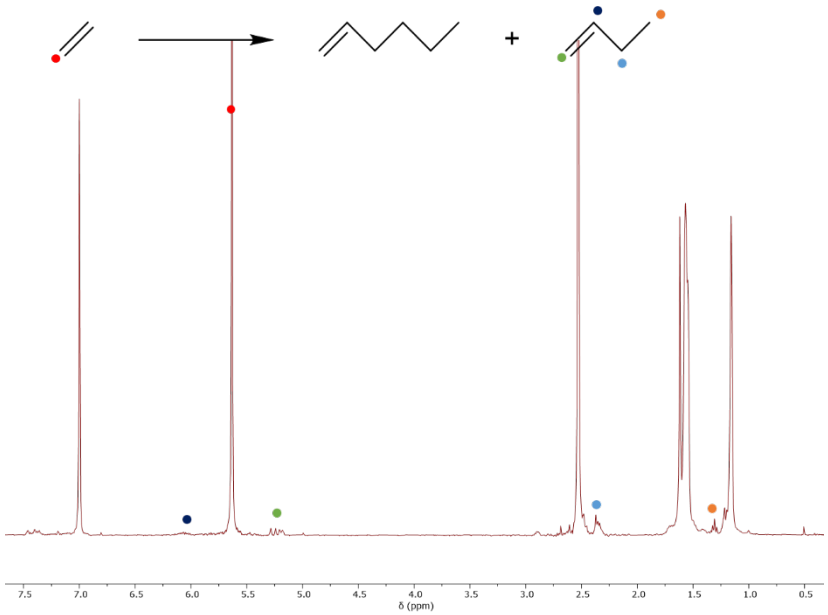

Figure A5.4. ^{1}H NMR spectrum of heterogeneous ethylene oligomerisation; 50 °C, d_{18}-octane, 1 h and $[Al]_0$:$[Nb]_0$ = 200:1.

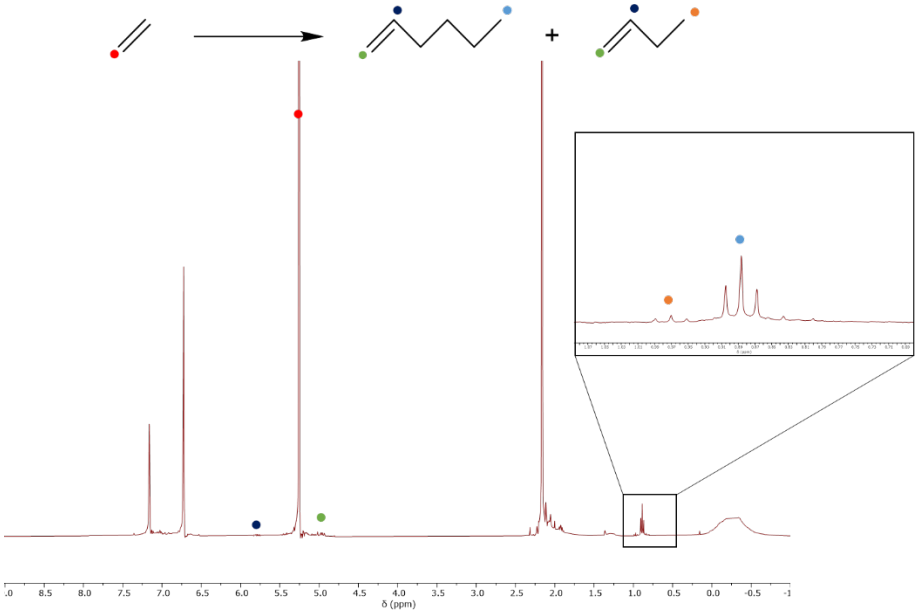

Figure A5.5. ^{1}H NMR spectrum of heterogeneous ethylene oligomerisation; 50 °C, d_6-benzene, 1 h, 100 equivalents MAO and $[Al]_0$:$[Nb]_0$ = 200:1.

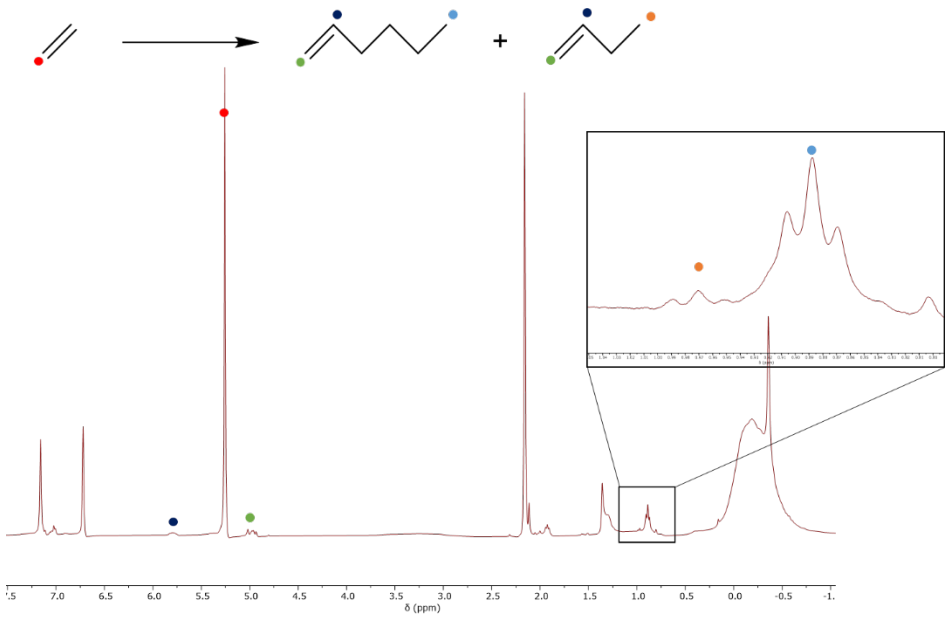

Figure A5.6. ^{1}H NMR spectrum of solution ethylene oligomerisation; 50 °C, d_6-benzene, 1 h and 100 equivalents MAO.

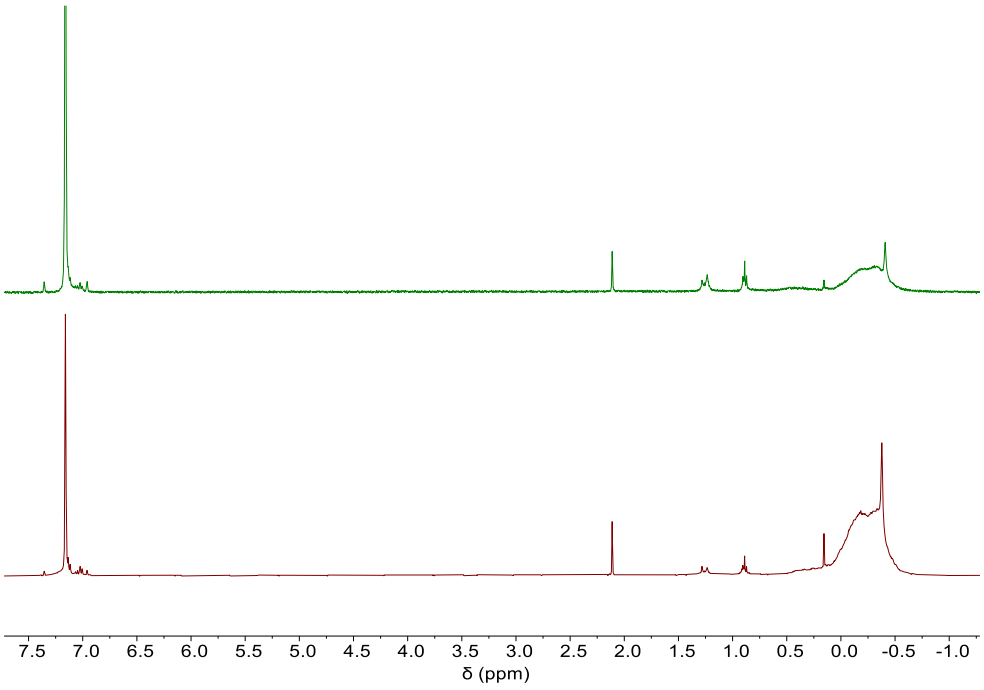

Figure A5.7. ^{1}H NMR spectra of sMAO-Nb(NDipp)Cl_3 with 100 equivalents of MAO after (top) 0 h and (bottom) 3 h of heating at 50 °C. Resonance at 7.16 ppm is attributable to d_6-benzene, 400 MHz, 298 K.

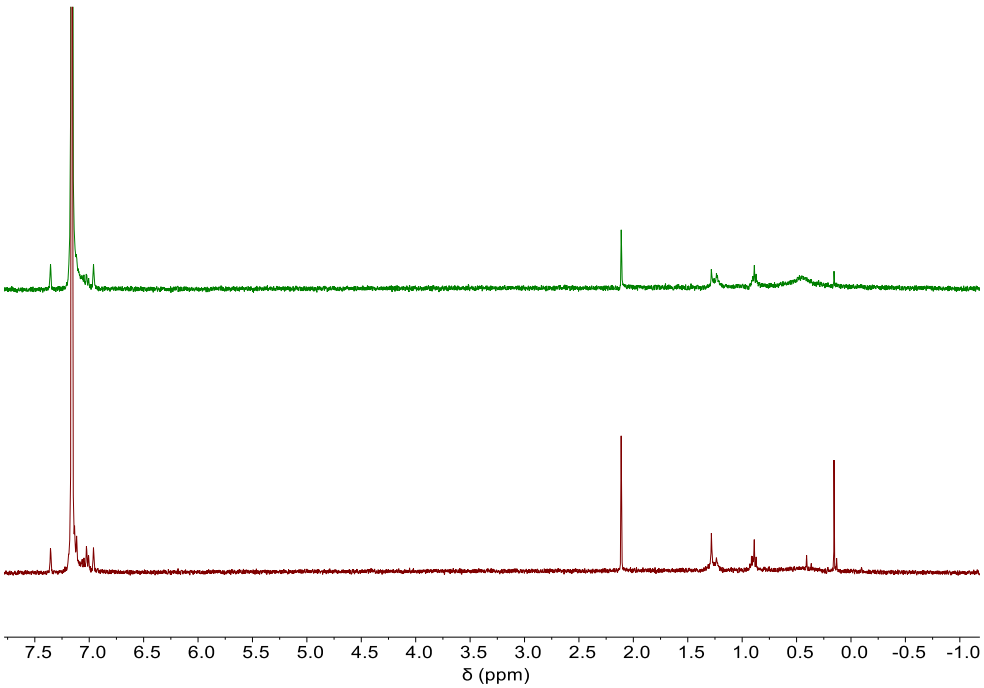

Figure A5.8. ^{1}H NMR spectra of sMAO-Nb(NDipp)Cl_3 after (top) 0 h and (bottom) 3 h of heating at 50 °C. Resonance at 7.16 ppm is attributable to d_6-benzene, 400 MHz, 298 K.

A6. References

1 F. Cataldo, *Eur. Chem. Bull.*, 2015, **4**, 92–97.

2 C. Reichardt and T. Welton, *Solvents and Solvent Effects in Organic Chemistry*, Wiley-VCH Verlag GmbH & Co. KGaA: Weinheim, Germany, Vol. 16., 2010.